

SPRINGER SERIES ON FLUORESCENCE

05

Series Editor O. S. Wolfbeis  
Volume Editor U. Resch-Genger

# Standardization and Quality Assurance in Fluorescence Measurements I

Techniques

 Springer

**5**

# **Springer Series on Fluorescence**

**Methods and Applications**

**Series Editor: O. S. Wolfbeis**

# **Springer Series on Fluorescence**

**Series Editor: O. S. Wolfbeis**

Recently Published and Forthcoming Volumes

**Standardization and Quality Assurance  
in Fluorescence Measurements II**  
Bioanalytical and Biomedical Applications  
Volume Editor: Resch-Genger, U.  
Vol. 6, 2008

**Standardization and Quality Assurance  
in Fluorescence Measurements I**  
Techniques  
Volume Editor: Resch-Genger, U.  
Vol. 5, 2008

**Fluorescence of Supermolecules,  
Polymers, and Nanosystems**  
Volume Editor: Berberan-Santos, M. N.  
Vol. 4, 2007

**Fluorescence Spectroscopy in Biology**  
Volume Editor: Hof, M.  
Vol. 3, 2004

**Fluorescence Spectroscopy, Imaging and Probes**  
Volume Editor: Kraayenhof, R.  
Vol. 2, 2002

**New Trends in Fluorescence Spectroscopy**  
Volume Editor: Valeur, B.  
Vol. 1, 2001

# Standardization and Quality Assurance in Fluorescence Measurements I

## Techniques

Volume Editor: Ute Resch-Genger

With contributions by

M. Ameloot · I. Billard · D. J. S. Birch · N. Boens · P. C. DeRose  
A. Duerkop · G. Flachenecker · A. K. Gaigalas · G. Gauglitz · G. Geipel  
A. A. Goulko · J. W. Guthrie · A. Hoffmann · K. Hoffmann · P. Kapusta  
J. Karolin · G. W. Kramer · X. C. Le · H. Lemmetyinen · G. E. Marti  
J. N. Miller · G. J. Mohr · C. Monte · S. Nagl · U. Ortmann · U. Panne  
M. Patting · D. Pfeifer · G. Proll · U. Resch-Genger · K. Rurack  
M. Schäferling · M. I. J. Stich · N. V. Tkachenko · B. Valeur  
R. F. Vogt Jr. · M. Wahl · L. Wang · O. S. Wolfbeis · V. Zenger  
Q. Zhao · H. Zou · J. Zwinkels



Fluorescence spectroscopy, fluorescence imaging and fluorescent probes are indispensable tools in numerous fields of modern medicine and science, including molecular biology, biophysics, biochemistry, clinical diagnosis and analytical and environmental chemistry. Applications stretch from spectroscopy and sensor technology to microscopy and imaging, to single molecule detection, to the development of novel fluorescent probes, and to proteomics and genomics. The Springer Series on Fluorescence aims at publishing state-of-the-art articles that can serve as invaluable tools for both practitioners and researchers being active in this highly interdisciplinary field. The carefully edited collection of papers in each volume will give continuous inspiration for new research and will point to exciting new trends.

ISBN 978-3-540-75206-6 e-ISBN 978-3-540-75207-3  
DOI 10.1007/978-3-540-75207-3

Springer Series on Fluorescence ISSN 1617-1306

Library of Congress Control Number: 2008934029

© 2008 Springer-Verlag Berlin Heidelberg

This work is subject to copyright. All rights are reserved, whether the whole or part of the material is concerned, specifically the rights of translation, reprinting, reuse of illustrations, recitation, broadcasting, reproduction on microfilm or in any other way, and storage in data banks. Duplication of this publication or parts thereof is permitted only under the provisions of the German Copyright Law of September 9, 1965, in its current version, and permission for use must always be obtained from Springer. Violations are liable to prosecution under the German Copyright Law.

The use of general descriptive names, registered names, trademarks, etc. in this publication does not imply, even in the absence of a specific statement, that such names are exempt from the relevant protective laws and regulations and therefore free for general use.

Cover design: WMXDesign GmbH, Heidelberg  
Typesetting and Production: le-tex publishing services oHG, Leipzig

Printed on acid-free paper

9 8 7 6 5 4 3 2 1 0

springer.com

---

## **Series Editor**

Prof. Dr. Otto S. Wolfbeis

Institute of Analytical Chemistry,  
Chemo- and Biosensors  
University of Regensburg  
93040 Regensburg, Germany  
*otto.wolfbeis@chemie.uni-regensburg.de*

## **Volume Editor**

Dr. Ute Resch-Genger

Bundesanstalt für Materialforschung und -prüfung (BAM)  
Arbeitskreis "Optical Spectroscopy"  
Richard-Willstaetter-Str. 11  
12489 Berlin  
Germany  
*ute.resch@bam.de*

---

## Preface

In the booming fields of the life and material sciences, advances are taking place on all fronts and often involve the use of luminescence techniques as analytical tools and detection methods due to their high sensitivity, intrinsic selectivity, noninvasive (or at least minimally invasive) character, comparative ease of use, potential for multiplexing applications, and remote accessibility of signals. Despite the fact that the measurement of fluorescence—with its birth marked by the study of Sir Stokes on quinine sulfate in 1852—is not a new technique and many fluorescence techniques have matured to a state where quantification is desired, standardization of the broad variety of fluorescence methods and applications is still in its infancy as compared to other prominent (bio)analytical methods.

It is still often overlooked that all types of fluorescence measurements yield signals containing both analyte-specific and instrument-specific contributions. Furthermore, the absorption and fluorescence of most fluorophores is sensitive to their microenvironment, and this can hamper quantification based on measurements of relative fluorescence intensities as well as accurate measurements of absolute fluorescence intensities. Hence, the realization of a truly quantitative measurement is inherently challenging. This situation renders quality assurance in fluorometry very important, especially with respect to the increasing complexity of instrumentation, and the blackbox-type of present-day instruments and software. This may compromise future applications of fluorescence techniques in strongly regulated areas like medical diagnostics and clinical chemistry that are within reach.

As a result, there is an ever increasing need for (a) recommendations and guidelines for the characterization and performance validation of fluorescence instrumentation and the performance of typical fluorescence measurements, and (b) for an improved understanding of fluorescence-inherent sources of error. This is closely linked to the availability of suitable and easily handled standards that can be operated under routine analytical conditions, are adequately characterized, and meet overall accepted quality criteria.

Within this context, the aim of this book is to provide a unique overview on the current state of instrumentation and application employed for steady state and time-resolved fluorometry and fluorescence polarization measurement as well as fluorescence techniques and materials used for fluorescent

chemical sensing thereby highlighting the present state of quality assurance and the need for future standards. Method-inherent advantages, limitations, and sources of uncertainties are addressed, often within the context of typical and upcoming applications. The ultimate goal is to make users of fluorescence techniques more aware of necessary steps to improve the overall reliability and comparability of fluorescence data to encourage the further broadening of fluorescence applications.

I wish to express my appreciation and special thanks to the individuals who insisted and encouraged me in the preparation of this book. These include Dr. K. Hoffmann, Dr. R. Nitschke, Dr. L. Wang, Dr. R. Zucker, and especially Prof. Dr. O. Wolfbeis for help with the choice of authors and reviewers. And finally, Jürgen and Claudia, for their continuous support and encouragement.

Berlin, July 2008

Dr. Ute Resch-Genger

---

# Contents

## Part I

### Need for Standardization of Fluorescence-Based Measurements

**Quantitative Fluorescence Calibration:  
a Tool for Assessing the Quality of Data Obtained  
by Fluorescence Measurements**  
R. F. Vogt Jr. · G. E. Marti · V. Zenger . . . . . 3

**Need for and Metrological Approaches  
Towards Standardization of Fluorescence Measurements  
from the View of National Metrology Institutes**  
P. C. DeRose · L. Wang · A. K. Gaigalas · G. W. Kramer  
U. Resch-Genger · U. Panne . . . . . 33

## Part II

### Steady State Fluorometry

**Linking Fluorometry to Radiometry  
with Physical and Chemical Transfer Standards: Instrument  
Characterization and Traceable Fluorescence Measurements**  
U. Resch-Genger · D. Pfeifer · K. Hoffmann · G. Flachenecker  
A. Hoffmann · C. Monte . . . . . 65

**Fluorescence Quantum Yields:  
Methods of Determination and Standards**  
K. Rurack . . . . . 101

---

<b>Long-Wavelength and Near-Infrared Fluorescence: State of the Art, Future Applications, and Standards</b> J. N. Miller . . . . .	147
<b>Surface Fluorescence: the Only Standardized Method of Measuring Luminescence</b> J. Zwinkels . . . . .	163
 <b>Part III</b> <b>Time Resolved Fluorometry</b>	
<b>Time-Resolved Fluorometry: Typical Methods, Challenges, Applications and Standards</b> N. V. Tkachenko · H. Lemmetyinen . . . . .	195
<b>Practical Time-Resolved Fluorescence Spectroscopy: Avoiding Artifacts and Using Lifetime Standards</b> N. Boens · M. Ameloot · B. Valeur . . . . .	215
<b>Evaluation of Time-Resolved Fluorescence Data: Typical Methods and Problems</b> M. Patting . . . . .	233
<b>Time-Resolved Fluorescence: Novel Technical Solutions</b> U. Ortmann · M. Wahl · P. Kapusta . . . . .	259
 <b>Part IV</b> <b>Fluorescence Polarization Techniques: Applications in the Material and the Life Sciences</b>	
<b>Fluorescence Depolarization Techniques in Materials Science</b> D. J. S. Birch · J. Karolin . . . . .	279
<b>Fluorescence Polarization: Recent Bioanalytical Applications, Pitfalls, and Future Trends</b> A. A. Goulko · Q. Zhao · J. W. Guthrie · H. Zou · X. C. Le . . . . .	303

**Part V****Fluorescent Chemical Sensors:  
Principles, Problems, and Need for Quality Assurance**

<b>Classification of Chemical Sensors and Biosensors Based on Fluorescence and Phosphorescence</b> S. Nagl · O. S. Wolfbeis . . . . .	325
<b>Fibre-Optic and Nanoparticle-Based Fluorescence Sensing Using Indicator Dyes: Pitfalls, Self- Referencing, Application, and Future Trends</b> G. J. Mohr . . . . .	347
<b>Intrinsically Referenced Fluorimetric Sensing and Detection Schemes: Methods, Advantages and Applications</b> M. Schäferling · A. Duerkop . . . . .	373
<b>Total Internal Reflection Fluorescence Sensing – Quality Assurance and Application to Water Analysis</b> G. Gauglitz · G. Proll . . . . .	415
<b>Fluorescence Sensing and Imaging Using Pressure-Sensitive Paints and Temperature-Sensitive Paints</b> M. I. J. Stich O. S. Wolfbeis · . . . .	429
<b>Part VI</b>	
<b>Fluorescence Analysis of Actinides</b>	
<b>Luminescence Analysis of Actinides: Instrumentation, Applications, Quantification, Future Trends, and Quality Assurance</b> I. Billard · G. Geipel . . . . .	465
<b>Subject Index . . . . .</b>	493

---

## Contributors

AMELOOT, MARCEL  
BIOMED  
Universiteit Hasselt  
Agoralaan, Building D  
3590 Diepenbeek, Belgium

BILLARD, I.  
IPHC/DRS  
Chimie Nucléaire  
Bat. 35, BP 28  
67037 Strasbourg Cedex 2  
France

BIRCH, DAVID J. S.  
Photophysics Research, Department of  
Physics  
Scottish Universities Physics Alliance  
University of Strathclyde  
Glasgow G4 0NG, UK

BOENS, NOËL  
Department of Chemistry  
Katholieke Universiteit Leuven  
Celestijnenlaan 200f, bus 02404  
3001 Heverlee, Belgium

DEROSE, P. C.  
National Institute of Standards  
and Technology (NIST)  
100 Bureau Drive  
Gaithersburg, MD 20899-8312, USA

DUERKOP, AXEL  
Institute of Analytical Chemistry,  
Chemo- and Biosensors  
University of Regensburg  
93040 Regensburg, Germany

FLACHENECKER, G.  
Federal Institute for Materials Research  
and Testing (BAM)  
Richard-Willstaetter-Str. 11  
12489 Berlin, Germany

GAIGALAS, A. K.  
National Institute of Standards  
and Technology (NIST)  
100 Bureau Drive  
Gaithersburg, MD 20899-8312, USA

GAUGLITZ, GUENTER  
Eberhard-Karls Universität  
Institut für Physikalische  
und Theoretische Chemie  
Auf der Morgenstelle 8  
72076 Tübingen, Germany

GEIPEL, G.  
Forschungszentrum Rossendorf  
Institute of Radiochemistry  
P.O. Box 510 119  
01314 Dresden, Germany

GOULKO, ALEVTINA A.  
Division of Analytical  
and Environmental Toxicology  
Department of Laboratory Medicine  
and Pathology  
Faculty of Medicine and Dentistry  
and School of Public Health  
University of Alberta  
Edmonton, Alberta, T6G 2G3, Canada



GUTHRIE, JEFFREY W.

Division of Analytical  
and Environmental Toxicology  
Department of Laboratory Medicine  
and Pathology  
Faculty of Medicine and Dentistry  
and School of Public Health  
University of Alberta  
Edmonton, Alberta, T6G 2G3, Canada

HOFFMANN, A.

Federal Institute for Materials Research  
and Testing (BAM)  
Richard-Willstaetter-Str. 11  
12489 Berlin, Germany

HOFFMANN, K.

Federal Institute for Materials Research  
and Testing (BAM)  
Richard-Willstaetter-Str. 11  
12489 Berlin, Germany

KAPUSTA, PETER

PicoQuant GmbH  
Rudower Chaussee 29  
12489 Berlin, Germany

KAROLIN, JAN

Photophysics Research, Department of  
Physics  
Scottish Universities Physics Alliance  
University of Strathclyde  
Glasgow G4 0NG, UK

KRAMER, G. W.

National Institute of Standards  
and Technology (NIST)  
100 Bureau Drive  
Gaithersburg, MD 20899-8312, USA

LE, X. CHRIS

Division of Analytical  
and Environmental Toxicology  
Department of Laboratory Medicine  
and Pathology  
Faculty of Medicine and Dentistry  
and School of Public Health  
University of Alberta  
Edmonton, Alberta, T6G 2G3, Canada

LEMMETYINEN, HELGE

Department of Chemistry  
and Bioengineering  
Tampere University of Technology  
P.O. Box 541  
33101 Tampere, Finland

MARTI, GERALD E.

Center for Biologics Evaluation  
and Research  
Food and Drug Administration  
Atlanta, GA 30341, USA

MILLER, JAMES N.

Department of Chemistry  
Loughborough University  
Loughborough LE11 3TU, UK

MOHR, GERHARD J.

Institute of Physical Chemistry  
Friedrich-Schiller University Jena  
Lessingstrasse 10  
07743 Jena, Germany

MONTE, C.

Physikalisch-Technische Bundesanstalt  
(PTB)  
Abbéstr. 2-12  
10587 Berlin, Germany

NAGL, STEFAN

Institute of Analytical Chemistry,  
Chemo- and Biosensors  
University of Regensburg  
Universitätsstr. 31  
D-93053 Regensburg, Germany

ORTMANN, UWE

PicoQuant GmbH  
Rudower Chaussee 29  
12489 Berlin, Germany

PANNE, U.

Federal Institute for Materials Research  
and Testing (BAM)  
Richard-Willstaetter-Str. 11  
12489 Berlin, Germany

**PATTING, MATTHIAS**

PicoQuant GmbH  
Rudower Chaussee 29  
12489 Berlin, Germany

**PFEIFER, D.**

Federal Institute for Materials Research  
and Testing (BAM)  
Richard-Willstaetter-Str. 11  
12489 Berlin, Germany

**PROLL, GUENTHER**

Eberhard-Karls Universität  
Institut für Physikalische  
und Theoretische Chemie  
Auf der Morgenstelle 8  
72076 Tübingen, Germany

**RESCH-GENGER, U.**

Federal Institute for Materials Research  
and Testing (BAM)  
Richard-Willstaetter-Str. 11  
12489 Berlin, Germany

**RURACK, KNUT**

Div. I.5  
Bundesanstalt für Materialforschung  
und -prüfung (BAM)  
Richard-Willstaetter-Str. 11  
12489 Berlin, Germany

**SCHÄFERLING, MICHAEL**

Institute of Analytical Chemistry,  
Chemo- and Biosensors  
University of Regensburg  
93040 Regensburg, Germany

**STICH, MATTHIAS I. J.**

Institute of Analytical Chemistry,  
Chemo- and Biosensors  
University of Regensburg  
93053 Regensburg, Germany

**TKACHENKO, NIKOLAI V.**

Department of Chemistry  
and Bioengineering  
Tampere University of Technology  
P.O. Box 541  
33101 Tampere, Finland

**VALEUR, BERNARD**

CNRS UMR 8531  
Laboratoire de Chimie Générale, CNAM  
292 rue Saint-Martin  
75141 Paris Cedex 03, France  
Laboratoire PPSM  
ENS-Cachan  
61 avenue du Président Wilson  
94235 Cachan Cedex, France

**VOGT JR., ROBERT F.**

Newborn Screening Branch  
Division of Laboratory Sciences  
Centers for Disease Control and Prevention  
CDC, Mailstop F19  
Atlanta, GA 30341, USA

**WAHL, MICHAEL**

PicoQuant GmbH  
Rudower Chaussee 29  
12489 Berlin, Germany

**WANG, L.**

National Institute of Standards  
and Technology (NIST)  
100 Bureau Drive  
Gaithersburg, MD 20899-8312, USA

**WOLFBEIS, OTTO S.**

Institute of Analytical Chemistry,  
Chemo- and Biosensors  
University of Regensburg  
Universitätsstr. 31  
D-93053 Regensburg, Germany

**ZENGER, VINCENT**

Center for Drugs Evaluation and Research  
Food and Drug Administration  
Atlanta, GA 30341, USA

**ZHAO, QIANG**

Division of Analytical  
and Environmental Toxicology  
Department of Laboratory Medicine  
and Pathology  
Faculty of Medicine and Dentistry  
and School of Public Health  
University of Alberta  
Edmonton, Alberta, T6G 2G3, Canada

ZOU, HANFA  
Dalian Institute of Chemical Physics  
Chinese Academy of Sciences  
Dalian, China

ZWINKELS, JOANNE  
National Research Council  
1200 Montreal Road  
Ottawa, Ontario  
K1A 0R6, Canada

**Part I**  
**Need for Standardization of Fluorescence-Based**  
**Measurements**

# Quantitative Fluorescence Calibration: a Tool for Assessing the Quality of Data Obtained by Fluorescence Measurements

Robert F. Vogt Jr.<sup>1</sup> (✉) · Gerald E. Marti<sup>2</sup> · Vincent Zenger<sup>3</sup>

<sup>1</sup>Newborn Screening Branch, Division of Laboratory Sciences, Centers for Disease Control and Prevention, CDC, Mailstop F19, Atlanta, GA 30341, USA  
*rvogt@cdc.gov*

<sup>2</sup>Center for Biologics Evaluation and Research, Food and Drug Administration, Atlanta, GA 30341, USA

<sup>3</sup>Center for Drugs Evaluation and Research, Food and Drug Administration, Atlanta, GA 30341, USA

<b>1</b>	<b>Laboratory Practice and Standardization of Fluorescence Measurements</b>	<b>4</b>
<b>2</b>	<b>Quantitative Fluorescence Calibration (QFC)</b>	<b>6</b>
2.1	Definition	6
2.2	Terminology	6
2.3	Formalization of QFC	13
2.3.1	The Fluorescence Measurement Equation	13
2.3.2	The FI Calibration Curve	13
2.3.3	Evaluation of the QFC Calibration Curve	15
2.4	Summary Considerations Regarding the Implications of QFC for Assessing Data Quality	15
<b>3</b>	<b>Standards for Quantitative Fluorescence Calibration</b>	<b>16</b>
3.1	Absolute and Relative Fluorescence Standards	16
3.2	Characterization of Fluorochrome Standards	16
3.2.1	Chemical Characterization of the Fluorochrome	16
3.2.2	Fluorescence Properties	17
3.2.3	Matrix	17
3.2.4	Assignment of Calibration Values	17
3.2.5	Stability	18
3.3	Biologic Calibrators and Other Binding Standards	19
3.4	Implications of Standards for QFC	20
<b>4</b>	<b>Procedures for QFC</b>	<b>20</b>
4.1	Assigning Values to QFC Calibrators	21
4.1.1	RFI Calibrators	21
4.1.2	MESF Calibrators	21
4.1.3	ABC Values	21
4.2	Constructing and Evaluating the Calibration Curve	22
4.2.1	Mathematical Construction	22
4.2.2	Evaluating Linearity and Goodness of Fit	23
4.2.3	Evaluating the Slope	24
4.3	Quantifying Fluorescence from Samples	24

4.3.1	Effects of Sample Preparation . . . . .	24
4.3.2	Extrapolation . . . . .	24
4.3.3	Choice of Distribution Parameter . . . . .	24
4.3.4	Expressing Results . . . . .	25
5	<b>Applications</b> . . . . .	25
5.1	Solid-Phase Particulate Ligand Binding Assays . . . . .	25
5.1.1	Immunophenotyping and Receptor Quantification . . . . .	26
5.1.2	Microbead Suspension Arrays and Multiplexed Analysis . . . . .	26
5.1.3	Microarrays . . . . .	27
5.2	Real-Time Polymerase Chain Reaction (PCR) . . . . .	28
6	<b>Summary</b> . . . . .	28
	<b>References</b> . . . . .	29

**Abstract** Over the last three decades, fluorescence has become the most widely used detection method in biomedical science. Fluorescence measurements are utilized in basic and translational research, method development, medical laboratory tests, clinical trials and epidemiologic studies. This renders the availability of objective methods to assess the quality of data obtained by these measurements very critical for research scientists, clinical laboratory personnel, and regulatory reviewers as is addressed in this chapter.

**Keywords** Flow cytometry · Fluorescence · Fluorescence intensity standard · Molecules of equivalent soluble fluorochrome · Quality assurance · Quantification

## 1

### Laboratory Practice and Standardization of Fluorescence Measurements

Over the last three decades, fluorescence has become the most widely used signal in biomedical science. Fluorescence measurements are utilized in basic and translational research, method development, medical laboratory tests, clinical trials and epidemiologic studies. Objective methods to assess the quality of data obtained by these measurements are critically important to research scientists, clinical laboratory personnel, and regulatory reviewers [1, 2].

Laboratory measurements typically depend on calibration systems as the most fundamental way of documenting the authenticity of the data. Because fluorescence is complex and its measurement is highly platform-dependent, calibration systems are not easily developed or evaluated. Fortunately, consensus methods and the standards required to use them have recently evolved to the point where they can provide a useful and accessible way of assessing the validity of data from fluorescence measurements. In this chapter, we will provide an overview of these methods and their ongoing development. An understanding of this evolution will reveal the power and limitations of quantitative fluorescence across any measurement platform.

The principles we describe are taken from a recent consensus document: the Approved Guideline for Fluorescence Calibration and Quantitative Measurements of Fluorescence Intensity [3] published by the Clinical and Laboratory Standards Institute (CLSI, formerly known as NCCLS). CLSI is a global, nonprofit, standards-developing organization comprising representatives from academia, government and industry, which promotes the development and use of voluntary consensus standards and guidelines within the healthcare community [4]. CLSI documents do in fact have regulatory implications, since the US Food and Drug Administration (FDA) is allowed to recognize certain CLSI consensus standards to satisfy identified portions of device review requirements [5]. Moreover, CLSI is the delegated Secretariat OF ISO Technical Committee 212, the scope of which is “Standardization and guidance in the field of laboratory medicine and in vitro diagnostic test systems. This includes, for example, quality management, pre- and post-analytical procedures, analytical performance, laboratory safety, reference systems and quality assurance” [6]. Because the CLSI process emphasizes scientific consensus and global harmonization, it provides a suitable framework for documenting areas of laboratory science in rapid technological transition.

The CLSI guideline describes the general principles for using standards in fluorescence measurements, and it details a number of practical issues that accompany such use. In this chapter, we will reprise the major features of that guideline, but we do recommend that scientific reviewers and end users consult the guideline itself when implementing or evaluating a fluorescence standardization system. The most important message in this chapter is that data based on measuring fluorescence intensity (FI) should be accompanied by a valid system of calibration that assures consistency across the entire range of time that the data was collected, and across the different laboratories that may have produced it. The most important goal of this chapter is to provide sufficient background that laboratory personnel and scientific reviewers can make an informed judgment about the validity of the calibration system employed and the data that comes from the measurements.

The material in this chapter is closely linked with other chapters in this volume [7–11]. Because the development of methods and standards for fluorescence calibration is ongoing and can be expected to expand, our emphasis is on general principles for evaluating data that derive from fluorescence measurements. Many of these principles, which have long been appreciated among optical physicists, came to the attention of biomedical scientists from the use of fluorescence measurements on flow cytometers, and this technology is the basis for most of our discussion. However, the general principles applied to fluorescence measurements by flow cytometry are relevant to any platform that measures FI.

## 2 Quantitative Fluorescence Calibration (QFC)

This term refers to the standardization of FI measurements by the use of fluorochrome standards in solution and on stained cells and microparticles. In principle, QFC involves quantifying all of the factors that influence the FI measurement: illumination, absorption, photodegradation, emission, quenching, photon collection (involving lens and optical filters), polarization (anisotropy), and electronic circuitry and software. In practice, the complex interactions among these factors are embodied in the QFC calibration curve that relates fluorochrome concentration to instrument response.

### 2.1 Definition

The CLSI guideline defines QFC as an “empiric system to calibrate FI in a way that preserves stoichiometry between the concentration of fluorochrome in solution and the equivalent molar quantity of fluorochrome on stained measurands such as cells, gels, microspheres, and microdots” [3]. The guideline specifically addresses analysis of cells and microspheres by flow cytometry, but the general principles of QFC apply to any fluorometric analysis.

Although QFC originated in attempts to apply FI measurements to particles, it carries with it the implicit need for attention to details in all quantitative fluorometry. FI measurements on solutions can be made with relatively simple instrumentation and methodologies. However, the simple approaches do not take into account the many vagaries of fluorescence, and this volume contains other chapters that deal with the arduous approaches required to assess and, if necessary, compensate for factors such as photodegradation, spectral shifts, anisotropy, and quenching. The good news is that such attention to detail is required only for the primary assignments of values for QFC standards. Given the availability of authoritative standards, scientific reviewers and end users can depend on the QFC calibration curve to determine whether FI measurements are consistent with QFC.

### 2.2 Terminology

Terminology is an important aspect of science and technology. While terms used in biomedical research are often at first somewhat ad hoc, a consensus for precise usage helps avoid confusion and lends clarity to research reports. Such precision is essential for effective communication and regulatory activities, where a misuse of terminology leads to confusion among reviewers and users. The first attempt to establish uniform terminology for QFC [12] led to the consensus definitions in the CLSI guideline. Even with this consensus,



certain terms are still frequently misconstrued, misused, or redefined. Among the terms peculiar in their usage to QFC, several deserve special attention. A careful review of their usage emphasizes both the evolution and the complexity of QFC and provides a cautionary alert for scientific reviewers.

*FI* is used in both a formal and practical sense. Formally, *FI* is a term for the radiant power of fluorescence emission. It may be viewed as a stream of photons (radiant flux) or a series of waves. In either case, it is expressed in units of energy per unit time. The conventions of radiometry can be applied to *FI*, in which case it is expressed in watts and normalized to a source area of  $1 \text{ m}^2$  and a solid angle of  $1 \text{ sr}$  [3]. This approach may be useful for instrument design and manufacturing, but it is not pertinent to either clinical or most biological applications. An additional formality concerns the spectral distribution of the radiant power. In radiometry, the *FI* measurement is often integrated across its entire spectral distribution and thus represents the total radiant power of the fluorescence emission. In clinical instruments, the *FI* is usually measured in a particular spectral region of fluorescence emission chosen by bandpass filters. This difference has important implications for *FI* calibration, discussed further below.

In the practical sense, *FI* is taken to mean the instrument reading from a fluorescence measurement. Such *FI* units depend on the instrument scale used for reporting; they range from actual photon counts to arbitrary units meant to convey only the relative strengths of *FI* signals. On flow cytometers, *FI* is expressed as the histogram distribution of the digitized signal, and the histogram channel number representing the central tendency of the distribution (the mean, median, or mode) is often used as the figure representing the *FI* of a fluorochrome-stained population [13]. Any such figure is arbitrary, since the distribution will depend on the particular instrument and settings under which the *FI* readings are taken. Earlier models of flow cytometers presented a special case of this arbitrary nature. Because the *FI* signals were logarithmically amplified before digitization and binning (Fig. 1), the resulting histogram representing a logarithmic distribution dependent on the gain of the log amplifier (logamp) [14]. On many of these cytometers, the software performed an antilog transformation and reported the *FI* as relative linear units. The problem with this approach was that a mathematical transformation assumed perfect logarithmic amplification, while logamps were notoriously inconsistent, especially at the extremes of *FI* signals. Further problems in standardizing *FI* scales arose when instruments went from 3-decade to 4-decade logamps, and from 8-bit (256 channel) to 10-bit (1024 channel) digitizers. These issues were somewhat mitigated by the use of a uniform scale based on the least common denominator (256 channel) histogram of the log-amplified *FI* signals [15], but they still led to confusion. Current flow cytometers use high-resolution (14–16 bit) converters to digitize *FI* signals without log amplification (Fig. 1), so the histogram channel number is a direct indicator of relative *FI* on a particular instrument with given settings.

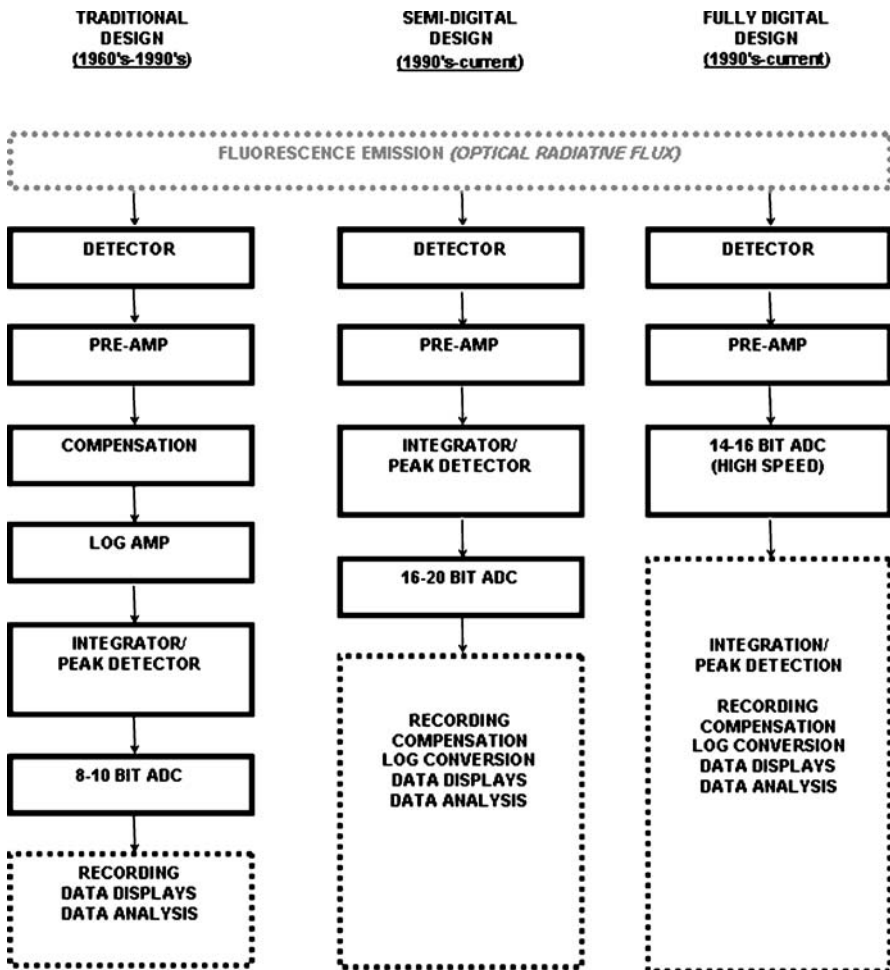


**Fig. 1** Block diagrams comparing signal processing in traditional, semidigital and fully digital flow cytometers (figure contributed by subcommittee participants). *ADC* Analog-to-digital converter *LOG AMP* logarithmic amplifier. *Solid outlines* indicate hardware/analog components, while *dashed outlines* indicate digital processing and software components. In the traditional models, signals were often amplified by logarithmic amplifiers (logamps), analog devices in which the output signal amplitude is proportionate to the logarithm of the input signal amplitude. This approach accommodated the wide dynamic range (>1000-fold) required for many fluorescence intensity (FI) measurements on fluorochrome-stained cells. The availability of affordable high-resolution ADCs allows linear data to be digitized directly across a wide dynamic range, obviating the need for logamps. High-speed ADCs further allow peak detection and integration to be handled by digital processing. (Reprinted from [3] with permission)

Once the FI signals have been processed and binned into histograms, the user must select the most relevant histogram statistic to represent the quantified value and to construct and interpolate from the calibration curve. The mean and the median are the most commonly used parameters for this purpose. The mean is the equivalent of a bulk measurement made in a cuvette, which is the process used to assign molecules of equivalent soluble fluorochrome (MESF) values to particulate standards, so it may be most appropriate in circumstances comparing solution and particulate measurements. However, the mean can be strongly influenced by outlying values and represents the central tendency of the histogram only if it is normally distributed. The median is a nonparametric statistic much less influenced by outlying readings and independent of distribution, so it may be the better choice for comparing data from different samples and assays. Other approaches such as the “trimmed mean” are also used; they may be helpful but should be viewed with caution, since outliers in the distribution may signal a biological anomaly or a technical problem. In any case, a complete understanding of the scale used to report FI is a critical component of QFC. We note that the final result reported to the operator depends largely on software, which is often obscure and may be modified without any apparent change in the instrument. Full disclosure of the algorithms used to report FI is an obligation of the instrument manufacturer and should be noted by those reviewing data from fluorescence measurements.

*Fluorescence yield* is defined as the product of the fluorochrome concentration and the quantum yield of the fluorochrome [16]. The fluorescence yield of a solution is a measure of the number of photons emitted per unit volume if every fluorochrome molecule absorbs a photon. The concept of fluorescence yield allows fluorochrome solutions to be compared in a meaningful way, which leads to the formalization of the MESF unit. This term has been used informally to convey various aspects of the same basic idea without attention to the details provided in the formal definition, so reviewers should be aware of alternative usages.

*MESF* is the basic unit of QFC, allowing the calibration of FI across different measurement platforms, instrument settings, and environmental influences. Although this term first appeared in published literature in 1989 [17], the same concept had been used in a 1986 paper under the term “free fluorescein equivalents” [18]. Using the concept of fluorescence yield, MESF is formally defined as the number of native (unconjugated) fluorochrome molecules in solution that gives the same fluorescence yield as a solution of fluorochrome conjugated to other molecules or a suspension of fluorochrome bound to microspheres or cells [3, 16]. It allows a fluorochrome solution to serve as a reference calibrator by which MESF values can be assigned to solutions of fluorochrome conjugates and suspensions of fluorochrome-labeled microparticles (Fig. 2).

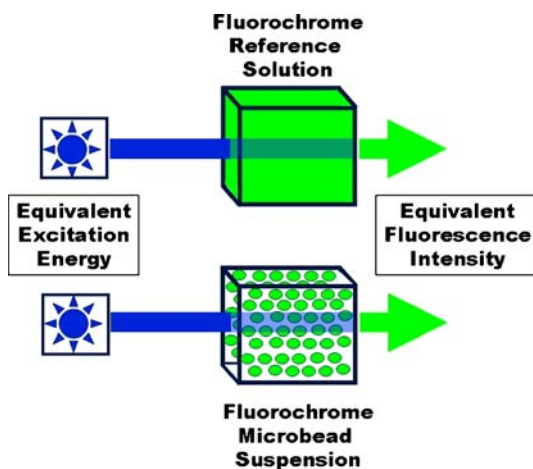


**Fig. 2** A schematic depiction of the process by which values for molecules of equivalent soluble fluorochrome (MESF) are assigned to microbead calibrators. A fluorochrome reference solution is used to establish a FI dose-response curve by cuvette fluorometry. The FI of a suspension of microbeads to which fluorochrome has been immobilized is determined under identical measurement conditions. The molarity of the fluorochrome reference solution and the molarity of the microbead suspension (where  $6 \times 10^{23}$  microbeads/L is 1 M) must be known, i.e., they are independent variables. See [23] and [24] for details of the assignment process

The original description of the MESF unit included the necessity for matching the absorption and emission spectra of the reference solution with those of the unknown solution or suspension to be assigned MESF [19, 20]. This restriction was made so that MESF-assigned calibrators could be used on any instrument regardless of the spectral properties of its illumination and emission collection optics. In principle, the FI measurements could be normalized by the molecular absorptivity of the reference and the unknown fluorochrome at the illumination wavelength, and emission could be integrated across the entire spectrum, allowing MESF equivalences to be made between any fluorochrome materials regardless of spectral characteristics. In practice, the use of spectrally matched materials provides the greatest confidence of consistency.

A series of reports from the US National Institute of Standards and Technology (NIST) [16, 21–23] provides further details on the formalization of MESF units and assignment of MESF values. These reports are available for downloading:

- <http://nvl.nist.gov/pub/nistpubs/jres/106/2/j62gai.pdf>
- <http://nvl.nist.gov/pub/nistpubs/jres/107/1/j71schw.pdf>
- <http://nvl.nist.gov/pub/nistpubs/jres/107/4/j74wan.pdf>
- <http://nvl.nist.gov/pub/nistpubs/jres/110/2/j110-2gai.pdf>

A useful summary of the formalization has also been presented [24].

Reviewers of research reports, device submissions and data from clinical trials that use MESF units must be cautious in their assessment. The methods of assigning MESF units to particulate standards are still evolving (see below), and authoritative standards for the reference solutions required to assign MESF are often lacking. As customarily used, MESF are fluorochrome-specific and cannot be compared directly; that is, 100 MESF of one fluorochrome may be brighter or dimmer than 100 MESF of a different fluorochrome. The most well-characterized fluorochrome for MESF calibration is fluorescein, but even for that, shifts over time in the values assigned to MESF standards make traceability difficult. Another caution concerns microsphere standards that employ surrogate dyes insulated from the aqueous environment. These standards are more stable and have less within-microsphere variability than MESF standards that are surface-labeled with the actual fluorochrome (or a close derivative). However, stable surrogate fluorochrome molecules do not have the matching spectral qualities or environmental responsivity required for true MESF calibration. It is possible on a particular instrument to establish an equivalence between a calibration curve from surrogate standards and one from MESF standards, then use the surrogate standards to read out MESF values for labeled analytes. However, any change in the optical configuration or the sample matrix can invalidate the relationship, so MESF values derived from surrogate calibrators should be evaluated with caution.

*Fluorochrome-labeled conjugate (FLC)* refers in general to the molecular species used in binding assays, where the fluorochrome is linked to either a protein (often an antibody) or an oligonucleotide [3]. The linkage is generally a covalent bond. The fluorescence properties of the fluorochrome are often altered by the linkage, and the binding properties of the protein or oligonucleotide may also be altered. These effects may lead to lot-to-lot variability in the binding properties and fluorescence of FLC, which should prompt scientific reviewers to look for careful assessment of FLC preparations used in medical devices. Such variability may be especially pronounced with tandem conjugates, i.e., those with multiple fluorochromes that use fluorescence energy resonance transfer (FRET) to shift the emission spectrum.

The *effective F/P ratio* is essentially the fluorescence yield of FLC expressed in MESF units per molecule of protein or oligonucleotide [3]. The term was adapted from the traditional molar F/P ratio used to characterize fluorescein-antibody conjugates in terms of the number of fluorochrome molecules per protein molecular. However, since FI from conjugated fluorochrome is often quenched by comparison with native fluorochrome, the molar F/P ratio does not provide the information needed to quantify FLC from FI measurements. The effective F/P ratio takes this into account. The term may be further generalized by letting “P” stand for “probe” rather than “protein”, so it can be applied to other conjugates such as oligonucleotides. The effective

F/P in principle can be determined by solution fluorometry comparing conjugate FI to the FI from fluorochrome reference materials. However, if the local microenvironment where the fluorochrome conjugate binds is different from the solution environment where it was calibrated, the effective F/P may shift [25]. The extent to which this effect biases FI measurements has not yet been widely explored.

*Antibody binding capacity (ABC)* is a special case of the general term “binding capacity” that was introduced to express the quantitative binding of FLC by cell surface proteins [26]. The term “antigen density” has been used to connote the degree of FLC binding, but the actual FI measurement is related to the amount of FLC, not the amount of antigen, and no determination of density can be made without a metric for cell surface area. Most immunophenotyping uses antibody conjugates, and prefixing “antibody” to “binding capacity” allowed the convenient acronym “ABC,” which has become widely used. However, the term is still misleading and ambiguous. The bound species measured is FLC, not native antibody, and the same antibody bound to different fluorochrome molecules can show striking differences in FLC binding to cells and microbead calibrators [27–29]. The term “capacity” was originally intended to mean saturated binding, so as to more nearly reflect the total antigen expression [26], but that distinction is not always made. Some authors have even redefined the acronym to signify “antibodies bound per cell,” so as not to imply saturation [30]. The meaning of this term must be put in the context of each particular report.

*Receptor* is generally considered a biological entity, meaning a biomolecule on a cell that binds a particular ligand. However, it can also refer to a binding species on a microbead or other solid-phase material.

*Sensitivity* is often taken as the ability of a laboratory assay to detect or quantify low levels of a measured substance. However, sensitivity is formally defined as the slope of the dose–response relationship [31], a steeper slope meaning a more sensitive measurement. The issue of measuring low levels of clinical analytes (properly referred to as limits of detection and limits of quantification) is addressed comprehensively in a recent CLSI guideline [32]. The principles described in this guideline are aimed at assays in general rather than specific instrumentation, so they apply to any fluorescence-based assay.

With respect to the instrumental sensitivity of a fluorometer, the ability of a fluorometer to detect weak fluorescence signals from a measurand cannot be captured by a single parameter, because it depends on both the optical background  $B$  (often equated with the term “noise”) and the detection efficiency  $Q$  [3, 33–35]. QFC provides an essential yardstick for  $Q$  and  $B$ , since they can be related to MESF by expressing  $Q$  in units of photoelectrons/MESF, and expressing  $B$  in units of MESF. A detailed procedure for measuring  $B$  and  $Q$  in terms of MESF is given in an appendix of the CLSI guideline [3].

## 2.3

### Formalization of QFC

Although QFC is an empiric system, the theoretical basis for its use has been carefully explored [3, 16, 21, 22].

#### 2.3.1

##### The Fluorescence Measurement Equation

QFC is based on a measurement equation that relates the FI produced by a given concentration of fluorochrome to the major chemical and instrument factors that determine the final reading on the fluorometer [3, 8]. In its most basic form, the equation is:

$$FI = [f]K ,$$

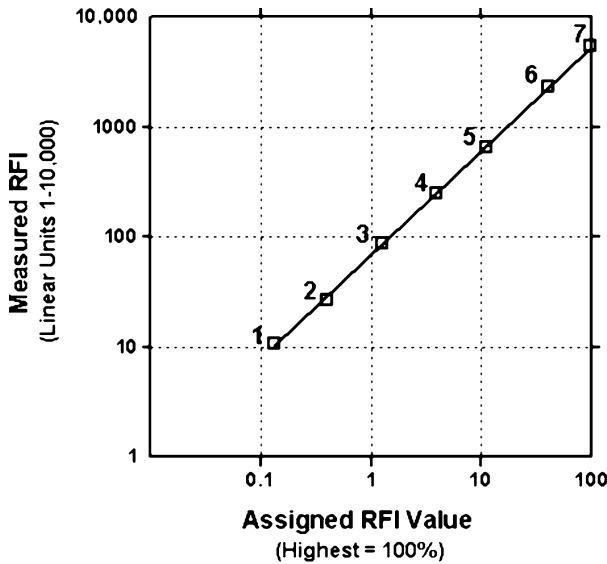
where FI is the measured value,  $[f]$  is the concentration of the fluorochrome, and  $K$  is a composite factor dependent on the properties of the fluorochrome and the fluorometer. The major fluorochrome factors are the absorptivity and the quantum yield, while the major instrument factors include gain, illumination flux, collection geometry, spectral responsivity, and quantum efficiency.

This measurement equation for QFC is a simplified treatment that ignores factors such as photodegradation and anisotropy. However, it makes an important prediction that constrains its use to situations that do not jeopardize its simplifying assumptions: the calibration curve that relates FI and fluorochrome concentration will be a straight line.

#### 2.3.2

##### The FI Calibration Curve

Scientific reviewers and laboratory researchers must have confidence that the readings produced by laboratory instruments lie within its boundaries of accurate measurements, and that they are consistent with the underlying assumptions of physics and chemistry. The most useful tool in this assessment is the calibration curve, also called the dose–response curve (Fig. 3). The CLSI guideline recommends that QFC curves use a log–log coordinate system for two reasons [3]. First, since the measurement equation for FI mathematically defines a linear relationship between signal strength and instrument response, the calibration curve will plot as a straight line with slope=1 in log space (in linear space, the slope of this line cannot be generally specified, since it is dependent on signal processing by the fluorometer). Second, since FI measurements typically extend over a wide dynamic range, simple linear regression will be more effective in log space than in linear space, where outlying points have a disproportionate impact on the regression line. Simple linear regression is preferred to the use of more complex curve-fitting models



Range of Standards	$r^2$	Slope	Average Absolute x-Residual	Standard Deviation y-Residual
1 - 7	>.999	0.94	3.3 %	0.022
2 - 7	>.999	0.96	2.0 %	0.015
3 - 7	>.999	0.95	1.6 %	0.013
1 - 6	>.999	0.94	3.2 %	0.023
2 - 6	>.999	0.93	1.2 %	0.012

**Fig. 3** Graphic depiction of data and the best-fit line from flow cytometric analysis of seven populations of fluorescent microspheres, each of which had an assigned value for relative FI (*RFI*). The independent (dose) variable is shown on the x-axis and the dependent variable (response) on the y-axis. This depiction is consistent with the linear regression, which used a simple least-squares method to determine the best-fit line. The accompanying table shows the parameters of the regression as performed with all seven standards and of other regressions in which the lowest and/or highest standards have been removed. The regression using standards 2 to 7 had the best combination of fit (low residuals), responsivity (slope closest to unity), and linear dynamic range (about 200-fold). (Reprinted from [3] with permission)



or weighting factors that may involve assumptions that mask departure from the simplified QFC model.

The QFC calibration curve is an idealized relationship between MESF and fluorometer response. Most biomedical assays measure an interaction that is only indirectly related to MESF, such as ligand binding or enzyme catalysis, where the shape of the dose–response curve depends on additional factors such as equilibrium constants. Scientific review of such assays should look for some assurance that the basic FI measurement lies within the constraints of QFC; that is, that fluorescence-specific factors such as quenching, anisotropy and photodegradation are not causing significant departure from the fundamentally linear relationship between fluorochrome concentration and instrument response. Moreover, the nonlinear ranges of such curves are often associated with larger confidence intervals, which at the lower end of the dose–response curve may well overlap into the “negative” dose region. While such factors can in theory be corrected through mathematical models, these approaches are more suited to (and often important components of) basic research and assay development, and their application in the biomedical laboratory can cause misleading results.

### 2.3.3

#### **Evaluation of the QFC Calibration Curve**

The CLSI document [3] offers specific criteria for evaluating the parameters of the QFC calibration curve based on empiric experience with FI measurements on flow cytometers and cuvette fluorimeters. Practical experience on other platforms, such as real-time PCR, will be required to establish relevant criteria. Within the limits of the simplifying assumptions of QFC, empiric FI measurements are remarkably linear, and any significant departure from unity in the slope of the log-space curve should trigger suspicion that confounding factors are influencing the dose–response relationship.

## 2.4

### **Summary Considerations Regarding the Implications of QFC for Assessing Data Quality**

QFC provides a framework whereby scientific reviewers can evaluate the ability of any platform or assay that uses FI as the response variable to provide consistently accurate results from the standpoint of the fluorescence measurement. However, QFC depends on the availability of standards with assigned values that are sufficiently accurate to detect anomalies in instrument or assay behavior, which is still a work in progress. Even as such standards evolve, reviewers will benefit from an understanding of the basic tenets of QFC as they review data obtained by fluorescence measurements.

### **3 Standards for Quantitative Fluorescence Calibration**

Like any approach to calibration based on a dose–response relationship, QFC requires standards with assigned values to use as the independent variable in the dose–response function. In particular, QFC requires two types of standards. Fluorochrome solutions of known concentration are used as standards for solution fluorometry, and they are also required as reference materials by which to assign MESF values to particulate materials such as microspheres, which can then be used as standards for other particles. Other chapters in this volume explore the details of fluorescence standards. Here we will limit the discussion to general principles.

#### **3.1 Absolute and Relative Fluorescence Standards**

For full implementation of QFC, standards with absolute mass-related values are required. With solution-based standards, the absolute calibration value is the concentration of fluorochrome; with solid-phase materials, it is the MESF per particle.

Values for relative fluorescence intensity (RFI) do not require absolute mass-related values. Typically, RFI values are assigned to a set of multiple standards in relation to each other. Assignment of such values does not require the complete characterization of fluorochrome property values such as purity and spectra that is necessary for assigning absolute mass-related values. However, even with “broad spectrum” standards, the RFI values are, at least to some extent, dependent on the excitation and emission wavelengths and the excitation energy used by the measurement system. Such dependence may be due to an “inner filter” effect, which could cause a red shift in the emission spectrum of only the brightest beads in the set (R. Hoffman, personal communication). This makes documented characterization of the exact conditions under which values were assigned prudent for using RFI standards in any FI measurement. With such prudence in mind, the following discussion is directed toward the complete characterization of absolute standards, which can be modified as appropriate for RFI standards.

#### **3.2 Characterization of Fluorochrome Standards**

##### **3.2.1 Chemical Characterization of the Fluorochrome**

The need for assessing the chemical purity of fluorochrome used to prepare primary standard solutions and solid-phase materials is obvious,

but still challenging. The assayed percentage of actual fluorochrome is important, but equally important is the characterization of impurities to insure that they do not alter the fluorescence by quenching the fluorochrome, inducing spectral shifts, or contributing their own fluorescence. The certificate of analysis (COA) for NIST SRM 1932 (available at [https://srmors.nist.gov/view\\_detail.cfm?srm=1932](https://srmors.nist.gov/view_detail.cfm?srm=1932)) provides a model for documentation of such preparations.

### 3.2.2

#### **Fluorescence Properties**

Fluorochrome preparations used as primary standard solutions and solid-phase materials should be characterized by high-resolution excitation and emission spectra. Ideally, the molar absorptivity, relative quantum yield, and fluorescence lifetime would be determined and compared with reference values. Some of these determinations that are straightforward in solution are not practical for solid-phase materials, but at least the original fluorochrome can be characterized before attachment to the solid phase.

### 3.2.3

#### **Matrix**

Since fluorescence is often affected by the environment of the fluorochrome, the matrix should be characterized as carefully as the fluorochrome itself. For solutions, this will include factors such as solvent content, pH, and salt concentration. For solid-phase materials, the support itself should be described, and the chemical linkage (if any) between it and the fluorochrome specified. Depending on the fluorochrome, the nature of the chemical linkage can have a significant influence on fluorescence properties.

### 3.2.4

#### **Assignment of Calibration Values**

A fluorochrome standard solution is generally assigned a concentration value (most rigorously a mass/mass concentration, since volume is not a constant parameter). A COA for such material should include a description of the means by which this value was obtained, and, ideally, an estimate of the uncertainty associated with it.

A particulate standard for QFC is assigned an MESF value. A COA for such material should also include a description of the means by which this value was obtained, and, ideally, an estimate of the uncertainty associated with it. Of critical importance is the reference solution to which comparisons were made in assigning the MESF value; it should be specified to the exact source, lot number, and even aliquot used for calibrating the particulate standard.

Multilevel calibrators may be assigned arbitrary relative values (e.g., RFI) that apply only to the suite of materials in the collection. The common use of multilevel calibrators is with particulate standards used in flow and image fluorescence measurements. Again, the COA for such material should include a description of the means by which the relative values were obtained, and, ideally, an estimate of the uncertainty associated with each of them. This is especially important since the RFI values may change under differing conditions of the FI measurement (e.g., excitation wavelength and power, emission collection optics) that produced them.

### **3.2.5 Stability**

Stability is especially worrisome for fluorochrome standards. Not only are many fluorochrome molecules inherently unstable, but also FI is so dependent on the measurement platform and fluorochrome environment that end users generally do not have the capacity to measure absolute property values that reveal degradation.

#### **3.2.5.1 Responsibilities of the Standard Providers**

Institutions or companies that provide fluorescence standards should conduct stability studies (including accelerated stability protocols) and assign an expiration date based on the results. They should specify explicit storage conditions and usage guidelines (e.g., single-use packages). Retention samples of each lot should be monitored for long-term stability. Since field use is often more demanding than is the idealized test laboratory, suppliers should track user inquiries and complaints and, when necessary, adjust expiration dates or even issue recalls if a standard does not remain stable in the hands of end users.

#### **3.2.5.2 Responsibilities of the End Users**

While end users should not have to conduct their own stability studies, they should monitor the consistency of FI signals under identical instrument settings, or, conversely, monitor the instrument settings required to achieve a target FI value. Trends or spikes that depart from normal variance require investigation that addresses the possibility of standard degradation. Moreover, monitoring the parameters of the calibration curve can reveal subtle shifts in FI caused by standard degradation. A prudent approach is to use two different fluorochrome standards read under the same instrument settings, so that variance in the FI or calibration parameters can be compared.

### 3.2.5.3

#### Using Multiple Fluorochrome Standards to Monitor Stability

Both suppliers and end users can benefit from using two difference fluorochrome standards to monitor stability. Some fluorochrome molecules are relatively stable and may provide more stable standards, but many (including two of those in most common use, fluorescein and phycoerythrin) do not fall into this category. Because the MESF units that are the basis of QFC require spectral matching (in principle, for both absorption and emission) as well as comparable environmental responsivity between fluorescence standards and unknowns, surrogate fluorochromes that offer greater stability are generally not suitable for measuring MESF. One way around this is to calibrate with both MESF and surrogate standards; if the calibration curves are parallel and instrument settings remain unchanged, MESF values can be read from the surrogate fluorochrome curve using a simple corrective factor that compensates for the distance between the two curves. In essence, this is equivalent to assigning MESF values to surrogate standards on an instrument-specific basis. A simplified version of this approach uses multipoint calibration for the surrogate fluorochrome and a single-point calibrator (a stained biologic material or an MESF standard) to obtain the MESF conversion factor. Single-point calibration is generally discouraged in laboratory practice; however, if the slope of the QFC calibration curve from the surrogate material is unity, a single-point correction to MESF is justified, but only within the FI range of the surrogate calibration curve. Monitoring the corrective factor then becomes the means by which instability in either the surrogate or the MESF standard can be revealed.

### 3.3

#### Biologic Calibrators and Other Binding Standards

For FI measurements that ultimately reflect the amount of fluorochrome bound (or somehow associated with) to a cell or microparticle, another QFC approach is to calibrate the extent of binding directly and disregard the vagaries of the fluorescence measurement. This approach has been widely used for standardizing the measurements of cell surface receptor expression. For such measurements, there is considerable appeal in using a biologic calibrator with a consensus value for receptor expression. The most detailed studies have been done with CD4 expression on helper T-cells, and a consensus value of about 100 000 CD4 molecules and 50 000 binding sites for divalent antibody per cell has emerged from multiple studies [26, 30, 36]. Microparticles that “capture” fluorochrome-labeled conjugates can also be used for direct calibration in ABC values. These approaches are certainly useful, but, other than

CD4 on helper T-cells, the values used for biologic calibrators and capture microbeads are not well documented.

### **3.4 Implications of Standards for QFC**

Laboratory workers and scientific reviewers should look carefully at the use of standards when fluorescence-based measurements are scrutinized. The production and characterization of fluorescence standards is continually evolving, and comparability cannot be assured across either time or sources. Most important is the internal consistency of the measurement system and compliance with the fundamental precept of the QFC calibration curve: linearity across the relevant dynamic range, so that residuals in the log–log curve are small and the slope is close to unity. If the measurement system does not comply with these parameters, the standards and the instrumentation require investigation.

These constraints apply only to the QFC calibration curve, and not necessarily to the calibration curve used to determine analyte concentrations in the measurand. In fact, the slope of the analyte calibration curve will often depart from unity because binding constants and other factors reduce the ideal generation of unit fluorescence per unit mass. Two major points for scientific reviewers emerge from this consideration. First, a QFC calibration curve is an essential component of the evaluation process, since it provides an analyte-independent indicator of the measurement system. Second, the use of mathematical curve-fitting algorithms, almost invariably bundled into the software that accompanies modern fluorimeters, may obscure weaknesses in the measurement system and ultimately do more harm than good. Our practical experience on a variety of platforms measuring FI has been that measurements taken outside the range of linearity in the log–log analyte calibration curve are inconsistent and unreliable.

## **4 Procedures for QFC**

This section will review the three fundamental procedures required for full implementation of QFC: assigning values to calibrators, using them to construct calibration curves, and applying them to the quantification of samples. Two general principles are paramount. The first principle is consistency within the measurement system (i.e., across different lots of standards calibrated with the same method and perhaps even restricted to measurement on the same platform). The second principal is to avoid generalizations that cannot be confirmed by explicit data.

## **4.1**

### **Assigning Values to QFC Calibrators**

#### **4.1.1**

##### **RFI Calibrators**

Although it may be the simplest of the calibration values to assign, there is at this time no standardized method for assignment and verification of RFI, nor are there any authoritative reference standards. RFI values assigned to microspheres for flow cytometric analysis have a long history of use and are generally reliable if they are analyzed under the conditions used to assign them. Even so, scientific reviewers should be cautious about flow cytometry systems that employ RFI calibrators without confirming their accuracy on that particular system. RFI values for image-based platforms are more likely to show platform-dependent variation, particularly with respect to fluorescence polarization.

#### **4.1.2**

##### **MESF Calibrators**

Figure 2 shows a schematic of the basic approach to assigning MESF values to particulate calibrators. This topic is detailed elsewhere in this volume as well as in the NIST publications [16, 22] and CLSI guideline [3]. Here we emphasize that the optimal approach to MESF assignment is still evolving, and that different approaches will likely give values that have significant methodologic bias, perhaps in the range of twofold or more. This makes comparisons across methods and time difficult to evaluate.

#### **4.1.3**

##### **ABC Values**

Binding capacity depends on a number of parameters of the complex interaction between ligand and receptor on a solid phase. These factors, which include avidity, valency, and receptor density, are themselves interactive, making model-dependent approaches unreliable. A general assignment of ABC values to solid phase materials is problematic because different conjugates can give widely varying results with the same solid phase. Moreover, there are no methods for assigning ABC values that can be considered definitive or authoritative. Each method of assignment must therefore be evaluated on its own merits. However, ABC values for a particular lot of capture microspheres assigned to a specific conjugate are likely to remain consistent. Even conjugate-specific values should be confirmed for each lot of microbeads and ideally for each lot of conjugate.

Of the published methods for assessing ABC, the use of fluorochrome-ligand conjugates that are also radiolabeled [36], whereby measurements can be related to the specific activity of the conjugate, may be the most reliable. Although this method is rarely used, it is the basis for one of the few commercially available systems that employ QFC [37]. One concern is that radiolabeling may alter the binding properties of the conjugate, so experimental evidence that this is not the case is desirable. Radioactivity is not the only alternative label that can be used; enzyme-labeled fluorochrome conjugates have also been employed [30].

An interesting approach for calibrating ABC on microspheres is isoparametric analysis [38], in which the results of a checkerboard titration are used to construct a model-independent series of equations from which a Scatchard-type plot and binding capacity can be derived. This method has the advantage of using unmodified conjugate and the fluorescence measurement itself in its determination; the major disadvantage may be the uncertain propagation of error through the series of constructed equations. The method did give results for CD4 ABC on helper T-cells in agreement with consensus values [26].

Perhaps the most well-documented system of assigned ABC uses unimolar conjugates of monoclonal antibodies and phycoerythrin [39, 40]. The relationship between phycoerythrin fluorescence and binding capacity is established either by use of CD4 binding on helper T-cells [39] or by use of microbeads labeled with a known molar quantity of phycoerythrin [40]. With this particular system, the fluorescence yield of phycoerythrin was equivalent whether it was conjugated to the monoclonal antibody or attached to microbead calibrators; therefore, no MESF calibration was required. The investigators who developed this system carefully documented each step in the chain of measurements in a series of peer-reviewed publications [39–41], allowing the scientific community at large to assess the validity of the system.

## 4.2

### Constructing and Evaluating the Calibration Curve

The basic method presented in the CLSI guideline [3] applies to calibrators assigned RFI values or absolute MESF values. It is summarized here and shown in Fig. 3; the CLSI guideline should be consulted for full details.

#### 4.2.1

##### Mathematical Construction

A simple linear regression without weighting factors applied to the log dose versus log response relationship is most informative, since QFC defines an ideal calibration curve that is linear and therefore has a slope of unity when constructed in log space. Departures from linearity and a unity slope are



indicators of departure from the QFC model, whether it is due to instrument factors or the generation of the fluorescence signal itself. Models that complicate the regression by assigning different confidence values (“weights”) of standards or employ nonlinear fitting algorithms may mask such departures. Such methods are appropriate if, and only if, an independent method has been used to determine confidence intervals for the assigned values or a consistent departure from linearity due to instrument factors.

An alternative approach to linear regression has become feasible with newer instruments that avoid the use of logamps. Because the requirement for unity slope in log space is a given parameter for QFC, the regression may be altered to fit the points around a line with a slope constrained to unity (R. Hoffman, personal communication). This approach has the advantage of limiting the evaluation to one parameter (goodness-of-fit); regions of the curve constructed from standards with residuals that lie outside the acceptable range would not be suitable for interpolation. In theory, this approach could be extended to instruments with logamps that were calibrated to give an accurate dynamic range, although departure from perfect log behavior within that range would still complicate the fitting (and may be revealed by high residuals). Such calibration would preferably be performed electronically, but in principle a calibration curve regressed without a fixed slope could be used to determine the true dynamic range. Empiric evidence is needed to evaluate this approach.

#### 4.2.2

##### **Evaluating Linearity and Goodness of Fit**

Because the dose–response relationship is very highly correlated even when the fit is poor, correlation coefficients offer little help in assessing the curve. The residuals (the distance between the observed point and the best-fit line) are much more informative. They should be small, approximately equal as a proportion of the dose, and randomly distributed on either side of the best-fit line (Fig. 3). When residuals become larger and biased to one side of the curve, as customarily seen in the extremes of the response scale, the relationship is no longer linear. As a rule of thumb, standards with accurately assigned values should lie within 5% of the best-fit line throughout the range of QFC validity [3].

The overall goodness of fit may be estimated by the average absolute percent residual, which is the average of the absolute values of each percent residual. The average absolute percent residual is equivalent to saying that the best-fit line lies within the stated percentage of the assigned values of the standards. The formal statistic often used to evaluate goodness-of-fit is the standard deviation of the  $y$ -residual, but this parameter does not have the intuitive interpretation of the average absolute residual.

### **4.2.3 Evaluating the Slope**

Unity slope in log space is a consequence of the QFC model, but the evaluation of this parameter is not straightforward. The extent of departure from unity becomes a more significant factor as the dose–response relationship increases. The evaluation is further complicated in instruments with logamps that must be properly calibrated to give a true value for dynamic range that will result in unity slope. The most helpful use of this parameter is in evaluating data from a series of standards that encompasses a sufficiently wide dynamic range: the portion of the QFC curve that fits closest to unity slope should be identified and quantitative measurements constrained to that region.

## **4.3 Quantifying Fluorescence from Samples**

The FI from a sample can be converted into RFI values, MESF values, or ABC values by interpolating from the respective calibration curve. Analyses, of course, must be conducted without any change in instrument settings. Beyond that, several precautions should be noted.

### **4.3.1 Effects of Sample Preparation**

The preparative methods used to obtain fluorescence signals from biologic material may have a profound impact on the results. For example, fixation of cells can change their autofluorescence and also their binding capacity for fluorochrome–antibody conjugates. Reviewers should look for complete descriptions of the preparative methods to be used with fluorescence measurements.

### **4.3.2 Extrapolation**

Results should not be extrapolated from beyond the lowest and highest standards that show suitable fit, as these extremes are not in compliance with the QFC model.

### **4.3.3 Choice of Distribution Parameter**

If data is obtained as a distribution, as with fluorescence measurements on cell populations analyzed by flow or image cytometry, the choice of parameter can influence the result. The median is the most robust parameter of the dis-

tribution if the sample size is sufficient. The mean may be strongly influenced by skewness and outlying values. However, if the analysis is meant to reflect the bulk fluorescence that would be obtained from measurement of a suspension in a cuvette, the mean is the correct parameter.

#### 4.3.4

#### Expressing Results

Relative fluorescence results should only be compared with results taken under exactly the same conditions. They may be considered proportionate arbitrary units. In some descriptive situations, semiquantitative terms such as “relatively dim” and “relatively bright” may be useful, but it is more precise to express the degree of proportionate difference between two measurements, such as twice or ten times as bright.

Results expressed as MESF or ABC units should reference the standards or calibration system used to obtain the numeric results. Scientific reviewers should be alert for any misuse of calibrator values that do not have an authoritative or at least consensus basis, such as publication in peer-reviewed literature.

## 5

### Applications

This chapter concludes with a brief review of some widely used applications for which the precepts of QFC can provide a sound basis for scientific review.

#### 5.1

#### Solid-Phase Particulate Ligand Binding Assays

A wide range of assays depends on detecting fluorescence signals from fluorochrome bound to a solid phase, such as microbeads or cells in suspension, or microarrayed features on a surface. Immunoassays include antibodies as part of the binding reaction, while hybridization assays are based on binding among oligonucleotides. The use of cells as the solid phase is a special case with wide applications including immunophenotyping and fluorescence in-situ hybridization (FISH).

Since QFC was developed in order to bridge the gap between fluorescence measurements made in solution and those made on particles, its principles apply to all the variants of these assays. The requirements for documenting the validity of the fluorescence measurement in the context of QFC are similar: the dose–response relationship should be linear throughout the relevant range of the assay, and the slope of a log–log calibration curve based on MESF calibrators should be close to unity.

### 5.1.1 Immunophenotyping and Receptor Quantification

This is the area where QFC was first developed, and is still the most active in terms of applications and technical development. The goal is to quantify the expression of cellular proteins in cells stained with antibody–fluorochrome conjugates by converting the fluorescence measurement into the number of antibody conjugate molecules bound by each cell. The proteins of interest are most often biological receptors, although the term receptor is used generically for any protein bound by the conjugate. Compared to simply dichotomizing cells into “positive” and “negative” populations, quantifying expression can give much more information about the state of differentiation and identify potential targets for therapeutics. Such analysis has been particularly fruitful for hematologic malignancies and remains an active area of technical development [42] and disease investigation [43]. However, applications in other areas such as infectious disease [44] also make use of receptor quantification.

Most cell receptor quantification assays use flow cytometry. While image platforms could, in principle, provide the same quantitative information, the simplifying assumptions of QFC do not hold up as well in image measurements on stained cells. Applications such as FISH depend on distinguishing presence from absence, or enumerating areas of discrete, highly localized staining; measuring overall quantitative differences is more difficult. Novel instrumentation, such as the laser scanning cytometer [45] and imaging flow cytometry [46], may provide a better platform for quantitative image measurements. This is an area of active development, as addressed elsewhere in this volume [47], and quantitative image measurements may become more widely used in the future.

Regardless of the platform, laboratory methods for quantifying cellular receptors through fluorescence measurements continue to evolve, and laboratorians and scientific reviewers will have to evaluate each data set in the context of the standardization method used. Comparisons across methods and studies may be difficult to validate, but consistency within a study should be well documented through the use of standards and controls. Standardized approaches across laboratories [41] and clinical trials [48] are especially welcomed.

### 5.1.2 Microbead Suspension Arrays and Multiplexed Analysis

This has been a very active growth area in the last several years [49] and is addressed in a separate chapter in this volume [50]. A number of regulatory approvals have been issued for particular assays on specific platforms. Applications include both protein measurements [51], usually by immunoassay,

and oligonucleotide detection for genotyping [52]. A microbead suspension array system recently became the first medical device approved by the FDA for the detection of mutations associated with cystic fibrosis [53].

Microbeads may be coated with antibodies, antigens, or oligonucleotides. The detection reagents may include directly labeled conjugates that are specific for particular analytes, or multilayer systems using a common reagent (such as fluorochrome-labeled avidin) that binds to a variety of secondary reagents (such as biotinylated antibodies). Multiple bead populations with different specificities may be used in a single suspension and separated during flow cytometric analysis by differences in bead-specific fluorescent signals or other parameters such as light scatter, reflecting differences in size and refractivity.

From the standpoint of QFC, the cautionary points about these assays are the same as those previously raised, with the added concern in multiplexed platforms over the large number of possible interactions among multiple analytes and multiple microbeads that may reduce specificity or sensitivity. In general, calibration curves should be linear, and, if MESF calibrators are used (rather than binding reactions with fluorochrome-labeled ligands), their slope should be near unity. In assay development, results from multiplexed suspensions should be confirmed by analysis in “uniplex”, i.e., with only a single bead population present. Even then, given the uncertainty of multiple analyte interactions that may be unique to particular samples, critical results may need confirmation by uniplex analysis.

### 5.1.3

#### Microarrays

Here we used this term to mean any highly dense surface array of targets for binding by oligonucleotide or protein analytes. This broad definition includes gene “chips”, mRNA expression microarrays, tissue microarrays, and protein microarrays for ligand-binding assays. While typically a single sample is exposed to the thousands of targets on the microarray, “reverse” microarrays have also been developed, where the array comprises thousands of unknown samples to be tested for reactivity with a single probe [54]. In every case, the challenge is to quantify the fluorescence signal from a small microdot or feature. Microarrays are in essence a form of image analysis, and they are addressed comprehensively in several chapters in this volume, including one on the regulatory perspective [9]. Evaluation from the standpoint of QFC is no different than with other applications, but the requirement to identify thousands of individual features and gather discrete information from each them presents special challenges. Many of the relevant concerns regarding the fluorescence measurement were cataloged in the early evolution of the technology [55], and commendable efforts toward standardization have since been made [56]. Still, the MESF concept has not been translated into microar-

ray measurements, and we would encourage officials at the standardization agencies to develop tools that would cultivate the use of QFC in this area.

## 5.2

### Real-Time Polymerase Chain Reaction (PCR)

This powerful technology, also called “quantitative PCR” and sometimes abbreviated Q-PCR, is addressed separately in this volume [57]. The fluorescence measurements in Q-PCR are done in solution, so the simplest precepts of QFC can be used to evaluate instrumentation without the need for MESF-calibrated particles. Some fundamental investigations would be required to characterize the effective fluorescence of the probe in the measurement matrix upon release from the region where it is quenched.

Surprisingly, there is little if any published material evaluating the fundamental fluorimetric characteristics of Q-PCR platforms. Issues remain with respect to the algorithms used to determine the “cycle threshold” and the ability to distinguish small differences in copy numbers, such as would be required to detect hemizygous deletions [58]. Characterization of the instrument measurements by QFC could help resolve these issues and improve reliability of Q-PCR measurements.

## 6

### Summary

Fluorescence is an evanescent signal, complex in its origins and sensitive to its environment, which resists the robust methods of standardization that serve well with simpler technologies. It is also the most widely used signal in biomedical science, illuminating the finely-tuned mechanisms that preserve life and allowing laboratory scientists to detect the cellular and molecular defects that cause disease. As laboratory scientists and regulatory reviewers try to strike the balance between harnessing innovative technologies and preventing the generation of misleading laboratory data, they need every available tool at their disposal. When evaluating devices that measure fluorescence or data from clinical trials that include such measurements, they can turn to the principles of QFC to determine whether the measurements lie within the simplifying constraints that give reliability to the results derived from them. These principles suggest that certain fundamental points be kept in mind while assessing the scientific quality of data from fluorescence measurements:

1. FI measurements should be validated by one of the standardization approaches described here and in the CLSI guideline.
2. The FI value used for quantification should be clearly defined, whether based on photon counts or arbitrary values representing instrument re-

sponse. If distributional data is used, the statistic (mean, median, or other) taken to represent the overall value should be specified. In some cases, the entire set of raw data (in flow cytometry often called “listmode”) should be made available to scientific reviewers.

3. The standards used for calibration should be specified by source, lot number, and dates of usage from start to completion of the data set. The calibration values (RFI, MESH, ABC) should be clearly indicated, and some traceability to the method used to assign them should be available, ideally in published reports. We emphasize that the methods for assigning values are still evolving, and only by specifying how the values for the particular standards were obtained can reviewers be confident of their usefulness for the intended purpose.
4. The methods used to construct calibration curves should be fully specified. Simple linear regression need not be further described, but any alterations such as weighting observations or fixing parameters should be explained.
5. The consistency of FI measurements should be documented by comparing two separate factors, such as the FI from two different fluorochrome standards, or instrument settings and FI response.
6. The preparative steps should be enumerated and the reagents defined by source and lot numbers. Process controls that undergo the entire preparative sequence should be included in all runs. Quantitative FI results on controls and samples should be tracked even if measurements are dichotomized into “positive” and “negative”, or otherwise classified into discrete categories, since trends in FI suggest possible bias in the classifications.
7. Those who generate or review data from fluorescence measurements should be aware of their complexity and use QFC to reveal artifacts created by instrument and reagent factors that might otherwise remain hidden.

## References

1. Mansfield E, O’Leary TJ, Gutman SI (2005) *J Mol Diagn* 7:2
2. Jezequel P, Pichon J, Magrangeas F, Minvielle S, Millour M, Ricolleau G, Malvaux S (2004) *Ann Biol Clin (Paris)* 62:361
3. Clinical and Laboratory Standards Institute (2004) *Fluorescence calibration and quantitative measurements of fluorescence intensity; approved guideline I/LA24-A* (ISBN 1-56238-543-7). CLSI, Pennsylvania
4. Tholen D (2006) *Med Lab Obs* 38:38, 40
5. FDA Modernization Act of 1997: Guidance for the recognition and use of consensus standards; availability. *Federal Register*: February 25, 1998, Vol. 63, No. 37. Notices, pp 9561
6. Kaplan LA (1999) *Scand J Clin Lab Invest* 59:479
7. DeRose P, Cramer G, Gaigalas A, Panne U, Resche-Genger U. This volume

8. Garsha K (2008) Quantification in fluorescence microscopy. This volume
9. Shi L, Goodsaid FM, Frueh FW, Tong W (2008) Microarray technology: unresolved issues and future challenges from a regulatory perspective. This volume
10. DeRose P, Wang L, Gaigalas A, Kramer G, Resch-Genger U, Panne U (2008) Need for and metrological approaches towards standardization of fluorescence measurements from the view of national metrological institutes. This volume
11. Resch-Genger U, Pfeifer D, Hoffmann K, Flachenecker G, Hoffmann A, Monte C (2008) Linking fluorometry to radiometry with physical and chemical transfer standards: instrument characterization and traceable fluorescence measurements. This volume
12. Henderson LO, Marti GE, Gaigalas A, Hannon WH, Vogt RF (1998) *Cytometry* 33:97
13. Coder DM, Redelman D, Vogt RF (1994) *Cytometry* 18:75
14. Muirhead KA, Schmitt TC, Muirhead AR (1983) *Cytometry* 3:251
15. Schwartz A, Repollet EF, Vogt RF, Gratama JW (1996) *Cytometry* 26:22
16. Schwartz A, Wang L, Early E, Gaigalas A, Zhang Y, Marti GE, Vogt RF (2002) *J Res Natl Inst Stand Technol* 107:83
17. Vogt RF, Cross GD, Henderson LO, Phillips DL (1989) *Cytometry* 10:294
18. Brown MC, Hoffman RA, Kirchanski SJ (1986) *Ann NY Acad Sci* 468:93
19. Schwartz A, Fernandez-Repollet E (1993) *Ann NY Acad Sci* 677:28
20. Schwartz A, Marti GE, Poon R, Gratama JW, Fernandez-Repollet E (1998) *Cytometry* 33:106
21. Gaigalas AK, Li L, Henderson O, Vogt R, Barr J, Marti G, Weaver J, Schwartz A (2001) *J Res Natl Inst Stand Technol* 106:381
22. Wang L, Gaigalas AK, Abbassi F, Marti GE, Vogt RF, Schwartz A (2002) *J Res Natl Inst Stand Technol* 107:339
23. Gaigalas AK, Wang L, Schwartz A, Marti GE, Vogt RF (2003) *J Res Natl Inst Stand Technol* 110:101
24. Schwartz A, Gaigalas AK, Wang L, Marti GE, Vogt RF, Fernandez-Repollet E (2004) *Cytom B, Clin Cytom* 57:1
25. Wang L, Abbasi F, Gaigalas A, Hoffman RA, Flagler D, Marti GE (2007) *Cytometry B, Clinical Cytom* 72:442–449
26. Vogt RF, Marti GE, Schwartz A (1995) Quantitative calibration of fluorochrome intensity for clinical and research applications of leukocyte immunophenotyping by flow cytometry. In: Tyrer HW (ed) *Critical issues in biotechnology and bioengineering*, vol. 1. Ablex, New Jersey, p 147
27. Gratama JW, D'hautcourt JL, Mandy F, Rothe G, Barnett D, Janossy G, Papa S, Schmitz G, Lenkei R (1998) *Cytometry* 33:166
28. Serke S, van Lessen A, Huhn D (1998) *Cytometry* 33:179
29. Lenkei R, Gratama JW, Rothe G, Schmitz G, D'hautcourt JL, Arekrans A, Mandy F, Marti G (1998) *Cytometry* 33:188
30. Davis KA, Abrams B, Iyer SB, Hoffman RA, Bishop JE (1998) *Cytometry* 33:197
31. International Organization for Standardization (1993) *International vocabulary of basic and general terms in metrology*. ISO, Geneva
32. Clinical and Laboratory Standards Institute (2004) *Protocols for determination of limits of detection and limits of quantitation; approved guideline EP17-A*. CLSI, Pennsylvania
33. Wood JC, Hoffman RA (1998) *Cytometry* 33:256
34. Wood JC (1998) *Cytometry* 33:260
35. Chase ES, Hoffman RA (1998) *Cytometry* 33:267
36. Poncelet P, Carayon P (1985) *J Immunol Methods* 85:65



37. Bikoue A, Janossy G.I, Barnett D (2002) *J Immunol Methods* 266:19
38. Chatelier RC, Ashcroft RG, Lloyd CJ (1986) *EMBO J* 5:1181
39. Hultin LE, Matud JL, Giorgi JV (1998) *Cytometry* 33:123
40. Iyer SB, Hultin LE, Zawadzki JA, Davis KA, Giorgi JV (1998) *Cytometry* 33:206
41. Schmitz JL, Czerniewski MA, Edinger M, Plaeger S, Gelman R, Wilkening CL, Zawadzki JA, Wormsley SB (2000) *Cytometry* 42:174
42. Wang L, Abbasi F, Gaigalas AK, Vogt RF, Marti GE (2006) *Cytometry* 70B:410
43. Kay S, Herishanu Y, Pick M, Rogowski O, Baron S, Naparstek E, Polliack A, Deutsch VR (2005) *Cytometry* 70B:218
44. Davis BH (2002) *Cytometry [Suppl]* 11:49
45. Mittag A, Lenz D, Gerstner AO, Tarnok A (2006) *Cytometry* 69A:691
46. Ortyн WE, Perry DJ, Venkatachalam V, Liang L, Hall BE, Frost K, Basiji DA (2007) *Cytometry A* 71(4):215–231
47. Xiao Y, Barker PE (2008) Cellular bioimaging in fluorescent cancer biomarker evaluation: validation, technologies and standards development. This volume
48. Purvis N, Stelzer G (1998) *Cytometry* 33:156
49. Earley MC, Vogt RE, Shapiro HM, Mandy FF, Kellar KL, Bellisario R, Pass KA, Marti GE, Stewart CC, Hannon WH (2002) *Cytometry* 50:239
50. Seydack M (2008) Particle-based assays: applications and unresolved issues. This volume
51. Keeney M, Barnett D, Gratama JW (2004) *J Biol Regul Homeost Agents* 18:305
52. Strom CM, Janaszco R, Quan F, Wang S, Buller A, McGinniss M, Sun W (2006) *J Mol Diagn* 8:371
53. Strom CM, Janaszco R, Quan F, Wang SB, Buller A, McGinniss M, Sun W (2006) *J Mol Diagn* 8:371
54. Wion E, Brantley M, Stevens J, Gallinger S, Peng H, Glass M, Hagopian W (2003) *Ann NY Acad Sci* 1005:400
55. Marti GE, Gaigalas A, Vogt RF (2000) *Cytometry* 42:263
56. Baker SC, Bauer SR, Beyer RP, Brenton JD, Bromley B, Burrill J, Causton H, and the External RNA Controls Consortium (2005) *Nature Methods* 2:731
57. Holden M, Wang L (2008) Quantitative real-time PCR: fluorescent probe options and issues. This volume
58. Weksberg R, Hughes S, Moldovan L, Bassett AS, Chow EW, Squire JA (2005) *BMC Genomics* 6:180

# Need for and Metrological Approaches Towards Standardization of Fluorescence Measurements from the View of National Metrology Institutes

P. C. DeRose<sup>1</sup> (✉) · L. Wang<sup>1</sup> · A. K. Gaigalas<sup>1</sup> · G. W. Kramer<sup>1</sup> ·  
U. Resch-Genger<sup>2</sup> (✉) · U. Panne<sup>2</sup>

<sup>1</sup>National Institute of Standards and Technology (NIST), 100 Bureau Drive,  
Gaithersburg, MD 20899-8312, USA  
*paul.derose@nist.gov*

<sup>2</sup>Federal Institute for Materials Research and Testing (BAM),  
Richard-Willstaetter-Str. 11, 12489 Berlin, Germany  
*ute.resch@bam.de*

1	Introduction . . . . .	34
2	Fluorescence Standards: Types, Requirements and Quality Criteria for Choice . . . . .	36
2.1	Classification of Fluorescence Standards . . . . .	36
2.2	Quality Criteria for Fluorescence Standards . . . . .	37
2.3	Fluorescence Calibration Standards . . . . .	39
2.3.1	Emission Standards with Certified Corrected Emission Spectra . . . . .	42
2.3.2	Interlaboratory Comparison on Corrected Emission Spectra . . . . .	45
2.3.3	Chromophore-Based Wavelength Standards . . . . .	45
2.4	Application-Specific Fluorescence Intensity Standards . . . . .	46
2.4.1	Fluorescence Quantum Yield Standards . . . . .	47
2.4.2	Standards that Relate Chemical Concentration to Instrument Response . . . . .	47
2.4.3	The MESF Concept . . . . .	48
2.5	Standards for Day-to-Day and Instrument-to-Instrument Intensity . . . . .	51
2.5.1	General Applications . . . . .	51
2.5.2	Selected Applications: Filter-Based Instruments . . . . .	53
3	Conclusion . . . . .	56
	References . . . . .	57

**Abstract** The need for standardization in fluorescence measurements to improve quality assurance and to meet regulatory demands is addressed from the viewpoint of National Metrology Institutes (NMIs). Classes of fluorescence standards are defined, including instrument calibration standards for the determination and correction of instrument bias, application-specific standards based on commonly used fluorescent labels, and instrument validation standards for periodic checks of instrument performance. The need for each class of standard is addressed and on-going efforts by NMIs and others are described. Several certified reference materials (CRMs) that have recently been developed by NMIs are highlighted. These include spectral correction standards, developed independently by both NIST and BAM (Germany), and fluorescence intensity standards for flow cytometry, developed by NIST. In addition, future activities at both institutes are addressed such as the development of day-to-day intensity standards.

**Keywords** Calibration · Emission standards · Fluorescence intensity standards · Fluorescence standards · Quality assurance

### Abbreviations

ABC	Antibody binding capacity
ASTM	ASTM International
BAM	Federal Institute for Materials Research and Testing, Germany
CRM	Certified reference material
EEM	Excitation-emission matrix
FDA	United States Food and Drug Administration
FL1	First fluorescence channel of a flow cytometer
ISO	International Organization for Standardization, Geneva
IUPAC	Union of Pure and Applied Chemistry
LED	Light emitting diode
MESF	Molecules of equivalent soluble fluorophore
NBS	National Bureau of Standards, USA
NIST	National Institute of Standards and Technology, USA
NMI	National Metrology Institute
NPL	National Physical Laboratory, UK
NRC	National Research Council, Canada
OLED	Organic light emitting diode
PTB	Physikalisch-Technische Bundesanstalt, Germany
R	Measured reference signal
S	Measured fluorescence signal, uncorrected
$S_{\text{cor}}$	Measured fluorescence signal, corrected for detection system responsivity
SOP	Standard operation procedure
SRM®	Standard Reference Material®

## 1

### Introduction

The use of fluorescence continues to increase in the life and material sciences with many techniques having matured to a state where quantification is desired [1–6]. Compared to other prominent analytical methods, however, standardization of fluorescence measurements is still in its infancy, despite the fact that it is not a new technique. Its birth was marked by Stokes' study of quinine sulfate in 1852 [7], where he used what can today be recognized as a basic fluorometric setup, but it was not until the appearance of the first commercial instruments in the late 1950s that fluorescence became a common analytical tool [8]. Since this time, the range of fluorescence-based techniques has expanded greatly with parameters measured including (integral) fluorescence intensities at selected excitation and emission wavelengths and polarization conditions, often in combination with spatial and temporal resolution, and increasingly at the single-molecule-detection level. However, what is often overlooked is that all types of fluorescence measurements yield

signals that contain both analyte- and instrument-specific contributions, and the resulting demand to remove the latter from the former to obtain fluorescence data comparable across instruments, laboratories, and over time is increasing [9]. Further fluorescence-inherent drawbacks relate to difficulties in accurately measuring absolute fluorescence intensities and hence in realizing true quantitative measurements [10]. In addition, the sensitivity of the absorption and fluorescence properties of most chromophores to their microenvironment can hamper quantification based on measurements of relative fluorescence intensities. Despite these problems and the ever-increasing complexity of fluorescence instrumentation, there are still very few commercially available reference materials to aid in the qualification of fluorescence instruments and the validation of related measurements or assays. Moreover, guidelines for the characterization of fluorescence instruments and for the performance and evaluation of selected measurements that were developed, mostly in the 1980s, e.g., by ASTM International, the Ultraviolet Spectrometry Group, a UK-based forum of spectrometer users from industry, academia and government, and the International Union of Pure and Applied Chemistry (IUPAC), focus mainly on steady-state fluorometry and do not include more modern fluorescence instrumentation and methods [11–16].

The present state of standardization of fluorescence measurements is closely linked to past and ongoing efforts of National Metrology Institutes (NMIs) in the development of fluorescence standards. In the late 1960s, the National Bureau of Standards (NBS), now known as the National Institute of Standards and Technology (NIST), became involved in fluorescence spectrometry to characterize “television” phosphors provided as NBS Standard Sample Phosphors [17]. By the early 1970s, NBS as the most active NMI in the fluorescence area<sup>1</sup> started to develop material standards for the calibration of fluorescence spectrometers and held related workshops to meet the demands of the clinical chemistry community [18, 19]. In addition, a high-accuracy fluorescence spectrophotometer was built and qualified to achieve the levels of precision and accuracy required for certified reference materials (CRMs) [20–22]. This instrument was used to certify the corrected emission spectrum, i.e., the instrument-independent spectrum, of Standard Reference Material® (SRM®) 936 Quinine Sulfate Dihydrate in 1979 [23], which covers the spectral region from about 395 to 565 nm.<sup>2</sup> This material was the first spectral correction standard for fluorescence to be released by an NMI and is still available as SRM 936a [9, 24]. In 1989, SRM 1931 [25] was released as a set of four solid spectral fluorescence standards in a cuvette format, but was restricted in measurement geometry and certified using polarizers [26]. These

---

<sup>1</sup> BAM (Federal Institute of Materials Research and Testing, Germany), NRC (National research Council, Canada), NPL (National Physics Laboratory, UK), and TTK (Metrology Resrach Institute, Finland) were mainly active in the area of colorimetry or so-called bispectral fluorescence at that time.

<sup>2</sup> Fluorescence intensities of  $\geq 10\%$  of the emission at the maximum of the band are required at least for spectral calibration with acceptable uncertainties.

efforts provided the basis to establish how and why users of fluorescence techniques should regularly calibrate their instruments and initiated the development of physical and chemical transfer standards of varying quality by a number of companies [9].

Despite the existing literature on instrument calibration [1, 5, 14, 19, 22], pressures from regulatory agencies, and the global trends of quality assurance, traceability, and accreditation [27, 28], many users of fluorescence techniques continue to restrict instrument characterization to calibration curves of fluorescence intensity versus concentration for quantifying analyte concentrations of unknowns. The influence of other instrument parameters on measured fluorescence quantities, such as emission spectra, is typically neglected, or the necessary corrections are expected to be included in the instrument manufacturer's software. At the same time, many of the newer fluorescence-based assays are employed in the highly regulated areas of clinical diagnostics, drug production, and environmental monitoring. In addition, the desire for analyte quantification from fluorescence measurements is ever-increasing in both conventional areas, e.g., spectrofluorometry, flow cytometry, and fluorescence assay technologies and newer areas with more complex instrumentation, e.g., fluorescence imaging techniques such as (confocal) fluorescence microscopy and fluorescence-based microarray technology. These developments demanded a reassessment of effective instrument calibration and qualification procedures and encouraged several NMIs, including the Federal Institute for Materials Research and Testing (BAM, Germany), NIST (USA), National Physical Laboratory (NPL, UK), National Research Council (NRC, Canada), and the Physikalisch-Technische Bundesanstalt (PTB, Germany), to become more active in the past several years in fluorescence standardization. In combination with the output from recent fluorescence workshops and questionnaires, organized by NIST [29–34] and BAM [35], this situation motivated BAM and NIST to dedicate research activities to the development of reliable instrument-type and application-specific fluorescence standards for various fluorescence techniques. In this chapter, recent, ongoing, and future standard activities at NIST and BAM are presented and directions still needing to be explored and addressed by NMIs in the fluorescence area are highlighted.

## 2

### **Fluorescence Standards: Types, Requirements and Quality Criteria for Choice**

#### 2.1

##### **Classification of Fluorescence Standards**

Fluorescence standards can be divided into three general types: (i) instrument calibration standards, both physical and chemical, i.e., chromophore-

based, for the determination and correction of instrument bias; (ii) application-specific fluorescence standards, based on routinely measured fluorophores or closely related<sup>3</sup> chromophores that take into account the fluorescence properties of typically measured samples and are thus particularly useful for the validation of methods involving such samples; and (iii) instrument validation standards, both physical and chemical, for periodic checks of instrument performance [9]. Standards of the first type include spectral fluorescence standards with known corrected, i.e., instrument-independent, spectra [9]. A classic example of application-specific fluorescence standards are fluorescence intensity standards that relate chemical concentration to instrument response. Such materials are fluorophore-specific. Fluorescence quantum yield standards [9], which belong to this class of standards as well, can be used to link fluorescence intensity to an absolute scale. Examples of instrument validation standards are day-to-day intensity standards, which test the instrument's day-to-day performance and long-term stability and may even enable correction for these variabilities. Such standards can also be applied as instrument-to-instrument intensity standards for the comparison of measured fluorescence intensities between instruments when measurement parameters are fixed. Requirements on different types of fluorescence standards, similar to those given here, have recently been defined by BAM [9].

## 2.2

### Quality Criteria for Fluorescence Standards

The value of a physical or chemical fluorescence standard depends on its suitability and reliability for the respective task, e.g., instrument characterization or quantification. Criteria for the production of reference materials – and thus also of fluorescence standards – are stated in *ISO Guide 34* [36] and *ISO Guide 35* [37], the calculation of uncertainties is described in the *Guide of the Measurement of Uncertainty* (GUM) [38], and traceability is defined in *EN ISO/IEC 17025* [28].

The reliability of a fluorescence standard is determined by the characterization of its calibration-relevant properties [9]. This includes the characterization of the instrument and the measurement conditions used for the determination of the calibration-relevant quantity or quantities, the standard's stability under application-relevant conditions that determine its shelf life and storage conditions, and the uncertainty of the certified/characterized quantity or quantities. Moreover, additional information relevant for proper use of the standard, a well-defined scope, limitations for use, and a tested standard operation procedure (SOP) should be mandatory. In principle, fit-for-purpose

---

<sup>3</sup> “Closely related” refers to spectral behavior, i.e., matching or similar absorption and emission spectra.

fluorescence standards, designed for a broad community of users of fluorescence techniques, need to consider typical samples to be encountered and measurement conditions commonly employed. These include measurement geometry, format of the sample, and common instrument settings. Also, the radiated/emitted intensity and the size and shape of the radiating volume of standard and sample should be comparable. This allows instrument calibration and fluorescence measurements to be made under similar conditions while the instrument's detection system is operated within its linear range.

To minimize standard-related uncertainties for the three types of fluorescence standards, information on the wavelength and temperature dependence of the application-relevant fluorescence properties is mandatory as well as on the concentration dependence of these features where applicable. Values of the fluorescence anisotropy should be provided as this quantity determines the need for the use of polarizers and the size of polarization-related contributions to the overall uncertainty. Also the determination of the standard's purity including method of analysis and respective uncertainty is important as dye purity can affect the standard's spectroscopic properties, photochemical and thermal stability, and reproducibility. Dye purity can vary substantially between different dye manufacturers and lots (see Fig. 1) and has historically contributed to errors in reported spectroscopic quantities, such as molar absorption coefficient [39] and fluorescence quantum yield [40]. For liquid standards, the solvent to be employed also needs to be characterized with respect to properties potentially affecting fluorescence, such as water content for hygroscopic solvents and pH and ionic strength for aqueous solvents. Alternatively, the solvent should be provided with the standard at a constant quality level. Solid standards require additional characterization of the homogeneity of the dye's distribution in the matrix to guarantee a uniform fluorescence. Additional requirements inherent to the respective application and type of fluorescence standard can be found in the corresponding sections.

The majority of fluorescence standards recommended in the literature, commercially available, or in-house prepared [9] do not meet these criteria. This results in an enhanced calibration or measurement uncertainty or, at worst, an instrument characterization that is not reliable. Also, these standards typically do not yield traceability to the spectral radiance or spectral responsivity scale relevant for fluorometry; see also Chap. 3 on the traceability of fluorometry in this book [41]. In contrast, reference materials from NMIs are supplied with certified values and uncertainties that apply to the individual or batch material and follow the *GUM*, are produced according to *ISO Guides 34* and *35*, and are traceable to SI units whenever possible. In addition, NMIs are typically required to have the highest confidence possible in the measured values for reference materials before these materials can be released as CRMs [42]. Measurement integrity of (certified) values is assured by the determination of these values with multiple, independent techniques, the investigation of all known or suspected sources of error, and the performance

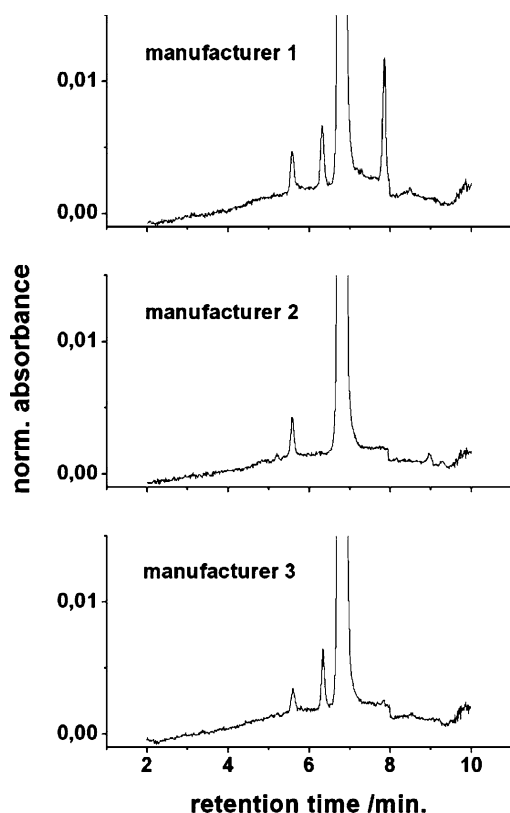


**Fig. 1** HPLC diagram of an exemplary organic dye revealing typical deviations in dye purity between batches from different dye manufacturers. Depending on the chemical nature and spectroscopic properties of the impurities, this can affect the spectroscopic properties of a dye, such as molar absorption coefficient (at a selected wavelength) and fluorescence quantum yield, as well as its photochemical and thermal long-term stability

of interlaboratory comparisons with other NMIs. At present, NIST and BAM are the only NMIs releasing CRMs for the characterization of fluorescence instruments [43–50].

### 2.3

#### Fluorescence Calibration Standards

Outcomes from recent workshops organized by NIST and BAM and results from distributed questionnaires have highlighted the importance of fluorescence calibration standards and certified, corrected fluorescence spectra to the fluorescence community [29–35]. This includes wavelength standards with multiple narrow emission bands spanning the UV/Vis/NIR spectral region to validate the wavelength accuracy of wavelength-selecting optical



components [51] and so-called emission and excitation standards having broad unstructured spectra for the determination of the spectral responsivity and intensity characteristics of fluorescence instruments [9, 52–54]. A number of spectral fluorescence standards have been reported in the literature and several are available from commercial (non-NMI) sources. However, none of these materials are supplied with traceable and certified, corrected fluorescence data and corresponding wavelength-dependent uncertainties [9, 55].<sup>4</sup> In particular, the reliability of the corrected emission spectra of emission standards is often questionable.

The importance of such fluorescence calibration standards, particularly of emission standards, is obvious as measured fluorescence signals are not only determined by the analyte's absorbance at the excitation wavelength and its spectral fluorescence yield, but also contain contributions from the instrument-specific spectral irradiance at the sample position and the instrument-specific spectral responsivity of the emission channel or detection system [9, 14, 56–58]. These two quantities are wavelength dependent (see Figs. 2 and 3 [58, 59]). This is a result of the combination of the wavelength dependence of the spectral radiance of the excitation light source, the transmittance of components like lenses, mirrors, filters, monochromator gratings and polarizers in the optical paths of the excitation and emission channels, and the spectral responsivity of the detector of the fluorescence instrument. In addition, they are polarization dependent, as discussed in Chaps. 3 and 6 in [41, 60], and time dependent, due to aging of instrument components.

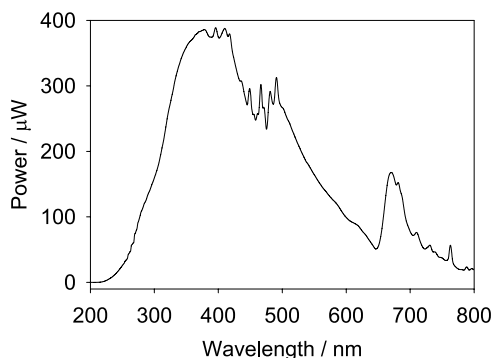


**Fig. 2** Excitation intensity or flux at the sample position of a typical spectrofluorometer measured with a calibrated detector

<sup>4</sup> See for instance Invitrogen or former Molecular Probes, Starna GmbH, Matech Precision Dynamics Corp., Labsphere Inc., LambdaChem GmbH and Photon Technology International Inc. (DYAG), FA-2036. Certain commercial equipment, instruments, or materials are identified in this chapter to foster understanding. Such identification does not imply recommendation or endorsement by the National Institute of Standards and Technology, nor does it imply that the materials or equipment identified are necessarily the best available for the purpose.

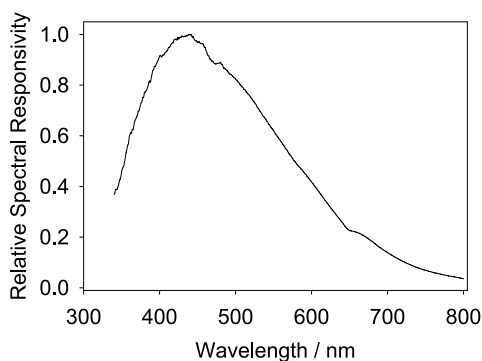


**Fig. 3** Relative spectral responsivity of the emission channel of a typical spectrofluorometer measured with a calibrated lamp

The influence of these instrument-specific quantities on fluorescence data is illustrated in Fig. 4 [58, 59] for an excitation-emission matrix (EEM) or so-called total fluorescence spectrum of tryptophan. This figure compares the measured uncorrected signal  $S$  (Fig. 4a), the excitation intensity-corrected signal  $S/R$  (Fig. 4b) that takes into account the wavelength dependence of the spectral irradiance of the instrument's excitation channel shown in Fig. 2, and the excitation- and emission corrected, i.e., instrument-independent, signal  $S_{\text{cor}}/R$  (Fig. 4c). The last considers both instrument-specific quantities. As follows from a comparison of these signals, without any spectral correction, two peaks are observed instead of one with both dramatically shifted by 100 nm or more (see Fig. 4a). When only the excitation intensity correction is applied, a single, qualitatively correct spectrum is obtained, but the peak is still shifted by about 12 nm (see Fig. 4b). The obvious differences between these data clearly demonstrate the need for and importance of the spectral correction of excitation and emission spectra and EEMs for comparable fluorescence data.

As only relative fluorescence intensities are typically measured, correction of measured data for the relative spectral irradiance of the excitation channel (termed excitation correction) and/or the relative spectral responsivity of the emission channel (termed emission correction) are sufficient [9, 56–58], as detailed in Chap. 3 in [41]. In most cases, there is no need to link fluorescence intensity to an absolute scale, i.e., to absolute radiometric units. When quantification from or longterm comparability of measured relative fluorescence intensities is desired, the requirements of most users can be satisfied using either a calibration curve for concentration or a (relative) day-to-day intensity standard, as described in a forthcoming section, in addition to the correction for the instrument's spectral characteristics.

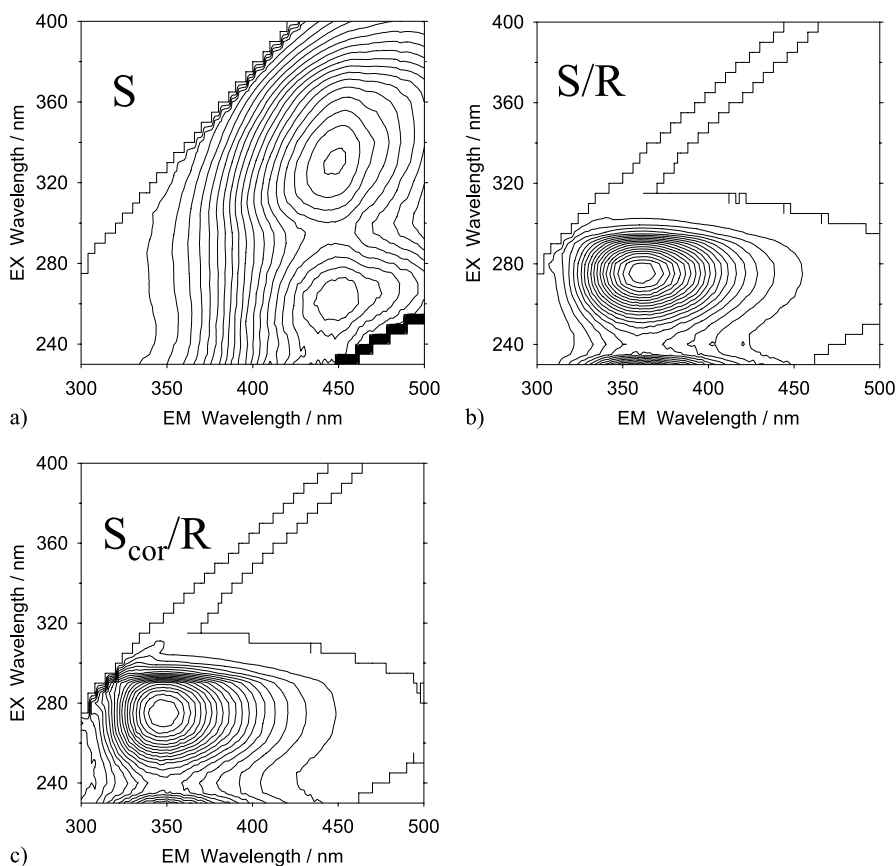


**Fig. 4** Comparison of contour-plotted EEM spectra for tryptophan, where the fluorescence intensity is **a**  $S$  the measured uncorrected signal, maxima at  $(\lambda_{EX}, \lambda_{EM}) = (265 \text{ nm}, 452 \text{ nm})$  and  $(330 \text{ nm}, 446 \text{ nm})$ , **b**  $S/R$  the signal corrected for the spectral irradiance at the sample position, shown in Fig. 2, maximum at  $(\lambda_{EX}, \lambda_{EM}) = (275 \text{ nm}, 358 \text{ nm})$ , and **c**  $S/R_c$  the instrument-independent signal, corrected for both the instrument's spectral irradiance and its spectral responsivity, displayed in Figs. 2 and 3, maximum at  $(\lambda_{EX}, \lambda_{EM}) = (275 \text{ nm}, 346 \text{ nm})$

### 2.3.1

#### Emission Standards with Certified Corrected Emission Spectra

The relative spectral responsivity of the emission channel of a fluorescence instrument can be most easily determined with chromophore-based emission standards, whose corrected, i.e., instrument-independent emission spectra are known and preferably certified. Accordingly, both BAM and NIST have responded to the increasing need for quality assurance in fluorescence in the past several years by qualifying fluorescence spectrometers for measuring

corrected fluorescence spectra [56, 58, 59]. These instruments have been and will be used for the certification of corrected fluorescence spectra with known uncertainties [44, 45, 61]. As a first step towards standardization of the spectral characteristics of fluorescence instruments on a broad level, BAM and NIST have independently developed new sets of standards for the determination of the relative spectral responsivity of fluorescence instruments and the spectral correction of emission data.

The BAM Calibration Kit *Spectral Fluorescence Standards* released in January 2006 [62, 63] consists of the five spectral fluorescence standards BAM-F001 through BAM-F005 (equaling the organic dyes A–E in earlier publications) with certified, normalized, corrected emission spectra covering the spectral range from 300 to 770 nm as a set (see Fig. 5). These dyes are provided as ready-made bottled solids, either as a kit [61–63] or individually [46–50]. They are readily transformed into dye solutions that can be measured without any additional dilution steps with routinely used settings of the fluorescence instrument to be calibrated. To minimize standard-related uncertainties, BAM developed the software *LINKCORR* for data evaluation and spectra linking [9, 61, 62].<sup>5</sup> The wavelength-dependent, expanded relative uncertainties supplied include uncertainties related to the calibration of the BAM fluorometer and to the measurement of fluorescence spectra with this instrument, as well as material-related uncertainties, such as batch-to-batch dye homogeneity and thermal stability [61–63]. The influence of other parameters, such as the bandwidth of the emission monochromator, temperature, and the excitation wavelength, was minimized by careful choice of standard materials [46–50, 61–63]. Due to their liquid nature and the minimum spectral overlap between their absorption and emission spectra, BAM-F001 through BAM-F005 offer a unique flexibility with respect to measurement geometry, format, and type of fluorescence instrument to be calibrated [63] and have been successfully used for the characterization of microplate readers and for the characterization of the spectral characteristics of spectral imaging systems [64]. Moreover, the BAM spectral fluorescence standards can be used in conjunction with all types of light sources (continuous and pulsed-lamps, lasers etc.) due to their short fluorescence lifetimes of a few nanoseconds.

The two new NIST standards, SRMs 2940 (*Orange Emission*) and 2941 (*Green Emission*) *Relative Intensity Correction Standards for Fluorescence Spectroscopy*, cover the spectral region from 395 to 780 nm, when combined with SRM 936a *Quinine Sulfate Dihydrate* as a set (see Fig. 6 [59]) [65]. SRMs 2940 and 2941 [44, 45] are ready-to-use, cuvette-shaped glasses with three long sides polished and one side frosted, allowing measurements using instruments with 0°/90°, front-face or epifluorescence geometries. Similar to

<sup>5</sup> BAM-F001–BAM-F005 ready-made from Sigma-Aldrich Production GmbH (former Fluka Production GmbH) are available from BAM or from Sigma-Aldrich. The corresponding product numbers from Sigma-Aldrich are 97003-1KT-F for the Calibration Kit and 72594, 23923, 96158, 74245, and 94053 for BAM-F001–BAM-F005, respectively.

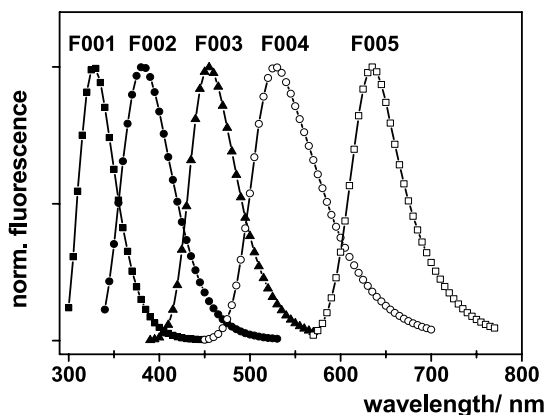


**Fig. 5** Normalized corrected emission spectra of the Calibration Kit *Spectral Fluorescence Standards* BAM-F001–BAM-F005

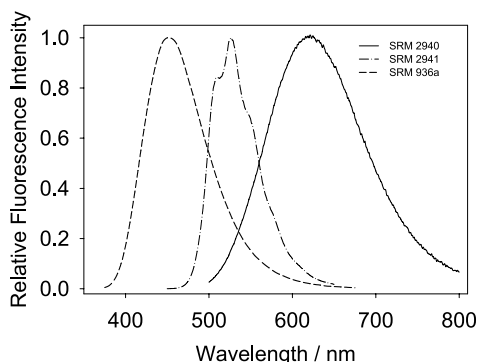


**Fig. 6** Normalized corrected emission spectra of the spectral correction standards SRMs 2940, 2941, and 936a

BAM-F001 through BAM-F005, the supplied uncertainties of the certified corrected emission spectra of the NIST SRMs arise from uncertainties related to the measurements by and calibration of the spectrofluorometer used for certification [58], as well as from material-related uncertainties. In the case of the new NIST SRMs, the latter includes the dependence of the emission spectra on excitation wavelength, spectral bandpass, concentration (inner filter effects), polarization of the excitation beam, responsivity of the detection system to fluorescence with different polarizations, and sample temperature. Information provided with each standard will include the temperature coefficient for fluorescence intensity and the anisotropy of the fluorescence at the peak maximum along with instructions for use. Software for calculating values and uncertainties of the certified spectra for any emission wavelength or wavelength interval will also be supplied. The certified values of these

SRMs are valid for ten years from the date of issue (April 2007). Due to the comparably long luminescence lifetimes of the dopants, inorganic metal ions, in the  $\mu\text{s}$  to  $\text{ms}$  region, use of these materials is recommended for instruments equipped with continuous light sources. In the case of pulsed light sources, the emission properties of these dopants can be affected by measurement parameters, such as pulse duration, delay, and gate [9], see also Sect. 2.5. For instance, the certified values for SRM 2941 can, but those for SRM 2940 cannot, be used, with pulsed light sources.

### 2.3.2

#### Interlaboratory Comparison on Corrected Emission Spectra

Along with the certification of their new spectral fluorescence standards, NIST and BAM organized a comparison amongst the NMIs (NRC, PTB, NIST, and BAM) active in the area of high precision spectrofluorometry to evaluate the comparability of their emission spectra measurements. This study, which will provide the basis for future steps towards instrument standardization and will be jointly published, focused on the determination of the relative spectral responsivity of spectrofluorometers in a  $0^\circ/90^\circ$  (PTB, BAM, and NIST) and  $45^\circ/0^\circ$  (NRC) measurement geometry using both physical transfer standards, i.e., calibrated lamps and detectors, and spectral fluorescence standards, here BAM-F001 through BAM-F005.

### 2.3.3

#### Chromophore-Based Wavelength Standards

Current research activities at NIST and BAM include the development of wavelength standards for the control of the wavelength accuracy and spectral resolution of fluorescence measuring systems in the UV/Vis/NIR spectral region [9, 51]. These materials are not intended as substitutes for atomic discharge lamps that, having extremely narrow emission lines and well known spectral band positions (including uncertainties) [65], are commonly used for the calibration of the wavelength scale of high precision spectrofluorometers to an accuracy of typically  $\pm 0.5$  nm [11, 67, 68]. However, chromophore-based wavelength standards present an elegant, easy-to-use alternative to such lamps, particularly for compact fluorescence instruments with a reduced spectral resolution, such as portable fluorometers, spectral imaging systems, or certain microplate readers, which are becoming increasingly more prevalent [9, 51]. Suitable materials should emit a multitude of narrow emission bands or lines in the UV/Vis/NIR region properly separated by at least 20 nm. Structured or very narrow bands may be used for the determination of the instrument's spectral resolution.

A variety of materials are potentially suited as chromophore-based wavelength standards, including inorganic crystals and glasses and organic-doped

polymers [9, 55, 69]. Both BAM and NIST are developing glass-based wavelength standards, such as cuvette-shaped glasses doped with a variety of different inorganic metal ions [9, 51]. Since the narrow spectra of these candidate wavelength standards are emitted as a consequence of absorption of the instrument's excitation light, and the intensity of the luminescence can be controlled via dopant concentration, the shape and size of the radiating volume and the spectral radiance/fluorescence intensity of such a solid standard can be made comparable to that of commonly measured samples. Accordingly, they can be used under routine measurement conditions. This may not necessarily be true for a comparatively bright atomic discharge lamp which must be attenuated to avoid detector saturation and where improper alignment of the lamp can lead to wavelength biases. BAM's candidate wavelength standards, which are currently tested with spectrofluorometers at a  $0^\circ/90^\circ$  measurement geometry, may be eventually provided in different formats for different fluorescence techniques including, for instance, fluorescence microscopy. As spectral bandpass can vary amongst instrument manufacturers, e.g., portable fluorometers or spectral imaging systems, and potential candidates for wavelength standards do not typically have symmetric emission bands, these wavelength standards will be certified at multiple bandwidths or spectral bandpasses, some narrow and some broad similar to the certification of the Calibration Kit Spectral Fluorescence Standards BAM-F001–BAM-F005 [46–50, 61, 62] and SRM 2034 *Holmium Oxide Solution* or SRM 2065 *UV/Vis/NIR Transmission Wavelength / Vacuum Wavenumber Standard*, wavelength standards for UV/Vis absorbance.

## 2.4

### Application-Specific Fluorescence Intensity Standards

Quantification of fluorophores from measurements of fluorescence intensities is hampered by two facts: the very challenging determination of absolute fluorescence intensities and the sensitivity of the molar absorption coefficients and fluorescence quantum yields of most chromophores to their microenvironment. Measurement of absolute fluorescence intensities imposes very strong requirements on instrument calibration because the spectral characteristics of the fluorescence instrument used need to be considered, as detailed in the previous section, as well as the collection efficiency of the instrument's detection system, a similarly instrument-specific property that is even more difficult to measure. Tedious measurements of absolute fluorescence intensities can be elegantly circumvented by the use of fluorescence intensity standards that link the measured fluorescence intensity of a sample to that of a standard, thereby defining a relative intensity scale comparable across instruments and laboratories. In the following, approaches to and examples of fluorescence intensity standards [9] from NIST and BAM, along with strategies to minimize the influence of dye microenvironment on quantification are

presented. Day-to-day and instrument-to-instrument intensity standards that have a similar scope are detailed in a later section.

#### 2.4.1

##### Fluorescence Quantum Yield Standards

Fluorescence quantum yield standards, which are employed as a reference for the determination of the (relative) fluorescence quantum yield of an analyte, are typically not based on the same fluorophore as the sample, contrary to the fluorescence intensity standards detailed in the next section that relate chemical concentration to instrument response [9]. They do not require matching of the spectra of the standard and the sample, but both systems should absorb and emit within comparable spectral regions [9]. However, spectrally corrected emission spectra for both the standard and the sample are mandatory in the vast majority of cases [1, 4, 5, 14]. The most stringent requirements on these standards are a reliable fluorescence quantum yield with a stated uncertainty and properly defined and reported measurement conditions, such as matrix, oxygen concentration, temperature, and excitation wavelength, as well as dye purity and applicable concentration range. These requirements are typically not fulfilled for most fluorescence quantum yield standards described and recommended in the literature [9] (see also Chap. 4 on fluorescence quantum yield standards) [70]. This encouraged BAM to investigate different strategies for the reliable determination of fluorescence quantum yields and to characterize existing and develop new fluorescence quantum yield standards. As a first step towards standards with certified fluorescence quantum yields, BAM is testing a set of fluorophores emitting in the UV/Vis/NIR region and characterizing a new, recently built reference fluorometer designed for the determination of absolute fluorescence quantum yields [57, 58]. Such standards and the measurement of absolute fluorescence quantum yields are likely to gain in importance due to an increasing desire for reliable relative and absolute fluorescence quantum yields of a variety of materials, including those used in LEDs and OLEDs [71],<sup>6</sup> as well as NIR fluorophores.

#### 2.4.2

##### Standards that Relate Chemical Concentration to Instrument Response

Standards that relate chemical concentration to instrument response compare the fluorescence intensity of a sample to that of a standard of known fluorophore content under identical measurement conditions to quantify the concentration or number of fluorophores. Accordingly, the same fluorophore as that to be quantified in the sample is used for the production of this type

---

<sup>6</sup> LED: light emitting diode; OLED: organic light emitting diode.



of intensity standard. To eliminate errors in quantification, the dye purity in the reference material needs to be determined (see Sect. 2.2 and Fig. 1) [39], aggregation should be avoided, and the chromophore(s) to be detected in the sample and in the standard have to be in the same microenvironment to guarantee identical molar absorption coefficients (at the excitation wavelength), fluorescence spectra, and fluorescence quantum yields [72]. In December 2004, NIST issued SRM 1932 *Fluorescein Solution*, a solution of high and well characterized purity of the most widely used fluorescent label, fluorescein, dissolved in a borate buffer at pH 9.5, and certified this solution for concentration. This included the identification of the chemical nature of impurities and the determination of their relative percentages, using at least seven different analytical techniques including  $^1\text{H-NMR}$ , HPLC, and a variety of elemental analyses [43], following the NIST guidelines for the traceable assessment of chemical purity [73].

### 2.4.3

#### The MESF Concept

For the majority of fluorescence techniques, the criterion of matching microenvironments between sample and standard can only be met to a certain degree. This is particularly true for the comparison of free and immobilized fluorophores, i.e., dyes attached to beads, particles or macro- and biomolecules, e.g., polymers, proteins, antibodies, and DNA. Accordingly, different concepts for fluorescence intensity standards have been developed that all aim at the consideration and minimization of the effect of dye microenvironment on fluorophore quantification. For flow cytometry, which has become a very prominent technique in clinical diagnostics for acquiring cell counts, such as the fraction of cells infected with a particular antigen in a blood sample, the concept of molecules of equivalent soluble fluorophore (MESF) has been introduced [74, 75] as an exemplary scheme for reliable quantification in complex microenvironments.

In flow cytometry, the antibody binding capacity (ABC) or absolute number of antibodies bound to a single cell is the most important quantity to be determined [76, 77]. However, the molar absorption coefficient at the excitation wavelength and especially the fluorescence quantum yield can change dramatically upon attachment to an antibody [78]. Moreover, the number of fluorophores bound to a particular antibody is both difficult to control and to determine, and the label density can vary within a batch of labelled antibodies and between different batches. In addition, flow cytometers can only measure fluorescence intensities of micrometer-sized structures such as cells suspended in a liquid. As fluorescently labelled cells are perishable, the calibration of the fluorescence channel number of flow cytometers is commonly performed with sets of microbeads with different amounts of surface-bound fluorophores and assigned MESF units. These units express

the nominal fluorescence intensity of each type of microbead in terms of the number of free fluorophores in a standard solution giving an equivalent fluorescence intensity in the same matrix under similar measurement conditions [9, 79–81] (see also chapters on flow cytometry in this book). The application and reliability of the MESF concept requires well characterized bead-type MESF standards for typical fluorescent labels [82–84], but few standards of this type and required quality are available. In response to this, the flow cytometry community has strongly expressed the need for better standards of this type in recent years to assign MESF values [29–33, 85]. As a first step to meet these demands, NIST developed SRM 1932 mentioned in the previous section [43],<sup>7</sup> a concentration standard for fluorescein, the first fluorescence channel, FL1, in flow cytometers. SRM 1932 enables the determination of concentration curves and assignment of MESF values of suspensions of fluorescein-labeled beads, which can then be used to calibrate the fluorescence intensity scale of FL1 in terms of MESF values, as illustrated in Fig. 7, with the number density of the microbeads being determined with a Coulter counter. Based on this intensity calibration, the fluorescence intensity of a single cell stained with fluorescein-labeled antibodies is then determined in terms of MESF values.

Even though the MESF concept provides a straightforward intensity scale comparable across instruments, laboratories, and over time, it is not designed to derive the absolute number of fluorophores in a sample. In addition, the instability of many organic dyes, such as fluorescein, which are known to degrade when exposed to oxygen or light, requires fresh fluorophore solutions for each calibration. Accordingly, results over time depend on the reproducibility of these solutions. When applied to integral (broad-band) fluorescence intensities, such as those typically detected in flow cytometry, the MESF approach relies on matching fluorescence spectra of the fluorophore in the standard and in the sample or at least knowledge of the spectral deviations. Here, the availability of corrected emission spectra of fluorophore-labeled microbeads and representative samples in typically used solvents, for instance from NMIs, such as BAM and NIST, may be helpful to estimate the size of these contributions to the overall uncertainty of quantification. Moreover, the MESF methodology needs to be extended to the simultaneous measurement of multiple fluorophores to enable the development of assay kits that calibrate each one of the multiple fluorescence channels in terms of MESF units. One way to approach these challenges with the limited resources of NMIs could involve collaborations with manufacturers of MESF standards and the organization of regular interlaboratory comparisons.

---

<sup>7</sup> A standard fluorescein solution similar to SRM 1932 is sold by Invitrogen. See the on-line publication by Molecular Probes at [http://probes.invitrogen.com/lit/bioprob45/bp45\\_16.pdf](http://probes.invitrogen.com/lit/bioprob45/bp45_16.pdf).

## MESF Assignment Process

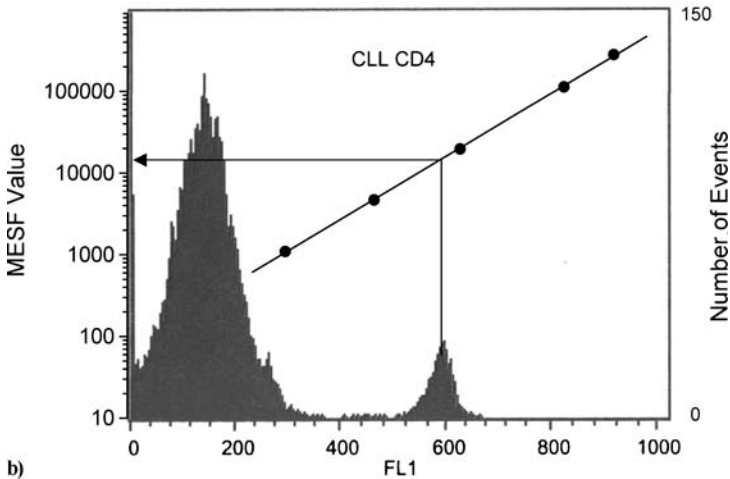
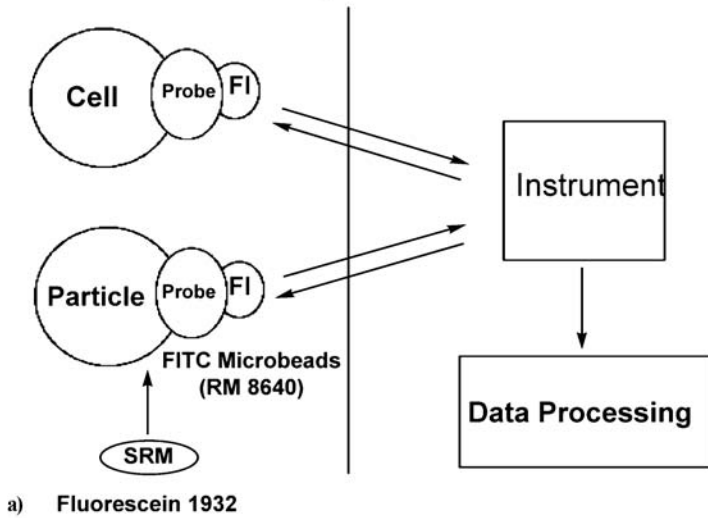


**Fig. 7** Illustration of the MESF assignment process. **a** MESF assignment of sets of microbeads with different amounts of surface-labeled fluorescein (RM 8640) with fluorescein solution (SRM 1932). These microbeads are used to calibrate the intensity axis of the fluorescence channel FL1 of flow cytometers thereby enabling the determination of the MESF values of fluorescein labeled cells. **b** Representative single-parameter histogram for CD4 T cells from a B-cell chronic lymphocytic leukemia (CLL) patient and a calibration curve generated with RM 8640 microbeads. The *vertical* and *horizontal* lines with *arrow* display the conversion of the channel number to the interpolated MESF values based on the calibration curve

## 2.5

### Standards for Day-to-Day and Instrument-to-Instrument Intensity

#### 2.5.1

##### General Applications

Most users of fluorescence techniques are not particularly interested in the measurement of absolute fluorescence intensities, but in the determination and consideration of the long-term stability of their fluorescence instrument and aging-induced changes in its absolute (spectral) sensitivity, as well as the comparability of fluorescence intensities across instruments. Accordingly, standards for day-to-day and instrument-to-instrument intensity are highly requested by many users of fluorescence techniques. Moreover, the availability of suitable standards of this type will strongly contribute to an improved quality assurance in fluorometry and eventually to the standardization of instrument qualification and method validation procedures for particular fluorescence techniques. Of equal interest for many users and especially for instrument manufacturers is the instrument's spectral sensitivity under a particular set of conditions or limit of detection for a particular analyte. Standard methods for measuring the range of linearity of fluorescence instruments, their dynamic range, and the limit of detection for particular analytes have been introduced by ASTM [12, 13], but the development of novel fit-for-purpose methods—preferably in combination with the supply of suited and well characterized materials to provide the necessary basis for the reliability and reproducibility of the respective procedure—along with their international acceptance is needed.

The significance of day-to-day and instrument-to-instrument standards is related not only to the ever-increasing use of fluorescence measurements and according need for the qualification of fluorescence instruments but also to the use of portable fluorometers, microplate and microarray readers, as well as fluorescence microscopes in drug discovery and clinical diagnostics. For these highly regulated areas, day-to-day and instrument-to-instrument standards are elegant tools to establish a comparable fit-for-purpose intensity scale as well as control charts [9, 10, 74, 79] for the comparison of fluorescence data over time and between laboratories. For the majority of these instruments, which are filter-based and accordingly perform integral and not spectrally resolved fluorescence measurements, spectral correction is not yet an issue.

Day-to-day and instrument-to-instrument intensity standards do not necessarily need to closely match routinely measured samples. However, they should be measurable with typical instrument settings to guarantee the reliability of the instrument performance and the determination of the spectral sensitivity under applicable conditions, e.g., at typical spectral irradiances, within a relevant spectral region [9]. The most stringent requirement is

either a sufficient, well-characterized stability under applicable conditions, or, for single-use standards, an excellent reproducibility, preferably in combination with an assigned uncertainty. Further prerequisites are known corrected spectra, if their intensities need to be compared with those of other fluorophores or between instruments with different spectral bandpasses.

The best-known day-to-day and instrument-to-instrument intensity standard of excellent stability is water (typically provided in a sealed cell to prevent the uptake of impurities) in combination with the so-called Raman test incorporated into the software of many spectrofluorometers [9, 54, 86].<sup>8</sup> Although very convenient, this method is effectively limited to excitation wavelengths below 400 nm due to the  $\lambda^{-4}$ -dependence of the intensity of scattered light. Fluorophores dissolved in a solvent or embedded into a solid matrix offer a greater flexibility with respect to the spectral region of excitation and emission. In the case of solutions of organic or inorganic dyes, their suitability is closely linked to the known purity of not only the dye, but also of the solvent. Depending on the chosen fluorophore, the close spectral match to typical fluorescent labels can be advantageous. Because many users of fluorescence techniques favor solid materials with an excellent long-term stability (desired shelf lives of two or more years) over liquid standards to be regularly replaced, inorganic fluorophores in a glass or polymer matrix are particularly attractive candidate materials [9, 51, 55, 69, 87]. As prerequisites for ease-of-use, such solid materials should be transparent, measurable without the use of polarizers, tested for the homogeneity of the fluorophore content and the long-term stability under application-specific conditions [36, 37],<sup>9</sup> and should come with an SOP for proper use. Ideally, they should also be usable for many different techniques and thus provided in different formats or shapes. Some materials are commercially available, but their corrected fluorescence spectra and other relevant information are typically not supplied or reported [9].

The significance of day-to-day and instrument-to-instrument intensity standards has motivated NIST and BAM to develop such materials in different formats for different fluorescence techniques ranging from steady-state fluorescence spectroscopy to fluorescence microscopy to fluorescence-based microarray technology. Attractive candidates currently tested by both institutes are inorganic glasses doped with inorganic fluorophores displaying either broad emission spectra, such as SRMs 2940 and 2941 [44, 45], or narrow line-shaped spectra covering the UV/Vis/NIR spectral regions [9, 51, 69]. These metal ion-doped glasses are very robust and do not photodegrade when excited by a fluorometer's conventional light source, even over long periods of

---

<sup>8</sup> This test, usually performed at an excitation wavelength of 350 nm and a detection wavelength of 397 nm, employs the Raman line of water to compare the long-term spectral sensitivity of a single fluorescence instrument or spectral sensitivities between instruments.

<sup>9</sup> The homogeneity of the dopant also needs to be considered as part of the photochemical stability studies to determine if local photo degradation effects are significant.

time. For instance, due to their excellent long-term stability, projected to be ten years, SRMs 2940 and 2941 are prescribed also for use as day-to-day intensity standards. Since many metal-ion-based dopants have comparably long emission lifetimes, on the order of milliseconds in many cases [88], when pulsed light sources are used, the emission properties of these dopants can be affected by measurement parameters, such as pulse duration, delay, and gate [9]. Accordingly, reference materials containing such dopants should be used as day-to-day intensity standards only for a constant set of measurement parameters. Their suitability as instrument-to-instrument intensity standards is linked to the application of comparable measurement conditions for the fluorescence instruments to be compared. As this is often difficult to guarantee, especially since many fluorescence users are not aware of the influence and control of the relevant instrument parameters, it is recommended to use materials containing such long lived emitters, as instrument-to-instrument intensity standards only with instruments using a continuous (non-pulsed) excitation source [9, 44, 45]. In addition to solid materials, BAM is investigating the potential of the liquid spectral fluorescence standards BAM-F001 to BAM-F005 for this application not only in a cuvette format, but also, e.g., in a slide-shaped microchannel device for fluorescence microscopy [9, 51, 64].

## 2.5.2

### **Selected Applications: Filter-Based Instruments**

The bright future of fluorescence-based assays and microarray experiments in medical diagnostics and drug discovery encouraged NIST and BAM to dedicate resources to the development of day-to-day intensity and instrument-to-instrument intensity standards for these areas. Moreover, instrument qualification is an important part of assay validation as required by regulatory agencies, such as the United States Food and Drug Administration (FDA). The majority of microplate readers, certain types of fluorescence microscopes, microarray readers and scanners, as well as portable fluorometers are filter-based instruments that use bandpass filters for wavelength and bandwidth selection of both excitation and emission. These filters typically have a maximum transmittance near the wavelength corresponding to the excitation or emission maximum of the dye of interest. However, the spectral transmittance of these filters often varies between manufacturers and on a batch-to-batch basis. This, combined with the instrument-specific, spectral responsivity of the detection system, makes fluorophore-specific intensity standards, based on the same fluorescent labels as used in assays, very attractive. When the standard and label are spectrally matched, neither a correction for filter transmittance nor for the spectral responsivity of the detection system has to be performed. Due to the ever-increasing number of fluorescent dyes, however, the production of a standard for every type of fluorescent label is not practical or straightforward and is thus not currently followed either by NIST

or BAM. Commercial fluorophore-specific standards are available, e.g., for the labels Cy3 and Cy5.

Day-to-day intensity standards for microplate readers can be made from solid materials, such as the chromophore-doped glasses already being studied at NIST and BAM. In principle, such standards can be produced by putting a mask over a glass slide, thereby mimicking, e.g., a 96-well microplate, or by filling the wells of a validation microplate with solid materials [87]. In addition, a microfluidic approach, which is generally gaining in importance in the assay area, may be suitable for the adaptation of liquid fluorescence standards to the characterization of microplate readers. Both NIST and BAM have tested existing liquid CRMs for the characterization of microplate readers. For instance, SRM 1932 fluorescein solution has been used in an interlaboratory comparison of NMIs to evaluate non-biological variations associated with 96-well microplate readers, i.e., for the determination of the limit of detection, dynamic range, and instrument variables [89].<sup>10</sup> BAM successfully employed BAM-F001 through BAM-F005 for the determination of the relative spectral responsivity of monochromator-based fluorescence microplate readers and for the determination of the range of linearity and limit of detection of both filter- and monochromator-based instruments [51, 64].

The variability in the spectral characteristics of filters does not affect the use of day-to-day intensity standards as long as the same filter is always employed. This variability, however, can affect the signals obtained with instrument-to-instrument intensity standards. To account for the influence of the wavelength dependence of the transmittance of such filters on measured fluorescence intensities, the transmittance spectra of individual filters, or batches of filters need to be known. One approach for producing an effective intensity standard currently discussed at NIST is the supply of a suitable reference material for a particular spectral region, similar to a spectral correction standard, along with software that can link the measured fluorescence intensity onto an absolute scale by considering the transmittance spectrum of the filters used, along with the corrected fluorescence spectrum of the standard. This is one possible way to compare spectral sensitivity and absolute intensity between instruments that use the same type of filter set, without relying on standards that must spectrally match specific fluorescent labels.

Generally, the quality assurance in the assay area could benefit from a closer collaboration of standard manufacturers with NMIs, in addition to the development of standards by NMIs. For instance, NMIs could aid in the determination of desirable characteristics of existing commercial standards and validation microplates, such as photostability, homogeneity of the fluorescence intensity across the plate, corrected emission spectra, and NMI

---

<sup>10</sup> CCQM P58 “Fluorescence measurement for the life sciences” with CCQM referring to the committee consultative de la matiere and mutual recognition agreement.

traceability. NMIs could also contribute to the development of guidelines for instrument performance validation, together with instrument and standard manufacturers, regulatory agencies, technical and scientific organizations, and users from industry and academics.

The obvious future importance of microarray technology in strongly regulated areas, such as medical diagnostics and homeland security, motivated NIST to get involved with the development of instrument-type and biological standards for this research area [9]. The logistics of developing, producing, and certifying day-to-day and instrument-to-instrument intensity standards for fluorescence-based microarray scanners are further complicated, beyond that of standards for microplate readers, by the use of a focused laser for the excitation of small blotted samples, on the order of 10 to 100  $\mu\text{m}$ , which are scanned similarly to a confocal microscope. Accordingly, a standard suitable for the characterization of a microarray scanner needs to be several orders of magnitude more photostable compared to a corresponding intensity standard for spectrofluorometry. In addition, the fluorescence intensity from the standard has to be independent of the instrument geometry at a constant laser spot volume and power, as some microarray readers use an epifluorescence and others a transmitting measurement geometry. Ideally, a fit-for-purpose standard should be made in a blotted pattern similar to a typically measured biochip. However, it is almost impossible to reach the necessary homogeneity and photostability with such a design. A fluorescent film is likely to be a better candidate for achieving these characteristics. Such a film should be comparable to or thinner than the size of the focused laser spot, typically having a 5  $\mu\text{m}$  to 10  $\mu\text{m}$  diameter, to render the fluorescence intensity independent of instrument geometry.

Only recently, a microarray standards interest group, which includes representatives from most of the major microarray reader manufacturers and from NIST, agreed on specifications for two standards for day-to-day and instrument-to-instrument intensity comparison and calibration. One standard should possess a typical medium intensity, corresponding to about 500 fluorophores per square micrometer, and the other a low intensity, corresponding to about 0.5 fluorophores per square micrometer (see Fig. 8). Both standards will be based on a continuous fluorescent thin film on a 1 mm thick glass slide with a coating thickness of less than 10  $\mu\text{m}$ . These standards will be certified as possessing an intensity uniformity of 99% or better averaged over areas of 250  $\mu\text{m}^2$ , when excited at 532 and 633 nm and supplied with the certified corrected emission spectrum. The same pair of standards can be used for both excitation wavelengths or one pair can be made for each wavelength, depending on the characteristics of the potential candidates. NIST is presently characterizing candidate materials in collaboration with commercial material manufacturers to determine if materials that appropriately fit the desired standards criteria can be found.



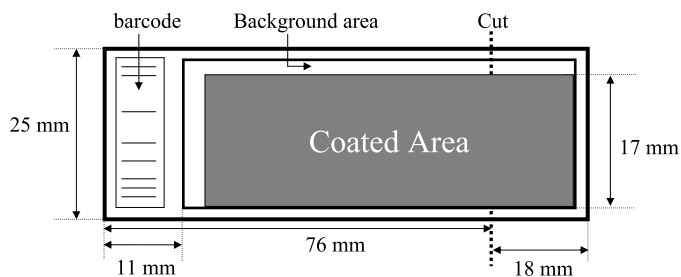


**Fig. 8** Design of consensus material standards for microarrays. Comprised of a glass slide (thickness of 0.7 to 1.0 mm) coated with a fluorescent thin film (thickness of 10  $\mu\text{m}$  or less) with a fluorescence intensity uniformity of 99% over 250  $\mu\text{m}$  scanning subareas. An uncoated background area and a barcode will be used to subtract substrate fluorescence and to identify the sample. To produce standards at the two most commonly used chip sizes the standard will be cut along the *dotted line*

Meanwhile, NIST is also testing a commercially available validation slide from Full Moon BioSystems<sup>11</sup> to assess the performance of an array scanner (see also Chap 26 [90]). This slide is composed of a series of known concentrations of either Cy3 or Cy5 embedded in a polymer matrix and, in principle, can be used to validate the scanners in terms of dynamic range, detection limit, and scanning uniformity [91, 92]. The emission spectrum of Cy5 fluorophores on oligonucleotide microarray slides matches that on the commercial validation slide and the spectrum of the Cy3 fluorophores on this slide is red-shifted by 5 nm in comparison to that on the oligonucleotide arrays [93]. This slide does photodegrade, but preliminary results suggest that fluorescence intensity changes with time and between instruments are detectable using this slide.

### 3

## Conclusion

The urgent need for fluorescence calibration standards and day-to-day intensity standards for the UV/Vis/NIR spectral region motivated NIST and BAM to develop certified reference materials to meet these demands and to perform a first interlaboratory comparison on spectral correction. The ultimate goal here is to make fluorescence measurements comparable across instruments, laboratories and over time. This comparison marks the beginning of a fruitful collaboration of NMIs in this area.

<sup>11</sup> Certain commercial equipment, instruments, or materials are identified in this chapter to foster understanding. Such identification does not imply recommendation or endorsement by the National Institute of Standards and Technology, nor does it imply that the materials or equipment identified are necessarily the best available for the purpose.

To improve the quality assurance in fluorometry and the comparability of fluorescence data on a broad level, reliable, yet fit-for-purpose, fluorescence standards with certified, calibration-relevant properties are mandatory, along with internationally accepted recommendations and guidelines for instrument calibration and performance validation. The fulfillment of these requirements encourages a close interaction and collaboration between NMIs, instrument manufacturers, and regulatory agencies. To help users of fluorescence techniques with the choice of fit-for-purpose standards, quality criteria for the different classes of fluorescence standards in need have been defined by NIST and BAM. Moreover, the determination of uncertainties for representative fluorescence measurements for different fluorescence techniques seems to be helpful, including interlaboratory comparisons between NMIs, expert laboratories, and routine users. These collaborations help to establish the achievable repeatability and accuracy of analyte determinations and assay results that can be eventually considered in recommendations and guidelines. Additionally, workshops and special training courses on drawbacks and sources of uncertainties of fluorescence techniques and instrument characterization—jointly organized by NMIs—may help to broaden the understanding for the need of an improved quality assurance in fluorometry within the fluorescence community.

**Acknowledgements** PCD would like to thank Doug Blackburn for producing a variety of metal ion-doped glasses, Dave Holbrook of the NIST Surface and Microanalysis Science Division for his EEM work including Fig. 4, and Steve Choquette and Mary Satterfield of the NIST Biochemical Science Division for helpful discussions and microarray related work. UR gratefully acknowledges financial support from the Federal Ministry of Economics and Technology (BMW; grants VI A 2-18/01 and VI A 2-17/03) and the German Ministry of Education and Research (BMBF; grant 13N8848).

## References

1. Lakowicz JR (ed) (1999) Principles of fluorescence spectroscopy, 2nd edn. Kluwer Academic/Plenum Press, New York
2. Lakowicz JR (ed) (1992–2004) Topics in fluorescence spectroscopy series, Vol. 1–8. Plenum Press, New York
3. Valeur B (ed) (2002) Molecular Fluorescence, Principles and Applications. Wiley-VCH, Weinheim
4. Wolfbeis OS (ed) (2001–2004) Springer series on fluorescence, methods and applications, Vol. 1–3. Springer, Berlin Heidelberg New York
5. Schulman SG (ed) (1985–1993) Molecular luminescence spectroscopy, Parts 1–3. Wiley Interscience, New York
6. Mason WT (1999) Fluorescent and luminescent probes for biological activity, 2nd edn. Academic Press, San Diego
7. Stokes GG (1852) On the change of refrangibility of light. *Phil Trans R Soc Lond* 142:463
8. Udenfriend S (1995) Development of the spectrophotofluorometer and its commercialization. *Protein Sci* 4:542

9. Resch-Genger U, Hoffmann K, Nietfeld W, Engel A, Ebert B, Macdonald R, Neukammer J, Pfeifer D, Hoffmann A (2005) How to improve quality assurance in fluorometry: fluorescence-inherent sources of error and suited fluorescence standards. *J Fluoresc* 15:337
10. Gaigalas AK, Li L, Henderson O, Vogt R, Barr J, Marti G, Weaver J, Schwartz A (2001) The development of fluorescence intensity standards. *J Res Nat Inst Stand Technol* 106:381
11. ASTM E 388-04 (2004) Spectral bandwidth and wavelength accuracy of fluorescence spectrometers. In: Annual book of ASTM standards, vol 03.06 (original version 1972)
12. ASTM E 578-01 (2001) Linearity of fluorescence measuring system. In: Annual book of ASTM standards, vol 03.06 (original version 1983)
13. ASTM E 579-04 (2004) Limit of detection of fluorescence of quinine sulfate. In: Annual book of ASTM standards, vol 03.06 (original version 1984)
14. Miller JN (ed) (1981) *Techniques in visible and ultraviolet spectrometry*, Vol. 2, Standards in fluorescence spectrometry. Chapman and Hall, New York
15. Eaton DF (1988) Reference compounds for fluorescent measurements. *Pure Appl Chem* 60:1107
16. Eaton DF (1990) Recommended methods for fluorescence decay analysis. *Pure Appl Chem* 62:1631
17. Shelton CF (1968) NBS Tech Note 417, Spectral emission properties of NBS standard phosphor samples under photo-excitation. US Government Printing Office, Washington, DC
18. Mavrodineanu R, Shultz JI, Menis O (eds) (1973) NBS Spec Pub 378, Accuracy in spectrophotometry and luminescence measurements. US Government Printing Office, Washington, DC (first appeared in (1972) *J Res Nat Bur Stand* 76A)
19. Mielenz KD, Velapoldi RA, Mavrodineanu R (eds) (1977) NBS Spec Pub 466, Standardization in spectrophotometry and luminescence measurements. US Government Printing Office, Washington, DC (first appeared in (1976) *J Res Nat Bur Stand* 80A)
20. Cehelnik ED, Mielenz KD, Velapoldi RA (1975) Polarization effects on fluorescence measurements. *J Res Nat Bur Stand* 79A:1
21. Mielenz KD, Cehelnik ED, McKenzie RL (1976) Elimination of polarization bias in fluorescence intensity measurements. *J Chem Phys* 64:370
22. Velapoldi RA, Mielenz KD (1980) NBS Spec Pub 260-64, A fluorescence standard reference material: quinine sulfate dihydrate. US Government Printing Office, Washington, DC
23. (1979) Certificate of analysis, Standard Reference Material 936, quinine sulfate dihydrate. National Bureau of Standards (This certificate is expired, replaced by [25])
24. (1994) Certificate of analysis, Standard Reference Material 936a, quinine sulfate dihydrate. National Institute of Standards and Technology (<http://ts.nist.gov/ts/htdocs/230/232/232.htm>)
25. (1989) Certificate of analysis, Standard Reference Material 1931, fluorescence emission standards for the visible region. National Institute of Standards and Technology (This SRM is no longer available.)
26. Thompson A, Eckerle KL (1989) Standards for corrected fluorescence spectra. *Proc SPIE-Int Soc Opt Eng* 1054:20
27. Saunders G, Parkes H (1999) *Analytical molecular biology: quality and validation*. RSC, Cambridge
28. (2005) ISO/IEC 17025, 2nd edn. International Organization for Standardization, Geneva

29. DeRose PC (2000) NIST workshop on luminescence standards for chemical analysis, Sept 1999. *J Res Nat Inst Stand Technol* 105:631 (<http://nvl.nist.gov/pub/nistpubs/jres/105/4/j54ce-der.pdf>)
30. Workshop (Jan 1998) Fluorescence intensity standards. NIST
31. Workshop (June 2000) New directions in fluorescence intensity standards. NIST
32. Workshop (March 2005) Towards national traceability in fluorescence intensity measurements. NIST
33. Workshop (Feb 2006) Improved antibody-based metrology in flow cytometry, NIST (comment: a ref. article should be available soon, the other 3 workshops, refs 31–33 were the precursors to this one)
34. Workshop (Dec 2002) Fluorescence standards for microarray assays. NIST (<http://www.cstl.nist.gov/biotech/fluormicroarray/FluorMicroarrayWkshp12-10-2002.html>)
35. Workshop (June 2003) Bioanalytical and biomedical applications of fluorescence techniques: instrument characterization and validation, traceability and need for reference materials. Resch-Genger U (BAM), Macdonald R (PTB), BERM-9
36. (2000) ISO; General Requirements for the Competence of Reference Material Producers, Second edition
37. (2003, draft) ISO; Reference materials — General and statistical principles for certification.
38. (1993) ISO; Guide to the expression of uncertainty in measurement; ISBN 92-67-10188-9, 1st edn. International Organization for Standardization, Geneva
39. DeRose PC, Kramer GW (2005) Bias in the absorption coefficient determination of a fluorescent dye, Standard Reference Material 1932 fluorescein solution. *J Luminesc* 113:314
40. Benson RC, Kues HA (1977) Absorption and fluorescence properties of cyanine dyes. *J Chem Eng Data* 22:379
41. Resch-Genger U, Pfeifer D, Hoffmann K, Flachenecker G, Hoffmann A, Monte C (2008) Linking fluorometry to radiometry: traceability and physical and fluorescence Standards. In: Resch-Genger U (ed) *Standardization in Fluorometry: State-of-the Art and Future Challenges*. Springer, Berlin Heidelberg
42. May W, Parris R, Beck C, Fassett J, Greenberg R, Guenther F, Kramer G, Wise S, Gills T, Colbert J, Gettings R, MacDonald B (2000) Definitions of terms and modes used at NIST for value-assignment of reference materials for chemical measurements, NIST Special Publication 260-136. US Government Printing Office, Washington, DC
43. (2004) Certificate of analysis, Standard Reference Material 1932, Fluorescein solution. National Institute of Standards and Technology (<http://ts.nist.gov/ts/htdocs/230/232/232.htm>)
44. (2007) Certificate of analysis, Standard Reference Material 2940, Relative intensity correction standard for fluorescence spectroscopy: Orange emission. National Institute of Standards and Technology. Certification of emission spectra in 1 nm-intervals. (<http://ts.nist.gov/ts/htdocs/230/232/232.htm>)
45. (2007) Certificate of analysis, Standard Reference Material 2941, Relative intensity correction standard for fluorescence spectroscopy: Green emission. National Institute of Standards and Technology. Certification of emission spectra in 1 nm-intervals. (<http://ts.nist.gov/ts/htdocs/230/232/232.htm>)
46. (2006) Certificate of analysis, Certified Reference Material BAM-F001, Spectral fluorescence standard for the determination of the relative spectral responsivity of fluorescence instruments within its emission range. Federal Institute for Materials Research and Testing (BAM)

47. (2006) Certificate of analysis, Certified Reference Material BAM-F002, Spectral fluorescence standard for the determination of the relative spectral responsivity of fluorescence instruments within its emission range. Federal Institute for Materials Research and Testing (BAM)
48. (2006) Certificate of analysis, Certified Reference Material BAM-F003, Spectral fluorescence standard for the determination of the relative spectral responsivity of fluorescence instruments within its emission range. Federal Institute for Materials Research and Testing (BAM)
49. (2006) Certificate of analysis, Certified Reference Material BAM-F004, Spectral fluorescence standard for the determination of the relative spectral responsivity of fluorescence instruments within its emission range. Federal Institute for Materials Research and Testing (BAM)
50. (2006) Certificate of analysis, Certified Reference Material BAM-F005, Spectral fluorescence standard for the determination of the relative spectral responsivity of fluorescence instruments within its emission range. Federal Institute for Materials Research and Testing (BAM)
51. Hoffmann K, Monte C, Pfeifer D, Resch-Genger U (2005) Standards in fluorescence spectroscopy: Simple tool for the characterization of fluorescence instruments, *GIT Lab J Eur* 9:29
52. Hofstraat JW, Latuhihin MJ (1994) Correction of fluorescence spectra. *Appl Spectrosc* 48:436
53. Gardecki JA, Maroncelli M (1998) Set of secondary emission standards for calibration of the spectral responsivity in emission spectroscopy. *Appl Spectrosc* 52:1179
54. Kovach RJ, Peterson WM (1994) The measurement of sensitivity in fluorescence spectroscopy. *Am Lab* 26:G32
55. Lifshitz IT, Meilman ML (1989) Standard sample for calibrating wavelength scales of spectral fluorimeters. *Sov J Opt Technol* 55:487
56. Hollandt J, Taubert DR, Seidel J, Resch-Genger U, Gugg-Helminger A, Pfeifer D, Monte C (2005) Traceability in fluorometry: Part I, Physical standards. *J Fluoresc* 15:301
57. Monte C, Resch-Genger U, Pfeifer D, Taubert RD, Hollandt J (2006) Linking fluorescence measurement to radiometric units. *Metrologia* 43:S89
58. DeRose PC, Early EA, Kramer GW (2007) Qualification of a fluorescence spectrometer for measuring true fluorescence spectra. *Rev Sci Instrum* 78:033107
59. DeRose PC, Early EA, Kramer GW (2008) Measuring and certifying true fluorescence spectra with a qualified fluorescence spectrometer. In: *Proc 5th Oxford Conf on spectrometry*. Crown, UK
60. Zwinkels J (2008) Surface fluorescence: the only standardized method of measuring luminescence. In: Resch-Genger U (ed) *Standardization in Fluorometry: State-of-the Art and Future Challenges*, Springer, Berlin Heidelberg
61. Resch-Genger U, Pfeifer D (2006) Certification report, Calibration kit Spectral fluorescence standards BAM-F001–BAM-F005, BAM, Berlin
62. (2006) Certificate of analysis, Certified reference materials BAM-F001–BAM-F005, Calibration Kit, Spectral Fluorescence Standards for the determination of the relative spectral responsivity of fluorescence instruments. Federal Institute for Materials Research and Testing (BAM). Certification according to ISO guides 34 and 35 in 1 nm-steps for three different spectral bandpasses of the BAM fluorometer.
63. Pfeifer D, Hoffmann K, Hoffmann A, Monte C, Resch-Genger U (2006) The calibration kit, Spectral fluorescence standards: A simple tool for the standardization of the spectral characteristics of fluorescence instruments. *J Fluoresc* 16:581

64. Hoffmann K, Resch-Genger U, Nitschke R (2005) Simple tool for the standardization of confocal spectral imaging systems. *GIT Imaging Microsc* 3:18
65. DeRose PC, Smith MV, Blackburn DH, Kramer GW (2008) Characterization of Standard Reference Material 2941, uranyl-ion-doped glass, spectral correction standard for fluorescence. *J Luminesc* 128:257
66. [www.physics.nist.gov/PhysRefData/Handbook/index.html](http://www.physics.nist.gov/PhysRefData/Handbook/index.html)
67. Harrison GR (1982) MIT wavelength tables, Vol. 2, Wavelengths by element. MIT Press, Cambridge, MA
68. Zaidel AN, Prokofev VK, Raikii SM, Slavnyi VA, Shreider EY (1970) Tables of spectral lines. Plenum Press, New York
69. Velapoldi RA, Epstein MS (1989) Luminescence standards for macro- and microspectrofluorimetry. In: Goldberg MC (ed) ACS symposium series 383, Luminescence applications in biological, chemical, environmental and hydrological sciences. American Chemical Society, Washington, DC, p 98
70. Rurack K (2008) Fluorescence quantum yields: traceability, methods of determination and standards. In: Resch-Genger U (ed) *Standardization in Fluorometry: State-of-the Art and Future Challenges*, Springer, Berlin Heidelberg
71. de Mello JC, Wittmann HF, Friend RH (1997) An improved experimental determination of external photoluminescence quantum efficiency. *Adv Mater* 9:230
72. Wise SA, Sander LC, May WE (1993) Determination of polycyclic aromatic hydrocarbons by liquid chromatography. *J Chromatogr* 642:329
73. Duewer DL, Parris RM, White V E, May WE, Elbaum H (2004) NIST Spec Pub 1012, An approach to the metrologically sound traceable assessment of the chemical purity of organic reference materials. US Government Printing Office, Washington, DC
74. Schwartz A, Gaigalas AK, Wang L, Marti GE, Vogt RF, Fernandez-Repollet E (2004) Formalization of the MESF unit of fluorescence intensity. *Cytometry* 57B:1
75. (2004) Report of Investigation, Reference Material 8640, Microspheres with immobilized fluorescein isothiocyanate. National Institute of Standards and Technology
76. Hultin LE, Matud JL, Giorgi JV (1998) Quantitation of CD38 activation antigen expression on CD8+ T cells in HIV-1 infection using CD4 expression on CD4+ T lymphocytes as a biological calibrator. *Cytometry* 33:123
77. Iyer SB, Hultin LE, Zawadzki JA, Davis KA, Giorgi JV (1998) Quantitation of CD38 expression using QuantiBRITE™ beads. *Cytometry* 33:206
78. Gruber HJ, Hahn CD, Kada C, Riener CK, Harms GS, Ahrer W (2000) Anomalous fluorescence enhancement of Cy3 and Cy3.5 versus anomalous fluorescence loss of Cy5 and Cy7 upon covalently linking to IgG and noncovalent binding to avidin. *Bioconj Chem* 11:696
79. Wang L, Gaigalas AK, Abbasi F, Marti GE, Vogt RF, Schwartz A (2002) Quantitating fluorescence intensity from fluorophores: Practical use of MESF values. *J Res Nat Inst Stand Technol* 107:339
80. Lenkei R, Mandy F, Marti G, Vogt R (eds) (1998) Special issue on quantitative fluorescence cytometry: An emerging consensus. *Cytometry* 33
81. Schwartz A, Wang L, Early E, Gaigalas AK, Zhang Y-Z, Marti GE, Vogt RF (2002) Quantitating fluorescence intensity from fluorophores: The definition of MESF assignment. *J Res Nat Inst Stand Technol* 107:83
82. Schwartz A, Marti GE, Gratama JW, Fernandez-Repollet E (1998) Standardizing flow cytometry: A classification system of fluorescence standards used for flow cytometry. *Cytometry* 33:106
83. Schwartz A, Mendez M, Santiago G, Diaz L, Fernandez-Repollet E (1997) Applications of common quantitative fluorescent standards to multiple platforms: Com-

- parison of commercial fluorescent calibration standards used in quantitative flow cytometry immunophenotyping analysis as a function of pH environment. *Clin Immunol* 17:14
84. Zenger VE, Vogt R, Mandy F, Schwartz A, Marti GE (1998), Quantitative flow cytometry: interlaboratory-variation. *Cytometry* 33:138
  85. Marti GE, Vogt RF, Gaigalas AK, Hixson CS, Hoffman RA, Lenkei R, Magruder LE, Purvis NB, Schwartz A, Shapiro HM, Waggoner A (2004) Fluorescence calibration and quantitative measurements of fluorescence intensity, Approved guideline, NCCLS, I/LA24-A, vol 24 No. 26
  86. Froehlich P (1989) Under the sensitivity specification for a fluorescence spectrophotometer. *Int Lab* 19:42
  87. Gibeler R, McGown E, French T, Owicki JC (2005) Performance validation of microplate fluorimeters. *J Fluoresc* 15:363
  88. Parke S, Watson AI, Webb RS (1970) Fluorescence decay times of divalent manganese in inorganic glasses. *J Phys D Appl Phys* 3:763
  89. Howarth P, Redgrave F (2003) *Metrology in short*, 2nd edn. MKom Aps, Denmark
  90. Sige Z, He H-J, Zong Y, Shi L, Wang L (2008) DNA microarrays: applications, future trends and need for standardization. In: Resch-Genger U (ed) *Standardization in Fluorometry: State-of-the Art and Future Challenges*. Springer, Berlin Heidelberg
  91. Zong Y, Wang Y, Zhang S, Shi Y (2003) How to evaluate a microarray scanner. In: Hardiman G (ed) *Microarrays methods and applications-nuts & bolts*. DNA Press, USA
  92. Shi L, Tong W, Su Z, Han T, Han J, Puri RK, Fang H, Frueh FW, Goodsaid FM, Guo L, Branham WS, Chen JJ, Xu ZA, Harris SC, Hong H, Xie Q, Perkins RG, Fuscoe JC (2005) Microarray scanner calibration curves: characteristics and implications. *BMC Bioinformatics* 6:S11
  93. Wang L, Gaigalas AK, Satterfield MB, Salit M, Noble J (2007) Evaluating the quality of data from microarray measurements. *Methods Mol Biol* 381:121

## **Part II**

# **Steady State Fluorometry**



# Linking Fluorometry to Radiometry with Physical and Chemical Transfer Standards: Instrument Characterization and Traceable Fluorescence Measurements

U. Resch-Genger<sup>1</sup> (✉) · D. Pfeifer<sup>1</sup> · K. Hoffmann<sup>1</sup> · G. Flachenecker<sup>1</sup> ·  
A. Hoffmann<sup>1</sup> · C. Monte<sup>2</sup>

<sup>1</sup>Federal Institute for Materials Research and Testing (BAM),  
Richard-Willstaetter-Str. 11, 12489 Berlin, Germany  
*ute.resch@bam.de*

<sup>2</sup>Physikalisch-Technische Bundesanstalt (PTB), Abbéstr. 2–12, 10587 Berlin, Germany

1	Introduction . . . . .	67
2	Quantities Affecting Photoluminescence . . . . .	68
3	Characterization of Fluorescence Instruments and Comparable Fluorescence Measurements . . . . .	71
3.1	Measurement Conditions and Requirements on Standards . . . . .	72
3.2	Linking Fluorescence Measurements to Radiometric and Physical Scales . .	73
3.3	Relative vs Absolute Instrument Characterization . . . . .	75
3.4	Guidelines and Recommendations on Instrument Qualification . . . . .	75
3.5	Linearity of the Detection System . . . . .	76
3.6	Wavelength Accuracy . . . . .	78
3.7	Spectral Responsivity of the Emission Channel . . . . .	80
3.8	Emission Standards . . . . .	82
3.9	Radiometric Reference Quantity and Photonic Nature of Emitted Light . .	86
3.10	Spectral Irradiance of the Excitation Channel . . . . .	87
3.11	Instrument Performance Validation (IPV) . . . . .	89
3.12	Future Trends: Absolute Fluorescence Measurements . . . . .	91
3.13	Impact on Other Fluorescence Techniques . . . . .	93
4	Conclusion . . . . .	93
	References . . . . .	94

**Abstract** Problems associated with the measurement of photoluminescence are briefly reviewed, including relevant instrument parameters affecting these measurements. Procedures for the characterization of relevant instruments are discussed, focusing on spectrofluorometers, and fit-for-purpose methods including suitable standards are recommended. The aim here is to increase the awareness of the importance of reliable instrument characterization and to improve the comparability of measurements of photoluminescence.

**Keywords** Calibration · Emission standards · Fluorescence intensity standards · Fluorescence standards · Quality assurance · Spectral correction

**Abbreviations**

ASTM	ASTM International
BAM	Federal Institute for Materials Research and Testing, Germany
CIPM	Comité Internationale des Poids et Mesures
CLSI	Clinical and Laboratory Standards Institute (formerly known as NCCLS)
CRM	Certified reference material
GUM	Guide to the expression of uncertainty of measurement
IPV	Instrument performance validation
ISO	International Organization for Standardization, Geneva
IUPAC	International Union of Pure and Applied Chemistry
MRA	Mutual recognition arrangement
NBS	National Bureau of Standards, USA
NIST	National Institute of Standards and Technology, USA (formerly NBS)
NMI	National Metrology Institute
NPL	National Physics Laboratory
NRC	National Research Council, Canada
PTB	Physikalisch-Technische Bundesanstalt, Germany
SI	Système International d'Unités
SOP	Standard operation procedure
SRM	Standard reference material
$f$	Absorption factor ( $f(\lambda_{ex})$ ); $f(\lambda_{ex})$ equals the absorbance $\alpha(\lambda_{ex})$
$\alpha$	Absorbance; $\alpha(\lambda_{ex})$ : absorbance at excitation wavelength
$r$	Emission anisotropy
$G$	Geometry factor
$\varepsilon$	Molar absorption coefficient at the excitation wavelength ( $\varepsilon(\lambda_{ex})$ )
$I_m(\lambda_{ex}, \lambda_{em})$	Measured fluorescence signal (excitation and emission) containing instrument-dependent and sample-specific contributions and background signals (e.g., scattering and fluorescence from the solvent and dark counts at the detector)
$I_c(\lambda_{em})$	Corrected, i.e., instrument-independent, fluorescence emission spectrum
$I_u(\lambda_{em})$	(Spectrally) uncorrected (background-corrected) emission spectrum
$Q^{F00x}(\lambda_{em})$	Quotient of corrected and uncorrected fluorescence spectrum for each component of the BAM Calibration Kit <i>Spectral Fluorescence Standards F00x</i> with $x = 1$ to $5$
$N_{em}$	Number of emitted photons
$N_{abs}$	Number of absorbed photons
$l$	Optical path length
$h$	Planck's constant
$\Phi_1$	quantum yield of photoluminescence
$F_\lambda(\lambda_{ex}, \lambda_{em})$	Spectral fluorescence yield relation to absolute quantum yield $\Phi_1$ : $\Phi_1(\lambda_{ex}) = \int_{\lambda_{ex}}^{\infty} \frac{\lambda}{\lambda_{ex}} F_\lambda(\lambda_{ex}, \lambda_{em}) d\lambda_{em}$
$L_\lambda$	Spectral radiance
$L_{p\lambda}$	Spectral photon radiance (equaling $L_\lambda \times \lambda / (hc)$ )
$E$	Irradiance; $E = \int_{\lambda_{ex}-\Delta\lambda/2}^{\lambda_{ex}+\Delta\lambda/2} E_\lambda(\lambda) d\lambda$ , where $E_\lambda$ is the spectral irradiance at wavelength $\lambda$ , $\lambda_{ex}$ the excitation wavelength, and $\Delta\lambda$ the spectral bandwidth used for excitation
$E_\lambda$	Spectral irradiance

$E_{p\lambda}$	Spectral photon irradiance (equaling $E_\lambda \times \lambda / (hc)$ )
$s$	Spectral responsivity
$c$	Velocity of light in vacuo
$\lambda$	Wavelength (e.g., emission wavelength $\lambda_{em}$ or excitation wavelength $\lambda_{ex}$ )

The subscript  $\lambda$  always denotes per nanometer or spectral. The only exception here is the spectral responsivity  $s$ . Due to radiometric convention,  $s$  always implies  $s_\lambda$ . The subscript  $p$  is used as a description for energy units related to photon energy denoting per second and photon. The indices  $ex$ ,  $em$ , and  $abs$  symbolize excitation, emission, and absorption. The term intensity that represents the recorded fluorescence signal is used as a description of radiant flux or radiant power.

## 1 Introduction

Fluorescence techniques that measure analyte-specific fluorescence quantities, such as emission and excitation spectra, fluorescence quantum yield, fluorescence lifetime, and emission anisotropy, are amongst the most widely used analytical techniques in materials science, environmental analysis, biology, clinical chemistry, and medical diagnostics [1–6]. Advantageous are their comparable ease of use, noninvasive character, potential for combining spectrally, temporally, and spatially resolved measurements, and suitability for multiplexing and remote sensing, as well as the sensitivity of fluorescence detection techniques down to the single molecule level. Drawbacks of all fluorescence-based analytical and detection methods are, however, intensity<sup>-1</sup>, wavelength-, polarization-, and time-dependent instrument-specific contributions to otherwise dye- or analyte-specific signals and general difficulties in accurately measuring absolute fluorescence intensities [7–16]. This limits the comparability of luminescence data across instruments and, for the same instrument, over time, especially if these instrument-specific effects are not properly removed. Simultaneously, these instrument-specific dependences—in conjunction with the dependence of the spectroscopic properties of most chromophores on their microenvironment—render quantitation from measurements of relative fluorescence intensities difficult. Critical with respect to these fluorescence-inherent drawbacks is the comparatively small number of reliable standards for instrument characterization and instrument performance validation (IPV) in combination with the few recommendations on instrument qualification and quality assurance in fluorometry [17–21]. With the exception of colorimetry or surface fluorescence [22–24] and in part flow cytometry [25, 26], the standardization of

---

<sup>1</sup> For the convenience of the majority of readers, the term intensity is not used in the correct radiometric sense, i.e., as flux per solid angle, but rather in the more common traditional sense as a description of radiant flux or radiant power.

fluorescence measurements is still in its infancy despite the frequent use and the importance of fluorescence techniques for strongly regulated areas, such as medical diagnostics and drug discovery [12], the often addressed need for the correction of fluorescence data for instrument-specific signal contributions [17–21, 27], pressure from regulatory agencies, and the globalization-induced trends of quality assurance, traceability, and accreditation [28, 29].

In this article, strategies and methods for the characterization and performance validation of fluorescence instruments are discussed employing physical and chemical, i.e., chromophore-based, transfer standards. Special emphasis is dedicated to linking fluorescence measurements to radiometric units and to steady-state fluorometry. Aiming at an improved quality assurance for fluorescence techniques on a broad level, criteria for the choice of fit-for-purpose standards are provided. Also, simple and straightforward procedures for instrument qualification under application-relevant conditions are presented that can be eventually standardized. These standards and procedures can be adapted to many different fluorescence techniques with proper consideration of the underlying measurement principles and method-specific requirements.

## 2 Quantities Affecting Photoluminescence

For each luminescence technique, measured fluorescence signals, which reflect the fluorescence intensity  $I_m(\lambda_{\text{ex}}, \lambda_{\text{em}})$  within the spectral bandwidth of excitation ( $\Delta\lambda_{\text{ex}}$ ) and emission ( $\Delta\lambda_{\text{em}}$ ), are determined by both instrument- and analyte-specific quantities, see Eq. 1.<sup>2</sup> *Instrument-specific quantities* include the spectral irradiance  $E_\lambda$  at the wavelength  $\lambda_{\text{ex}}$  reaching the sample, i.e.,  $E_\lambda(\lambda_{\text{ex}})$ , and the spectral responsivity  $s(\lambda_{\text{em}})$  of the emission or detection channel within the spectral bandwidth of excitation ( $\Delta\lambda_{\text{ex}}$ ) and emission ( $\Delta\lambda_{\text{em}}$ ) [10, 11, 20, 30].  $E_\lambda(\lambda_{\text{ex}})$  is controlled by the spectral radiance  $L_\lambda(\lambda_{\text{ex}})$  of the excitation light source and the transmittance of optical components like lenses, mirrors, filters, monochromator gratings, beam splitters, and polarizers in the excitation channel.  $s(\lambda_{\text{em}})$  is determined by the transmittance of the optical components in the emission channel and the spectral responsivity of the detector. Accordingly, both quantities strongly depend on wavelength. For a typical spectrofluorometer equipped with a xenon lamp,  $E_\lambda$  changes by more than an order of magnitude from a maximum around 400 nm to the minima below 250 nm and above 750 nm (see inset of Fig. 1). The wavelength dependence of  $s$  is most pronounced in the UV region and at wavelengths

---

<sup>2</sup> Eq. 1 assumes very dilute solutions, negligible inner filter effects, and validity of the Beer–Lambert law as is typically fulfilled for the majority of fluorescence measurements.

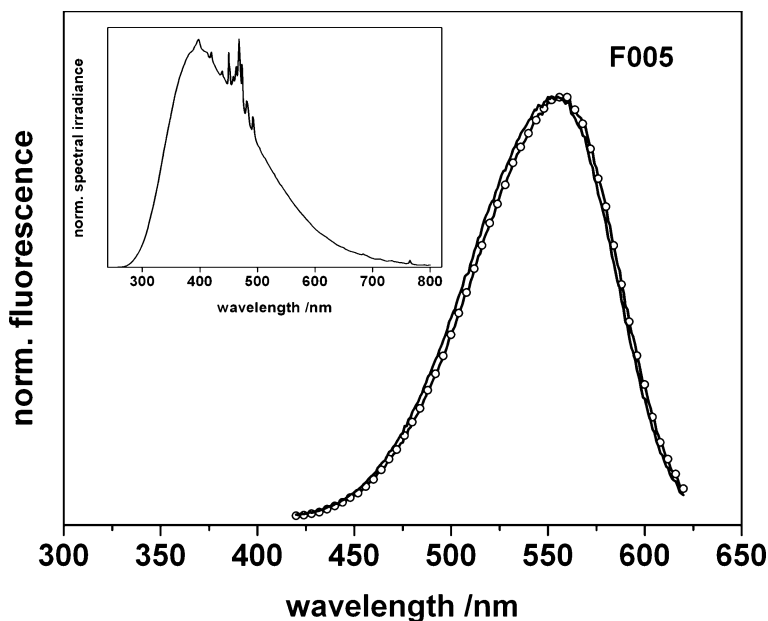


**Fig. 1** Wavelength dependence of the spectral irradiance  $E_{\lambda}(\lambda)$  of a typical fluorometer (*inset*) determined with a calibrated detector at sample position and comparison of the measured uncorrected excitation spectrum (*solid line*) of exemplary chosen dye F005 and the corresponding corrected, i.e., instrument-independent, excitation spectrum (*symbols*). Both excitation spectra represent quotients of signals from the emission detector and the reference detector accounting for fluctuations of the excitation light source as are typically measured with the majority of spectrofluorometers. Accordingly, the observed differences between the corrected and uncorrected spectra can be mainly attributed to the spectral responsivity of the reference channel that is not considered in the case of the uncorrected spectrum

of above ca. 520 nm, as displayed in the inset of Fig. 2 for five common fluorescence measuring systems. Coincidentally, these spectral regions are of particular interest, e.g., for the detection of naturally occurring fluorescent biological molecules, such as tryptophan, and for (bio)analytically relevant red-emitting fluorescent probes and labels. In addition to their wavelength dependences, both  $E_{\lambda}$  and  $s$  are polarization-dependent and, due to aging of optical and optoelectronic instrument components, also time-dependent. For the correction of relative fluorescence intensities for the instrument-dependent spectral characteristics, knowledge of the relative values of  $s$  and  $E_{\lambda}$  is sufficient (see Sects. 2, 3.7, and 3.10). For measurements of absolute fluorescence intensities, however, the irradiance in the volume of detection and the geometry factor  $G$  in Eq. 1 have to be considered. The geometry factor  $G$ , which accounts for the ratio of the solid angle of fluorescence emission, the solid angle of detection, and the size of the illuminated volume, depends on

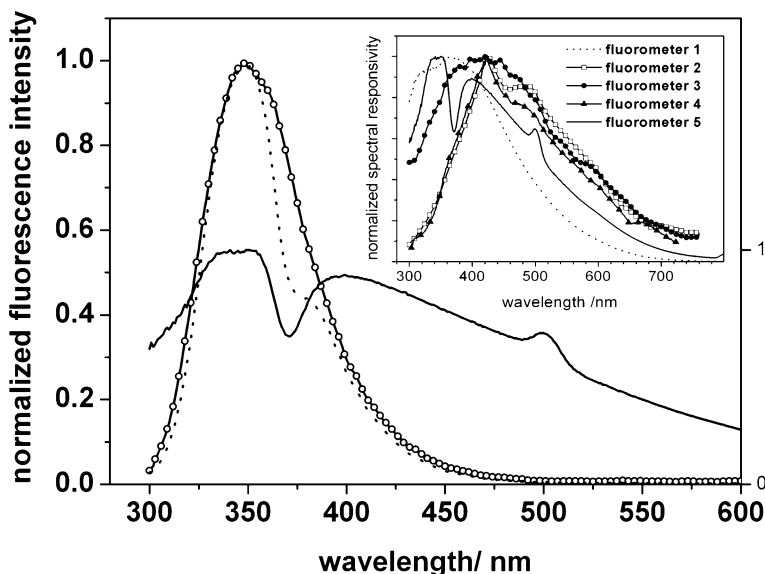


**Fig. 2** Effect of the spectral responsivity  $s(\lambda)$  of the emission channel (*solid line*) of a typical fluorometer on the measured emission spectra of D,L-tryptophan in phosphate butter (pH 7.0): uncorrected emission spectrum (*dotted line*) of tryptophan vs corrected emission spectrum (*symbols*).  $s(\lambda)$  was determined with a calibrated source. The indentation at ca. 370 nm in  $s(\lambda)$  and, less pronounced, in the uncorrected spectrum result from diffraction effects (Wood anomalies) of the instrument's monochromator gratings and can be corrected for (see indentation-free corrected spectrum). *Inset*: Normalized spectral responsivities of five different fluorescence measuring systems

both the instrument and the sample [7, 31]

$$I_m(\lambda_{\text{ex}}, \lambda_{\text{em}}) \Delta\lambda_{\text{ex}} \Delta\lambda_{\text{em}} = f(\lambda_{\text{ex}}) F_\lambda(\lambda_{\text{ex}}, \lambda_{\text{em}}) E_\lambda(\lambda_{\text{ex}}) s(\lambda_{\text{em}}) G \Delta\lambda_{\text{ex}} \Delta\lambda_{\text{em}} . \quad (1)$$

*Analyte-specific quantities*, which control measured fluorescence signals from the sample side, are the analyte's absorption factor at the excitation wavelength  $f(\lambda_{\text{ex}})$ , which is equivalent to the absorbance  $\alpha(\lambda_{\text{ex}})$  [32], and its spectral fluorescence yield  $F_\lambda(\lambda_{\text{ex}}, \lambda_{\text{em}})$  [1–6, 10, 11, 20, 33], see Eq. 1.  $F_\lambda(\lambda_{\text{ex}}, \lambda_{\text{em}})$  reveals the spectral shape of the fluorescence spectrum of the analyte. For systems consisting of a single (nonaggregated) chromophore with simple photophysics (including also, e.g., the absence of dye–dye interactions and exciplex formation) in a homogeneous matrix,  $F_\lambda$  commonly does not depend on excitation wavelength. Both absorption factor  $f$  and  $F_\lambda$  are typically sensitive to dye microenvironment. The absorption factor  $f$  is nonlinearly linked to absorbance  $A$  and thus to the concentration  $c$  by the Beer–Lambert law, see Eq. 2 (with  $\varepsilon$  equaling the molar absorption coefficient at the excitation wavelength and  $l$  the optical path length).  $F_\lambda$  is linked to the quantum yield

of photoluminescence  $\Phi_1$  that represents the number of emitted photons  $N_{em}$  per number of absorbed photons  $N_{abs}$  [34, 35], see Eq. 3.  $\Phi_1$  is one of the most important parameters in luminescence analysis. It characterizes a radiative transition in combination with the luminescence lifetime and the luminescence spectrum, and determines the sensitivity for the detection of a certain analyte from the sample or material side together with the analyte's molar absorption coefficient at the excitation wavelength

$$f(\lambda_{ex}) = 1 - 10^{-A(\lambda_{ex})} = 1 - 10^{-\varepsilon(\lambda_{ex})cl}, \quad (2)$$

$$\Phi_1 = N_{em}/N_{abs}. \quad (3)$$

To illustrate the influence of  $E_\lambda(\lambda_{ex})$  and  $s(\lambda_{em})$  on measured fluorescence excitation and emission spectra in Figs. 1 and 2, for typical spectrofluorometers and exemplary chosen chromophores, instrument-specific uncorrected fluorescence excitation and emission spectra are compared to the corresponding spectra (spectrally) corrected for the wavelength and polarization dependences of  $E_\lambda$  and  $s$ . The observed considerable differences underline the need for spectral correction of measured (or apparent) spectra as a prerequisite for fluorescence data that are comparable across instruments and, for the same instrument, over time. In the literature, such corrected spectra are also referred to as technical spectra. Spectral correction, however, typically does not include correction for uncertainties introduced by the sample itself, such as pre- and post- or so-called inner filter effects, quenching by oxygen, and refraction at the sample boundaries (refractive index of the matrix) [8, 36]. Such effects need to be considered by the proper choice of measurement conditions and additional corrections.

### 3 Characterization of Fluorescence Instruments and Comparable Fluorescence Measurements

A fit-for-purpose qualification of a fluorescence instrument has to be performed with properly characterized physical and chemical transfer standards under commonly used, i.e., application-relevant, measurement conditions [37]. In addition, all the instrument parameters that can influence fluorescence signals need to be kept constant in between instrument characterization and subsequent fluorescence measurements. Only this guarantees reliable and truly comparable fluorescence data. Simultaneously, it imposes stringent requirements on suitable standards. However, this is the prerequisite for the eventually desired traceable measurements of photoluminescence, thereby linking fluorometry to radiometric or other physical units as required, e.g., by ISO/IEC 17025. According to this written standard, which is relevant for laboratory accreditation, an instrument qualification needs to be

traceable to the relevant SI units if possible or to other accepted primary standards via an unbroken chain of comparisons with given uncertainties [29, 31].

### 3.1

#### Measurement Conditions and Requirements on Standards

*Instrument parameters* affecting fluorescence signals are, e.g., spectral resolution [38, 39], detector voltage, and, for measurements with pulsed light sources, also delay, gate, and (integration or scanning) time [10], as well as polarizer settings and measurement geometry [1, 4, 5, 11, 20]. Accordingly, a straightforward instrument qualification has to be performed for commonly used measurement conditions to minimize calibration-related measurement uncertainties. As the calibration-relevant radiometric or fluorometric properties of a standard are similarly affected by the instrument settings and measurement conditions chosen for their determination, a *standard* is solely then well characterized when not only its calibration-relevant properties are reported, but also all the parameters that can influence these properties and their uncertainty [10, 37, 40].<sup>3</sup> Only this enables the evaluation of the standard's suitability. This criterion is typically fulfilled for physical standards such as lamps and detectors calibrated by National Metrology Institutes (NMIs), but scarcely for chromophore-based standards. In addition to the influence of instrument parameters, for such chemical transfer standards it needs to be kept in mind that, similarly to commonly measured fluorophores, the absorption and emission spectra, molar absorption coefficients, and fluorescence quantum yields of these standards can also depend on microenvironment, i.e., solvation, solvent polarity, and, in aqueous media, pH value and ionic strength as well as viscosity and temperature. Moreover, the fluorescence quantum yields and lifetimes of standards can be sensitive to the presence of fluorescence quenchers such as oxygen [41]. Accordingly, the measurement conditions used for the characterization of the standard need to be well defined and reported as well as the standard's scope and limitations for its use. This includes information on, e.g., concentration-dependent absorption and emission properties, an excitation wavelength-dependent spectral shape of the emission spectrum, excitation wavelength-dependent fluorescence quantum yields, the standard's emission anisotropy, and dye purity [42–44].<sup>4</sup> For commercial chromophore-based standards, in addition, the criteria for the production of reference materials as stated in ISO Guide 34 [45] and ISO Guide 35 [46] should be fulfilled.

---

<sup>3</sup> The calculation of uncertainties is described in the ISO Guide to the Expression of Uncertainty in Measurement (GUM) [40].

<sup>4</sup> Values of the fluorescence anisotropy should be provided as this quantity determines the need for the use of polarizers and the size of polarization-related contributions to the overall uncertainty.



### 3.2

#### Linking Fluorescence Measurements to Radiometric and Physical Scales

The choice of the method and the standard(s) used for the characterization of the fluorescence instrument determine whether all the subsequent fluorescence measurements are traceable to the relevant physical unit(s) [29–31]. As illustrated in Fig. 3, traceability in the case of fluorometry implies at least linking of fluorescence spectra or (integral) fluorescence intensities (fluxes) to radiometric quantities, i.e., to the *spectral radiance scale* and/or the *spectral responsivity scale* with the aid of accordingly calibrated physical or chemical transfer standards. Other radiometric quantities that can play a role include, e.g., the *diffuse reflectance* or *spectral radiance factor* for the calibration of diffuse reflectance standards. These so-called white standards are often applied for the characterization of fluorescence instruments in combination with source- and/or detector-based transfer standards [24, 30].

For the determination of  $s(\lambda_{em})$ , source or so-called spectral radiance transfer standards with known wavelength-dependent spectral radiances (or emission intensities in the case of chemical standards) are used, as detailed in Sect. 3.7 [47]. Physical-type source standards, such as tungsten ribbon lamps or integrating sphere radiators, are calibrated, via working standards, against a high-temperature black body radiator in the Vis/NIR spectral region and in

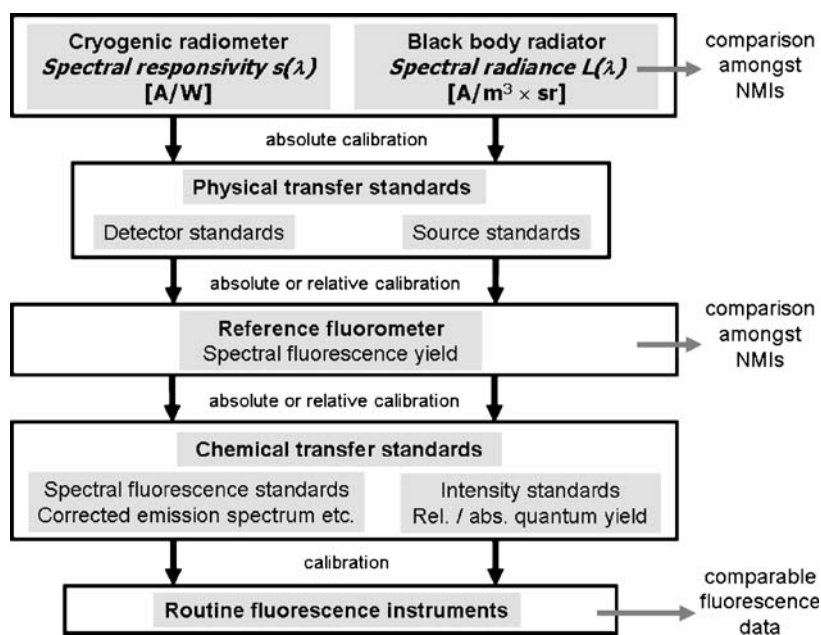


**Fig. 3** Linking fluorometry to radiometry: traceable instrument characterization and fluorescence measurements

the UV region against an electron storage ring or a high-temperature black body radiator as the primary standards for the realization and dissemination of the spectral radiance [30], see Fig. 3 (top). The spectral radiance is traced back to the SI unit of temperature, the Kelvin, in the case of a high-temperature black body radiator. For the characterization of chemical source standards or so-called emission standards, as described in Sects. 3.7 and 3.8, additionally, a reference fluorometer is mandatory, see Fig. 3 (middle). This reference fluorometer must be traceably calibrated with physical transfer standards with a known measurement uncertainty.

Measurement of  $E_\lambda(\lambda_{\text{ex}})$  detailed in Sect. 3.10 requires standards with a known spectral responsivity and calibrated aperture. *Spectral responsivity standards*, e.g., detector standards, are measured against a cryogenic radiometer as the primary standard for the spectral responsivity [30], as illustrated in Fig. 3 (top). For the traceable characterization of the (corrected) excitation spectra of chemical transfer standards with a known uncertainty, a reference fluorometer is needed similarly to emission standards, see Fig. 3 (middle).

To guarantee the international equivalence of source- and detector-based primary standards between the NMIs,<sup>5</sup> in particular as signatories of the CIPM Mutual Recognition Arrangement (MRA) of 1999,<sup>6</sup> regular comparisons of measurement capabilities are performed [48], see Fig. 3 (top). These comparisons are often referred to as key comparisons. Only recently, the importance of the determination of the spectral characteristics of fluorescence instruments and the availability of reliably corrected emission spectra recently motivated all the NMIs active in the area of high precision spectrofluorometry to evaluate the comparability of their emission measurements. This is highlighted in the middle of Fig. 3. Participants in this soon to be jointly published comparison included the National Research Council (NRC), Canada, the Physikalisch-Technische Bundesanstalt (PTB), Germany, the National Institute of Standards and Technology (NIST), USA, and the Federal Institute for Materials Research and Testing (BAM), Germany.

For other fluorescence techniques, additionally, the traceable determination of fluorometric quantities, such as fluorescence lifetime or traceable microscopic measurements, is gaining in importance. The traceable measurement of fluorescence lifetimes implies linking of time-resolved fluorescence measurements, i.e., the time axis of fluorescence instruments, to the time or length scale defined by the natural constants of the frequency of a selected

<sup>5</sup> A National Metrological Institute (NMI) is an institute designated by national decision to develop and maintain national measurement standards for one or more quantities.

<sup>6</sup> In October 1999, the CIPM (Comité Internationale des Poids et Mesures) Mutual Recognition Agreement (MRA) for national standards and calibration and measurement certificates issued by National Metrological Institutes was signed. By the end of 2003, NMIs of 44 signatory states of the Metre Convention, two international organizations, and 13 associates of CGPM had signed CIPM MRA.

atomic transition of the Cs atom and the velocity of light, respectively, via suitable transfer standards. For spatially resolved fluorescence measurements as performed in fluorescence microscopy, the (additional) characterization of the instrument's spatial resolution traceable to the length scale is eventually desired. For the microscopically relevant nanometer up to micrometer length domain, a metrologically combined optical/X-ray interferometer and scanning probe microscope can be used in conjunction with (structured) masks and gratings as transfer standards [49, 50].

### 3.3

#### **Relative vs Absolute Instrument Characterization**

In a typical fluorescence experiment, only relative fluorescence intensities are measured. Accordingly, for the vast majority of applications, it is sufficient to link fluorescence measurements to the spectral radiance and/or the spectral responsivity scale via relative measurements, i.e., to determine only the relative spectral responsivity and the relative spectral irradiance of the respective fluorescence instrument. This still yields traceable measurements [30], but circumvents the very challenging determination of absolute fluorescence intensities that requires the determination of the geometry factor  $G$  in Eq. 1 [30, 31, 47]. When comparable values of fluorescence intensities are needed, this can be realized either with a suitable fluorescence instrument in conjunction with a very sophisticated absolute instrument characterization [7, 51] or, for the broad users of fluorescence techniques, with the extra use of fluorescence intensity standards such as fluorescence quantum yield standards [37].

### 3.4

#### **Guidelines and Recommendations on Instrument Qualification**

Only in 2004, in the area of laboratory medicine, was a consensus document published by the Clinical and Laboratory Standards Institute (CLSI): the Approved Guideline for Fluorescence Calibration and Quantitative Measurements of Fluorescence Intensity [25, 26]. This document, which has regulatory implications, focuses on quantitative fluorescence calibration and specifically addresses analysis of cells and microspheres by flow cytometry [26]. For other fluorescence techniques, there currently exist only comparably few guidelines and recommendations for the characterization of the respective instrumentation and the performance and evaluation of fluorescence measurements. These documents were developed mostly in the 1980s, e.g., by ASTM International, the UK-based Ultraviolet Spectrometry Group, and the International Union of Pure and Applied Chemistry (IUPAC) [17–21]. This includes, for instance, methods for the determination of the wavelength accuracy and spectral resolution of fluorescence instruments and their linear

and dynamic range, as well as the limit of detection for particular analytes introduced by ASTM [17–19] and methods for the evaluation of fluorescence lifetime measurements from IUPAC [52]. Also, only comparably few recommendations on emission and excitation standards as well as fluorescence quantum yield and lifetime standards are available [1–5, 11, 20, 21]. Often, these recommendations are based on non- or only partially evaluated literature data. Moreover, the recommended standards are typically not fully characterized (see Sect. 3.1, with, e.g., data on dye purity missing). As the existing ASTM and IUPAC guidelines and recommendations do not consider the current state of the art in fluorescence instrumentation and more recent research on and development of standards and reference materials [10, 37], current activities, e.g., from ASTM and IUPAC are dedicated to their update and improvement. The aim here is to review and at least partly evaluate existing standards and to develop novel fit-for-purpose recommendations focusing on modern fluorescence instrumentation and techniques.

### 3.5

#### Linearity of the Detection System

The first step toward a reliable instrument characterization and fluorescence measurements is the determination of the linear range of the instrument's detection system(s). Otherwise, measured fluorescence intensities can be distorted resulting in considerable measurement uncertainties. For fluorescence instruments equipped with a reference channel and a reference detector that accounts for fluctuations of the excitation light intensity (flux), this applies to both detection systems [53].

Typical methods for the determination of the linear range of a detection system include (1) the variation of the spectral radiance of a lamp by means of attenuators such as optical filters with certified or known transmission characteristics or polarizers (via polarizer settings) [24] and (2) the double aperture method [54, 55] or, by far more common, (3) the variation of the light intensity via chromophore concentration. The latter is recommended in ASTM E 578-83 in conjunction with quinine sulfate dihydrate emitting in the visible region and displaying little spectral overlap between its absorption and emission band [18]. Drawbacks of the physical approaches (1) and (2) are the costs for the necessary optical components as well as often an enhanced uncertainty due to the introduction of additional spectral distortions and the nonideal reproducibility of positioning of the optical components [53]. The reliability of the chemical approach (3) depends on the chosen chromophore(s). A suitable dye should display well-separated absorption and emission bands to minimize inner filter effects (reabsorption) and should not be prone to concentration quenching and aggregation. Also, the use of very dilute dye solutions with, e.g., absorbances below 0.05 (for 1-cm

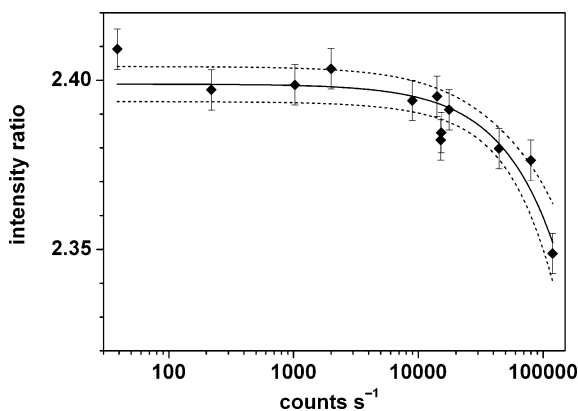


**Fig. 4** Example of the method of signal ratioing for determination of the linear range of detection systems: ratio of the light intensities recorded at two settings of the emission polarizer vs registered photon counts of the detector. The spectral radiance/intensity of the fluorometer's excitation light varied by the use of neutral density filters was scattered by a white standard at sample position toward the emission channel and measured at emission polarizer settings of 0 and 90°. Operation of the detector in its linear range should yield a constant intensity ratio within the measurement uncertainty illustrated by the bars. The *solid line* represents a modified exponential fit (quotient of two exponential saturation curves) to the overall measured data. The *dotted line* is the corresponding statistical uncertainty

cells) is recommended as only then can a linear dependence of fluorescence intensity on dye concentration be anticipated [53].<sup>7</sup>

An elegant method recently proposed by us [53] is the measurement of ratios of signal intensities, as illustrated in Fig. 4. This method is robust, simple, and not very susceptible to additional measurement uncertainties. It can be realized, e.g., via controlled modulation of the spectral radiance of the instrument's excitation light source or a second lamp with attenuators in front of the light source, a white standard at sample position, and an emission polarizer. Then, the ratios of the light fluxes of the lamp scattered from the white standard at sample position toward the detection system are determined for two different emission polarizer settings as a function of lamp intensity. This is revealed in Fig. 4. Deviations from a constant value exceeding the (previously determined) uncertainty of fluorescence measurements (bars in Fig. 4) reveal the upper limit of the linearity of the emission detection system. A straightforward alternative for the broad majority of fluorescence users presents the variation of the light intensity reaching the detector via a fluorescent sample and chromophore concentration and the subsequent measurement of signal ratios either at different settings of an emission polarizer or at different

<sup>7</sup> The absorbance  $\alpha(\lambda)$  in Eq. 1 in Sect. 2 can be replaced by absorbance that is linearly linked to concentration by the Beer-Lambert law with a reasonable uncertainty ( $\leq 5\%$ ) only for very dilute solutions with an absorbance below 0.05.

emission wavelengths. Signal ratioing can also be achieved with an attenuator in the emission channel. Then, its reproducibility of positioning should be determined additionally and the attenuation factor should be in the order of 3 to 5.

### 3.6 Wavelength Accuracy

For spectrofluorometers and the vast majority of fluorescence instruments, each instrument qualification must include the verification and control of the wavelength accuracy of the excitation and/or emission channel [12]. A physical or chemical wavelength standard suitable for this purpose, and also for the determination of the spectral resolution of the instrument, must emit a multitude of very narrow emission bands in the UV/Vis/NIR spectral region at known spectral positions with a given uncertainty [56]. Accordingly, the corrected emission spectrum of this standard must be known. Within the recently developed framework of the classification of fluorescence standards (see also Sect. 2) such a wavelength standard represents an instrument calibration standard [37] or spectral fluorescence standard [10].

For the calibration of the wavelength scale of high precision spectrofluorometers, where typically an accuracy of about  $20 \text{ cm}^{-1}$  ( $\pm 0.5 \text{ nm}$  at  $500 \text{ nm}$ ) is desired, the best and most common choice is atomic discharge lamps that display extremely narrow emission lines, see Fig. 5 (left panel). Such lamps

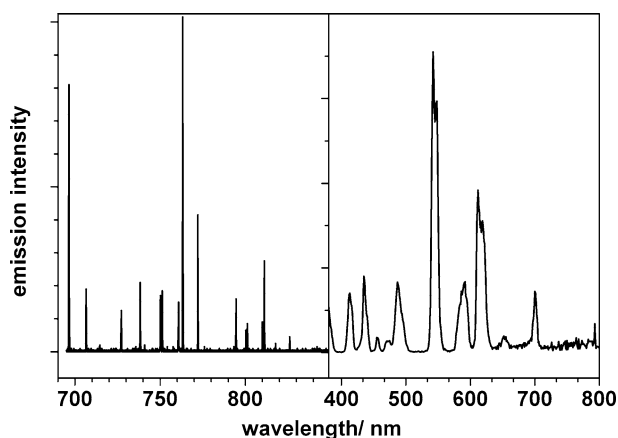


**Fig. 5** Emission spectra of an atomic discharge lamp containing a mixture of mercury and argon (*left panel*) and a fluorescent glass doped with a multitude of rare earth (RE) metal ions (*right panel*)

often contain gas mixtures to cover the UV/Vis/NIR spectral region [57–61].<sup>8</sup> This procedure has also been recommended by, e.g., ASTM E 388-04 [17]. The spectral positions of the atomic emission lines (including uncertainties) of, e.g., mercury, argon, and neon used as filling gases are reliably known [57, 59, 60]. However, as these positions are affected by gas pressure, this parameter should be reported by the standard's manufacturer and supplier. Traceability typically does not play a role in the determination of the wavelength accuracy in fluorometry. Since atomic discharge lamps exhibit typically a very large spectral radiance as compared to fluorescent samples, the use of an attenuator such as a white standard or diffuse scatterer is often mandatory to avoid detector saturation.

Easy-to-use chemical alternatives for the determination of the wavelength accuracy are chromophore-based wavelength standards. Such reference materials are particularly attractive for fluorescence instruments with a reduced spectral resolution, such as confocal spectral imaging systems or certain microplate readers [10, 56], where control of this parameter does not require the high accuracy provided by low pressure atomic discharge lamps. Examples include glass-based materials currently developed by NIST and BAM [37], adaptation of a reflectance standard such as SRM 2036 [62] to fluorescence measurements, and  $Y_{3-x}Dy_xA_{15}O_{12}$ , a dysprosium-activated yttrium garnet [63, 64]. In addition, although questionable, the potential of luminescent nanocrystals or so-called quantum dots as wavelength standards for fluorescence instruments with a low spectral resolution has been tested [65]. Different manufacturers of steady-state fluorometers also recommend the determination of the wavelength accuracy via scanning of the emission lines of the instrument's xenon excitation source or the transmission minima in the spectrum of a solution of holmium perchlorate. This, however, typically requires a specific calibration accessory and measurement geometry which limits the widespread use of this procedure.

The right-hand panel of Fig. 5 reveals the corrected emission spectrum of a very promising candidate wavelength standard currently tested by BAM [10, 56]. This material, a glass doped with a mixture of rare earth ions, will eventually be provided in a variety of formats for different fluorescence techniques such as, e.g., cuvette shaped for spectrofluorometry and slide shaped for fluorescence microscopy, with corrected emission spectra certified for different application-relevant excitation wavelengths,<sup>9</sup> temperatures, and different spectral bandpasses/spectral resolutions of the BAM reference fluorometer. Since the luminescence intensity of such a material can be controlled

---

<sup>8</sup> Certain commercial equipment, instruments, or materials are identified in this chapter to foster understanding. Such identification does not imply recommendation or endorsement by the Federal Institute for Materials Research and Testing (BAM), nor does it imply that the materials or equipment identified are necessarily the best available for the purpose.

<sup>9</sup> Mixtures of different fluorophores such as rare earth ions always display excitation wavelength-dependent emission spectra.

by dopant concentration, not only the shape and size of its radiating volume, but also its spectral radiance or fluorescence intensity can be matched to that of commonly measured samples.

The *spectral bandwidth* of the monochromator(s) of fluorescence instruments and the instrument's spectral resolution follow from measurements of the full width at half height of the maximum of selected emission bands of a wavelength standard. This is described, e.g., in ASTM E 388-04 for spectrofluorometers and an atomic discharge lamp [17]. As the spectral bandpass is usually wavelength-dependent, the instrument's spectral resolution should be obtained within the typically measured wavelength region. In the case of chromophore-based wavelength standards, similarly structured or narrow bands, such as the band at ca. 612 nm displayed by the BAM candidate material (see right-hand panel of Fig. 5), can be used for this purpose.

### 3.7

#### **Spectral Responsivity of the Emission Channel**

The (relative) spectral responsivity of the emission channel of a fluorescence instrument, see Eq. 1, can be obtained with a source-based standard that emits a broad, preferably unstructured spectrum in the UV/Vis/NIR spectral region [10, 11, 20, 30, 31, 37, 47, 53, 56, 66]. The wavelength-dependent spectral radiance or corrected emission spectrum of this instrument calibration [37] or spectral fluorescence standard [10] must be known and should be preferably certified.

Typical methods for the determination of the relative spectral shape of the spectral responsivity of the emission channel include the use of:

1. A calibrated physical source-based transfer standard, such as a tungsten ribbon lamp or an integrating sphere-type radiator
2. The previously characterized excitation channel, see Sect. 3.10, as calibrated light source in a synchronous scan of the excitation and emission channel with a calibrated white standard at sample position [11, 20] or
3. Chromophore-based spectral fluorescence or so-called emission standards [37, 53, 67–72]

All these approaches are all principally traceable to a radiometric scale [29]. Tungsten ribbon lamps and integrating sphere-type spectral radiance transfer standards reveal a very broad unstructured emission spectrum covering the UV/Vis/NIR spectral region [30]. Drawbacks of these source standards calibrated, e.g., by NMIs (see Fig. 3) are a tedious alignment, regular and expensive recalibrations [73], restrictions on measurement geometry, and a considerable size that can hamper their application for compact fluorescence instruments. Moreover, their spectral radiances exceed those of typical fluorescent samples by at least four (tungsten ribbon lamp) to two (integrating sphere radiator) orders of magnitude [31, 53], as illustrated



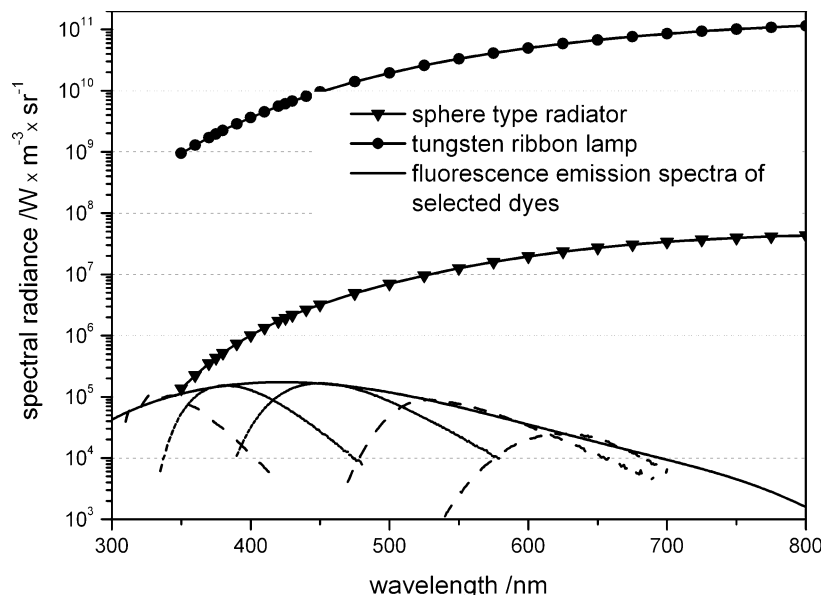


**Fig. 6** Comparison of the typical spectral radiances of a tungsten ribbon lamp (*top, circles*), an integrating sphere-type radiator (*middle, triangles*), and typical fluorophores (*bottom, solid line and dashed lines for emission spectra*)

in Fig. 6. Accordingly, to still operate the fluorometer's detection system within its linear range and avoid the introduction of additional spectral effects, such source standards can only be used in conjunction with sophisticated attenuation procedures [53]. Method 2 relies on the use of a white standard, the wavelength dependence of the spectral radiance factor of which was determined (and certified) for the employed measurement geometry, and on a synchronized behavior of the emission and excitation monochromator. Due to the smaller calibration uncertainties of detector-based compared to source-based transfer standards [30], this approach may eventually yield a smaller calibration uncertainty if, e.g., uncertainties related to fluctuations of the spectral radiance of the excitation light source and the different radiating volumes and spectral radiances of the calibrated excitation channel and typically measured samples can be minimized [51].

The broad community of fluorescence users can be reached only with the chromophore-based procedure 3. Here, the close match of the spectral radiance and the size and shape of the radiating volume of both standard(s) and samples enables a straightforward determination of the instrument's relative spectral responsivity under application-relevant conditions [31].

### 3.8 Emission Standards

The use of a fluorescent dye as a chemical equivalent of a spectral radiance transfer standard was first proposed by Kortüm and Finckh in 1944 [69]. However, only recently, requirements on and quality criteria for emission standards have been derived [10, 53, 71] that belong to the class of instrument calibration standards. This includes, e.g., broad and unstructured emission spectra to minimize the dependence of the shape of the spectra on instrument resolution/spectral bandpass, minimum overlap between absorption and emission for a moderate influence of dye concentration and measurement geometry on spectral shape, and moderate to high fluorescence quantum yields to enhance the signal-to-noise ratio and to reduce the influence of stray light, solvent emission, and fluorescent impurities on the spectral shape of the standard's emission spectrum. A small emission anisotropy ( $r$ ), e.g.,  $r \leq 0.05$  within the analytically relevant room temperature region, is desirable to circumvent additional material-related polarization effects and reduces uncertainties for use without polarizers [53, 74, 75]. The standard's thermal and photochemical stability must be adequate under application-relevant conditions and should be preferentially reported in a comprehensible way. Also, the shelf life of the standard should be given.

Though a number of emission standards have been recommended in the literature [11, 20, 21, 67, 68, 71, 72] and several are available from commercial (non-NMI) sources,<sup>10</sup> none of these materials is supplied with traceable and certified, corrected fluorescence data. Often, information on the calibration of the instrument and measurement conditions employed for the characterization of the standards is missing and measurement uncertainties are scarcely provided, rendering the reliability of the provided spectra questionable. Also, most of the recently derived quality criteria on fluorescence standards and their characterization [10, 37, 53, 71] are not fulfilled. At present, the only emission liquid standards that provide the necessary reliability and traceability are standard reference material (SRM) 936 quinine sulfate dihydrate from NIST [76–78]<sup>11</sup> and BAM-F001 to BAM-F005 (equaling the organic dyes A–E in earlier publications) recently certified by BAM [79], see Fig. 7 (bottom) used as solutions. This is also true for the solid emission standards SRM 2940 (*Orange Emission*) and SRM 2941 (*Green Emission*) *Relative Intensity Correction Standards for Fluorescence Spectroscopy* released by NIST in April 2007 (see also Sect. 2) that are ready-to-use, cuvette-shaped glasses with three long sides polished and one side frosted, allowing measurements using instruments with  $0^\circ/90^\circ$  and front-face

<sup>10</sup> See, for instance, Invitrogen or former Molecular Probes, Starna GmbH, Matech Precision Dynamics Corp., Labsphere Inc., and LambdaChem GmbH.

<sup>11</sup> SRM 936 is still available as SRM 936a.

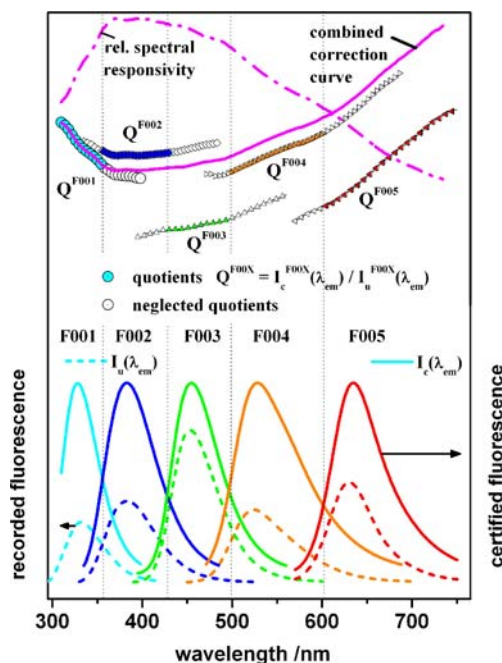


**Fig. 7** Determination of the relative spectral responsivity of a typical fluorescence instrument with the Calibration Kit Spectral Fluorescence Standards BAM-F001 to BAM-F005. *Bottom:* Normalized certified corrected emission spectra  $I_c(\lambda_{em})$  of BAM-F001 to BAM-F005 (solid lines) and corresponding spectrally uncorrected (background-corrected) emission spectra  $I_u(\lambda_{em})$  measured with the instrument to be calibrated. *Middle:* quotients  $Q^{F00x}(\lambda_{em}) = I_c(\lambda_{em})/I_u(\lambda_{em})$ . *Top:* weighted combination of  $Q^{F00x}(\lambda_{em})$  to the inverse relative spectral responsivity  $1/s(\lambda_{em})$  and its reciprocal  $s(\lambda_{em})$

geometries [80, 81]. The slightly structured emission spectrum of SRM 2941, however, may be problematic as this can introduce a considerable dependence on spectral bandpass and spectral resolution. Due to the comparably long luminescence lifetimes of the inorganic metal ions used as dopants for these glasses, which are in the microsecond to millisecond region, use of these materials is recommended for instruments equipped with continuous light sources. In the case of pulsed light sources, the emission properties of these dopants can be affected by measurement parameters, such as pulse duration, delay, and gate. For instance, the certified values for SRM 2941 can, but those for SRM 2940 cannot, be used with pulsed light sources. As the organic dyes quinine sulfate dihydrate and BAM-F001 to BAM-F005 display short fluorescence lifetimes of a few nanoseconds, these materials can be principally employed for all types of light sources (continuous and pulsed lamps, lasers etc.).

The emission spectra of typical organic or inorganic chromophores cover only a small spectral region<sup>12</sup> compared to a physical source standard (see, e.g., Fig. 6). For instance quinine sulfate dihydrate, which reveals a very broad emission spectrum for a chromophore, covers only the spectral region of 395 to 565 nm [76].<sup>13</sup> Accordingly, a dye-based emission calibration within the UV/Vis/NIR region requires the combination of emission standards to sets [53, 67, 68, 70, 71, 82].<sup>14</sup> Although such a chromophore-based strategy was first applied by Lippert et al. [70], suitable combinations of emission standards are still very rare. For such sets, not only must each component fulfill the criteria discussed in this section, but also the spectra of the set dyes must cross at points of sufficient fluorescence intensity, e.g., at least at 20% of the relative maximum fluorescence intensity [53, 71]. To the best of our knowledge, at present, the only dye set that meets these stringent criteria and is traceable is the Calibration Kit *Spectral Fluorescence Standards* BAM-F001 to BAM-F005 [83–85]<sup>15</sup> covering the spectral range from 300 to 770 nm. The NIST standards SRM 936, SRM 2940, and SRM 2941 cover the spectral region from 395 to 780 nm as a set. However, it is not yet clear whether these emission standards can be used in a similar fashion to the BAM dye set [76, 80, 81].

The working principle of a set of emission standards is illustrated for BAM-F001 to BAM-F005 in Fig. 7. For each spectral standard F00x ( $x$  equaling 1 to 5), the quotients  $Q^{F00x}(\lambda_{em})$  of the certified normalized corrected emission spectra  $I_c(\lambda_{em})$  (Fig. 7, bottom, solid lines) and the spectrally uncorrected (background-corrected<sup>16</sup>) emission spectra  $I_u(\lambda_{em})$  (Fig. 7, bottom, dashed lines; measured with the instrument to be calibrated) are calculated. These quotients  $Q^{F00x}(\lambda_{em})$  shown in the middle part of Fig. 7 represent the corresponding inverse spectral responsivities  $1/s(\lambda_{em})$ . The inverse relative spectral responsivity  $1/s(\lambda_{em})$  of the instrument to be calibrated (Fig. 7, top) follows from the statistically weighted combination of  $Q^{F00x}(\lambda_{em})$ . Corrected, instrument-independent, and comparable data are obtained upon subsequent

<sup>12</sup> For instance, the emission spectrum of quinine sulfate dihydrate in 0.105 M perchloric acid, which is very broad for an organic dye, can be used for spectral correction only from ca. 395 to 565 nm where the emission intensity is at least 10% of the intensity at the emission maximum.

<sup>13</sup> Typically, for the determination of the spectral responsivity of fluorescence instruments with a reasonable uncertainty, only fluorescence intensities  $\geq 10\%$  of the intensity at the emission maximum are used. Otherwise the signal-to-noise ratio can be poor.

<sup>14</sup> Standard Reference Material 1931: this set of four solid spectral fluorescence standards in a cuvette format was restricted in measurement geometry and certified using polarizers.

<sup>15</sup> BAM-F001, BAM-F002, BAM-F003, BAM-F004, and BAM-F005 ready-made from Sigma–Aldrich GmbH (former Fluka GmbH) are available from BAM or from Sigma–Aldrich. The corresponding product numbers from Sigma–Aldrich are 97003–1KT-F for the Calibration Kit and 72594, 23923, 96158, 74245, and 94053 for BAM-F001, BAM-F002, BAM-F003, BAM-F004, and BAM-F005, respectively.

<sup>16</sup> Removal of background signals, such as scattering and fluorescence from the solvent and dark counts at the detector, from measured fluorescence spectra by subtraction of a background spectrum,  $I_b(\lambda_{ex}, \lambda_{em})$ , which was recorded under identical measurement conditions for a blank solvent sample  $I_m(\lambda_{ex}, \lambda_{em})$ , yields spectrally uncorrected spectra,  $I_u(\lambda_{ex}, \lambda_{em})$ :  $I_u(\lambda_{ex}, \lambda_{em}) = I_m(\lambda_{ex}, \lambda_{em}) - I_b(\lambda_{ex}, \lambda_{em})$ .

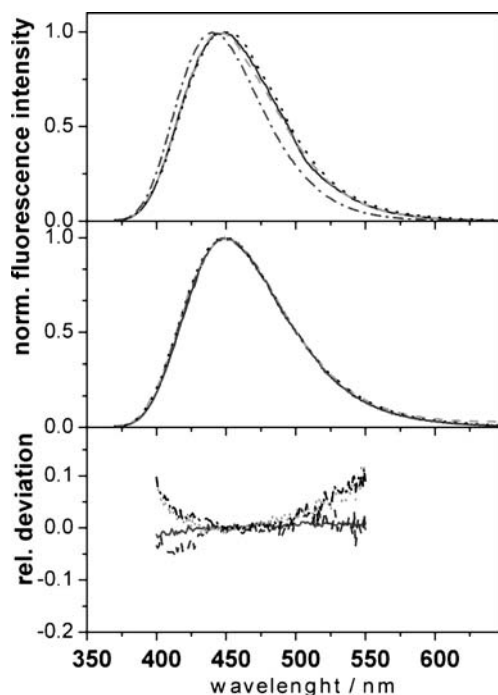


**Fig. 8** Comparability of fluorescence data without and with dye-based (spectral) emission correction. *Top*: uncorrected emission spectra of quinine sulfate dihydrate SRM 936a measured with four different fluorometers. *Middle*: corresponding corrected spectra obtained with a dye-based (F001 to F005) emission correction curve. *Bottom*: relative deviations of corrected spectra from certified reference spectrum

multiplication of measured spectra with  $1/s(\lambda_{em})$ . A critical step of this procedure is the reliable and comparable linking of  $Q^{F00x}(\lambda_{em})$ . To achieve this for the broad majority of users, software is mandatory that performs this linking procedure. Accordingly, we developed the software *LINKCORR* for data evaluation to minimize standard- and calibration-related uncertainties in conjunction with the BAM reference materials.

The corrected emission spectra of BAM-F001 to BAM-F005 and the determination of a dye-based emission correction with the BAM Calibration Kit and the BAM software *LINKCORR* were both validated in an interlaboratory comparison of the NMIs NIST, NRC, PTB, and BAM. In addition, the performance of these reference materials and the data evaluation procedure were tested by selected laboratories from academia and industry by comparing the uncorrected spectra and kit-based corrected spectra of three test dyes. The results from such a comparison are shown in Fig. 8 for the test dye quinine sulfate dihydrate. As follows from this figure, the uncorrected emission spectra of this dye measured with four typical spectrofluorometers clearly differ as

expected, whereas the corresponding kit dye-based corrected emission spectra are in excellent agreement with relative deviations of at maximum 5% for signals  $\geq 10\%$  of the maximum intensity. This provides a hint for the achievable comparability of emission spectra upon widespread use of this new calibration tool.

### 3.9

#### Radiometric Reference Quantity and Photonic Nature of Emitted Light

Traceability of the instrument's emission channel can be established to the spectral radiance  $L_\lambda$  or to the spectral photon radiance  $L_{p\lambda}$  equaling  $L_\lambda \times \lambda / (hc)$ . Though trivial and often neglected, the choice of the radiometric quantity can affect the spectral shape of corrected fluorescence spectra and especially integral fluorescence intensities and fluorescence quantum yields [86, 87]. This is illustrated in Fig. 9, which compares the normalized corrected emission spectra of three organic dyes 1–3 emitting in the UV/Vis/NIR spectral region determined traceable to  $L_\lambda$  and  $L_{p\lambda}$ , respectively, and the corresponding non-normalized spectra reflecting the respective

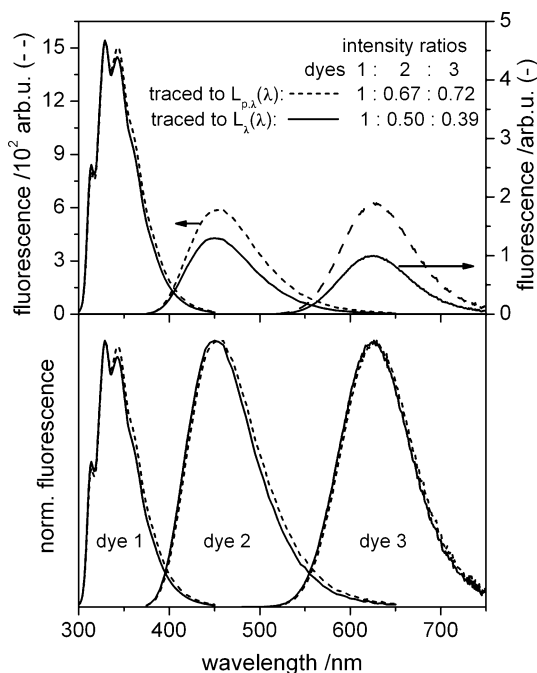


**Fig. 9** Comparison of the relative corrected emission spectra (*top*) and the normalized corrected emission spectra (*bottom*) of dyes 1–3 referenced to the spectral radiance  $L_\lambda(\lambda)$  (*solid lines*) and the spectral photon radiance  $L_{p\lambda}(\lambda)$  (*dashed lines*)

intensity ratios. Whereas the spectral deviations are comparatively small, the differences in intensity, and thus eventually in fluorescence quantum yield, are intriguing with intensity ratios of 1 : 0.67 : 0.72 and 1 : 0.50 : 0.39 resulting for dye 1, dye 2, and dye 3 referring to  $L_\lambda$  and  $L_{p\lambda}$ , respectively.

Unfortunate for this otherwise trivial problem is the fact that despite its obvious influence, the radiometric reference quantity employed for spectral correction is typically not explicitly quoted and it is not clear from measured dimensionless spectra or quantum yields. This can additionally affect the comparability of fluorescence data, especially in the case of fluorescence quantum yields. Similarly, it underlines the importance of properly reported and eventually standardized procedures for instrument characterization and the determination of relevant fluorometric quantities. In our opinion, the spectral radiance is to be favored as reference quantity for corrected emission spectra, as the physical source-based transfer standards used by the majority of instrument manufacturers for the determination of the spectral characteristics of their instrumentation, as well as certified and recommended emission standards, are typically referenced to the spectral radiance [71, 76, 79, 83]. Moreover,  $L_\lambda$  is also used in closely related colorimetry (see also Chap. 6 in [24]). For the determination of fluorescence quantum yields, however, the energy of the emitted photons should be taken into account as illustrated in Fig. 8, as the fluorescence quantum yield is the ratio of the number of emitted to absorbed photons and not a ratio of radiated fluxes or powers. Accordingly, corrected emission spectra referenced to  $L_\lambda$  have to be multiplied by the wavelength prior to integration on a wavelength scale to consider the photonic nature of the emitted light. For the BAM Calibration Kit, this is correspondingly described in the certificates [79, 83].

### 3.10

#### Spectral Irradiance of the Excitation Channel

Instrument-independent excitation spectra and the comparison of (integral) emission intensities measured at different excitation wavelengths require knowledge and consideration of the spectral irradiance at sample position. For the determination of the relative spectral shape of  $E_\lambda(\lambda_{\text{ex}})$ , which is sufficient in the majority of cases, the wavelength and polarization dependence of the flux reaching the sample (in relative units) needs to be obtained. Here, it is typically assumed that the illuminated volume does not change in between instrument characterization and measurement of fluorescent samples to be corrected. For the few cases where the absolute values of  $E_\lambda(\lambda_{\text{ex}})$  are desired, such as the direct comparison of fluorescence intensities generated by different instruments or absolute fluorescence quantum yields, additional knowledge of the illuminated volume of the spectral responsivity transfer standard (and the sample) is mandatory.

The most common method (1) for the traceable measurement of the spectral shape of  $E_\lambda(\lambda_{\text{ex}})$  is the use of a calibrated spectral responsivity transfer standard, such as a calibrated detector, typically a silicon photodiode (simple or integrating sphere-type, trap detector [47, 88]) as also pursued by us, see Fig. 1. In the case of a flux-calibrated detector, this method can yield absolute values of  $E_\lambda(\lambda_{\text{ex}})$  in combination with a known volume or cross section of the illuminated detection area. An alternative method (2) that can principally lead to the relative spectral shape of  $E_\lambda(\lambda_{\text{ex}})$  and absolute values is the application of the previously characterized emission channel, see Sect. 3.7, as a “calibrated detector” in a synchronous scan of the excitation and emission channel with a white standard at sample position [11, 20]. A prerequisite here is that for both the characterization of the spectral responsivity of the emission channel and the spectral irradiance at sample position, the angle under which the white standard is illuminated (either with a spectral radiance transfer standard or the excitation channel), the illuminated area of the white standard, and the angle of detection are either kept constant or are known and are accordingly considered. Knowledge of the illuminated area is mandatory for absolute measurements of  $E_\lambda(\lambda_{\text{ex}})$ . Method 3, the use of chromophore-based so-called excitation standards with known corrected excitation spectra [11, 20, 53], which assumes comparable illuminated and detected volumes for standard(s) and samples, yields only the relative values of  $E_\lambda(\lambda_{\text{ex}})$ . This approach relies on suitable excitation standards that have to fulfill all the requirements previously derived for emission standards [53], the combination of these standards to a set to cover a broad spectral region as described for emission standards in Sect. 3.8, and dilute dye solutions. The latter is related to the proportionality of fluorescence intensity to absorption factor  $f$  or absorptance  $\alpha$ , see Eq. 2, which results in a concentration dependence of the spectral shape of excitation spectra and introduces a dependence on measurement geometry. For instance, for a  $0^\circ/90^\circ$  measurement uncertainty, the chromophore absorbance should not exceed 0.05. At present, drawbacks of method 3 are the lack of certified excitation standards, with the first set of excitation standards being only recently presented by us [53] and, generally, the limited reliability of literature data.

Of much less importance and not advisable are the application of (4) a pyroelectric detector,<sup>17</sup> (5) a quantum counter prone to polarization and geometry effects [34, 68, 89, 90], and (6) an actinometer [53, 91, 92].<sup>18</sup> Also, the most simple method (7), the comparison of the absorption and excitation spectra of a chromophore [20], can lead to a comparatively high calibration

<sup>17</sup> A pyroelectric detector measures the energy of absorbed photons with a wavelength-independent responsivity (gray detector), but with a drastically reduced sensitivity and accuracy compared to, for instance, a Si photodiode.

<sup>18</sup> An actinometer relies on the wavelength-independent quantum yield of a photochemical reaction, yielding a measurable and well-characterized product.



uncertainty<sup>19</sup> if the dye photophysics are not very well known and, e.g., the fluorescence quantum yield of the dye depends on the excitation wavelength for excitation at two different electronic transitions [13, 53].

Also for the excitation correction, the chosen radiometric reference quantity, either the spectral irradiance  $E_\lambda$  or the spectral photon irradiance  $E_{p\lambda}$  equaling  $E_\lambda(\lambda) \times \lambda / (hc)$ , can influence spectrally corrected fluorescence data. On our opinion, the characterization of a fluorometer should be performed traceable to radiometric reference quantities. For the comparison of excitation and absorption spectra, however, the photonic nature of the exciting light needs to be taken into account upon division by the corresponding photon energies. This is similarly true for the determination of relative fluorescence quantum yields employing different excitation wavelengths for sample and standard.

### 3.11

#### Instrument Performance Validation (IPV)

Quality assurance in fluorometry requires validation and regular control of instrument performance at fixed application-relevant measurement conditions to, e.g., account for changes of the optical and optoelectronic components of the instrument. This ensures the measurement accuracy and the ability to carry out meaningful comparisons of data acquired from multiple instruments as well as from the same instrument over time. Especially for clinical trials, not only instrument calibration but also performance validation are mandatory [12, 25, 26]. To the best of our knowledge, however, there exist no overall accepted procedures for instrument characterization and IPV for the broad majority of fluorescence techniques at present.

For steady-state fluorometry, which is the focus of this article, regular validation of instrument performance should include control of the wavelength accuracy of the excitation and the emission channel and the (relative) spectral responsivity and sensitivity of the emission channel. In many cases, the (relative) spectral irradiance of the excitation channel at sample position is not that critical. Often, only emission spectra or integral fluorescence intensities at a fixed excitation wavelength are measured, and the spectral radiance of the excitation channel is typically controlled for each fluorescence measurement via a reference channel or reference detector that accounts for its short-term fluctuations. In addition, fluorescence intensity standards can be used [37]. Regular measurement of  $E_\lambda$  is mandatory, however, for the proper correction of excitation spectra and for the comparison of fluorescence intensities measured at different excitation wavelengths.

---

<sup>19</sup> Prerequisites for method 7 are a pure compound and an excitation wavelength-independent emission spectrum and quantum yield, and thus a straightforward excited-state photochemistry can yield a comparatively high calibration uncertainty.

The instrument performance can be validated with physical and chemical standards [10, 37]. These so-called instrument validation standards can be identical to the instrument calibration standards presented in the previous sections as is typically the case for, e.g., the determination of the wavelength accuracy. They can also represent standards exclusively employed for periodic controls. For frequent use to capture any drift in instrument performance under application-relevant conditions, simple yet reliable standards are to be favored to reduce costs and measurement time. Aside from application-specific requirements, suitable well-characterized (in-house or commercial) standards must reveal an excellent long-term stability or excellent reproducibility [10, 84].

Different manufacturers of steady-state fluorometers recommend the so-called Raman test [93, 94] for the control of the long-term stability and spectral sensitivity of fluorescence instruments. This simple test measures the intensity of the Raman band from nonfluorescent water (available in sealed cuvettes) at an excitation wavelength of 350 nm and a detection wavelength of 397 nm. It responds to changes in both the instrument's excitation and emission channel and is well suited for daily use. Generally, the Raman test is recommended for excitation at 350 nm and detection at 397 nm for water, and the Raman bands lose intensity at longer wavelengths which hampers their application. The use of other solvents aside from water does not really improve this situation. We routinely use the Raman test only for the recommended measurement conditions. Accordingly, extra tools are desired for IPV for the huge majority of fluorescence instruments and applications in the Vis/NIR spectral region. For the long-term comparability of fluorescence intensities that require control of the instrument's spectral sensitivity within the typically used wavelength region, additional application of one or several fluorescence intensity standards is advisable. These standards are often referred to as day-to-day intensity standards [37] (see also Sect. 2), and account simultaneously for changes in the spectral irradiance reaching the sample and the spectral sensitivity of the emission channel, similarly to the Raman test. A versatile tool here can be the very robust chromophore-based wavelength standard shown in Fig. 5 (right panel) with its multitude of emission lines and excellent long-term stability. This standard represents not only a fluorescence intensity standard for a very broad spectral region, but also communicates changes in the instrument's spectral responsivity via changes in the intensity pattern of its emission spectrum. Special care has to be taken here, however, for use with pulsed light sources, especially in the case of mixtures of metal ions differing in fluorescence lifetime. Since many metal-ion-based dopants have comparably long emission lifetimes in the microsecond to millisecond region, the emission properties of these dopants are influenced by the pulse duration, delay, and gate for instruments equipped with pulsed light sources like many routine spectrofluorometers. Accordingly, reference materials containing such long-lived emitters should be used as day-to-day intensity stan-

dards only for a constant set of measurement parameters. Moreover, the use of such materials as instrument-to-instrument intensity standards should be limited to instruments using a continuous (nonpulsed) excitation source. For pulsed light sources, comparable measurement conditions have to be guaranteed, which can be very difficult to realize and to control.

A clear distinction between drifts arising from changes of the excitation and emission channel requires tools for the independent measurement of  $E_\lambda(\lambda_{\text{ex}})$  and  $s(\lambda_{\text{em}})$ . The long-term stability of the spectral characteristics of the emission channel can be determined, e.g., by regular measurement and comparison of the (uncorrected) emission spectra of certified or in-house emission standards. Such standards can also be suitable as day-to-day intensity standards. The long-term stability of  $E_\lambda(\lambda_{\text{ex}})$  is best controlled with a detector standard.

### 3.12

#### Future Trends: Absolute Fluorescence Measurements

Currently, one of the future trends in fluorometry is the enhanced interest in measuring absolute fluorescence intensities with quoted uncertainties, e.g., for the characterization of LED and OLED materials [95–98]<sup>20</sup> and NIR chromophores [44] increasingly applied in the life sciences. This trend also aims at the evaluation of literature data on fluorescence quantum yield standards [21, 91, 99, 100] and eventually at the direct comparison of fluorescence intensities generated by different instruments. Measurement of absolute fluorescence requires the additional determination of the geometry factor  $G$  in Eq. 1 [31].  $G$  depends strongly on the solid angle for the detection of fluorescence and the numerical apertures for excitation as well as on the type of sample (e.g., translucent or nontranslucent with emission from the surface) and the anisotropy of its emission [7, 24, 101], i.e., the angular distribution of its luminescence [74]. Also, for instance, the wavelength dependence of the refractive index of the solvent or matrix and of the container walls play a role. Accordingly, all these properties have to be known.

Absolute measurements of fluorescence include measurements of absolute fluorescence spectra and absolute luminescence quantum yields, i.e., the number of emitted per absorbed photons, see Eq. 2, without the use of a standard, see also Sect. 4. The choice of a suitable optical measurement technique depends on the type of sample, e.g., dilute dye solutions with a nearly isotropic emission vs solid samples such as polymer films or inorganic phosphors (powders) with a strongly polarized, i.e., anisotropic, emission and a strong angular dependence of their photoluminescence. Absolute fluorescence intensities of dilute solutions and cuvette-shaped trans-

<sup>20</sup> LED: light-emitting diode; OLED: organic light-emitting diode.

parent solid materials such as glasses can be measured with an accordingly designed and characterized spectrofluorometer in  $0^\circ/90^\circ$  geometry or with an integrating-sphere setup [102]. In the case of solid anisotropic and scattering or strongly absorbing materials, typically an integrating-sphere setup is used [96–98], e.g., in conjunction with a laser and a detection system or a spectrofluorometer [103].

A spectrofluorometer suitable for the measurement of absolute fluorescence intensities must reveal minimum chromatic and geometrical aberrations and thus, ideally, a wavelength-independent illuminated and detected volume of simple, symmetrical, and well-defined shape [104]. This imposes very stringent requirements on instrument design and suitable optical components, e.g., for wavelength selection, illumination, and imaging. Also, for instance, the reproducibility of the apertures must be adapted to the desired reproducibility of the illuminated and detected volume. An instrument that fulfills these requirements is being currently established at BAM for the determination of absolute fluorescence quantum yields. Requirements on integrating-sphere setups as well as their advantages and limitations are beyond the scope of this article. With the increasing commercial availability of such integrating-sphere accessories for spectrofluorometers, similarly the radiometric characterization of such setups will increase in importance in the near future.

Generally, absolute fluorescence quantum yields need to be carefully evaluated. The first step here should be the determination of absolute fluorescence quantum yields of very well characterized chromophores, such as rhodamines and fluorescein as well as quinine sulfate [7, 67, 105–107], the quantum yields of which have been independently obtained by different groups with different optical and calorimetric measurement techniques to validate the chosen setup and method of determination. Eventually, the performance of interlaboratory comparisons of measurements of (absolute) quantum yields of application-relevant chromophores should be encouraged. The ultimate goal should be to establish a set of fluorescence quantum yield standards for the UV/Vis/NIR spectral region, to improve the reliability of relative fluorescence quantum yield measurements and to identify reliable methods for the measurement of the photoluminescence quantum yields of different types of samples, such as nearly isotropic, anisotropic, scattering, and/or strongly absorbing materials. This could be done following an approach only recently initiated in the area of (nanosecond) time-resolved fluorometry. Here, a round robin was initiated by expert laboratories from academia to establish a set of fluorescence lifetime standards displaying lifetimes in the nanosecond region [108].

### 3.13

#### Impact on Other Fluorescence Techniques

Equation 1 in Sect. 2 is valid for every method or technique measuring photoluminescence. The vast majority of the procedures for instrument characterization and IPV revealed in the previous sections can be transferred to other fluorescence techniques with proper consideration of the respective method-inherent requirements on, e.g., standards and method-specific limitations. This includes, for instance, adaptation of measurement geometry, sample/standard format, excitation wavelength(s), and (photochemical and thermal) stability [10, 109]. Though often overlooked, the luminescence lifetime of the standard can also affect its suitability as briefly discussed, e.g., in Sects. 3.8 and 3.11. For instance, for standards containing single long-lived chromophores or a mixture of chromophores displaying fluorescence lifetimes in the microsecond to millisecond time domain, limitations to their use can be imposed by pulsed light sources [37]. Generally, standards are very attractive that are method-adaptable, e.g., with respect to their format, and can be accordingly used for a wide variety of fluorescence techniques. This may eventually enable a comparison of fluorescence data between different fluorescence techniques.

One approach currently pursued by us is the adaptation of BAM-F001 through BAM-F005 to other fluorescence techniques. Due to their use as dye solutions, the minimum spectral overlap between absorption and emission, and the excellent photostability, these spectral fluorescence standards offer a unique flexibility with respect to measurement geometry, format, and type of fluorescence instrument to be calibrated, as has been revealed by first studies with different fluorescence instruments [84]. Meanwhile, BAM-F001 through BAM-F005 have been successfully employed, e.g., for the characterization of microplate readers [10] as well as for the determination of the spectral characteristics of both a colorimeter in front face, i.e.,  $45^\circ/0^\circ$  measurement geometry [24] and confocal spectral imaging systems, here in conjunction with a microchannel device [110] (see also Chapter by Hoffmann et al., 2008, in this volume). Similarly, the potential of glass-based standards is being currently evaluated for different fluorescence techniques ranging from conventional fluorometry over microfluorometry to fluorescence microscopy and Raman spectroscopy [10, 37, 56, 111, 112].

## 4

### Conclusion

Quality assurance in fluorometry and the comparability of fluorescence data on the desired broad level are closely linked to the availability of reliable and simple fluorescence standards with certified, calibration-relevant properties

designed for use under application-relevant conditions, along with internationally accepted recommendations and guidelines for instrument calibration and performance validation. This also includes overall accepted requirements on and quality criteria for fluorescence standards. In addition, uncertainties for typical instrument calibrations and fluorescence measurements should be determined, e.g., by NMIs and expert laboratories, for different levels of accuracy of instrument characterization to define state-of-the-art uncertainties and to help users with the choice of instrument qualification strategies and fit-for-purpose standards. Here, interlaboratory comparisons on application-relevant fluorescence quantities and measurements are a straightforward tool. Accordingly, the improvement of quality assurance in fluorometry requires a close collaboration between NMIs, instrument manufacturers, regulatory agencies, scientific organizations, and fluorescence users.

**Acknowledgements** UR gratefully acknowledges financial support from the Federal Ministry of Economics and Technology (BMWi; grants VI A 2-18/01 and VI A 2-17/03) and the German Ministry of Education and Research (BMBF; grant 13N8848).

## References

1. Lakowicz JR (1999) Principles of fluorescence spectroscopy, 2nd edn. Kluwer Academic/Plenum, New York
2. Lakowicz JR (ed) (1992–2004) Topics in fluorescence spectroscopy series, vols 1–8. Plenum, New York
3. Valeur B (ed) (2002) Molecular fluorescence: principles and applications. Wiley-VCH, Weinheim
4. Wolfbeis OS (ed) (2001–2004) Springer series on fluorescence, methods and applications, vols 1–3. Springer, Berlin
5. Schulman SG (ed) (1985–1993) Molecular luminescence spectroscopy, parts 1–3. Wiley Interscience, New York
6. Mason WT (1999) Fluorescent and luminescent probes for biological activity, 2nd edn. Academic, San Diego
7. Mielenz KD (1982) Optical radiation measurements, vol 3. Measurement of photoluminescence. Academic, New York
8. Burgess C, Jones DG (1995) Spectrophotometry, luminescence and colour. Elsevier, Amsterdam
9. Gaigalas AK, Li L, Henderson O, Vogt R, Barr J, Marti G, Weaver J, Schwartz A (2001) The development of fluorescence intensity standards. *J Res Natl Inst Stand Technol* 106:381
10. Resch-Genger U, Hoffmann K, Nietfeld W, Engel A, Ebert B, Macdonald R, Neukammer J, Pfeifer D, Hoffmann A (2005) How to improve quality assurance in fluorometry: fluorescence-inherent sources of error and suited fluorescence standards. *J Fluoresc* 15:337
11. Parker CA (1968) Photoluminescence of solutions. Elsevier, Amsterdam
12. Marin NM, MacKinnon N, MacAulay C, Chang SK, Atkinson EN, Cox D, Serachitopol D, Pikkula B, Follen M, Richards-Kortum R (2006) Calibration standards

- for multicenter clinical trials of fluorescence spectroscopy for in vivo diagnosis. *J Biomed Opt* 11:014010-1
13. Jameson DM, Croney JC, Moens PDJ (2003) Fluorescence: basic concepts, practical aspects, and some anecdotes. *Methods Enzymol* 360:1
  14. Nickel B (1996) Pioneers in photochemistry: from the Perrin diagram to the Jablonski diagram. *EPA Newsletter* 58:9
  15. Nickel B (1997) Pioneers in photophysics: from the Perrin diagram to the Jablonski diagram. Part 2. *EPA Newsletter* 61:27
  16. Nickel B (1998) Pioneers in photophysics: from Widemann's discovery to the Jablonski diagram. Part 2. *EPA Newsletter* 64:19
  17. ASTM E 388-04 (2004, original version 1972) Spectral bandwidth and wavelength accuracy of fluorescence spectrometers. In: *Annual book of ASTM standards*, vol 03.06
  18. ASTM E 578-01 (2001, original version 1983) Linearity of fluorescence measuring system. In: *Annual book of ASTM standards*, vol 03.06
  19. ASTM E 579-04 (2004, original version 1984) Limit of detection of fluorescence of quinine sulfate. In: *Annual book of ASTM standards*, vol 03.06
  20. Miller JN (ed) (1981) *Techniques in visible and ultraviolet spectrometry*, vol 2. *Standards in fluorescence spectrometry*. Chapman and Hall, New York
  21. Eaton DF (1988) Reference compounds for fluorescent measurements. *Pure Appl Chem* 60:1107
  22. Commission Internationale de l'Éclairage (1986) *Colorimetry*, 2nd edn. CIE-Publ 15.2. CIE, Vienna
  23. Rich DC, Martin D (1999) Improved model for improving the inter-instrument agreement of spectrophotometers. *Anal Chim Acta* 380:263
  24. Zwinkels J (2007) Surface fluorescence: the only standardized method of measuring luminescence. In: Resch-Genger U (ed) *Standardization in fluorometry: state of the art and future challenges*. Springer, Berlin
  25. Vogt RF Jr, Marti GE, Zenger VE (2007) Need for standardization of fluorescence measurements from the regulator's view. In: Resch-Genger U (ed) *Standardization in fluorometry: state of the art and future challenges*. Springer, Berlin
  26. (2004) Approved guideline for fluorescence calibration and quantitative measurements of fluorescence intensity. *Clinical and Laboratory Standards Institute (CLSI)*, USA
  27. Chapman JH, Förster T, Kortüm G, Parker CA, Lippert E, Melhuish WH, Nebbia G (1963) Proposal for the standardization of reporting fluorescence emission spectra. *J Am Chem Soc* 17:171
  28. Saunders G, Parkes H (1999) *Analytical molecular biology: quality and validation*. RSC, Cambridge
  29. (2005) ISO/IEC 17025, General requirements for the competence of testing and calibration laboratories, 2nd edn. *International Organization for Standardization*, Geneva
  30. Hollandt J, Taubert DR, Seidel J, Resch-Genger U, Gugg-Helminger A, Pfeifer D, Monte C (2005) Traceability in fluorometry: part I. Physical standards. *J Fluoresc* 15:301
  31. Monte C, Resch-Genger U, Pfeifer D, Taubert RD, Hollandt J (2006) Linking fluorescence measurement to radiometric units. *Metrologia* 43:S89
  32. Braslavsky SE (2007) Glossary of terms used in photochemistry, 3rd edn (IUPAC recommendations 2006). *Pure Appl Chem* 79:293

33. Nighswander-Rempel SP (2006) Quantum yield calculation from strongly absorbing chromophores. *J Fluoresc* 16:483
34. Verhoeven JW (1996) Glossary of terms used in photochemistry. *Pure Appl Chem* 68:2223
35. Melhuish WH (1984) Nomenclature, symbols, units and their usage in spectrochemical analysis VI: molecular luminescence spectroscopy. *Pure Appl Chem* 56:231
36. Mielenz KD (1978) Refraction correction for fluorescence spectra of aqueous solutions. *Appl Opt* 17:2876
37. DeRose PC, Wang L, Cramer G, Gaigalas A, Resch-Genger U, Panne U (2007) Need for and metrological approaches toward standardization of fluorescence measurements from the view of national metrological institutes. In: Resch-Genger U (ed) *Standardization in fluorometry: state of the art and future challenges*. Springer, Berlin
38. Williams ATR, Winfield SA, Miller JN (1983) Relative fluorescence quantum yields using a computer controlled luminescence spectrometer. *Analyst* 108:1067
39. Boivin LP (2002) Study of bandwidth effects in monochromator-based spectral responsivity measurements. *Appl Opt* 41:1929
40. (1995) ISO; Guide to the expression of uncertainty in measurement; ISBN 92-67-10188-9, 1st edn. International Organization for Standardization, Geneva
41. Melhuish WH (1965) Quantum efficiencies of fluorescence of organic substances: effect of solvent and concentration of the fluorescent solute. *J Phys Chem* 65:229
42. Chauvin A-S, Gumy F, Imbert D, Bünzli J-C (2004) Europium and terbium tris(dipicolinates) as secondary standards for quantum yield determination. *Spectrosc Lett* 37:517
43. DeRose PC, Kramer GW (2005) Bias in the absorption coefficient determination of a fluorescent dye, Standard Reference Material 1932 fluorescein solution. *J Luminesc* 113:314
44. Benson RC, Kues HA (1977) Absorption and fluorescence properties of cyanine dyes. *J Chem Eng Data* 22:379
45. (2000, corrigendum 2003) ISO; General requirements for the competence of reference material producers, 2nd edn. International Organization for Standardization, Geneva
46. (2006) ISO; Reference materials—general and statistical principles for certification. International Organization for Standardization, Geneva
47. DeRose PC, Early EA, Kramer GW (2007) Qualification of a fluorescence spectrometer for measuring true fluorescence spectra. *Rev Sci Instrum* 78:033107
48. Howarth P, Redgrave F (2003) *Metrology in short*, 2nd edn. MKom Aps, Denmark
49. Bosse H, Wilkening G (2005) Developments at PTB in nanometrology for support of the semiconductor industry. *Meas Sci Technol* 16:2155
50. Dai G, Koenders L, Pohlenz F, Dziomba T, Danzebrink H-U (2005) Accurate and traceable calibration of one-dimensional gratings. *Meas Sci Technol* 16:1241
51. Monte C, Pilz W, Resch-Genger U (2005) Linking fluorescence to the scale of spectral sensitivity—the BAM reference fluorometer. *Proc SPIE* 5880:588019-1
52. Eaton DF (1990) Recommended methods for the fluorescence decay analysis. *Pure Appl Chem* 62:1631
53. Resch-Genger U, Pfeifer D, Monte C, Pilz W, Hoffmann A, Spieles M, Rurack K, Taubert DR, Schönenberger B, Nording P (2005) Traceability in fluorometry: part II. Spectral fluorescence standards. *J Fluoresc* 15:315
54. Mielenz KD, Eckerle KL (1972) Spectrophotometer linearity testing using the double-aperture method. *Appl Opt* 11:2294



55. Zwinkels JC, Gignac DS (1991) Automated high precision variable aperture for spectrophotometer linearity testing. *Appl Opt* 30:1678
56. Hoffmann K, Monte C, Pfeifer D, Resch-Genger U (2005) Standards in fluorescence spectroscopy: simple tool for the characterization of fluorescence instruments. *GIT Lab J Eur*, p 29
57. Salit CJML et al (1996) Wavelengths of spectral lines in mercury pencil lamps. *Appl Opt* 35:74
58. [www.physics.nist.gov/PhysRefData/Handbook/index.html](http://www.physics.nist.gov/PhysRefData/Handbook/index.html) last visit: August 2007
59. Harrison GR (1982) MIT wavelength tables, vol 2. Wavelengths by element. MIT, Cambridge
60. Zaidel AN, Prokofev VK, Raiskii SM, Slavnyi VA, Shreider EY (1970) Tables of spectral lines. Plenum, New York
61. Calibration light source CAL-2000, MIKROPACK GmbH (<http://www.mikropack.de>) or Ocean Optics Inc (<http://www.oceanoptics.com>)
62. (2003) Certificate of analysis, Standard Reference Material 2036, near-infrared wavelength/wavenumber reflection standard. National Institute of Standards and Technology, Gaithersburg
63. Lifshitz IT, Meilman ML (1989) Standard sample for calibrating wavelength scales of spectral fluorometers. *Sov J Opt Technol* 55:487
64. Photon Technology International Inc. (DYAG) FA-2036
65. Knight A, Gaunt J, Davidson T, Chechik V, Windsor S (2004) Evaluation of the suitability of quantum dots as fluorescence standards. NPL report DQL-AS 007
66. Bartholomeusz D, Andrade JD (2002) Photodetector calibration method for reporting bioluminescence measurements in standardized units. In: *Bioluminescence & chemiluminescence: progress & current applications*. Proceedings of the Symposium on Bioluminescence and Chemiluminescence, World Scientific, Singapore, p 189
67. Velapoldi RA, Tonnesen HH (2004) Corrected emission spectra and quantum yields for a series of fluorescent compounds in the visible spectral region. *J Fluoresc* 14:465
68. Hofstraat JW, Latuhihin MJ (1994) Correction of fluorescence spectra. *Appl Spectrosc* 48:436
69. Kortüm G, Finckh B (1941–1944) Eine photographische Methode zur Aufnahme quantitativer vergleichbarer Fluoreszenzspektren. *Spectrochim Acta* 2:137
70. Lippert E, Nägele W, Seibold-Blankenstein I, Staiger U, Voss W (1959) Messung von Fluoreszenzspektren mit Hilfe von Spektralphotometern und Vergleichsstandards. *Z Anal Chem* 170:1
71. Gardecki JA, Maroncelli M (1998) Set of secondary emission standards for calibration of the spectral responsivity in emission spectroscopy. *Appl Spectrosc* 52:1179
72. Thompson A, Eckerle KL (1989) Standards for corrected fluorescence spectra. *Proc SPIE Int Soc Opt Eng* 1054:20
73. Eppeldauer G (1998) Spectral response based calibration method of tristimulus colorimeters. *J Res Natl Inst Stand Technol* 103:615
74. Mielenz KD, Cehelnik ED, McKenzie RL (1976) Elimination of polarization bias in fluorescence intensity measurements. *J Phys Chem* 64:370
75. Azumi T, McLynn SP (1962) Polarization of the luminescence of phenanthrene. *J Chem Phys* 37:2413
76. (1979) Certificate of analysis, Standard Reference Material 936, quinine sulfate dihydrate. National Bureau of Standards, Gaithersberg
77. (1994) Certificate of analysis, Standard Reference Material 936a, quinine sulfate dihydrate. National Institute of Standards and Technology, Gaithersberg

78. Velapoldi RA, Mielenz KD (1980), A fluorescence standard reference material: quinine sulfate dihydrate. NBS Spec Publ 260–64, PB 80132046, Springfield
79. (2006) Certificates of analysis, Certified Reference Materials BAM-F001, BAM-F002, BAM-F003, BAM-F004, and BAM-F001. Spectral fluorescence standard for the determination of the relative spectral responsivity of fluorescence instruments within its emission range. Certification of emission spectra in 1-nm intervals. Federal Institute for Materials Research and Testing (BAM), Berlin
80. (2006) Certificate of analysis, Standard Reference Material 2940. Relative intensity correction standard for fluorescence spectroscopy: orange emission. Certification of emission spectra in 1-nm intervals. National Institute of Standards and Technology. <http://ts.nist.gov/ts/htdocs/230/232/232.htm>
81. (2006) Certificate of analysis, Standard Reference Material 2941. Relative intensity correction standard for fluorescence spectroscopy: green emission. Certification of emission spectra in 1-nm intervals. National Institute of Standards and Technology. <http://ts.nist.gov/ts/htdocs/230/232/232.htm>
82. (1989) Certificate of analysis, Standard Reference Material 1931, fluorescence emission standards for the visible region. National Institute of Standards and Technology. (This SRM is no longer available)
83. (2006) Certificate of analysis, Certified Reference Materials BAM-F001–BAM-F005, Calibration Kit Spectral Fluorescence Standards for the determination of the relative spectral responsivity of fluorescence instruments. Certification according to ISO guides 34 and 35 in 1-nm steps for three different spectral bandpasses of the BAM fluorometer. Federal Institute for Materials Research and Testing (BAM), Berlin
84. Pfeifer D, Hoffmann K, Hoffmann A, Monte C, Resch-Genger U (2006) The Calibration Kit Spectral Fluorescence Standards: a simple tool for the standardization of the spectral characteristics of fluorescence instruments. *J Fluoresc* 16:581
85. Resch-Genger U, Pfeifer D (2006) Certification report, Calibration Kit Spectral Fluorescence Standards BAM-F001–BAM-F005. BAM, Berlin
86. Ejder E (1969) Methods of representing emission, excitation, and photoconductivity spectra. *J Opt Soc A* 59:223
87. Parker CA, Rees WT (1960) Correction of fluorescence spectra and measurement of fluorescence quantum efficiency. *Analyst* 85:587
88. Fox NP (1991) Trap detectors and their properties. *Metrologia* 28:197
89. Melhuish WH (1975) Modified technique for determining the wavelength-sensitivity curve of a spectrofluorometer. *Appl Opt* 14:26
90. Hart SJ, Jones PJ (2001) Fiber-optic quantum counter for incident excitation correction in fluorescence measurements. *Appl Spectrosc* 55:1717
91. Demas JN, Crosby GA (1971) The measurement of photoluminescence quantum yields. A review. *J Phys Chem* 75:991
92. Mielenz KD, Velapoldi RA, Mavrodineanu (1977) Standardization in spectrophometry and luminescence measurements. NBS Special Publication 466, Gaithersfield
93. Froehlich P (1989) Under the sensitivity specification for a fluorescence spectrophotometer. *Int Lab* 42
94. Kovach RJ, Peterson WM (1994) The measurement of sensitivity in fluorescence spectroscopy. *Am Lab* 32G
95. Greenham NC, Samuel IDW, Hayes GR, Phillips RT, Kessener YARR, Moratti SC, Holmes AB, Friend RH (1995) Measurement of absolute photoluminescence quantum efficiencies in conjugated polymers. *Chem Phys Lett* 241:89
96. de Mello JC, Wittmann HF, Friend RH (1997) An improved experimental determination of external photoluminescence quantum efficiency. *Adv Mater* 9:230

97. He L, Hattori R, Kanicki J (2000) Light output measurements of the organic light-emitting devices. *Rev Sci Instrum* 71:2104
98. Rohwer LS, Martin JE (2005) Measuring the absolute quantum efficiency of luminescent materials. *J Luminesc* 115:77
99. Madge D, Brannon JH, Cremers TL, Olmsted J III (1979) Absolute luminescence yield of cresyl violet. A standard for the red. *J Phys Chem* 83:696
100. Chen RF (1972) Measurements of absolute values in biochemical fluorescence spectroscopy. *J Res Natl Bur Stand* 76A:593
101. Greenham NC, Friend RH, Bradley DDC (1994) Angular dependence of the emission from a conjugated polymer light-emitting diode: implications for efficiency calculations. *Adv Mater* 6:491
102. Porrès L, Holland A, Pålson L-O, Monkman AP, Kemp C, Beeby A (2006) Absolute measurements of photoluminescence quantum yields of solutions using an integrating sphere. *J Fluoresc* 16:267
103. Pålsson L-O, Monkman AP (2002) Measurements of solid state photoluminescence quantum yields of films using a fluorimeter. *Adv Mater* 14:757
104. Monte C, Pilz W, Resch-Genger U (2005) Linking fluorescence spectroscopy to the scale of spectral sensitivity: the BAM reference fluorometer. *Proc SPIE* 5880:588019-1
105. Fischer M, Georges J (1996) Fluorescence quantum yield of rhodamine 6G in ethanol as a function of concentration using thermal lens spectrometry. *Chem Phys Lett* 260:115
106. Magde D, Wong R, Seybold PG (2002) Fluorescence quantum yields and their relation to lifetimes of rhodamine 6G and fluorescein in nine solvents: improved absolute standards for quantum yields. *Photochem Photobiol* 75:327
107. Kubin RF, Fletcher AN (1982) Fluorescence quantum yields of some rhodamine dyes. *J Luminesc* 27:455
108. Boens N, Qin W, Basaric N, Hofkens J, Ameloot M, Pouget J, Lefevre J P, Valeur B, Gratton E, vandeVen M, Silva ND, Engelborghs Y, Willaert K, Sillen A, Rumbles G, Phillips D, Visser AJWG, vanHoek A, Lakowicz JR, Malak H, Gryczynski I, Szabo AG, Krajcarski DT, Tamai N, Miura A (2007) Fluorescence lifetime standards for time and frequency domain fluorescence spectroscopy. *Anal Chem* 77:2137
109. Giebeler R, McGown E, French T, Owicki JC (2005) Performance validation for microplate fluorimeters. *J Fluoresc* 15:363
110. Hoffmann K, Resch-Genger U, Nitschke R (2005) Simple tool for the standardization of confocal spectral imaging systems. *GIT Imaging Microsc*, p 18
111. Ray KG, McCreery RL (1997) Simplified calibration of instrument response function for Raman spectrometers based on luminescence intensity standards. *Appl Spectrosc* 51:108
112. Frost KJ, McCreery RL (1998) Calibration of Raman spectrometer instrument response function with luminescence standards: an update. *Appl Spectrosc* 52:1614

# Fluorescence Quantum Yields: Methods of Determination and Standards

Knut Rurack

Div. I.5, Bundesanstalt für Materialforschung und -prüfung (BAM),  
Richard-Willstätter-Str. 11, 12489 Berlin, Germany  
*knut.rurack@bam.de*

1	Introduction . . . . .	102
2	Scope and Terminology . . . . .	105
3	Absolute Fluorescence Quantum Yields . . . . .	106
3.1	Optical Methods . . . . .	107
3.2	Calorimetric Methods . . . . .	115
3.2.1	Photoacoustic Spectroscopy . . . . .	116
3.2.2	Thermal Lensing . . . . .	119
3.2.3	Actinometry . . . . .	122
4	Relative Fluorescence Quantum Yields . . . . .	123
4.1	Measurements at Room Temperature . . . . .	126
4.2	Measurements as a Function of Temperature . . . . .	133
5	Fluorescence and Phosphorescence Quantum Yields . . . . .	136
6	Fluorescence Quantum Yield Standards . . . . .	136
7	Outlook . . . . .	137
	References . . . . .	140

**Abstract** The fluorescence quantum yield  $\Phi_f$  is a key property that characterizes the ability of a fluorophore to convert absorbed photons into emitted photons under various environmental conditions. Knowledge of it is important for the successful development of fluorometric indication and visualization methods and for the understanding of light-driven processes in the natural sciences.  $\Phi_f$  is a molecule- or material-related parameter and can thus significantly differ from the fraction of absorbed photons that are actually measured as the fluorescence signal of a certain sample, e.g., when the signal is modulated by reabsorption, self-quenching or polarization effects. The determination of  $\Phi_f$  can be performed in absolute measurements or relative to a fluorescent standard material with a known  $\Phi_f$  by optical or calorimetric methods. Here the different procedures and techniques are described and compared, and the suitability of a representative number of dyes that have been proposed as fluorescence reference materials in the past 25 years is discussed. Besides addressing specific issues such as low-temperature measurements and the appropriate choice of standards and measurement conditions, we conclude with recommendations for better standardization and quality management in this area.

**Keywords** Actinometry · Calorimetry · Fluorescence · Photoacoustic spectroscopy · Quantum yield · Standard · Thermal lensing

### Abbreviations

9,10-DPA	9,10-Diphenylanthracene
BL	Bioluminescence
BP(OH) <sub>2</sub>	2,2'-Bipyridyl-3,3'-diol
CH	Cyclohexane
CL	Chemiluminescence
DANS	1-Dimethyl-aminonaphthalene-5-sulfonate
DCM	4-Dicyanomethylene-2-methyl-6- <i>p</i> -dimethylaminostyryl-4 <i>H</i> -pyran
DMF	Dimethyl formamide
DMSO	Dimethyl sulfoxide
ECL	Electrochemiluminescence
EG	Ethylene glycol
IUPAC	International Union of Pure and Applied Chemistry
MCH	Methylcyclohexane
NIST	National Institute of Standards and Technology (US)
PAS	Photoacoustic spectroscopy
PBS	Phosphate-buffered saline
POPOP	<i>p</i> -Bis[2-(5-phenyloxazolyl)]-benzene
PPO	2,5-Diphenyloxazol
PTB	Physikalisch-Technische Bundesanstalt (D)
PVA	Polyvinylalcohol
QS	Quinine sulfate
RT	Room temperature
TPB	Tetraphenylbutadiene
TPE	Tetraphenylethylene
TRITC	Tetramethyl rhodamine isothiocyanate

## 1

### Introduction

Quantitative fluorometry and the measurement of fluorescence intensities are intrinsically connected to the fluorescence quantum yield ( $\Phi_f$ ) of an excited target substance. The knowledge of the fluorescence quantum yield of a compound or material is thus important for the successful development of fluorometric indication and visualization methods or for the understanding of processes in the natural sciences that rely or depend on, operate with or involve the conversion of (excitation) energy into light [1–4]. For instance, sensitive analytical and imaging techniques essentially rely on molecular probes or labels that possess high intrinsic fluorescence quantum yields [5–7]. Research on laser or scintillator materials involves the determination of fluorescence quantum yields as one of the primary steps [8, 9]. Charge and energy transfer processes play an important role in areas such

as solar energy conversion and molecular electronics, the efficiency of the processes often being connected to the fluorescence quantum yields of key species involved [10–13]. Basic research in photophysics and photochemistry is essentially unimaginable without consideration of one of the four experimental parameters of fluorescence, the spectrum, lifetime, polarization and quantum yield [14–16].

The fluorescence quantum yield generally represents the fraction of photons that is emitted from an ensemble of excited species after optical excitation [Eq. 1;  $N_{\text{em}}(\lambda_{\text{ex}})$  = number of emitted photons,  $N_{\text{abs}}(\lambda_{\text{ex}})$  = number of absorbed photons]. For fluorescent molecules under ideally dilute conditions it is identical to the quantum efficiency ( $\eta$ ) of this primary photochemical process and is intrinsically related to the fluorescence lifetime ( $\tau_f$ ) through the radiative and the nonradiative transition probabilities  $k_f = \Phi_f \tau_f^{-1}$  and  $k_{\text{nr}} = (1 - \Phi_f) \tau_f^{-1}$  [17]. The fluorescence quantum yield is a molecule- or material-related parameter and can thus significantly differ from the fraction of absorbed photons that are actually measured as the fluorescence signal of a certain sample. For solution-based measurements in conventional cuvettes, reabsorption, self-quenching or polarization effects, for example, can influence the results

$$\Phi_f = N_{\text{em}}(\lambda_{\text{ex}}) / N_{\text{abs}}(\lambda_{\text{ex}}). \quad (1)$$

Quantum yields of fluorescence can be measured in two different ways: relative to a fluorescent standard material with a known  $\Phi_f$  or as an absolute quantity. The methods that have been employed for such measurements can be divided into optical methods, which directly measure the emitted photons, and calorimetric methods, which allow an indirect determination through the heating of a sample, i.e., through the efficiency with which the energy of absorbed photons is converted into heat. Since Vavilov first introduced both the term “fluorescence quantum yield” and a method for its determination for fluorescent organic dyes dissolved in liquid solution [18], numerous papers have appeared that deal with measurements of fluorescence quantum yields and/or fluorescent compounds that can be used as standards. Reference materials with verified and approved fluorescence quantum yields are essentially important for all users of fluorescence methods since the most popular method of  $\Phi_f$  determination is still by far the relative measurement of an unknown sample against such a fluorescence standard with a conventional fluorometer, frequently referred to as the Parker–Rees method [19].

Various review and feature articles have discussed the many issues related to the determination of fluorescence quantum yields as well as the requirements on and reliability of several fluorescence quantum yield standards proposed during the past 80 years. Most of these papers appeared in

the 1970s and 1980s during the time when the use of commercial fluorometers was routine and lasers and computers became widely established in many research laboratories. One of the first landmark articles was the above-mentioned publication by Parker and Rees that introduced the determination of  $\Phi_f$  relative to that of a known standard [19], quinine sulfate in 0.1 N  $\text{H}_2\text{SO}_4$  with  $\Phi_f = 0.55$  as given by Melhuish in his first paper on absolute fluorescence quantum yields [20]. In 1969, Testa reported and critically commented on a collection of fluorescence quantum yield standards [21]. A key review article in the field appeared in 1971, with Demas and Crosby discussing in detail the various methods of absolute and relative fluorescence quantum yield determinations [22]. A series of articles was published in the following year in the November/December issue of the Journal of Research of the National Bureau of Standards dealing with absolute fluorometry and quantum efficiencies, as well as with organic and inorganic compounds in the liquid or solid state as potential reference materials [23–27]. In mid 1976, another series of papers on similar issues was published again in the National Bureau of Standards' journal [17, 28–30]. Demas updated the review of 1971 [22] in 1982 as part of a monograph on *Optical Radiation Measurements* [31]. Five years later, a monograph on *Advances in Standards and Methodology in Spectrophotometry* contained two contributions on liquid and solid standards in fluorometry [32, 33]. Also in 1982, Grum highlighted the requirements on and the need for fluorescence standards from the point of view of industrial use [34]. In 1989, Velapoldi and Epstein broadened their scope and reported on standards for macro- and microspectrofluorometry [35]. Based on this broad history of collective work on fluorescence standards, quantum yields and absolute fluorometry, IUPAC's *Commission on Photochemistry* published some recommendations on reference materials for fluorescence measurements, prominently including standards for fluorescence quantum yields [36, 37]. In 1999, Fery-Forgues and Lavabre also brought the issue to the attention of people involved in the education of young scientists [38].

It is probably no coincidence that the last very active period (1982–1989) of general publications on issues of quantitative fluorometry and  $\Phi_f$  standards for classical fluorometer-based applications and methods overlaps with the emergence and/or virtually exponential growth of other formats in quantitative fluorometry such as fluorescence microscopy, flow cytometry, biochemical amplification techniques and other assays based on fluorescence scanners and readers. Moreover, although a substantial body of work existed on fluorescence quantum yield measurements and the respective standards (see preceding paragraph), considerable efforts were still necessary to establish first standard procedures, reference materials and recommendations on quality assurance in these emerging areas of fluorescence spectroscopy (see, e.g., [39] and references therein). The more classical field of research on fluorescence quantum yield standards has thus been drifting

out of focus in the recent past. Nonetheless, when keeping in mind the list of unresolved issues in connection with fluorescence quantum yields as addressed in the IUPAC recommendations—the two most prominent remarks being: “far-red and near-infrared standards are not known” and “no good standards exist for low intensity emitters”—it is not surprising that quality assurance in the traditional areas of fluorometry has recently seen its revival [40].

All the issues and details discussed in the seminal reviews on the absolute measurement of fluorescence and the determination of fluorescence quantum yields [22, 31] will not be repeated here. Instead, the work on absolute and relative measurements of, as well as fluorescence standards proposed for,  $\Phi_f$  that has appeared in the last 25 years will be summarized.

## 2

### Scope and Terminology

The present chapter deals with the quantum yield of the most widespread type of luminescence, fluorescence, that is, with the photon efficiency of the radiative transition between an excited singlet state (usually the first excited singlet state  $S_1$ ) and the singlet ground state ( $S_0$ ) after optical excitation of the emitter. Many of the issues discussed here also pertain to phosphorescence quantum yields ( $\Phi_p$ ) that characterize the radiative transition between an excited triplet state (usually  $T_1$ ) and  $S_0$  after optical excitation. However,  $\Phi_p$  are not treated in detail here and only some aspects are described in Sect. 5. Luminescence phenomena such as bioluminescence (BL), chemiluminescence (CL) or electrochemiluminescence (ECL) where the determination of quantum yields is less frequently attempted are also not subject of this paper. Basic considerations and experimental details can be found in authoritative original works such as [41] on CL, [42] on BL and [43] on ECL or recent comprehensive reviews such as [44, 45], [46] and [47, 48] on CL, BL and ECL respectively. Other luminescence methods such as sono-, tribo-, thermo- or radioluminescence where emission involves ionization/ion recombination, surface effects or bubble dynamics and collapse after excitation with high-energy particles or electron beams, friction or ultrasound are additionally not the subject of this article [49–57].

Fluorescence quantum yields have been mostly determined for substances in solution and the present contribution will restrict itself to this subject. The peculiarities associated, for instance, with the determination of absolute quantum yields of organic molecules in the gas phase will not be discussed [58–60]. Likewise, neither will quantum yield measurements of organic emitters in the crystalline state or adsorbed on solid surfaces [61–65] as well as of multichromophoric biomacromolecules [66, 67] be described here. Owing to the complexity of the method, the problems in the preparation



of comparable and homogeneous samples and a general lack of reliable reference materials, organic dyes in polymer matrices [68–73] and inorganic solid-state emitters [25, 74–76] are not subjects of this article.

Throughout the literature, the terms “fluorescence quantum yield”, “fluorescence yield”, “fluorescence efficiency”, “photon yield”, “photon efficiency” and “quantum yield” are often used for the same quantity. Moreover, frequently “(photo)luminescence” (“(photo)luminescence quantum yield” and “(photo)luminescence yield”, etc.) are used synonymously for “fluorescence”. Some terms are more frequently or exclusively used in radiometry, others, for example, in applied chemistry. For consistency, only the term “fluorescence” in combination with “quantum yield” ( $\Phi_f$ ) is used in this text.  $\Phi_f$ , the *fluorescence quantum yield* of a certain species, is by definition independent of sample absorption, excitation intensity and wavelength.

(Note: although in 1984, IUPAC’s *Commission on Spectrochemical and Other Optical Procedures for Analysis* published recommendations on the use of terms in molecular luminescence spectroscopy [77], e.g., to use the term “luminescence quantum yield” only for the ratio of the number of the emitted to the absorbed photons of a species in a sample and to use the term “luminescence quantum efficiency” only for the fraction of molecules in a particular excited state that emit luminescence, the rather arbitrary choice of terminology in research papers did not change very much. Last year’s update by IUPAC’s *Organic and Biomolecular Chemistry Division (III)* and *Physical and Biophysical Chemistry Division (I)* gives the following definitions. *Quantum efficiency*: “Useful energy delivered or bound divided by the energy supplied, i.e., energy output/energy input. It is also used in the sense of a quantitative measure of the relative rate of a given step,  $k_i$ , involving a species with respect to the sum of the rates of all of the parallel steps, which depopulate that species.” *Quantum yield*: “Number of defined events occurring per photon absorbed by the system.” and “Note: for a primary photochemical process, *quantum efficiency* is identical to *quantum yield*.” [78].)

### 3

#### **Absolute Fluorescence Quantum Yields**

The majority of fluorometric applications measure signals from fluorophores in optically dilute solutions. Moreover, the most common methods of the relative determination of fluorescence quantum yields (Parker–Rees and adapted methods) also rely on the measurement of samples with low optical densities. Thus, when the aim of an absolute fluorescence measurement is the introduction and provision of a fluorescence standard, it is important that such measurements are performed on those chemical species that have to be used later on by others for dilute conditions. Regardless of the use of

calorimetric, optical or other methods, it has to be assured that only isolated (monomeric) molecules of the emitter are present in solution. Aggregation or other concentration-induced effects that already alter the ground-state properties of a fluorescent compound and consequently lead to a different excited state or emission behavior must be strictly avoided.

When one considers fluorescent dyes that are widely commercially available in the most important solvents (water, basic/acidic aqueous solutions, methanol, ethanol,  $\text{CH}_2\text{Cl}_2$ , dimethyl sulfoxide (DMSO)—often used for near-infrared emitting compounds—and toluene and cyclohexane as nonpolar representatives), ca. one-third of the absolute fluorescent quantum yields published to date were obtained in the 1950s and 1960s, more than 50% in the 1970s and 1980s and only about 15% later than 1990. Among the methods employed, ca. 40% of the studies used optical techniques, ca. 25% classical calorimetric techniques and ca. 10–15% photoacoustic and thermal lensing methods (with others methods including e.g., actinometric ones, covering the rest). Table 1 lists a representative selection of widely popular fluorophores for which absolute  $\Phi_f$  have been determined in the past 25 years together with those of the dyes recommended by the IUPAC Commission where the recommendation is based on an absolute value measured (Table 1, entries 1-1, 1-4, 1-6, 1-17, 1-64 and 1-65).

### 3.1

#### Optical Methods

Because the first work on the determination of fluorescence quantum yields utilized an optical method [18], optical approaches will be discussed first. When scrutinizing the literature, it is noticeable that the traditional techniques using a solid-state scatterer such as magnesium oxide or barium sulfate in combination with front-face excitation/detection under acute angles, as introduced by Vavilov [18] and established by Melhuish [20, 79, 80], has not seen a great revival in the last 25 years (Fig. 1A). Although lasers have become a common tool in optical spectroscopy in the past decades, the prediction made by Demas in 1982 that the decline of the use of this method during the 1970s would be overcome by the availability of potent laser excitation sources was not met by reality [31]. In 1982, Galanin et al. published a study on the determination of absolute fluorescence quantum yields of a series of well-known dyes in which they compared the results obtained by the Vavilov/Melhuish method with those employing the same solid-state scatterer in an integrating sphere (Table 1, entries 1-7, 1-11, 1-12, 1-23, 1-24, 1-35, 1-36, 1-50, 1-51, 1-62 and 1-63) [81]. In general, these researchers found good agreement between the values obtained with both methods, although the integrating sphere yielded somewhat lower values in most cases. The authors attributed this fact to the influence of and type of the correction employed for reabsorption for the considerably high dye

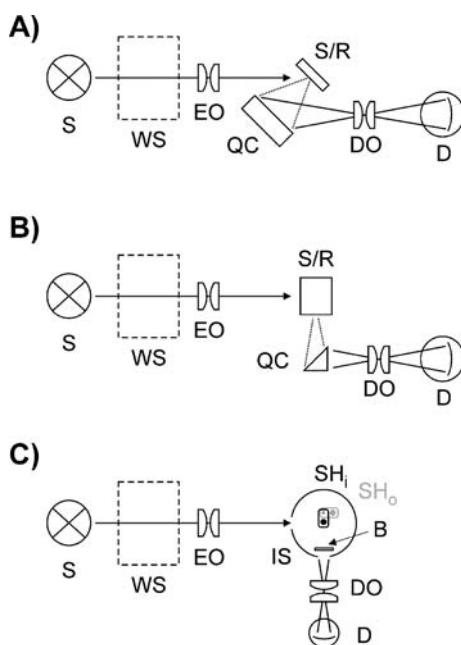


**Fig. 1** Schematic setup of instruments for optically measuring absolute fluorescence quantum yields by **A** front-face geometry (Vavilov–Melhuish approach), **B** 90° geometry (Weber–Teale approach) and **C** employing an integrating sphere. *S* Light source, *WS* device for selecting monochromatic light (optional, e.g., in the case of *S* being a laser), *EO* excitation optics, *S/R* position of sample or reference, *QC* quantum counter, *DO* detection optics, *D* detector, *IS* integrating sphere, *SH<sub>i</sub>* sample holder positioned in the excitation beam, *SH<sub>o</sub>* sample holder positioned out of the excitation beam, *B* baffle

concentrations they used, 20  $\mu\text{M}$  at minimum. The results also agree well with the generally accepted values of the fluorescence quantum yields of the compounds as obtained by other researchers. It should be noted that Galanin et al. used a conventional lamp and not a laser for excitation. Solution scatterers such as colloidal silica particles or glycogen, which were commonly used in combination with the classical 90° measurement geometry (the so-called Weber–Teale method [82], Fig. 1B), have also not been used in  $\Phi_f$  determinations latterly, again in contrast to predictions by Demas that common availability of laser sources and photon-counting detectors would overcome the strongest limitation of this method, its relatively low sensitivity [31].

Before taking a closer look at the few approaches that have been made toward the measurement of absolute fluorescence quantum yields by optical methods in recent years, the potential sources of error will be looked at. Many publications, including various contributions to this monograph, have discussed these potential errors in detail so that the following description will be

**Table 1** Fluorescence quantum yields of various popular or common fluorescent dyes as obtained by absolute methods in the last 25 years

Entry	Compound	Solvent	Conditions <sup>a</sup>	$\lambda_{exc}/nm^b$	$\Phi_f^c$	Method <sup>d</sup>	Standard <sup>e</sup>	Refs.
1-1	Benzene	CH	296 K, deg.	254	$0.053 \pm 0.008$	Optical <sup>f</sup>	Colloidal silica soln. <sup>f</sup>	[36, 181]
1-2	Azulene	Ethanol	RT, deg.	337	$0.04 \pm 0.01$	PAS <sup>g</sup>	2-Hydroxybenzophenone	[119]
1-3	PPO	Ethanol	RT, deg.	337	$0.89 \pm 0.03$	PAS <sup>g</sup>	2-Hydroxybenzophenone	[119]
1-4	Anthracene	Ethanol	296 K, deg.	366	$0.27 \pm 0.01$	Optical <sup>f</sup>	Colloidal silica soln. <sup>f</sup>	[36, 181]
1-5	Anthracene	Ethanol	RT, deg.	337	$0.22 \pm 0.06$	PAS <sup>g</sup>	2-Hydroxybenzophenone	[119]
1-6	9,10-DPA	CH	298 K, deg.	325	$0.90 \pm 0.04$	Actinom.	$K_3[Fe(C_2O_4)_3]$	[36, 137]
1-7	9,10-DPA	Toluene	293 K, air	365	$0.70 \pm 0.02$	Optical (V)	MgO scatterer	[81]
1-8	DANS amide	CH	RT, air	337	$0.59 \pm 0.01$	PAS <sup>g</sup>	Ferrocene/TPE	[115]
1-9	DANS amide	Ethanol	RT, air	337	$0.47 \pm 0.01$	PAS <sup>g</sup>	Ferrocene/TPE	[115]
1-10	DANS amide	Water	RT, air	337	$0.04 \pm 0.01$	PAS <sup>g</sup>	Ellman's reagent	[115]
1-11	2-Aminophthalimide	Ethanol	293 K, air	365	$0.60 \pm 0.02$	Optical (V)	MgO scatterer	[81]
1-12	2-Aminophthalimide	Ethanol	293 K, air	365, 405	$0.62 \pm 0.02$	Optical (IS)	MgO scatterer	[81]
1-13	Coumarin 1	EtOH:H <sub>2</sub> O 8 + 2	RT, air	n.r.	$0.48 \pm 0.03$	PAS <sup>h</sup>	none	[121]
1-14	Coumarin 6	Ethanol	RT, air	n.r.	$0.82 \pm 0.03$	PAS <sup>i</sup>	none	[120]
1-15	Coumarin 340	Ethanol	RT, air	n.r.	$0.62 \pm 0.03$	PAS <sup>i</sup>	none	[120]
1-16	Coumarin 500	Methanol	RT, air	390	$0.68 \pm n.r.$	Optical (IS)	none	[111]
1-17	Quinine sulfate	1.0 N H <sub>2</sub> SO <sub>4</sub>	298 K, deg.	Hg lines	$0.546 \pm 0.01$	Optical <sup>j</sup>	MgO scatterer	[36, 79]
1-18	Quinine sulfate	1.0 N H <sub>2</sub> SO <sub>4</sub>	RT, air	337	$0.51 \pm 0.05$	Optical <sup>k</sup>	none	[109]
1-19	Quinine sulfate	1.0 N H <sub>2</sub> SO <sub>4</sub>	RT, air	n.r.	$0.48 \pm 0.03$	PAS <sup>h</sup>	none	[121]
1-20	Quinine sulfate	0.1 N H <sub>2</sub> SO <sub>4</sub>	295 K, air	337	$0.55 \pm 0.02$	PAS <sup>h</sup>	none	[122]
1-21	Quinine sulfate	0.1 N H <sub>2</sub> SO <sub>4</sub>	RT, air	390	$0.51 \pm n.r.$	Optical (IS)	none	[111]
1-22	Fluorescein	0.1 N NaOH	RT, air	337	$0.91 \pm 0.04$	Optical <sup>k</sup>	none	[109]
1-23	Fluorescein	0.1 N NaOH	293 K, air	450–465	$0.90 \pm 0.02$	Optical (V)	MgO scatterer	[81]
1-24	Fluorescein	0.1 N NaOH	293 K, air	490	$0.86 \pm 0.02$	Optical (IS)	MgO scatterer	[81]

Table 1 (continued)

Entry	Compound	Solvent	Conditions <sup>a</sup>	$\lambda_{exc}/nm$ <sup>b</sup>	$\Phi_f^c$	Method <sup>d</sup>	Standard <sup>e</sup>	Refs.
1-24	Fluorescein	0.1 N NaOH	293 K, air	490	$0.86 \pm 0.02$	Optical (IS)	MgO scatterer	[81]
1-25	Fluorescein	0.1 N NaOH	RT, air	488, 514	$0.91 \pm 0.04$	Therm. lens.	Dichromate	[127]
1-26	Fluorescein	0.01 N NaOH	RT, air	470	$0.92 \pm 0.02$	Optical (IS)	Calibration set	[112]
1-27	Fluorescein	EtOH:1 N NaOH 8 + 2	RT, air	n.r.	$0.82 \pm 0.03$	PAS <sup>h</sup>	none	[121]
1-28	Fluorescein	Methanol, Et <sub>3</sub> N	RT, air	488, 514	$0.91 \pm 0.015$	Therm. lens.	Basic fuchsin	[127]
1-29	Fluorescein	Ethanol, Et <sub>3</sub> N	RT, air	488, 514	$0.92 \pm 0.02$	Therm. lens.	Basic fuchsin	[127]
1-30	Fluorescein	PVA	RT, air	n.r.	$0.83 \pm n.r.$	PAS	Phenol red	[116]
1-31	DCM	DMF	RT, air	n.r.	$0.82 \pm 0.04$	PAS <sup>i</sup>	none	[120]
1-32	Acridine orange	PVA	RT, air	n.r.	$0.55 \pm n.r.$	PAS	Phenol red	[116]
1-33	Eosin	EG:1 N NaOH 97 + 3	RT, air	n.r.	$0.35 \pm 0.04$	PAS <sup>h</sup>	none	[121]
1-34	Eosin	PVA	RT, air	n.r.	$0.75 \pm 0.02$	PAS	Phenol red	[116]
1-35	Rhodamine 6G	Ethanol	293 K, air	546	$0.97 \pm 0.02$	Optical (V)	MgO scatterer	[81]
1-36	Rhodamine 6G	Ethanol	293 K, air	530	$0.95 \pm 0.02$	Optical (IS)	MgO scatterer	[81]
1-37	Rhodamine 6G	Ethanol	RT, air	n.r.	$0.88 \pm 0.04$	PAS <sup>i</sup>	none	[120]
1-38	Rhodamine 6G	Ethanol	RT, air	488	$0.94 \pm n.r.$	Therm. lens.	<i>m</i> -Cresol purple	[123]
1-39	Rhodamine 6G	Ethanol	RT, air	480–540	$0.94 \pm 0.02$	Therm. lens.	Ferrocene	[128]
1-40	Rhodamine 6G	Ethanol	RT, air	532	$0.95 \pm 0.005$	Therm. lens.	Basic fuchsin	[127]
1-41	Rhodamine 6G	Ethanol	RT, air	488	$0.88 \pm n.r.$	Optical (IS)	none	[111]
1-42	Rhodamine 6G	EtOH:H <sub>2</sub> O 8 + 2	RT, air	n.r.	$0.85 \pm 0.02$	PAS <sup>h</sup>	none	[121]
1-43	Rhodamine 6G	Methanol	RT, air	532	$0.93 \pm 0.005$	Therm. lens.	Basic fuchsin	[127]
1-44	Rhodamine 6G	EG	RT, air	480–540	$0.95 \pm 0.02$	Therm. lens.	Co(NO <sub>3</sub> ) <sub>2</sub>	[128]
1-45	Rhodamine 6G	Water	RT, air	532	$0.86 \pm 0.09$	Optical <sup>k</sup>	none	[109]
1-46	Rhodamine 6G	Water	RT, air	532	$0.90 \pm 0.02$	PAS <sup>g</sup>	n.r.	[129]
1-47	Rhodamine 6G	Water	RT, air	480–540	$0.93 \pm 0.02$	Therm. lens.	Co(NO <sub>3</sub> ) <sub>2</sub>	[128]
1-48	Rhodamine 6G	Water	RT, air	532	$0.90 \pm 0.02$	Therm. lens.	Dichromate	[127]

Table 1 (continued)

Entry	Compound	Solvent	Conditions <sup>a</sup>	$\lambda_{exc}/nm^b$	$\Phi_f^c$	Method <sup>d</sup>	Standard <sup>e</sup>	Refs.
1-49	Rhodamine 6G	PVA	RT, air	n.r.	0.85 ± 0.02	PAS	Phenol red	[116]
1-50	Rhodamine B	Ethanol	RT, air	546	0.77 ± 0.02	Optical (V)	MgO scatterer	[81]
1-51	Rhodamine B	Ethanol	RT, air	520–540	0.73 ± 0.02	Optical (IS)	MgO scatterer	[81]
1-52	Rhodamine B	Ethanol	RT, air	n.r.	0.94 ± 0.05	PAS <sup>i</sup>	none	[120]
1-53	Rhodamine B	Ethanol	RT, air	532-cw	0.96 ± n.r.	Therm. lens. <sup>l</sup>	none	[130]
1-54	Rhodamine B	Ethanol	RT, air	532-pulsed	0.99 ± n.r.	Therm. lens. <sup>l</sup>	none	[130]
1-55	Rhodamine B	Methanol	RT, air	532-cw	0.96 ± n.r.	Therm. lens. <sup>l</sup>	none	[130]
1-56	Rhodamine B	Methanol	RT, air	532-pulsed	0.99 ± n.r.	Therm. lens. <sup>l</sup>	none	[130]
1-57	Rhodamine B	Water	RT, air	532-cw	0.95 ± n.r.	Therm. lens. <sup>l</sup>	none	[130]
1-58	Rhodamine B	Water	RT, air	532-pulsed	0.99 ± n.r.	Therm. lens. <sup>l</sup>	none	[130]
1-59	Rhodamine B	PVA	RT, air	n.r.	0.80 ± 0.02	PAS	Phenol red	[116]
1-60	Rhodamine 101	Acidic ethanol	297 K, air	590, 600	0.935 ± 0.015	Therm. ph. gr.	Crystal violet	[136]
1-61	Rhodamine 101	Acidic methanol	RT, air	535	1.00 ± 0.05	Optical (IS)	Calibration set	[112]
1-62	Rhodamine 110	Ethanol	293 K, air	436	0.95 ± 0.02	Optical (V)	MgO scatterer	[81]
1-63	Rhodamine 110	Ethanol	293 K, air	470–530	0.91 ± 0.02	Optical (IS)	MgO scatterer	[81]
1-64	Cresyl violet	Methanol	295 K, air	Hg lines	0.56 ± 0.03	Calorim.	Azulene, dienone	[36, 124]
1-65	Cresyl violet	Methanol	295 K, air	632	0.52 ± 0.03	Therm. lens.	CuSO <sub>4</sub> , Malachite green	[36, 124]
1-66	Cresyl violet	Methanol	297 K, air	590, 600	0.54 ± 0.04	Therm. ph. gr.	Crystal violet	[136]
1-67	Cresyl violet	Methanol	RT, air	514	0.54 ± 0.03	Therm. lens.	Crystal violet	[132]
1-68	Cresyl violet	Ethanol	297 K, air	590	0.60 ± 0.04	Therm. ph. gr.	Crystal violet	[136]
1-69	Cresyl violet	Ethanol	297 K, air	600	0.57 ± 0.03	Therm. ph. gr.	Crystal violet	[136]
1-70	Cresyl violet	Ethanol	295 K, air	601	0.59 ± 0.03	PAS <sup>h</sup>	none	[122]
1-71	Cresyl violet	Ethanol	RT, air	632	0.49 ± 0.06	Therm. lens.	Methylene blue	[135]
1-72	Oxazine 1	Ethanol	297 K, air	600	0.16 ± 0.04	Therm. ph. gr.	Crystal violet	[136]

**Table 1** (continued)

Entry	Compound	Solvent	Conditions <sup>a</sup>	$\lambda_{\text{exc}}/\text{nm}$ <sup>b</sup>	$\phi_f$ <sup>c</sup>	Method <sup>d</sup>	Standard <sup>e</sup>	Refs.
1-73	Oxazine 1	Ethanol	RT, air	632	$0.15 \pm 0.02$	Therm. lens.	Methylene blue	[135]
1-74	Nile blue	Ethanol	297 K, air	600	$0.23 \pm 0.04$	Therm. ph. gr.	Crystal violet	[136]
1-75	Nile blue	Ethanol	RT, air	632	$0.47 \pm 0.06$	Therm. lens.	Methylene blue	[135]
1-76	Oxazine 17 <sup>m</sup>	Ethanol	297 K, air	600	$0.58 \pm 0.03$	Therm. ph. gr.	Crystal violet	[136]
1-77	Ru(bipy) <sub>3</sub> Cl <sub>2</sub>	Water	RT, air	514	$0.36 \pm 0.01$	Therm. lens.	Crystal violet	[132]
1-78	Ru(bipy) <sub>3</sub> Cl <sub>2</sub>	Methanol	RT, air	514	$0.31 \pm 0.01$	Therm. lens.	Crystal violet	[132]
1-79	Ru(bipy) <sub>3</sub> (ClO <sub>4</sub> ) <sub>2</sub>	Water	RT, air	514	$0.80 \pm 0.01$	Therm. lens.	Crystal violet	[132]
1-80	Ru(bipy) <sub>3</sub> (ClO <sub>4</sub> ) <sub>2</sub>	Methanol	RT, air	514	$0.80 \pm 0.01$	Therm. lens.	Crystal violet	[132]

<sup>a</sup> air = non-degassed, deg. = degassed

<sup>b</sup> Hg lines = mercury lamp with lines not explicitly specified, cw = continuous wave, pulsed = pulsed laser excitation

<sup>c</sup> n.r. = uncertainty not reported

<sup>d</sup> actinom. = actinometric, calorim. = calorimetric, therm. lens. = thermal lensing or blooming,

optical (V) = Vavilov method, optical (IS) = employing an integrating sphere, therm. ph. gr. = thermal phase grating

<sup>e</sup> dienone = tetraphenylcyclopentadienone, n.r. = not reported

<sup>f</sup> 90° geometry with Rhodamine B as quantum counter and colloidal silica solution as scatterer

<sup>g</sup> Pulsed laser PAS

<sup>h</sup> Quenching method

<sup>i</sup> Double wavelength method

<sup>j</sup> Acute angel front face geometry with Rhodamine B as quantum counter

<sup>k</sup> Referenced on the differential Raman scattering cross section of the solvent

<sup>l</sup> Dual beam technique

<sup>m</sup> Oxazine 17 is equivalent to Nile red, the first being the trivial name used in the Russian literature,

the second the trivial name used in the English literature.

brief and will cite only a few representative references

$$I_m(\lambda_{\text{ex}}, \lambda_{\text{em}}) = \int_{\Delta\lambda} s(\lambda_{\text{em}}) P_\lambda(\lambda_{\text{ex}}, \lambda_{\text{em}}) d\lambda_{\text{em}}, \quad (2)$$

$$P_{p,\lambda}(\lambda_{\text{ex}}, \lambda_{\text{em}}) = \varepsilon(\lambda_{\text{ex}}) c F_{p,\lambda}(\lambda_{\text{em}}) \int_{\Delta\lambda} \int E_{\text{ex},\lambda}(\lambda_{\text{ex}}, \mathbf{r}) \mathbb{P}(\mathbf{r}) dV d\lambda_{\text{ex}}, \quad (3)$$

$$\Phi_f = \int_{\lambda_{\text{em}}} F_{p,\lambda}(\lambda_{\text{ex}}, \lambda_{\text{em}}) d\lambda_{\text{em}}. \quad (4)$$

Equation 2 is the general equation relevant for the measurement of an emission spectrum and Eq. 3 is the basic equation for the optical determination of fluorescence quantum yields.  $I_m(\lambda_{\text{ex}}, \lambda_{\text{em}})$  is the actual measured emission spectrum and transforms into the *spectral radiant power*,  $P_\lambda(\lambda_{\text{ex}}, \lambda_{\text{em}})$ , by taking into account the *spectral responsivity* of the emission channel,  $s(\lambda_{\text{em}})$ , and the *spectral bandwidth*  $\Delta\lambda$  [83]. Because  $\Phi_f$  is the ratio of emitted to absorbed photons (cf. Eq. 1), the spectral radiant power that reaches the emission channel from the illuminated volume is best expressed as the photon quantity with  $P_{p,\lambda} = P_\lambda \lambda / hc$ .  $P_{p,\lambda}$  is determined by the sample-specific quantities  $\varepsilon(\lambda_{\text{ex}})$ , the *molar absorption coefficient* at the excitation wavelength, the *concentration*  $c$  and the *spectral fluorescence photon yield*  $F_{p,\lambda}(\lambda_{\text{ex}}, \lambda_{\text{em}})$ , as well as  $E_{\text{ex},\lambda}(\lambda_{\text{ex}}, \mathbf{r})$ , the *spectral irradiance* at the position  $\mathbf{r}$  in the sample, and  $\mathbb{P}(\mathbf{r})$ , the detection probability of a photon emitted at the position  $\mathbf{r}$ . The spectral fluorescence photon yield is then related to the fluorescence quantum yield by Eq. 4. Since  $\Phi_f$  is a photon ratio, the actual absorption of the sample volume observed by the detector is important. Depending on the measurement geometry (front-face,  $90^\circ$ , etc.) and method (reference scatterer, integrating sphere, etc.), the determination of the actual absorption (at  $\lambda_{\text{ex}}$ ) can be done in various ways and harbors different degrees of uncertainty. Moreover, if the absorption of a sample is measured separately, different monochromator slits in absorption (i.e., of the spectrophotometer employed) and excitation (i.e., of the excitation channel/source of the fluorescence apparatus) can introduce an additional uncertainty [84, 85]. The effect of the width of the excitation slits itself on the determination of  $\Phi_f$  has been discussed in [86]. A formalism to estimate the error has been provided in [87]. With regard to the nature of exciting and emitted light, polarization errors have to be avoided or adequately corrected for [88]. This is especially important when using lasers as excitation sources because of their almost perfect polarization. Additionally, optical components of the spectrofluorometer employed can alter the polarization in the excitation and/or emission channel [89]. Polarization problems can be of paramount importance for many near-infrared dyes, which tend to possess a considerable anisotropy in solvents with a moderate or high viscosity or with (partially) slow sol-



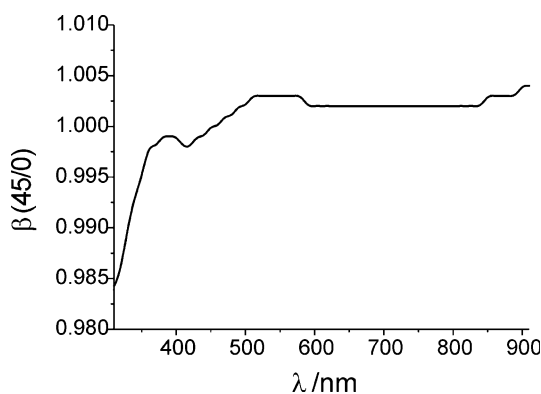


**Fig. 2** Spectral radiance factor for  $0^\circ/45^\circ$  irradiation/detection geometry of a commercial barium sulfate solid state scatterer

vent relaxation dynamics. This possible error is of outstanding importance when organic dyes in solid transparent organic or inorganic matrices are used [90]. Besides the spectral irradiance at sample position [ $E_{\text{ex},\lambda}(\lambda_{\text{ex}})$ , see Eq. 3] and the spectral responsivity of the detection channel, the linearity of the response of the detector is critical [91, 92]. When solid-state or solution scatterers are used as reference materials, their spectral reflectance (and anisotropic scattering properties) has to be taken into account, especially in the UV (see, e.g., Fig. 2 [93]). Moreover, such materials might fluoresce under UV excitation [94]. Concerning the use of quantum counters, various requirements have to be met, as discussed, for instance in [95]. If different types of sample and standard or different solvents are used, the differences in refractive indices must be corrected for. Advantages and problems of front-face versus right-angle excitation in the recording of fluorescence spectra for optically dense solutions or samples with a strongly absorbing background have been discussed by Eisinger, as well as by Bendig, for different types of emitters, i.e., for dyes with resonant and Stokes' shifted fluorescence [96–98]. Sample-related sources of error pertain to the purity of the dyes and standards used (e.g., [99]) as well as the autofluorescence of the solvent or stabilizers/impurities contained therein, quenching by oxygen (e.g., for 9,10-diphenylanthracene [100]) or halides (e.g., for quinine sulfate [101]), the temperature dependence of fluorescence (e.g., [102, 103]), the dependence of  $\Phi_f$  on the excitation wavelength used (e.g., [104]), self- or concentration quenching (e.g., for rhodamines [105]), inner-filter or reabsorption effects [106, 107], other types of concentration-induced effects such as dimer or aggregate formation of the fluorophore (e.g., for rhodamines [108]) or photobleaching during measurement.

The spontaneous Raman scattering signal of the solvent has been proposed by Chekalyuk et al. to serve as the internal standard for absolute fluorescence measurements of very dilute dye solutions (0.1–10 nM) [109]. These

authors used attenuated laser excitation to avoid saturation effects in fluorescence and referenced the fluorescence signal on the Raman signal of the 3440  $\text{cm}^{-1}$  line of water. By using tabulated data of the differential Raman scattering cross section of the solvent at the respective excitation wavelength and determining the absorption cross section of the chromophore on a conventional spectrophotometer, they reproduced within experimental error the fluorescence quantum yields of rhodamine 6G, fluorescein and quinine sulfate in aqueous solution (Table 1, entries 1-18, 1-22 and 1-45). The method is rather convenient, but has not been applied to other solvents. It is limited to dilute solutions of strong emitters so that the Raman signal can be readily quantified, yet it might harbor potential for the determination of fluorescence quantum yields of weakly emissive compounds. However, recently doubts arose with respect to the applicability of Raman signals as calibration tools in laser-induced fluorescence measurements [110].

Two other approaches toward absolute  $\Phi_f$  utilize integrating spheres and dispense with a standard by using different geometries and sample in/out positions in the sphere (Fig. 1C). Three signals have to be measured, the sample under direct excitation, the sample under excitation by diffuse light as reflected from the sphere's wall and the signal from the empty sphere [111, 112]. Since this approach follows the basic considerations of the fluorescence quantum yield determination of thin films [69], microcuvettes are used and the samples must be checked on a conventional fluorometer for reabsorption or other sample-related effects. The advantage of the use of an integrating sphere is the elimination of polarization effects—the multiple reflections in the sphere depolarize the radiation—and of the need for refractive index correction. The most critical factor in such measurements is the reflectivity of the sphere's inner coating, the sphere's efficiency. Whereas Porrès et al. used direct excitation of the sample in one of the three necessary experiments [112], Shea Rohwer and Martin only employed excitation with diffuse light [111]. In the first case, the agreement of the measured values with the commonly accepted  $\Phi_f$  of fluorescein and rhodamine 101 is excellent (Table 1, entries 1-26 and 1-61), while in the second case, the  $\Phi_f$  lie at the lower limits of the previously reported ones (Table 1, entries 1-21 and 1-41).

### 3.2

#### Calorimetric Methods

In the past 25 years, classical calorimetric measurements of absolute fluorescence quantum yields have not been reported for the dyes listed in Table 1 (for a comparative determination of  $\Phi_f$  of fluorescein by calorimetric and optical methods see, for example, [113]). Instead, researchers preferred to use photoacoustic methods and thermal lensing techniques for the indirect determination of the quantity in question. The latter means that all calorimetric

approaches try to measure the amount of excitation energy that is not emitted by the fluorophore, but converted into heat and dissipated into the surrounding medium. This conversion efficiency is 100% for an entirely nonfluorescent compound and correspondingly lower for an emitter with a certain  $\Phi_f$ . In calorimetric measurements, the heating effect of the fluorophore under consideration is usually compared to that of a nonemissive dye in the same solvent and absorbing at the same wavelength. The calorimetric experiment provides a certain radiant yield determined by the ratio of emitted to absorbed power. This yield can be converted to the fluorescence quantum yield by taking into account the excitation and emission spectra.

Calorimetric methods are free of polarization errors and detailed corrections for measurement geometries do not have to be performed. Refractive index correction is also less crucial, as for optical methods. Reabsorption effects on the other hand can have a severe influence on the calorimetric signal. Another disadvantage is the fact that signal ratios are analyzed so that the difference between the sample signal (the emitter with unknown  $\Phi_f$ ) and the reference signal (the nonfluorescent compound) should be as large as possible, preventing the measurement of weakly emissive dyes. Moreover, the corrected emission spectrum of the fluorophore in question has to be known.

### 3.2.1

#### Photoacoustic Spectroscopy

Photoacoustic spectroscopy (PAS) techniques use modulated excitation of the sample that is placed in a sealed cell with a microphone or acoustic transducer attached to it. The absorbed energy that is not emitted heats the sample, which itself produces a periodic pressure wave of a certain magnitude at the excitation frequency that is directly related to the temperature rise in the sample medium. Similar to conventional calorimetry, the emitter with unknown  $\Phi_f$  is measured against a nonfluorescent reference compound. Alternatively, the reference sample can consist of the emitter in the presence of an excess of a quencher (e.g., oxygen, iodide salt), i.e., of the same dye under totally quenched conditions. In PAS, all nonradiative processes contribute to the acoustic signal, including the energy loss due to the Stokes' shift. The PAS signal  $S_x$  of a sample  $x$  is given by [114, 115]

$$S_x = \kappa P_0 (1 - 10^{-A}) \left( \frac{\bar{\nu}_{\text{ex}} - \Phi_f \bar{\nu}_{\text{em}}}{\bar{\nu}_{\text{ex}}} \right), \quad (5)$$

where  $\kappa$  is a sample- and instrument-related constant and includes the scaling factor between amplitude of the pressure wave and amplitude of the measured voltage, as well as solvent-specific contributions such as molecular weight, adiabatic expansion coefficient, density and heat capacity [115].  $P_0$  is the *ra-*

diant power of the incident pulse,  $A$  the absorbance of the sample,  $\bar{\nu}_{\text{ex}}$  the wavenumber of excitation and  $\bar{\nu}_{\text{em}}$  the average emission wavenumber from the corrected fluorescence spectrum. For the nonfluorescent reference compound with  $\Phi_f = 0$ , Eq. 5 transforms to

$$S_r = \kappa P_0 (1 - 10^{-A}). \quad (6)$$

Since the procedure is a relative measurement of emissive versus nonemissive sample in the same solvent,  $\kappa$  cancels out. Under the precondition that both sample  $i$  and reference  $r$  are dissolved in the same solvent and possess the same absorbance at the excitation wavelength, Eqs. 5 and 6 give the following expression for the fluorescence quantum yield

$$\Phi_f = \frac{\bar{\lambda}_{\text{em}}}{\lambda_{\text{ex}}} \left( 1 - \frac{S_i}{S_r} \right). \quad (7)$$

The main problems of PAS methods are a good contact between the liquid sample and the acoustic transducer, the difficulty of detecting small temperature fluctuations (e.g., in the milli-Kelvin (mK) domain), the thermal isolation from the surrounding and the realization of similar thermal transport coefficients for sample and standard. Another problem, especially for measurements at shorter excitation wavelengths is the availability of nonemissive reference absorbers. A comprehensive discussion of the contribution of the single errors to the uncertainty budget is given in [116]. Reference [115] discusses several other problematic aspects of PAS.

As mentioned above, the use of PAS for measuring low fluorescence quantum yields is problematic. For instance, Rockley and Waugh reported a  $\Phi_f = 0.02 \pm 0.10$  for crystal violet in water as determined by PAS [117]. Although this value agrees fairly well with the value determined for crystal violet by relative optical methods ( $0.016 \pm 0.002$  [118]), the large error points directly to the high uncertainty of the method for such weak emitters. Moreover, from Table 1 it is interesting to see that crystal violet is frequently used as a reference compound in PAS that should ideally be nonemissive (*vide ante*) (see entries 1-60, 1-66 to 1-69, 1-72, 1-74 and 1-76 to 1-80).

Despite the results of Rockley and Waugh, the uncertainty of PAS measurements can be distinctly improved when using pulsed-laser excitation and photoacoustic waveform deconvolution techniques [119]. This technique not only allows one to gain deeper insight into and separate fast and slow processes such as, for instance, vibrational relaxation on one hand and triplet-state decay on the other, but it represents a technique that is complimentary to time-resolved fluorescence measurements. Employing pulsed-laser PAS, Rudzki Small et al. were able to determine the absolute fluorescence quantum yield of azulene to  $\Phi_f = 0.04 \pm 0.01$  with 2-hydroxybenzophenone as the reference compound (Table 1 entry 1-2). However, the wealth of information provided by this method has to be critically considered for every

compound to be measured. Dyes with straightforward singlet-state photo-physics and negligible intersystem crossing rates such as the well-known scintillator dye 2,5-diphenyloxazol (PPO), readily yield reliable values of  $\Phi_f$  (Table 1, entry 1-3). Chromophores with potentially more complex photo-physics and long fluorescence lifetimes and/or long-lived triplet states such as anthracene or pyrene, on the other hand, yield values of  $\Phi_f$  that are at the lower end of the commonly accepted range of fluorescence quantum yields (e.g., Table 1, entry 1-5) or that are very difficult to approximate as in the case of pyrene [119].

Other recent reports on absolute fluorescence quantum yields of common organic emitters that have been determined by PAS with a nonemissive reference absorber are listed as entries 1-8 to 1-10 (also with a pulsed nitrogen laser as Rudzki Small et al. used) [115] and 1-30, 1-32, 1-34, 1-49 and 1-59 (with lamp excitation) [116] in Table 1. Whereas Grabowski and coworkers found slightly higher  $\Phi_f$  values for dansylamide in many solvents than obtained with relative optical methods [115], Görtz and Perkampus obtained fluorescence quantum yields for the popular fluorophores fluorescein, rhodamine 6G and rhodamine B in a PVA matrix that are again at the lower limit of the commonly accepted values [116].

PAS measurements that dispense with reference compounds but either work according to the quenching method mentioned above or with a so-called double-wavelength technique have been published by Zhang et al. (Table 1, entries 1-13 to 1-15, 1-19, 1-27, 1-31, 1-33, 1-37, 1-42 and 1-52) [120, 121] and Sabol and Rockley (Table 1, entries 1-20 and 1-70) [122]. For the quenching method, Zhang et al. used saturated aqueous KI solutions as the quenching medium and Sabol and Rockley used ethyl iodide. The latter researchers did not quench their fluorophores completely but used a series of low-level concentrations of the quencher and analyzed the different slopes obtained for the quenching instead of comparing measured PAS intensities. Whereas the method employing KI produces fluorescence quantum yields that are at the lower limit of the commonly accepted values, as in, e.g., entries 1-19, 1-27 and 1-42 for quinine sulfate, fluorescein and rhodamine 6G (note that they used aqueous ethanol for the two latter instead of pure water or ethanol) in Table 1, the low-level luminescence quenching method revealed excellent agreement for quinine sulfate (Table 1, entry 1-20).

The double-wavelength technique is based on the assumption that the fluorescence quantum yield is independent of the excitation wavelength and that two separated wavelengths of equal absorption exist. Furthermore, if intersystem crossing is neglected and PAS signals far from saturation are recorded, the PAS signal ratio allows the extraction of the fluorescence quantum yield. The results obtained by Zhang et al. for rhodamine 6G (entry 1-37) and rhodamine B (entry 1-52) as shown in Table 1 suggest that the performance of the method is difficult to assess at present; whereas the value for rhodamine 6G ( $\Phi_f = 0.88$ ) lies at the lower limit, that of rhoda-

mine B ( $\Phi_f = 0.94$ ) is considerably high as compared to the generally accepted values.

### 3.2.2

#### Thermal Lensing

Thermal lensing or thermal blooming has been frequently used for the determination of absolute  $\Phi_f$  in recent years. It is based on the special characteristics of a laser beam passing through a liquid of absorbing molecules. Commonly, the laser beam has a Gaussian intensity profile that is radially symmetric and thus heats an absorbing medium through which it passes unevenly. Since the refractive index of a solvent depends on temperature, the resulting temperature gradient leads to a gradient in refractive index—produces the thermal lens—which in turn alters the dispersion of the traveling beam (Fig. 3). When monitored from a distant target with a suitable detector, the change in beam expansion leads to a change in intensity registered by the detector. Accordingly, different heating rates lead to different thermal lenses and the development of the thermal lens (the “blooming” of the beam) until a thermal equilibrium where heat loss from the illuminated volume equals the heat diffusion rate into the surrounding medium (typically in the microsecond time regime) can be traced on an oscilloscope or equivalent recorder. Since thermal lensing is a very sensitive method—refractive index changes down to  $10^{-8}$ , corresponding to micro-Kelvin temperature variations, can be measured—the precision of the method is usually very good. Again, as for the other calorimetric methods, a nonfluorescent reference compound is commonly used in the  $\Phi_f$  measurements.

The fraction of laser power  $\theta$  that is converted into heat can be obtained in two ways, (1) directly from the linear initial slope  $m$  of the decay of the photocurrent  $I(t)$  after the abrupt initial rise (Fig. 3) by an expansion of Eq. 8 to Eq. 9 for short times  $t$  or (2) from the initial and the steady state photocurrents  $I_0$  and  $I_\infty$  according to Eq. 10 and Eq. 11 [123, 124]. Owing to the comparative nature of the method,  $\theta$  has to be determined separately for sample  $i$ , reference  $r$  and blank  $b$  and, assuming constant laser intensity, yields  $\Phi_f$  according to Eq. 12. The other parameters in Eqs. 8–12 are the *thermal relaxation time*  $t_c$ , the *thermal conductivity*  $k$ , the *density*  $\rho$ , the *specific heat capacity*  $C$ , the *beam waist*  $\omega_0$ , the (photometric) *absorbance*  $A_x$  at  $\lambda_{ex}$ , the

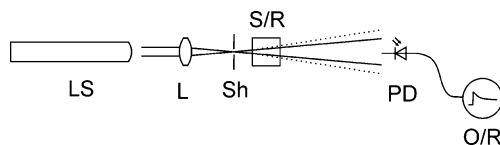


**Fig. 3** Schematic setup of a thermal lensing instrument. LS Laser source, L lens, Sh shutter, S/R position of sample or reference, PD photodiode, O/R oscilloscope/recorder

average *emission wavelength* from the corrected fluorescence spectrum  $\bar{\lambda}_{em}$  and the excitation wavelength  $\lambda_{ex}$

$$I(t) = I_0 \left[ 1 - \theta \left( 1 + \frac{t_c}{2t} \right)^{-1} + \frac{1}{2} \theta^2 \left( 1 + \frac{t_c}{2t} \right)^{-2} \right]^{-1}, \quad (8)$$

$$I(t) = I_0 + mt \quad \text{with} \quad m = \frac{8\theta k}{I_0 \rho C \omega_0^2}. \quad (9)$$

If similar solvents are used for sample and reference,  $k$ ,  $\rho$ ,  $C$  and  $\omega_0$  cancel out in the relative measurements

$$I = \frac{(I_0 - I_\infty)}{I_\infty}, \quad (10)$$

$$\theta = 1 - \sqrt{1 + 2I}, \quad (11)$$

$$\Phi_f = \left( 1 - \frac{A_r - A_b}{A_i - A_b} \frac{\theta_i - \theta_b}{\theta_r - \theta_b} \right) \frac{\bar{\lambda}_{em}}{\lambda_{ex}}. \quad (12)$$

If the absorbances of the sample and reference solutions are adjusted, the  $A$  term in the brackets also cancels out.

The advantages of thermal lensing include the advantages of calorimetric methods in general (no polarization errors and no need for refractive index correction) as well as specific aspects such as no influence of radiation trapping and reabsorption in the sample. Drawbacks and limitations of the method can be as follows. First, a Gaussian behavior of the TEM<sub>00</sub> (fundamental Transverse ElectroMagnetic) mode has to be assumed. Second, thermal convection or spherical aberrations of the thermal lens have to be avoided by using low excitation power. Third, some geometric requirements such as a small detector surface with respect to the beam size at target position and a cell that is long compared to the laser beam diameter have to be guaranteed. Finally, being a comparative calorimetric method, its sensitivity is not as good as in conventional fluorometry.

The absolute fluorescence quantum yields of fluorescein in basic aqueous (Table 1, entry 1-25) as well as in basic organic solution (Table 1, entries 1-28, 1-29) have been reassessed by Magde and coworkers several years ago and excellent agreement with the values obtained by optical (Table 1, 1-22, 1-23, 1-26 and [82] or [125]) and other calorimetric techniques (e.g., [126]) has been reached [127]. The same kind of agreement was found for rhodamine 6G in alcohols and water (Table 1, entries 1-40, 1-43, 1-48). Whereas Magde et al. used dichromate as the nonluminescent standard, Fischer and Georges employed *m*-cresol purple and could reproduce well the result for rhodamine 6G in ethanol (Table 1, entry 1-38) [123]. This group additionally used ferrocene for the calibration of their set-up. In a second work published in 1996, the French researchers also investigated rhodamine 6G in ethylene glycol (Table 1, entry 1-44) and water (Table 1, entry 1-47), and found again

a very good agreement of the  $\Phi_f$  values with the generally accepted data [128]. In that article, the limitations arising from optical saturation effects are also discussed in detail. The absolute fluorescence quantum yield of rhodamine 6G in water has also been verified by Sathy et al. by thermal lensing using a Nd:YAG laser as excitation source (Table 1, entry 1-46) [129].

Bindhu and Harilal devoted their attention to the influence of the type of laser source used for thermal lensing, i.e., if continuous wave (cw) or pulsed excitation is employed [130]. To accomplish this, a dual beam experiment was set up in which either a cw argon laser beam (at 514 nm) or a pulsed Nd:YAG beam (at 532 nm) were guided through the sample collinearly with a HeNe laser (at 632 nm) for monitoring purposes [131]. A filter that only allows the HeNe beam to pass was placed between sample and detector. In this way, these researchers investigated rhodamine B in alcohols and water by the quenching method (Table 1, entries 1-53 to 1-58). Despite the fact that they measured absolute fluorescence quantum yields that are considered too high for this dye (0.96 to 0.99), they always found a slightly higher yield for pulsed excitation. Bindhu and Harilal attributed these findings to different thermal lensing dynamics and the possibility or impossibility of achieving thermal equilibration. Moreover, various other factors such as the induction of excited-state absorption or two photon processes as a function of the mode of excitation can complicate the measurement. Although their application of the technique in the case of rhodamine 6G gave more reliable values [108], further research in this direction is necessary to be able to better judge the potential of these dual beam techniques.

Cresyl violet in methanol (Table 1, entry 1-67) served as a model compound to evaluate the performance of a setup that Degen et al. utilized in 1992 for the determination of the absolute fluorescence quantum yields of the popular ruthenium bipyridyl emitters  $\text{Ru}(\text{bipy})_3\text{Cl}_2$  and  $\text{Ru}(\text{bipy})_3(\text{ClO}_4)_2$  (entries 1-77 to 1-80, Table 1) [132]. This group found an excellent agreement of  $\Phi_f$  of cresyl violet with the generally accepted values as recommended by the IUPAC (Table 1, entries 1-64, 1-65), rendering the  $\text{Ru}(\text{bipy})_3^{2+}$  values reliable. However, these studies pose two important questions: (1) crystal violet was used a reference (see discussion in Sect. 3.2.1), and (2) distinctly different  $\Phi_f$  values of ca. 0.04 have been obtained by relative methods for  $\text{Ru}(\text{bipy})_3^{2+}$  before [133, 134]. A somewhat lower value for cresyl violet in ethanol (Table 1, entry 1-71), was reported by Wang et al. who measured the absolute quantum yields of several popular oxazine dyes (entries 1-73, 1-75, Table 1) [135].

The absolute fluorescence quantum yields of several oxazine dyes have also been measured by a modified thermal lensing technique, thermal phase grating [136]. This is a triple-beam technique in which two beams of the same wavelength are guided in such a way onto the sample that they form an interference pattern. After absorption and heating of the sample, a phase grating of the refractive index is formed which, after a temporal interval sufficient for thermal equilibration, is probed by a third (pulsed) beam incident on the



sample/phase grating at a certain angle (e.g., the Bragg angle). The diffraction efficiency is then a measure for the heating of the sample and accordingly allows calculation of the fluorescence quantum yield as for any calorimetric method. The method harbors a few difficulties such as the depth (or special profile) of the grating in the sample (determining the dye concentration that has to be used) and the precise detection of the changes of the diffraction efficiency. An advantage of the method is the possibility of using high dye concentrations, since for total absorption of the exciting radiation the diffraction efficiency is independent of dye concentration and only determined by the fraction of the excitation energy that is converted into heat. Limitations also reside in the photochemical processes that can happen or can be induced in the sample, such as trapping of excitation energy in triplet states or excited state as well as triplet-triplet absorption and the careful timing of the sampling pulse. As can be deduced from entries 1-60, 1-66, 1-68 and 1-69 in Table 1, the agreement of the data obtained by this method with those generated by traditional thermal lensing, conventional calorimetry or PAS is very good. Moreover, although the  $\Phi_f$  values for oxazine 1 in ethanol as determined by Petukhov et al. [136] and Wang et al. [135] match well (Table 1, entries 1-72 and 1-73), they differ considerably for cresyl violet (Table 1, entries 1-70 and 1-71) and Nile blue (Table 1, entries 1-74 and 1-75) in ethanol. Since both groups use reference compounds which are not nonfluorescent but show residual emission of a few percent—crystal violet (see discussion in [117]) and methylene blue (see [126] for data)—the quality of the absolute  $\Phi_f$  is difficult to judge. On the other hand, as detailed above, the German group also used crystal violet, and yet obtained very good agreement with the  $\Phi_f$  values determined independently by other methods [132]. The role of the residual emissivity of the reference compound and the suitability of the various modified thermal lensing techniques described here thus clearly need further investigation and verification.

### 3.2.3

#### Actinometry

The actinometric approach to measure absolute  $\Phi_f$  has been less popular recently. Experimentally, an actinometer solution surrounds the sample chamber that contains the fluorescent compound. The excitation light is coupled into the solution through a small port. The actinometer solution can thus absorb all the emitted photons and its decomposition rate is proportional to the latter. The excitation beam is measured in the same way with a blank sample. Without a reference compound, the ratio of exciting to emitted photons yields  $\Phi_f$ . Employing proper cell design, the method is free of refractive index and polarization errors. A disadvantage is the loss of emitted light through the excitation port and end windows and the fact that certain actinometer systems are only applicable in specific wavelength ranges [31].

Hamai and Hirayama used the well known potassium ferrioxalate actinometer for the determination of the absolute fluorescence quantum yield of 9,10-diphenylanthracene (9,10-DPA) in degassed cyclohexane and found a value that lies within the commonly accepted range (Table 1, entry 1-6) [137].

In general, due to the experimental peculiarities and the considerably small amount of data on specific pairs of dye and solvent in Table 1 it is not possible to make a final statement on the comparison of absolute fluorescence quantum yields determined by the different methods.

## 4

### Relative Fluorescence Quantum Yields

The measurement of relative fluorescence quantum yields has exclusively been done by optical methods, most prominently using a spectrofluorometer and the comparative method as proposed by Parker and Rees [19]. The methodology can best be derived from the basic equation (Eq. 14) according to which the fluorescence quantum yield of a compound  $i$  is determined relative to that of a standard  $s$  with known  $\Phi_f^s$

$$\Phi_f^i = \Phi_f^s \frac{f_s(\lambda_{\text{ex}}) \int_{\lambda_{\text{em}}} P_{p,\lambda}^i(\lambda_{\text{em}}) n_i^2}{f_i(\lambda_{\text{ex}}) \int_{\lambda_{\text{em}}} P_{p,\lambda}^s(\lambda_{\text{em}}) n_s^2}, \quad (13)$$

$$f_x(\lambda_{\text{ex}}) = 1 - 10^{-A_x(\lambda_{\text{ex}})} = 1 - 10^{-\varepsilon_x(\lambda_{\text{ex}})c_x l}. \quad (14)$$

In a first step, the *absorbances*  $A_x(\lambda_{\text{ex}})$  ( $= \varepsilon_x(\lambda_{\text{ex}})c_x l$ ; cf. Beer–Lambert law, Eq. 14) of both sample ( $x = i$ ) and standard ( $x = s$ ) at the respective *excitation wavelength*  $\lambda_{\text{ex}}$  are adjusted, yielding the corresponding *absorption factor*  $f_x(\lambda_{\text{ex}})$ .  $f_x(\lambda_{\text{ex}})$  is equivalent to the *absorptance*,  $\alpha_x(\lambda_{\text{ex}})$ , although use of the latter is not recommended anymore [78]. Then, the fluorescence spectra of both solutions are measured and corrected for all instrument-specific contributions, introducing the spectral radiant power term to Eq. 13. If the solvent has to be different for both sample and standard, a refractive index correction term ( $n_x^2$ ) also has to be applied. (Note: although having generally been accepted for several decades [31], the refractive index correction as shown in Eq. 13 was questioned again in the 1970s, e.g., in [138]. However, a series of experiments by Meech and Phillips verified the original approach [139]. If in doubt for his/her own fluorometer, a researcher should repeat these experiments on his/her in-lab equipment.)

Concerning potential errors and sources of uncertainty of the method, in principle, most of the points mentioned above in Sect. 3.1 for the absolute optical methods have to be considered in relative measurements as well. However, some additional comments are necessary. The relative determination of fluorescence quantum yields is often employed for moderately or weakly

emissive fluorophores, since many conventional spectrofluorometers today are sufficiently sensitive to measure optically dilute solutions of compounds with  $\Phi_f \sim 10^{-4}$  with acceptable accuracy. The problems that can arise when the standard of choice, for instance, possesses a  $\Phi_f \sim 0.5$  and the target compound a  $\Phi_f$  that is two or three orders of magnitude lower are the following: (1) the linear dynamic working range of the fluorometer might be a limiting factor, (2) if the standard is employed in very high dilution in order to circumvent problem (1), the precision and reliability of the absorption measurement might be insufficient, and (3) to be able to use optimum excitation conditions, it might be necessary to use two different excitation wavelengths for sample and standard. Concerning (1), the linearity range of the detection system of the fluorometer employed has to be measured. Point (2) can be circumvented when a larger quantity of the solution is prepared and absorption is measured in a longer path cell. With respect to (3), the excitation correction curve of the instrument employed, i.e., the spectral irradiance at sample position  $E_{\text{ex},\lambda}(\lambda_{\text{ex}})$ , has to be known or determined [91] and has to be introduced as an additional term to Eq. 13. The choice of the right wavelength of excitation is of paramount importance in the measurement of relative fluorescence quantum yields, especially when compounds with narrow and structured absorption bands are concerned. Consider for instance the case of using anthracene as the fluorescence standard for determining the  $\Phi_f$  value of *p*-bis[2-(5-phenyloxazolyl)]-benzene (POPOP), a well-known scintillator and brightening dye. Figure 4 shows the absorption and fluorescence spectra of both compounds in ethanol. At first it is

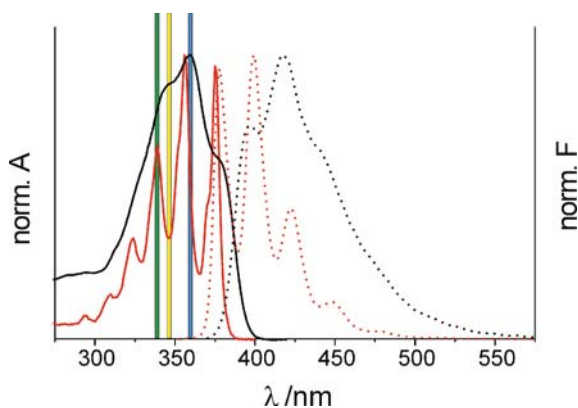


**Fig. 4** Absorption (*solid*) and fluorescence (*dotted*) spectra of *p*-bis[2-(5-phenyloxazolyl)]-benzene ( POPOP) (*black*) and anthracene (*red*) in ethanol at 298 K. The *blue bar* indicates a 2-nm band centered around the absorption maximum of POPOP, the *green bar* a 2-nm band centered around the absorption maximum of the third of the vibronic bands of anthracene and the *yellow bar* a 2-nm band encompassing two rather plateau-like regions in both absorption spectra. The 2-nm band should symbolize the region of absorption or excitation for narrow slit widths

apparent that for anthracene, as a dye with a very small Stokes shift, excitation wavelengths shorter than ca. 360 nm should be employed so that the emission spectrum is not truncated on the high-energy side. Second, the narrowness of the anthracene bands renders choice of the POPOP absorption maximum as the excitation wavelength not very suitable (blue bar in Fig. 4). Small errors in the wavelength accuracy of the spectrophotometer and/or fluorometer as well as differences in the slit functions could easily lead to errors because of the steep slope in the standard's spectrum. The same could be encountered when choosing the shortest wavelength vibronic band of anthracene (green bar, Fig. 4). The best choice in this example would be an excitation wavelength within the yellow bar that crosses both spectra in an almost plateau-like region.

In the second example, 4-dicyanomethylene-2-methyl-6-*p*-dimethylaminostyryl-4*H*-pyran (DCM) in methanol is measured relative to fluorescein in 0.1 N NaOH (Fig. 5). This is one of the many cases where both dyes possess very different photophysical characteristics, i.e., the standard (here fluorescein) shows narrow and only slightly Stokes' shifted spectra while the compound with unknown  $\Phi_f$  shows broad and structureless absorption and emission bands that are well separated. Many so-called charge-transfer active dyes such as electron donor–electron acceptor-substituted stilbene, styryl or coumarin dyes display similar characteristics as DCM in medium and highly polar solvents. As Fig. 5 suggests, in the present case, the wavelength of excitation should at best lie within the yellow region where the absorption spectrum of DCM is almost in a plateau and where the slope in the spectrum of fluorescein is also considerably flat.

The third case of fluorescein (in 0.1 N NaOH) and rhodamine 101 (in ethanol) as shown in Fig. 6 describes a situation that is common, for example,

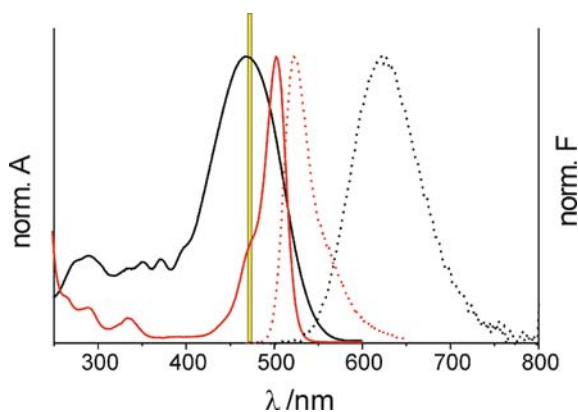


**Fig. 5** Absorption (*solid*) and fluorescence (*dotted*) spectra of 4-dicyanomethylene-2-methyl-6-*p*-dimethylaminostyryl-4*H*-pyran (DCM) in methanol (*black*) and fluorescein in 0.1 N NaOH (*red*) at 298 K. The *yellow bar* indicates a 2-nm band where excitation would produce minimum errors as detailed in the text

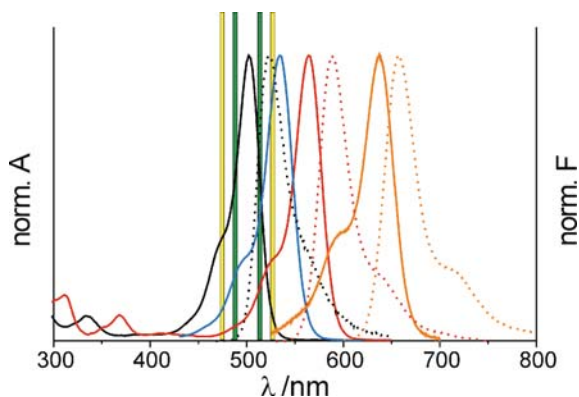


**Fig. 6** Absorption (*solid*) and fluorescence (*dotted*) spectra of fluorescein in 0.1 N NaOH (*black*) and rhodamine 101 in ethanol (*red*) at 298 K. Also displayed are the absorption spectrum of a hypothetical chemical transfer standard dye (*blue*) and the absorption and fluorescence spectra of the Cy5 parent indodicarbocyanine (C5) in methanol (*orange*) taken from [180]. The *yellow bars* indicate the 2-nm bands for optimum excitation of fluorescein and rhodamine with two different excitation wavelengths. The *green bars* indicate the two excitation wavelengths that would be most suitable when first measuring fluorescein with the chemical transfer standard dye and then measuring rhodamine 101 against that dye

in the wavelength range  $> 650$  nm, where no reliable standards exist yet where many popular labeling dyes (e.g., Cy5, Indocyanine Green, several Alexa dyes) absorb and emit with their characteristically narrow and only slightly Stokes' shifted bands. If the fluorescence quantum yield of rhodamine 101 should be determined relative to that of fluorescein, two methods are possible. First, two different excitation wavelengths can be used as indicated by the two yellow bars in Fig. 6. In this case, an excitation correction as mentioned above has to be employed. Second, if possible, a so-called chemical transfer standard dye can be used that possesses, for instance, an absorption band between the two dyes in question and shows sufficient overlap with the spectra of both other dyes in a region that can be used for excitation. This is exemplified by the hypothetical blue spectrum and the green bars in Fig. 6. When aiming at the determination of the fluorescence quantum yield of Cy5 (the spectra of the parent compound are shown in Fig. 6) relative to that of rhodamine 101, it is obvious that a similar procedure as for rhodamine 101 and fluorescein has to be employed.

#### 4.1 Measurements at Room Temperature

As has been discussed above for the absolute fluorescence quantum yields, again, the high time of the determination of relative fluorescence quantum

yields for widely used commercial fluorescent dyes in the most important solvents were the 1970s with ca. 35% and the 1980s with ca. 25% of the data reported. The 1960s as well as the 1990s and the 2000s each share ca. 10–15% of the values published. Table 2 lists a representative selection of widely popular fluorophores for which  $\Phi_f$  have been determined in the past 25 years by relative methods, together with those of the dyes recommended by the IUPAC Commission where the recommendation is based on a value obtained by relative methods (Table 2, entries 2-2, 2-5, 2-14, 2-15, 2-18 and 2-54) and several promising dyes that have been advertised as fluorescence standards during the past decades (e.g., acridinium salts and perylenebis(dicarboximides)). It is obvious from Table 2 that quinine sulfate is by far the most popular fluorescence standard for relative determinations, followed by 9,10-DPA, fluorescein and several rhodamines. Interestingly, quinine sulfate has also been used frequently as a relative standard for red-emitting dyes such as rhodamines, entailing even more dramatic consequences than detailed above for the fluorescein/rhodamine case. Figure 7 shows that there is a 200-nm gap between the lowest energy absorption bands of both compounds and that the molar absorptivity of quinine sulfate is considerably low. The overlap with the higher energy bands of rhodamine at ca. 370 and 315 nm is also not optimum. Moreover, in general, excitation into higher excited states (e.g.,  $S_3$  or higher at  $\lambda_{\text{ex}} < 370$  nm for rhodamines) should be avoided since additional nonradiative deactivation routes might compete with internal conversion from  $S_n$  to  $S_1$ . Moreover, when using quinine sulfate for the red region, rigorous care has to be taken of the correction of the excitation and emission channels of the instrument used.

Although the majority of the works cited in Table 2 explicitly aims at providing reference data or introducing a potential new fluorescence quantum yield standard dye, a comprehensive description of the methodology em-

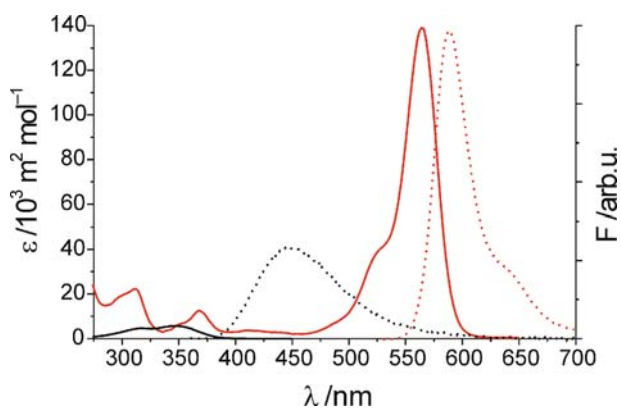


**Fig. 7** Absorption (*solid*) and fluorescence (*dotted*) spectra of quinine sulfate in 0.1 N  $\text{H}_2\text{SO}_4$  (*black*) and rhodamine 101 in ethanol (*red*) at 298 K

**Table 2** Fluorescence quantum yields of various popular or common fluorescent dyes as obtained by relative optical methods in the last 25 years

Entry	Compound <sup>a</sup>	Solvent	Conditions <sup>b</sup>	$\lambda_{exc}/nm$ <sup>c</sup>	$\Phi_f$ <sup>d</sup>	Standard/solvent ( $\Phi_f$ ) <sup>e</sup>	Refs. Std.Refs.
2-1	Benzene	MCH	RT, air	254	0.03 ± 0.03	9,10-DPA/CH (1.00)	[147] [85]
2-2	Naphthalene	CH	RT, deg.	256	0.23 ± 0.02	9,10-DPA/CH (1.00)	[182] [36, 183]
2-3	2-Aminopyridine	1.0 N H <sub>2</sub> SO <sub>4</sub>	RT, air	n.r.	0.65 ± 0.04	QS/1.0 N H <sub>2</sub> SO <sub>4</sub> (0.546)	[79] [139]
2-4	2-Aminopyridine	0.1 N H <sub>2</sub> SO <sub>4</sub>	RT, deg.	n.r.	0.66 ± 0.05	QS/1.0 N H <sub>2</sub> SO <sub>4</sub> (0.546)	[79] [139]
2-5	2-Aminopyridine	0.1 N H <sub>2</sub> SO <sub>4</sub>	RT	285	0.60 ± 0.05	9,10-DPA/CH (1.00) QS/ 0.1 N H <sub>2</sub> SO <sub>4</sub> (0.46)	[100] [36, 184]
2-6	Fluorene	MCH	RT, air	265	0.71 ± 0.03	9,10-DPA/CH (1.00)	[147] [85]
2-7	Sodium salicylate	1.0 N NaOH	RT, air	302	0.25 ± 0.03	QS/0.1 N HClO <sub>4</sub> (0.59)	[185] [85]
2-8	Sodium salicylate	Phosphate buffer, pH 7	RT, air	299	0.32 ± n.r.	QS/1.0 N H <sub>2</sub> SO <sub>4</sub> (0.546)	[79] [145]
2-9	Retinol (Vitamin A2)	Water, pH 7	RT, air	n.r.	0.03 ± n.r.	QS/1.0 N H <sub>2</sub> SO <sub>4</sub> (0.546)	[79] [186]
2-10	Pyrene	CH	RT, air	241	0.31 ± 0.03	9,10-DPA/CH (1.00)	[147] [85]
2-11	TPB	CH	RT, air	346	0.84 ± 0.03	9,10-DPA/CH (1.00)	[147] [85]
2-12	DANS	Phosphate buffer, pH 7	RT, air	326	0.34 ± n.r.	QS/1.0 N H <sub>2</sub> SO <sub>4</sub> (0.546)	[79] [145]
2-13	Anthracene	MCH	RT, air	252	0.31 ± 0.03	9,10-DPA/CH (1.00)	[147] [85]
2-14	Anthracene	Ethanol	298 K, deg.	Hg lines	0.27 ± n.r.	QS/1.0 N H <sub>2</sub> SO <sub>4</sub> (0.546)	[79] [36, 79]
2-15	9,10-DPA	CH	RT, deg.	n.r.	0.91 ± 0.02	QS/1.0 N H <sub>2</sub> SO <sub>4</sub> (0.546)	[79] [36, 139]
2-16	9,10-DPA	CH	RT, air	n.r.	0.70 ± 0.04	QS/1.0 N H <sub>2</sub> SO <sub>4</sub> (0.546)	[79] [139]
2-17	9,10-DPA	CH	RT, air	262	1.00 ± 0.03	QS/0.1 N HClO <sub>4</sub> (0.59)	[185] [85]
2-18	Quinine sulfate	0.1 N H <sub>2</sub> SO <sub>4</sub>	298 K, air	n.r.	0.52 ± 0.02	QS/1.0 N H <sub>2</sub> SO <sub>4</sub> (0.546)	[79] [36, 139]
2-19	Quinine sulfate	0.1 N H <sub>2</sub> SO <sub>4</sub>	RT, air	347	0.51 ± 0.02	QS/0.1 N HClO <sub>4</sub> (0.59)	[185] [140]
2-20	Sulfonatoalkyl-quinolinium salt	Water, pH 7	RT, air	340–345	0.53 ± n.r.	QS/1.0 N H <sub>2</sub> SO <sub>4</sub> (0.546)	[79] [146]
2-21	$\beta$ -Carboline (nor-harmane)	1.0 N H <sub>2</sub> SO <sub>4</sub>	298 K, air	330–370	0.60 ± 0.02	QS/1.0 N H <sub>2</sub> SO <sub>4</sub> (0.546)	[79] [142]
2-22	$\beta$ -Carboline (nor-harmane)	0.1 N H <sub>2</sub> SO <sub>4</sub>	298 K, air	330–390	0.58 ± 0.02	QS/1.0 N H <sub>2</sub> SO <sub>4</sub> (0.546)	[79] [141]

Table 2 (continued)

Entry	Compound <sup>a</sup>	Solvent	Conditions <sup>b</sup>	$\lambda_{\text{exc}}/\text{nm}^c$	$\Phi_f^d$	Standard/solvent ( $\Phi_f$ ) <sup>e</sup>	Refs. Std.	Refs.
2-23	Harmaline	0.1 N H <sub>2</sub> SO <sub>4</sub>	298 K, air	330–390	0.83 ± 0.03	$\beta$ -Carboline/0.1 N H <sub>2</sub> SO <sub>4</sub> (0.58)	[141]	[141]
2-24	Harmine	0.1 N H <sub>2</sub> SO <sub>4</sub>	298 K, air	330–390	0.45 ± 0.03	$\beta$ -Carboline/0.1 N H <sub>2</sub> SO <sub>4</sub> (0.58)	[141]	[141]
2-25	2-Methyl-harmine	0.1 N H <sub>2</sub> SO <sub>4</sub>	298 K, air	330–390	0.45 ± 0.03	$\beta$ -Carboline/0.1 N H <sub>2</sub> SO <sub>4</sub> (0.58)	[141]	[141]
2-26	Sulfonatoalkyl-harmanium salt	Water, pH 7	RT, air	340–345	0.80 ± n.r.	QS/1.0 N H <sub>2</sub> SO <sub>4</sub> (0.546)	[79]	[146]
2-27	Coronene	MCH	RT, air	303	0.18 ± 0.03	9,10-DPA/CH (1.00)	[147]	[85]
2-28	Perylenebisimide dye	CH <sub>2</sub> Cl <sub>2</sub>	293 K, air	466	1.02 ± 0.05	Diazaperylene/EtOH (0.83)	[149]	[150]
2-29	Perylenebisimide dye	CH <sub>2</sub> Cl <sub>2</sub>	293 K, air	469	0.98 ± 0.07	Diazaperylene/EtOH (0.83)	[149]	[150]
2-30	Sulfonatoalkyl-acridinium salt	Water, pH 7	RT, air	340–345	1.00 ± n.r.	N-Methylacridinium chloride/Water (1.01)	[187]	[146]
2-31	9-Aminoacridinium chloride	Phosphate buffer, pH 7	RT, air	327	0.97 ± n.r.	QS/1.0 N H <sub>2</sub> SO <sub>4</sub> (0.546)	[79]	[145]
2-32	Harmaline	0.01 N H <sub>2</sub> SO <sub>4</sub>	298 K, air	330–390	0.32 ± 0.02	$\beta$ -Carboline/0.1 N H <sub>2</sub> SO <sub>4</sub> (0.58)	[141]	[141]
2-33	Lucifer yellow	Water, pH 7	RT, air	430	0.20 ± 0.03	QS/0.1 N HClO <sub>4</sub> (0.59)	[185]	[85]
2-34	Diazaperylene	Ethanol	298 K, air	n.r.	0.83 ± 0.05	Fluorescein/0.1 N NaOH (0.92)	[82]	[149]
2-35	BP(OH) <sub>2</sub>	CH	293 K, air	351	0.315 ± 0.024	QS/1.0 N H <sub>2</sub> SO <sub>4</sub> (0.546)	[79]	[154]
2-36	BP(OH) <sub>2</sub>	CH	293 K, air	354	0.336 ± 0.028	9,10-DPA/CH,air (0.7)	[139]	[154]
2-37	Fluorescein	0.1 N NaOH	RT, air	460	0.82 ± 0.03	QS/0.1 N HClO <sub>4</sub> (0.59)	[185]	[85]
2-38	Fluorescein	Borate buffer, pH 9.1	298 K, air	n.r.	0.92 ± 0.02	QS/0.1 N HClO <sub>4</sub> (0.59)	[185]	[140]
2-39	Perylenebisimide dye	CH <sub>2</sub> Cl <sub>2</sub>	293 K, air	488	0.99 ± 0.05	Fluorescein/0.1 N NaOH (0.92)	[82]	[150]
2-40	Perylenebisimide dye	CHCl <sub>3</sub>	RT	n.r.	1.00 ± n.r.	Rhodamine 101	n.r.	[143]
2-41	Perylenebisimide dye	CHCl <sub>3</sub>	RT	n.r.	0.83 ± n.r.	Perylenebisimide dye/CHCl <sub>3</sub> (1.00)	[151]	[152]
2-42	Perylenebisimide dye	CHCl <sub>3</sub>	RT	n.r.	1.00 ± n.r.	Rhodamine 101	n.r.	[151]



Table 2 (continued)

Entry	Compound <sup>a</sup>	Solvent	Conditions <sup>b</sup>	$\lambda_{\text{exc}}/\text{nm}^c$	$\Phi_f^d$	Standard/solvent ( $\Phi_f$ ) <sup>e</sup>	Refs. Std.	Refs.
2-43	Perylenebisimide dye	DMF	RT	n.r.	0.84 ± n.r.	Perylenebisimide dye/ CHCl <sub>3</sub> (1.00)	[151]	[152]
2-44	Perylenebisimide dye	CHCl <sub>3</sub>	290 K, air	437	1.03 ± 0.04	Perylene/EtOH (0.87)	[188]	[153]
2-45	Perylenebisimide dye	CHCl <sub>3</sub>	290 K, air	492	1.03 ± 0.05	Perylenebisimide dye/ CH <sub>2</sub> Cl <sub>2</sub> (0.99)	[150]	[153]
2-46	Rhodamine 6G	Hexane	RT, air	514	0.92 ± 0.09	Rhodamine 6G/EtOH (0.95)	[105]	[156]
2-47	Rhodamine 6G	Ethanol	298 K, air	248–528	0.95 ± 0.05	QS/1.0 N H <sub>2</sub> SO <sub>4</sub> (0.546)	[79]	[105]
2-48	Rhodamine 6G	Ethanol	293 K, air	n.r.	0.95 ± n.r.	n.r.	n.r.	[144]
2-49	Rhodamine 6G	Water	RT, air	514	0.45 ± 0.05	Rhodamine 6G/EtOH (0.95)	[105]	[156]
2-50	Rhodamine B	Ethanol	293 K, air	n.r.	0.50 ± n.r.	n.r.	n.r.	[144]
2-51	Rhodamine B	Basic ethanol	298 K, air	259–542	0.65 ± 0.03	QS/1.0 N H <sub>2</sub> SO <sub>4</sub> (0.546)	[79]	[105]
2-52	Rhodamine B	Methanol	298 K, air	n.r.	0.69 ± 0.02	QS/0.1 N HClO <sub>4</sub> (0.59)	[185]	[140]
2-53	Rhodamine 3B	Ethanol	298 K, air	257–556	0.45 ± 0.02	QS/0.1 N HClO <sub>4</sub> (0.59)	[185]	[140]
2-54	Rhodamine 101	Ethanol	RT, deg.	450–565	1.00 ± n.r.	Rhodamine 101/EtOH (1.00)	[189]	[36, 81]
2-55	Rhodamine 101	Ethanol	293 K, air	n.r.	0.96 ± n.r.	n.r.	n.r.	[144]
2-56	Rhodamine 101	Basic ethanol	298 K, air	265–563	0.96 ± 0.05	QS/1.0 N H <sub>2</sub> SO <sub>4</sub> (0.546)	[79]	[105]
2-57	Rhodamine 110	Basic ethanol	298 K, air	267–501	0.92 ± 0.05	QS/1.0 N H <sub>2</sub> SO <sub>4</sub> (0.546)	[79]	[105]
2-58	Rhodamine 123	Ethanol	298 K, air	245–510	0.90 ± 0.05	QS/1.0 N H <sub>2</sub> SO <sub>4</sub> (0.546)	[79]	[105]
2-59	Rhodamine 19	Basic ethanol	298 K, air	245–516	0.95 ± 0.05	QS/1.0 N H <sub>2</sub> SO <sub>4</sub> (0.546)	[79]	[105]
2-60	TRITC	Hexane	RT, air	514	0.14 ± 0.02	Rhodamine 6G/EtOH (0.95)	[105]	[156]
2-61	TRITC	Ethanol	RT, air	514	0.26 ± 0.03	Rhodamine 6G/EtOH (0.95)	[105]	[156]
2-62	TRITC	Water	RT, air	514	0.15 ± 0.02	Rhodamine 6G/EtOH (0.95)	[105]	[156]
2-63	Texas red	Hexane	RT, air	585	0.20 ± 0.02	Rhodamine 6G/EtOH (0.95)	[105]	[156]
2-64	Texas red	Ethanol	RT, air	585	0.93 ± 0.09	Rhodamine 6G/EtOH (0.95)	[105]	[156]
2-65	Texas red	Water	RT, air	585	0.35 ± 0.03	Rhodamine 6G/EtOH (0.95)	[105]	[156]
2-66	Cy3	PBS buffer	RT, air	n.r.	0.04 ± n.r.	Rhodamine 6G/MeOH (0.95)	[190]	[160, 161]

Table 2 (continued)

Entry	Compound <sup>a</sup>	Solvent	Conditions <sup>b</sup>	$\lambda_{\text{exc}}/\text{nm}^c$	$\phi_f^d$	Standard/solvent ( $\phi_f$ ) <sup>e</sup>	Refs. Std.	Refs.
2-67	Cy5	PBS buffer	RT, air	n.r.	0.27 ± n.r.	3,3'-diethylthiadicarbocyanine/MeOH (0.33)	[191]	[160, 161]
2-68	IR 125	Ethanol	298 K, air	n.r.	0.05 ± n.r.	IR 125/DMSO (0.13)	[99]	[158]
2-69	IR 125	Methanol	298 K, air	n.r.	0.04 ± n.r.	IR 125/DMSO (0.13)	[99]	[158]
2-70	IR 125	Water, pH 7	298 K, air	n.r.	0.01 ± n.r.	IR 125/DMSO (0.13)	[99]	[158]
2-71	IR 132	Ethanol	298 K, air	n.r.	0.09 ± n.r.	IR 125/DMSO (0.13)	[99]	[158]
2-72	IR 132	Methanol	298 K, air	n.r.	0.07 ± n.r.	IR 125/DMSO (0.13)	[99]	[158]
2-73	IR 132	Water, pH 7	298 K, air	n.r.	< 0.005 ± n.r.	IR 125/DMSO (0.13)	[99]	[158]
2-74	IR-1048	CH <sub>2</sub> Cl <sub>2</sub>	RT, air	980, 1064	0.0017 ± 0.0005	Rhodamine B/0.1 N NaOH (0.97)	[82]	[159]
2-75	IR-1048	Acetonitrile	RT, air	980, 1064	0.001 ± 0.0002	Rhodamine B/0.1 N NaOH (0.97)	[82]	[159]
2-76	IR-1048	Ethanol	RT, air	980, 1064	0.004 ± 0.001	Rhodamine B/0.1 N NaOH (0.97)	[82]	[159]
2-77	IR-1050	CH <sub>2</sub> Cl <sub>2</sub>	RT, air	980, 1064	0.0015 ± 0.0004	Rhodamine B/0.1 N NaOH (0.97)	[82]	[159]
2-78	IR-1050	Acetonitrile	RT, air	980, 1064	0.0011 ± 0.0003	Rhodamine B/0.1 N NaOH (0.97)	[82]	[159]
2-79	IR-1050	Ethanol	RT, air	980, 1064	0.004 ± 0.001	Rhodamine B/0.1 N NaOH (0.97)	[82]	[159]
2-80	IR-1040	CH <sub>2</sub> Cl <sub>2</sub>	RT, air	980, 1064	0.006 ± 0.002	Rhodamine B/0.1 N NaOH (0.97)	[82]	[159]
2-81	IR-1040	Acetonitrile	RT, air	980, 1064	0.004 ± 0.001	Rhodamine B/0.1 N NaOH (0.97)	[82]	[159]
2-82	IR-1040	Ethanol	RT, air	980, 1064	0.012 ± 0.004	Rhodamine B/0.1 N NaOH (0.97)	[82]	[159]
2-83	IR-1061	CH <sub>2</sub> Cl <sub>2</sub>	RT, air	980, 1064	0.009 ± 0.003	Rhodamine B/0.1 N NaOH (0.97)	[82]	[159]
2-84	IR-1061	Acetonitrile	RT, air	980, 1064	0.005 ± 0.001	Rhodamine B/0.1 N NaOH (0.97)	[82]	[159]
2-85	IR-1061	Ethanol	RT, air	980, 1064	0.017 ± 0.005	Rhodamine B/0.1 N NaOH (0.97)	[82]	[159]

<sup>a</sup> Lucifer yellow = substituted 4-aminonaphthalimide, Texas red = substituted rhodamines, IR-125, IR-132, IR-1048, IR-1050, IR-1040 and IR-1061 = various tricarboyanine dyes

<sup>b</sup> air = non-degassed, deg. = degassed

<sup>c</sup> n.r. = not reported

<sup>d</sup> n.r. = uncertainty not reported

<sup>e</sup> n.r. = not reported

ployed for instrument correction, dye purification or other technical details is only given in some of them (e.g., [85, 140–142]). Furthermore, in several cases, the mentioning of the exact excitation conditions has also been omitted (e.g., [143, 144]) and some of the works do not provide details on the uncertainty of measurement (e.g., [145, 146]). Unfortunately, the overlap of the data in Tables 1 and 2 is not so good in the UV region so that a direct comparison cannot be done. Taking older data into account, some peculiarities can be found. For instance, the data for sodium salicylate differ between 0.25 and 0.32 (Table 2, entries 2-7 and 2-8) with an absolute  $\Phi_f$  having been obtained to  $0.28 \pm 0.02$  by Weber and Teale in 1957 [82]. Entries 2-15 to 2-17 show that the inconsistencies in the reports on the fluorescence quantum yields of 9,10-DPA continue to exist, despite the amount of work that has been invested on this dye, see, e.g., [100, 102, 138, 147, 148]. Entries 2-21 to 2-26 and 2-32 as well as 2-28, 2-29, 2-34 and 2-39 to 2-45 report the data of two classes of compounds, harmans and derivatives as well as perylenebis(dicarboximides), that have been frequently advertised as potential fluorescence quantum yield standards in the last years but have not been the subject of absolute studies yet [141–143, 146, 149–153]. The harmanes lie in the same wavelength range as quinine sulfate but do not possess the latter's complex chemistry (*vide infra*). The perylenebis(dicarboximides) are photo- and chemically very stable dyes with a very high emissivity in almost any solvent that they can be dissolved in. Acridinium dyes (Table 2, entries 2-30 and 2-31) are water soluble and also possess  $\Phi_f$  close to unity so that they should in principle also constitute potent standards [145, 146]. BP(OH)<sub>2</sub> (Table 2, entries 2-35 and 2-36) is interesting from the point of view that it emits with a large Stokes' shift (ca. 10 000 cm<sup>-1</sup>) and that its fluorescence quantum yield is only weakly susceptible to changes of solvent polarity [154]. The data for fluorescein (Table 2, entries 2-37 and 2-38) support the sensitivity of this compound toward its environment (see, e.g., [155]). Whether NaOH or a borate buffer is used, significantly different  $\Phi_f$  have been reported by two groups that, according to the descriptions in the papers, have carried out the relative determinations with great care [85, 140].

In the case of the rhodamine dyes, the picture is also diverse. Whereas the data agree well for rhodamine 101 in ethanol (Table 2, entries 2-54 to 2-56) and rhodamine 6G in organic solvents (entries 2-46 to 2-48), Soper et al. found a significantly lower  $\Phi_f = 0.45$  for this dye in water (Table 2, entry 2-49) [156], in contrast to the data obtained by absolute methods which yield  $\Phi_f$  between 0.86 and 0.93 (Table 1, entries 1-45 to 1-48). Similar differences are obvious when one compares the entries for rhodamine B. Whereas the absolute measurements either report values of ca. 0.95 (Table 1, entries 1-52 to 1-58) or ca. 0.77 (entries 1-50, 1-51 and 1-59, Table 1), the relative measurements give  $\Phi_f$  of 0.50, 0.65 and 0.69 (entries 2-50 to 2-52, Table 2) [105, 140, 144]. Apparently, the well-known temperature dependence of the fluorescence quantum yield of this compound alone cannot be responsible for such dramatic dif-

ferences [105, 157] so that the problem might lie in the application of the correction for reabsorption; in some of the absolute measurements, rather high dye concentrations of  $> 10 \mu\text{M}$  were employed [81, 120]. The data for the near-infrared dyes included in Table 2 (entries 2-66 to 2-85) also have to be treated carefully. First, the publications lack information on the use of or the setting of polarizers despite the fact that these rather large and rod-like molecules are known to often possess a non-negligible anisotropy [158–161]. Second, the data of Soper et al. are based on a  $\Phi_f$  value published by Benson and Kues for IR-125 in DMSO, which is not very reliable as the authors themselves state in [99]. The fluorescence quantum yields of the IR-10XX series are referenced on a high value of rhodamine B (0.97), which harbors all the above-mentioned uncertainties. Moreover, rather concentrated solutions ( $20 \mu\text{M}$ ) of such dyes with small Stokes shift and high molar absorptivity have been measured so that reabsorption effects should have been considered. Finally, the seminal works on the Cy dyes do not give a comprehensive account of the experimental details and at least in the case of Cy5, the reference value for 3,3'-diethylthiadicarbocyanine is not well established.

Most of the data discussed in this chapter were determined with the classical method of using optically dilute solutions. In the early 1980s, however, an alternative approach was proposed that compares the fluorescences of a target dye and a  $\Phi_f$  standard under highly concentrated, optically dense conditions [145, 162]. Although the method is very straightforward, it has all the chemical problems connected to concentrated dye solutions. Unfortunately, in both works not much information is provided on instrument calibration, dye characteristics and uncertainties of measurement and the dyes chosen to test the approach have not been measured in standard solvents (see, e.g., Table 2, entries 2-8, 2-12, 2-31) so that a profound evaluation of the method is not possible yet.

## 4.2

### Measurements as a Function of Temperature

One of the important tasks in luminescence spectroscopy and photochemistry is the elucidation of the processes that lead to the partial quenching for most emissive compounds in solution at room temperature. Only a very few dyes, such as 9,10-substituted anthracenes, acridinium salts, perylenebis(dicarboximides) or some rhodamine dyes possess fluorescence quantum yields close to unity at room temperature. One source of quenching can be the presence of oxygen, the influence of which can be elegantly assessed by a comparison of the  $\Phi_f$  obtained under inert and normal atmospheric conditions. In most cases however, internal quenching channels such as photoisomerization, charge shift or charge transfer processes can compete more or less successfully with fluorescence. To get access to the nature of the quenching process, measurements of the fluorescence quantum yield

(and lifetime, which will not be discussed here) as a function of temperature are often performed. Many works in this field scan, for instance, the temperature range from room temperature to 77 K and work with liquid nitrogen as the cooling medium. To be able to extract reliable fluorescence quantum yield data from such experiments, several issues have to be considered. The interference of increased scattering due to cracks in the solid matrix at low temperature must be avoided. The experiment thus has to be carried out in a solvent or in solvent mixtures that form optically transparent glasses below the glass temperature. Information on suitable media can be found, for example, in [163–165]. Additionally, the temperature dependence of the refractive index of the solvent has to be taken into account. Such data are tabulated, e.g., in the Landolt–Börnstein compendium [166]. Since for most dyes, the shape of the absorption spectrum also changes as a function of temperature—often the bands are bathochromically shifted due to an increase of the solvent’s dielectric constant and narrowed due to a freezing of vibronic modes (Figs. 8 and 9)—knowledge of the actual absorbance at every point of the temperature run is required. At best, the absorption of the sample is directly measured in the cryostat mounted in the fluorometer (Fig. 9). If this is not possible, the following procedure can be applied for fluorophores with a well-separated  $S_1 \leftarrow S_0$  transition and matching absorption and fluorescence excitation spectra.

The initial solution can be measured on a spectrophotometer and the absorbance at the excitation wavelength can be determined from these data. Afterwards, the sample is placed in the cryostat and fluorescence emission and excitation spectra are measured at the same temperature. After cooling the sample to a desired temperature, fluorescence excitation and emission

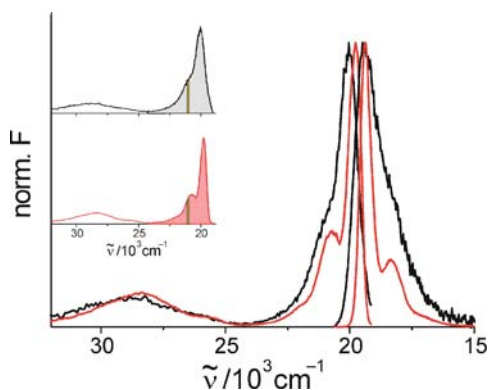


**Fig. 8** Fluorescence excitation (*left*) and emission (*right*) spectra of a typical polymethine dye in ethanol at 300 K (*black*) and 80 K (*red*). The *inset* shows the integrals of the bands corresponding to the  $S_1 \leftarrow S_0$  transition and the *yellow bar* denotes the idealized excitation interval. It is obvious that the bathochromic shift and narrowing of the band upon cooling to 77 K results in a relative decrease in absorbance at the excitation wavelength

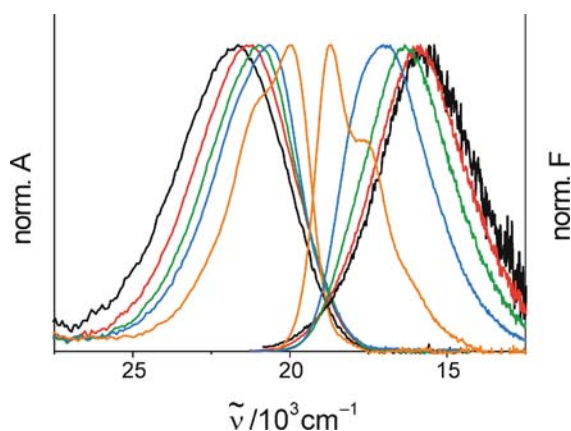


**Fig. 9** Absorption (*left*) and fluorescence (*right*) spectra of a typical electron donor-acceptor-substituted charge-transfer-active dye in ethanol at 290 K (*black*), 230 K (*red*), 185 K (*green*), 150 K (*blue*) and 50 K (*orange*)

spectra are recorded again. Then the ratio of the integral of the fluorescence excitation spectrum and the intensity reading at the excitation wavelength is calculated for both temperatures (Fig. 8, inset). Since the oscillator strength of an electronic transition does not change as a function of temperature, comparison of the two ratios allows estimation of the change in absorbance at the excitation wavelength. For common charge-transfer-active dyes as the one shown in Fig. 9, use of a single excitation wavelength is not possible over the entire temperature range and thus the excitation correction curve of the instrument has to be taken into account as well. Furthermore, the density of the solvent is also altered as a function of temperature, and this change in concentration of the emissive solute also has to be corrected. As mentioned above in Sect. 3.1, polarization effects have to be considered when increasing the viscosity of solvents upon decreasing the temperature or when measuring the fluorophore in the glassy solvent. Additionally, based on the commonly observed spectral changes as a function of temperature—narrowing and decrease of the Stokes' shift—reabsorption errors can be more significant at low temperatures, see e.g., [167]. Measurement of a mixture of fluorophores with known and unknown fluorescence quantum yields to account for increased scattering as proposed in [168] is less recommended here, since the requirements for the standard are very difficult to meet. The absorption spectrum should be well-separated from that of the dye in question so that exclusive excitation is guaranteed; the differences in  $E_{\text{ex},\lambda}(\lambda_{\text{ex}})$  then have to be accounted for. However, both emission spectra should overlap as much as possible to avoid the influence of the wavelength dependence of the intensity of the scattering light. At the same time, any energy transfer between the two dyes also has to be strictly avoided.

## 5 Fluorescence and Phosphorescence Quantum Yields

The determination of phosphorescence quantum yields is experimentally very similar to the determination of  $\Phi_f$ . However, due to the intrinsically longer lifetime of phosphorescence decays, special attention has to be paid to the exclusion of quenchers and when pulsed excitation sources are used. A comprehensive review has been published in the field only recently, highlighting the peculiarities connected with the measurement of  $\Phi_p$  [169]. Difficulties in the determination of  $\Phi_p$  can arise when a compound is able to decay through both channels, phosphorescence and fluorescence. This is frequently observed for (poly)cyclic hydrocarbons at low temperatures in the glass [170]. If the two luminescence spectra are not well separated, spectral deconvolution in connection with lifetime measurements or time-gated detection can be used to separate the slowly decaying from the fast decaying species. A detailed discussion of the measurement of absolute quantum yields of phosphorescence and fluorescence at 77 K in the glass is given in [171]. However, in most cases,  $\Phi_p$  is determined by relative optical methods.

## 6 Fluorescence Quantum Yield Standards

The discussion in the previous chapters suggests that 25 years after the publication of Demas' review [31] and almost 20 years after the publication of the IUPAC recommendations [36], it is not possible to report essential advances with respect to the establishment of reliable and approved fluorescence quantum yield standards. Quinine sulfate with all its problematic features—complicated ground-state chemistry [172, 173], dependence of emission band position on excitation wavelength [104]—is still the most popular standard, together with fluorescein for the visible region. The latter, however, is also not an optimum candidate since it is sensitive to acid–base chemistry and is photochemically not very stable [31]. Anthracene and 9,10-DPA are not ideal due to their susceptibility toward the presence of oxygen, their sharp and narrow bands and small Stokes shifts. Moreover, as has been reported above, the literature still disagrees on a reference value for their fluorescence quantum yields. The situation is not much different for rhodamines. Here, rhodamine 6G and especially rhodamine B seem to be less suitable standards while rhodamine 101 is probably the most promising one. Cresyl violet seems to be an equally good candidate as rhodamine 101. Some of the oxazine dyes might qualify as potent fluorescence quantum yield standards as well, but further verification of their data is necessary. The same holds for the promising compounds listed in Table 2—acridinium salts, harmanes, perylenebis(dicarboximides)—where the basis of the available data is still too

little to seriously judge their suitability. Further research is also required for coumarin or stilbene dyes. For both classes of dyes, many derivatives are known that partly show very different fluorescence quantum yields, photostability and/or excitation-wavelength-dependent photophysics. For instance, Olmsted III found  $\Phi_f = 0.64 \pm 0.02$  for coumarin I in ethanol with an absolute calorimetric method [126], but Drexhage reported a value of 0.5 [174]. Fluorinated coumarins, a class of stable laser dyes proposed by Demas as potential standard materials [31], have not been the subject of intensive studies in this respect in the past two decades. Their potential thus remains to be assessed.

Focusing on the red visible and near-infrared spectral region, unfortunately, the last 25 years have also not improved the availability of standards significantly. Cyanine dyes are expected to be the most promising candidates because the majority of fluorescent stains, labels and probes in the near infrared stem from this class of compounds. However, the amount of data published so far does not allow the recommendation of a particular compound in a particular solvent. Many cyanine dyes are known to already aggregate at micromolar concentrations, restricting the use of such compounds to methods for the measurement of  $\Phi_f$  that operate well in very dilute solutions. Additionally, cyanine dyes show characteristically narrow and weakly Stokes-shifted bands, further complicating their use at higher concentrations. Styryl dyes that show broad and distinctly Stokes-shifted absorption and emission bands in the 600–1000 nm region might also be potential standards for this region—selected styryl derivatives have been proposed as reference materials for the correction of the spectral responsivity of the emission channel of fluorimeters [175]—yet the amount of fluorescence quantum yields published is also rather sparse. Furthermore, application of such dyes in alcoholic or aqueous solution is generally hampered by the fact that hydrogen bonding usually quenches the emission of such charge-transfer dyes dramatically [176]. Finally, the  $\Phi_f$  values published in the past for  $\text{Ru}(\text{bipy})_3^{2+}$  salts are still too scattered and unreliable, so that these dyes can also not be recommended without further validation.

## 7

### Outlook

The last 25 years have seen the publication of several fluorescence quantum yields determined either by absolute or by relative methods. In general, the data provided in this period of time are not significantly different from or better than the data obtained between the 1950s and the 1980s, despite all of the technological and instrumental advances that have been made in the past decades. Besides dye-specific issues such as purity, stability and final concentration used in the measurement, instrument calibration is most probably the key to more reliable data. The quality of correction methods and chemical ref-



erence materials has to be assured, at best with a chain of transfer standards fully traceable to the primary metrological standards held for instance at National Institute of Standards and Technology (US) or Physikalisch-Technische Bundesanstalt (Germany) [83, 177, 178]. As an alternative, Round Robin tests or key comparisons of qualified laboratories can be carried out to establish and verify specific compounds in certain solvents as suitable fluorescence quantum yield standards. Such tests or comparisons should at best include all three major methods of fluorescence quantum yield determination, optical ones, PAS and thermal lensing. Moreover, it has to be assured that participants of these tests provide a comprehensive uncertainty budget for their method and provide evidence for traceability. A related procedure has very recently been followed for fluorescence lifetime standards [179].

In retrospect, it is amazing how few things have changed since the last authoritative review on the measurement of fluorescence quantum yields appeared in 1982 [31]. This observation concerns the quantum yield data or their scattering as well as the information on experiment and data treatment provided in most of the articles cited in Tables 1 and 2. Data presentation is still one of the major problems in truly judging the quality and reliability of the values listed in the tables. Before reprinting here Demas' recommendations for data presentation that are as relevant as they were in 1982, it should also be noted that the two major remarks of the IUPAC recommendations mentioned already in the Introduction—"far-red and near-infrared standards are not known" and "no good standards exist for low-intensity emitters"—unfortunately are still valid. Being alerted by the fate of Demas' predictions as mentioned in Sect. 3.1, only the hope can be expressed here that at least some of the unresolved issues will be tackled by the scientific community in the coming years.

Recommendations for data presentation taken from [31]:

1. What method of photon yield determination was used? How were the data reduced?
2. In relative photon yield determinations, what standard was employed? How was it used? What yield was assumed?
3. If a standard scattering solution was used, how was it prepared and how soon after preparation was it used? How was the sample absorbance measured? Over what wavelength range did it obey Raleigh law? Was there evidence for fluorescence and absorption?
4. What wavelengths were used to excite the sample and the standard? If the two wavelengths were different, what method was used to ascertain the relative intensities? How were stray-light errors avoided, especially when using optically dilute methods? What methods were used to eliminate short- and long-term drift in the source?
5. If a quantum counter was used, what was the material, its source and purification? What solvent and concentration were employed? What was the

- history of the counter, especially the frequency of dye replacement and exposure to light? Was purity verified? Was the response assumed to be quantum flat and why? If not, what corrections were applied and why?
6. How were absorption measurements made? Were the errors from scattered or fluorescence radiation as the detector assessed and avoided?
  7. What luminescence instrument was used? Were special cuvette, cell placement or sample compartment designs used? Was the cuvette blackened on all sides not used for optical transmission? What stops and lenses were used, especially in the emission paths?
  8. What excitation bandpass was used? What was the extent of the bandpass errors, and what corrections were made?
  9. What techniques were used to calibrate the excitation and emission systems? Were checks of the excitation and emissions systems made on reference samples with well-characterized excitation and emission spectra and over what wavelength ranges? How strongly did the corrections vary with wavelength?
  10. If an integrating sphere was used, how was it prepared? How was the combined spectral response of sphere and detector determined? How was deterioration of the sphere coating prevented and how often was the system calibrated?
  11. Were solvent blanks corrected for? Were the blanks a significant portion of the sample signal? Where blank contributions were large, the blank and sample spectra should both be presented to permit the reader to estimate errors of any subtractions.
  12. What refractive index correction was made? Is this correction appropriate for the instrument used? Did the detection system see beyond the region of uniform luminescence?
  13. What concentrations and temperatures were used? Did the yield vary with excitation wavelength?
  14. Was oxygen quenching present? If so provide Stern–Volmer oxygen quenching constants.
  15. What were the lifetimes of the species studied under the conditions used in the yield determination? With increasing availability of (nanosecond) decay-time instruments, lifetime information will permit workers to verify that they are studying the same systems.
  16. Was concentration quenching present? If so provide self-quenching constants.
  17. Was any unusual chemical or spectroscopic behavior observed? Was photolysis, association or dissociation observed? Were stock solutions stable with time and were emission intensities stable on prolonged irradiation?
  18. What were the observed statistical uncertainties and confidence levels (preferably 95–99%)? Precision and accuracy should be listed separately, along with an explanation of how they were calculated.

19. What standards were run to verify system performance and what were their measured yields? Failure to present satisfactory evidence casts doubts on all results.

**Acknowledgements** I thank Dr. Christian Monte (AG 7.31 Temperaturstrahlung, PTB, Berlin) for fruitful discussions, comments and suggestions.

## References

1. Lakowicz JR (2006) Principles of fluorescence spectroscopy, 3rd edn. Springer, Berlin
2. Valeur B (2001) Molecular fluorescence. Wiley-VCH, Weinheim
3. Lakowicz JR (ed) (1992–2006) Topics in fluorescence spectroscopy series, vols 1–11. Plenum, New York and Springer, Berlin
4. Wolfbeis OS (ed) (2001–2008) Springer series on fluorescence, vols 1–4. Springer, Berlin
5. Mycek MA, Pogue BW (eds) (2003) Handbook of biomedical fluorescence. Marcel Dekker, New York
6. de Silva AP, Tecilla P (eds) (2005) *J Mater Chem* 15:2637
7. Pawley JB (ed) (2006) Handbook of biological confocal microscopy, 3rd edn. Springer, Berlin
8. Duarte FJ, Hillman LW (eds) (1990) Dye laser principles. Academic Press, New York
9. Ross H, Noakes JE, Spaulding JD (eds) (1991) Liquid scintillation counting and organic scintillators. Lewis, Chelsea, MI
10. Balzani V, Piotrowiak P, Rodgers MAJ, Mattay J, Astruc D, Gray HB, Winkler J, Fukuzumi S, Mallouk TE, Haas Y, de Silva AP, Gould I (eds) (2001) Electron transfer in chemistry. Wiley-VCH, Weinheim
11. De Cola L (ed) (2005) *Top Curr Chem* 257
12. May V, Kuhn O (2004) Charge and energy transfer dynamics in molecular systems. Wiley-VCH, Weinheim
13. Earp AA, Smith GB, Swift PD, Franklin J (2004) *Sol Energ* 76:655
14. Birks JB (1970) Photophysics of aromatic molecules. Wiley-Interscience, London
15. Klessinger M, Michl J (1995) Excited states and photochemistry of organic molecules. Wiley-VCH, Weinheim
16. Lanzani G (ed) (2005) Photophysics of molecular materials. Wiley-VCH, Weinheim
17. Birks JB (1976) *J Res Natl Bur Stand* 80A:389
18. Vavilov SI (1924) *Z Phys* 22:266
19. Parker CA, Rees WT (1960) *Analyst* 85:587
20. Melhuish WH (1955) *N Z J Sci Technol B* 37:142
21. Testa AC (1969) *Fluoresc News* 4:1
22. Demas JN, Crosby GA (1971) *J Phys Chem* 75:991
23. Melhuish WH (1972) *J Res Natl Bur Stand* 76A:547
24. Crosby GA, Demas JN, Callis JB (1972) *J Res Natl Bur Stand* 76A:561
25. Reisfeld R (1972) *J Res Natl Bur Stand* 76A:613
26. Velapoldi RA (1972) *J Res Natl Bur Stand* 76A:641
27. Chen RF (1972) *J Res Natl Bur Stand* 76A:593
28. Demas JN, Blumenthal BH (1976) *J Res Natl Bur Stand* 80A:409
29. Bril A, Jagerveinis AWD (1976) *J Res Natl Bur Stand* 80A:401
30. Callis JB (1976) *J Res Natl Bur Stand* 80A:413

31. Demas JN (1982) In: Mielenz KD (ed) Measurement of photoluminescence, optical radiation measurements, vol 3. Academic Press, New York, p 195
32. Velapoldi RA (1987) In: Burgess C, Mielenz KD (eds) Advances in standards and methodology in spectrophotometry. Elsevier, Amsterdam, p 175
33. McKinnon RA (1987) In: Burgess C, Mielenz KD (eds) Advances in standards and methodology in spectrophotometry. Elsevier, Amsterdam, p 195
34. Grum F (1982) *Color Res Appl* 7:253
35. Velapoldi RA, Epstein MS (1989) *ACS Symp Ser* 383:98
36. Eaton DF (1988) *Pure Appl Chem* 60:1107
37. Eaton DF (1988) *J Photochem Photobiol B* 2:523
38. Fery-Forgues S, Lavabre D (1999) *J Chem Educ* 76:1260
39. Resch-Genger U, Hoffmann K, Nietfeld W, Engel A, Neukammer J, Nitschke R, Ebert B, Macdonald R (2005) *J Fluoresc* 15:337
40. Resch-Genger U (2005) *J Fluoresc* 15:205
41. Hastings JW, Riley WH, Massa J (1965) *J Biol Chem* 240:1473
42. Lee J (1972) *Biochemistry* 11:3350
43. Wallace WL, Bard AJ (1979) *J Phys Chem* 83:1350
44. Barnett NW, Francis PS (2005) In: Worsford P, Townshend A, Poole C (eds) *Encyclopedia of analytical sciences*, vol 1, 2nd edn. Elsevier, Amsterdam, p 506
45. Barnett NW, Francis PS (2005) In: Worsford P, Townshend A, Poole C (eds) *Encyclopedia of analytical sciences*, vol 1, 2nd edn. Elsevier, Amsterdam, p 511
46. Kricka LJ (2005) In: Worsford P, Townshend A, Poole C (eds) *Encyclopedia of analytical sciences*, vol 1, 2nd edn. Elsevier, Amsterdam, p 277
47. Richter MM (2004) *Chem Rev* 104:3003
48. Kankare J, Kulmala S (2005) In: Worsford P, Townshend A, Poole C (eds) *Encyclopedia of analytical sciences*, vol 1, 2nd edn. Elsevier, Amsterdam, p 528
49. Beese W, Zink JI (1984) *J Luminesc* 29:119
50. Vass I, Govindjee (1996) *Photosynth Res* 48:117
51. Peto A (1996) *Radiat Prot Dosim* 65:123
52. McKeever SWS, Chen R (1997) *Radiat Meas* 27:625
53. Hilgenfeldt S, Grossmann S, Lohse D (1999) *Nature* 402:398
54. Bourhill G, Palsson LO, Samuel IDW, Sage IC, Oswald IDH, Duignan JP (2001) *Chem Phys Lett* 336:234
55. Didenko YT, Suslick KS (2002) *Nature* 418:394
56. Abrams BL, Holloway PH (2004) *Chem Rev* 104:5783
57. Furetta C, Kitis G (2004) *J Mater Sci* 39:2277
58. Hall LM, Hunter TF, Stock MG (1976) *Chem Phys Lett* 44:145
59. Rockley MG (1977) *Chem Phys Lett* 50:427
60. Sonnenschein M, Amirav A, Jortner J (1984) *J Phys Chem* 88:4214
61. Ates S, Yildiz A (1983) *J Chem Soc Faraday Trans 1* 79:2853
62. Alimarin IP, Durnev VE, Runov VK (1987) *Teor Eksp Khim* 23:705
63. Ferreira LFF, Freixo MR, Garcia AR, Wilkinson F (1992) *J Chem Soc Faraday Trans* 88:15
64. Haynes DR, Tokmakoff A, George SM (1993) *Chem Phys Lett* 214:50
65. Miranda M, Lagorio MG, Roman ES (2004) *Langmuir* 20:3690
66. Brody M, Brody SS (1971) *Photochem Photobiol* 13:293
67. Kurian E, Prendergast FG, Rudzki Small J (1997) *Biophys J* 73:466
68. Greenham NC, Samuel IDW, Hayes GR, Phillips RT, Kessener Y, Moratti SC, Holmes AB, Friend RH (1995) *Chem Phys Lett* 241:89
69. deMello JC, Wittmann HF, Friend RH (1997) *Adv Mater* 9:230

70. Mattoussi H, Murata H, Merritt CD, Iizumi Y, Kido J, Kafafi ZH (1999) *J Appl Phys* 86:2642
71. Nollau A, Hoffmann M, Floreck K, Fritz T, Leo K (2000) *J Appl Phys* 87:7802
72. Nonell S, Marti C, Garcia-Moreno I, Costela A, Sastre R (2001) *Appl Phys B* 72:355
73. Palssson LO, Monkman AP (2002) *Adv Mater* 14:757
74. Weidner VR, Mavrodineanu R, Eckerle KL (1986) *Appl Opt* 25:832
75. Seelert W, Strauss E (1987) *J Luminesc* 36:355
76. Torchia GA, Munoz JA, Cusso F, Jaque F, Tocho JO (2001) *J Luminesc* 92:317
77. Melhuish WH (1984) *Pure Appl Chem* 56:231
78. Braslavsky SE (2007) *Pure Appl Chem* 79:293
79. Melhuish WH (1961) *J Phys Chem* 65:229
80. Melhuish WH (1964) *J Opt Soc Am* 54:183
81. Galanin MD, Kut'envok AA, Smorchkov VN, Timofeev YP, Chizhikov ZA (1982) *Opt Spektrosk* 53:683
82. Weber G, Teale FWJ (1957) *Trans Faraday Soc* 53:646
83. Hollandt J, Taubert RD, Seidel J, Resch-Genger U, Gugg-Helminger A, Pfeifer D, Monte C, Pilz W (2005) *J Fluoresc* 15:301
84. Fletcher AN (1969) *Photochem Photobiol* 9:439
85. Rhys Williams AT, Winfield SA, Miller JN (1983) *Analyst* 108:1067
86. Bendig J, Kreysig D, Schöneich R (1979) *Z Chem* 19:151
87. Demas JN (1973) *Anal Chem* 45:922
88. Cehelnik ED, Mielenz KD, Velapoldi RA (1975) *J Res Natl Bur Stand* 79A:1
89. Minato H, Nanjo M, Nayatani Y (1983) *Color Res Appl* 8:238
90. Levitus M, Bourdelande JL, Marqués G, Aramendía PF (1999) *J Photochem Photobiol A* 126:77
91. Resch-Genger U, Pfeifer D, Monte C, Pilz W, Hoffmann A, Spieles M, Rurack K, Hollandt J, Taubert D, Schönenberger B, Nording P (2005) *J Fluoresc* 15:315
92. Credi A, Prodi L (1998) *Spectrochim Acta* 54A:159
93. Kim CS, Kong HJ (1997) *Color Res Appl* 22:275
94. Eastman JW (1967) *Photochem Photobiol* 6:55
95. Cundall RB, Evans GB (1968) *J Phys E* 1:305
96. Eisinger J, Flores J (1979) *Anal Biochem* 94:15
97. Bendig J, Kreysig D (1979) *Z Phys Chem* 260:149
98. Bendig J, Csongar C, Kreysig D (1979) *Z Phys Chem* 260:312
99. Benson RC, Kues HA (1977) *J Chem Eng Data* 22:379
100. Rusakowicz R, Testa AC (1968) *J Phys Chem* 72:793
101. Barrow DA, Lentz BR (1984) *Chem Phys Lett* 104:163
102. Eastman JW (1970) *Spectrochim Acta* A26:1545
103. Chen RF (1967) *Anal Lett* 1:35
104. Fletcher AN (1968) *J Phys Chem* 72:2742
105. Kubin RE, Fletcher AN (1982) *J Luminesc* 27:455
106. Lutz H-P, Luisi PL (1983) *Helv Chim Acta* 66:1929
107. De Jersey J, Jeffers Morley P, Martin RB (1981) *Biophys Chem* 13:233
108. Bindhu CV, Harilal SS, Nampoori VPN, Vallabhan CPG (1999) *Mod Phys Lett B* 13:563
109. Chekalyuk A, Fadeev V, Georgiev G, Kalkanjiev T, Nickolov Z (1982) *Spectrosc Lett* 15:355
110. Sivaprakasam V, Killinger DK (2003) *J Opt Soc Am B* 20:1980
111. Shea Rohwer L, Martin JE (2005) *J Luminesc* 115:77

112. Porrès L, Holland A, Palsson LO, Monkman AP, Kemp C, Beeby A (2006) *J Fluoresc* 16:267
113. Seybold PG, Gouterman M, Callis J (1969) *Photochem Photobiol* 9:229
114. Adams MJ, Highfield JG, Kirkbright GF (1977) *Anal Chem* 49:1850
115. Grabowski JJ, Bertozzi CR, Jacobsen JR, Jain A, Marzluff EM, Suh AY (1992) *Anal Biochem* 207:214
116. Görtz W, Perkampus HH (1983) *Fresenius Z Anal Chem* 316:180
117. Rockley MG, Waugh KM (1978) *Chem Phys Lett* 54:597
118. Vogel M, Rettig W (1985) *Ber Bunsenges Phys Chem* 89:962
119. Rudzki Small J, Hutchings JJ, Small EW (1989) *Proc SPIE Int Soc Opt Eng* 1054:26
120. Zhang G, Li Z, Yan J (1985) *Kexue Tongbao* 30:1158
121. Zhang G, Li Z, Yan J (1986) *Chin Phys Lett* 3:9
122. Sabol JE, Rockley MG (1987) *J Photochem Photobiol A* 40:245
123. Fischer M, Georges J (1996) *Chem Phys Lett* 260:115
124. Magde D, Brannon JH, Cremers TL, Olmsted J III (1979) *J Phys Chem* 83:696
125. Hercules DM, Frankel H (1960) *Science* 131:1611
126. Olmsted J III (1979) *J Phys Chem* 83:2581
127. Magde D, Wong R, Seybold PG (2002) *Photochem Photobiol* 75:327
128. Georges J, Arnaud N, Parise L (1996) *Appl Spectrosc* 50:1505
129. Sathy P, Philip R, Nampoori VPN, Vallabhan CPG (1990) *Pramana* 34:585
130. Bindhu CV, Harilal SS (2001) *Anal Sci* 17:141
131. Bindhu CV, Harilal SS, Varier GK, Issac RC, Nampoori VPN, Vallabhan CPG (1996) *J Phys D* 29:1074
132. Degen J, Reinecke K, Schmidtke HH (1992) *Chem Phys* 162:419
133. Van Houten J, Watts RJ (1975) *J Am Chem Soc* 97:3843
134. Nakamaru K, Nishio K, Nobe H (1979) *Sci Rep Hirosaki Univ* 26:57
135. Wang T, Zhang BQ, Pan JL, Gu P, Xu Q, Sun Q (1989) *Chin Sci Bull* 34:1756
136. Petukhov VA, Popov MB, Krymova AI (1986) *Kvantovaya Elektron* 13:777
137. Hamai S, Hirayama F (1983) *J Phys Chem* 87:83
138. Morris JV, Mahaney MA, Huber JR (1976) *J Phys Chem* 80:969
139. Meech SR, Phillips D (1983) *J Photochem* 23:193
140. Velapoldi RA, Tønnesen HH (2004) *J Fluoresc* 14:465
141. Pardo A, Reyman D, Poyato JML, Medina F (1992) *J Luminesc* 51:269
142. Ghiggino KP, Skilton PE, Thistlethwaite PJ (1985) *J Photochem* 31:113
143. Icil H, Uzun D, Pasaogullari N (1998) *Spectrosc Lett* 31:667
144. Deltau G, Kringel U, Peros D, Runde B, Drexhage KH (1989) In: Kirov N, Simova P, Jordanov B (eds) *Recent developments in molecular spectroscopy: proceedings of the tenth national conference on molecular spectroscopy with international participation*. World Scientific, Hackensack, NJ, p 539
145. O'Neal JS, Schulman SG (1986) *Anal Lett* 19:495
146. Wolfbeis OS, Urbano E (1982) *J Heterocycl Chem* 19:841
147. Heinrich G, Schoof S, Güsten H (1974) *J Photochem* 3:315
148. Mardelli M, Olmsted J III (1977) *J Photochem* 7:277
149. Johansson LB-Å, Karolin J, Langhals H, Reichherzer S, von Fünér N, Polborn K (1993) *J Chem Soc Faraday Trans* 89:49
150. Langhals H, Karolin J, Johansson LB-Å (1998) *J Chem Soc Faraday Trans* 94:2919
151. Icli S, Icil H (1996) *Spectrosc Lett* 29:1253
152. Icil H, Arslan E (2001) *Spectrosc Lett* 34:355
153. Kalinin S, Speckbacher M, Langhals H, Johansson LB-Å (2001) *Phys Chem Chem Phys* 3:172

154. Bulska H (1988) *J Luminesc* 39:293
155. Wang L, Gaigalas AK, Abbasi F, Marti GE, Vogt RF, Schwartz A (2002) *J Res Natl Bur Stand* 107:339
156. Soper SA, Nutter HL, Keller RA, Davis LM, Shera EB (1993) *Photochem Photobiol* 57:972
157. Karstens T, Kobs K (1980) *J Phys Chem* 84:1871
158. Soper SA, Mattingly QL (1994) *J Am Chem Soc* 116:3744
159. Casalboni M, De Matteis F, Proposito P, Quatela A, Sarcinelli F (2003) *Chem Phys Lett* 373:372
160. Mujumdar RB, Ernst LA, Mujumdar SR, Lewis CJ, Waggoner AS (1993) *Bioconjugate Chem* 4:105
161. Ernst LA, Gupta RK, Mujumdar RB, Waggoner AS (1989) *Cytometry* 10:3
162. Renschler CL, Harrah LA (1983) *Anal Chem* 55:798
163. Hurtubise RJ (1990) *Phosphorimetry*. VCH, New York, p 104
164. Meyer C (1971) *Low temperature spectroscopy*. Elsevier, New York, p 203
165. Pestemer M (1964) *Anleitung zum Messen von Absorptionsspektren im Ultraviolett und Sichtbaren*. Thieme, Stuttgart
166. <http://www.springer.com/east/home/laboe?SGWID=5-10113-0-0-0&referer=www.landolt-boernstein.com&SHORTCUT=www.springer.com> Accessed 11. February 2008
167. Bendig J, Siegmund M (1981) *Z Phys Chem* 262:834
168. Bendig J (1983) *Z Phys Chem* 264:807
169. Hurtubise RJ, Thompson AL, Hubbard SE (2005) *Anal Lett* 38:1823
170. Li R, Lim EC (1972) *J Chem Phys* 57:605
171. Gilmore EH, Gibson GE, McClure DS (1952) *J Chem Phys* 20:829
172. Schulman SG, Threatte RM, Capomacchia AC, Paul WL (1974) *J Pharm Sci* 63:876
173. Chen RF (1967) *Anal Biochem* 19:374
174. Drexhage KH (1976) *J Res Natl Bur Stand* 80A:421
175. Gardecki JA, Maroncelli M (1998) *Appl Spectrosc* 52:1179
176. Hebert P, Baldacchino G, Gustavsson T, Mialocq JC (1994) *J Photochem Photobiol A* 84:45
177. Pfeifer D, Hoffmann K, Hoffmann A, Monte C, Resch-Genger U (2006) *J Fluoresc* 16:581
178. Monte C, Resch-Genger U, Pfeifer D, Taubert DR, Hollandt J (2006) *Metrologia* 43:S89
179. Boens N, Qin W, Basaric N, Hofkens J, Ameloot M, Pouget J, Lefevre J-P, Valeur B, Gratton E, vandeVen M, Silva ND Jr, Engelborghs Y, Willaert K, Sillen A, Rumbles G, Phillips D, Visser AJWG, van Hoek A, Lakowicz JR, Malak H, Gryczynski I, Szabo AG, Krajcarski DT, Tamai N, Miura A (2007) *Anal Chem* 79:2137
180. Du H, Fuh RCA, Li J, Corkan LA, Lindsey JS (1998) *Photochem Photobiol* 68:141
181. Dawson WR, Windsor MW (1968) *J Phys Chem* 72:3251
182. Bowen EJ, Sahu J (1959) *J Phys Chem* 63:4
183. Berlman IB (1971) *Handbook of fluorescence spectra of aromatic molecules*. Academic Press, New York
184. Rusakowicz R, Testa AC (1968) *J Phys Chem* 72:2680
185. Velapoldi RA, Mielenz KD (1980) NBS Special Publication No 260-64. US Government Printing Office, Washington, DC
186. Tsin ATC, Pedrozo-Fernandez HA, Gallas JM, Chambers JP (1988) *Life Sci* 43:1379
187. Weber G, Teale FWJ (1958) *Trans Faraday Soc* 54:640

188. Murov SL, Carmichael I, Hug GL (1993) Handbook of photochemistry, 2nd edn. Marcel Dekker, New York
189. Drexhage KH (1990) In: Schäfer FP (ed) Dye lasers, 3rd edn. Springer, Berlin, p 155
190. Drexhage KH (1997) NBS Special Publication 466, Paper 80A3-894. Washington, DC
191. Roth NJL, Craig AC (1974) J Phys Chem 78:1154



# Long-Wavelength and Near-Infrared Fluorescence: State of the Art, Future Applications, and Standards

James N. Miller

Department of Chemistry, Loughborough University, Loughborough LE11 3TU, UK  
*J.N.Miller@lboro.ac.uk*

1	Introduction . . . . .	147
2	Long-Wavelength Fluorophores . . . . .	150
3	Tandem Long-Wavelength Fluorophores . . . . .	153
4	Long-Wavelength Fluorescence Instrumentation . . . . .	154
5	Selected Applications . . . . .	156
6	Long-Wavelength Standards . . . . .	158
7	Conclusions . . . . .	160
	References . . . . .	161

**Abstract** Near-infrared fluorescence (i.e. at wavelengths above 600 nm) provides many advantages over conventional measurements at shorter wavelengths. This chapter highlights the availability of simple and robust solid-state instrumentation and the great reduction in unwanted background fluorescence and scattered light signals. A wide range of long-wavelength fluorophores suitable as labels and probes are available. Some are naturally occurring proteins, while others are newly synthesised organic molecules, many of them commercially available: tandem fluorophores, providing larger Stokes shifts, may also be valuable. Examples of instrument systems using laser or light-emitting diode light sources and photodiode and other detectors are provided. Some example applications are summarised, and the need for further high-quality fluorescence standards in the long-wavelength region is highlighted. Particularly important are new standards for the correction of emission spectra at >700 nm, and lifetime standards.

**Keywords** DNA sequencing · Fluorescence standards · Immunoassays · Instrumentation · Lifetime assays · pH sensing · Western blotting

## 1 Introduction

One of the most striking features of the rapid development of fluorescence spectrometry in recent years has been the increased use of the long-wavelength visible and near-infrared (NIR) regions of the spectrum [1].

In this chapter we define such studies as those with emission wavelengths above ca. 600 nm: in practice the upper wavelength limit is generally about 900 nm, as significant solvent interference may occur at higher wavelengths (see below). This spectral range includes the red end of the visible spectrum and the shorter-wavelength end of the NIR region, so research papers sometimes use the terms “long wavelength” and NIR interchangeably for molecules emitting above ca. 750 nm. A significant impetus for the use of the 600–900-nm region in fluorescence studies has been the availability of simple, stable, long-lived, and low-cost solid-state light sources and detectors with properties very well matched to the requirements of this area of spectroscopy. While such devices, especially diode laser and high brightness light-emitting diode (LED) sources, are also now widely available in the wavelength region below 600 nm, their contribution to the development of long-wavelength fluorescence has been crucial. They have encouraged the development of a wide range of compact and robust single- or multi-wavelength instruments with many applications. Several other advantages of working in the long-wavelength region may conveniently be summarised here:

- Relatively few organic compounds have significant fluorescence emission in this region. The practical effect of this is that, while several groups of synthetic fluorophores are available for use as labels and probes, the background auto-fluorescence from naturally occurring samples such as blood plasma is much smaller than it is at lower wavelengths. Very low limits of detection are thus available in quite simple detection devices.
- Background signals from solvent Rayleigh and Raman scattering are very much reduced at longer wavelengths. The well-known inverse-fourth-power law means that, for example, the intensity of scattering from a given sample excited at 650 nm is only ca. 8.5% of the intensity scattered at 350 nm. Moreover, solvent Raman shifts in the long-wavelength region are so large in wavelength terms that interference from Raman scattering is usually negligible. The principal water Raman band at ca.  $3400\text{ cm}^{-1}$  often causes interference in the UV and visible regions (e.g. with excitation at 400 nm, the water Raman band is at ca. 463 nm), but with an excitation wavelength of 650 nm, the water Raman scattering occurs at ca. 834 nm, a Stokes shift much greater than that of most fluorophores. The same advantage is rightly claimed by Raman spectroscopists working in this region: their Raman signals suffer from little fluorescence interference!
- Absorption of incident light by the solvent is generally negligible. Overtones and harmonics of the main mid-infrared absorption modes can occur, but are mainly confined to wavelengths above ca. 900–1000 nm. The background fluorescence from the solvent, and from cuvettes and storage containers, which often causes problems in UV and visible region fluorescence studies, is also minimal.

- The use of longer excitation wavelengths is expected to minimise photodecomposition effects.

At the same time, some possible disadvantages of working at long wavelengths must be recognised. These all relate to the fact that the fluorophores used as labels or probes are, as is to be expected, very large organic molecules with extended delocalised  $\pi$ -orbital systems. The consequences of this are that:

- The fluorophores may show limited solubility and/or a tendency to aggregate, especially in water and other polar solvents. Even if the solubility problems are addressed, e.g. by the incorporation of sulphonic acid or other polar substituent groups or by the use of mixed aqueous–organic solvents,  $\pi$ -orbital system interactions can still occur if two or more fluorophore groups are incorporated into the same labelled molecule. Such effects may cause wavelength shifts and intensity changes.
- Almost all the established groups of long-wavelength fluorophores have very small Stokes shifts (emission–excitation wavelength differences), in some cases only about 10 nm. If laser excitation is combined with the use of efficient cut-off filters in the emission beam, this effect may not cause serious difficulties, but if a broader-band light source such as an LED is used there may be a significant scattered light background signal, despite the lower intensities of scattering in this wavelength region (see above). A simple though clearly only partly satisfactory solution is to use sub-optimal excitation and/or emission wavelengths to minimise scattered light problems. Fluorophores based on metal complexes (lanthanides, Ru, Os, Re etc.) do not suffer this disadvantage, and can in any case be studied using time-resolved methods which minimise background signals.
- As expected from established theory [2], longer-wavelength organic fluorophores tend to have rather shorter fluorescence lifetimes than UV–visible emitters. The result is that fluorescence phenomena which depend on changes or interactions of the molecule during its excited state lifetime are harder to detect. In particular, fluorescence polarisation measurements may be harder. Even with conventional UV–visible fluorophores, changes in polarisation resulting from altered rotational correlation times, e.g. when a labelled molecule binds to a large receptor such as an antibody, are relatively small. At longer wavelengths they are likely to be smaller still. Again, metal-chelate complexes may circumvent this problem, some of them having very long lifetimes and also high polarisation/anisotropy values.

Despite these problems long-wavelength fluorescence studies continue to develop, with the frequent synthesis of new fluorophore families and the development of new instruments. Applications to fields such as the health and environmental sciences indicate the need for good standards such as those already in use in UV–visible fluorescence measurements.

## 2 Long-Wavelength Fluorophores

The evident advantages of long-wavelength fluorescence measurements, coupled with the rapidly developing technologies that allow their full exploitation, have encouraged much research into the development of fluorophores suitable for use at wavelengths above 600 nm. As already noted, long-wavelength fluorescence measurements are mostly based on the use of synthetic molecules as probes and labels, naturally occurring long-wavelength fluorophores being relatively rare. Two exceptions to this generalisation are the phycobiliprotein allophycocyanin (APC), one of a family of proteins isolated from bacterial or algal sources, and the red fluorescent proteins (RFPs) derived from coral reef organisms. All the phycobiliproteins have very high molar absorbances ( $\epsilon$  values in the range 700 000–2.5 million have been reported) and high quantum yields. Their role in photosynthesis utilises their linked tetrapyrrole groups, and they have evolved so that energy losses by intra-molecular energy transfer and quenching by changes in their environment (pH, ionic strength etc.) are minimal. They are also highly water soluble, carry numerous surface groups useful for derivatisation, and are resistant to photodecomposition [3]. APC has an  $\epsilon$  value of ca. 700 000 and a quantum yield of ca. 0.7. Its excitation maximum is 650 nm, with a pronounced shoulder at ca. 630 nm, so it is well suited to excitation by a number of red lasers (see below): the Stokes shift is small, the emission maximum being at about 660 nm. The protein is available in a purified form, conjugated to various antibodies or to streptavidin, and is also used in tandem fluorescent conjugates (see below). A potential problem in the use of APC–protein conjugates is that the large APC molecule might give rise to steric interference with the functionality of the second protein. Smaller fluorescent proteins have been used for many years for live cell imaging and other applications. The first to be isolated was green fluorescent protein (GFP) from *Aequorea victoria*, but more recently the search for longer-wavelength analogues—RFPs—has led to the production of genes expressing a range of proteins emitting at wavelengths up to ca. 660 nm. These are often given names corresponding to red-coloured fruits (strawberry, plum, cherry etc.). Their potential value lies in the ease with which they are combined with fluorescence microscope systems, and the greater transparency of tissues at these wavelengths. However, they have been found to have some disadvantages, including a tendency to form oligomers, and significant toxicity. Recent studies have shown that quite brightly fluorescent monomeric red proteins can be produced [4], though their quantum yields are mostly less than that of GFP.

The remaining long-wavelength fluorescent labels and probes in common use are synthetic organic or organometallic compounds. Several major series of long-wavelength fluorophores have been made commercially available. Here we consider briefly some of the more commonly used materials and

their major properties. Most of these fluorophores are based either on carbocyanine dyes or on modified and extended xanthene dyes. The carbocyanines vary from tricarbocyanines to heptacarbocyanines, i.e. with a varying number of polymethine groups between the aromatic functions. As always, the various substituents in the aromatic ring systems have major effects on their fluorescence properties, as well as on their solubility and tendency to aggregate (see above). However, it should be noted that in several cases the full structures of the fluorophores have not yet been released by their originators.

The BODIPY® dyes (patented by Molecular Probes Inc.) have found many uses in fluorescence spectroscopy over more than a decade [5]. They are all based on the highly conjugated BODIPY nucleus, 4,4-difluoro-4-bora-3a,4a-diaza-*s*-indacene. A dozen labels from this family are available, but only three of them emit at long wavelengths. BODIPY-TR is designed to be similar in properties to Texas Red, sulphorhodamine 101, and has a slightly longer emission wavelength of ca. 618 nm. The other two long-wavelength BODIPY dyes, with closely similar substituent groups, are named simply by using their approximate excitation and emission wavelengths, i.e. BODIPY 630/650 and BODIPY 650/655. These fluorophores can clearly be excited with red diode lasers, He-Ne or Ar-Kr lasers, or possibly even bright red LEDs. For each of these dyes the Stokes shift is in practice about 15 nm—quite low, but not untypical at these wavelengths. They all have solvent-dependent lifetimes of 4–5 ns.

The Alexa Fluor series of dyes (also Molecular Probes Inc.) contains six members that are excited at wavelengths above 600 nm. These fluorophores, with suffixes 633, 647, 660, 680, 700 and 750 corresponding to their approximate excitation wavelengths, are available as succinimidyl esters and in most cases in the form of kits for labelling proteins, nucleotides and DNA. Alexa Fluor 633 is a sulphonated rhodamine dye, while the higher-wavelength members of the series are sulphonated carbocyanines. They have molar absorbance values of ca. 200 000. The excitation and emission spectra of the Alexa Fluor 647, 680 and 750 are similar to those of Cy5, Cy5.5 and Cy7, respectively. However, the Alexa Fluor dyes are claimed to have major advantages in terms of their photostability, lower tendency to aggregate, and most importantly their ability to produce more heavily labelled and more fluorescent protein conjugates without self-quenching or energy transfer phenomena occurring [5]. These advantages probably arise from the use of different substituents on the carbocyanine nucleus.

Another extensive group of commercially available dyes that includes several long-wavelength fluorophores are the Atto Dyes (Sigma-Aldrich). Almost 20 of these materials have been made available, again named by a number that approximates to their excitation wavelengths. About half of the dyes have excitation wavelengths above 600 nm. Of these fluorophores, those excited at lower wavelengths are probably extended or modified rhodamine or phenoxazine derivatives [6]. Most of the long-wavelength dyes

have  $\epsilon$  values of ca. 120 000 and modest Stokes shifts of 20–25 nm. Their quantum yields and lifetimes tend to fall as the excitation wavelength increases, but they are very photostable, and it is claimed that their rigidity and the absence of the *cis-trans* isomerisation, as found in some of the carbocyanine-based dyes, contribute to this advantage. They are generally available as *N*-hydroxysuccinimide (NHS) or maleimide derivatives, allowing labelling of a range of peptides, proteins and amino-oligonucleotides.

A very large group of dyes (“DY nnn” where nnn is the approximate excitation wavelength) is available from Dyomics GmbH. The range includes 13 dyes classified as “red”, i.e. with excitation wavelength >600 nm, six “far red” dyes (excitation above 675 nm) and no fewer than 14 dyes excited at wavelengths from 700 to as high as 840 nm. Most of these dyes are available in the form of NHS or maleimide labels, as well as carboxylic acid and amino derivatives. Unusually the full structures, based on benzopyrylium groups with a great range of substituents and additional conjugated groups, are readily available for all the dyes [7]. Although chemically very different from some other groups of dyes, these molecules seem to share the properties of very modest Stokes shifts, substantial  $\epsilon$  values of 100 000–200 000, and short (ca. 1 ns) lifetimes. However, the same company also markets a smaller number of “mega-Stokes” dyes, which are heavily substituted coumarins emitting at wavelengths up to about 660 nm. Their molar absorbance values are about 50 000 L mol<sup>-1</sup> cm<sup>-1</sup>, and published applications are relatively few thus far. Some pyridinium substituted cyanines also show larger Stokes shifts, but in general the use of dyes with small Stokes shifts seems to have been both common and acceptable up to now.

In the area of gene technology the long-wavelength fluorescent labels offered by Li-Cor Biosciences are well established, and are often used with the dedicated instrumentation summarised below. These labels are excited at ca. 689 and 774 nm in water with  $\epsilon$  values of ~165 000 and 240 000, respectively, so are well suited to excitation with widely available diode lasers. (In methanol the excitation wavelengths are slightly different, and the  $\epsilon$  values significantly higher.) They have lifetimes of about 1.5 and 0.8 ns, respectively, so polarisation studies would be problematical, especially with the higher-wavelength dye. The Stokes shift in each case is extremely small ( $\leq 15$  nm). The excitation wavelengths of the two dyes are very well separated, so the use of “two-colour” assays for different targets is very feasible (though the term is completely inappropriate at these long wavelengths!) [8]. As well as the applications in the genomics area, the usual kits are available to expedite the labelling of peptides, antibodies and other proteins.

Yet another group of dyes of interest in the long-wavelength regions are the Puretime® dyes marketed by Assaymetrics. The products of this company are oriented towards fluorescence lifetime-based methods, and three of them have excitation and emission wavelengths in the red and NIR regions. Puretime® 5, 3 and 1 have excitation wavelengths of ca. 680, 652 and 658 nm,

respectively, and emission wavelengths of 722, 700 and 709 nm, respectively. These Stokes shifts are quite large compared with other long-wavelength dyes, and the lifetimes of 4.7, 2.8 and 1.2 ns are also usefully longer than those of many other far-red fluorophores. Excellent photostability is claimed [9], but the  $\epsilon$  values of ca. 75 000 are lower than those of other dyes in this region, and the dyes do not seem to have been functionalised thus far, being used for cell staining (they are membrane-permeable). Chemical structures are apparently not available.

In summary, there are clearly numerous long-wavelength organic fluorophores available for a variety of applications. A good deal of ingenuity in synthetic chemistry has been applied to generate several series of potentially useful materials. But despite presumably substantial differences in chemical structure between the dye families, the practical outcomes are often fairly similar, especially in the genuine NIR region above ca. 700 nm. In many cases the dyes are characterised by small—sometimes extremely small—Stokes shifts and short lifetimes. These properties are the consequence of inescapable photochemical principles, and must affect the nature of the instruments used to measure the fluorescence of the dyes, and their applications. Lanthanide and other metal complexes, and their implementation using nanoparticles etc., offer substantially different properties. Complexes of europium and terbium (the lanthanides most commonly used), and of heavy metals such as ruthenium, osmium and rhenium, have found use in the development of immunoassays in particular—some examples are given below.

### 3 Tandem Long-Wavelength Fluorophores

A striking benefit of using long-wavelength labels, thus effectively extending the practical wavelength range of fluorescence spectrometry, is the possibility of tandem or multiple labelling of cellular and other targets. This is achieved using the well-known phenomenon of fluorescence resonance energy transfer (FRET), which permits the excitation of two or more fluorophores with just one primary energy absorber. Such systems can be elaborated using both soluble fluorophores and micro- or nanoparticles. One approach to tandem labelling in solution uses the phycobiliprotein R-phycoerythrin (R-PE) as the primary absorber and one or more fluorescent dyes as acceptors. R-PE, a 240 000 molecular weight protein with an  $\epsilon$  value of ca. two million and a fluorescence quantum yield of more than 0.8, has absorption bands at 565, 545 and 495 nm: although the last is the weakest of the three it is very well matched to the Ar<sup>+</sup> laser line at 488 nm. The relatively narrow emission spectrum of R-PE is centred at ca. 580 nm. If the protein is labelled with a fluorophore, the excitation spectrum of which overlaps the R-PE emission

spectrum, FRET can take place from the R-PE to the bound fluorophore. If the degree of labelling of the latter is carefully controlled a large proportion of the observed fluorescence will come from this acceptor molecule. A number of different acceptor dyes, including sulphorhodamine 101 and some Cy and Alexa Fluor dyes, have been used in tandem with R-PC, so multi-colour labelling and staining methods are available [10]. One elegant approach appropriate for flow cytometric studies involves coupling the R-PE tandem dye with avidin or streptavidin, and using the conjugates to bind to biotinylated antibodies of the desired specificity for cell surface markers [11]. Allophycocyanin (APC, see above) can also be used as the energy transfer donor: its higher excitation and emission wavelengths allow the use of long-wavelength acceptors such as Cy7 or Alexa Fluor 750 [12]. In all these cases the potential for multi-colour studies is clearly important, and there is the further bonus that the effect of the FRET is to produce a much larger Stokes shift, thus minimising scattered light problems in filter-based instruments.

The tandem labelling approach has been extended to the production of fluorescent polystyrene microspheres 1  $\mu\text{m}$  in diameter or less. (The smallest particles are not much larger than quantum dots.) The micrometre-sized particles are designed for use in flow cytometers or confocal microscopes that use laser excitation. They contain energy donors suitable for excitation by argon-ion or green or red He–Ne lasers and a range of acceptor fluorophores, again providing large Stokes shifts and multi-colour capacity. Conventional carbodiimide methods are used to conjugate antibodies and other bioactive molecules to carboxylic acid groups on the particle surfaces. These and other tandem labelling technologies, already well established for cell characterisation, seem likely to have many other applications [5].

## 4

### Long-Wavelength Fluorescence Instrumentation

It is entirely possible to carry out long-wavelength and NIR fluorescence measurements using a conventional fluorescence spectrometer fitted with a xenon light source, excitation and emission monochromators and a photomultiplier as a detector. However, the photomultiplier must be a “red-sensitive” one, giving a reasonable response up to wavelengths of ca. 800 nm. Most manufacturers of fluorescence detectors provide such facilities and some modern instruments of this type are fitted with adaptors so that a laser source can be used instead of the broad-band xenon lamp, the excitation monochromator then being redundant. Two laser sources useful for exciting red fluorescence are the He–Ne laser (output at 633 nm) and the  $\text{Kr}^+$  laser (647 nm). Low-power He–Ne lasers are available at a cost similar to that of diode lasers (see below), but they tend to be larger and heavier than solid-state lasers and their output power may drift rather more over periods of



hours. In many instances equipment capable of excellent analytical sensitivity, combined with small size, simplicity and low cost, can be constructed from solid-state components. Fluorescence plate-readers, microscopes, both confocal and conventional, and flow cytometry devices are all very readily used in the long-wavelength region.

In most cases diode lasers provide ideal light sources for long-wavelength work [13]. They are currently available at a large number of wavelengths, though most commercially available units emit in the ranges 630–690 nm or above ca. 780 nm. Power outputs range from a few milliwatts to several watts, but in practice the lower powered lasers, which minimise the necessary safety precautions, are sufficient for many purposes. Such sources are available for only a few tens of euros, yet have a useful life of 10 000–100 000 hours (i.e. in practice they might last longer than the working careers of many researchers!). Their output is extremely stable, with intensity fluctuations as low as ca. 0.2%, so for most purposes the use of a reference detector to monitor source intensity changes is not necessary. The bandwidth emitted is a small fraction of a nanometre, with obvious advantages in terms of minimising scattered light signals and ensuring that all the emitted photons are available for absorption by the selected fluorophore. The emitted wavelength is temperature dependent, but usually the shifts observed are small (ca. 0.25 nm °C<sup>-1</sup>) compared with the width of the fluorophore absorption band. A power supply delivering only a few volts is sufficient, so low-powered lasers can be powered by a battery pack, an important advantage for portable instruments. Pulsing and/or modulation of the lasers are straightforward, and such facilities are often provided by manufacturers' power supplies, so pulsed-source or phase-resolved lifetime methods can readily be used. Very wide ranges of beam shapes and divergences, and laser/fibre optic interfaces, are available. Systems using two or more lasers to excite multiple fluorophores are very feasible: the emitted fluorescence signals can be differentiated by pulsing or modulating the lasers at different frequencies, or simply by the selection of appropriate filters in the emission beam(s).

Successful fluorescence instruments, including commercially available ones, have been developed using high-brightness LEDs as light sources. Most important in the present context are the red LEDs that emit at about 640 nm. Their spectral output has a typical width (at half-maximum intensity) of ca. 20 nm, so there may be a few instances in which they are more suitable than diode lasers for exciting two or more fluorophores simultaneously. On the other hand, they are more likely to need monochromators or (much more commonly) filters to minimise scattered light interferences.

High-quality filters often comprise a crucial part of the emission beam in the instrumental setup, and both narrow-band interference filters and notch filters, cut-off filters with steep gradients in their characteristic curves, can be used as alternatives or in combination. Such devices are available over the wavelength interval of interest, and polarisers are also readily obtainable.

Solid-state (silicon) detectors are used most commonly in the long-wavelength region, their sensitivity characteristics being excellent at 700–900 nm. In particular, avalanche photodiodes have been used frequently [14], though miniaturised photomultiplier tubes are also suitable, especially in the wavelength region up to ca. 700 nm.

Amongst many papers describing the design and construction of purpose-built instruments, the following are a few examples. A simple instrument using diode laser sources, emission beam cut-off filters and a silicon detector was described by Hu et al. [15]. The light source had a pulsed 5-V power supply, the pulse frequency generator providing five options. The detector had a rise time of less than 50 ns and a surface area of 100 mm<sup>2</sup>. This instrument was suitable for the detection of picomolar levels of cyanine dyes in both conventional cuvettes and in a flow cell for use in flow-injection analysis. Thrush et al. [16] described a miniaturised and integrated fluorescence detection system with laser excitation, emission filters and PIN photodetectors, designed for use with micro-fluidic devices: the detection area was only 10<sup>4</sup> μm<sup>2</sup>. A single photon counting system was described that utilised a 780-nm diode laser source, pulsed at 80 Hz with a pulse width of 150 ps. An integrated microscope and large-area avalanche photodiode were used to detect fluorescence: the overall response time of the instrument allowed lifetimes of 500 ps and above to be measured, and nanomolar detection limits were achieved [17]. A laser-based instrument designed as a detector for near-IR solid-phase immunoassays was described [18]. A commercially available instrument (“Odyssey”, LiCor® Biosciences) incorporates two long-wavelength diode lasers and is suitable for (amongst many applications) the detection of DNA and protein arrays, the spatial resolution being under operator control. The same company provides a DNA sequencer using a long-wavelength nucleotide terminator.

## 5 Selected Applications

As already noted, the dearth of naturally occurring long-wavelength fluorophores means that virtually all the applications of fluorescence spectrometry in this region are based on the use of synthetic labels, probes or enzyme substrates. The range of published applications is enormous and growing rapidly: in general it is probably fair to claim that most applications of UV-visible fluorescence can be transferred, as it were, to the long-wavelength region, frequently with the many advantages summarised above. Here it is possible to describe only a minute selection of the areas, most of them inevitably in the areas of biomedical science, in which long-wavelength measurements have been used in practice.

A simple example of the advantages of using long-wavelength fluorophores is provided by the development of dye-binding methods for the determination of serum albumin. Several new probes for this purpose, excited by He–Ne or red diode lasers and yielding large fluorescence enhancements, have been described [19]. Detection limits are below  $1 \text{ mg L}^{-1}$  and the method has been extended to studies of albuminuria [20]. The fluorescence signal varies from one species to another, but there is virtually no interference arising from dye binding by other proteins, or from other serum or urine components. Analogous assays using shorter-wavelength fluorophores are much more likely to suffer from such problems. Bovine serum albumin has been determined using the fluorescence enhancement of Nile Blue [21], and the principle has been extended to the analysis of the total protein content of serum using a cyanine dye in the presence of the detergent CTAB [22]. Protein determination using Western blotting has been shown to be facilitated using antibodies labelled with long-wavelength fluorophores. The combination of Alexa Fluor 680 and IRDye 800 seems to be popular for “two colour” applications [23], and has been used in protein micro-array studies [24]. Sensitivity, linearity and reproducibility are all claimed to be superior to the use of lower-wavelength dyes, and to chemiluminescence methods. Long-wavelength dyes have also been used in conjunction with DNA dendrimers (also applied in fluorescence in situ hybridisation) for the ultra-sensitive detection of protein micro-arrays [25].

An interesting and potentially powerful group of methods is based on the finding that tryptophan residues in proteins and peptides quench a number of different long-wavelength dyes from the groups described above. In many cases the quenching effect is due to photoinduced electron transfer (PET) and has a very short range (shorter than that involved in conventional FRET), possibly requiring contact between the two chromophores involved. Potential applications to the development of enzyme and other assays have been outlined [26]. Rather similar quenching interactions occur between rhodamine or oxazine dyes and guanosine residues in nucleotides. If a hairpin-shaped oligonucleotide has the quenched dye group attached at its 5' terminus and then undergoes a conformational change on binding to a complementary sequence, the quenching effect is reduced and an enhanced fluorescence signal is seen. This method of monitoring hybridisation may be superior to a conventional molecular beacon requiring two extrinsic probes, a fluorescent donor and a “dark” acceptor [27].

Many papers describe the development and use of long-wavelength fluorescence immunoassays: most of the assay types originally developed for use in the UV–visible regions are replicated at longer wavelengths. For example, an intrinsically simple assay for prostate-specific antigen (PSA) based on the sandwich principle and utilising microtitre plates was adapted to use europium chelate nanoparticles about 100 nm in diameter and coated with antibodies as the label. The limit of detection of the assay was as low as

$0.04 \text{ ng L}^{-1}$  (fewer than  $10^6$  molecules  $\text{mL}^{-1}$ ), and was set by the non-specific binding of the antibody-labelled fluorescent particles to the microtitre plate surface [28]. Solid-phase assays using long-wavelength cyanine dyes without lifetime discrimination have also been described [29,30], and a fibre-optic based biosensor for sandwich assays was developed using Alexa Fluor 647 as the laser excited label [31]. Mathis has devoted much research to lanthanide cryptate complexes, and has shown how they can be used as donors in an energy transfer immunoassay, with allophycocyanin as the acceptor [32]. Rather more conventional long-wavelength labels have also been used in energy transfer assays: good spectral overlap makes Cy5 and Cy5.5 a good pair of donor and acceptor dyes, with a Förster distance (i.e. the distance at which donor-acceptor transfer is 50% efficient) of over 8 nm [33]. Fluorescence polarisation immunoassays have been developed to utilise the long lifetimes of heavy metal chelate complexes. An osmium complex with a lifetime of 19 ns could be excited at wavelengths of ca. 700 nm and was used in a simple assay for human serum albumin [34]. A rhenium(I) complex with a lifetime of over  $1 \mu\text{s}$  was used in a similar assay and it was shown that in principle such labels could be used in polarisation immunoassays for molecules with molecular weights up to 100 million. This opens up a new field of application, as analogous assays using conventional fluorophores can normally be used only for low molecular weight analytes [35]. An extremely promising recent development has been the use of fluorescence up-conversion methodology, most commonly used for the study of very short emission lifetimes, as the basis of an energy transfer immunoassay. Using continuous laser diode excitation at 980 nm with an up-converting phosphor as the energy transfer donor, emission of the acceptor at 600 nm has been measured in a sub-nanomolar assay for oestradiol. The up-conversion approach avoids many of the problems of other homogeneous (separation-free) assays, and opens up the possibility of measurements on problematic samples such as whole blood [36].

Fluorescence methods have been used for 20 years or more in the field of DNA sequencing, providing sensitive detection methods for gel electrophoresis and more recently capillary electrophoresis separations. A variety of approaches are available using one, two or four fluorophores and one or more light sources, but it is evident that laser excitation of long-wavelength fluorophores provides ample opportunities [37,38]. Similarly, applications abound in areas such DNA arrays, fluorescence in situ hybridisation (FISH) and other areas related to nucleotide chemistry.

## 6 Long-Wavelength Standards

In the UV-visible region of the spectrum fluorescence standards are required for a range of tasks. These include the calibration of grating monochromators

by means of wavelength standards; quantum counters to allow the correction of excitation spectra; standard light sources for the correction of emission spectra with the aid of an efficient reflecting material in the sample position; fluorophores with agreed corrected emission spectra to permit the direct correction of other emission spectra by comparison; quantum yield standards; and lifetime standards [39]. In principle there is a need for similar standards for use in the long-wavelength and NIR regions, so that the photochemical properties of existing and new fluorophores can be fully characterised, even though routine measurements made in these regions often dispense with any form of spectral discrimination.

On occasion the standardisation methods used in the UV-visible region can be extended to longer wavelengths very readily. For example, monochromator wavelength scales can be calibrated well into the long-wavelength region by the use of fluorescent lanthanide ions, usually provided in the form of glassy polymer matrices. The emission spectra of these ions are extremely narrow so their peak wavelengths are not significantly affected by spectral correction effects. For the correction of emission spectra, calibrated dual source (deuterium and tungsten-halogen) lamps are available to cover the wavelength range 210–1050 nm. The reflectance standards used in conjunction with such lamps to characterise the emission beam optics (the grating monochromator plus the photomultiplier tube) of a scanning fluorescence spectrometer have a very flat reflectance across the whole long-wavelength and NIR region. Such systems can be used to provide emission spectrum correction factors for this region, but they are rather tedious to set up and use.

The modern approach to the correction of emission spectra is to use a series of standard fluorophores with agreed or certified spectra, which overlap substantially with each other to minimise the uncertainty of the correction over a wide spectral range. Comparison of the agreed spectra with the results obtained on any given instrument for these fluorophores allows the correction factors for that instrument to be calculated. These factors can then be used to correct the spectra of any other solutes obtained on the same instrument in the same optical conditions. Such methods can be applied routinely without the use of specialised equipment, but require the availability of sets of fluorophores with a range of critical properties, such as good chemical and photostability, featureless spectra, not too great an overlap between excitation and emission spectra, and negligible anisotropy. A set covering the emission spectrum range of 360–700 nm has been proposed, using quinine, fluorescein, rhodamine B and sulphorhodamine 101 [40]. The recommended quantum yield values for these four compounds are also given. In practice the emission spectrum of sulphorhodamine 101 is quite weak beyond ca. 670 nm (its emission intensity at 675 nm is <10% of the maximum intensity at ca. 595 nm): since many conventional instruments using grating monochromators and photomultiplier detectors show a substantial loss of sensitivity at wavelengths above 600 nm, it is probably best to limit the use of this

compound to the 570–670 nm region. Moreover, fluorescein and rhodamine have spectra with some fine structure, substantial excitation–emission overlap and are not very photostable. A different set of five fluorophores has recently become available, the longest wavelength member of which emits at ca. 635 nm [41]. The certified emission spectrum of this dye extends to about 730 nm, but the uncertainty of the resulting correction curve deteriorates sharply above about 700 nm, and this wavelength is perhaps a safer upper limit for accurate correction. A welcome feature of this set of fluorophores is the provision of software which effectively calculates and links the correction factors obtained from each of the five dyes to provide a continuous correction curve across a wide wavelength range. This facility should greatly ease the burdens of determining corrected emission spectra up to ca. 700 nm. Moreover, an analogous set of dyes is available for excitation spectral correction, the longest excitation wavelength accessible being ca. 600 nm. However, quite a number of fluorophores in regular modern use emit at wavelengths well above 700 nm (see above), and may well be studied using instruments with monochromators and photomultiplier or avalanche photodiode detectors, so there is some need for an extension of the spectral correction factors still further into the far-red and NIR regions.

Reliable fluorescence lifetime standards [42] have not been well established in any part of the UV–visible–NIR range, and this is especially true for long-wavelength fluorophores. Such standards are more urgently needed now that lifetime-based assays are coming into routine use. The lifetimes of some long-wavelength dyes are known (though often only in a single set of solvent conditions). Of the dyes mentioned in previous sections, ATTO 655, Alexa Fluor 633, Alexa Fluor 647, Alexa Fluor 680, Cy5 and Cy5.5 have lifetimes of 3.6, 3.2, 1.0, 1.2, 1.0 and 1.0 ns, respectively.

Since plate readers represent one of the commonest fluorescence measurement formats, the availability (Matech) of some intensity reference standards is valuable. These contain inorganic phosphors and are suitable for top-reading 96- and 384-well plates and bottom-reading 96-well plates. The longest wavelength available at present seems to be 613 nm.

## 7

### Conclusions

Measurements in the long-wavelength and NIR regions provide a range of new and promising measurement methods which retain the intrinsic sensitivity and selectivity of fluorescence spectroscopy, while offering simplified and possibly miniaturised instrumentation based on solid-state optical components. Almost all the applications of UV–visible fluorescence can be replicated advantageously with long-wavelength fluorophores, and it is quite evident that this area of fluorescence studies will continue to expand rapidly.

## References

1. Miller JN, Brown MB, Seare NJ, Summerfield S (1993) In: Wolfbeis OS (ed) *Fluorescence spectroscopy: new methods and applications*. Springer, Berlin, p 189
2. Lakowicz J (2006) *Principles of fluorescence spectroscopy*, 3rd edn. Springer, New York
3. Glazer AN (1994) *J Appl Phycol* 6:105
4. Fischer M, Haase I, Simmeth E, Gerisch G, Muller-Taubenberger A (2004) *FEBS Lett* 577:227
5. Haugland RP (2002) *Handbook of fluorescence probes and research products*, 9th edn. Molecular Probes, Eugene
6. Neumann M, Herten DP, Sauer M (2001) In: Valeur B, Brochon JC (eds) *New trends in fluorescence spectroscopy: applications to chemical and life sciences*. Springer, Berlin
7. Czerney P, Lehmann F, Wenzel M, Buschmann V, Dietrich A, Mohr GJ (2001) *Biol Chem* 382:495
8. McWhorter S, Soper SA (2000) *Electrophoresis* 21:1267
9. <http://www.assaymetrics.com>. Accessed December 2006
10. Glazer AN, Stryer L (1983) *Biophys J* 43:383
11. POugnard C, Catala P, Drocourt J-L, Legastelois S, Pernin P, Pringuez E, Lebaron P (2002) *Appl Environ Microbiol* 68:3102
12. Beavis AJ, Pennline KJ (1996) *Cytometry* 24:390
13. Nagaraj S, Karnes HT (2000) *Biomed Chromatogr* 14:234
14. Legendre BL Jr, Moberg DL, Williams DC, Soper SA (1997) *J Chromatogr A* 779:185
15. Hu SJ, French MT, Palmer DA, Evans M, Zhou SM, Sarpara GH, Miller JN (2002) *Anal Chim Acta* 454:31
16. Thrush E, Levi O, Ha W, Wang K, Smith SJ, Harris JS Jr (2003) *J Chromatogr A* 1013:103
17. Zhang Y, Soper SA, Middendorf LR, Wrump JA, Erdmann R, Wahl M (1999) *Proc SPIE* 3602:403
18. Silzel JW, Cercek B, Dodson C, Tsay T, Obremski RJ (1998) *Clin Chem* 44:2036
19. Kessler MA, Wolfbeis OS (1992) *Anal Biochem* 200:254
20. Kessler MA, Meinitzer A, Petek W, Wolfbeis OS (1997) *Clin Chem* 43:996
21. Lee SH, Suh JK, Li M (2003) *Bull Korean Chem Soc* 24:45
22. Zheng H, Zhu CQ, Li DH, Chen QY, Yang HH, Chen XL, Xu JG (2000) *Fresenius J Anal Chem* 368:511
23. Schutz-Geschwender A, Zhang Y, Holt T, McDermitt D, Olive DM (2004) *LiCor® Biosciences*. [www.licor.com](http://www.licor.com). Accessed 10.04.2008
24. Calvert VS, Tang Y, Boveia V, Wulfkuhle J, Schutz-Geschwender G, Zhang Y, Holt T, Olive DM, Litoa LA, Petricoin EF III (2004) *Clin Proteomics* 1:181
25. Stears RL, Getts RC, Gullans SR (2000) *Physiol Genomics* 3:93
26. Marmé N, Knemeyer J-P, Sauer M, Wolfrum J (2003) *Bioconjug Chem* 14:1133
27. Heinlein T, Knemeyer J-P, Piestert O, Sauer M (2003) *J Phys Chem B* 107:7957
28. Soukka T, Paukunnen J, Härmä H, Lönnberg S, Lindroos H, Lövgren T (2001) *Clin Chem* 47:1269
29. Williams RJ, Narayanan N, Casay GA, Lipowska M, Strekowski L, Patonay G, Peralta JM, Tsang VCW (1994) *Anal Chem* 66:3102
30. Williams RJ, Peralta JM, Tsang VCW, Narayanan N, Casay GA, Lipowska M, Strekowski L, Patonay G (1997) *Appl Spectrosc* 51:836
31. Anderson GP, Nerurkar NL (2002) *J Immunol Methods* 271:17

32. Mathis G (1993) *Clin Chem* 39:1953
33. Schobel U, Egelhaaf H-J, Brecht A, Oelkrug D, Gauglitz G (1999) *Bioconjug Chem* 10:1107
34. Terpetschnig E, Szmecinski H, Lakowicz JR (1996) *Anal Biochem* 240:54
35. Guo X-Q, Castellano FN, Li L, Lakowicz JR (1998) *Anal Chem* 70:632
36. Kuningas K, Ukonaho T, Pääkkilä H, Rantanen T, Rosenberg R, Lövgren T, Soukka T (2006) *Anal Chem* 78:4690
37. Williams DC, Soper SA (1995) *Anal Chem* 67:3427
38. Woolley AT, Mathies RA (1995) *Anal Chem* 67:3676
39. Miller JN (ed) (1981) *Standards in fluorescence spectrometry*. Chapman and Hall, London
40. Velapoldi R, Tonnesen HH (2004) *J Fluoresc* 14:465
41. Resch-Genger U, Pfeifer D, Monte C, Pilz W, Hoffmann A, Spieles M, Rurack K, Hollandt J, Taubert D, Schönenberger B, Nording P (2005) *J Fluoresc* 15:315
42. Chen RF (1974) *Anal Biochem* 57:593



# Surface Fluorescence: the Only Standardized Method of Measuring Luminescence

Joanne Zwinkels

National Research Council, 1200 Montreal Road, Ottawa, Ontario, K1A 0R6, Canada  
*Joanne.Zwinkels@nrc-cnrc.gc.ca*

1	Introduction and Color Measurement Concepts . . . . .	164
2	Measurement of Surface Fluorescent Colors . . . . .	171
3	Standardization of Fluorescent Color . . . . .	172
3.1	Historical Background . . . . .	172
3.2	One-Monochromator Method . . . . .	176
3.3	Two-Monochromator Method . . . . .	177
3.3.1	Instrumentation for Two-Monochromator Method . . . . .	180
4	Standard Procedures for Surface Fluorescence Measurements . . . . .	181
4.1	Standard Spectrophotometric Procedures . . . . .	181
4.1.1	Standard Geometric Conditions . . . . .	182
4.1.2	Standard Polarization Conditions . . . . .	183
4.1.3	Standard Radiometric Calibration Procedures . . . . .	183
4.1.4	Spectral Irradiance of the Excitation Unit . . . . .	184
4.1.5	Spectral Responsivity of the Emission Unit . . . . .	186
4.1.6	Determination of Reflected Radiance Factor . . . . .	187
4.1.7	Determination of Bispectral Luminescent Radiance Factor . . . . .	187
4.2	Uncertainties . . . . .	189
5	Conclusions . . . . .	190
	References . . . . .	190

**Abstract** The measurement of surface fluorescence is used to determine the color properties of a wide variety of materials containing fluorescent dyes and colorants, to enhance their apparent whiteness or colorfulness. The accurate evaluation of these colorimetric properties is important to quality control and color specification of a number of products, such as fluorescence-whitened paper, textiles and plastics, and fluorescent safety goods. The increasing importance of these industrial applications and the increasing use of fluorescent dyes and colorants due to their improved performance, has motivated the development of standard methods for precisely and accurately measuring surface fluorescence. The historical background of these standardization efforts is briefly described here, beginning with the important contributions of Donaldson in 1954. Since then, several standardizing organizations, including the Commission Internationale de l'Éclairage (CIE) and American Society of Testing and Materials (ASTM), have documented recommendations and standard methods for calibrating instrumentation for the measurement of fluorescent materials. This paper describes the current status of the standardization of surface fluorescence measurements for colorimetric applications, with emphasis on the two-monochromator method.

**Keywords** Colorimetry · Photoluminescence · Reflection spectrophotometry · Spectrofluorimetry metrology · Surface fluorescence · Two-monochromator method

### Abbreviations

ASTM	American Society of Testing and Materials
BAM	Federal Institute for Materials Research and Testing, Berlin
CIE	Commission Internationale de l'Eclairage
FWA	Fluorescent whitening agent
ISO	International Standards Organization
M/P mode	Monochromatic illumination, polychromatic detection
M/M mode	Monochromatic illumination, monochromatic detection (two-monochromator method)
NMI	National Measurement Institute
NPL	National Physical Laboratory, UK
NRC	National Research Council, Canada
P/M mode	Polychromatic illumination, monochromatic detection
TC	Technical committee
TKK	Metrology Research Institute, Helsinki University of Technology
$\beta_i$	Radiance factor ( $i = T, L, R$ , or $std$ for total, luminescent, reflected, or standard, respectively)
$\beta_{L\lambda}$	Bispectral luminescent radiance factor
CCD	Charge-coupled device
$d\Omega$	Solid angle
$D(\mu, \lambda)$	Donaldson matrix of radiance data for excitation at wavelength $\mu$ and emission at wavelength $\lambda$
$E_i(\lambda)$	Spectral irradiance distribution ( $i = s$ or $ref$ for sample or reference, respectively)
$I(\lambda)$	Analyzing detector signal
$I_{mon}(\mu)$	Monitor detector signal
$K$	Coverage factor (for calculating expanded uncertainty)
$L_\lambda(\lambda)$	Spectral radiance
$\mu(\lambda)$	Spectral quantum efficiency
$p$ -polarized	Polarized parallel to the plane of incidence
PRD	Perfect reflecting diffuser
$P(\lambda)$	Spectral radiant flux
$R(\lambda)$	Spectral reflectance factor
$R_{sys}(\lambda)$	Relative spectral responsivity of detection system
$s$ -polarized	Polarized perpendicular to the plane of incidence
$S(\lambda)$	Relative spectral power distribution
$T(\lambda)$	Spectral transmittance

## 1

### Introduction and Color Measurement Concepts

A discussion of standard methods for measuring surface fluorescence requires a brief introduction to the basic principles and concepts of color measurements since this field of metrology, known as colorimetry, spurred

the development of standard procedures to deal with the special problems of fluorescence.

The physical stimulus that evokes the sensation of color from an object is the combined subjective effect of three essential ingredients: the source of light, the object, and the observer. If any one of these ingredients changes, the color appearance changes. The perceived color also depends upon the geometry of illumination and viewing and on the angular subtense of the viewed area. To enable unambiguous specification of object color, it is necessary to standardize these influencing conditions.

In the early twentieth century, there was a great deal of research activity on quantifying these influencing parameters and defining an acceptable method of objectively measuring and communicating color [1]. This research laid the foundation for modern colorimetry. The development and documentation of these colorimetric standards and procedures was carried out by the Commission Internationale de l'Eclairage (CIE), the leading authority involved in the standardization of physical measurements of optical radiation, including color. CIE colorimetry continues to be the fundamental basis for the objective description of color and has been widely adopted as the normative reference for color measurement practices in test methods prepared by other standardizing bodies, including the American Society for Testing and Materials (ASTM) and the International Standards Organization (ISO). The CIE has established the following important colorimetric standards and methods of operation:

1. Two standard illuminants, standard illuminant A representing light from a tungsten lamp at a color temperature of 2856 K, and standard illuminant D65, which represents a phase of natural daylight with a color temperature of 6500 K, plus several other D illuminant conditions representing other phases of daylight and illuminant C, which is intended to represent an average daylight with a correlated color temperature of approximately 6800 K; in practice, illuminant C is often used as an approximation to an indoor daylight condition. Whereas a source is a physical entity, the CIE illuminants are a table of relative spectral power distributions,  $S(\lambda)$ . In the case of standard illuminant A and the D illuminants, the  $S(\lambda)$  is normalized to the value 100 (exactly) at the wavelength of 560 nm (exactly) [2, 3].
2. Two standard colorimetric observers for two different fields of view ( $2^\circ$ ,  $10^\circ$ ). The spectral tristimulus values for these two standard observers are designated  $\bar{x}(\lambda)$ ,  $\bar{y}(\lambda)$ ,  $\bar{z}(\lambda)$ , and  $\bar{x}_{10}(\lambda)$ ,  $\bar{y}_{10}(\lambda)$ ,  $\bar{z}_{10}(\lambda)$ , for the  $2^\circ$  and the  $10^\circ$  standard observers, respectively, and are defined in tabular form [2, 4].
3. Two standard illuminating and viewing geometries: diffuse/normal (d/0 or 0/d) or directional/normal (45/0 or 0/45), where the first term gives the direction of illumination and the second term gives the direction of viewing [2, 5].

4. Standard methods for calculating colorimetric quantities (tristimulus values,  $X$ ,  $Y$ , and  $Z$  and chromaticity coordinates,  $x$  and  $y$ ). Since the human eye only responds to optical radiation in the visible portion of the spectrum, the essential spectral range for calculating these colorimetric quantities is from 380 to 780 nm [2].

These three essential ingredients of the color stimulus for an opaque object and representative CIE standard conditions for the source and observer conditions for specifying its colorimetric properties are depicted in Fig. 1, where  $E_i(\lambda)$  is the spectral irradiance distribution. The product of the relative spectral distributions of the standard illuminant, the spectral properties of the material and the spectral sensitivity of the standard colorimetric ob-

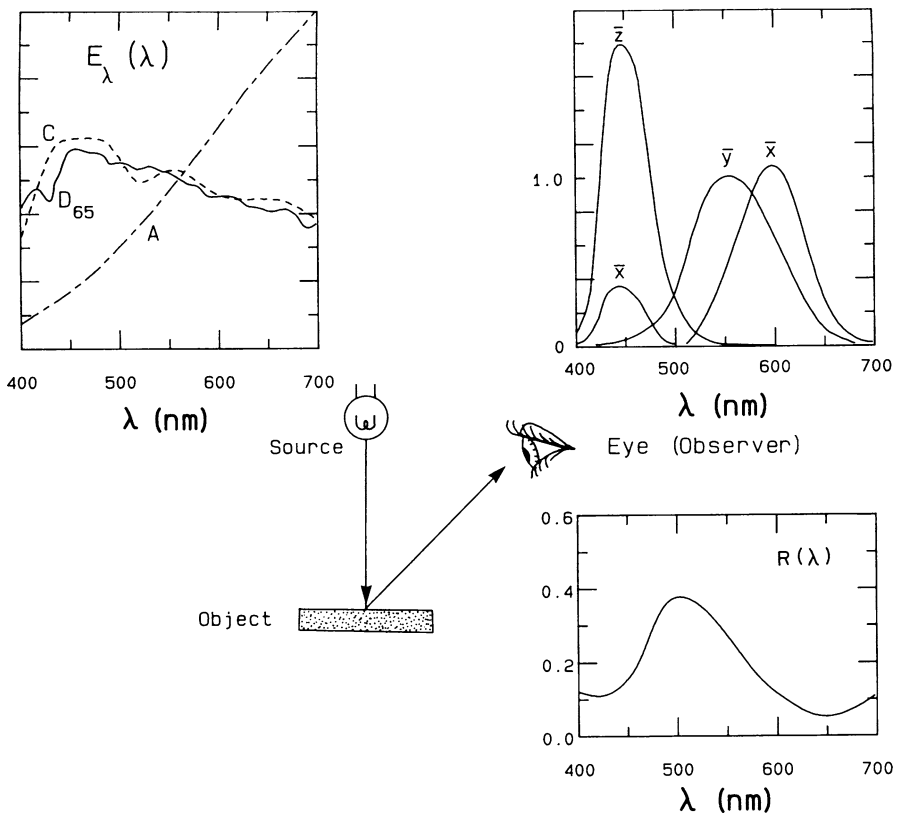


**Fig. 1** The three essential ingredients for an object color stimulus. The color stimulus is produced by the product of the relative spectral power distribution of the illuminating source,  $S(\lambda)$ , the spectral reflectance of the object,  $R(\lambda)$  and the trichromatic spectral sensitivity of the human observer,  $\bar{x}(\lambda)$ ,  $\bar{y}(\lambda)$ ,  $\bar{z}(\lambda)$ . Standardized spectral curves are shown for representative Commission Internationale de l'Éclairage (CIE) standard illuminants and colorimetric observer.

server now define unambiguously this CIE color stimulus. The only quantity that needs to be measured is the optical property of the object.

For an opaque nonfluorescent material, the predominant optical interaction is the reflection or forward scattering of the light, where the wavelength remains unchanged. The wavelength-selective reflection of the light by the object is the physical stimulus that produces the sensation of object color. In instrumental color measurements, at each wavelength  $\lambda$ , this reflected spectral radiance by the sample,  $L_{\lambda s}$ , is not measured directly but by reference to that of a white standard,  $L_{\lambda w}$ , where the subscripts s and w refer to the sample and white standard, respectively. This radiance factor,  $\beta$ , is defined as:

$$\beta(\lambda) = \frac{[L_{\lambda s}]}{[L_{\lambda w}]} \quad (1)$$

The CIE primary standard for reflection measurements is the perfect reflecting diffuser (PRD), which is defined as an ideal isotropic diffuser (Lambertian) with a reflectance of unity for all wavelengths and geometries and is assumed to be nonfluorescent. This ideal reflecting diffuser does not exist and, in practice, secondary white reflection standards, such as pressed tablets of barium sulfate or polytetrafluoroethylene powder are used, whose reflectance is known from absolute reflectance methods defined in CIE Publication No. 44 [6].

For the ideal PRD, the spectral radiance factor is independent of the direction of viewing. However, for most real reflecting and diffusing materials, this optical property is not intrinsic to the material and depends upon the measurement geometry. Thus, the more general description of the measured optical quantity of an opaque reflecting object is the spectral reflectance factor,  $R(\lambda)$ , which is the ratio of the spectral radiant flux,  $P(\lambda)$ , reflected by the specimen in the directions delimited by a cone of solid angle,  $d\Omega$  to that reflected in the same directions by the perfect reflecting diffuser identically irradiated. If the solid angle  $d\Omega$  approaches  $2\pi$  steradians (sr), the spectral reflectance factor approaches the spectral hemispherical reflectance,  $\rho(\lambda)$  and if  $d\Omega$  approaches 0 sr, the spectral reflectance factor approaches the spectral radiance factor,  $\beta(\lambda)$ .

Once the reflecting properties of the sample have been measured according to these CIE procedures, the color properties can be calculated using well-standardized methods. The standard colorimetric quantities of the CIE system are the CIE tristimulus values, X, Y and Z. For an opaque nonfluorescent material, these coordinates are calculated from the following equations:

$$X = k \int_{\lambda} R(\lambda)S(\lambda)\bar{x}(\lambda) d\lambda, \quad (2a)$$

$$Y = k \int_{\lambda} R(\lambda)S(\lambda)\bar{y}(\lambda) d\lambda, \quad (2b)$$

$$Z = k \int_{\lambda} R(\lambda)S(\lambda)\bar{z}(\lambda) d\lambda, \quad (2c)$$

where  $S(\lambda)$  is the relative spectral power distribution of the illuminant, and  $k$  is a normalization factor.

The CIE color coordinates,  $x$  and  $y$  of this object color on a CIE standard chromaticity diagram are given by:

$$x = \frac{X}{X + Y + Z}, \quad y = \frac{Y}{X + Y + Z}. \quad (2d)$$

The color properties of an object are completely specified by its three tristimulus values so that if two different objects have different spectral reflectance curves but identical CIE tristimulus values for given CIE standard illuminant/observer and geometric conditions, they will be perceived as matching in color. This colorimetric property is a commercially important basis of color reproduction technologies and colorant formulation. The CIE recommended standards and methods of operation for basic colorimetry have been published in fundamental CIE technical reports and standards [2–5]. More detailed accounts of CIE colorimetry concepts and applications can be found in the literature [7, 8]

A variety of instruments are available for color measurement and can be broadly classified as tristimulus colorimeters, spectroradiometers and spectrophotometers. Tristimulus colorimeters use a filtered light source and three or four filtered detectors whose modified spectral response approximates that of a particular CIE standard illuminant/observer combination. They give a direct measure of colorimetric quantities but provide no information on the underlying spectral data. A spectroradiometer is an instrument designed to measure radiometric quantities (irradiance, radiance) in a defined waveband as a function of wavelength. These instruments are used to measure the color of self-luminous colors. A spectrophotometer is designed to compare, at each wavelength, the radiant power leaving an object to that incident on it. These radiance power ratios are dimensionless quantities used for color measurement of object colors. [9]. The usual measured quantity is spectral transmittance,  $T(\lambda)$ , for transparent object colors (volume color) or spectral reflectance,  $R(\lambda)$ , for opaque object colors (surface color).

For the vast majority of colorimetric applications, the color specification is for a surface color, such as paint, plastic, paper and textile samples. High accuracy surface color measurements are required in several applications. These include analytical analysis in the pharmaceutical industry, color formulation, color specification and critical color quality control in the manufacture of colored goods. The incorporation of fluorescent dyes and colorants

in these materials produces fluorescent surface colors with apparent enhancement of their whiteness or colorfulness (saturation). They are widely used for applications requiring enhanced brightness of white materials, such as the manufacture of fluorescence-whitened papers, textiles and detergents, or those requiring improved visibility and conspicuity such as the production of safety and security goods. They are also used in the manufacture of fluorescent lamps, LEDs, TV screens and displays.

For the physical measurements of a nonfluorescent material to correlate with visual appearance evaluations, the spectral and geometric requirements for the measuring instrument are well documented in standard test methods and

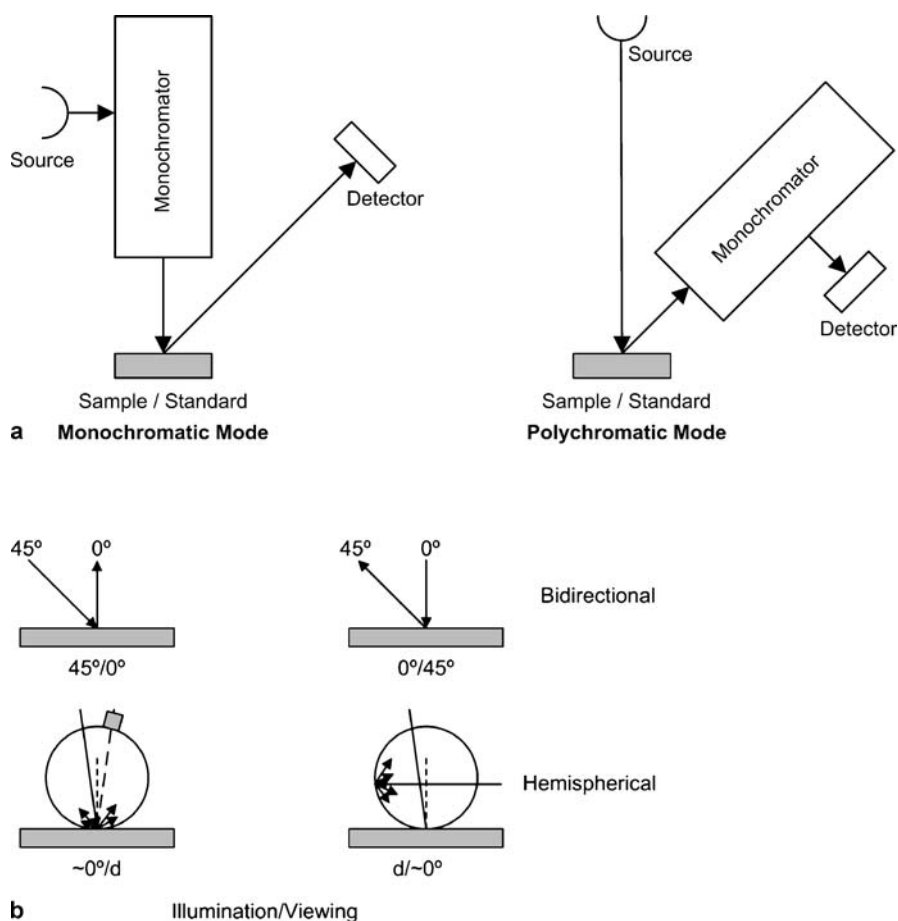


**Fig. 2** a Schematic representation of conventional spectrophotometer design configurations: monochromatic illumination/polychromatic viewing (M/P mode) and polychromatic illumination/monochromatic viewing (P/M mode). b CIE-recommended geometries of illumination and viewing for measurement of surface color

CIE publications [2, 10]. The instrumental arrangement can be monochromatic illumination, polychromatic detection (M/P mode) or polychromatic illumination, monochromatic detection (P/M mode) for any one of the four CIE-specified illuminating and viewing geometries, where reciprocal geometries, e.g., 45/0 and 0/45, give identical results. These instrumental arrangements and CIE-recommended geometries of illumination and viewing for reflectance factor measurements are shown in Fig. 2. It should be noted that some color-measuring instruments replace the scanning monochromator and detector with a fixed grating and diode array detector or charge-coupled device (CCD).

The exact nature of the illuminating source is immaterial, provided that it has adequate output over the visible (color) range. It is recommended in these standards that this spectral range extend from 380 to 780 nm and that the instrument spectral bandpass be equal to the wavelength measurement interval. Since the spectral curves of most object colors are smooth, the CIE has recommended that adequate colorimetric accuracy is achieved with a 5-nm bandpass.

A large number of instruments have been designed to measure surface color and the general interinstrument agreement using these CIE standard colorimetric methods is good for measuring nonfluorescent materials. However, this not the case for the measurement of fluorescent materials. The problems of measuring fluorescent surface colors and the refinements and

**Table 1** Terminology to describe surface fluorescence measurements

Symbol	Physical quantity	Units
$\beta$	Radiance factor	1
$\beta_R$	Reflected radiance factor	1
$\beta_L$	Luminescent radiance factor	1
$\beta_{L\lambda}(\mu)$	Bispectral luminescent radiance factor	$\text{nm}^{-1}$
$\beta_L(\mu, \lambda)$	Weighted bispectral luminescent radiance factor at emission wavelength, $\lambda$ and emission waveband, $\Delta\lambda$	1
$\eta_L(\mu)$	Spectral quantum efficiency of the fluorescent process	1
$D(\mu, \lambda)$	Donaldson matrix representation of reflected and weighted bispectral luminescent radiance factor data	1
$L_{L\lambda}$	Luminescent radiance concentration (per unit waveband at emission wavelength, $\lambda$ )	$\text{Wm}^{-2} \text{sr}^{-1} \text{nm}^{-1}$
$E_\mu$	Spectral irradiance concentration (per unit waveband at excitation wavelength, $\mu$ )	$\text{Wm}^{-2} \text{nm}^{-1}$
$\alpha(\mu)$	Relative spectral irradiance distribution of excitation source referenced to an arbitrary normalization wavelength, $\lambda_c$ in excitation range of fluorescent sample under test	1

The functional dependence on detection wavelength,  $\lambda$  is implicitly assumed for the above quantities.



restrictions to these standard methods to improve the measurement of luminescence, are described below. The terminology and symbols used in this chapter for describing colorimetric measurements of surface fluorescence are according to the CIE International Lighting Vocabulary [11] and CIE Publication 182:2007 on Calibration methods and photoluminescent standards for total radiance factor measurements [12]. This terminology for describing surface fluorescence measurements is summarized in Table 1.

## 2 Measurement of Surface Fluorescent Colors

We have seen that the perceived color of an object depends upon the spectral nature of the light leaving the sample and reaching the observer. In the case of a fluorescent opaque material, the light leaving the specimen is a combination of reflected and diffusely emitted (luminescent) radiation. Since the human eye cannot distinguish between these different types of nonthermal radiation, the color evoked by a fluorescent object is the combined subjective effect of this reflected and luminescent radiation. For instrumental measurements of surface fluorescent color to correlate with this visual assessment, they need to measure this same physical stimulus.

Conventional instrumentation used for colorimetry cannot discriminate between emitted radiation due to fluorescence (less than 10 ns) or phosphorescence (greater than 10 ns), so the more correct terminology is surface photoluminescence which is the generic term that includes fluorescence, phosphorescence and related phenomena. To simplify the following discussion, the term surface fluorescence is used to describe this color effect.

The ratio of the total spectral radiance leaving a surface element of the fluorescent reflecting sample in a given direction to that of the perfect reflecting diffuser, identically irradiated and viewed, is termed the total spectral radiance factor,  $\beta_T(\lambda)$ :

$$\beta_T(\lambda) = \beta_R(\lambda) + \beta_L(\lambda) \quad (3)$$

where  $\beta_R(\lambda)$  is the reflected spectral radiance factor and  $\beta_L(\lambda)$  is the luminescent spectral radiance factor. This measured quantity on a reflection spectrophotometer is sometimes referred to as the apparent sample reflectance or radiance and can exceed 100%.

To underline the importance of the spectral quality of the illuminating source,  $S(\lambda)$  on the luminescent component, Eq. 3 can be rewritten, to show this functional dependence more explicitly:

$$[\beta_T(\lambda)]_{S(\lambda)} = \beta_R(\lambda) + [\beta_L(\lambda)]_{S(\lambda)}. \quad (4)$$

Whereas the reflected radiation corresponds to the same incident wavelength,  $\mu$ , as the exciting radiation, the emitted radiation,  $\lambda$ , is usually of

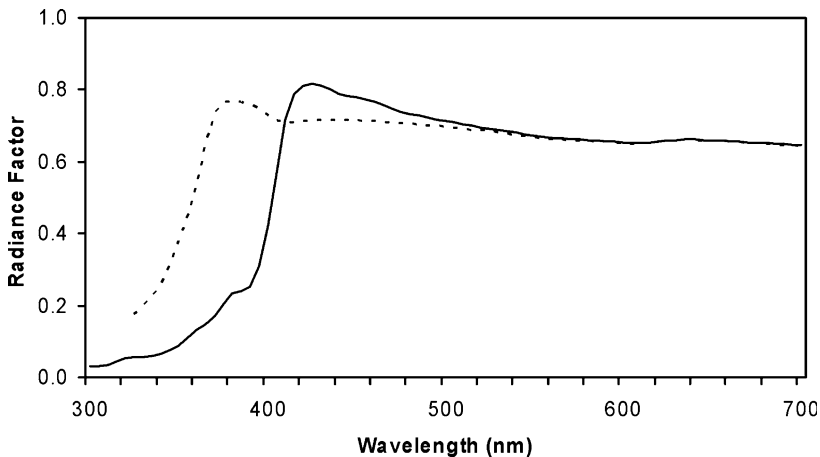


**Fig. 3** Measured apparent radiance of a fluorescence-whitened fabric sample recorded on a conventional one-monochromator spectrophotometer in M/P mode (*dashed*) and P/M mode (*solid*)

longer wavelength (Stoke's law). For this reason, it is not meaningful to measure surface fluorescence using a conventional spectrophotometer with monochromatic illumination, polychromatic detection (M/P mode) since the emitted radiation is incorrectly attributed to the excitation wavelength. This effect is illustrated in Fig. 3, which shows the measured apparent radiance of a fluorescence-whitened fabric sample using the two different design modes shown in Fig. 2a. This sample contains fluorescent whitening agents (FWAs) that are excited by UV radiation and emit in the shortwave visible (blue) to produce an enhanced whiteness perception. It can be seen that in M/P mode (dashed line), the detector has incorrectly recorded the enhanced reflectance in the UV portion of the spectrum, at the wavelengths of excitation, instead of in the blue portion of the spectrum, where the light is emitted. This choice of instrument design can result in large colorimetric errors. The more meaningful colorimetric result is obtained in the P/M mode measurement (solid line), which correctly shows the enhanced radiance in the blue.

### 3 Standardization of Fluorescent Color

#### 3.1 Historical Background

The development of standard methods for measuring surface fluorescence began in the 1950s with the work of Donaldson at the National Physical La-

boratory (NPL) [13]. Donaldson investigated the spectrophotometry of fluorescent pigments and introduced the classical two-monochromator method of separating the reflected from the fluorescent component by using one monochromator in the excitation beam and one monochromator in the detection beam (the so-called two-monochromator method, or M/M mode), which is illustrated in Fig. 4. Donaldson also introduced the useful two-dimensional matrix concept for completely describing the reflected and luminescent components as a function of excitation and emission wavelengths. This Donaldson radiance factor matrix notation is shown in Table 2 for a fluorescent red ink sample [13].

The compensation of the instrument characteristics by the two-monochromator method allowed the sample's total radiance properties to be calculated from the Donaldson radiance data for any illumination of interest. The separation of the reflected and luminescent components also enabled colorant formulation for fluorescent surface colors. Because of the complexity of the two-monochromator method, it was not implemented in many laboratories and most practical colorimetrists still relied on one-monochromator methods.

With the increasing use of fluorescent colorants, particularly FWAs, in the early 1970s, other authors designed reference instruments based on the two-monochromator method for colorimetric applications, notably Grum [14] and Clarke [15]. Clarke is also responsible for introducing the term bispectral luminescent radiance factor.

During most of this period, the CIE monitored this work, but made no explicit recommendation on instrument geometry for surface fluorescence

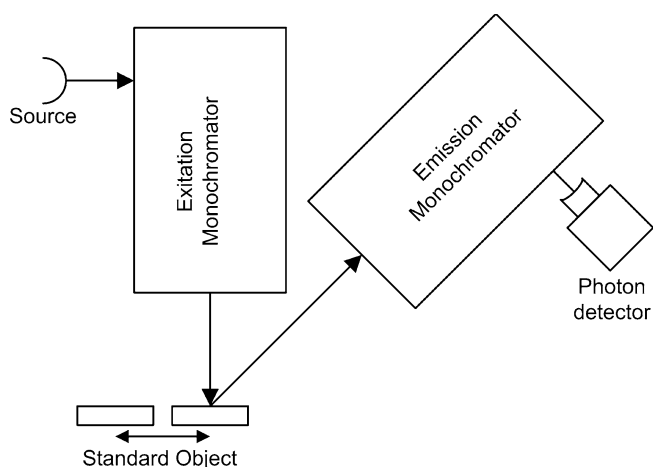


**Fig. 4** Schematic representation of a reference spectrofluorimeter design configuration based on the two-monochromator method: monochromatic illumination/monochromatic viewing (M/M mode)

**Table 2** Donaldson radiance factor (as a percentage) matrix representation,  $D(\mu, \lambda)$  of a red fluorescent ink [13]

Excitation wavelength (nm)	Emission wavelength (nm)											
	300	340	380	420	460	500	540	580	620	660	720	760
300	3.5	-	-	-	-	-	-	1.9	5.6	2.1	0.5	0.1
340		6.7	-	-	-	-	-	1.6	5.8	2.2	0.6	0.1
380			6.8	-	-	-	-	2.3	7.0	2.5	0.8	0.2
420				2.8	-	-	-	2.9	8.6	3.2	1.0	0.2
460					4.4	-	-	2.7	8.3	3.4	0.8	0.2
500						4.3	-	3.0	8.3	3.4	0.8	0.3
540							2.4	3.7	8.8	3.6	0.9	0.3
580								8.0	9.3	3.9	1.0	0.4
620									80.0	0.4	0.1	-
660										84.0	-	-
700											85.0	-
740												86.0

measurements. In principle, these measurements could be performed on any general-purpose color-measuring instrument, provided that it conformed to one of the CIE recommended geometries. The critical requirement was that the relative spectral power distribution of the instrument irradiating system match that of the desired standard illuminant. The color of the fluorescent materials was then calculated from the measured radiance factor substituted into Eq. 2, as in the case of nonfluorescent materials.

During the period 1975–1980, the Luminescence Subcommittee of the CIE technical committee (TC) 2.3 carried out a comparative study of luminescence measurements to determine the state-of-the-art variability among instruments [16]. It was found that the colorimetric errors were significant and largely attributable to the lack of practical instrument sources that simulated the desired standard illuminant conditions. To address this issue of nonstandard sources, the CIE developed a standard method for assessing the quality of daylight simulators for colorimetry (1981) but were unsuccessful in recommending a practical source for simulating these standard conditions [17].

Researchers, like Alman and Billmeyer [18], Simon [19], Allen [20] and others [21] proposed modifications of the one-monochromator method to improve colorimetric accuracy in the measurement of fluorescent materials. During this time period, a one-monochromator integrating-sphere spectrophotometer was widely used for industrial color measurement of fluorescent materials, since this geometry minimizes the effects of surface structure and/or directional characteristic. However, in 1976, it was reported by Alman and Billmeyer [18] that a sphere was not ideal for the measurement of fluorescent materials, since the spectral radiance from the sample modified the

---

**Table 3** A selection of CIE, ASTM and ISO publications and standards dealing with color measurement of fluorescent materials

---

## CIE

CIE Publication No. 76 (1988) Intercomparison on Measurement of (Total) Radiance Factor of Luminescent Specimens;

CIE Publication No. 51 (TC 1.3), 1981. A Method for Assessing the Quality of Daylight Simulators for Colorimetry;

CIE Publication No. 182:2007 (TC 2-25) Calibration Methods and Photoluminescent Standards for Total Radiance Factor Measurements.

## ASTM

E991 Color Measurement of Fluorescent Specimens;

E1247 Identifying Fluorescence in Object-Color Specimens by Spectrophotometry;

E2152 Standard Practice for Computing the Colors of Fluorescent Objects from Bispectral Photometric Data;

E2301 Standard Test Method for Daytime Colorimetric Properties of Fluorescent Retroreflective Sheeting and Marking Materials for High Visibility Traffic Control and Personal Safety Applications Using 45° Normal Geometry;

E2153 Standard Practice for Obtaining Bispectral Photometric Data Evaluation of a Fluorescent Object;

E1247 Standard Practice for Detecting Fluorescence in Object-Color Specimens by Spectrophotometry.

## ISO

2470 Paper and Board: Measurement of Diffuse Reflectance Factor (ISO Brightness);

2469 Paper, Board and Pulps – Measurement of Diffuse Reflectance Factor;

16693 Paper and Board – Measurement of D65 Brightness (Diffuse Blue Reflectance Factor Under UV(D65) Condition).

---

spectral distribution of the irradiating sphere–source system. There was also a problem with self-absorption of the fluoresced radiation. Because of these complications, the CIE recommended the use of 45/0 (0/45) geometry and the two-monochromator method as the preferred condition for the measurement of surface fluorescence [2].

In the 1980s, there was another surge of research activity on fluorescence standardization as the use of fluorescent colorants became more widespread due to their increased stability and gamut of available colors. This research was carried out by several authors including Alman and Billmeyer [18], Zwinkels and coworkers [22, 23], Mielenz [24], and Minato et al. [25].

Over the past 20 years, the CIE, ASTM, ISO and other standardizing bodies have developed documentary standards to specify the requirements for measuring fluorescent surface colors for various applications. A selection of these documentary standards is given in Table 3. Despite the growing commercial importance of fluorescent surface colors, only a few standardizing laboratories have developed two-monochromator method spectrofluorimeters that conform with these standard recommendations [22, 26, 27].

## 3.2

### One-Monochromator Method

As we have seen the one-monochromator method, with (P/M) mode, measures the total radiance factor directly. In principle, it gives a simple, rapid method of determining the color of fluorescent surface colors and can provide accurate results when the source is well controlled and conforms with the desired standard illumination condition. To achieve this standard condition, the instrument source is generally filtered or adjusted so that its spectral power distribution matches that of the desired CIE illuminant. Although the CIE has developed standard methods for assessing the quality of these simulated illuminant conditions [17], the lack of recommendations on practical methods of simulating the CIE daylight illuminants, notably D65, has greatly limited the accuracy of one-monochromator methods.

A number of authors have developed procedures to separate the total radiance factor data measured using a one-monochromator method to give the reflected and uncorrected fluorescent components. The fluorescent component is then adjusted by the known mismatch between the instrument source and desired illuminant condition to give corrected total spectral radiance factor values. These one-monochromator methods of separating the two components are referred to as predictor methods. The four accepted predictor methods are the two-mode method of Simon [19], the filter reduction method of Eitle and Ganz [28], the adjustment method of Alman and Billmeyer [18] and the fluorescent-weakening method of Allen [20]. The fluorescent-weakening method is considered to be the most accurate of these predictor methods where the fluorescent sample is measured under two different filtered sources for which the ratio of the irradiances is known. This method gives fairly accurate colorimetric results when the instrument source is already a close approximation to the desired CIE standard illuminant distribution.

However, most practical measurements of surface colors are performed on one-monochromator instruments with some means of adjusting the source spectral distribution. For the measurement of materials containing FWAs, these one-monochromator instruments commonly employ a UV adjustment filter with a steep absorption edge at 400 nm. The UV adjustment filter is used to alter the ratio of UV to visible source output so that the illumination more closely approximates the desired CIE illuminant condition. This adjustment is accomplished using calibrated fluorescent reference standards that have been calibrated with a two-monochromator instrument for the desired CIE standard illuminant. For this instrument adjustment to give accurate colorimetric results, the fluorescent transfer standard must have similar excitation and emission spectral profiles to the fluorescent samples under test. Other desirable properties of these fluorescent transfer standards are described by Grum [29] However, standard procedures for the selection and use of these

fluorescent standards has not been developed and this discussion is outside the scope of this chapter.

A serious limitation of the one-monochromator methods is that they only provide very limited colorimetric information that pertains to a single illuminant. Additional measurements must be performed with other sources of illumination to obtain color information for other illumination conditions. The only definitive method that provides complete information on the color properties of a fluorescent material for any illumination condition is the two-monochromator method where the spectral radiance factor spectrum is measured for each incident wavelength. The remainder of this chapter will focus on a discussion of the basic principles, terminology, instrumentation, standards and experimental procedures for accurate surface fluorescence measurements via the two-monochromator method.

### 3.3

#### Two-Monochromator Method

The two-monochromator method is defined by the CIE as the standard method for the determination of the colorimetric properties of fluorescent materials. In this method, the measuring instrument has two separated monochromators. The first monochromator, referred to here as the excitation monochromator, irradiates the specimen with monochromatic light at wavelength  $\mu$ . The second monochromator, referred to here as the emission monochromator, analyzes the radiation leaving the specimen monochromatically at wavelength  $\lambda$ . This design of instrument is shown schematically in Fig. 4. This basic design is similar to that used in analytical fluorimetry. However, for colorimetric applications of surface fluorescence, the radiance of the sample is compared to that of a reflection standard and the measured quantity is expressed on a reflectance or radiance factor scale. The two-monochromator method allows for the complete separation of the reflected and fluorescent components. Although this is not strictly required for color appearance evaluation, it is essential for colorant formulation applications.

The reflected radiance factor,  $\beta_R$ , is determined by synchronous scanning of both excitation and emission monochromators and having them set to the same wavelength. The reflected radiance of the sample is compared at each wavelength,  $\lambda$ , to that of a white nonfluorescent reflectance standard that has been calibrated for the same geometric conditions of irradiation and viewing. This ratio is then multiplied by the known spectral radiance factor of the standard,  $\beta_{std}(\lambda)$ , to give an absolute value for the reflected radiance factor.

The luminescent radiance factor,  $\beta_L$  is determined by setting the excitation monochromator at a fixed wavelength  $\mu$  in the excitation band of the specimen and scanning with the emission monochromator through all wave-

lengths  $\lambda$  in the emission spectrum. This process is repeated for each incident wavelength in the excitation region of the fluorescent sample. The result is a two-dimensional array of uncorrected bispectral fluorescent radiance data,  $L_\lambda(\mu, \lambda)$  which is distorted by the spectral characteristics of the measuring instrument. The standard methods for correcting for these instrument effects are similar to those used in analytical fluorimetry. However, for colorimetric applications, absolute values of the reflected and bispectral luminescent radiance factor are required on a reflectance or radiance scale so that the correction procedures for the excitation and emission spectra are not independent and must be applied to all readings. The details of this instrument calibration procedure are described later in this chapter.

When these bispectral luminescent data have been corrected for the spectral effects of the excitation and emission unit, and compared to the known spectral radiance of the white reflectance standard, the result is the instrument-independent, bispectral luminescent radiance factor,  $\beta_{L\lambda}(\mu)$  [15]. This quantity describes the radiance per unit waveband at wavelength  $\lambda$  due to luminescence of the sample when irradiated per unit waveband at wavelength  $\mu$ , compared to the radiance of the perfect reflecting diffuser identically irradiated and viewed. Whereas the reflected radiance factor is dimensionless, the bispectral luminescent radiance factor is an absolute differential radiometric quantity and has dimensions of  $\text{nm}^{-1}$ . To determine the total luminescent radiance factor over an emission waveband,  $\Delta\lambda$ , at an emission wavelength,  $\lambda$ , it is necessary to sum the bispectral luminescent radiance factor across this waveband. This weighted bispectral luminescent radiance factor,  $\beta_L(\mu, \lambda)$ , is a dimensionless quantity, given by:

$$\beta_L(\mu, \lambda) = \sum_{\lambda} \beta_{L\lambda}(\mu) \Delta\lambda. \quad (5)$$

A convenient method for presenting both the reflected and weighted bispectral luminescent radiance factor data is the so-called Donaldson matrix,  $D(\mu, \lambda)$  representation of the radiance factor data. This representation developed by Donaldson [13] and illustrated in Table 2, has the excitation wavelengths tabulated in the vertical direction, and the emission wavelengths in the horizontal direction. The diagonal elements,  $D(\mu, \lambda)$  where  $\mu = \lambda$  are the reflected radiance factors,  $\beta_r(\lambda)$ , and the off-diagonal terms,  $D(\mu, \lambda)$  where  $\mu \neq \lambda$  are the weighted bispectral luminescent radiance factors,  $\beta_L(\mu, \lambda)$ . The advantage of the Donaldson matrix representation of the radiance factor data is that it provides a complete color specification for a fluorescent surface color for any desired illumination condition, without the inaccuracies of simulator sources or mathematical corrections.

The spectral luminescent radiance factor of the sample is obtained by weighting the bispectral luminescent radiance factors by the relative spectral distribution of the desired CIE standard illuminant,  $E_{\text{std},\lambda}(\mu)$ , and integrat-



ing (or summing) this product for all wavelengths  $\mu$  in the excitation range according to Eq. 6

$$\beta_L(\lambda) = \frac{\int_{\mu} E_{\text{std},\lambda}(\mu)\beta_{L\lambda}(\mu) d\mu}{E_{\text{std},\lambda}(\lambda)} \tag{6}$$

This quantity is added to the reflected radiance factor to give the total spectral radiance factor for the specified CIE standard illuminant condition. Figure 5 shows an application of this process giving the calculated total radiance factor of a fluorescence-whitened paper sample corresponding to excitation by two different illuminating conditions: CIE illuminants C and D65. From these CIE illuminant spectral irradiance distributions shown in Fig. 1, it can be seen that the reciprocal spectrum of the standard illuminant is imprinted on the fluorescent component. The source-independent reflected radiance factor for this sample is also given and compared with the reflected radiance factor of a nonfluorescent paper sample.

The spectral quantum efficiency of the fluorescent process,  $\eta_1(\mu)$  is the ratio of the total number of photons of all wavelengths emitted from the sample by the fluorescent process for an excitation at wavelength  $\mu$  to the number of photons at wavelength  $\mu$  reflected from the perfect reflecting diffuser identically irradiated and viewed. This quantum efficiency is calculated from the bispectral luminescent radiance factor data, by integrating (summing) this

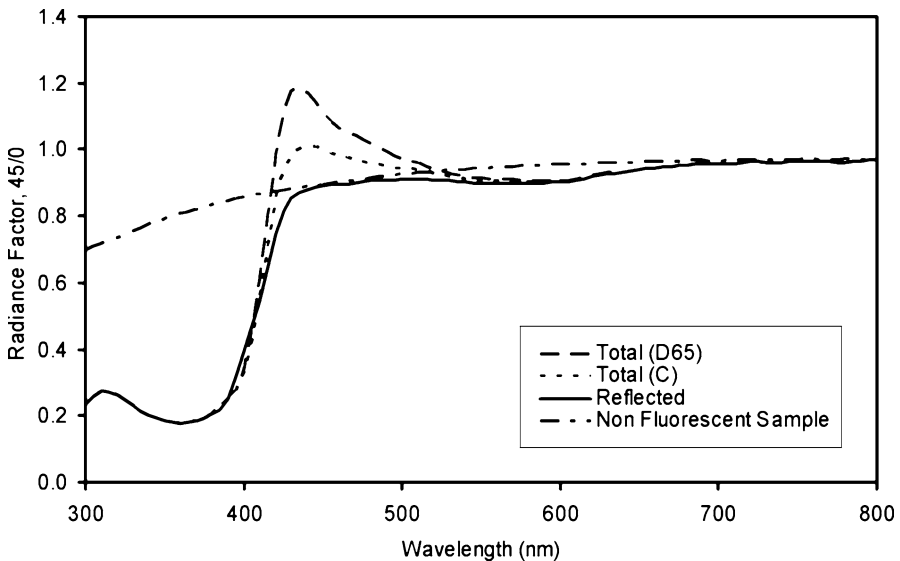


**Fig. 5** Total radiance factor of a fluorescence-whitened paper sample for CIE Illuminant D65 and C conditions. The reflected radiance factor is also given and compared with that of a nonfluorescent paper sample

quantity for a fixed excitation wavelength  $\mu$  across the wavelengths of emission  $\lambda$  according to:

$$\eta_L(\mu) = \int_{\lambda} \beta_{L\lambda}(\mu) d\lambda. \quad (7)$$

The colorimetric quantities for the fluorescent sample,  $X$ ,  $Y$ ,  $Z$  and  $x$ ,  $y$ , are calculated by simply substituting the value of  $\beta_T(\lambda)$  for  $R(\lambda)$  in the CIE equations Eqs. 2a–2d.

Thus, the two-monochromator method provides a complete analysis of the spectral properties of a fluorescent surface color: its reflectance, fluorescence, quantum yield and colorimetric value, independent of the spectral distribution of the measuring instrument.

### 3.3.1

#### Instrumentation for Two-Monochromator Method

Despite the commercial importance of fluorescent surface color measurements, there has not been much progress in the development of new or improved instrumentation for these measurements since the two-monochromator design introduced by Donaldson in 1954 [13]. To date, only two manufacturers have developed commercial spectrofluorimeters for colorimetric applications. The Labsphere BFC/450 instrument has a 45°/0° design geometry and is based on a diode array spectrofluorimeter developed by Ver-rill and Williams at the NPL [27]. Minolta developed a more conventional two-monochromator spectrofluorimeter with a diffuse/normal geometry to conform with the standard instrument geometry specified by ISO for measuring optical properties of paper [30]. These commercial instruments are traceable to reference spectrofluorimeters developed by National Measurement Institutes (NMIs).

Currently, there are only a few standardizing laboratories that have designed and built reference spectrofluorimeters based on the two-monochromator method for the measurement of fluorescent surface colors. These laboratories include the Federal Institute for Materials Research and Testing in Berlin (BAM) [26], the NPL [27], the National Research Council, of Canada (NRC) [23] and most recently, the Metrology Research Institute, Helsinki University of Technology in Finland (TKK) [31]. These instruments all use a xenon source to provide high spectral irradiance for the wavelengths of interest in fluorescence color measurements and have been designed to conform to the CIE preferred standard geometric condition of 45/0 (or 0/45). The instruments largely differ in their means of illuminating and viewing the sample monochromatically. The NRC and BAM instruments use a conventional second monochromator and photomultiplier detector in the analyzing beam, whereas the NPL and TKK instruments use a diode array and CCD

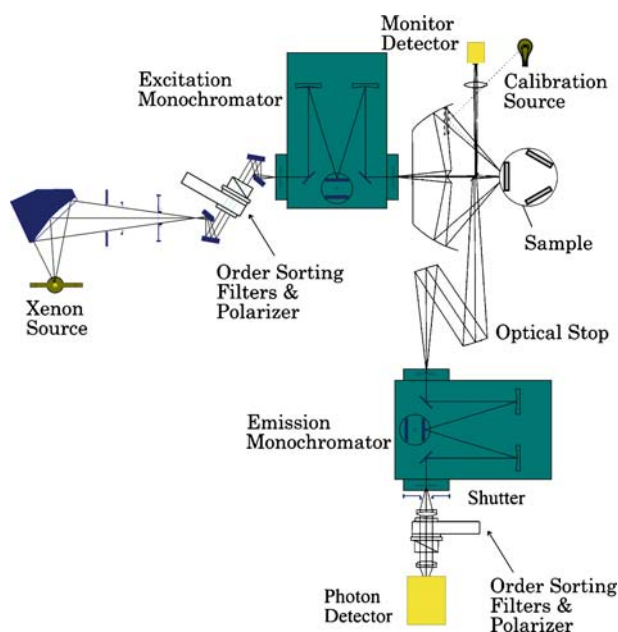


**Fig. 6** Design of the National Research Council, Canada (NRC) reference spectrofluorimeter for the two-monochromator method calibration of fluorescent surface colors for 45/0 geometry. The physical transfer standards for radiometric calibration of the instrument characteristics are: standard and monitor detectors, standard lamp and standard reflector (45/0 geometry)

spectrometer, respectively. However, the key requirements for calibrating these bispectral instruments are similar and the following section discusses the important steps in standardizing the procedures for instrument correction. To aid this discussion, a schematic of the NRC reference spectrofluorimeter is given in Fig. 6, and the details of its standardization procedures are given below.

## 4

### Standard Procedures for Surface Fluorescence Measurements

#### 4.1

##### Standard Spectrophotometric Procedures

Since a two-monochromator spectrofluorimeter evaluates both the relative spectral reflectance of a material and its absolute spectral emission, it functions as both a spectrophotometer and a spectroradiometer. Thus, its calibration involves many of the standard procedures that are commonly used for

these two different types of spectral measuring instruments. The procedures for calibrating the spectrophotometric errors of wavelength scale, photometric scale, stray light, polarization, and beam geometry errors are well known and described in several references [32, 33].

The wavelength scale of the monochromator or spectrometer is calibrated using spectral line lamps, e.g., Hg, Cd, Cs and He. Wavelength accuracies of 0.1 nm throughout the spectral range of use are achievable using polynomial correction functions. The photometric scale of the analyzing detector needs to be verified throughout the dynamic range of measurement. Since the fluorescent signals are typically much weaker than the reflected signals for most surface colors, it is also important to take special precautions to reduce stray light interference effects. Calibrated white and neutral gray reflectance standards can be used to check the photometric scale of the instrument up to a reflectance level of about 100%. Since fluorescent surface colors can have reflectances exceeding 100%, it is necessary to check the photometric scale at these higher values. Photometric linearity over this wide dynamic range can be checked using a variety of methods based on the light addition principle. This light summation can be accomplished using multiple apertures, multiple sources, or multibeam optics. The light addition method used at NRC, involving a high-precision variable aperture is a variant of the double-aperture method [34].

The requirements for the reflection standard are described in several references. It is important to verify that the standard is nonphotoluminescent. It has been found that some white standards used commonly as reflection standards for color measurements of nonfluorescent samples exhibit weak photoluminescence that can compromise the accuracy of colorimetric results [35].

#### 4.1.1

##### Standard Geometric Conditions

As mentioned earlier, for surface fluorescence measurements, the instrument geometry must conform to one of the CIE-recommended standard geometric conditions for reflection colorimetry shown in Fig. 2. For reference measurements, the preferred geometries are illumination or detection at  $45^\circ$  to the sample normal. For a unidirectional geometry, designated  $45^\circ x:0$  (or reverse configuration of  $0^\circ:45^\circ x$ ), the color measurement is sensitive to the effects of texture and directionality. This error is reduced with an annular illumination geometry in which the sample is illuminated or detected at all azimuthal angles, designated  $45^\circ a:0$  ( $0^\circ:45^\circ a$ ) [4]. For both these geometric conditions, the sampling aperture is a cone with a half-angle of  $5^\circ$ .

The accuracy of the spectral measurements will depend on the conformance of the instrument geometry with the CIE standard geometric conditions and tolerances. However, the error due to nonconformance is very sam-

ple dependent and varies with both the opacity/translucency and anisotropy of the sample. For diffusely reflecting fluorescent colors, such as the Lab-sphere Spectralon-based fluorescence standards, the sensitivity to geometric errors is small. However, for retroreflective fluorescent marking material or fluorescent lacquer-on-paint samples, the error can be quite large. A geometric error can also be caused by inaccurate sample positioning. Since the color measurements involve a comparison with a white reflectance standard to minimize geometric transfer errors, it is essential that the fluorescent sample and the standard are positioned at exactly the same reflecting plane. This can be accomplished by direct substitution of the sample and reference at the same specimen port or by using a standard laser alignment procedure and precision adjustments on the sample and standard mounts. The latter approach has been used by the NRC [36].

#### 4.1.2

##### **Standard Polarization Conditions**

Surface fluorescent measurements need to be carried out with a defined state of polarization incident on the sample. The instrument degree of polarization, due to polarization properties of the source, monochromator and other optical components, can be quite significant. To produce *s*- or *p*-polarized radiation, a polarizing filter or prism is placed in the beam and oriented vertically or horizontally to the optical axis and these two measurements are averaged to obtain the result corresponding to unpolarized conditions. Alternatively, polarizing filters are placed in both the incident and viewing beams, and oriented so that they are at  $45^\circ$  to make the horizontal and vertical components equal in intensity and, thereby, equivalent to unpolarized conditions.

Minato et al. have extensively investigated the influence of instrument polarization on surface fluorescence measurements and found that, while it affects the accurate shape of the measured reflected or luminescent radiance factor, it has a negligible influence on the accuracy of the derived colorimetric results [37].

#### 4.1.3

##### **Standard Radiometric Calibration Procedures**

The radiometric calibration of a spectrofluorimeter for colorimetric applications is very similar to that used for correcting analytical fluorimeters for the influencing characteristics of the instrument. These standard procedures use physical transfer standards that are traceable to primary radiometric scales and have been calibrated under identical experimental conditions as used for the fluorescent sample measurements. The critical experimental parameters that must be controlled are the spectral bandwidth, incident geometry,

polarization orientation and photometric level. Generally, the first step in this instrumental spectral characterization is to calibrate the relative spectral irradiance of the excitation unit. Thus, the following physical transfer standards are required, as a minimum:

1. A calibrated nonphotoluminescent white reflectance standard
2. A calibrated detector of relative spectral responsivity.

To dynamically correct for fluctuations or drifts in the excitation unit irradiance, a beamsplitting device can be used to direct a portion of the incident beam to a monitor detector [23, 27, 31], or the excitation unit irradiance can be compared to that of a more stable incandescent reference lamp [26]. Once the spectral power distribution at the sample position is known, it is possible to use this information to determine the spectral responsivity of the emission unit. This detector-based calibration of the emission unit is used by some NMIs [27, 31]. However, many spectrofluorimeters use a xenon source that has an irregular distribution that is susceptible to bandpass errors. To eliminate this bandpass error, the calibration system should also include a third item: a calibrated source of relative spectral radiance that has a smooth spectral power distribution. This source can be either an incandescent spectral irradiance lamp and standard diffuser reflector or an integrating sphere type radiator. For colorimetric applications, it is strictly only necessary to calibrate the emission unit over the spectral range 380–780 nm, so the fact that the output of an incandescent lamp is very low at wavelengths below 340 nm is not a problem for this source-based radiometric calibration of the emission unit.

#### 4.1.4

##### Spectral Irradiance of the Excitation Unit

As mentioned above, the standard procedure for calibration of the excitation unit involves the use of a standard detector and/or monitor detector. Figure 7 shows representative *s*- and *p*-polarized spectral responsivity data for a standard silicon detector, calibrated for 45° incidence (underfilled mode). This reference detector is then placed at the sample position in the excitation unit and used to calibrate the monitor detector for *s*- and *p*-polarized illumination conditions (see Fig. 8). If the detector aperture is smaller than the beam diameter (underfill mode), the total beam power is measured and if it is larger (overfill mode), the relative spectral irradiance is measured. For each polarization, the normalized spectral distribution of the excitation source,  $\alpha(\mu)$  is defined as the ratio of the spectral irradiance at the sample position for all wavelengths  $\mu$  in the excitation range,  $E_\mu(\mu)$ , to the spectral irradiance at an arbitrary normalization wavelength,  $\lambda_c$ ,  $E_\mu(\lambda_c)$ . This quantity can be determined for each instrument polarization, from the monitor detector signal,  $i_{\text{mon}}(\mu)$  referenced to the value at wavelength  $\lambda_c$ , corrected by its as-

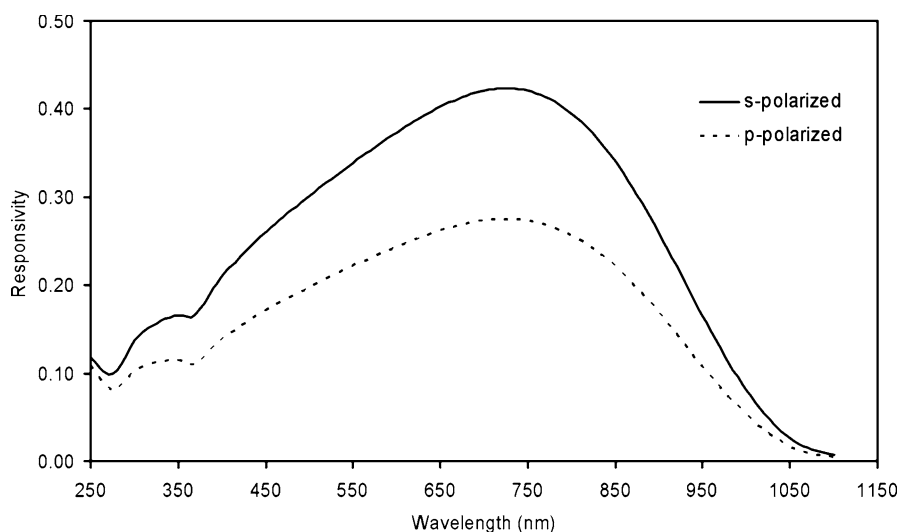


**Fig. 7** Representative standard detector calibration data for traceable calibration of the NRC reference spectrofluorimeter for 45° incidence and *s*- and *p*-polarized incident conditions

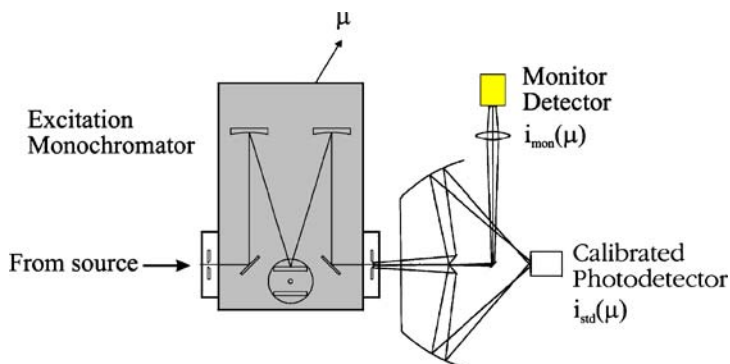


**Fig. 8** Schematic diagram of experimental set-up for detector-based calibration of excitation unit of the NRC reference spectrofluorimeter

sociated spectral responsivity of the monitor detector calibrated for this state of polarization,  $R_{\text{mon}}(\mu)$  or  $R_{\text{mon}}(\lambda_c)$ , where

$$\alpha(\mu) = \frac{E_{\mu}(\mu)}{E_{\mu}(\lambda_c)} = \frac{i_{\text{mon}}(\mu)/i_{\text{mon}}(\lambda_c)}{R_{\text{mon}}(\mu)/R_{\text{mon}}(\lambda_c)}. \quad (8)$$

This relative spectral distribution of the excitation unit will be superimposed on the measured excitation curves. These raw data can be corrected for instrument spectral effects by dividing the measured sample excitation spectra

by this spectral function. However, the instrumental characteristic of interest for obtaining corrected surface fluorescence values is the instrument spectral efficiency of detected energy per unit bandpass to incident energy per unit bandpass.

A standard method for determining this quantity is to measure the quantum yield for a known standard. For a nonluminescent reflectance standard, the spectral quantum efficiency at each wavelength is the corresponding absolute radiance factor under specified geometric conditions of illumination and viewing. Because of the bandpass error discussed above, the reflected radiance signal for this reflectance standard will be divided between the wavelengths across the detection waveband. There is also an error due to mismatch in the wavelength scales of the two monochromators. Different standard procedures have been used to correct for these effects, including the method of Burns et al. [38] in which a trapezoidal bandpass is set in the emission monochromator to include entirely the triangular bandpass of the excitation monochromator. The standard method used at NRC is similar to that presented by Minato et al. [25], in which the emission monochromator is scanned at 1-nm intervals centered on an arbitrary wavelength,  $\lambda_c$ , in the excitation range of the fluorescent sample, and integrated or summed over the instrument's effective spectral width. For equal 5-nm excitation and emission monochromator bandwidth settings, this spectral width,  $\Delta\lambda$ , extends 20 nm, centered on the nominal wavelength setting. The total reflected radiance signal,  $I_{mw}(\lambda_c)$  is then given by:

$$I_{mw}(\lambda_c) = \int i_{mw}(\lambda_c) d\lambda = \sum_{\lambda_c - \Delta\lambda}^{\lambda_c + \Delta\lambda} i_{mw}(\lambda_c) \Delta\lambda. \quad (9)$$

This measured signal is proportional to the monochromatic spectral irradiance at wavelength  $\lambda_c$ , according to:

$$I_{mw}(\lambda_c) \approx kE_\mu(\lambda_c)\beta_{std}(\lambda_c)R_{sys}(\lambda_c), \quad (10)$$

where  $R_{sys}(\lambda)$  is the relative spectral responsivity of the emission unit and  $k$  is an instrument-specific constant dependent upon the instrument bandpass. The procedure for calibrating  $R_{sys}(\lambda)$  is described below.

#### 4.1.5 Spectral Responsivity of the Emission Unit

To calibrate the spectral responsivity of the emission unit,  $R_{sys}(\lambda)$ , it is necessary to use a source of known spectral radiance at the sample position. As mentioned previously, this can be the previously calibrated excitation unit. At NRC, an incandescent spectral irradiance standard,  $E_{ref}(\lambda)$  is used in combination with a white standard of known spectral reflected radiance factor,



$\beta_{\text{std}}(\lambda)$ . The measured signal of the analyzing detector,  $i_{\text{sw}}(\lambda)$  is then given by:

$$i_{\text{sw}}(\lambda) = k_2 E_{\text{ref}}(\lambda) \beta_{\text{std}}(\lambda) R_{\text{sys}}(\lambda), \quad (11)$$

where  $k_2$  is an instrument-specific constant dependent upon the emission unit bandpass.

#### 4.1.6

##### Determination of Reflected Radiance Factor

The reflected radiance factor,  $\beta_r(\lambda)$  is measured using a procedure similar to standard spectrophotometric methods for measuring spectral reflected radiance of nonphotoluminescent materials. The two monochromators are set at the same wavelength setting and are scanned synchronously. However, the measurement of reflected radiance factor with a two-monochromator spectrofluorimeter does not necessarily give the same result as a conventional one-monochromator spectrophotometer, even for a nonfluorescent material. This is because the shape of the spectral bandpass is modified by passing through two monochromators. If each monochromator has a triangular slit function, the spectral bandpass will be Gaussian-shaped after passing through the second monochromator. Also if the spectral slit width settings of both monochromators are equal, the effective spectral width of the radiation passing through the second monochromator is double this nominal setting. To determine the reflected radiance, it is necessary to sum the measured signals across this effective spectral width. Gundlach and Terstiege [26] describe how to carry out this bandpass correction by using mathematical deconvolution and Minato et al. [25] describe how to reduce this error by reducing the bandpass of the emission monochromator. Alternatively, to avoid this complication the measurement interval for detecting the reflected and emitted radiation can be increased to twice the value of the nominal slit-width setting and the measured data interpolated with a Lagrangian or cubic-order function. This is the strategy used by NRC to separate the reflected and fluorescent components and to correct for this bandpass effect [35].

#### 4.1.7

##### Determination of Bispectral Luminescent Radiance Factor

After the instrument characteristics have been determined via Eqs. 8–11, the measured raw bispectral luminescent data,  $i_f(\mu, \lambda)$  for a fluorescent surface color can be corrected to give source and instrument-independent bispectral luminescent radiance factors. At NRC, this determination for a specified excitation and emission wavelength,  $(\mu_c, \lambda_c)$ , is carried out according to:

$$\beta_{L\lambda}(\mu_c) = \left[ \frac{i_f(\mu_c, \lambda_c)}{i_{\text{sw}}(\lambda_c)} \right] \left[ \frac{i_{\text{sw}}(\lambda) \beta_{\text{std}}(\lambda_c) E_{\text{ref}}(\lambda)}{I_{\text{mw}}(\lambda_c) E_{\text{ref}}(\lambda_c) \alpha(\mu_c)} \right]. \quad (12)$$

Because of short-term fluctuations in the source output between the measurements of  $i_f(\mu, \lambda)$  and  $I_{mw}(\lambda)$ , the latter is adjusted by the ratio of the monitor detector signals recorded at the time of these two measurements.

The application of these standard procedures for correcting the bispectral luminescent radiance factor for the instrument characteristics is shown in Fig. 9, which compares the raw measured and corrected bispectral luminescent radiance factor data for a fluorescent red paper sample for *s*-polarized conditions. The large dip in the raw data is due to this grating instrument's

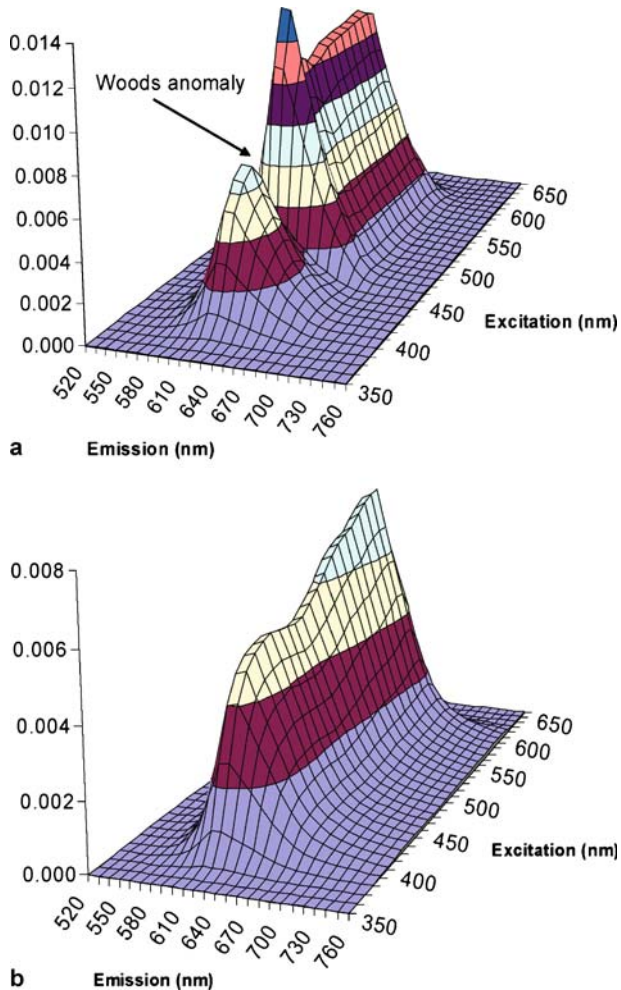


**Fig. 9** Bispectral luminescent radiance factor data for a fluorescent red paint sample (*s*-polarized). **a** Raw measured data. **b** Corrected for instrument characteristics and normalized for unit emission bandpass. Measurements are for horizontal polarization

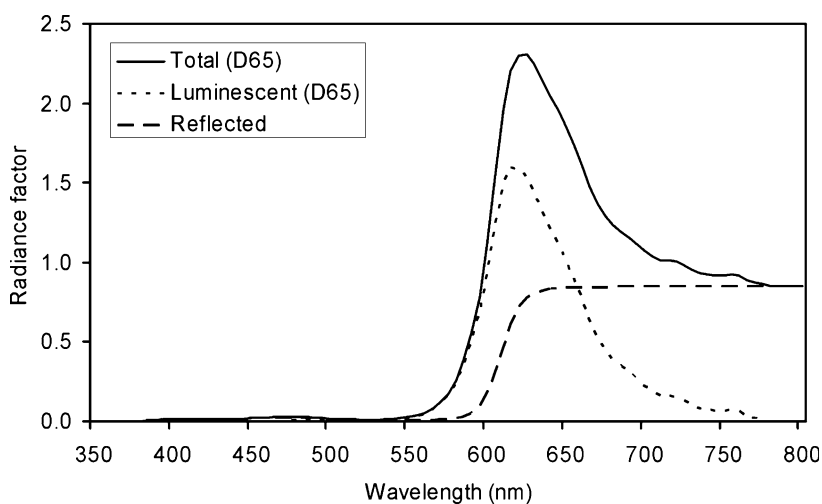


**Fig. 10** Total (CIE D65), luminescent (CIE D65) and reflected radiance factors of a fluorescent red paper sample for 45a:0 geometry

characteristic Wood's anomalies, which have been effectively removed in the corrected data. The measured reflected radiance factor and calculated total radiance factor for this fluorescent sample for CIE illuminant D65 conditions are shown in Fig. 10.

## 4.2

### Uncertainties

The measurement of total spectral radiance factors of fluorescent surface color using the two monochromator method is a complicated procedure involving several calibration steps. The principal components of uncertainty are listed below:

1. Geometric errors (includes nonconformance with CIE standards, polarization effects, beam nonuniformity)
2. Wavelength scale errors
3. Photometric scale nonlinearity
4. Spectral bandpass effects
5. Stray light errors
6. Instrument polarization error
7. Reflectance standard effects (includes photoluminescence, non uniformity, stability)
8. Transfer errors from standard lamp, detector and reflector
9. Monitor detector effects (includes transfer error, noise and drift)
10. Excitation source effects (includes noise and drift)

Many of these sources of uncertainty are common to analytical fluorimetry instrumentation. However, colorimetric measurements are subject to additional sources of error due to the requirement for absolute values of the bispectral luminescent radiance factor spectrum and, therefore the normalization of the excitation and emission spectra to radiance units. The absolute correction of these spectra involves additional uncertainties due to the diffuse reflecting standard and to the instrument bandpass.

The current state-of-the-art accuracies in the measurement of total spectral radiance factors of surface colors depend upon the material and the respective contributions from reflectance and fluorescence. In the case of fluorescent paper standards, NRC reports an expanded ( $k = 2$ ) uncertainty of 1%, excluding sample-induced effects [23], where  $k$  is the coverage factor for a certain level of confidence; a coverage factor of 2 is approximately a 95% confidence level. However, for the measurement of highly saturated fluorescent paint samples, where the radiance due to fluorescence exceeds that due to reflectance at some wavelengths (see Fig. 10), the uncertainties can be as high as 5%.

## 5 Conclusions

The problems of measuring fluorescent surface color using traditional colorimetric instrumentation, standards and methods has been extensively studied over the past 50 years. These research findings have contributed to the development of new instrumentation, fluorescence standards and experimental procedures for accurately measuring these fluorescent materials. Documentary standards detailing these methods, notably the two-monochromator method and a 45/0 (0/45) reference measurement geometry, have been prepared by the CIE and other standardizing bodies. The current status of these standardized methods has been summarized for both the one-monochromator and two-monochromator methods.

**Acknowledgements** The author would like to acknowledge the significant contributions of François Gauthier, Denis Gignac and Monica Nevins for experimental assistance in this work and to thank Mario Noël and Eric Côté for preparing several of the figures.

## References

1. Wyszecki G (1973) Colour 73:21
2. Commission Internationale de l'Eclairage CIE (2004) Publication 15.3, Colorimetry, 3rd edn. CIE Central Bureau, Vienna
3. Commission Internationale de l'Eclairage (2006) CIE S014-2/E2006. Colorimetry, Part 2: CIE Standard Illuminants. CIE Central Bureau, Vienna

4. Commission Internationale de l'Éclairage (2006) CIE S014-1/E2006. Colorimetry, Part 1: CIE Standard Colorimetric Observer. CIE Central Bureau, Vienna
5. Commission Internationale de l'Éclairage (2006) Publication 176:2006. Geometric Tolerances for Color Measurements. CIE Central Bureau, Vienna
6. Commission Internationale de l'Éclairage (1979) Publication 44. Absolute methods for reflection measurements. CIE Central Bureau, Vienna
7. Wyszecki G, Stiles WS (eds) (1982) Color science: concepts and methods, quantitative data and formulae. Wiley, New York
8. Ohta N, Robertson AR (2005) Colorimetry fundamentals and applications. Wiley, West Sussex
9. Zwinkels J (1996) Displays 16:163
10. American Society for Testing and Materials (1996) ASTM E179, Guide for the selection of geometric conditions for measurement of reflection and transmission properties of materials. ASTM, West Conshohocken, PA
11. Commission Internationale de l'Éclairage (1987) Publication 17.4, International lighting vocabulary, 4th edn. CIE Central Bureau, Vienna
12. Commission Internationale de l'Éclairage (2007) CIE Publication 182:2007. Calibration methods and photoluminescent standards for total radiance factor measurements. CIE Central Bureau, Vienna
13. Donaldson R (1954) Brit J Appl Phys 5:210
14. Grum F (1980) Colorimetry of fluorescent materials. In: Grum F, Bartleson CJ (eds) Optical radiation measurements, vol 2. Academic, New York, p 235
15. Clarke FJJ (1975) Problems of spectrofluorimetric standards for reflection and colorimetric use. In: NPL Report MOM 12. NPL, Teddington, UK, pp 1–28
16. Commission Internationale de l'Éclairage (1988) Publication 76. Intercomparison on measurement of (total) spectral radiance factor of luminescent specimens. CIE Central Bureau, Vienna
17. Commission Internationale de l'Éclairage (1981) Publication 51, A method for assessing the quality of daylight simulators for colorimetry. CIE Central Bureau, Vienna
18. Alman DH, Billmeyer FW Jr (1976) Color Res Appl 1:141
19. Simon FT (1999) Anal Chim Acta 380:417
20. Allen E (1973) Appl Opt 12:289
21. Billmeyer FW Jr (1994) Color Res Appl 6:413
22. Zwinkels J, Gignac D (1995) Development of a new reference spectrofluorimeter. In: Burgess C, Jones DG (eds) Spectrophotometry, luminescence and colour: science and compliance. Elsevier, Amsterdam, p 97
23. Zwinkels J, Gignac D, Nevins M, Powell I, Bewsher A (1997) Appl Opt 36:892
24. Mielenz KD (1987) Fluorescence Spectrometry in analytical chemistry and color science. In: Burgess C, Mielenz KK (eds) Advances in standards and methodology in spectrophotometry. Elsevier, Amsterdam, p 49
25. Minato H, Nanjo M, Nayatani Y (1979) Acta Chromatica 3:153
26. Gundlach D, Terstiege H (1994) Color Res Appl 6:47
27. Verrill JE, Williams DC (1995) The development of a new reference spectrofluorimeter at the National Physical Laboratory. In: Burgess C, Jones DG (eds) Spectrophotometry, luminescence and colour: science and compliance. Elsevier, Amsterdam, p 111
28. Eitel D, Ganz E (1968) Textilveredlung 3:389
29. Grum F (1982) Color Res Appl 7:253
30. International Standards Organization (1994) ISO 2469, Paper, board and pulps—measurement of diffuse reflectance factor. ISO, Geneva

31. Holopainen S, Manoocheri F, Laurila M, Ikonen E (2006) Goniofluorimeter for spectrum quantum yield measurements. In: 5th Oxford Conference on Spectrometry, NPL website. Queens Printer for Scotland, Edinburgh, pp 15–19
32. Zwinkels JC (1989) *Textile Chem Colorist* 21:23
33. American Society for Testing and Materials (2000) Standards on color and appearance measurement, 6th edn. ASTM, West Conshohocken, PA
34. Zwinkels J, Gignac D (1991) *Appl Opt* 30:1678
35. Zwinkels J, Gauthier F (2003) *Proc SPIE* 4826:70
36. Zwinkels J, Gauthier F (1999) *Anal Chim Acta* 380:193
37. Minato H, Nanjo M, Nayatani Y (1983) *Color Res Appl* 8:238
38. Burns RA, Clarke FJJ, Verrill JF (1980) *Proc SPIE* 234:48

**Part III**  
**Time Resolved Fluorometry**

# Time-Resolved Fluorometry: Typical Methods, Challenges, Applications and Standards

Nikolai V. Tkachenko · Helge Lemmetyinen (✉)

Department of Chemistry and Bioengineering, Tampere University of Technology,  
P.O. Box 541, 33101 Tampere, Finland  
*helge.lemmetyinen@tut.fi*

<b>1</b>	<b>Introduction</b> . . . . .	195
<b>2</b>	<b>Principles of Time-Resolved Fluorometry</b> . . . . .	196
<b>3</b>	<b>Typical Methods</b> . . . . .	200
3.1	Direct Time-Resolved Measurements . . . . .	201
3.2	Time-Correlated Single Photon Counting . . . . .	201
3.3	Modulation or Frequency Domain Method . . . . .	207
3.4	Streak Camera . . . . .	208
3.5	Up-Conversion . . . . .	209
<b>4</b>	<b>Comparison of the Methods</b> . . . . .	212
	<b>References</b> . . . . .	214

**Abstract** The ability of fluorescence to obtain temporal information on chemical and physical processes in molecules and supramolecular systems is of major importance. A time resolution of a few tens of picoseconds can nowadays be easily achieved by pulse and phase fluorometries, and the time resolution can be extended to femtosecond phenomena by more recent techniques based on fluorescence up-conversion.

In this chapter the most common methods used in time-resolved fluorometry will be discussed. The purpose is to introduce the techniques and highlight their application range, typical problems to be solved and the limitations imposed by each method.

**Keywords** Direct measurements · Fluorescence kinetics · Phase of frequency domain method · Streak camera · Time-correlated single photon counting · Up-conversion

## 1 Introduction

Two main directions in advancing emission spectroscopy techniques during the past few decades have been time resolution and sensitivity. The latter has focused on studies of smaller and smaller amounts of substance and has reached the single molecule limit [1, 2]. The former was driven by the desire to investigate the dynamics of the most fundamental processes caused



by interaction of light with matter, and has progressed to a new scientific direction called femtochemistry [3]. Nowadays, time-resolved fluorometry can solve a wide range of problems extending in time to femtosecond phenomena and scaling in space to a single molecule.

In this chapter the most common methods used in time-resolved fluorometry will be discussed. The purpose is to introduce the techniques and highlight their application range, typical problems to be solved and the limitations imposed by each method. Also this chapter does not pretend to provide complete information on the subject, which is covered by a number of books already published [4–6].

## 2 Principles of Time-Resolved Fluorometry

Absorption of a photon by a molecule triggers a chain of intramolecular processes, which are typical for photoreactions. As a simple example let us consider a scheme nominated as a Jablonski diagram and presented in Fig. 1. It shows typical processes found in organic dye molecules upon photoexcitation. The initial electronic state of the molecule is the ground singlet state,  $S_0$ . After excitation (by a photon with energy  $h\nu_{ex}$ ) the molecule enters a new energetic state. In the scheme this state is the first excited singlet state,  $S_1$ . The excited singlet state has numerous vibrational and rotational modes, which are indicated by thinner lines at slightly higher energies. Typically the absorption maximum of dye molecules is at a wavelength slightly shorter (at high energy) than that corresponding to the energy differences between the involved electronic states. This indicates that vibrational sublevels are involved in the transition from the ground to the excited state. In the scheme an arrow

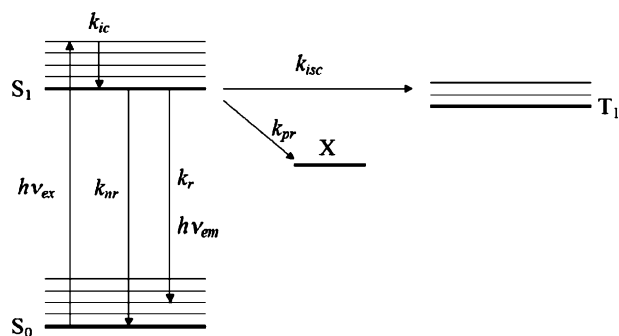


**Fig. 1** Jablonski diagram presenting the relaxation of the photoexcited ( $h\nu_{ex}$ ) first singlet state ( $S_1$ ). The initial state is the singlet ground state ( $S_0$ ); the excitation relaxation products are the triplet excited state ( $T_1$ ) and an inter-chromophore interaction product ( $X$ ). See text for details

upwards marks this transition from the lowest vibrational level  $S_0$  to one of the sublevels above  $S_1$ .

The vibrational modes of the dye interact efficiently with vibrational modes of the environment, resulting in a fast relaxation to the lowest vibrational sublevel of the electronically excited molecule. The short arrow in the scheme indicates this process and has a rate constant of  $k_{ic}$ . Typically this relaxation lasts less than a picosecond. Relaxation of the electronically excited state is slower than the vibrational relaxation, since the energy gap between the initial and final states is much bigger and all this energy must be withdrawn at once. The molecule can relax by emitting a photon,  $h\nu_{em}$ . The rate constant of this process is called the radiative rate constant,  $k_r$ . Alternatively, it can relax non-radiatively, which is indicated by the rate constant  $k_{ic}$  in the scheme. In addition to the relaxation to the ground state, an intersystem crossing may occur, yielding the triplet excited state with the rate constant  $k_{isc}$ .

The reactivity of many compounds is enhanced when the molecule is excited. There are also a few classes of reactions or processes which happen exclusively in excited states. The most important examples of such processes are excited state energy transfer, formation of exciplex and excimer, and photoinduced electron transfer (PET). The product of such a reaction is denoted in the scheme as  $X$  and the corresponding rate constant is  $k_{pr}$ . This reaction is an additional quenching mechanism of the excited state, and often it is the focus of investigation, e.g. when PET is the subject of study. In this case the reaction rate,  $k_{pr}$ , is the parameter to be determined. To illustrate how this can be achieved with the help of time-resolved measurements, let us first consider the excited state relaxation in the absence of additional quenching processes. Let us also assume that the thermal relaxation is much faster than all other reactions, so that one can consider the molecule to be in the lowest vibrational level of the electronically excited state right after the excitation. Then the relaxation rate of the excited state is the sum of rates

$$k_0 = k_r + k_{ic} + k_{isc} . \quad (1)$$

The rate of relaxation of the population,  $n$ , of the excited molecules is

$$dn/dt = -k_0 n . \quad (2)$$

This equation is also called the rate equation. Solution of the equation is a mono-exponential decay

$$n(t) = n(0) \exp(-k_0 t) , \quad (3)$$

where  $n(0)$  is the excited state population at  $t = 0$  (which is usually assumed to be the time of the excitation, thus  $n(t) = 0$  at  $t < 0$ ). The lifetime of the excited state is  $\tau_0 = k_0^{-1}$ .

The intensity of the emission is proportional to the population of the excited state; therefore the emission will decay exponentially<sup>1</sup>

$$I(t) = I(0) \exp(-k_0 t). \quad (4)$$

One may notice that even if the radiative rate constant is  $k_r$ , the emission decays with the rate constant  $k_0 = k_r + k_{ic} + k_{isc}$ . From the point of view of the emission efficiency, the rates of non-radiative decay ( $k_{ic}$ ) and intersystem crossing ( $k_{isc}$ ) are losses, and the emission quantum yield is

$$\Phi = k_r/k_0 = k_r/(k_r + k_{ic} + k_{isc}). \quad (5)$$

The additional photoreaction,  $S_1 \rightarrow X$ , increases the relaxation rate of the excited state, so that Eq. 2 reads

$$dn'/dt = -(k_0 + k_{pr})n'. \quad (6)$$

The solution of the equation is again a mono-exponential decay

$$n'(t) = n'(0) \exp[-(k_0 + k_{pr})t], \quad (7)$$

and the corresponding emission decay is

$$I'(t) = I'(0) \exp[-(k_0 + k_{pr})t], \quad (8)$$

where the decay rate constant is

$$k_q = k_0 + k_{pr}. \quad (9)$$

Comparing the two decay rate constants, with and without quenching reaction, one can calculate the rate of the reaction of interest,  $k_{pr} = k_q - k_0$ .

If the same number of molecules are excited in the presence and absence of the quenching reaction, the initial populations are the same,  $n(0) = n'(0)$ , and the initial emission intensities are the same,  $I(0) = I'(0)$ . This makes time-resolved measurements different from steady-state measurements, where the detected emission intensity will be lower in the presence of the quenching reaction. The quantum yield of the steady-state emission in the case of quenching is

$$\Phi' = k_r/(k_0 + k_{pr}). \quad (10)$$

The effect of the photoreaction on the time profile of the emission decay and on the steady-state spectra is illustrated in Fig. 2, where the rate constants were assumed to be  $k_0 = 0.2$  and  $k_{pr} = 0.8$  (arbitrary time units). It is also worth noticing that the emission intensities have different meanings in the case of the time-resolved and spectrum measurements. For the time-resolved measurements the intensity is the number of photons per unit time, whereas

<sup>1</sup> Formally speaking, accounting for all the photons emitted by the sample the emission intensity measured as number of photons per unit time is  $I(t) = k_r n(t) \exp(-k_0 t)$ . The total number of emitted photons is the integral of  $I(t)$  from zero time to infinity, which gives  $N_{ph} = k_r n(0)/k_0$ . The emission quantum yield is  $\Phi = N_{ph}/n(0) = k_r/k_0$ , which is Eq. 5.

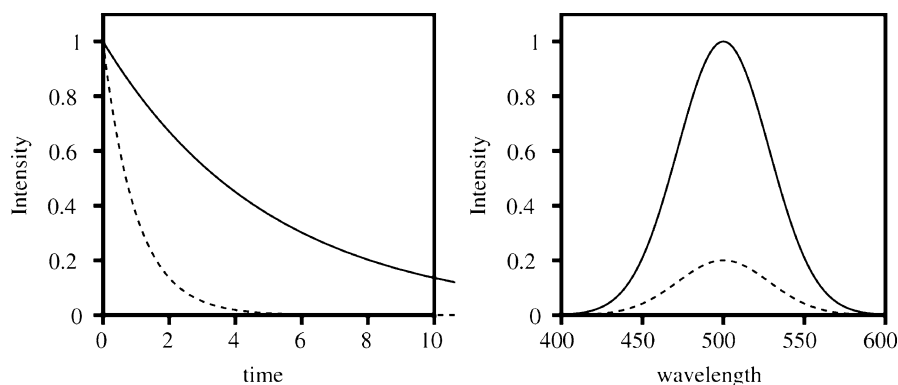


**Fig. 2** Fluorescence decays (*left*) and steady-state fluorescence spectra (*right*) of a sample in the absence (*solid lines*) and in the presence (*dashed lines*) of a quenching reaction,  $S \rightarrow X$ . The reaction rate constants are  $k_0 = 0.2$  and  $k_{pr} = 0.8$

in the case of the spectrum measurements the intensity is the number of photons per unit wavelength. However, both intensities come to a common denominator when the total number of photons is calculated. For the time-resolved measurements this is given by integration over time, whereas for the spectrum measurements it is over wavelength. Both integrals give the total number of photons.

From a practical point of view, one can measure the fluorescence decay profile of the compound in conditions where the excited state relaxes via natural pathways (without additional quenching reaction). This corresponds to the decay marked by the solid line in Fig. 2. Then the measurement is repeated in conditions where an activating additional photoreaction takes place, e.g. adding an electron acceptor to create PET. This will result in a decay marked by the dashed line in Fig. 2. Using a fitting algorithm the lifetimes of the fluorescence can be calculated for the first,  $\tau_0$ , and second,  $\tau_q$ , experiments, and the rate constant of the reaction of interest can be calculated as  $k_{pr} = \tau_q^{-1} - \tau_0^{-1}$ , in accordance with Eq. 9.

Based on the results of the steady-state fluorescence measurements one can calculate the ratio of the rate constants  $k_q/k_0 = \Phi/\Phi'$ , but in order to obtain the rate constant of the reaction of interest one still needs to know either  $k_0$  or  $k_q$ , then  $k_{pr} = \tau_0(\Phi/\Phi' - 1)$ . In other words, for the considered example the time-resolved measurements provide all the information needed to obtain the rate constant of the reaction, whereas steady-state measurements give only a relative estimation of the reaction rate. A similar strategy can be used to study many different problems associated with excited state photochemistry and photophysics.

The required time resolution of fluorescence decay measurements depends on the problem at hand. The vibrational relaxation and internal conversion in organic chromophores and thermal relaxation of hot carriers in semicon-

ductor structures are examples of processes that may take less than 100 fs. The primary photoreactions in natural photosynthesis, such as the energy transfer in an antenna subsystem and the primary charge separation, and intramolecular exciplex formation are examples of reactions taking place in picosecond and subpicosecond timescales. The typical lifetime of the singlet excited state of organic dyes is in the nanosecond time domain, e.g. for anthracene, rhodamine, coumarin, phthalocyanine etc. Thus, one can find different kinds of photoinduced reactions in a subnanosecond time domain for these chromophores: e.g. intra- and intermolecular charge separation, energy transfer and exciplex formation. For some systems the lifetime of the excited singlet state can fall into a microsecond timescale, e.g. for metal ions in a solid matrix. Then a sufficient time resolution of the fluorometer can be in the submicrosecond time domain.

### 3 Typical Methods

Similar to the instruments used for steady-state emission spectroscopy, two main components of time-resolved fluorometers are the source of the excitation light and the emission detection subsystem, although these two components must have certain specific features to attain the desired time resolution. A simplified scheme of an instrument for time-resolved emission measurements is presented in Fig. 3. For most of the time-resolved methods the excitation light source is a pulsed source. The width of the pulse is one obvious factor limiting time resolution. The time response of the detection system is usually the second limiting factor.

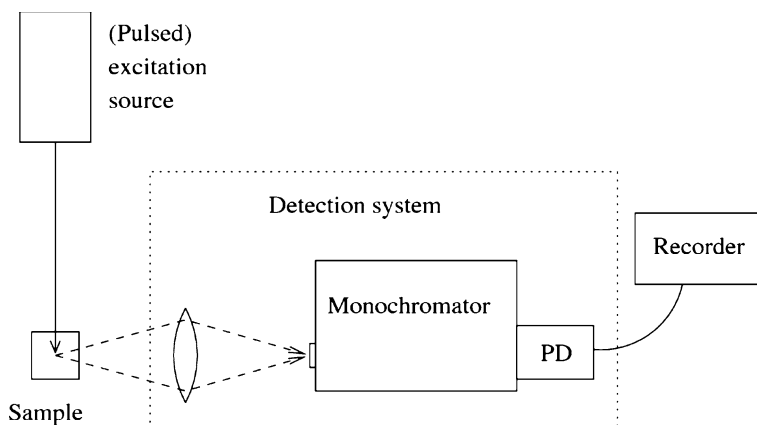


**Fig. 3** Generic scheme for time-resolved emission measurements. PD: photodetector; L: emission collection component, e.g. a lens

Using a pulsed excitation source, e.g. a pulsed laser, and a photodetector, e.g. a fast photodiode, one can monitor the emission decay after a short pulse excitation at a wavelength selected by the detection monochromator. This is the most straightforward or direct method to carry out time-resolved emission decay measurements. In the endless race for speed and higher sensitivity, new methods were developed. The difference between the methods comes from the choice of the excitation sources, types and methods used to detect (and record) the signal.

### 3.1

#### Direct Time-Resolved Measurements

The most straightforward approach to the problem is to use the scheme presented in Fig. 3 with a photodetector capable of measuring fast variations of the light intensity. This can be a photomultiplier tube (PMT) or a photodiode, although the former is preferred as the PMTs are generally more suitable for low light intensity measurements. The excitation source can be a pulsed laser.

Potentially a single-shot excitation is enough to record the emission decay profile. However, to achieve a reasonable signal-to-noise ratio the emissions should be rather strong, which requires high emission quantum yields and high densities of the emitting centres in the sample. If this is not the case the measurements can be repeated a few times, summing all individual decays to improve the signal-to-noise ratio.

The monitoring spectrum range of the method depends on the type of photodetector used. PMTs can be used in the UV, visible and near-IR spectral ranges (roughly 200–1000 nm). At shorter wavelengths photodiodes can replace PMTs. Silicon diodes can operate up to 1100 nm and GaAs diodes up to 1700 nm.

Pulsed lasers are typical sources of excitation light for this method. There is a great choice of pulsed lasers, which can produce pulses of a few nanoseconds and much shorter in a wide spectrum range. The actual time resolution-limiting components of the method are the photodetector and the transient recorder, which stores the signal. The typical time resolution of a fast PMT is a few nanoseconds, which seems to be a reasonable time-resolution limit for the instruments of this type. Although it is possible to extend the time resolution to the subnanosecond time domain, the price and complexity of the system increases drastically making it less attractive compared to other methods.

### 3.2

#### Time-Correlated Single Photon Counting

In order to achieve the highest sensitivity and accuracy in optical measurements, photon counting methods can be employed. In application to time-

resolved emission spectroscopy the single photon detection strategy means that instead of measuring light intensity, which is a cooperating effect of many photons, one needs to deal with photon statistics. In particular, one can measure the distribution of the delay times of emission photons relative to the excitation pulse. This is implemented in a method called time-correlated single photon counting (TCSPC). In terms of the scheme presented in Fig. 3, the photodetector of the TCSPC instrument consists of a PMT operating in photon counting mode and a time-to-amplitude converter (TAC). An emission photon at the PMT entrance generates an electric pulse on its output. The role of the TAC is to measure the delay time between the excitation pulse and the pulse produced by the emitted photon. The TAC operates as a pulse control generator of linearly rising voltage. It converts the time delay between the excitation pulse (start pulse) and the pulse produced by the photon (stop pulse) to a potential signal, whose value is proportional to the delay between pulses (thus the name: time-to-amplitude converter).

A multichannel analyser (MCA) is used as the recorder (Fig. 3). The analyser has a memory—a multichannel array, which collects the delay statistics. Each channel corresponds to a short voltage interval in increasing order. For example, if the intervals are 0.1 V and the input signal is 1.3 V, the signal is attributed to channel 13 and the value in this channel is incremented by one. If the output signal of the TAC is 4.3 V, the channel 43 is incremented by one. Initially all the channels are zeroed. Since the TAC output signal is proportional to the delay time between excitation pulse and emitted photon, the channels collect a number of photons detected at certain delays after the excitation.

Figure 4 presents snapshots modelling the emission decay measurements by the TCSPC method. The measurements can be viewed as an experiment with a single molecule. A negligibly short pulse excites the molecule and the interest is in the probability that it will emit a photon at delay time  $\Delta t$ . In the case of the simple model considered in Sect. 2, this probability is given by Eq. 4 or Eq. 8, e.g. it is decaying exponentially

$$p(\Delta t) \sim \exp(-\Delta t/\tau), \quad (11)$$

where  $\tau$  is the lifetime of the excited state. In accordance with the statistical nature of the problem, one cannot predict when the photon will be emitted after a particular excitation pulse. After the first excitation pulse the photon was detected at a delay time corresponding to channel 6 (top diagram in Fig. 4). Clearly, no reliable conclusion can be drawn about the excited state lifetime yet. The next diagram shows the result after repeating the experiments a few more times and collecting 20 photons. Still the picture does not show what the emission decay may look like. After collecting 500 photons the diagram starts to resemble an exponential decay. When 10 000 photons are collected the exponential decay profile becomes apparent. The exponential

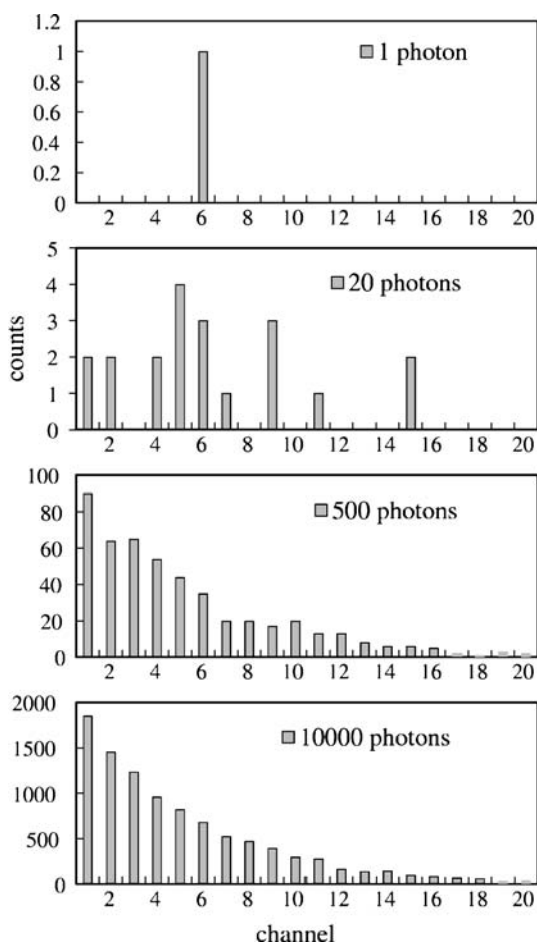


**Fig. 4** Snapshots of emission decay measurements using the TCSPC method. The singlet excited state lifetime corresponds to five channels. The plots show (from top to bottom) the state of MCA after collecting 1, 20, 500 and 10 000 emission photons

fitting of the decay is shown in Fig. 5. It gives a lifetime of  $4.9 \pm 0.2$ , which is reasonably close to the actual lifetime of 5.

There are a few important points to notice from this example. First of all, only one photon is detected after each excitation pulse. If there are more photons, as may happen when many molecules are excited at the same time, the second and following photons are lost. Therefore the experiments must be arranged in such way that the probability to see more than one photon after each excitation pulse will be negligibly small.<sup>2</sup>

<sup>2</sup> This means that for most of the excitation pulses there will be no detected photons at all. Typically the counting rate should be 100 times lower than the excitation rate to reduce so-called peak-up distortions to a level lower than 1% (see example 8.1 in [6]).



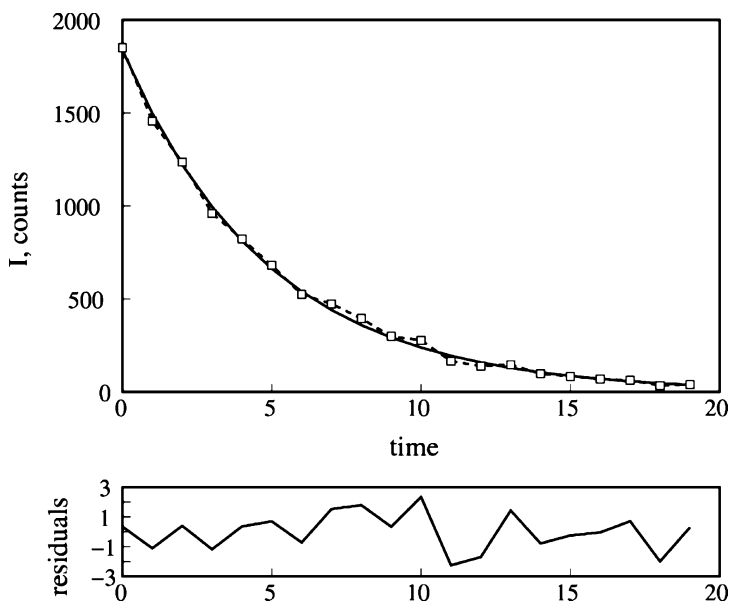


**Fig. 5** Exponential fit of the emission decay presented in the bottom plot of Fig. 4 (measured by the TCSPC method). Experimental data are indicated by the *squares* connected by a *dashed line*. The *solid line* represents the fitting curve. The *bottom plot* shows the weighted residuals of the fit

Secondly, TCSPC measurements rely strongly on repeating the excitation many times. Referring to the example considered above (Fig. 4), in order to collect 10 000 photons one has to excite the molecule at least 10 000 times. In actual measurements, the instruments may have more than 1000 channels, the desired signal can be 10 000 counts at maximum (to achieve better signal-to-noise ratio), and the counting rate can be selected to 1/100 of the excitation rate to avoid pile-up distortions. In such conditions the sample has to be excited  $10^9$  times (in order of magnitude) during the measurements [6]. In order to perform that many excitation cycles the excitation pulse rate must be relatively high. A typical range of the excitation frequency for TCSPC measurements is 1–40 MHz, and the typical signal collection time is from a minute to tens of minutes.

Thirdly, since not more than one photon has to be detected per excitation pulse, the excitation pulse energy can be relatively low. Typical pulse energies for TCSPC instruments are less than 1 nJ, but depending on the sample under study it can be lower than picojoules. Not only the excitation pulse energy, but also the sample concentration can be very low. In the extreme case one can study single molecules. For single molecule time-resolved spectroscopy applications, the TCSPC instruments are combined with confocal microscopes and the samples are prepared at such low concentrations that a single molecule

can be excited. It was possible to collect a few thousand counts during a 10-s measurement and calculate the lifetimes of individual dye molecules embedded in a thin polymer film [7].

The utilization of the photon counting technique makes the TCSPC method a very accurate tool. Practically the only source of noise and uncertainty is the quantum statistics of photons. The quantum noise follows Poisson statistics, and its relative contribution decreases as the number of counts increases. For example, at a signal intensity of 10 000 counts (typical for TCSPC measurements) the noise level is just 1%. Therefore the emission decay parameters, e.g. lifetimes, can also be determined with high accuracy, i.e. a few percent or better.

The time resolution of the TCSPC method is typically a few times better than that of the direct emission intensity measurements (Sect. 3.1) under otherwise equal conditions. This is due to the fact that for direct measurements the time resolution is determined by the signal rise and decay times of the detector, but for the TCSPC method the time resolution depends on so-called transient time spread, which specifies deviation in response delay from pulse to pulse and is usually a few times shorter than the signal rise time. Time resolution of 50–100 ps is widely available for TCSPC instruments.

For a long time, PMTs were the only detectors suitable for TCSPC measurements. The principal feature of PMTs is their ability to detect single photons. An important modification of PMTs is the microchannel plate (MCP) photomultiplier. These devices were developed for high-speed applications and can reach a time resolution of a few tens of picoseconds when used in the TCSPC mode. The spectrum range of monitoring wavelength depends on the type of photocathode and covers the UV, visible and near-IR parts of the spectrum (200–950 nm).<sup>3</sup>

Recently, new types of avalanche photodiodes (APDs) were developed which can also be used in the single photon mode. These devices can be used in the visible and near-IR ranges (400–1000 nm), with time resolution approaching 100 ps in the TCSPC mode.

The most important requirements imposed on the excitation sources are reasonably short pulse widths (typically a few tens of picoseconds) and high repetition rate (preferably 1–40 MHz), but the pulse energy or average power can be relatively low. Low-pressure pulsed N<sub>2</sub> or H<sub>2</sub> lamps coupled with a monochromator were a usual excitation source in TCSPC instruments a few decades ago. A nanosecond time resolution was a common feature of these devices. The invention of pulsed mode-locked lasers and MCP PMTs made possible time resolution as short as 25 ps (as specified for the Hamamatsu R3809U series of MCP PMTs). Recently, pulsed semiconductor laser diodes and similar light-emitting devices were developed and they can replace the

---

<sup>3</sup> There are PMTs with the spectrum sensitivity extended to 1100 nm. However, they require cooling of the photocathodes to achieve an acceptable dark counting rate.

mode-locked laser systems without significant compromise in time resolution, allowing resolution as short as 60 ps to be obtained.

An example of routine lifetime measurements using a TCSPC instrument is presented in Fig. 6. The fluorescence of porphyrin in solution can be quenched by addition of quinone. The quenching mechanism is the PET from the porphyrin donor to the quinone acceptor. First, the sample was a pure porphyrin solution (top decay curve in Fig. 6), and using a mono-exponential fit the lifetime of the porphyrin singlet state was determined to be  $\tau_0 = 9.23 \pm 0.02$  ns. An addition of quinone to the porphyrin solution at a concentration of 5 mM decreased the lifetime to  $\tau_q = 5.98 \pm 0.02$  ns. Following the procedure described in Sect. 2 one can determine the quenching rate to be  $k_{pr} = \tau_q^{-1} - \tau_0^{-1} = 5.89 \pm 0.3 \times 10^8$  s<sup>-1</sup>. In this particular case the quenching reaction is diffusion controlled; therefore, the increase in the quinone concentration results in a proportional increase in the quenching rate, but the decay law stays mono-exponential.

The plots in the left frame of Fig. 6 show the decrease in the intensities of the steady-state fluorescence. This figure is the real life example of the simulation presented in Fig. 2, illustrating correlation between time-resolved and steady-state measurements.

The sharp short pulse in Fig. 6 shows the instrument response function, which was measured by monitoring scattered excitation pulses. The half width of the instrument response was 90 ps for these measurements. The instrumental response is used during data fitting to account for the limited time resolution of the instrument and to improve the quality of the fit.

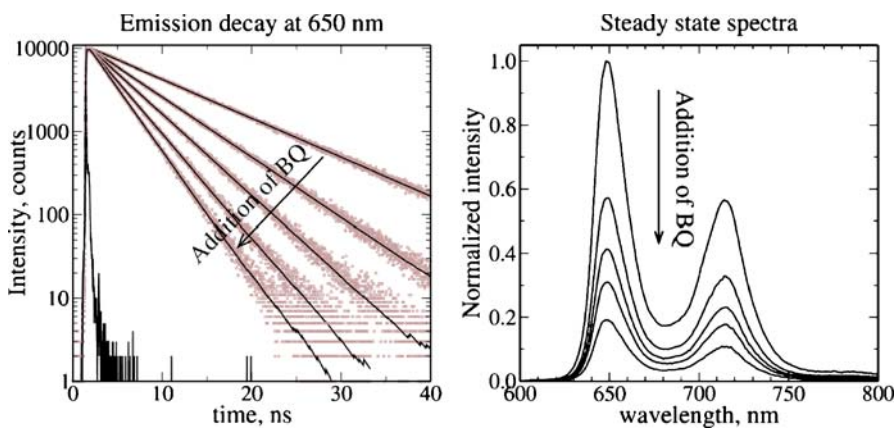


**Fig. 6** Fluorescence decays measured by the TCSPC method (*left*) and steady-state fluorescence spectra (*right*) of porphyrin solution in the absence of benzoquinone (BQ) (the *top curve*) and after successive additions of 5 mM BQ to the sample

### 3.3 Modulation or Frequency Domain Method

This method relies on the mathematical fact that any time-dependent function,  $f(t)$ , has an equivalent representation in frequency domain,  $F(\nu)$ . This means that for any function  $f(t)$  there is unique function  $F(\nu)$ , and vice versa. The transition from time to frequency domain is done by Fourier transform, and from frequency to time domain by inverse Fourier transform.

Formally speaking, instead of using pulse excitation and measuring the time response of the sample,  $f(t)$ , one can use sinusoidal excitation, scan the frequency,  $\nu$ , and measure the frequency response of the sample,  $F(\nu)$ . Then, using the inverse Fourier transform one can convert the frequency domain measurements,  $F(\nu)$ , to the time domain measurements,  $f(t)$ .

The scheme of the instrument for the frequency domain measurements is similar to the one shown in Fig. 3, except the excitation source is a continuous light source modulated at some frequency, and the recorder is a synchronous detector to record the frequency response of the sample. All other parts are similar to those of any other fluorometer. This is an advantage of the method, since it can be easily combined with steady-state fluorometry, opening the possibility to measure lifetimes with otherwise the same instrument. The measurements are carried out at a series of modulation frequencies. At each frequency two values are determined for the sample emission: the phase shift relative to the excitation and the modulation amplitude, as illustrated in Fig. 7.

On the downside of this approach is the fact that although the mathematically inverse Fourier transform is well defined it requires accurate knowledge of the function  $F(\nu)$  in an infinite range of frequencies,  $\nu$ . In a limited frequency range and/or accuracy of the frequency response measurements the

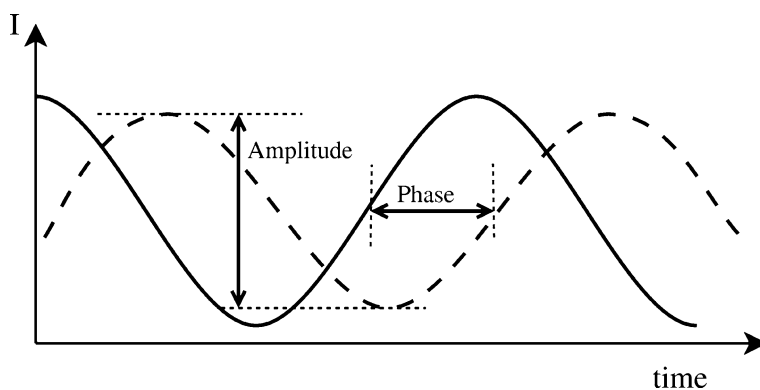


**Fig. 7** Frequency domain emission measurements: excitation (solid line) and emission (dashed line) time courses

inverse transform may become ill defined. Therefore, the analysis of the frequency domain measurements is usually reduced to the determination of the lifetime, which assumes an exponential decay in the time domain,  $f(t) \sim \exp(-t/\tau)$ . In more complex cases a biexponential decay model can be used, but still it implies strong limitations of the shape of function  $f(t)$ , and thus function  $F(\nu)$ .

A typical light modulation frequency range for the method is 1–300 MHz, which allows determination of lifetimes in the range from subnanoseconds to milliseconds. When acousto-optic or electro-optic modulators are used the excitation source can be a lamp coupled with a monochromator. Then the excitation wavelength can be tuned in a wide spectrum range, which is another advantage of the method.

The sensitivity of the method is also compatible with that of steady-state fluorometers, since there are no additional losses due to the modulation in the detection part of the system. An apparent disadvantage of the method is that the lifetime is difficult to monitor in real time. Additionally, if the emission time profile of the sample is complex, the data analysis may appear to be a complex mathematical problem with no unambiguous solution.

### 3.4

#### Streak Camera

Streak cameras are a type of special electronic tube developed to achieve as short as possible time resolution. They utilize photocathodes to convert a photon flow to an electron flow. If the photon flow changes in time, then the electron flow after the photocathode also changes in time. To measure the time dependence of the electron flow, the electron beam is swept over a phosphorus screen. When the electrons hit the screen they produce light with an intensity proportional to the density of the electrons. As a result, the time dependence of the input photon flow is converted to spatial light dependence on the streak camera screen. This spatial dependence can now be measured using, e.g., a CCD detector, and analysed.

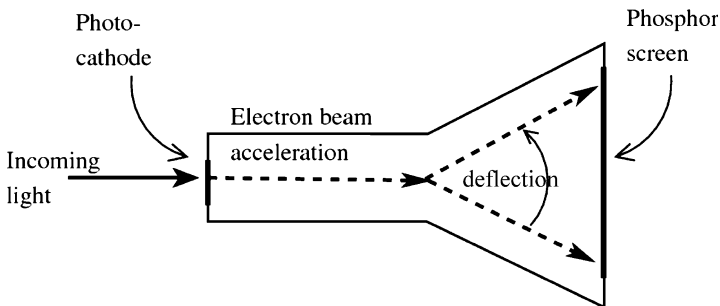


**Fig. 8** Scheme of a streak camera

Accelerating the electron beam generated by the photocathode and then passing it for high-speed deflection can achieve a system with high time resolution in the streak camera. In a single-shot regime this allows subpicosecond time resolution to be achieved.<sup>4</sup> However, if signal averaging has to be performed, the limiting step becomes the trigger jitter, and the time resolution is reduced to a few picoseconds at best.

Unlike PMTs, streak cameras have no amplification of the electron beam, although there are special devices developed for spectroscopy applications that combine a streak camera with an image intensifier (MCP amplifier). These devices have sensitivity approaching that of photon counting devices.

In addition to high time resolution, streak cameras have an advantage of being able to measure time and wavelength dependences at the same time. This is achieved by passing the light beam through a polychromator, which spreads the beam across the photocathode in a direction perpendicular to the direction of the electron beam deflection. As a result, a two-dimensional image is formed on the camera output screen with one direction presenting the time and the other the wavelength dependence.

The spectrum range of streak cameras depends on the type of photocathode used. From this point of view they are similar to PMTs. The typical sensitivity range covers the near-UV–visible–near-IR part of the spectrum (200–950 nm).

Using streak cameras one can carry out single-shot experiments which, however, require a relatively high concentration (or density) of emitting centres and relatively high excitation energy. In single-shot mode the cameras provide the best time resolution. Also most spectroscopy-oriented cameras are designed to be able to average many excitation pulses. This reduces the requirements to sample concentration and/or excitation density, but limits the time resolution to roughly 10 ps.

### 3.5

#### Up-Conversion

All previously discussed methods reach the limit of model electronics in time resolution, but there are reactions which take place in subpicosecond or even shorter time domains. These reactions can be studied using femtosecond lasers and optical methods to time-resolve them. In emission spectroscopy the optical gating methods, and in particular an up-conversion technique, are widely used for this purpose [8]. The basic principle of optical gating is to use short light pulses and non-linear optical phenomena to gate the sample emission. The gating window is shifted in time scanning the emission profile, which is then detected by a photodetector with a low time resolution.

The detection part of an instrument utilizing the up-conversion method is shown in Fig. 9. The key component of the scheme is the non-linear crystal

---

<sup>4</sup> The FESCA-200 (Hamamatsu Photonics K. K.) camera has a time resolution of 200 fs.

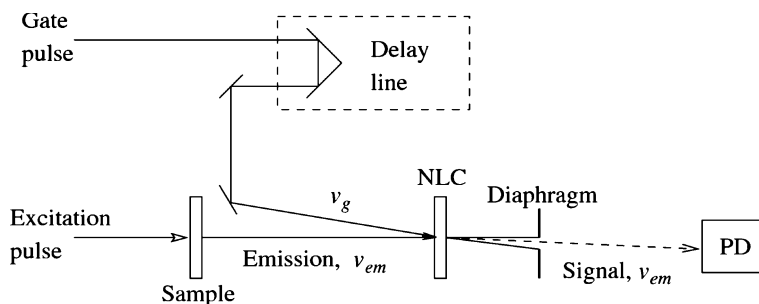


**Fig. 9** Optical scheme of the up-conversion method. NLC: non-linear crystal; PD: photodetector

(NLC), which receives emission at frequency  $\nu_{em}$ , gate pulses at frequency  $\nu_g$ , and generates the signal at sum frequency

$$\nu_s = \nu_{em} + \nu_g. \quad (12)$$

The signal intensity is proportional to the product of the gate pulse and emission intensity at the gating delay. The gate pulse intensity is kept constant during the measurements. Moving the delay line the gate pulse interacts with emission (in NLC) at different delay times; therefore, the signal intensity is proportional to the emission intensity at the delay time determined by the position of the delay line. Since the actually measured signal is shifted up in frequency by value  $\nu_g$ , the method is called up-conversion.

The photodetector does not need to resolve the signal in time, since after gating only the average signal amplitude is of interest. Therefore, almost any sensitive enough detector can be used in this method. To avoid light at all undesired wavelengths, colour-rejecting filters and monochromators are usually used in front of the detector.

The delay line is formed by a right-angle reflector placed on the translation line. To change the delay time, e.g. by  $\Delta t = 1$  ps, the translation line displacement must be  $d = c\Delta t/2 = 1.5$  mm. Moving the translation line with small steps, one can scan the whole emission decay profile.

A typical flow of measurements starts from the determination of a suitable timescale (how long the delay line must go), the starting point (at which position of the delay line the gate pulse will match the beginning of the emission), and a suitable time step (delay line displacement from point to point). Then the measurements of the signal intensity are repeated at each delay time to provide the emission decay time profile.

The time resolution of the method depends on the pulse width, both of the excitation and the gate, and on group velocity dispersion, which leads to a pulse broadening when a short light pulse propagates in condensed media. The latter implies some limitations on the samples and optics used. The sample must be as thin as possible to achieve the best time resolution. The lenses

used in the optical scheme must be as thin as possible, as well, or replaced by mirrors. To achieve a 100–200 fs time resolution one should use a laser system generating 50-fs pulses or shorter, and the preferable sample thickness is 1 mm or thinner [6].

Short laser pulses are widely available for Ti:sapphire lasers operating in the self mode-locking regime. The pulses from Ti lasers can be used directly for up-conversion measurements if the laser wavelength (tuneable in the range 750–1000 nm) is suitable for excitation. Alternatively, the second harmonic (380–500 nm) can be used for the excitation and the fundamental harmonic for gating. The excitation wavelength range can be further extended by using a more complex laser system combining Ti:sapphire amplifiers and optical parametric amplifiers (OPAs), which are able to generate pulses at virtually any wavelength from UV to IR.

The sensitivity range of the photodetector basically determines the available emission wavelength range; also one has to keep in mind that the signal wavelength is shifted to a shorter wavelength. For example, if the emission and the gate pulse wavelengths are  $\lambda_{em} = 600$  nm and  $\lambda_g = 800$  nm, respectively, the signal wavelength is, according to Eq. 12,

$$\lambda_s = (\lambda_g^{-1} + \lambda_{em}^{-1})^{-1} = 343 \text{ nm} . \quad (13)$$

In other words, for the emission in the visible part of the spectrum the signal detection wavelength is shifted to the UV range, where PMTs can be used successfully.

Similarly to the TCSPC method, the up-conversion methods requires repeating excitations of the sample many times to collect signals at a series of delay times and to achieve a desired signal intensity (signal-to-noise ratio) at each delay time. Also similarly to the TCSPC method, photon counting can be used to determine the signal intensity at each delay time. From this point of view the up-conversion method combines high time resolution with high accuracy of measurements.

An example of the up-conversion study of a PET reaction is presented in Fig. 10. The studied compound is a covalently linked porphyrin–fullerene dyad [9]. Photoexcitation at 420 nm (second harmonic of a Ti:sapphire laser) populates the second singlet excited state of the porphyrin chromophore, which decays rapidly ( $< 200$  fs) to the first singlet excited state. The emission of the sample is monitored at 605 nm, which is the porphyrin fluorescence wavelength. The fluorescence lifetime of the reference porphyrin compound was a few nanoseconds, but for the dyad it is reduced to 2 ps only. This fast quenching of the porphyrin singlet excited state is attributed to the rapid electron transfer from porphyrin to the fullerene moiety. The electron transfer was also confirmed by transient absorption pump–probe measurements, where specific spectral features of the charge separated state were identified. In this particular case the emission decay time constant is the time constant



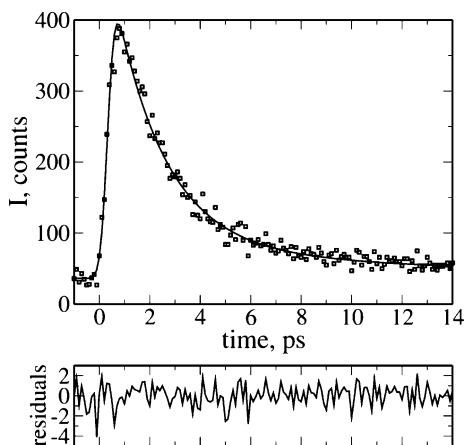


**Fig. 10** Fluorescence decay of porphyrin chromophore (at 650 nm) in a porphyrin-fullerene donor-acceptor dyad measured by the up-conversion method

of the electron transfer reaction, since all other relaxation reactions of porphyrin are slower by three orders of magnitude.

The sensitivity of the up-conversion method is much lower than that of the TCSPC method, since only the photons emitted in a narrow time window of the gate pulse can be detected. Also there are some additional losses associated with the method, such as the efficiency of the non-linear crystal.<sup>5</sup> This is the price one has to pay for the high time resolution.

The up-conversion method is usually used to record emission decays at a single wavelength, since phase matching conditions for NLCs are sensitive to the wavelength. However, the method has been modified to enable measurements of time-resolved spectra [10]. This was achieved by using a thin (0.1 mm) crystal and long wavelength gating (1300 nm).

Although the up-conversion method is the most widely used optical gating technique, there are other non-linear optical phenomena that can be used for time-resolved emission measurements. For example, the optical Kerr effect can provide subpicosecond time resolution with proper selection of the Kerr media. The advantage of the optical Kerr effect is that it is not sensitive to the wavelength and allows one to measure time-resolved spectra [11, 12].

## 4 Comparison of the Methods

Probably the most widely used method for fluorescence decay measurements is TCSPC. It is relatively inexpensive, covers the timescales of interest for most

<sup>5</sup> An estimation of the method sensitivity can be found in [6].

organic dye compounds, and can be used in a wide spectrum range and with a very small amount of substance. This method can serve as a reference for other methods. The most important parameters for comparison and factors for selecting one or another method for time-resolved emission spectroscopy are the time resolution and timescale, excitation and emission wavelength range, and the sensitivity, which determines, e.g., the amount of substance required to conduct the measurements.

At present the fastest method available is the up-conversion method. It can routinely be used with time resolution up to 200 fs. After taking special measures to reduce the effects of group velocity dispersion, the time resolution can be improved a few times. The next fastest method is based on streak camera detection, which can provide better than 1 ps time resolution in single-shot experiments. In the case of repeating mode measurements (more practical for spectroscopy applications) the time resolution can reach 10 ps. The latter is a few times better than the best time resolution available for TCSPC instruments. For the TCSPC method the practically good result is at the level of 30–50 ps. From these three methods, TCSPC provides the best sensitivity and has the smallest demands of excitation source. The sensitivity of the best streak cameras approaches that of TCSPC instruments, being close to single photon detection. Still, streak cameras can hardly be used for single molecule time-resolved spectroscopy as TCSPC has been used, since in single molecule applications most of the excitation pulses are left without photon detection. This is the normal operation mode for the TCSPC method, but causes background noise collection in streak camera measurements.

The least sensitive method from those considered above is the up-conversion method. This is due to its gating nature—from all the emitted photons only those which fall in the time window of the gate pulse are detected. For example, if the emission lifetime is 10 ps, not more than 1% of photons will fall into the 100-fs window of the gate pulse and 99% of photons will be lost. For a 1-ns lifetime the number of lost photons increases to 99.99%. Therefore, if picosecond (or faster) time resolution is not required, other methods are preferred.

Frequency domain measurements are usually considered as an inexpensive replacement of the TCSPC method [13], since they do not require a high-repetition pulsed excitation source (which were rather expensive laser systems until the recent invention of ultra-short pulsed diode lasers), and can be used for lifetime measurements in the nanosecond to subnanosecond time domain. Theoretical estimations show that the frequency domain method can be as sensitive as TCSPC [14]. However, there are no reports on experimental single molecule studies using frequency domain techniques. Also, the TCSPC method has an advantage of direct measurement of the emission time profile, which becomes an important issue when the decay is multi-exponential or non-exponential in nature, as is the case in polymer films, for example [15, 16].

In some cases the high repetition rate of the excitation source can be a problem, for example when the emission lifetime is extended to a microsecond. Then the direct method is an inexpensive and easy to implement solution of the problem. In fact, traditional flash photolysis systems can be successfully used for this purpose.

From the point of view of the emission spectrum range, the direct, frequency domain, TCSPC and streak camera methods are rather equivalent—the most important factor is the sensitivity range of the photodetector. PMTs are available in the spectrum range of 200–950 nm, and in some cases up to 1100 nm. Also one has to keep in mind that the noise level (dark current or dark counting rate, depending on application) increases with extending the sensitivity to the red side of the spectrum. The up-conversion method differs from the others, since the actual wavelength of the measurements is shifted to the blue part of the spectrum relative to the emission. Using the up-conversion technique one can easily carry out measurements of a sample emitting at 1500 nm or longer wavelengths [17].

## References

1. Macklin JJ, Trautman JK, Harris TD, Brus LE (1996) *Science* 272:255
2. Vallee RAL, Marsal P, Braeken E, Habuchi S, De Schryver FC, Van der Auweraer M, Beljonne D, Hofkens J (2005) *J Am Chem Soc* 127:12011
3. Zewail AH (2000) *J Phys Chem A* 104:5660
4. Lakowicz JR (1999) *Principles of fluorescence spectroscopy*, 2nd edn. Kluwer/Plenum, New York
5. Valeur B (2002) *Molecular fluorescence: principles and applications*. Wiley-VCH, Weinheim
6. Tkachenko NV (2006) *Optical spectroscopy: methods and instrumentations*. Elsevier, Amsterdam
7. Maus M, Cotlet M, Hofkens J, Gensch T, De Schryver FC, Schaffer J, Seidel CAM (2001) *Anal Chem* 73:2078
8. Sash J (1988) *IEEE J Quant Electron* 24:276
9. Kesti TJ, Tkachenko NV, Vehmanen V, Yamada H, Imahori H, Fukuzumi S, Lemmetyinen H (2002) *J Am Chem Soc* 124:8067
10. Zhao L, Lustres JLP, Farztdinov V, Ernsting NP (2005) *Phys Chem Chem Phys* 7:1716
11. Kinoshita S, Ozawa H, Kanematsu Y, Tanaka I, Sugimoto N, Fujiwara S (2000) *Rev Sci Instrum* 71:3317
12. Schmidt B, Laimgruber S, Zinth W, Gilch P (2003) *Appl Phys B* 76:809
13. Booth MJ, Wilson T (2004) *J Microsc* 214:36
14. Philip J, Carlsson K (2003) *J Opt Soc Am A* 20:368
15. Gulbinas V, Chachisvilis M, Valkunas L, Sundström V (1996) *J Phys Chem* 100:2219
16. Kalinin S, Johansson LB-Å (2004) *J Phys Chem B* 108:3092
17. Dhaka VDS, Tkachenko NV, Lemmetyinen H, Pavelescu E-M, Suomalainen S, Pessa M, Aarsila K, Nordlund K, Keinonen J (2006) *J Phys D Appl Phys* 39:2659

# Practical Time-Resolved Fluorescence Spectroscopy: Avoiding Artifacts and Using Lifetime Standards

Noël Boens<sup>1</sup> (✉) · Marcel Ameloot<sup>2</sup> · Bernard Valeur<sup>3,4</sup>

<sup>1</sup>Department of Chemistry, Katholieke Universiteit Leuven,  
Celestijnenlaan 200f, bus 02404, 3001 Heverlee, Belgium  
*Noel.Boens@chem.kuleuven.be*

<sup>2</sup>BIOMED, Universiteit Hasselt, Agoralaan, Building D, 3590 Diepenbeek, Belgium

<sup>3</sup>CNRS UMR 8531, Laboratoire de Chimie Générale, CNAM, 292 rue Saint-Martin,  
75141 Paris Cedex 03, France

<sup>4</sup>Laboratoire PPSM, ENS-Cachan, 61 avenue du Président Wilson, 94235 Cachan Cedex,  
France

<b>1</b>	<b>Introduction</b> . . . . .	216
<b>2</b>	<b>Principles of Time and Frequency-Domain Fluorometries</b> . . . . .	217
2.1	Two Major Methods: Single-Photon Timing and Multifrequency Phase-Modulation Fluorometry . . . . .	217
2.2	Basic Equations for Time-Resolved Fluorescence in SPT and MPF . . . . .	217
<b>3</b>	<b>Artifacts and Remedies to Pitfalls</b> . . . . .	218
3.1	Introduction . . . . .	218
3.2	Inner Filter Effects . . . . .	219
3.3	Autofluorescence . . . . .	219
3.4	Polarization Effects. Magic Angle Configurations . . . . .	220
3.5	Color Effect . . . . .	221
3.6	Photobleaching Effects . . . . .	223
3.7	Deoxygenation . . . . .	223
3.8	Artifacts Specific to Pulse Fluorometry . . . . .	224
3.8.1	Pulse Pile-Up Effect . . . . .	224
3.8.2	Linearity of the Time Response of the TAC . . . . .	224
3.9	Artifacts Specific to Frequency-Domain Fluorometry . . . . .	224
<b>4</b>	<b>Fluorescence Lifetime Standards</b> . . . . .	225
4.1	Need for Lifetime Standards . . . . .	225
4.2	Criteria for the Choice of Fluorescence Lifetime Standards and Solvents . . . . .	225
4.3	Requirements for the Standardization of Lifetime Measurements . . . . .	226
4.4	Experimental . . . . .	227
4.5	Comparison of Accuracy of Lifetime Data Obtained by Time and Frequency-Domain Fluorometries . . . . .	228
4.6	List of Lifetime Standards . . . . .	230
<b>5</b>	<b>Concluding Remarks</b> . . . . .	231
	<b>References</b> . . . . .	231

**Abstract** In this chapter we describe how artifacts can be avoided in the two most commonly used time-resolved fluorometries, namely the single-photon timing and the multifrequency phase-modulation techniques. The most frequently encountered artifacts (inner filter effect, autofluorescence, polarization effects, color effect, photobleaching, deoxygenation, pulse pile-up, and linearity of the time response in the time-to-amplitude converter) are described in detail and remedies are presented to avoid these pitfalls. An extensive list of fluorescence lifetime standards is presented, which allows the spectroscopist to calibrate and test time-resolved instruments for systematic errors.

**Keywords** Frequency-domain fluorometry · Lifetime standard · Single-photon timing · Time-resolved fluorometry

### Abbreviations

cw	Continuous wave
FD	Frequency domain
MCP	Microchannel plate
MPF	Multifrequency phase-modulation fluorometry
SPT	Single-photon timing
TAC	Time-to-amplitude converter
TD	Time domain

## 1

### Introduction

Time-resolved fluorescence spectroscopy provides essential information for investigating the dynamics of photophysical, photochemical, and photobiological processes. The two principal methods commonly used for recording time-resolved fluorescence data are the single-photon timing technique [1, 2] (also called time-correlated single-photon counting) and multifrequency phase-modulation fluorometry [3, 4]. Both techniques yield essentially the same information and differ mainly in how the time-resolved fluorescence data are obtained, namely in the time domain versus the frequency domain.

Over recent decades, extraordinary progress has been made in both time-resolved fluorometries as a result of the use of high repetition rate (sub)picosecond lasers, microchannel plate (MCP) photomultipliers, and global data analysis software. However, reliable time-resolved fluorescence measurements are not straightforward to carry out because of the many potential pitfalls. As far as possible, it is preferable to eliminate these experimental distortions by experimental techniques rather than to correct for them in data analysis. The various artifacts in data collection and analysis, and the approaches to prevent or rectify them have been the subject of numerous contributions in the literature.

The aim here is to give the reader a good understanding of the most important artifacts encountered in time-resolved fluorometries together with

the precautions to avoid them or the remedies to amend them. Moreover, a list of fluorescence lifetime standards is provided. The use of such standards is imperative for evaluating the performance of time-resolved fluorescence instrumentation so that the experimental setup is properly tuned before running an experiment.

Data analysis will not be considered here because this topic is extensively discussed in Chap. 3b (Time-resolved fluorometry. Evaluation of time-resolved fluorescence data: Typical methods and problems).

## 2 Principles of Time and Frequency-Domain Fluorometries

### 2.1 Two Major Methods: Single-Photon Timing and Multifrequency Phase-Modulation Fluorometry

The single-photon timing technique (SPT) [a time domain (TD) technique: pulse fluorometry] uses very short, repetitive, optical exciting pulses to obtain the sample fluorescence decay (a convolution of the instrument response function with the fluorescence  $\delta$ -response of the sample, Eq. 2). In multifrequency phase-modulation fluorometry (MPF) [a frequency domain (FD) method] a continuous wave (cw) light source associated with an electrooptical modulator (Pockels cell) delivers a sinusoidally modulated excitation of variable frequency. Using a set of modulation frequencies, the time-resolved fluorescence response of the sample is obtained in MPF. Pulse fluorometry and phase-modulation fluorometry give, in theory, equivalent results because they are coupled by a Fourier transform [5]. Optical pulse trains can therefore also be used in MPF. The time resolution of a phase-modulation fluorometer using the harmonic content of a mode-locked picosecond laser and a MCP photomultiplier is comparable to that of a SPT instrument using the same type of excitation source and detector. For detailed information on the two methods, we refer to Chap. 3 in this book and several excellent monographs and reviews [1–4, 6–14].

### 2.2 Basic Equations for Time-Resolved Fluorescence in SPT and MPF

For a fluorophore that decays monoexponentially with lifetime  $\tau$ , the fluorescence  $\delta$ -response function  $f(t)$  is

$$f(t) = \alpha \exp(-t/\tau), \quad (1)$$

where  $\alpha$  is the preexponential factor or amplitude.

In an ideal SPT experiment, the observed fluorescence decay of the sample,  $d(t)$ , is a convolution of  $f(t)$  and the instrument response function  $u(t)$ :

$$d(t) = \int_0^t f(t')u(t-t') dt' = \int_0^t f(t-t')u(t') dt' = f(t) \otimes u(t), \quad (2)$$

where  $\otimes$  denotes the convolution operator, and  $t$  and  $t'$  represent time. The wavelength dependence of  $d(t)$  and  $u(t)$  is discussed in Sect. 3.5.

In the frequency domain, the values of the phase shift (or phase difference) between excitation and emission light,  $\phi$ , and the relative modulation,  $m$ , for a fluorophore with lifetime  $\tau$ , are given by

$$\phi = \tan^{-1}(\omega\tau) \quad (3)$$

$$m = m_{\text{em}}/m_{\text{ex}} = (1 + \omega^2\tau^2)^{-1/2}, \quad (4)$$

where  $\omega = 2\pi f$  is the angular frequency of the harmonically modulated excitation light,  $f$  the generator-set frequency (expressed in hertz) and  $m_{\text{ex}}$  and  $m_{\text{em}}$  stand for the modulation of excitation and emission light, respectively. For a range of frequencies, phase differences,  $\phi$ , and relative modulations,  $m$ , are measured. The lifetime can thus be independently determined from the phase shift (Eq. 3) and the relative modulation (Eq. 4). For a single-exponential  $f(t)$  (Eq. 1), the lifetime obtained from the phase data,  $\tau_\phi$ , and that from the modulation values,  $\tau_m$ , has to be equal for all frequencies:  $\tau_\phi = \tau_m = \tau$ . This is an easy approach to quickly check the instrument performance for a fluorescent lifetime standard with known single-exponential decay under well-controlled experimental conditions.

In the case of multiexponential decays, the expressions for  $\phi$  and  $m$  in MPF can be found in the books cited in the introduction [3, 4].

### 3

## Artifacts and Remedies to Pitfalls

### 3.1

#### Introduction

In this section we describe only the most important artifacts together with their corresponding remedies. The error sources discussed here are related to measurements of time-resolved fluorescence of bulk samples. Hence, artifacts attributable to microscopy measurements and single-molecule fluorescence are not considered here. A comprehensive list of possible pitfalls in time-resolved fluorescence measurements is given elsewhere [14].

### 3.2

#### Inner Filter Effects

When the concentration of a solution containing identical fluorophores is high, a fluorescence photon emitted in the region overlapping the absorption spectrum may be absorbed by another fluorophore. This process, called *radiative energy transfer*, results in a reduction of the steady-state fluorescence intensity in this spectral region. The larger the spectral overlap, the larger the distortion. Such a deformation of the fluorescence spectrum is called the *inner filter effect*. Because of this distortion, the fluorescence decay following a pulse excitation is slower than in a dilute solution due to successive reemissions and reabsorptions. Moreover, the fluorescence anisotropy decay becomes faster because the excitation energy is transferred to another molecule with a different orientation of the transition moment.

The inner filter effects depend on the concentration and on the geometry of the sample cell arrangement. For the usual right-angle observation, a theoretical correction is difficult, and it is recommended to work as much as possible with dilute solutions (absorbance < ca. 0.1). When the use of high concentrations is required, the fluorescence should be monitored in the front-face configuration by using very thin cells. It is recommended that the illuminated surface is oriented at 30° to reduce the amount of stray light reaching the detection system.

### 3.3

#### Autofluorescence

Given the extreme sensitivity of fluorescence spectroscopy, it is of the utmost importance to avoid fluorescence arising from species other than the fluorophore(s) under study. This kind of fluorescence is called autofluorescence. This is of major importance for investigations in cellular biology because many cellular components are fluorescent [15, 16], especially when the excitation wavelength is shorter than 400 nm. For investigations of fluorophores in solvents, it is crucial that the neat solvents are nonfluorescent at the used excitation wavelength. It is good practice before starting any time-resolved experiment to observe the fluorescence signal of the system without the extrinsic fluorophore (e.g., the neat solvent, the biological sample without the added fluorescent dye) under the excitation conditions to be used for the sample. Indeed, a preliminary experiment in the absence of extrinsic fluorophore can provide the amount of autofluorescence at the excitation wavelength that will be used for exciting the fluorophore. If this amount is not negligible but reasonably small with respect to the overall fluorescence in the presence of the fluorophore, the lifetime(s) of the autofluorescence can be determined and taken into account in further experiments using the fluorophore. The best



remedy is, of course, to use fluorophores excitable at long wavelengths so that the autofluorescence is negligible.

### 3.4

#### Polarization Effects. Magic Angle Configurations

The transmission efficiency of a monochromator depends on the polarization of the incident light. Consequently, the observed fluorescence intensity depends on the polarization of the emitted fluorescence, i.e., on the relative contribution of the vertically and horizontally polarized components. This problem can be circumvented in the following way.

Let  $I_x$ ,  $I_y$ , and  $I_z$  be the respective intensity components of the fluorescence (see Fig. 1). If no polarizer is placed between the sample and the emission monochromator, the light intensity at the entrance of the monochromator is  $I_z + I_y$ , which is not proportional to the total fluorescence intensity ( $I_x + I_y + I_z$ ). Moreover, the transmission efficiency of the monochromator depends on the polarization of the incident light and is thus not the same for  $I_z$  and  $I_y$ .

For the determination of fluorescence lifetimes, the measured fluorescence response must be proportional to the total fluorescence intensity, independently of the fluorescence polarization. This can be achieved by using polarizers under “magic angle” conditions (see details in the appendix of Chap. 6 of [3]). The three main configurations are the following (the first two are displayed in Fig. 1):

- A polarizer is introduced between the excitation monochromator and the sample and set in the vertical position, and another one between the sample and the emission monochromator and set at the magic angle (i.e., with the principal axis oriented at  $54.7^\circ$  with respect to the vertical).
- The excitation polarizer is set at the magic angle, and the emission polarizer in the vertical position.
- In the particular case where an optical filter is used instead of a monochromator for selecting the emission wavelength, no emission polarizer is required but the excitation polarizer must be set at  $35.3^\circ$  with respect to the vertical.

Any polarization of the excitation light will induce a photoselection. The emitted fluorescence will be at least partially polarized if the ensemble of excited molecules does not acquire an isotropic distribution before emission. In other words, the fluorescence emission will be partially polarized when the molecular rotational correlation time is of the same order of the fluorescence decay time. This implies that the observed fluorescence emission is not proportional to the total fluorescence. The measured fluorescence decay curve reflects the combined effect of fluorescence and rotational relaxation. This can be avoided by using one of the three optical configurations described above.

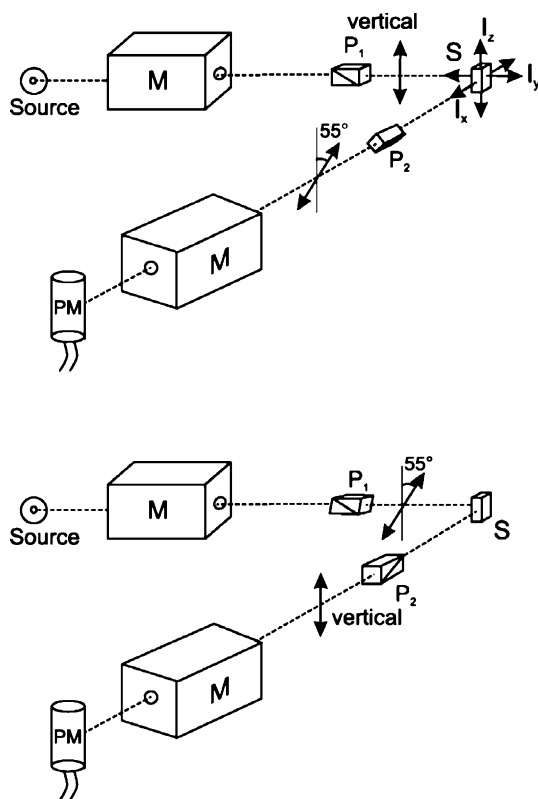


**Fig. 1** Configuration of the excitation and emission polarizers for observing a signal proportional to the total fluorescence intensity. *M*: monochromator; *S*: sample; *P1*, *P2*: polarizers (from [3])

In conclusion, when fluorescence is polarized, it is important to use properly oriented polarizers in order to get the true fluorescence response for lifetime measurements.

### 3.5

#### Color Effect

The explicit wavelength dependence of the measured fluorescence decay of the sample  $d(t)$  (Eq. 2), due to excitation at wavelength  $\lambda_{ex}$  and observed at wavelength  $\lambda_{em}$  [i.e.,  $d(\lambda_{ex}, \lambda_{em}, t)$ ] is given by Eq. 5:

$$d(\lambda_{ex}, \lambda_{em}, t) = u(\lambda_{ex}, \lambda_{em}, t) \otimes f(t). \quad (5)$$

An accurate recovery of the fluorescence parameters of  $f(t)$  needs the instrument response function  $u(\lambda_{ex}, \lambda_{em}, t)$  measured at  $\lambda_{em}$  and caused by excitation at  $\lambda_{ex}$ . Unfortunately,  $u(\lambda_{ex}, \lambda_{em}, t)$  cannot be measured directly,

because the excitation light pulse at  $\lambda_{\text{ex}}$  cannot normally be observed at  $\lambda_{\text{em}}$ . When the instrument response function is weakly wavelength dependent (e.g., when using a MCP photomultiplier), one can substitute  $u(\lambda_{\text{ex}}, \lambda_{\text{ex}}, t)$  [i.e.,  $u(t)$  measured at  $\lambda_{\text{ex}}$  by recording the scattered excitation pulse profile] for  $u(\lambda_{\text{ex}}, \lambda_{\text{em}}, t)$ . However, many photodetectors such as common photomultipliers and avalanche photodiodes exhibit a clear wavelength-dependent effect on their transit time and transit time spread. This leads not only to a time shift between the sample fluorescence signal observed at  $\lambda_{\text{em}}$  and the signal from the scattering solution measured at  $\lambda_{\text{ex}}$ , but, more importantly, also to a different pulse shape of  $u(t)$  as a function of wavelength. Such distortions are called the *color effect*. In SPT experiments, if the wavelength dependence consists only of a time shift, this can be corrected simply by using a time-shift parameter or a time-shifted  $u(t)$  in the curve-fitting analysis program [2]. In MPF experiments, if the wavelength dependence only results in a frequency-independent time shift, this time shift can be experimentally determined and its value can be used to correct the phase and modulation data before analysis [11].

In addition to a wavelength-triggered time shift there might be a dependence of the detector response upon the position of the illuminated area of the photocathode (targeting) and a temporal broadening induced by the emission monochromator.

The most efficient way to overcome these difficulties is to use a reference fluorophore instead of a scattering solution. The method requires a reference compound that absorbs light at the same wavelength  $\lambda_{\text{ex}}$  and fluoresces at the same wavelength  $\lambda_{\text{em}}$  as that used for the sample. Moreover, the fluorescence  $\delta$ -response function of the reference compound,  $f_r(t)$ , should be single-exponential:

$$f_r(t) = \alpha_r \exp(-t/\tau_r), \quad (6)$$

where  $\tau_r$  stands for the lifetime of the reference compound and  $\alpha_r$  is a scaling factor. Finally, the fluorescence decays of reference,  $d_r(t)$ , and sample,  $d(t)$ , must be recorded under identical experimental conditions ( $\lambda_{\text{ex}}$ ,  $\lambda_{\text{em}}$ , optical and electronic settings) [17–23], so that  $u(\lambda_{\text{ex}}, \lambda_{\text{em}}, t)$  is the same for both decays. The measured decays of the sample and the reference [ $d(t)$  and  $d_r(t)$ , respectively] are related according to:

$$d(t) = \tilde{f}(t) \otimes d_r(t) \quad (7)$$

with

$$\tilde{f}(t) = [f(0)\delta(t) + f'(t) + \tau_r^{-1}f(t)]/\alpha_r, \quad (8)$$

where  $\delta(t)$  denotes the Dirac delta function and  $f'(t)$  represents the time derivative of the fluorescence  $\delta$ -response function  $f(t)$ . When  $f(t)$  is single-

exponential (Eq. 1),  $\tilde{f}(t)$  is given by Eq. 9:

$$\tilde{f}(t) = \beta [\delta(t) + (\tau_r^{-1} - \tau^{-1}) \exp(-t/\tau)] \quad (9)$$

with  $\beta = \alpha/\alpha_r$ .

To correct for the photomultiplier color effect in FD measurements, the phase shift and relative modulation are measured under identical instrumental settings for a reference fluorophore and the sample fluorophore. The values for the phase difference  $\Delta\phi$  and modulation ratio  $m/m_r$  between two fluorophores which decay monoexponentially are given by [24]

$$\Delta\phi = \tan^{-1}(\omega\tau) - \tan^{-1}(\omega\tau_r) \quad (10)$$

$$\frac{m}{m_r} = \sqrt{\frac{1 + \omega^2\tau_r^2}{1 + \omega^2\tau^2}} \quad (11)$$

where  $m_r$  denotes the modulation of the reference.

A time-shift between the decay profiles recorded for sample and reference is still possible because the light paths for the sample and the reference may have slightly different lengths because of differences in refractive index, physical sample/reference placement, or sample/reference cuvette dimensions. These resulting time shifts can be accounted for in the data analysis.

### 3.6

#### Photobleaching Effects

Organic fluorophores are more or less stable upon extensive illumination. Degradation by light is called photobleaching. It is thus recommended to reduce the intensity of the incident light as much as possible (by using neutral density filters, for instance). In the SPT technique, where fluorescence detection is achieved photon after photon, such a reduction is easier than in the phase-modulation technique, which requires analog signals for zero-crossing detection and modulation measurements.

Removal of  $O_2$  can also help to decrease the efficiency of photobleaching.

Finally, the best remedy against photobleaching is to use a metering pump delivering continuously fresh sample to the illuminated volume.

### 3.7

#### Deoxygenation

Molecular oxygen ( $O_2$ ) is a well-known quencher of fluorescence. It is ubiquitous in solutions, and attention should be paid to its effect on time-resolved fluorescence. The contribution of  $O_2$  quenching to the decay of an excited state can be expressed by a quenching term  $k_q[O_2]$  to be added to the rate constants of deexcitation. Under atmospheric pressure, the concentration of  $O_2$  in the usual solvents is  $10^{-3} - 10^{-4} \text{ mol L}^{-1}$ . Therefore, since

$k_q \approx 10^{10} \text{ L mol}^{-1} \text{ s}^{-1}$  (for a diffusion-controlled process at ambient temperature), the lifetime of a fluorophore in the presence of  $\text{O}_2$  cannot be longer than  $10^{-6}$ – $10^{-7}$  s in air-saturated solutions. The longer the lifetime in the absence of  $\text{O}_2$ , the stronger its sensitivity to the presence of  $\text{O}_2$ , and for some applications, solutions must be deoxygenated by bubbling  $\text{N}_2$  (or rather Ar) through the solution or, preferably, by the freeze–pump–thaw technique which is more efficient.

### 3.8

#### Artifacts Specific to Pulse Fluorometry

##### 3.8.1

##### Pulse Pile-Up Effect

It is important to note that the number of pulses arising from the detection of fluorescence photons must be kept much smaller than the number of exciting pulses ( $<0.01$ – $0.05$  pulse per exciting pulse), so that the probability of detecting two fluorescence pulses per exciting pulse is negligible. Otherwise, since the time-to-amplitude converter (TAC) will take into account only the first fluorescence pulse, the counting statistics will be distorted: the decay will appear shorter than it is in reality. This effect is called the pulse pile-up effect.

##### 3.8.2

##### Linearity of the Time Response of the TAC

The linear time response of the TAC is critical for obtaining accurate fluorescence lifetime values. Indeed, the fluorescence lifetimes are traceable to the appropriate SI unit (time, in this instance). The accuracy of fluorescence lifetime measurements depends critically upon the calibration of the time axis of the TAC. The response of the TAC is more linear when the time during which the TAC is in operation and unable to respond to another signal (dead time) is minimized. For this reason, it is better to collect the data in the reverse configuration: the fluorescence pulse acts as the start pulse and the corresponding excitation pulse (delayed by an appropriate delay line) as the stop pulse. In this way, only a small fraction of start pulses result in stop pulses and the collection statistics are better.

### 3.9

#### Artifacts Specific to Frequency-Domain Fluorometry

When zero-crossing detectors are used, artifacts appear if the intensities of light from the sample and reference cuvettes are not matched, because the detectors operate then on different gain settings and different noise characteristics. It is thus recommended to adjust the concentration of the reference

cuvette (containing in general the less expensive material) for matching as well as possible the intensities so that the detectors operate on near-identical gain settings and identical noise characteristics in both sample and reference channels.

Matching to operate with the same gain settings is also recommended for digital acquisition analog-to-digital converting cards.

## 4

### Fluorescence Lifetime Standards

#### 4.1

##### Need for Lifetime Standards

Fluorescence lifetime standards are needed most in the areas of photophysics, photobiology, chemical sensing, physical chemistry, fluorescence lifetime imaging microscopy, flow cytometry, and single-molecule spectroscopy. Fluorophores with known lifetimes are necessary for testing the time-resolved instruments for systematic errors, for calibration of fluorescence lifetime equipment, and for use as reference compounds to avoid the wavelength-dependent time response (the color effect) of photomultipliers [25, 26]. Although these wavelength-dependent effects are less pronounced with MCP photomultipliers [27–31], it is still necessary to verify that such effects are not present or to correct for them by the use of fluorescence lifetime standards [14].

To provide the research community with reliable fluorescence lifetime standards, an international, cooperative project involving nine research groups active in the field of time-resolved fluorescence was undertaken [32]. Because a reliable lifetime value for a standard should be independent of the measurement method used, research groups using either pulse (TD) or phase-modulation (FD) fluorometry participated in the study. Moreover, this allowed verification of the comparability of time- and frequency-domain techniques. The results of this collaborative study are presented here.

#### 4.2

##### Criteria for the Choice of Fluorescence Lifetime Standards and Solvents

Although any compound with single-exponential fluorescence decay kinetics can theoretically serve as a lifetime standard, for the sake of standardization the following criteria for the choice of possible lifetime standards in liquid solution must be applied:

- The first, obvious condition for a fluorescence lifetime standard is that it should show single-exponential decay kinetics, independent of excitation and emission wavelengths.

- The compound should be commercially available in sufficiently high purity so that additional purification steps can be avoided (unfortunately, some potential lifetime standards showed dual exponential fluorescence decays when used as received, requiring purification before the lifetime measurements).
- From a practical point of view, an ideal fluorescence lifetime standard should have a (relatively) large Stokes shift (to ensure minimal spectral overlap of excitation and emission spectra) and a (relatively) large quantum yield.
- To cover the picosecond and nanosecond timescales, a series of fluorescence standards with lifetimes matching that range should be on hand.
- A variety of fluorescence standards should be available to cover different spectral regions.
- Chemical stability and photostability during the fluorescence measurements
- In so far as possible, the standards should not pose health, safety, or environmental problems.

Based on these criteria, the dyes that can serve as fluorescence lifetime standards for time-domain and frequency-domain measurements were found to be anthracene, 9-cyanoanthracene, 9,10-diphenylanthracene, *N*-methylcarbazole, coumarin 153, erythrosin B, *N*-acetyl-L-tryptophanamide (NATA), 1,4-bis(5-phenyloxazol-2-yl)benzene (POPOP), 2,5-diphenyloxazole (PPO), rhodamine B, rubrene, *N*-(3-sulfopropyl)acridinium (SPA), and 1,4-diphenylbenzene (*p*-terphenyl).

The choice of solvents was guided by their availability for fluorescence measurements. Water is an environment-benign solvent. Ultrahigh quality water, delivered by a properly maintained Milli-Q system (Millipore), meets all the requirements of fluorescence spectroscopy. Methanol and cyclohexane were chosen as organic solvents because they can be procured from several chemical suppliers in sufficiently high (spectroscopic) purity.

### 4.3

#### Requirements for the Standardization of Lifetime Measurements

To minimize systematic errors in the fluorescence lifetime determinations all sources of variation must be taken into account and eliminated where possible. To standardize the experimental conditions for the measurement of the fluorescence lifetimes, the following prerequisites were set:

- Since temperature may affect the fluorescence lifetime, the temperature was set fixed at 20 °C.
- To avoid the quenching effect of the ubiquitous quencher O<sub>2</sub>, all solutions had to be deoxygenated prior to the measurements.

- The concentration of the solute in the solution had to be low enough to avoid systematic errors that depend on the concentration of the lifetime standard (such as inner filter effects, aggregate formation, etc.) and the absorbance of the solutions was therefore kept very low (typically around 0.05).
- Obviously, the impurity of both the lifetime standard and the solvent used to prepare the solutions can contribute to systematic errors, hence the use of standards and solvents of the highest possible purity commercially available was mandatory.
- To obtain reliable lifetime values, it is extremely important to collect high-quality experimental data, as well as to use sensitive criteria for judging the quality of the fit. First-rate data can be obtained only with state-of-the-art instrumentation that is free of systematic errors (see Sect. 3 for the most important experimental distortions) and that is expertly maintained and run. Systematic errors can be introduced into lifetime measurements by several factors [due to the fluorescent sample (purity, preparation, concentration, and geometry), the electronic and optical components of the time-resolved instrumentation, and the data analysis].

#### 4.4

#### Experimental

Multifrequency phase and modulation measurements were performed using lasers as the excitation source, either mode-locked lasers or cw lasers associated with a Pockels cell. Between 11 and 60 frequencies  $f$  (an average of 25) were used in the measurements. The number of frequencies that is required to recover “correct” values for the decay parameters depends on the complexity of the function  $f(t)$ . In principle, a few frequencies suffice for a single-exponential  $f(t)$  whereas at least 50 or more frequencies (producing  $\geq 50 \phi$  and  $\geq 50 m$  values) are necessary for a distribution of exponentials. Laser excitation was similarly used in the single-photon timing measurements. The decay traces were collected in the channels (between 1/4 K and 4 K) of a (computer-integrated) multichannel analyzer. The excitation and emission wavelength ranges used are compiled in Table 1. The absorbance of the fluorophores in all solutions at the excitation wavelength  $\lambda_{\text{ex}}$  was less than 0.15, typically around 0.05. Magic angle (54.7°) detection (see Sect. 3.4) was used to eliminate polarization effects on the fluorescence decays. If that preventative measure is not taken, the measured time-resolved fluorescence trace will be at least biexponential. Dissolved O<sub>2</sub> was removed from all solutions by purging the solutions with N<sub>2</sub> or Ar or, preferably, by repetitive freeze–pump–thaw cycles. All measurements were done at 20 °C. To remove any bias in the lifetime data, each research group analyzed its own experimental time-resolved fluorescence data, using its individual data analysis software. Moreover, the fluorescence lifetime values obtained by



**Table 1** Mean lifetime  $\bar{\tau}$  and sample standard uncertainty  $u$  [33,34] of the fluorescent lifetime standards in fluid solution at 20 °C [32]

Compound <sup>a</sup>	Solvent	Lifetime $\bar{\tau} \pm u$ (ns) <sup>b</sup>	100 $u/\bar{\tau}$	$\lambda_{\text{ex}}$ (nm)	$\lambda_{\text{em}}$ (nm)	$n^c$
Anthracene	Methanol	5.1 ± 0.3	6.1	295–360	375–442	7
	Cyclohexane	5.3 ± 0.1	2.6	295–360	375–442	7
9-Cyanoanthracene	Methanol	16 ± 1	9.3	295–360	400–480	7
	Cyclohexane	12.7 ± 0.7	5.5	295–360	400–450	4
DPA	Methanol	8.7 ± 0.5	5.6	295–360	400–475	8
	Cyclohexane	7.5 ± 0.4	5.8	295–360	400–475	7
<i>N</i> -methylcarbazole	Cyclohexane	14.1 ± 0.9	6.2	290–325	350–400	6
Coumarin 153	Methanol	4.3 ± 0.2	4.5	295–442	495–550	5
Erythrosin B	Water	0.089 ± 0.003	3.6	488–568	550–580	6
	Methanol	0.47 ± 0.02	4.0	488–568	550–590	6
NATA	Water	3.1 ± 0.1	3.6	295–309	330–410	7
POPOP	Cyclohexane	1.12 ± 0.04	3.6	295–360	380–450	8
PPO	Methanol	1.65 ± 0.05	2.7	295–330	340–400	8
	Cyclohexane	1.36 ± 0.04	2.6	290–325	360–450	8
Rhodamine B	Water	1.74 ± 0.02	0.9	488–575	560–630	5
	Methanol	2.5 ± 0.1	4.0	295, 488–568	550–630	8
Rubrene	Methanol	9.9 ± 0.3	3.2	300,488,514	550–610	5
SPA	Water	31.2 ± 0.4	1.4	300–330	466–520	5
<i>p</i> -Terphenyl	Methanol	1.17 ± 0.08	6.5	284–315	330–380	7
	Cyclohexane	0.98 ± 0.03	3.3	290–315	330–390	7

<sup>a</sup> Abbreviations used: DPA: 9,10-diphenylanthracene, NATA: *N*-acetyl-L-tryptophanamide, POPOP: 1,4-bis(5-phenyloxazol-2-yl)benzene, PPO: 2,5-diphenyloxazole, SPA: *N*-(3-sulfopropyl)acridinium. All solutions are deoxygenated by repetitive freeze-pump-thaw cycles or by bubbling N<sub>2</sub> or Ar through the sample solutions

<sup>b</sup> Average (mean) lifetime  $\bar{\tau}$ . The quoted errors are sample standard uncertainties  $u = \sqrt{\frac{1}{n-1} \sum_{i=1}^n (\tau_i - \bar{\tau})^2}$ . Both time and frequency domain data were used to determine  $\bar{\tau}$  and  $u$  [33, 34]

<sup>c</sup> Number of lifetime data used in the calculation of  $\bar{\tau}$  and  $u$  [33, 34]

the different laboratories were hidden from each other for the duration of the research project.

#### 4.5

##### Comparison of Accuracy of Lifetime Data Obtained by Time and Frequency-Domain Fluorometries

To find out if the pulse TD and FD fluorometries yield the same or, conversely, significantly different results, replicate analyses with each fluorometric tech-

nique must be carried out by the participating laboratories. A  $t$ -test can be applied to investigate whether the differences between the mean lifetimes  $\bar{\tau}_{\text{TD}}$  and  $\bar{\tau}_{\text{FD}}$  obtained with the TD and FD methods, respectively, are significant or not. The variances for the replicate analysis of each sample by the two methods can be compared using the  $F$ -test. These statistical tests demonstrated that for all investigated (fluorescent lifetime standard/solvent) combinations no difference between the mean lifetimes  $\bar{\tau}_{\text{TD}}$  and  $\bar{\tau}_{\text{FD}}$  and their respective variances  $u^2$  obtained with the two time-resolved fluorescence techniques could be observed (according to ISO [33] and Taylor and Kuyatt [34], the estimated standard deviation  $s_i$  evaluated by statistical methods should be termed standard uncertainty with suggested symbol  $u_i$  (i.e.,  $u_i = s_i$ ) and is equal to the positive square root of the estimated variance  $u_i^2$ ).

An easier way of assessing the comparability of the two methods is by least-squares fitting [35]. When the mean lifetimes  $\bar{\tau}_{\text{FD}}$  obtained for the samples with the FD method (MPF) are plotted against  $\bar{\tau}_{\text{TD}}$  obtained with the TD technique (SPT), a straight line should be found. Theoretically, this line should have a slope,  $b$  (Eq. 12), of exactly unity and an intercept on the ordinate,  $a$ , of exactly zero.

$$y = a + bx. \quad (12)$$

By fitting Eq. 12 to the data, one obtains estimates  $\hat{a}$  and  $\hat{b}$  of  $a$  and  $b$ , respectively, and by a goodness-of-fit test one can find out if Eq. 12 really describes the experimental observations. Since none of the two techniques yields error-free lifetime data, one should use the orthogonal regression because it takes into account errors in  $x$  and  $y$  [36]. The best general least-squares fit according to Eq. 12 of  $\bar{\tau}_{\text{FD}}$  ( $y$ , subject to error) versus  $\bar{\tau}_{\text{TD}}$  ( $x$ , subject to error) obtained for 18 samples gives the following estimates:  $\hat{a} = -0.001 \pm 0.005$  ( $s_a$ ),  $\hat{b} = 1.02 \pm 0.01$  ( $s_b$ ). Figure 2 shows the results of the best straight-line fit of  $\bar{\tau}_{\text{FD}}$  ( $y$ ) versus  $\bar{\tau}_{\text{TD}}$  ( $x$ ) when both variables contain errors.

The correlation coefficient  $r = 0.978$  reveals that the correlation between  $\bar{\tau}_{\text{TD}}$  and  $\bar{\tau}_{\text{FD}}$  is very good.

To investigate whether  $\hat{a}$  and  $\hat{b}$  differ significantly from zero and unity, respectively, one must apply  $t$ -tests. The  $t$ -test on the estimate  $\hat{a}$  (of the intercept) indicates that  $\hat{a}$  is not significantly different from 0, implying that there is no method bias. Similarly, the  $t$ -test on the estimate  $\hat{b}$  (of the slope) shows that  $\hat{b}$  is not significantly different from 1.

To conclude, the values of slope, intercept, and correlation coefficient estimated by the appropriate least-squares regression of  $\bar{\tau}_{\text{FD}}$  and  $\bar{\tau}_{\text{TD}}$  (both variables have uncertainties) demonstrate that the pulse and multifrequency phase-modulation fluorometries have very similar precision. Therefore, the two major time-resolved fluorometries are not only theoretically equivalent: they provide the same type of information [because the harmonic response is the Fourier transform of the  $\delta$ -response function  $f(t)$ ], and do this with very similar precision.

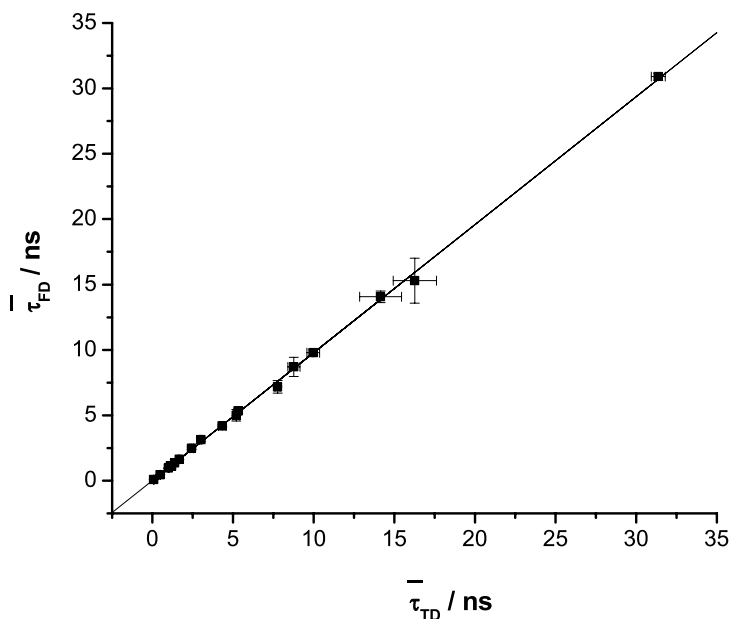


**Fig. 2** Linear least-squares fitting when both variables have uncertainties for assessing the comparability of the pulse (TD) and phase-modulation (FD) fluorometries. The mean  $\bar{\tau}_{\text{FD}}$ -values ( $y$ ) are plotted against the corresponding mean  $\bar{\tau}_{\text{TD}}$ -values ( $x$ ). The regression equation is:  $y = (-0.001 \pm 0.005) + (1.02 \pm 0.01)x$  (correlation coefficient  $r = 0.978$ ). Number of observations  $n = 18$ . The quoted errors represent one standard error for the intercept and the slope. The standard uncertainties [33] on  $\bar{\tau}_{\text{FD}}$  and  $\bar{\tau}_{\text{TD}}$  are also displayed (when they are larger than the used symbols) (from [32])

To summarize, the two leading time-resolved fluorometries have their own advantages and drawbacks. They appear to be complementary methods rather than competitive ones.

#### 4.6

##### List of Lifetime Standards

Table 1 summarizes the mean lifetimes  $\bar{\tau}$  and the associated sample standard uncertainties  $u$  [33, 34] for 20 fluorescence lifetime standards in the solvents used. To have an idea of the precision of the measured lifetime data, we calculated the relative standard uncertainty (the ratio of the sample standard uncertainty  $u$  over the mean lifetime  $\bar{\tau}$ ) expressed as a percentage, that is,  $100u/\bar{\tau}$ . These percentages range from 0.9% for rhodamine B in water to 9.3% for 9-cyanoanthracene in methanol.

The small relative standard uncertainties expressed as percentages ( $100u/\bar{\tau}$ , Table 1) indicate that the interlaboratory uncertainty and the systematic error introduced by the use of the SPT and MPF methods are rather insignificant.

The lifetime values  $\bar{\tau}$  of Table 1 agree very well those of the following seven lifetime standards reported in the literature: (1) anthracene in cyclohexane, (2) erythrosin B in water, (3) NATA in water, (4) POPOP in cyclohexane, (5) PPO in cyclohexane, (6) rhodamine B in water, and (7) rhodamine B in methanol.

## 5

### Concluding Remarks

Time-resolved fluorescence experiments should be performed with great care because of many potential pitfalls and error sources. Many items must be carefully checked before running an experiment. When preparing a sample, attention should be paid to inner filter effects and to the possible effects of dissolved O<sub>2</sub>, temperature, photobleaching, autofluorescence, etc. Optical and electronic artifacts can have many origins and it is sometimes difficult to track them. However, we have shown in the present chapter that in most cases, their effects can be minimized, eliminated or corrected. Then, using appropriate strategies for data analysis, time-resolved measurements of fluorophores with decay times of only a few picoseconds are possible with superb reliability and excellent goodness-of-fit statistics. Fluorescence lifetime standards can be used to test time-resolved instrumentation for systematic errors, for calibration of fluorescence lifetime equipment, and for use as reference compounds to avoid the wavelength-dependent time response of photomultiplier tubes.

### References

1. O'Connor DV, Phillips D (1984) Time-correlated single photon counting. Academic Press, London
2. Boens N (1991) In: Baeyens WRG, De Keukeleire D, Korkidis K (eds) Luminescence techniques in chemical and biochemical analysis. Marcel Dekker, New York, p 21
3. Valeur B (2002) Molecular fluorescence. Principles and applications. Wiley, Weinheim
4. Lakowicz JR (2006) Principles of fluorescence spectroscopy, 3rd edn. Springer, New York
5. Gratton E, Jameson DM, Hall RD (1984) Ann Rev Biophys Bioeng 13:105
6. Demas JN (1983) Excited-state lifetime measurements. Academic Press, New York
7. Cundall RB, Dale RE (eds) (1983) Time-resolved fluorescence spectroscopy in biochemistry and biology. Plenum Press, New York
8. van Hoek A, Visser AJWG (1985) Anal Instrum 14:359
9. Jameson DM, Gratton E, Hall RD (1984) Appl Spectrosc Rev 20:55
10. Eaton DF (1988) Pure Appl Chem 60:1107
11. Pouget J, Mugnier J, Valeur B (1989) J Phys E: Sci Instrum 22:855
12. Eaton DF (1990) Pure Appl Chem 62:1631
13. Lakowicz JR (ed) (1991) Topics in fluorescence spectroscopy, vol 1: techniques. Plenum Press, New York

14. vandeVen M, Ameloot M, Valeur B, Boens N (2005) *J Fluoresc* 15:377
15. König K, Tirlapur UK (2002) In: Diaspro A (ed) *Confocal and two-photon microscopy. Foundations, applications and advances*. Wiley-Liss, New York, p 191
16. Gill EM, Palmer GM, Ramanujam N (2003) In: Marriotti G, Parker I (eds) *Methods in enzymology. Biophotonics, part B*. Academic Press, Amsterdam, p 452
17. Gauduchon P, Wahl P (1978) *Biophys Chem* 8:87
18. Wijnaendts van Resandt RW, Vogel RH, Provencher SW (1982) *Rev Sci Instrum* 53:1392
19. Libertini LJ, Small EW (1984) *Anal Biochem* 138:314
20. Zuker M, Szabo AG, Bramall L, Krajcarski DT, Selinger B (1985) *Rev Sci Instrum* 56:14
21. Van den Zegel M, Boens N, Daems D, De Schryver FC (1986) *Chem Phys* 101:311
22. Kolber ZS, Barkley MD (1986) *Anal Biochem* 152:6
23. Boens N, Ameloot M, Yamazaki I, De Schryver FC (1988) *Chem Phys* 121:73
24. Thompson RB, Gratton E (1988) *Anal Chem* 60:670
25. Wahl P, Auchet JC, Donzel B (1974) *Rev Sci Instrum* 45:28
26. Rayner DM, McKinnon AE, Szabo AG, Hackett PA (1976) *Can J Chem* 54:3246
27. Murao T, Yamazaki I, Yoshihara K (1982) *Appl Opt* 21:2297
28. Yamazaki I, Tamai N, Kume H, Tsuchiya H, Oba K (1985) *Rev Sci Instrum* 56:1187
29. Bebelard D (1986) *Rev Sci Instrum* 57:1116
30. Kume H, Koyama K, Nakatsugawa K, Suzuki S, Fatlowitz D (1988) *Appl Opt* 27:1170
31. Boens N, Tamai N, Yamazaki I, Yamazaki T (1990) *Photochem Photobiol* 52:911
32. Boens N, Qin W, Basariæ N, Hofkens J, Ameloot M, Pouget J, Lefèvre JP, Valeur B, Gratton E, vandeVen M, Silva ND, Engelborghs Y, Willaert K, Sillen A, Rumbles G, Phillips D, Visser AJWG, van Hoek A, Lakowicz JR, Malak H, Gryczynski I, Szabo AG, Krajcarski DT, Tamai N, Miura A (2007) *Anal Chem* 79:2137
33. International Organization for Standardization (1993) *Guide to the expression of uncertainty in measurement*. Geneva, Switzerland (<http://www.iso.org/iso/home.htm>)
34. Taylor BN, Kuyatt CE (1994) *NIST Technical Note 1297*
35. Massart DL, Vandeginste BGM, Deming SN, Michotte Y, Kaufman L (1988) *Chemometrics: a textbook*. Elsevier, Amsterdam
36. Lybanon M (1984) *Am J Phys* 52:22

# Evaluation of Time-Resolved Fluorescence Data: Typical Methods and Problems

Matthias Patting

PicoQuant GmbH, Rudower Chaussee 29, 12489 Berlin, Germany  
*photonics@pq.fta-berlin.de*

1	Structure of the Data . . . . .	233
2	Modelling Temporal Behaviour . . . . .	236
3	Data Inversion . . . . .	238
4	Assessment of Results . . . . .	242
5	Error Estimation . . . . .	244
6	Resolving Lifetimes . . . . .	248
7	Analysis of FLIM Data . . . . .	249
8	Visualising FLIM Data . . . . .	252
9	Accuracy of Fitting Parameters in FLIM . . . . .	255
10	Outlook . . . . .	257
	References . . . . .	257

**Abstract** The temporal characterisation of the light emission by fluorescing molecules can be used to extract a variety of different parameters, such as intramolecular distances or environmental changes. However, deriving a set of lifetimes from given raw data may prove to be a complex task, depending on influences such as the dynamics of the underlying process, the separation of the lifetime parameters or the statistical properties of the measurement. Whereas nowadays computational power provides the possibility to extract the lifetime parameters with sufficient speed, aspects like parameter accuracy and the interpretation of the extracted values can still be challenging. In this contribution, the underlying mathematical approaches to the analysis of time-resolved fluorescence data are outlined with emphasis on time-correlated single photon counting (TCSPC). Some peculiarities of these approaches are discussed with respect to their impact on recently emerging techniques like fluorescence lifetime imaging (FLIM).

**Keywords** Data analysis · FLIM · TCSPC · Time-resolved fluorescence

## 1 Structure of the Data

Two alternative methods are primarily used for recording time-resolved fluorescence. In time-domain measurements the fluorescence intensity is directly

recorded as a function of time: a pulsed light source is used to repeatedly excite an ensemble of fluorophores. The arrival times of the fluorescence photons are recorded relative to the preceding excitation pulse. This may be done by actually evaluating single photon events as in time-correlated single photon counting (TCSPC), but also analogue methods are available. The resolution of time-domain methods is mainly limited by the pulse width of the exciting light and the time resolution of the detectors used to record the decay.

In contrast to time-domain measurements, frequency-domain measurements work by exciting the fluorophores with intensity modulated light. The fluorescence light emitted by the fluorophores will have the same frequency as the excitation light, but there will be a phase shift and a change in amplitude with respect to the excitation light, which can be used to extract lifetime information.

For a more detailed introduction see Chapter “Time Resolved Fluorometry: Typical Methods, Challenges, Applications and Standards”.

The following discussion will mainly take the viewpoint of time-domain data analysis; nevertheless, most of the principles described here can also be applied to frequency-domain methods.

Figure 1 shows a typical time-domain measurement. The plot comprises a single exponential decay and the “lamp function” or instrument response function (IRF), recorded with TCSPC.

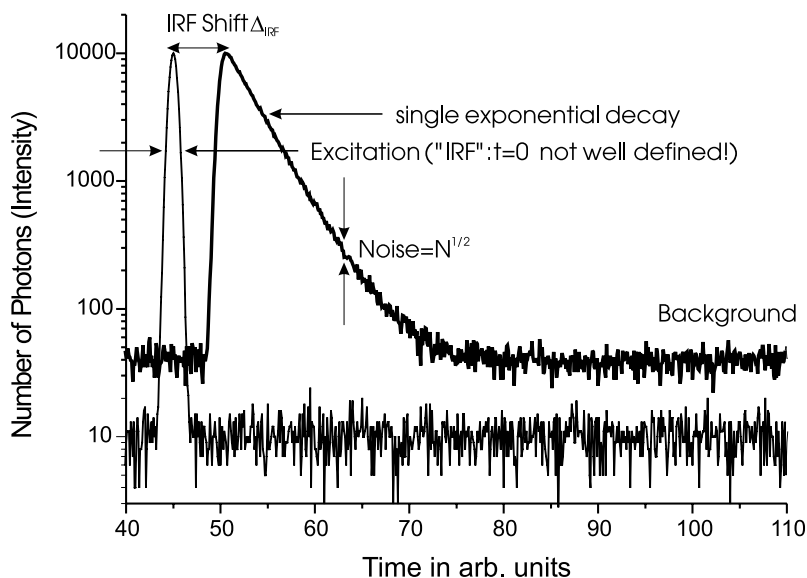


**Fig. 1** A time-domain measurement (TCSPC). The IRF shift is exaggerated for clarification. In a typical experiment  $\Delta_{\text{IRF}}$  is a few channels or less

There are some deviations from the straight line expected for a single exponential decay. First of all, there is an “onset” to the decay at  $\sim 50$  ns, where the intensity increases. This is due to the influence of the finite width of the IRF.

The IRF is the response of a perfect scatterer (which can for visualisation be regarded as a fluorophore with zero lifetime) to the light source as seen by the instrument. For the following discussion it can be regarded as solely originating from the finite width of the excitation light pulse: The ensemble of fluorophores will be “charged” with energy during the pulse, which is the origin of the initial onset in Fig. 1. Excited fluorophores will immediately start to emit light. As a consequence the observed decay  $D^{\text{exp}}$  will be the convolution of the “real” decay  $D$  and the IRF:

$$D^{\text{exp}}(t) = \int_{-\infty}^t \text{IRF}(\hat{t})D(t - \hat{t}) d\hat{t}. \quad (1)$$

Note that due to the convolution the maximum of the observed decay  $D^{\text{exp}}$  is generally shifted to longer lifetimes with respect to the IRF.

Another artefact in Fig. 1 is the presence of a time-independent background both for IRF and decay. This background originates (besides other effects) from the so-called dark counts: The detector will produce photon events even if not exposed to any light.

TCSPC measurements exhibit experimental noise which is governed by Poisson statistics. If the number of events  $N_i$  in a given TCSPC channel is large enough (in practice  $> 10$ ) the noise distribution in this channel can be approximated by a Gaussian and scales with  $N_i^{1/2}$ .

For most detectors the absolute position of the curves in time shows a more or less pronounced dependency of the wavelength. Because IRF and decay are always measured at different wavelengths, there will be a shift  $\Delta_{\text{IRF}}$  between IRF and decay.

All the artefacts mentioned above are intrinsic to time-domain measurements. Some other phenomena can be avoided by careful design of the experimental set-up.

Especially when the spectral separation between IRF and decay is narrow, a scattered fraction of the IRF intensity may leak through the emission filter. It shows in the decays as an intensity contribution equivalent to a hypothetical fluorophore with lifetime zero. It is easily mistaken for a very short lifetime and reduces the resolution of short lifetimes, because it introduces parameter correlations in a later analysis, even if the effect is included in the models.

When the time interval between two pulses of the excitation light is smaller than necessary for the fluorescence light to reach background level, in the decay there will be residual fluorescence originating from the preceding excitation pulses. If possible, this situation should be avoided by decreasing the repetition frequency of the excitation light.



## 2 Modelling Temporal Behaviour

Obviously, analysis of time-resolved fluorescence data will mainly be concerned with extracting the lifetime of the excited states. In the simplest case one might think of an ensemble of identical fluorophores in the same excited state. By emitting a photon each fluorophore may relax to some ground state. If the probability of emitting a photon is time independent and the same for all fluorophores, the observed intensity emitted by the ensemble will decay exponentially with a given lifetime  $\tau$ :

$$D = e^{-\frac{t}{\tau}}. \quad (2)$$

For a mixture of  $n$  different fluorophores with decay times  $\tau_i$  the observed decay will be simply a sum of the exponential decays for each fluorophore:

$$D = \sum_{i=1}^n A_i e^{-\frac{t}{\tau_i}}. \quad (3)$$

The exponential decays are weighted with an amplitude  $A_i$ .

In some cases the transition rate of a given fluorophore may depend on its environment, e.g. on some properties of the solvent in the immediate vicinity of each individual fluorescent molecule. These properties may be subject to fluctuations throughout the solvent. As a consequence, the observed ensemble will show rather a distribution of lifetimes:

$$D = \int_{-\infty}^{+\infty} \alpha(\tau) e^{-\frac{t}{\tau}} d\tau. \quad (4)$$

The shape of the lifetime distribution  $\alpha(\tau)$  may be arbitrary, for example, a Gaussian of width  $\Delta\tau$  centred around some lifetime  $\tau_0$ :

$$\alpha(\tau) = e^{-\left(\frac{\tau-\tau_0}{\Delta\tau}\right)^2}. \quad (5)$$

It should be mentioned that the exact shape of the distribution can never be derived from the data. In fact, a three-exponential model with the right lifetime and amplitude parameters can adequately describe data known to show a lifetime distribution. Thus, some knowledge of the underlying process is always necessary to sensibly choose  $\alpha(\tau)$ . Sometimes instead of a single Gaussian as in Eq. 5 a sum of two or more Gaussians with individual  $\tau_0$  and  $\Delta\tau$  values are used as a model. It is extremely difficult to derive these parameters from the data with acceptable accuracy. Often methods like global analysis (see Sect. 6) have to be used.

Any series or sum of exponentials may be interpreted in terms of energy conversions (radiant or other) with fixed conversion probabilities. This makes this kind of decay model most widely applicable. Even some more complex

decay models as the stretched exponentials [1]:

$$D = e^{-\left(\frac{t}{\tau}\right)^\beta} . \quad (6)$$

( $0 < \beta \leq 1$ ), which are used, e.g. in polymer physics, can be regarded as life-time distributions [2].

The previous discussion completely neglected polarisation effects. Once an ensemble of fluorophores is excited using linearly polarised light, the temporal behaviour of the anisotropy of the fluorescence light yields information about the rotational behaviour of the fluorophores. The time-resolved fluorescence anisotropy is defined as:

$$r(t) = \frac{i_{\parallel}(t) - i_{\perp}(t)}{i_{\parallel}(t) + 2i_{\perp}(t)} , \quad (7)$$

where  $i_{\parallel}(t)$  and  $i_{\perp}(t)$  denote the plane-polarised component of emission having its electric vector polarised parallel, respectively, perpendicular, to the electric vector of the plane-polarised excitation light. The anisotropy decay as defined by Eq. 7 is expected to decay multi-exponentially. For a realistic set-up (especially if separate detectors are used for recording  $i_{\parallel}$  and  $i_{\perp}$ ) the detection efficiency differences have to be taken into account by introducing a phenomenological factor  $G$ , which has to be estimated experimentally:

$$r(t) = \frac{i_{\parallel}(t) - Gi_{\perp}(t)}{i_{\parallel}(t) + 2Gi_{\perp}(t)} . \quad (8)$$

$G$  may be estimated as a freely varying fitting parameter. This assumes the anisotropy decay is much faster than the fluorescence decay. This approach is equivalent to the so-called tail matching, which estimates  $G$  so that  $i_{\perp}(t) = i_{\parallel}(t)$  on the “tail” of both decays not influenced by anisotropy effects. Another method would be exciting the sample with the polarisation direction changed by  $90^\circ$ . For an ideal instrument, where  $G$  would be one, the integral fluorescence intensity measured in both polarisation directions should be equal. Any differences observed in a realistic instrument may be used to define  $G$  as the ratio of the integral over  $i_{\parallel}(t)$  and the integral over  $i_{\perp}(t)$ .

Note that by using Eqs. 7 and 8, the effects of the IRF cannot be taken into account. For this purpose the parallel and perpendicular data set have to be regarded directly:

$$\begin{aligned} i_{\parallel}^{\text{exp}}(t) &= G \int_{-\infty}^t \text{IRF}_{\perp}(t) \frac{1}{3} \text{FLUOR}(t - \hat{t}) [1 + 2\text{ANISO}(t - \hat{t})] d\hat{t} , \\ i_{\perp}^{\text{exp}}(t) &= \int_{-\infty}^t \text{IRF}_{\perp}(t) \frac{1}{3} \text{FLUOR}(t - \hat{t}) [1 - \text{ANISO}(t - \hat{t})] d\hat{t} . \end{aligned} \quad (9)$$

IRF<sub>||</sub> and IRF<sub>⊥</sub> denote the IRF in the parallel and perpendicular polarised direction, FLUOR and ANISO the fluorescence and anisotropy decay. Technically the parallel and perpendicular polarisation directions are analysed simultaneously. This can be regarded as an example of a global analysis (see Sect. 6).

This approach is more powerful not only with regard to IRF effects. Imagine a mixture of fluorophores showing different fluorescence lifetimes and different rotational diffusion times. Calculating the anisotropy decay according to Eq. 8 the correlation between lifetimes and rotational diffusion times is lost while it can still be included in the models that apply Eq. 9. As a drawback, the number of model parameters significantly increases, since a description is needed for the fluorescence decay. Parameter accuracy can be improved by including the magic angle decay in Eq. 9, allowing to recover the fluorescence decay parameters more precisely. Generally, a scan over the polarisation angle of the emitted light followed by global analysis allows for improving parameter resolution. See [3] for a detailed description of these techniques.

### 3

#### Data Inversion

For a mono-exponential decay direct extraction of the lifetime is possible. Let the excitation process be infinitely short, then the barycentre of the resulting decay is located exactly at the lifetime  $\tau$  [4, 5]:

$$\frac{\int_0^{+\infty} t D^{\text{exp}}(t) dt}{\int_0^{+\infty} D^{\text{exp}}(t) dt} = \frac{\int_0^{+\infty} t e^{-\frac{t}{\tau}} dt}{\int_0^{+\infty} e^{-\frac{t}{\tau}} dt} = \tau. \quad (10)$$

If the excitation process (i.e. the IRF) is of finite width both the decay as well as the previously sharp “time zero” will be convolved with the IRF. Since the convolution is a linear operation, the average lifetime is now the distance between the barycentre of the IRF and the barycentre of the decay curve:

$$\tau = \frac{\int_{-\infty}^{+\infty} t D^{\text{exp}}(t) dt}{\int_{-\infty}^{+\infty} D^{\text{exp}}(t) dt} - \frac{\int_{-\infty}^{+\infty} t \text{IRF}(t) dt}{\int_{-\infty}^{+\infty} \text{IRF}(t) dt} + \Delta_{\text{IRF}}. \quad (11)$$

This method provides a good measure of the lifetime if the following two conditions are met:

1. The shift between IRF and decay  $\Delta_{\text{IRF}}$  is either negligible or known and taken into account when calculating the “true” barycentre of the IRF.
2. The background of both IRF and decay is small enough not to contribute significantly to the calculation of the barycentre.

While in time-domain measurements this equation can be applied directly, in frequency-domain measurements the average lifetime has to be related to phase shift  $\phi_\omega$  and  $m_\omega$  modulation of the fluorescent light:

$$\begin{aligned}\tan \Phi_\omega &= \omega\tau, \\ m_\omega &= (1 + \omega^2\tau^2)^{-1/2}.\end{aligned}\tag{12}$$

Both in time-domain measurements and frequency-domain measurements analysing multi-exponential decays is more involved. As a first approach the methods discussed above may be used to extract a kind of average lifetime. This will disregard the true nature of the underlying process, but in some situations this approach has striking advantages. The computation time is greatly reduced (by more than a factor of 100) in comparison to fitting. Also the average lifetime will be estimated with much higher accuracy. Sometimes this simple approach is the only possibility of extracting any useful information at all. In the case of TCSPC, if the number of photon events is no more than 10–100 for the complete decay fitting would produce extremely noisy and inaccurate results even for a mono-exponential model. Both advantages are of interest when analysing FLIM data (see Sect. 7).

Let us consider Fig. 1 again. The artefacts discussed in Sect. 1 have to be taken into account in the models:

1. The background of the IRF has to be estimated and subtracted from the IRF and the IRF shift has to be compensated for.
2. The model decay has to be convolved according to Eq. 1 with the experimentally measured IRF (“reconvolution”).
3. The background of the experimental decay has to be added to the reconvolved model decay.

The results of these calculations then have to be compared to the experimental data.

In the above procedure the IRF effects are taken into account by reconvolving the model decay before comparing it to the experimental data. Sometimes a different approach is used: The IRF is used to deconvolve the experimental data before comparison. This is a valid approach, but it should be stressed that deconvolving of any data is always an ill conditioned process with a high probability of producing artefacts. For time-domain data it is possible to use deconvolution routines which work via Fourier transform. Besides the computational effort necessary for such operations, it should be noted that the deconvolution does not yield any information about the model parameters yet. Thus a fit has to be applied anyway. For these reasons deconvolution is very rarely used in comparison to reconvolution techniques.

As a measure for the accordance between fitted curve and experimental decay the sum of their squared difference over all data points may be used. This sum has to be minimised in a least-squares fit by adjusting the model

parameters, e.g. lifetimes, amplitudes, IRF shift and IRF and decay background.

The desired result of the fit would be the parameter set with the maximum probability of being correct. This is indeed the outcome of a least-squares fit, if the following preconditions are met [6]:

1. All data points are independent observations.
2. The number of data points is sufficient (i.e. the model parameters are overdetermined).
3. The experimental noise follows a Gaussian distribution.
4. There are no systematic errors, i.e. the model describes the data correctly.
5. The experimental noise along the time axis is negligible.

In the following, these preconditions are verified for TCSPC data: The acquisition of a curve is done by sorting photon events into a TCSPC histogram. All electronics used to convert the arrival time of a photon to a TCSPC channel are subject to noise which may have a spread broader than the channel spacing. Therefore, the photon numbers in adjacent channels are not independent observations, so (1) does *not* hold. Luckily there is a workaround for this problem: If the error distribution along the time axis was the same for every TCSPC channel it would lead to an additional convolution of the data with the error distribution. By recording the excitation light pulse with such a set-up, one would get an IRF which is already the excitation pulse convolved with all these effects. It can be taken for the “real” excitation pulse profile throughout the analysis. Thus the timing errors are included in the model, and the photon numbers can technically be regarded as independent, but one has to keep in mind that an absolutely necessary prerequisite for doing so is the homogeneity of the timing errors, which has to be ensured by careful design of the electronics.

Note that also the independency of adjacent channels does not hold once the data are “smoothed”, e.g. by a gliding average. As a consequence, smoothed data are, strictly speaking, not fit for least-squares fitting. Part (2) is typically fulfilled because the usual TCSPC measurement contains about 400–1000 data points, while the number of parameters is less than 30 even for the most complex models. Part (3) is not strictly fulfilled, because the noise originates from a counting process and thus follows a Poisson distribution. Luckily, in the limit of a large number of events in each TCSPC channel, the Poisson noise approaches a Gaussian distribution. Consequently, for data with high number of counts per channel, a least-squares fit may be applied. Part (4) has to be fulfilled by carefully choosing the model. Systematic errors either point to an invalid choice or indicate the presence of artefacts not described in the model (e.g. ripple). For (5), the error along the time axis is defined by the spread of the histogramming bin width. It is on the order of a percent and can indeed be neglected.

In conclusion, for TCSPC data a least-squares fit may be applied, and we arrive at the following measure for the goodness of fit:

$$\chi_{\text{red}}^2 = \frac{1}{N - n_{\text{par}}} \sum_{i=1}^N \left[ \frac{(D(\text{model parameters}, t_i) - D_i^{\text{exp}})}{\sqrt{D_i^{\text{exp}}}} \right]^2. \quad (13)$$

The differences between the experimental data points  $D_i^{\text{exp}}$  and the model curve  $D(\text{model parameters}, t_i)$  are normalised to the expected noise level, which for TCSPC data is  $D_i^{\text{exp}1/2}$ , i.e. Poisson noise in the Gaussian limit. Usually the sum of Eq. 13 is normalised to the degrees of freedom, i.e. the number of data points minus the number of freely varying parameters  $N - n_{\text{par}}$ . The result, the normalised, or reduced,  $\chi^2$ , serves as the optimisation parameter and is expected to be near 1.0 for a good fit.

An introduction to the algorithms used for the least-squares minimisation is beyond the scope of this section and can be found elsewhere [7]. Usually an optimisation algorithm of the Marquardt–Levenberg type [8] is used. Any optimisation algorithm needs an initial set of model parameters as a starting point for the optimisation. It is recommendable to use, e.g. a Monte Carlo search (i.e. trying a large number of random parameter sets and selecting the one with the best  $\chi^2$ ) to estimate these initial parameters, or any other method minimising the risk of arriving at a local optimum instead of the global one.

Least-squares fitting is not the method of choice when dealing with TCSPC data which suffer from poor statistics, i.e. have a significant amount of channels with less than about ten photon events. While least-squares will yield some “nearly acceptable” parameters, it will not yield the parameter set with the maximum probability of being correct, which means it will introduce systematic errors to the fitted parameters.

The least-squares measure for the goodness of fit,  $\chi^2$ , has to be replaced by

$$\chi_{\text{MLE}} = \sum_{i=1}^N [D(\text{model parameters}, t_i) - D_i^{\text{exp}} \ln(D(\text{model parameters}, t_i))]. \quad (14)$$

This approach is referred to as maximum likelihood estimation (MLE). This term may be misleading, as for Gaussian distributed data least-squares would also be a maximum likelihood estimator [7]. MLE stresses the fact that it is applicable to Poisson distributed data, even if the Gaussian limit is not reached. As long as the Gaussian limit still holds, least-squares is by far the preferable method, because the fast Marquardt–Levenberg algorithm depends on the specific least-squares definition of the optimisation parameter as in Eq. 13 and is not directly applicable to MLE. For MLE, slower methods, for example the simplex method [9], have to be used instead.

## 4

### Assessment of Results

As a summary of the last section a typical time-resolved data analysis would probe the parameter space of the applied decay model to find the parameter set with the maximum probability of being correct. Several topics are not covered by this process:

1. Is the model indeed applicable to the data?
2. What are the confidence limits for the fitted parameters?

Assessing (1) is crucial for any analysis. For illustration purposes, let a double-exponential model as in Eq. 3 describe the data. Then, of course, also a three-exponential model could be applied: A trivial solution would lead to amplitude zero for the third exponential, and often the  $\chi^2$  can even be slightly improved by allowing the third amplitude to be different from zero. But is the model really justified by the data, and is the three-exponential model describing any physical reality?

The first question can easily be answered: If a double-exponential model already described the data well, there is absolutely no way of extracting useful information by applying a three-exponential one. An exception from this rule would be allowed if information from another experiment can be used, e.g. to reduce the number of freely varying parameters, but then that very same information would have to lead to an insufficient description of the data by the double-exponential model.

A simple rule of thumb summarises the above example: Always use the simplest model that adequately describes the data and the physical reality. Especially if the mono-exponential model sufficiently describes any data set, there is no chance of extracting more information than a single lifetime, even if the investigated process is expected to be of multi-exponential nature. In this case the physical meaning of the single lifetime is the average lifetime of the process.

Question (2) is usually much more difficult to answer and involves thorough knowledge of the investigated process. Regardless of the answer to question (2), question (1) is already sufficient to reject a model.

What are the criteria for a model to describe the data “sufficiently”? Obviously, the goodness of fit parameter (e.g. the  $\chi^2$ ) alone is not appropriate for this purpose, since it only shows the overall agreement with the data without recognising small, but maybe significant regions, where the accordance may be very bad. A far better measure would be the trace of the weighted residuals:

$$\text{Res}(t_i) = \frac{(D(\text{model parameters}, t_i) - D_i^{\text{exp}})}{\sqrt{D_i^{\text{exp}}}}. \quad (15)$$

For a good fit the residuals should be randomly distributed around zero. There should be no trends or recognisable features like oscillations.

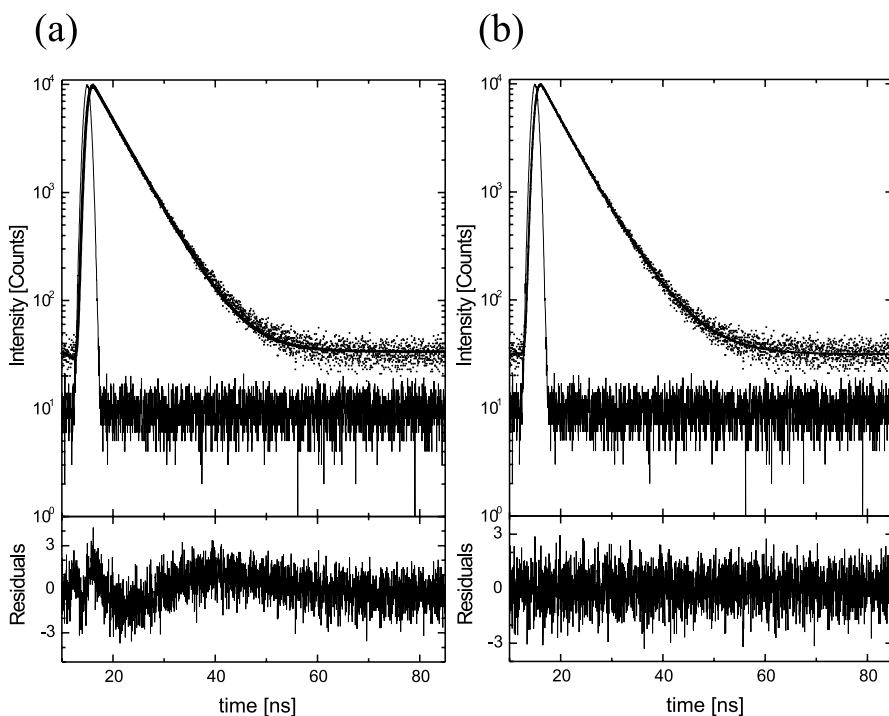
Figure 2 shows an example of a poor fit (a). A mono-exponential model was applied. Although the differences between the fitted curve (bold black line) and the experimental decay (dots) is barely visible in the intensity plot, the weighted residuals trace shows clear oscillations. This leads to the rejection of the mono-exponential model. For the double-exponential model (b) the residuals are perfectly distributed around zero. No trends are visible, thus the double-exponential model is acceptable.

Small trends in the residuals can be “magnified” by examining the normalised autocorrelation function of the residuals:

$$A(t) = \frac{\int_{-\infty}^{+\infty} R(\tau + t)R(\tau) d\tau}{\int_{-\infty}^{+\infty} R(\tau)^2 d\tau}. \quad (16)$$

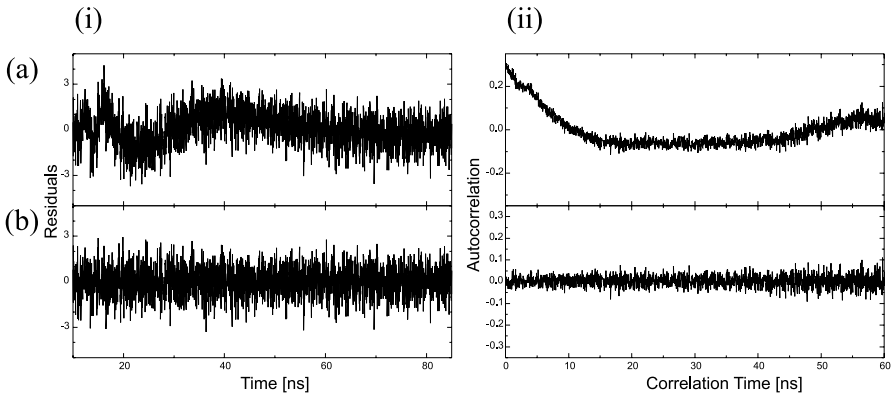
It should be randomly distributed around zero as well; trends show much more clearly than in the residuals trace.

Figure 3 illustrates the residuals of Fig. 2 (i). Although the distortions of the residuals for fit (a) are already visible in the residuals trace, the effect is much more pronounced in the corresponding autocorrelation functions (ii). For fit (a) the deviations of the autocorrelation function from zero are well



**Fig. 2** Residuals traces as a measure for the goodness of fit. **a** Poor fit as indicated by systematic trends in the residuals trace. **b** Acceptable fit





**Fig. 3** Comparison residuals trace (i) versus autocorrelation function of the residuals trace (ii). Systematic distortions in the residuals trace show much more pronounced in the autocorrelation function (a). A featureless residuals trace leads to an equally featureless autocorrelation function (b)

above the noise level. For the acceptable fit the autocorrelation function does not show any trends, same as the residuals trace.

Now let us assume the fit was perfect. Is the model really appropriate then? Actually, it matches the data, but it may still be overdetermined, i.e. it could try to extract information not present in the data. There is only one way to rule this out: The confidence intervals of the fitted parameters have to be considered. If they are too wide compared to a given required precision, the model is overdetermined. Of course this involves a reliable estimation of the confidence intervals, which is not trivial.

## 5 Error Estimation

Most least-squares fitting algorithms will produce some error estimates for the fitted parameters, which are a “built-in” outcome of the optimisation. These errors are the so-called asymptotic standard errors [10].

In principle the estimation of asymptotic standard errors works as discussed in the following: One takes a given parameter from the best fit parameter set, removes it from the optimum and calculates a new  $\chi^2$  for this new constellation. It will of course be greater than for the best fit parameter set. How far can the parameter be removed from the optimum without the corresponding  $\chi^2$  crossing a given tolerance level? The maximum distance from the optimum in both directions defines the boundaries of the confidence interval. Since the  $\chi^2$  will be a nearly quadratic function of the change of the parameter near the optimum, it is sufficient to calculate its second derivative

for estimating the confidence intervals, which is what is intrinsically done by the fitting algorithm.

The asymptotic standard errors are valid if, and only if, the parameters are uncorrelated, that means, changing one parameter, the optimum of all the other parameters does not change. Unfortunately this is almost never the case for time-resolved analysis. For example, take a mono-exponential time-domain data set. If the best fit amplitude would be forcefully reduced, the best fit lifetime would try to compensate for that change by becoming larger: The minimised squared differences between fitted curve and experimental curve would force the area under both curves to be the same, forcing the product of best fit lifetime and best fit amplitude to be constant.

The asymptotic standard errors as estimated by the least-squares algorithm will systematically underestimate the true parameter errors. There exists a variety of methods which will give more accurate results, two of which will be shortly discussed in the following.

The so-called support plane analysis works essentially the same way the asymptotic standard errors are defined. Again one takes a given parameter from the best fit parameter set, removes it from the optimum and calculates a new  $\chi^2$  for this new constellation.

Of course simply calculating the new  $\chi^2$  for the removed parameter would, as mentioned before, underestimate the true errors, because it neglects correlations between the parameters. Having crossed the  $\chi^2$  boundary with this approach, there probably exists another parameter set, which has a far smaller  $\chi^2$ , thus the parameter of interest could be removed even further from the optimum. The question is how to find it. The principle is simple: Just keep the removed parameter fixed and fit all the other parameters. Then take the  $\chi^2$  of this fit as a criterion for the definition of the confidence intervals. The  $\chi^2$  confidence limit can be related to the probability of the true parameter set being located within the confidence interval, see, for example [6, 11, 12].

Figure 4 compares the asymptotic standard error estimation and the support plane analysis for the lifetime parameter of a mono-exponential fit. The contour plot (i) shows  $\chi^2$  as a function of the amplitude and lifetime parameter, normalised to the  $\chi^2$  value of the best fit parameter set,  $\chi_0^2$ . In this example the confidence intervals for the lifetime parameter are investigated. Shown within (i) are the pathways chosen in parameter space for the asymptotic standard error method and the support plane analysis: The pathway for the asymptotic standard error method is a straight line parallel to the lifetime axis, because only the lifetime parameter is changed (a), in contrast to the pathway for the support plane analysis (b), where the amplitude parameter is optimised and thus changes as a function of the lifetime parameter. Note that by construction the pathway for the support plane analysis intersects with the  $\chi^2$  contour lines at the point where their tangent is perpendicular to the lifetime parameter axis. Part (ii) shows the  $\chi^2$  values along (a) and (b). The

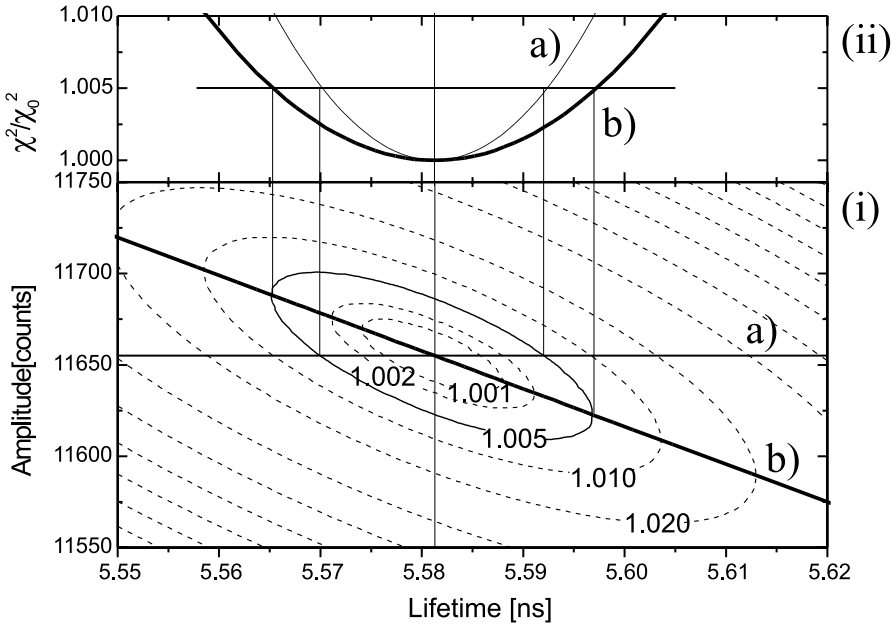


**Fig. 4** (i) Contour plot of  $\chi^2$  as a function of the two parameters of a single exponential fit and (ii)  $\chi^2$  surface slices along the lines (a) and (b)

intersections with the  $\chi^2/\chi_0^2$  confidence limit of 1.005 establish the confidence interval for the lifetime parameter.

Another straightforward way of estimating parameter errors would be performing repeated measurements and repeating the fit for all data sets. Instead of a single parameter set a “cloud” of parameter sets would be generated (one parameter set for each measurement). The errors could simply be derived from the spread of this cloud. Of course repeating the measurement, say, a thousand times would be very time consuming. To save time, the computer can be used to produce simulated data sets based on the experimental data. This leads to error estimation methods known as Monte Carlo methods, because a random element is needed for a realistic simulation.

An ab initio simulation would need thorough knowledge about the measurement process to reproduce realistic noise. Often it is rather time consuming. It is far more convenient to produce the “simulated” data set by selecting a subset of points from the experimental one. This is the approach of the bootstrap method [13].

Let the original data set contain  $N$  points. To preserve the statistical properties of the original data set,  $N$  data points are randomly picked out of the original data set. If one picks  $N$  times some randomly chosen point out of a set of  $N$  points, some points of the set will never be selected, others more than once. Thus the simulated data set is not identical to the original one. As

for all Monte Carlo methods one has to fit about one thousand simulated data sets for a reliable estimation of the parameter errors. This may seem more time consuming than support plane analysis, but note that using the bootstrap analysis all parameter errors are estimated at once, while for the support plane analysis a separate series is needed for each parameter error.

Furthermore, support plane analysis is limited to the least-squares definition of a  $\chi^2$ , while the bootstrap analysis can be used with any optimisation algorithm, which is valuable for MLE fitting, for example.

Figure 5 shows the results of a bootstrap analysis for a mono-exponential fit (same data set as for Fig. 4). Each point represents the best fit parameter set for a simulated data set. Correlations between the parameters lead to a trend in the shape of the cloud, visible as a slight “tilting” to the left in Fig. 5. The contour lines of the  $\chi^2$  surface corresponding to Fig. 4 are drawn for comparison. Although the spread of the cloud is reminiscent of the shape of the  $\chi^2$  surface it originates rather from the slight differences in the simulated data sets: Each point is located in the optimum of an individual  $\chi^2$  surface.

When deriving error intervals from the cloud of parameters, usually a certain probability  $P$  of an individual parameter of being correct is required. The confidence interval for this parameter has to be chosen to include a fraction of  $P$  points of the cloud. In other words, the actual choice is arbitrary, as long as it includes the right number of points. A suitable choice would be to select the shortest interval meeting the condition of containing a fraction of  $P$

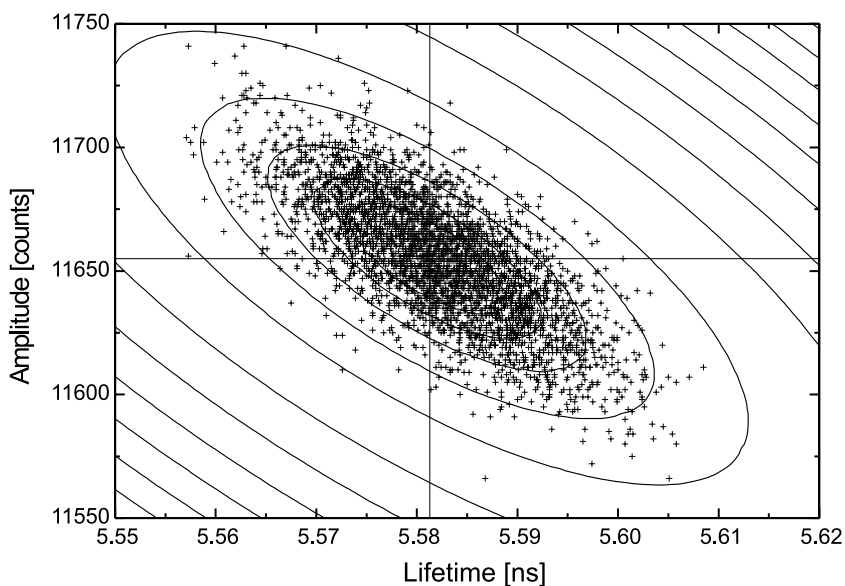


**Fig. 5** The cloud of best fit parameter sets for a bootstrap error analysis compared with the contour plot of  $\chi^2$  (same analysis as previous figure)

points. Note that the error intervals derived on this basis may be asymmetric with respect to the best fit parameter value of the original data set.

## 6 Resolving Lifetimes

Consider a double-exponential model with narrowly spaced decay times. Let the amplitudes be comparable. Obviously this decay would only slightly differ from a single exponential decay. If the difference is smaller than the noise level, the two decay times cannot be resolved anymore.

As a rule of thumb, lifetimes which are separated by a factor of two can be resolved, if the statistics of the data is at least of average quality. If the separation becomes less than a factor of 1.5, resolving the lifetimes becomes increasingly difficult. There exists a region where accumulating more counts, i.e. improving the statistics, will solve this problem, but there is a limit to this approach: The necessary measurement time will diverge quadratically, and reducing more and more of the statistical noise, what remains is non-statistical, systematic noise, e.g. differential non-linearity effects for TCSPC.

Figure 6 illustrates the dependency of resolution limits on the statistics of the data set. All data sets shown here are generated by a simulation based

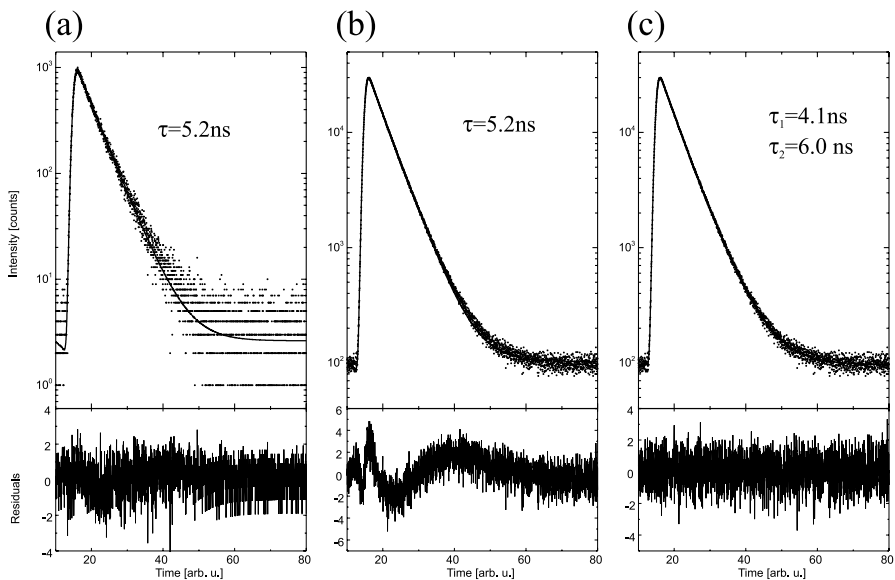


**Fig. 6** Effect of statistics on resolving lifetimes (simulated data). **a** Double-exponential decay recorded with poor statistics. A single exponential model describes the data sufficiently. **b** The same decay recorded with enhanced statistics. The single exponential model does not describe the data sufficiently. **c** A double-exponential model has to be applied

on a double-exponential decay (the IRF is omitted in the plots). The relative amplitudes and the lifetime parameters (6.0 ns and 4.0 ns) were the same for all data sets, but (a) was accumulated to an extent of 1000 photons in the maximum channel, while the data set used in (b) and (c) was accumulated to 30 000 photons in the maximum channel. In (a) the data were fitted using a mono-exponential model. The model decay (solid line) and the simulated data (dots) are in good accordance, as is also visible in the residuals. Although it is known from the simulation that the decay was truly based on double-exponential dynamics, it behaves perfectly mono-exponentially in the analysis due to the poor statistics.

For comparison, consider the same mono-exponential model for the 30 000 photon data set (b): Here the residuals clearly show data and model are inconsistent. A double-exponential model has to be applied: Both lifetimes are well resolved (c).

A very powerful approach to overcome resolution limitations is global analysis [14–19]. Instead of a single decay, a series of decays is recorded. If the experimental conditions were the same for each of these data sets, this would be equivalent to recording a single one with the same integral acquisition time. But if some experimental parameter changes, additional information can be gained from each individual data set. Usually the emission wavelength is scanned in such an experiment. While the decay times are expected to be the same in each data set, their amplitudes may be dependent on the emission wavelength.

Let, for example, a double-exponential model describe the data. The idea in a global analysis is to analyse all data sets, e.g. recorded as a function of the emission wavelength, simultaneously. Each data set has its individual model parameters in the optimisation. To make use of the fact that the lifetimes do not change with the emission wavelength, the lifetime parameters are forced to have the same value for all data sets during the fit. Thus the number of freely varying parameters per data point is effectively reduced. As an important side effect, the correlation between the global parameters (i.e. usually the lifetimes) is reduced. Finally, since every individual data set has a different shape, the systematic noise will have different effects for each data set. Its influence on the analysis is thus reduced.

## 7

### **Analysis of FLIM Data**

In fluorescence lifetime imaging (FLIM), timing behaviour of fluorescence light is measured as a function of image coordinates. It yields additional contrast in addition to mere fluorescence intensity imaging and can be used for a variety of methods, from enhancing spectral resolution to investigations based on Förster resonance energy transfer (FRET), to name only a few.

A prerequisite of FLIM is performing a lifetime measurement for an array of image pixels as shown in Fig. 7. If an average image consists of about  $500 \times 500$  pixels and a typical decay data set contains 1000 data points of four bytes each, an image takes about 1 Gbyte storage space. Compression is often necessary.

For TCSPC data advantage can be taken of the fact that in most images there will be dark regions, which contain only a few photons per pixel. Rather than recording TCSPC curves for each pixel, each individual photon may be recorded. Thus for dark pixels only a few bytes are needed for data representation in comparison to 4 kbyte for a complete TCSPC histogram. A prerequisite for this method is the possibility of recording individual photon events [20], see also Sect. 10. This mode of operation is called TTTR (time-tagged time-resolved) or sometimes list mode.

Be it in time domain or frequency domain, the main task is dealing with thousands of data sets. The analysis may be very time consuming. In many cases one would only be interested in an additional lifetime contrast, so using one of the methods described in Sect. 3 as a fast means of calculating just the average lifetime would be sufficient. This typically takes only a few seconds, even for large images. When fully resolving all information present, e.g. performing a multi-exponential fit, image analysis may take several minutes.

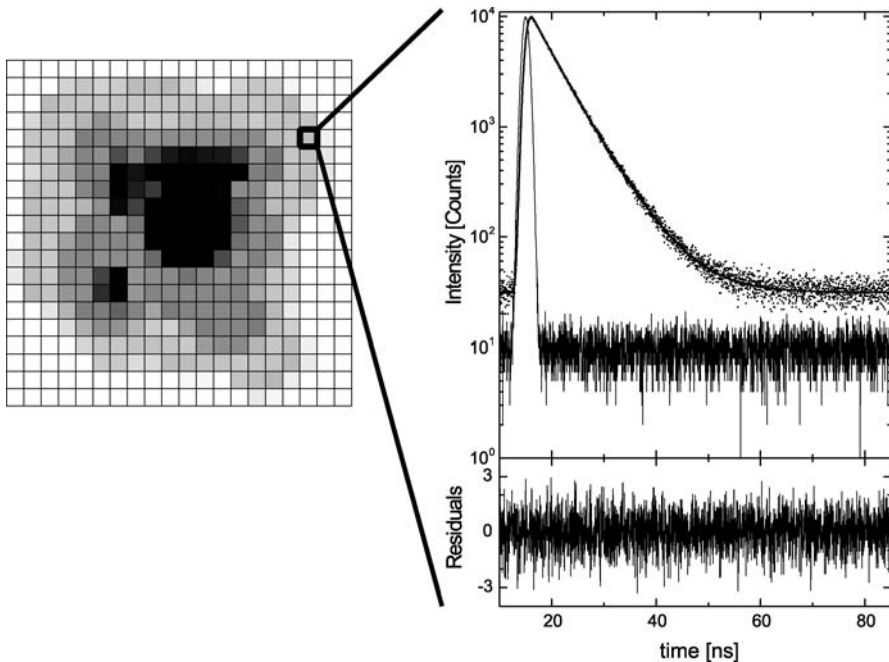


**Fig. 7** A FLIM image is an array of pixels, each pixel containing a time resolved fluorescence measurement

When the lifetimes are expected to be constant throughout the image, one may try to fit all pixel data sets in one huge global fit, which may take up to several hours. Although this will yield the lifetimes with the utmost resolution possible for a given data set, a similar effect can be achieved by estimating the lifetimes in advance and keeping them as fixed parameters in the image fit, while performing a non-global analysis. The lifetime parameters can be estimated conveniently based on the image data. The idea is to take the sum of all pixel data sets. All exponential decays present in the image can be found in the resulting “overall” data set and the lifetimes can be determined with a high accuracy due to the excellent signal to noise ratio (which is better by a factor of  $\sim 10\,000$  compared to a single pixel). It should be stressed that this approach is not fully equivalent to a global analysis. However, it greatly reduces the computational effort at a comparably low price regarding the precision of the lifetimes.

Assessing FLIM data is mainly done by means of the lifetime histogram. The frequency of a given lifetime in the image can be histogrammed either by counting the number of pixels exposing this lifetime or by weighting each pixel by the product of lifetime and amplitude, i.e. the amount of photons a given lifetime contributes. This intensity weighting suppresses dark regions which often give rise to outliers in the fits due to the bad statistics and is therefore the preferable method. For a multi-exponential analysis the frequencies of the lifetime of each exponential may be histogrammed or the frequency of the average lifetime. Comparison between the maxima of the

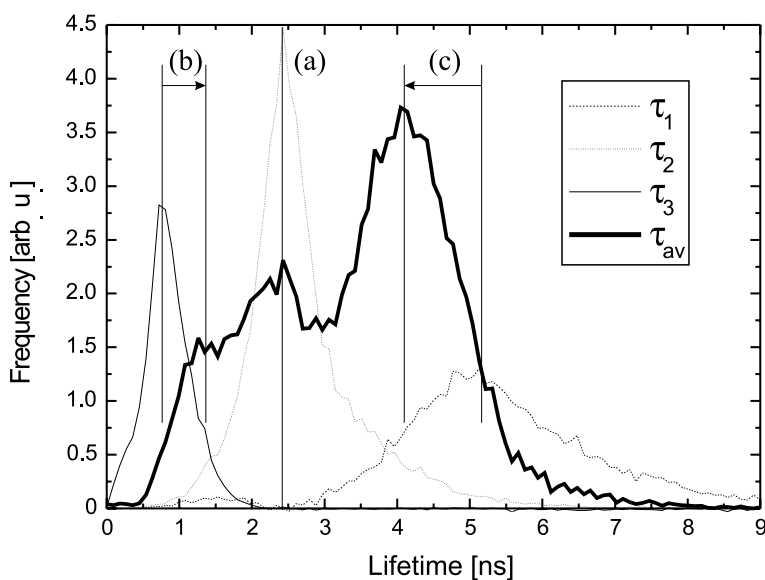


**Fig. 8** Lifetime histogram of a FLIM image; a three-exponential model was applied (see text)



histograms for each separate exponential and the average lifetime histogram yields information about the spatial correlation of the lifetimes: If there are shifts of the maxima or if some maxima even merge in the average lifetime histogram, there are pixels in the image, which show more than one lifetime.

Figure 8 shows an example of a lifetime histogram. The FLIM image was fitted with a three-exponential model. While the maximum of the histogram for  $\tau_2$  (a) remains at the same position in the average lifetime histogram ( $\tau_{av}$ ), the maxima for  $\tau_1$  (b) and  $\tau_3$  (c) show a pronounced shift towards the peak of  $\tau_2$ : In the image there are some regions where  $\tau_2$  is found exclusively, while  $\tau_1$  and  $\tau_3$  always intermix with  $\tau_2$ .

## 8

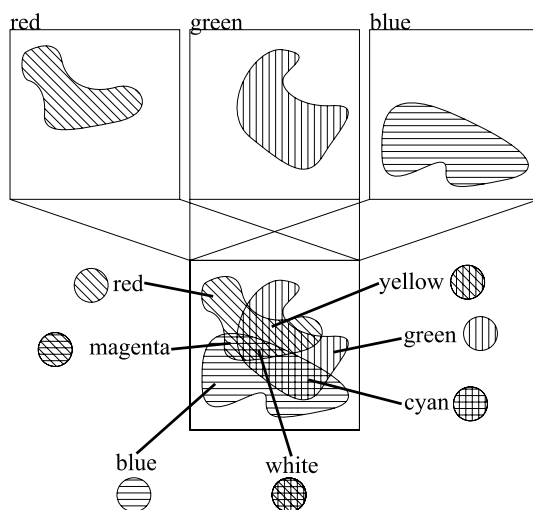
### Visualising FLIM Data

In a steady-state fluorescence image there is only one channel of information, namely, the fluorescence intensity. In a FLIM image there are as many channels of information as there are fitting parameters, in addition to the fluorescence intensity. Visualisation of a FLIM image thus always means selecting information from this vast data stream. The most common visualisation is a false colour plot of the average lifetime. Usually the lifetimes are represented by a rainbow colour scheme while the fluorescence intensity is represented by the brightness of a pixel.

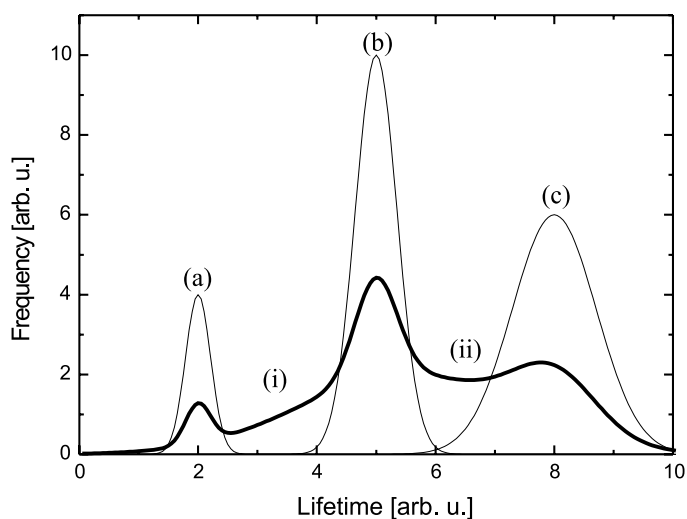
Especially when visualising multi-exponential FLIM data, the rainbow false colour plot neglects information which might be useful to locate each individual exponential component in the image. Imagine a distribution of three different fluorescent species, each showing an individual lifetime. The image has to be analysed with a three-exponential model. One might be interested in the concentration of the three species as a function of the image coordinates. In this case the lifetime information only serves as a filter for separating the fluorescence contributions of each species and does not need to be visualised. Assigning, for example, the amplitude parameters to the red, green or blue channel of a RGB colour model would at once result in a map of the concentrations.

Figure 9 shows how to interpret the RGB image. While the separate red, green or blue channel shown in the upper part of the image represents a kind of “dyed” greyscale image of the fluorescence intensities of the separated species, the mixture of the channels shows the colocalisation of the species. Regions showing in pure red, green or blue only contain species one, two or three. Yellowish regions appear where species one and two intermix, magenta regions show intermixing of species one and three, etc.

Figure 10 shows a hypothetical lifetime histogram of the image of Fig. 9. The maxima of the histograms for each separate exponential (a–c) are visible in the histogram of the average lifetime (bold line), because there are regions,



**Fig. 9** RGB visualisation of a FLIM image (see text)



**Fig. 10** Schematic lifetime histogram as expected for the FLIM image of the previous figure

where the exponentials do not intermix. The intermixing regions will show as a shapeless broad background in the average lifetime histogram, as seen at (i) and (ii).

Now imagine that a mixture of two species was investigated, one of which shows two lifetimes. Again a three-exponential model has to be applied, but this time there is a one-to-one correlation of two of the lifetimes.

Figure 11 illustrates how the FLIM image would look in RGB visualisation. The green and blue channel were chosen to represent the two lifetimes of the double-exponential species. Since there is a one-to-one correlation between both colour channels, some colours are “missing” in the overlaid image. In fact there is only red, where only the first species is present, cyan, where only

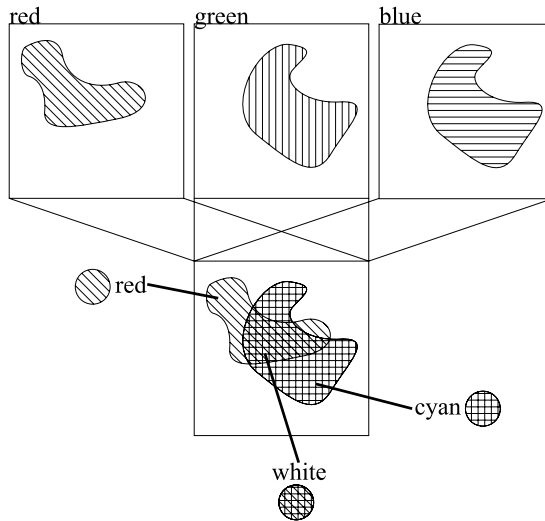


**Fig. 11** Correlating lifetimes as visualised by the RGB false colour scheme (see text)

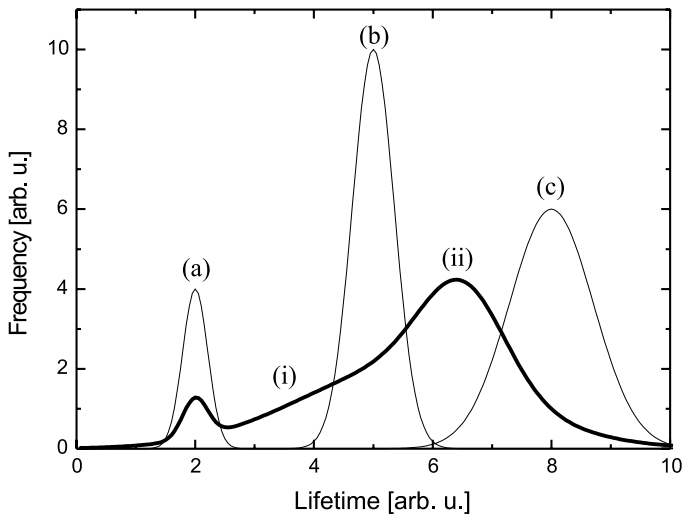


**Fig. 12** Schematic lifetime histogram as expected for the FLIM image of the previous figure

the double-exponential species is present and white (or at least, nearly white), where both species are found. Correspondingly, the lifetime histogram looks quite different from that of Fig. 9.

Figure 12 shows the hypothetical lifetime histogram of the image shown in Fig. 11. Only the position of the maximum corresponding to the mono-exponential species is preserved in the average lifetime histogram. Since the maxima (b) and (c), corresponding to the green and blue channel, are originating from the double-exponential species and show a one-to-one spatial correlation, there are no regions, where the corresponding exponential is exclusively found in the image. Wherever there is exponential “blue”, there is also exponential “green”. Therefore, their maxima combine to a fairly sharp maximum in between of (b) and (c), visible in Fig. 12 at (ii). Again, regions where both species intermix give rise to a more or less featureless background (i).

## 9

### Accuracy of Fitting Parameters in FLIM

The error analysis methods discussed in Sect. 5 typically take some minutes for calculation. While this is not a limitation in the analysis of a single decay, it is by far too slow for an array of about 10 000 pixels. The “built-in” asymptotic standard errors of the fitting algorithm may be used at least as a rough estimate of the real errors, but especially for FLIM data, which intrinsically suffer from bad statistics in dark regions of the image, where the model might easily be overdetermined, strong correlations between the parameters have to be expected.

An acceptable workaround would be the estimation of the errors from the local noise of the parameters. Assuming there are no large spatial jumps in the properties of the image, as lifetimes and amplitudes of the single pixel decays, adjacent pixels should show at least similar values for these parameters. The limited precision of the parameters should become apparent as additional noise, thus the errors of a given parameter can be deduced from the differences between adjacent pixels. This is also a rough estimate, but has a better potential of correctly monitoring correlated parameter errors.

The spread especially of the lifetime parameters also significantly contributes to the shape of the lifetime histogram by broadening its features. Figure 13 illustrates this effect. Both lifetime histograms are calculated from the same image. While in (a) the data is taken with its original spatial resolution, in (b)  $4 \times 4$  pixels are binned. Thus for (b) there are more photons in a single pixel by a factor of approximately 16. Consequently, the accuracy of the estimated lifetimes is enhanced. This is visible as a reduction in the width of the maxima in (b). In addition, because the diameter of an image pixel became larger by a factor of four, the data can be expected to show more pro-

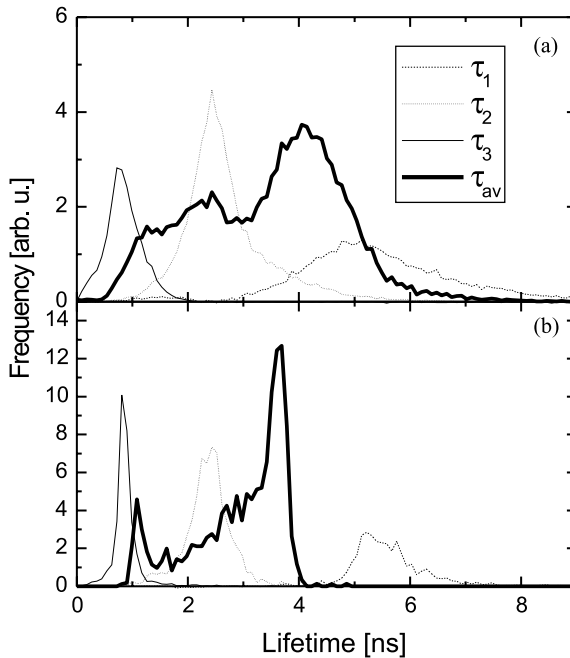


**Fig. 13** Comparison of the lifetime histograms for a FLIM image calculated without pixel binning (a) and with a pixel binning of  $4 \times 4$  (b). The narrowing of peaks in (b) indicates improved fitting parameter accuracy; the vanishing of the peak at 2 ns indicates an increase of the spatial correlation of the lifetimes

nounced spatial correlations. This is visible in the shift of the maxima in the average lifetime histogram of (b) with respect to (a).

As a consequence of the above discussion the precise shape of the peaks in any lifetime histogram is strongly influenced by the fitting precision and thus cannot be analysed quantitatively (say, when deducing distance distributions from a FRET experiment) without a preceding error analysis.

Another aspect is very important to consider. Since most images show an intensity contrast in addition to a lifetime contrast, there almost unavoidably will be pixels which have only very few photons. For these pixels a least-squares fit is no longer applicable, so MLE fitting should be used. Unfortunately MLE fitting is markedly more time consuming. Actually, least-squares is often applied regardless of the problematic statistics of the pixel data. This is a valid approach, as long as the absolute values of the lifetimes are not of crucial importance. However, it should be stressed that especially the lifetimes will be systematically underestimated by 10–20% when not using MLE. These systematic errors will in most cases be markedly above the errors introduced by the limited fitting precision. Whenever lifetimes are evaluated quantitatively, as for example in lifetime based FRET, MLE fitting is an absolute must.

## 10 Outlook

Increasing computational power constantly reduces the time needed for even the most complex analyses. Therefore, the applicability of time-resolved fluorescence will extend to fields, where fast data analysis is of crucial importance, as medical or pharmaceutical applications. Improved mass storage will allow accumulating more and larger data sets, especially in FLIM.

Techniques like TTTR mode measurements allowing one to record every individual photon event, steadily gain importance due to their ability of monitoring temporal effects on a “mesoscopic” scale, like bursts of diffusing single molecules, and a “microscopic” scale, like a fluorescence decay, in a single measurement. Combining TCSPC information with classical methods, as, for example, the extension of FCS (fluctuation correlation spectroscopy) to FLCS (fluorescence lifetime correlation spectroscopy) [21–23] opens completely new fields.

Conversely, commercially available software packages more and more make the analysis of time-resolved fluorescence data a routine task, increasing throughput in both laboratory and industrial applications.

## References

1. Berberan-Santos MN, Bodunov EN, Valeur B (2005) *Chem Phys* 315:171
2. Lindsay CP, Patterson GD (1980) *J Chem Phys* 73:3348
3. Crutzen M, Ameloot M, Boens N, Negri RM, De Schryver FC (1993) *J Chem Phys* 97:8133
4. Yang H, Xie XS (2002) *J Chem Phys* 117:10965
5. Yang H, Luo G, Karnchanaphanurach P, Louie T-M, Rech I, Cova S, Xun L, Xie XS (2003) *Science* 302:262
6. Straume M, Frasier-Cadoret SG, Johnson ML (1991) Least-squares analysis of fluorescence data. In: Lakowicz JR (ed) *Topics in Fluorescence Spectroscopy*, vol 2, Principles. Plenum Press, New York
7. Press WH, Teukolsky SA, Vetterling WT, Flannery BP (1992) *Numerical Recipes in C*, 2nd edn. Cambridge University Press, New York
8. Marquardt DW (1963) *J Soc Ind Appl Math* 11:431
9. Nelder JA, Mead R (1965) *Comput J* 7:308
10. Johnson ML (1994) *Methods Enzymol* 240:1
11. Lakowicz JR (1999) *Principles of Fluorescence Spectroscopy*, 2nd edn. Kluwer Academic/Plenum Press, New York
12. Box GEP (1960) *Ann NY Acad Sci* 86:792
13. Efron B (1982) CBMS-NSF Regional Conf Ser in Appl Math 38
14. Beecham JM, Knutson JR, Ross JBA, Turner BW, Brand L (1983) *Biochemistry* 22:6045
15. Beecham JM, Ameloot M, Brand L (1985) *Chem Phys Lett* 120:466
16. Knutson JR, Beecham JM, Brand L (1983) *Chem Phys Lett* 102:501
17. Beecham JM (1989) *Chem Phys Lipids* 50:237

18. Beechem JM, Gratton E, Ameloot M, Knutson JR, Brand L (1991) The global analysis of fluorescence intensity and anisotropy decay data: Second-generation theory and programs. In: Lakowicz JR (ed) *Topics in Fluorescence Spectroscopy*, vol 2, Principles. Plenum Press, New York, p 241
19. Beecham JM (1992) *Methods Enzymol* 210:37
20. Wahl M, Erdmann R, Lauritsen K, Rahn H-J (1998) *Proc SPIE* 3259:173
21. Böhmer M, Wahl M, Rahn H-J, Erdmann R, Enderlein J (2002) *Chem Phys Lett* 353:439
22. Benda A, Hof M, Wahl M, Patting M, Erdmann R, Kapusta P (2005) *Rev Sci Instrum* 76:033106
23. Enderlein J, Gregor I (2005) *Rev Sci Instrum* 76:033102

# Time-Resolved Fluorescence: Novel Technical Solutions

Uwe Ortmann (✉) · Michael Wahl · Peter Kapusta

PicoQuant GmbH, Rudower Chaussee 29, 12489 Berlin, Germany  
*info@picoquant.com*

1	<b>Introduction</b> . . . . .	259
2	<b>Excitation Sources</b> . . . . .	260
2.1	Picosecond Diode Lasers . . . . .	260
2.2	Fibre Laser . . . . .	262
2.3	Turn-key Ti:Sapphire Laser Systems . . . . .	262
2.4	Light-Emitting Diodes . . . . .	263
2.5	Example of the Use of LEDs in Spectroscopy . . . . .	263
3	<b>Detectors</b> . . . . .	264
4	<b>TCSPC Electronics and “High Information Content” Data Formats</b> . . . . .	266
4.1	Fluorescence Lifetime Correlation Spectroscopy . . . . .	270
5	<b>Conclusion</b> . . . . .	274
	<b>References</b> . . . . .	274

**Abstract** Time-resolved techniques are more and more accepted as versatile and powerful tools for the investigation, analysis and online process control of chemical and biological processes. In the past, the common understanding was that the technique was complicated and complex. However, this has changed dramatically and technical advantages in the field of time-resolved studies are manifold. New laser materials and types have been developed that now ensure a turn-key operation; the measurement electronics have been improved and simplified and the detectors have also evolved into more sensitive, yet easier to handle, devices. Especially, simplifications and reduction of system cost have boosted the acceptance of time-resolved fluorescence techniques in routine laboratory work. In this contribution we would like to focus only on areas where large improvements have been made in the past. We will mainly focus on small and low-cost excitation sources, novel detector types and the use of modern data acquisition electronics that preserve the full photon information. Examples will briefly give some reference to the use of these novel techniques in the field of time-resolved spectroscopy.

**Keywords** FLCS, fluorescence lifetime correlation spectroscopy · Gain switching · Pulsed diode lasers · SPAD · Time-resolved fluorescence · Time tagging · TTTR

## 1 Introduction

Time-resolved fluorescence techniques are more and more accepted as versatile and powerful tools for the investigation, analysis and online process



control of chemical and biological processes. In the past, the common understanding was that the technique was complicated and complex, requiring instrumentation that could be handled only by well-trained scientists with a strong background in physics.

However, this has changed dramatically and technical advantages in the field of time-resolved studies are manifold. New laser materials and types have been developed that now ensure a turn-key operation. The measurement electronics have been improved and simplified and the detectors have also evolved into more sensitive, yet easier to handle, devices. Especially, simplifications and reduction of system cost have boosted the acceptance of time-resolved fluorescence techniques in routine laboratory work.

In the following we will focus only on areas where large improvements have been made in the past 10 years. This can be only a small fraction and should not give a full description of what has been done. A full survey of technical features will breach the size of this chapter. We will only concentrate on the currently most frequently used technique for time-resolved measurements, which is based on the time domain approach. Frequency domain techniques are not discussed here, but some of the discussed topics do also apply to them, especially in the area of new laser materials.

## 2

### Excitation Sources

A key component in time-resolved techniques is the pulsed light source. Generally, they can be separated into coherent sources like lasers and “lamps” like light-emitting diodes (LEDs) or flashlamps. In the following we will give a short review of useful novel light sources for time-resolved spectroscopy. We therefore pick from our perspective the best-suited new light sources, while other new or improved laser sources, such as MicroChip lasers, Nd:YAG lasers or disc lasers, will not be discussed.

### 2.1

#### Picosecond Diode Lasers

Diode lasers cannot exactly be regarded as “novel” light sources as they have been in use since 1996 [1] in the field of time-resolved spectroscopy. However, they are still one of the most frequently used sources because they involve a low cost factor and are reliable, easy to use, and no maintenance or alignment is needed during operation. Consequently, these features make them one of the best tools suited for untrained users in the area of time-resolved spectroscopy.

The commonly used technique to generate the light pulses is “gain switching”, where a short electrical pulse is applied to a laser diode. This allows one

to generate laser pulses with a repetition rate up to 80 MHz and a pulse width down to 50 ps. Besides this short pulse width, one often overlooked but very important feature of pulsed diode lasers is the ability to tune the repetition rate freely without large frame optics, such as pulse pickers or Pockel's cells. The adaptation of the experimental setup to the corresponding sample conditions, e.g. to permit lifetime measurements of long-lived samples, is therefore straightforward.

Unfortunately, the first diode laser systems were only available in the red to infrared spectral region, which limited the usage of these otherwise very nice laser systems. This situation finally changed in 1998 with the introduction of the first GaN laser diode [2]. Today, pulsed diode lasers are available at many different wavelengths, covering the spectral range from 375 to 1550 nm. However, despite all efforts, there are still no laser diodes available in the green/yellow spectral range between 470 and 630 nm, although this region is of high importance due to the large number of available fluorophores.

One possibility to overcome these limitations is to use frequency conversion techniques. This requires that the output power of pulsed diode lasers has to be amplified first to allow an efficient conversion. The developed solution therefore consists of a gain switched picosecond diode laser as the seed laser along with a tapered amplifier in a master oscillator power amplifier (MOPA) arrangement (PicoTA [3]; see Fig. 2). This configuration yields

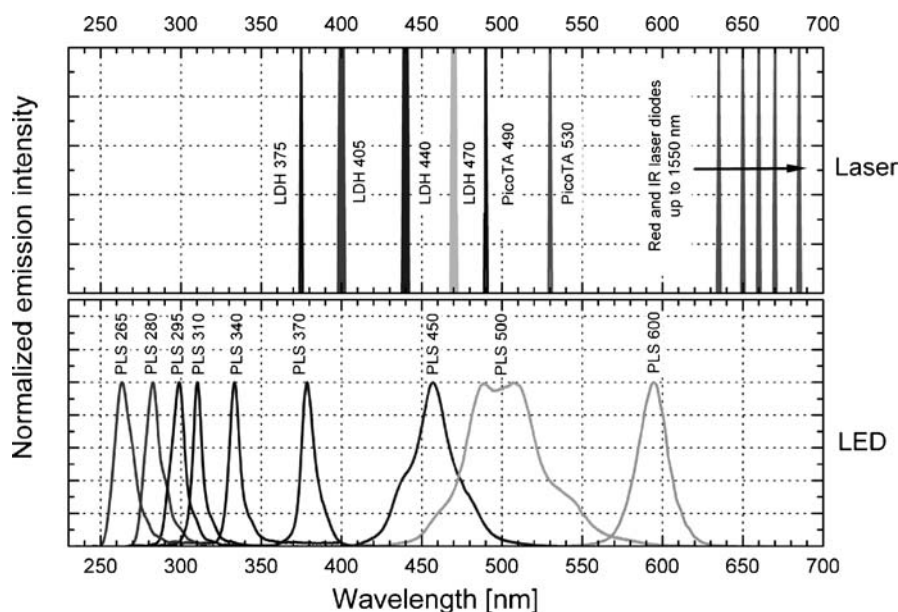


**Fig. 1** Excitation wavelength ranges of available diode lasers, LEDs and frequency-doubled diode lasers

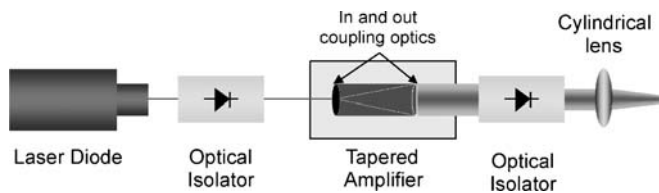


**Fig. 2** Scheme of the PicoTA setup

a boost in power by a factor of typically 50 and the output power of the amplified diode laser pulse is then high enough to be efficiently doubled to either 490 or 532 nm, yielding average power levels of more than 4 mW. In analogy to the pulsed diode laser, this amplified system allows any repetition rate up to 80 MHz. Of course, the system can also work without frequency doubling to yield powerful pulses in the red/infrared.

Today, the development of new laser material has come to a practical standstill. The current development focuses mainly on the improvement of laser power, beam quality and laser durability. This development is mostly driven by the use of these laser diodes in non-spectroscopy applications, e.g. in data storage.

## 2.2

### Fibre Laser

Another emerging new laser system is the fibre laser. It consists mainly of a diode pump laser and a doped fibre of a fixed length. Such a laser system is quite reliable and does not need any maintenance. The laser delivers several hundred femtosecond- to picosecond-long laser pulses in the range from 1060 to 1600 nm with a fixed repetition rate of typically several tens of megahertz to more than 100 MHz. The power of the laser system is sufficient for frequency conversion to generate laser pulses in the visible spectral range as well as for two-photon spectroscopy. However, the design making it such a robust source also makes it quite limited in its use. The optical setup is mostly fixed and no changes are possible after the laser has been supplied. If there is any need for an alteration, e.g. of the quite crucial laser parameter repetition rate, it can not be fulfilled.

## 2.3

### Turn-key Ti:Sapphire Laser Systems

One of the most often used laser sources in the field of time-resolved spectroscopy is clearly the Ti:sapphire (Ti:Sa) laser. In the past, such a laser system consisted of a large pump laser and a Ti:Sa oscillator. This combination was very bulky and expensive and needed very high maintenance

during daily operation. Consequently, such a laser system could mainly be used only by well-trained staff. During the past few years, almost all large Ti:Sa laser manufacturing companies have developed simpler to use turn-key Ti:Sa lasers. These excitation sources have the pump laser incorporated in the frame and feature self-alignment and computer-controlled tuning. Such systems have the same optical properties as the “old” Ti:Sa systems, e.g. 700 to 980 nm tuning range and typically 20 to 200 fs pulse width. Therefore, they are ideal but costly tools for near-infrared and two-photon spectroscopy. The spectral range can also be further extended in the visible by using frequency conversion as well as optical parametric oscillators (OPOs). The repetition rate of these laser systems is typically fixed at 78 to 92 MHz, which is acceptable in applications where the decay time of the sample does not exceed 3 to 5 ns. Again, to measure decays of long-lived samples, an adjustment of the excitation rate by means of a pulse picker is needed. Compared to diode lasers, the high price tag is still one of the largest drawbacks of such laser systems.

## 2.4

### Light-Emitting Diodes

During the last few years, LEDs have become progressively important in time-resolved spectroscopy. Their robustness and very low cost make them a welcome tool and they are able to fill in the gaps in the spectra covered by diode lasers (Fig. 1). As a current development, the spectral range of LEDs is more and more pushed towards the deep-UV range [4] and LEDs with wavelengths down to 260 nm are available today. They have been commercialized mainly for use in water purification [5], but many applications in spectroscopy also benefit from these novel materials.

With special driving electronics, these new UV LEDs can be pulsed up to 10 MHz, yielding average powers around  $1 \mu\text{W}$  at pulse widths down to 500 ps. This is still broad compared to laser sources with pulses down to femtoseconds, but much smaller than the decay times of most fluorophores, which are typically on the order of several nanoseconds.

## 2.5

### Example of the Use of LEDs in Spectroscopy

One of the most striking examples of the use of these new light sources in time-resolved spectroscopy is the investigations done in the area of the intrinsic fluorescence of proteins due to tryptophan, tyrosine and their derivatives, which absorb far below 375 nm. Until now the necessary UV excitation could only be achieved either with slow and bulky lamp systems (e.g. gas-filled flash-lamps) or complex large-scale laser systems such as tripled Ti:Sa lasers. The new generation of UV LEDs has solved this problem for many applications.

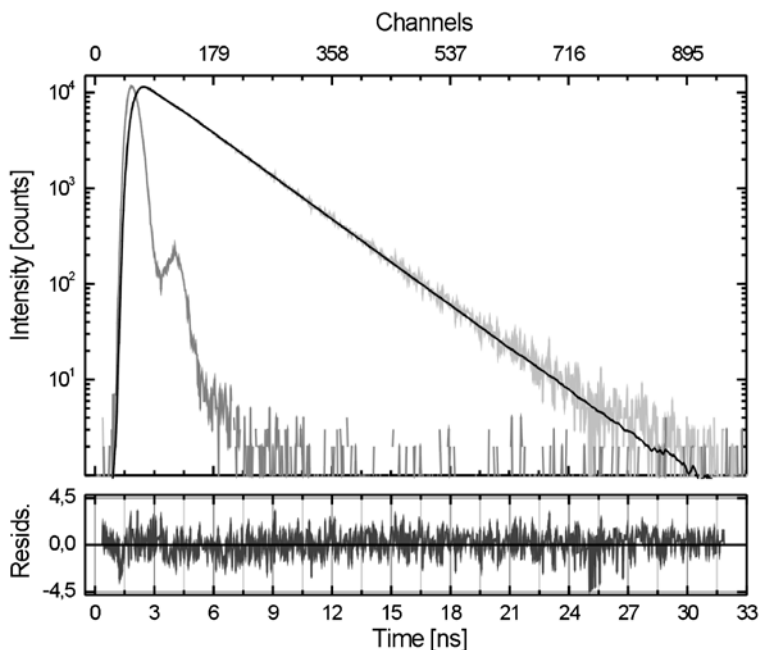


**Fig. 3** Time-resolved fluorescence decay of a 10  $\mu\text{M}$  non-degassed aqueous solution of NATA (*N*-acetyl-L-tryptophanamide) at 24  $^{\circ}\text{C}$ . The fluorescence decay is fitted with a single exponential decay function. The estimated fluorescence lifetime is 2.88 ns

As an example of the use of pulsed UV LEDs, the investigation of a 10  $\mu\text{M}$  aqueous solution of NATA (*N*-acetyl-L-tryptophanamide) at 24  $^{\circ}\text{C}$  is shown in Fig. 3. The sample was excited with a pulsed LED at 280 nm, driven at a 2.5 MHz repetition rate using a time domain fluorescence lifetime spectrometer. Within 60 s 1.3 million counts were collected by a photomultiplier tube (PMT), corresponding to an average detection rate of 21.7 kHz, i.e. less than 1% of the excitation rate, thereby avoiding pulse pile-up effects. The measured instrument response function (IRF) has a FWHM of 700 ps. The IRF, the decay and the fitted single exponential curve are shown. The estimated lifetime is 2.88 ns and the reduced chi-square equals 1.065. The quality of the fit can also be judged by the residual distribution plotted in the bottom panel.

### 3 Detectors

Solid-state photon counting devices, mostly known under the name single-photon avalanche diodes (SPADs), have been extensively used in time-

resolved fluorescence spectroscopy in the past. For a long time the only commercially available detector type was the SPCM-AQR module from Perkin-Elmer (formerly EG&G). Those SPCM-AQR modules feature a very high quantum efficiency in the red spectral range of up to 65%, but only a moderate time resolution of typically 350 to 500 ps IRF width (FWHM). Further limitations of these detectors are signal intensity dependent IRF broadening, limited signal rate and general reliability problems. Nonetheless, they have been widely used in application areas where high quantum efficiency is needed, such as fluorescence correlation spectroscopy (FCS) and other related single-molecule spectroscopy (SMS) techniques. Recently, however, a new type of SPAD has become available which shows in many areas a much better performance than the SPCM-AQR modules. These new SPADs are based on a shallow-junction Geiger mode design in comparison to the SPCM-AQR “reach-through” structure. They are characterized by a very small depletion area, which allows faster timing down to 50 ps, lower operation voltage and higher count rate up to 15 Mcps. The achievable maximum quantum efficiency does not reach the 65% maximum value of the SPCM-AQR design, but is still much higher than that of conventional PMTs. A comparison of the typical quantum efficiencies is shown in Fig. 4.

The biggest advantages of this new type of SPAD are the very fast timing and the superior pulse stability and reliability. Even exposure to room light when powered on will not destroy these detector types. The timing response of these SPADs is comparable to the currently fastest single photon counting detectors available, the micro-channel plate photomultiplier tubes (MCP-PMTs) (Fig. 5).

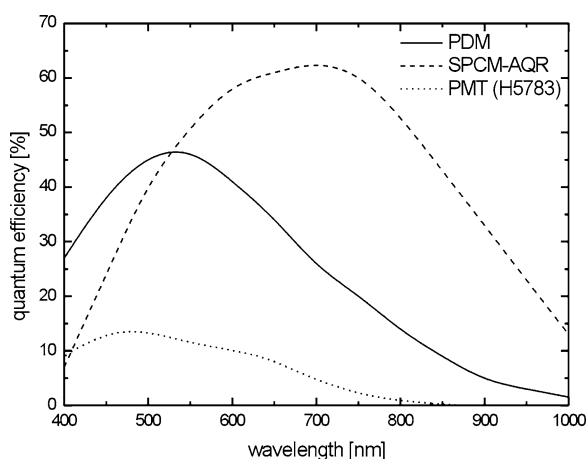


**Fig. 4** Comparison of the typical spectral quantum efficiencies of a new CMOS SPAD of the manufacturer Micro Photon Devices, Bolzano, Italy (PDM module), the SPCM-AQR of Perkin-Elmer and a standard H5783 Hamamatsu PMT

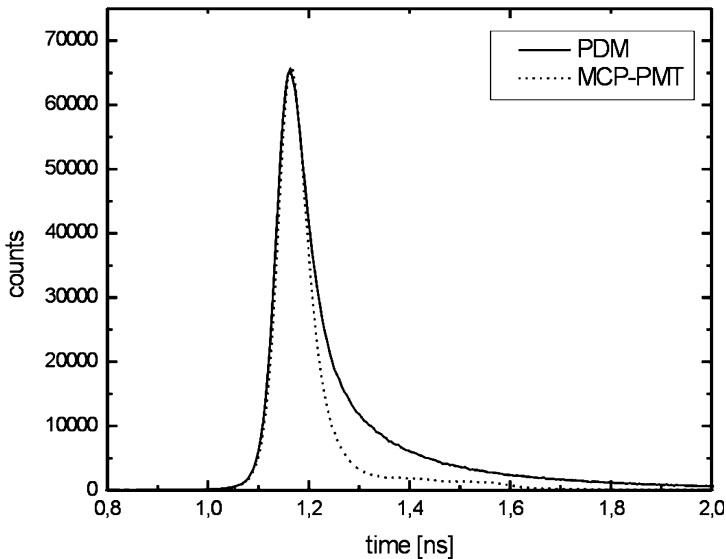


**Fig. 5** Comparison of the IRF of a PDM SPAD and an MCP-PMT R3809 from Hamamatsu

The potential of this new detector type does not lie only in its better performance, but can be further boosted by the fact that its production uses standard complementary metal-oxide-semiconductor (CMOS) procedures. These procedures have been optimized over the years; devices can be produced in monolithic arrays and with fully integrated control and read-out circuitry. It is predictable that the manufacturing cost can be reduced strongly with volume, and therefore the usage of such detectors will not be limited to time-resolved spectroscopy.

#### 4

### TCSPC Electronics and “High Information Content” Data Formats

Originally, time-correlated single photon counting (TCSPC) evolved as a method of measuring fluorescence decays upon pulsed excitation. TCSPC data were collected usually with just one number in mind: the fluorescence lifetime. Obtaining fluorescence decays by TCSPC required only histogramming time differences between excitation and photon emission. Histogramming was implemented in hardware, so that it would meet the counting rate demands required for reasonably speedy data acquisition. This approach was sensible and efficient when instrumentation resources were limited in terms of electronics and data processing power. However, histogramming in this context is a form of early data reduction. When the TCSPC technique received a fresh boost from its applications in SMS in the 1990s, it was realized

that there is valuable information beyond the fluorescence lifetime which, in principle, could be obtained from the raw photon timing data if they were processed more flexibly. While the fluorescence lifetime very elegantly provided the required discrimination of a fluorescence decay against scattered light, the lack of information on the photon intensity dynamics in classic TCSPC, due to histogramming, was a problem. The intensity dynamics on a millisecond scale were important in identifying single molecules in a liquid flow, which show distinct bursts of fluorescence photons. First approaches of overcoming these limitations were therefore aimed at combining existing instrumentation, so that one was able to record the time differences between excitation and photon emission, as well as the inter-photon times [6]. Despite the elegant approach, those early instruments were lacking throughput, due to excessive dead-times upon processing a photon event. The method was greatly improved over time, notably in terms of data analysis algorithms, but still involved combinations of independent instruments with accompanying throughput shortcomings [7].

At the same time, new families of integrated TCSPC instruments had been evolving that allowed much faster processing, although still with conventional histogramming. Another approach to the problem of intensity dynamics was therefore the modification of such fast TCSPC hardware, so that it would allow collection of histograms repeatedly, in a fast sequence, without any gaps [8]. This concept of continuous histogramming is still used today for some applications, notably because of its direct way of delivering lifetime data. However, it has the severe shortcoming of massive redundancy in the data. Notably with sparsely filled histograms, the amount of data versus true information content can be enormous. It was therefore another logical consequence that modern integrated TCSPC electronics evolved, which had the capability of recording individual photon events with a dual time-tagging: one timing figure for the difference between excitation and photon emission and another for the photon arrival on an overall experiment timescale [9]. This concept is referred to as the time-tagged time-resolved (TTTR) mode. Figure 6 shows a timing diagram for this “classic” TTTR mode.

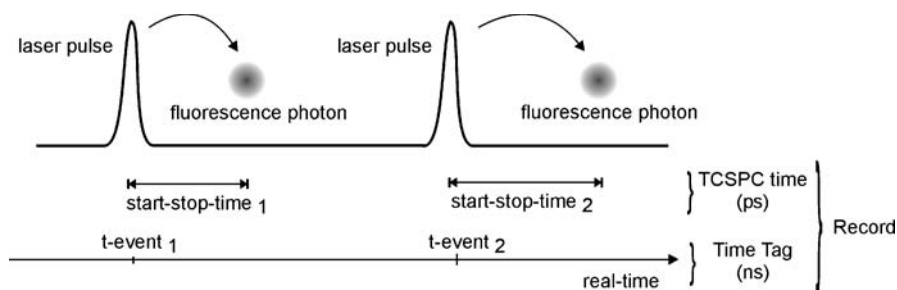


**Fig. 6** Scheme of the “classic” TTTR mode



Collecting the photon arrival time with respect to the start of the experiment as opposed to inter-photon times is a small modification of the original idea for mere convenience in the data processing. The more powerful additions to the concept were the introduction of detector coding in the event records and the introduction of special event markers. The latter can be used to synchronize the photon data with experimental signals, such as pixels and lines in an image scan. The TTTR mode in this recent form has proven extremely powerful. Today it is the method of choice if time-resolved fluorescence is to be used in the most flexible way. It has become the foundation for data collection in a whole new class of time-resolved fluorescence microscopes for applications not only in SMS but also in general fluorescence lifetime microscopy [10, 11] (also see Chap. 7, in this volume). Furthermore, it is the basis for powerful extensions of laser scanning microscopes (LSMs) for time-resolved fluorescence imaging [12]. Nevertheless, TTTR-based TCSPC instrumentation has evolved even further. The separation of TTTR data into separate time tags on two different timescales is not strictly necessary. In fact, it originated from the evolution of the instruments, where a second, coarser timing was added for access to the intensity dynamics in SMS. Similarly, it is due only to the conventional technology of time-to-amplitude converters (TACs) that the instruments must work with pairs of signals (start and stop).

Having realized the power of a much more general approach of using photon arrival times and synchronization events, one can design an instrument that simply collects events on independent input channels and then pro-

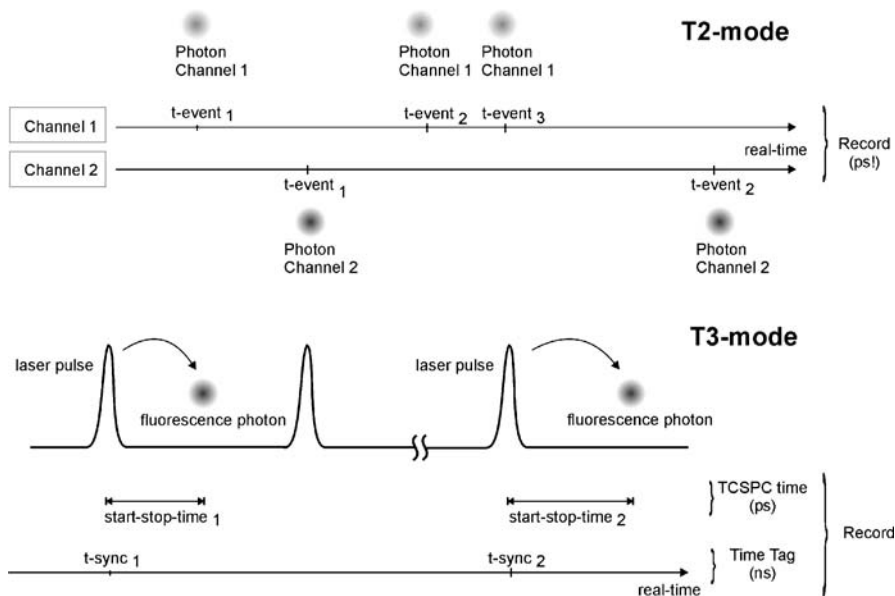


**Fig. 7** Scheme of the T2 and T3 modes of the PicoHarp 300

cesses them according to the nature of the experiment. This allows one to, for example, connect either detectors or laser sync signals, just as required. Start–stop differences are then obtained by a simple subtraction. Coincidence correlations can then be calculated not only between successive events but also across any sequence of events. The first instrument of this kind is the PicoHarp 300 [13]. It uses two independent time digitizers based on fast digital counters with picosecond interpolators. Both time digitizers are locked to the same crystal clock, so that their readings are always synchronous for synchronous events. All processing of relative times is done arithmetically in a field programmable gate array (FPGA) or by the host computer. This provides ultimate flexibility in data analysis. For instance, one can use the two inputs for two detectors and obtain a cross-correlation between them, which covers the lag time range from picoseconds to infinity. This mode of collecting single number time tags (picosecond-resolved signal arrival times) on independent and functionally identical inputs is called T2 mode.

Although the two time digitizers used in the PicoHarp design have the shortest dead time of any comparable instrument today, there is a limitation when using very fast sync sources (e.g. lasers with excitation rates over 10 MHz). This problem is solved by a sync divider at one input. When this dedicated sync input is used, the instrument is operated in so-called T3 mode, which is conceptually more similar to the original TTTR concept. Each photon event is recorded with two figures: a time difference between excitation and photon emission and the number of the excitation cycle. Knowing the excitation period, the latter directly translates to the coarse scale arrival time of the classic TTTR mode. This is an important improvement, because the classic TTTR mode would not easily allow one to know the excitation period a given photon belonged to.

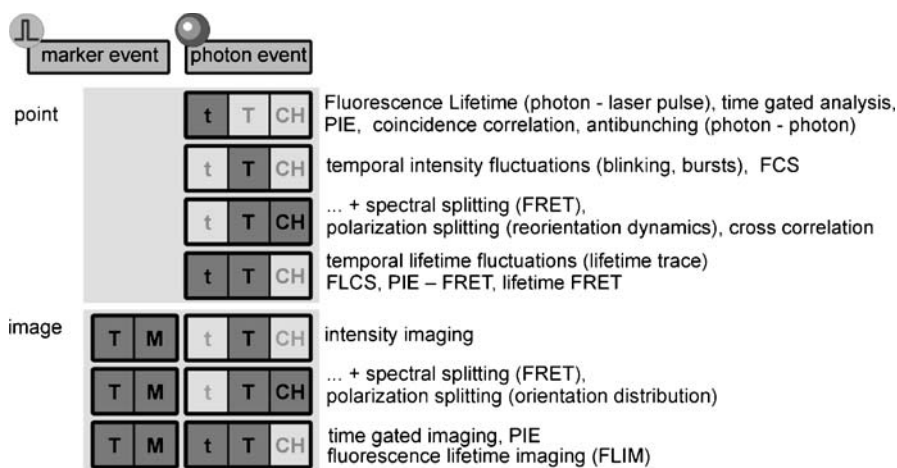


**Fig. 8** Analysis possibilities based on a single TTTR file

While the instrument internally always processes data as independent T2 mode events, the conventional histogramming as well as T3 mode are implemented on top of this layer. By choosing between any of the three modes, the user can solve almost any problem in time-resolved fluorescence measurement with one instrument.

In summary, new developments in electronic design have resulted in very versatile TCSPC instruments, which gain their power from a very generic approach to photon data collection. This time tagged data collection allows very innovative concepts of fluorescence photon processing. The range of methods of data analysis based on TTR raw data is virtually unlimited. It ranges from plain fluorescence lifetime measurements, over FLIM to FRET and FCS. Figure 8 summarizes the most common analysis possibilities based on TTR data. While these classical methods are well documented in the literature, one especially ingenious and powerful new method will be shown in more detail in the next section.

## 4.1

### Fluorescence Lifetime Correlation Spectroscopy

An elegant example is the fusion of time-correlated single photon counting (TCSPC) and fluorescence correlation spectroscopy (FCS), called fluorescence lifetime correlation spectroscopy (FLCS). FLCS is a method that uses picosecond time-resolved photon detection for separating different FCS contributions [14, 15].

Conventional FCS is based on recording and subsequent correlation analysis of intensity fluctuations caused by molecular movement (e.g. diffusion) and/or photophysical processes (such as association–dissociation, isomerization, etc.). Essentially, photon bursts with typical durations on the microsecond timescale are observed. Although individual photon arrival times can be resolved down to nanoseconds, FCS is in principle still a steady-state method because the fluorescence decay kinetics is not taken into account. The standard light source in FCS is a cw laser and typically photon-to-photon delays are measured and recorded. The global photon arrival time is sufficient for autocorrelation calculation, but it is important to realize that there is no way to guess the origin of the photon. The main problem in FCS is that the detected photon signal always contains various unwanted contributions. For example, at very low sample concentration (which is typical for FCS) a considerable portion of the detected intensity is generated by Rayleigh and Raman scattered excitation light and by dark counts (thermal noise). Detector after-pulsing is also a serious issue. All these contributions affect the shape of the resulting autocorrelation function (ACF). The subsequent mathematical analysis (fitting) is then complicated and/or can lead to misleading results due to parameter correlation.

FLCS provides a solution to many inherent problems of FCS. The main feature of FLCS is the statistical separation of a selected signal component

matching a certain TCSPC decay behaviour. This is done before the autocorrelation analysis, hence the result is a separated, component ACF instead of the linear combination as usual in FCS. The selected signal component can be, for example, the fluorescence emitted by one of the species present in the sample, provided its decay curve is known. Alternatively, the method can be used merely to suppress various parasitic components (again, with known TCSPC histograms), without any further assumptions on the rest of the signal.

The key to this is the high information content of the TTTR data file. Namely, the photon delay time measured relative to the onset of the excitation pulse is now available in addition to the previously mentioned global photon arrival time. It is evident that sub-nanosecond pulsed excitation should be used instead of cw radiation.

The principle of FLCS is illustrated in the example below. The experimental data were acquired with the MicroTime 200 confocal time-resolved fluorescence microscope [11] equipped with a pulsed diode laser. The timing electronics of this system are based on the TimeHarp 200 or PicoHarp 300 TCSPC modules operated in the above described TTTR mode [16].

In a typical FCS-like experiment, the fluorescence from diffusing molecules comes in bursts of photons. Such photon bursts are often presented as a so-called multi-channel scaling (MCS) trace (Fig. 9). It is the bare number of photons plotted against the global arrival time, which shows the intensity evo-

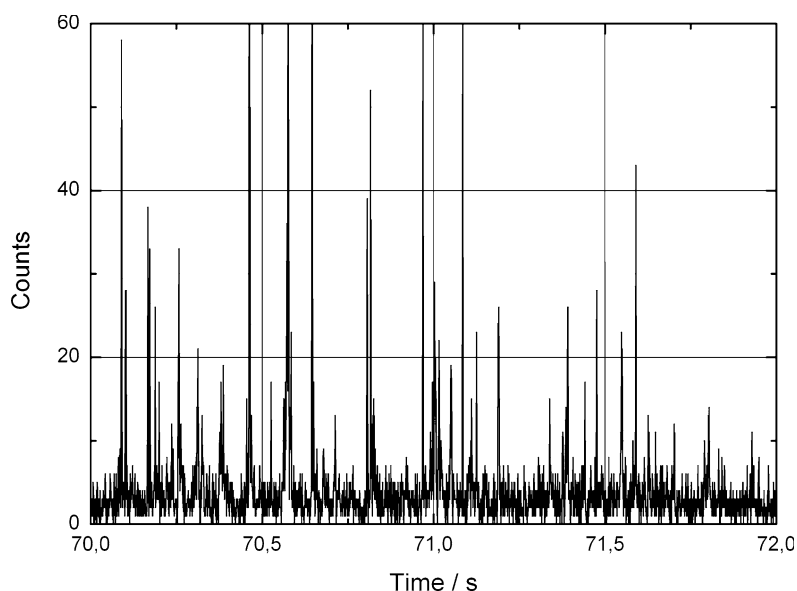


**Fig. 9** A 2-s period of intensity fluctuations caused by diffusing fluorescent molecules. Sample: a drop of 50 pM aqueous solution of Atto655 on a glass cover slip at room temperature, excited at 635 nm with a 20-MHz pulsed laser diode (LDH-635B)

lution (i.e. fluctuations). In the standard FCS approach, this intensity trace is autocorrelated to give an ACF. During this calculation, only the global arrival time of the photon is relevant and each photon contributes equally as a unit intensity carrier.

However, the previously disregarded TCSPC timing information can be used to obtain the conventional decay histogram of the same photons. An important feature of such a TCSPC histogram (Fig. 10) is that it is possible to decompose it (e.g. by reconvolution fitting) into well-defined signal contributions. A quick view on the TCSPC histogram reveals that a large portion of the detected intensity originates from scattered light (Rayleigh and Raman, see the sharp spike at the beginning). The fraction of detector dark counts and after-pulsing (on this timescale appearing as an offset) can also be determined. Only the remaining photons can be attributed to the fluorescence originating from molecules.

Using the fitted component histograms and the overall decay curve, filter functions can be calculated [12] for each intensity contribution (Fig. 11). In the FLCS approach, these filter functions are used as photon weighting schemes during the autocorrelation calculation (Fig. 9). Contrary to the standard FCS, the TCSPC timing is now taken into account. The software looks up the weight (i.e. the sign and the magnitude) of the photon contribution, which then enters the calculation of the selected component ACF. Note that the weight is generally a real number. Dependent on which ACF component

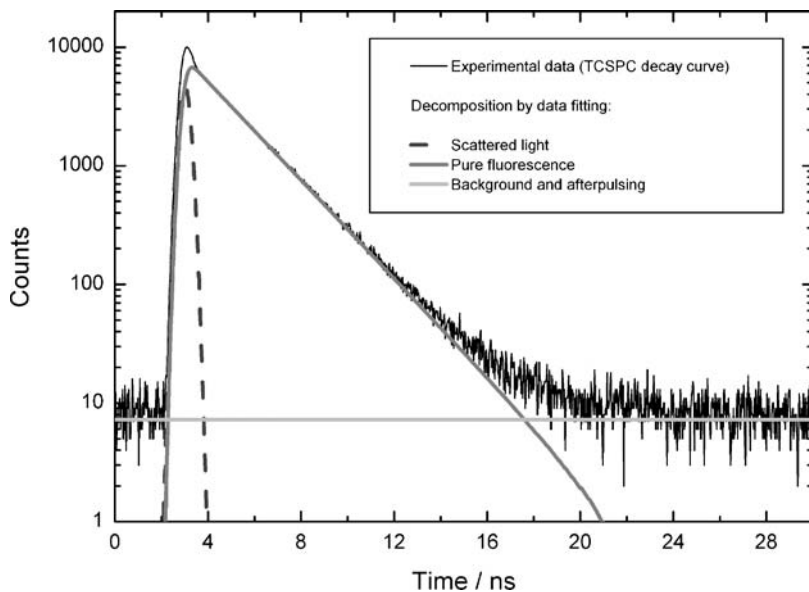


**Fig. 10** TCSPC histogram of all photons collected in the FCS experiment (see Fig. 9) and the result of its decomposition

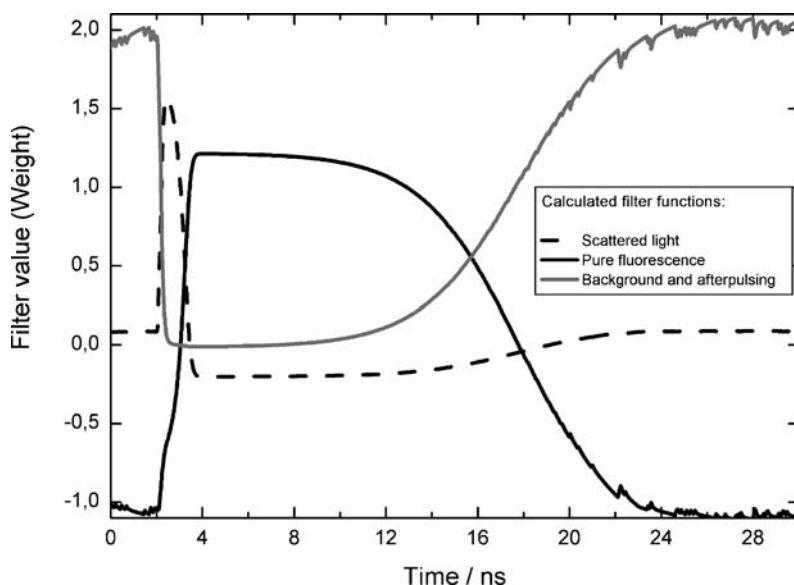


**Fig. 11** Calculated filter functions for the various signal contributions

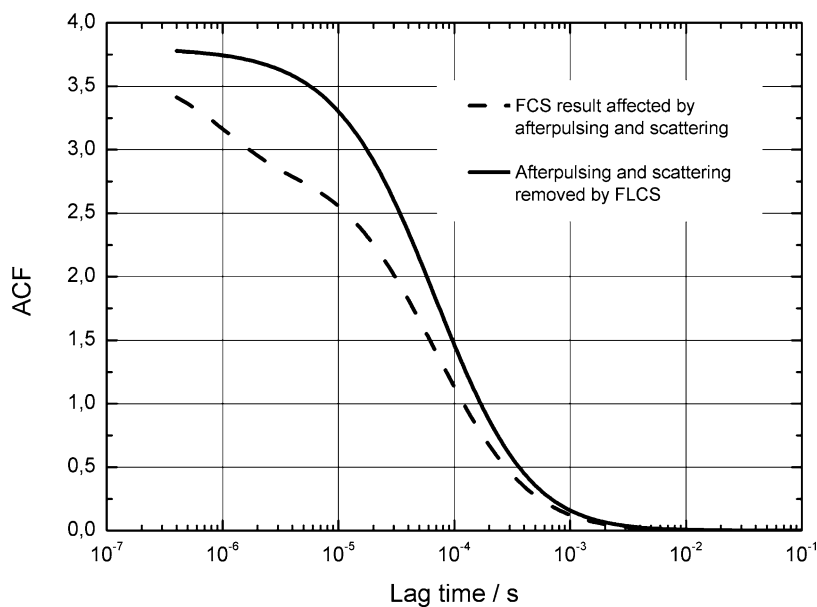


**Fig. 12** Comparison of FCS and FLCS results

is calculated, the same photon contributes with different weights. However, the sum of all weights corresponding to a single photon (characterized by its TCSPC delay time) is exactly 1, since it carries a unit intensity.

Continuing with the above example, it is interesting to see the effect of the use of the filter function for pure fluorescence on the resulting ACF. Figure 12 compares the ACF calculated by a standard FCS approach with that separated (“filtered”) by FLCS. The increase of the ACF amplitude at the shortest lag times is due to filtering out the effect of scattered light and dark noise. This is very important because the initial ACF amplitude is interpreted as a reciprocal value of the average number of molecules inside the detection volume, and is thus related to the absolute concentration. Another effect visible in Fig. 12 is the change of the ACF shape. An initial fast decay is completely absent in the FLCS result, proving that the FCS result is affected by detector after-pulsing and not, for example, by triplet dynamics. In a nutshell, FLCS provides correct results in cases where FCS fails.

## 5

### Conclusion

The development of novel turn-key instrumentation based on integrated semiconductor devices, along with tremendous improvements in data processing and analysis, will continue to boost the power of time-resolved fluorescence methods. For instance, the concept of collecting single number time tags on independent and functionally identical inputs (T2 mode) is extremely powerful, due to the absence of dead times across channels. Work is in progress to extend this concept to more than two inputs. This will allow parallelization of high-throughput applications, as well as novel approaches to general photon coincidence correlation in general quantum physics and quantum information processing research. At the same time, data analysis software is evolving rapidly towards a generalized approach based on time tagged single-photon records. This development will lead to more powerful solutions in key applications, such as sensitive fluorescence detection, fluorescence assays and functional studies of biomolecules.

### References

1. Legendre BL Jr, Williams DC, Soper SA, Erdmann R, Ortmann U, Enderlein J (1996) *Rev Sci Instrum* 67:3984
2. Nakamura S, Senoh M, Nagahama S, Iwasa N, Yamada T, Matsushita T, Kiyoku H, Sugimoto Y (1996) *Jpn J Appl Phys* 35:L74
3. Erdmann R, Langkopf M, Lauritsen K, Bülter A, Wahl M, Wabnitz H, Liebert A, Möller M, Schmitt T (2005) *Proc SPIE* 5693:43
4. Khan A (2000) *Appl Phys Lett* 76:273
5. SET Inc (2003) *Comp Semicond* 9:24
6. Wilkerson CW Jr, Goodwin PM, Ambrose WP, Martin JC, Keller RA (1993) *Appl Phys Lett* 62:2030

7. Brand L, Eggeling C, Zander C, Drexhage KH, Seidel CAM (1997) *J Phys Chem A* 101:4313
8. Erdmann E, Ortmann U, Enderlein J, Becker W, Wahl M, Klose EO (1966) *Proc SPIE* 2680:176
9. Wahl M, Erdmann R, Lauritsen K, Rahn HJ (1998) *Proc SPIE* 3259:173
10. Böhmer M, Pampaloni F, Wahl M, Rahn HJ, Erdmann R, Enderlein J (2001) *Rev Sci Instrum* 72:4145
11. Wahl M, Koberling F, Patting M, Rahn HJ, Erdmann R (2004) *Curr Pharm Biotechnol* 05:299
12. Ortmann U, Dertinger T, Wahl M, Patting M, Erdmann R (2004) *Proc SPIE* 5325:179
13. Wahl M (2005) *PicoHarp 300 user manual*. PicoQuant GmbH, Berlin
14. Böhmer M, Wahl M, Rahn HJ, Erdmann R, Enderlein J (2002) *Chem Phys Lett* 353:439
15. Kapusta P, Wahl M, Benda A, Enderlein J (2007) *J Fluoresc* 17:043–048
16. Böhmer M, Enderlein J (2003) *ChemPhysChem* 04:792



**Part IV**  
**Fluorescence Polarization Techniques:**  
**Applications in the Material and the Life Sciences**

# Fluorescence Depolarization Techniques in Materials Science

David J. S. Birch (✉) · Jan Karolin

Photophysics Research, Department of Physics, Scottish Universities Physics Alliance,  
University of Strathclyde, Glasgow G4 0NG, UK  
*djs.birch@strath.ac.uk*

1	Introduction . . . . .	279
2	Probe Brownian Depolarization . . . . .	280
3	Probe Depolarization on Silica Nanoparticles . . . . .	284
3.1	Stable Silica Nanoparticles (Ludox) . . . . .	285
3.2	Surface-Contour Diffusion (SCOD) . . . . .	289
3.3	Silica Hydrogel Nanoparticle Growth Kinetics . . . . .	290
3.4	The Multiphoton Advantage . . . . .	291
3.5	Sources of Error . . . . .	293
4	Depolarization Due to Protein Structure and Dynamics . . . . .	293
4.1	Intrinsic Amino Acid Fluorescence . . . . .	293
4.2	Extrinsic Probe FRET . . . . .	296
5	Conclusions . . . . .	298
	References . . . . .	299

**Abstract** We review the different approaches available to materials science using time-resolved fluorescence depolarization. Performance, limitations and challenges in this emerging area of nanometrology are discussed using the exemplars of sol-gel nanoparticle growth and protein dynamics.

**Keywords** Depolarization · Nanoparticles · Silica · Nanometrology · Ludox · FRET · Sol-gel

## 1 Introduction

When it comes to tracking rapidly changing phenomena on the scale of molecular dimensions, fluorescence lifetime techniques have few equals. This is because they can be performed in-situ, have an appropriate time-scale (ps to ns), offer high sensitivity (even down to the single-molecule level) and benefit from a wide-range of well-characterized fluorescence probes with which to customize a study of the problem of interest. The associated equipment is

also now extremely easy to use and reliable. Nevertheless, it is fair to say that interpretation of data still requires skill and experience.

Nowhere is interpretation more important than in one of the increasingly important uses of fluorescence lifetimes, namely the association of time information with distance information to describe the nanometrology of molecular structures and how it changes with time. Quite simply, the fluorescence lifetime enables the advantages of fluorescence to be brought to bear on distance measurement in a reproducible way, which offers considerable scope for standardization. Dynamic nanometrology can perhaps be best-facilitated by fluorescence lifetime measurements using interpretations based on quenching caused by fluorescence resonance energy transfer (FRET) and fluorescence depolarization leading to the decay of fluorescence anisotropy. Both approaches offer sub-nm resolution, but span different distance scales. FRET is useful in the range  $\sim 1$ – $10$  nm and anisotropy decay in the range  $\sim 0.1$  nm to  $>10$  nm. This complementarity comes about because FRET has a distance-dependent rate constant that falls off rapidly as  $\sim r^{-6}$ , and the anisotropy decay has a rotational correlation time  $\phi$ , in the simplest case of free Brownian rotation increasing as  $\sim r^3$  to give an equivalent rate of  $\sim r^{-3}$ , which falls off less rapidly than FRET. Both are sometimes closely connected, as we will also discuss here, which sometimes leads to misinterpretation, but, given careful design, are also capable of revealing important structural information.

There are numerous early reviews of fluorescence depolarization [1–5], but it is perhaps fair to say that it is only quite recently that the standing of this technique, alongside those of more traditional methods such as small angle X-ray and neutron scattering, electron microscopy, etc., has started to be fully appreciated by those outside the immediate field. This has come about through successful demonstration of the power of fluorescence depolarization in applications, which draw heavily on other techniques. Here we choose two such applications, sol-gel ceramics and proteins, as paradigms, in order to illustrate what is already known which might contribute to the setting-up of standards while pointing out some of the present limitations, assumptions, ambiguities, errors and challenges needing to be overcome to advance the field.

## 2 Probe Brownian Depolarization

In the simplest case, a free and rigid fluorescent dye molecule undergoing Brownian isotropic rotation in a solvent is capable of complete fluorescence depolarization, which can be described by a single rotation correlation time  $\phi$ .

In terms of the widely used fluorescence anisotropy function  $R(t)$

$$R(t) = \frac{D(t)}{S(t)} = \frac{F_V(t) - F_H(t)}{F_V(t) + 2F_H(t)}, \quad (1)$$

where  $F_V(t)$  and  $F_H(t)$  refer, respectively, to the vertical and horizontal orientation of the emission polarizer, with respect to vertically polarized excitation. The decay of anisotropy due to Brownian rotation following the initial photo-selection due to polarized excitation can be described by

$$R(t) = R_0 \exp(-t/\phi). \quad (2)$$

Here,  $R_0$  indicates the maximum value the anisotropy can take and the rotational correlation time  $\phi$  can be described by the Stokes–Einstein equation

$$\phi = \frac{\eta V}{kT}, \quad (3)$$

where  $\eta$ ,  $V$ ,  $k$  and  $T$  are the viscosity, hydrodynamic volume, Boltzmann constant, and temperature, respectively.

The very nature of Eq. 1 whereby the information concerning depolarization is carried by the numerator in the difference of two fluorescence decay curves (as compared with the absolute measurement of decay time being contained in the difference between a decay curve and the baseline or indeed the sum given in the denominator), leads to an important limit to the precision of measurement.

Even in this simplest implementation of a dye in a solvent, a number of assumptions and potential sources of error come into play. Most noteworthy is the effect of the solvent shell on the rotational correlation time such that frequently measurements [1] do not translate from solvent to solvent. Other assumptions concern the absence of dye aggregation and FRET, the need for isotropic rotation and a rigid rotor. However, having made these points there is no doubt that the depolarization characteristics of several fluorescent probes are well enough quantified to be able to contribute to any debate concerning standards.

In the following we will focus on the use of fluorescence depolarization to measure both the size of and distances within macromolecules. An ideal fluorophore for these applications should have a high quantum yield, well-defined and co-linear absorption and emission transition dipoles, which implies no intra-molecular depolarization due to “hidden” electronic states or conformational re-arrangement; have emission characteristics independent of the surrounding environment as well as having a fluorescence lifetime  $\tau$  on a comparable scale to the rotation of interest described by  $\phi$ . Further, labelling of macromolecules adds additional constraints regarding fluorophore solubility and rarely can a fluorophore be found that maximally fulfils all these criteria. Figure 1 shows a selection of commonly used extrinsic fluorophores that we will mainly be referring to in this review. The sizes of the fluorophores

are indicated by the solvent excluded volume,  $V_{\text{sev}}$ , and by the corresponding radius of a sphere,  $R_{\text{sev}}$ .

Two of the fluorophores presented in Fig. 1 belong to the xanthene family, i.e., Rhodamine 6G (R6G) and Rhodamine 700 (R700) [6], which have found application in silica colloids [7–18]. Both R6G and R700 are highly water soluble with similar fluorescence lifetimes in the region 2–4 ns, making them compatible with the rotational correlation time of colloidal particles at the lower limit of detection. (See the following discussion of the relative magnitudes of  $\tau$  and  $\phi$ ). One striking difference between these two dyes is their pH stability. While R6G can be used over extraordinary range of pH (1–14), which makes it ideal for sol–gel studies, R700 will degrade in alkaline and acidic environments. However, the absorption peak of R700 is centered around 640 nm, for which inexpensive and compact diode laser sources are available, while R6G absorption is centered around 520 nm and requires the use of either lower power light emitting diode or complex main-frame laser non-linear techniques for excitation. A further advantage of R700 is the reduced Rayleigh light scattering ( $\sim\lambda^{-4}$ ) at longer wavelengths, minimizing an

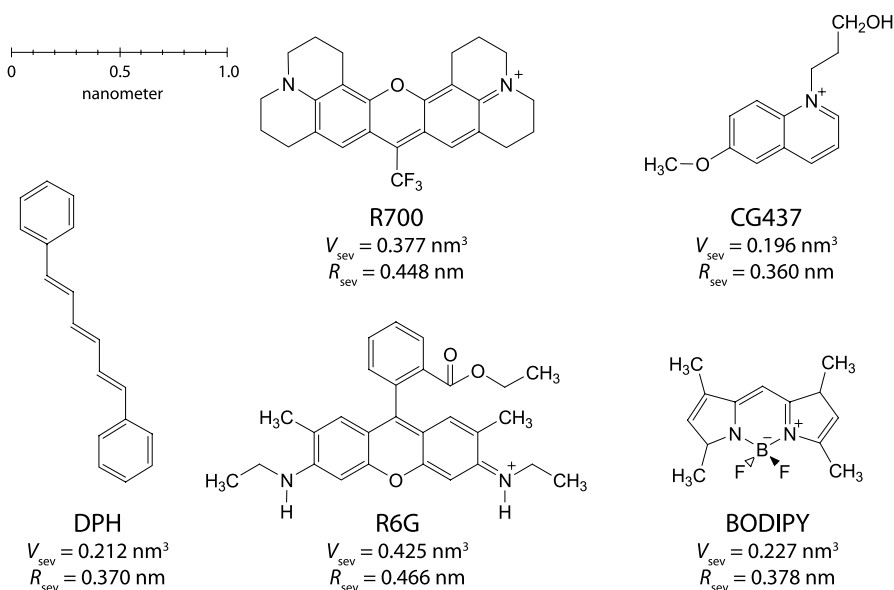


**Fig. 1** Molecular structures of fluorophores discussed. DPH (1,6-Diphenyl-1,3,5-hexatriene), R700 (Rhodamine 700), CG437 (6-methoxy-1-(3-propanol) quinolinium), R6G (Rhodamine 6G) and BODIPY (4,4-difluoro-1,3,5,7-tetramethyl-4-bora-3a,4a-diaza-s-indacene). The solvent excluded volume,  $V_{\text{sev}}$ , is calculated for structures energetically minimized in a MM+/MM2 force field [83–85] using the method of Connolly [86, 87]. The corresponding radius of a sphere  $R_{\text{sev}}$  is also given. Note that  $V_{\text{sev}}$  often is smaller than the experimentally measured hydrodynamic volume due to solvent “sticking” to the fluorophore

often major source of interference with fluorescence measurements. Note that for all these dyes, their physical dimensions presented in Fig. 1 clearly determine the measurable lower size limit of any nanoparticle to which they are attached as a probe (see the next section).

The quinolinium group in CG437 has the advantage of minimal intrusion, being the smallest of all the probes considered, and has a relatively long fluorescence lifetime, often bi-exponential, but with a component up to  $\sim 30$  ns [19], making it possible to track the rotation of larger colloidal particles up to  $\sim 10$  nm radius. Concomitant with its size is of course the need for ultraviolet excitation, which brings with it increased Rayleigh scattering and greater probability of exciting background fluorophores.

Diphenyl hexatriene (DPH) and its derivatives have been extensively studied in membrane systems [20–31], for molecular structure see Fig. 1.

It is informative for a moment to compare and contrast the characteristics of DPH and R6G in the light of their enduring popularity. R6G is water soluble, whereas DPH is not, making the latter more useful in probing lipid bilayers. R6G is ionic whereas DPH is not making the former easier to bind to structures such as those of silica. Both can have a high fluorescent quantum yield approaching unity and are believed to be isotropic rotors, giving one dominant rotational correlation time in common solvents. Ideal diode laser excitation sources are presently lacking for both. However, DPH has a complex fluorescence decay attributed to its closely coupled  $^1A_g$  and  $^1B_u$  excited states [32] in polar environments and membranes [33], whereas R6G shows a much more robust fluorescence decay time and indeed can be used over an extraordinary range of pH (1–14), which makes it ideal for sol–gel studies. Interestingly though, the form (though not the duration) of the fluorescence decay is irrelevant in anisotropy studies as the fluorescence just provides a tracer with which to track the depolarization, irrespective of whether it has a mono or multi-exponential decay.

The BODIPY (4,4-difluoro-3a,4a-diaza-*s*-indacene) fluorophore shows a spectral profile similar to that of fluorescein at alkaline pH. The quantum yield and the fluorescence lifetime are  $>0.8$  and  $\sim 5.5$  ns respectively, and nearly independent of polarity. Transition dipoles for absorption and emission, i.e.,  $S_0 \rightarrow S_1$ , are nearly parallel and polarized along the long axis of the chromophore [34]. The probe is zwitterionic and in that sense resembles an amino acid, which is believed to be advantageous in site-specific labelling of proteins using reactive derivatives of the probe shown in Fig. 1.

Knowing the accurate hydrodynamic radius of the depolarization probe is of crucial importance if viscosity is the measurand of interest (cf. Eq. 3). Because of their extensive study over many years, both R6G and DPH are probably as close as we have available for depolarization standards, their dimensions being determined from their anisotropy decay in an isotropic solvent such as paraffin oil and using appropriate versions of Eq. 3. Anisotropy decay measurements of the hydrodynamic radius and theoretical predictions

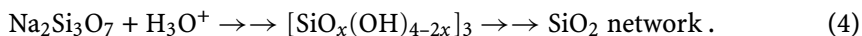
when treating R6G as an oblate ellipsoid of axes 0.7 nm and 0.2 nm are consistent at  $\sim 0.53 \pm 0.03$  nm [10, 35, 36]. By contrast, DPH is a prolate ellipsoid with fairly consistent reports of a long-axis measured to be  $\sim 1.3$  nm [37, 38] and short axis 0.17 nm [37] and 0.13 nm [38]. However, care should be taken when using the theoretical molecular dimensions in experiments (Fig. 1) as they make no allowance for conformational changes associated with solvation of probes under experimental conditions. Indeed, the volume of DPH derived from anisotropy measurements has been reported to be 20 times less than the Van der Waal volume [38].

### 3 Probe Depolarization on Silica Nanoparticles

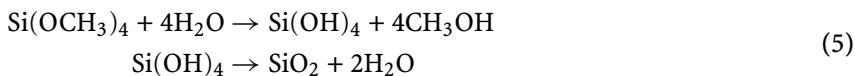
Early use of bound fluorescent probes in depolarization studies mainly concerned proteins using the fluorescence of the intrinsic amino acid tryptophan and membranes using the fluorescence of extrinsic probes, particularly DPH. There have been a number of excellent reviews on these topics to which the reader is referred [1–4], but here we will concentrate on probes bound to nanoparticles as a means of determining the hydrodynamic radius. A principle requirement for this kind of study is that the fluorescence lifetime  $\tau \sim \phi$ . If  $\tau \gg \phi$  the depolarization is too fast to measure accurately during the fluorescence lifetime and if  $\tau \ll \phi$  too little depolarization occurs during the fluorescence lifetime. Recent results summarized in this article suggest this criterion is not so strictly applicable as it appears at face-value.

Silica has advantages in nanoparticle standardization as it is optically transparent to below 200 nm and is photophysically benign in comparison to metal colloids where surface plasmon effects are an unwanted complication. Silica nanoparticles are also much smaller than readily available organic polymer particles.

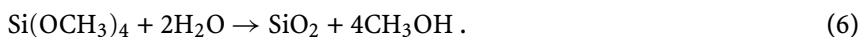
In the following sections we will discuss fluorescence depolarization observed from probe molecules introduced into two different categories of silica systems. The first system is a commercially available stable sol of nanometer-sized silica particles, e.g., Ludox. The stability of the sol is achieved by adjusting pH and ionic strength to values where particles have a negative surface charge and therefore repel each other. Next we examine less-stable silica sols prepared under conditions where mutual repulsion between particles is not great enough to prevent agglomeration and growth of more ramified silica clusters therefore occurs. At a certain time,  $t_g$ , the clusters are joined together to span the containing vessel and the sol enters a gel state, hence this category of samples are often referred to as sol-gels. Starting from sodium silicate, the reaction can schematically be written:



This hydrogel reaction pathway is complex and still under debate [39]. Alternatively silica alcogels can be prepared starting from an orthosilicate [40], e.g., TMOS (tetramethyl orthosilicate) where the reaction can be written as



and taken together



Compared to the silicate route the orthosilicate reaction is free from salt and can be prepared close to physiological conditions of interest in biological/medical applications. The produced alcohol can be removed under vacuum [41, 42] and replaced with other solvents.

The molecular picture of silica sol-gels is an interlinked network of  $\text{SiO}_2$  particles that spans the containing vessel. Initially the network is fragile, i.e., at  $t_g$ , but gains mechanical strength by aging and syneresis, i.e., solvent is expelled by capillary forces. By controlling the synthesis optical transparent sol-gels can be prepared that can host a variety of guest molecules within its pores [40, 43]. Here we will concentrate on the particles in the precursor state prior to  $t_g$ .

### 3.1

#### Stable Silica Nanoparticles (Ludox)

Dyes can be covalently bound to silica particles [44] but here we consider the general convenience of post-doping a nanoparticle. Figure 2 shows polarization data recorded on Ludox AM30 non-covalently labelled with the dye CG437 which has fluorescence decay components of  $\tau_1 = 8.5 \pm 1.7$  ns (45%) and  $\tau_2 = 26.5 \pm 0.7$  ns (55%). If one assumes that AM30 is a monodispersed sol of silica particles of radius 6 nm (mean value quoted by the manufacturer Dupont) and that the dye is rigidly attached to particles dissolved in water at 20 °C one would expect a single correlation time given by Eq. 3 of  $\sim 220$  ns. However, data analyzed using such an idealized model shows a significant mismatch and can be ruled out. A systematic analysis of data shows that three different Ludox, SM30, AM30 and AS40 of radii given by the manufacturer of 3.5 nm, 6.0 nm and 12 nm, respectively, require a two exponential model with a limiting anisotropy for an adequate fit:

$$R(t) = b_1 \exp\left(-\frac{t}{\phi_1}\right) + b_2 \exp\left(-\frac{t}{\phi_2}\right) + R_\infty . \quad (7)$$

Typical fitting values are shown in Table 1. Interestingly, it can be noted that one of the correlation times,  $\phi_2$ , corresponds to what is expected for



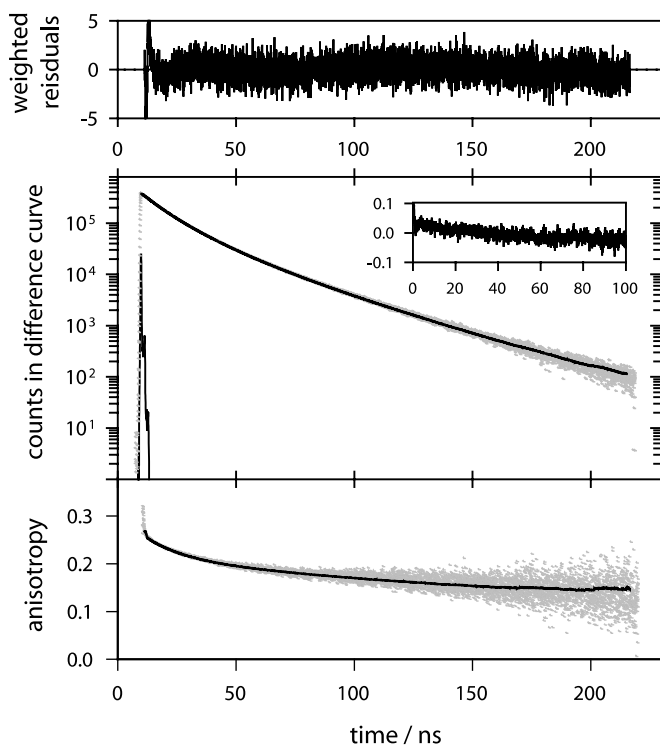


**Fig. 2** Depolarization data recorded on a Ludox AM30 sample (radius 6 nm as specified by Dupont) diluted to 2% w/w SiO<sub>2</sub> and non-covalently labelled with the dye CG437. The excitation source was an IBH NanoLED-11 ( $\lambda = 374$  nm, FWHM = 120 ps) and the emission was recorded through a monochromator centered at 450 nm. The number of counts in the peak of the difference curve is  $5 \times 10^5$ . Data was fitted to two exponential functions and a limiting value, a total of six fitting parameters including a time-shift parameter. The quality of the fit was judged by inspecting the weighted residuals (*upper graph*) the autocorrelation function, inserted graph, as well by the calculated reduced  $\chi^2$  that should equal 1 for an ideal fit to data with only Poissonian distributed noise. In the present case,  $\chi^2 = 1.23$ . As can be seen from the weighted residuals, there is a small mismatch observed at the excitation peak. This can be explained by the large number of counts recorded exposing small systematic errors otherwise hidden in the statistical noise. Also, the sample most likely contains a fraction of unbound dye with an estimated correlation time of  $\sim 50$  ps at the measurement temperature 20 °C, which is not included in the analysis. The time per channel in the time-correlated single-photon experiment was set to 0.28 ps and data was recorded over 8192 channels

Brownian rotation of a dye rigidly attached to the SiO<sub>2</sub> particle and with no additional depolarization mechanisms occurring. In Table 2 we show a comparison between the particle radius obtained from  $\phi_2$  via the Stokes–Einstein relationship (Eq. 3) and values quoted by the manufacturer, which were most probably obtained by electron microscopy. These results demonstrate the po-

**Table 1** Typical fitting parameters obtained in analyzing depolarization data recorded on Ludox. Ludox has a finite shelf life and data presented here is measured on fresh samples diluted to 2% w/w SiO<sub>2</sub> and labelled with CG437 at  $\sim 1 \mu\text{M}$  bulk concentration. It has been noticed that there are differences in recovered parameters between samples prepared from different batches of Ludox. These mainly concern the fraction of the limiting anisotropy value, probably reflecting different degrees of agglomeration, however, the value of  $\phi_2$  stays approximately constant

Ludox	$R_0$	$b_1$	$\phi_1/\text{ns}$	$b_2$	$\phi_2/\text{ns}$	$R_\infty$	$\chi^2$	$\text{pc}^a$
SM30	0.24	0.08	24	0.04	65	0.12	1.26	$1 \times 10^5$
AM30	0.28	0.06	17	0.16	273	0.06	1.23	$5 \times 10^5$
AS40	0.28	0.05	10	0.16	1400	0.07	1.27	$1 \times 10^6$

$\text{pc}^a$  – number of counts recorded in the peak of the difference curve

**Table 2** Comparison between calculated particle sizes,  $r_{\text{calc}}$ , i.e.,  $\phi_2$  Table 1 and Eq. 3 and values reported by the manufacture,  $r_m$

Ludox	$r_m/\text{nm}$	$r_{\text{calc}}/\text{nm}$
SM30	3.5	$4.0 \pm 0.4$
AM30	6.0	$6.4 \pm 0.5$
AS40	12	$11 \pm 1.6$

tential use of Ludox as a readily available nanometrology standard, but it always needs to be kept in mind that Ludox is an industrial-grade colloid and with this can come background fluorescence, particle aggregation, and batch differences.

Indeed, the nature of the limiting value is most likely due to a fraction of SiO<sub>2</sub> particles agglomerated into a larger cluster with a correlation time that cannot be resolved during the fluorescence lifetime of CG437, i.e.,  $\phi \gg \tau$ . Consistent with this explanation it should be noted that destabilizing the sample by adding salt, i.e., by inducing aggregation, causes this fraction to increase. The shorter correlation time,  $\phi_1$ , may reflect a distribution of particle sizes in the sol [45] however if one follows the argument used in analyzing depolarization data recorded on fluorescent probes dissolved in lipid bilayers and proteins, it is likely that the probe has a certain degree of freedom to wobble in its binding site [46], as is illustrated in Fig. 3. Wobbling is characterized by an effective cone angle that reflects the local environment. It must here be noted that the overall Brownian diffusion of the particle and the local wobbling motion of the probe are coupled [47], however, Eq. 7 is a valid approximation if  $\phi_2 \gg \phi_1$ , which is the case here.

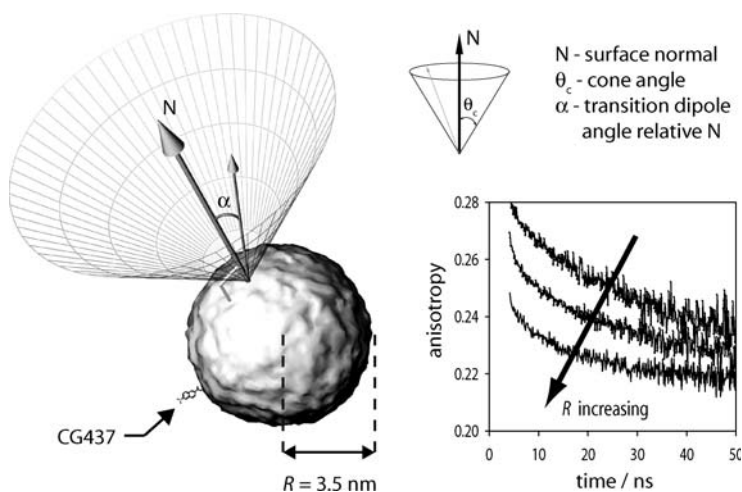


**Fig. 3** Part A of the figure illustrates a fluorophore attached to a particle, e.g., Ludox SM30 ( $r = 3.5$  nm), free to undergo a local motion within a cone. Notice the relative size of the chromophore CG437 shown to scale. Part B shows anisotropy decays recorded on silica particles of different sizes

Previously it has been found that fluorescence anisotropy recorded on silica samples could be described assuming that a fraction of the dye was unbound and free to rotate in solution [48]. Most likely this is the case for the CG437/Ludox systems discussed here, and if we are strictly rigorous Eq. 7 should therefore be expanded to include one additional correlation time corresponding to the size of CG437. However, estimating this correlation time from the solvent excluded volume of the probe, see Fig. 1, gives  $\sim 50$  ps that approximately corresponds to two channels (28 ps) in the recorded photon counting histogram. Thus, if the fraction of free dye is small in comparison to the fraction bound, one cannot expect to resolve this component. In analyzing data, it was found that including one additional correlation time only marginally improved the quality of the fit. However, the low  $R_0$  values shown in Table 1 with respect to the theoretical value of 0.4 might reflect an additional depolarization mechanism such as free dye or indeed intra-molecular dipole re-orientation in the excited state.

From Table 1 it can also be seen that despite the presence of a complex anisotropy decay and a large departure from the rigid requirement of  $\tau \sim \phi$ , reliable particle size measurements can be obtained up to  $\tau \sim \phi/50$  provided that depolarization data can be recorded with sufficient high statistics, i.e., a large number of counts in the difference curve exceeding  $10^5$ . Stable silica colloids such as Ludox would thus seem to offer useful possibilities as an in-situ fluorescence polarization metrology standard for nanoparticles provided the anisotropy is carefully interpreted.

### 3.2

#### Surface-Contour Diffusion (SCOD)

Translational diffusion of fluorophores in solution will not contribute to a change in the fluorescence anisotropy; however, the situation is different if the translational motion is restricted to a curved surface, thereby imparting excited state dipole rotation. This effect has been investigated for fluorophores localized in curved lipid phases and to take lateral diffusion into account a hopping constant was included in anisotropy models reported by Van Der Meer [49]. Further experimental investigations by Chen et al. [50] showed that the time-resolved fluorescence anisotropy decay contained morphological information in terms of the curvature of the lipid phase that agreed with X-ray diffraction data. Krishna et al. [51] used Monte-Carlo simulations to investigate translational diffusion of fluorophores on spherical surfaces, i.e., micelles and vesicles. It was found that depolarization due to translational diffusion could be described by a sum of three exponentials containing 3 independent parameters, the angle,  $\alpha$ , of the emission transition dipole relative to the surface normal, the curvature of the surface, i.e., the radius  $r$ , and the translation diffusion constant  $D_{tr}$ :

$$\begin{aligned}
 R(t) = & \frac{2}{5} \left( \cos^2 \alpha - \frac{1}{2} \sin^2 \alpha \right)^2 \exp(-6D_{tr}t/r^2) \\
 & + \frac{6}{5} \sin^2 \alpha \cos^2 \alpha \exp(-5D_{tr}t/r^2) \\
 & + \frac{3}{10} \sin^4 \alpha \exp(-2D_{tr}t/r^2).
 \end{aligned} \tag{8}$$

It is interesting to make a comparison with a dye molecule non-covalently attached to a silica particle as depicted in Fig. 3A, because we may expect a similar effect to occur although it has not hitherto been identified as such in fluorescence anisotropy studies of silica nanoparticles. The translational diffusion coefficient reported for Nile Red when dissolved in the hydrophobic interior of micelles is  $\sim 1 \times 10^{-10} \text{ m}^2 \text{ s}^{-1}$  [51]. If one assumes a similar diffusion coefficient when localized on a  $\text{SiO}_2$  surface and that the emission transition dipole moment adopts an orientation parallel with the surface normal, i.e.,  $\alpha = 0^\circ$ , then Eq. 8 is reduced to a single exponential term and a correlation time of  $\sim 20 \text{ ns}$  can be estimated in the case of Ludox SM30 ( $r = 3.5 \text{ nm}$ ). This is remarkably close to the value of  $\phi_1 = 24 \text{ ns}$  measured for SM30 and hitherto attributed by default to dye wobbling on the surface. However, in general, if dye molecules are undergoing surface contour diffusion (SCOD) one can expect this to constitute an additional depolarization channel to wobbling and to the overall Brownian rotational motion and should be taken into account in any full treatment. In Fig. 3B we show a comparison of depolarization recorded on a set of Ludox of different radii. It is reasonable to assume that the surface conditions are nearly identical between the

Ludox and if local wobbling is contributing to the depolarization it should be similar between the samples. However, as can be seen from  $\phi_1$  in Table 1 and Fig. 3B, there is a strong dependence of the shorter correlation time on the radius of the particle. On one hand this suggests SCOD is the more dominant over wobbling, but on the other hand the trend whereby  $\phi_1$  decreases as  $r$  increases is perhaps counter-intuitive. Either way the data analysis is complicated by the unknown angle  $\alpha$  and by coupled depolarization motions and further work is presently needed to confirm the relative magnitudes of these competing pathways to depolarization. Nevertheless, the potential of Ludox as a nanometrology standard is clear.

### 3.3

#### Silica Hydrogel Nanoparticle Growth Kinetics

Although the search for improved nanometrology standards for fluorescence anisotropy decay is still ongoing, the field has already progressed using the rotation of free dye as the standard for comparison, even though dye molecules are not of comparable size to most nanoparticles of interest [10, 11, 19, 48, 52–60]. Figure 4 shows the growth of silica nanoparticles at pH 10, which are the precursors to reaching the gel point  $t_g$  at which the silica network spans the containing vessel. In this case, the free dye (R700, see Fig. 1) radius and rotational correlation time were used effectively as standards with which to determine the microviscosity, which in turn enabled the dye-particle size to be determined from Eq. 3. The anisotropy expression then takes the form

$$R(t) = (1 - f)R_0 \exp(-t/\phi_f) + f R_0 \exp(-t/\phi_b), \quad (9)$$

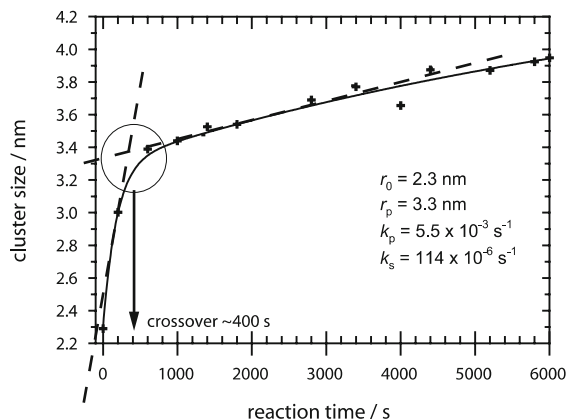


**Fig. 4** Particle growth in a 2% w/w  $\text{SiO}_2$  sample at pH 10 as probed with R700. The crossover between what is suggested to be different mechanisms of polymerization is indicated. The *solid curve* is Eq. 10 fitted to data with parameters as listed

where  $(1 - f)$  is the fraction of free dye in solution undergoing Brownian rotational diffusion characterized by  $\phi_f$ , and correspondingly  $f$  and  $\phi_b$  reflects dye bound to silica particles. Interestingly, the particle size data presented in Fig. 4 shows two different growth regions, an initial rapid phase followed by slower region reflecting different reaction mechanisms involved in the underlying silica polymerization. It is generally believed that particle growth at high pH occurs by Ostwald ripening [39], i.e., larger particles grow at the expense of smaller clusters that dissolve, and one could speculate that at the crossover point the silicic acid initially released is consumed and the slower dissolution process becomes dominant. Consistent with this the crossover point is also coincident with the time  $t_{\text{pH}}$  at which the pH stabilizes [18]. Taken together, if one assumes a two-step process for the particle growth one can write

$$r(t) = r_0 + (r_p - r_0)(1 - \exp(-k_p t)) + (r_s - r_p)(1 - \exp(-k_s t)), \quad (10)$$

where  $r_0$  is the initial particle radius that the measuring technique can resolve, i.e., if data could be taken at time zero defined by the time of mixing the reactants then  $r_0 = 0$ . Such an experiment is possible to realize through a continuous flow system [52], however, for practical reason the data presented in Fig. 4 was recorded under stationary conditions.  $r_p$  and  $r_s$  indicate the size reached by the silica particles during the different time-regions to denote primary “p” and secondary “s” particles and  $k_p$  and  $k_s$  indicate the corresponding rate constants. Equation 10 is fitted to the data presented in Fig. 4 and the best fitted parameters are listed.

With respect to the last section on Ludox colloids, which are hard silica spheres, it seems unlikely that SCOD depolarization will occur to the same extent in the more ramified and hence more diffusion limited local environment of silica nanoparticles during their formation. However, dye wobbling would still of course be expected to occur.

### 3.4

#### The Multiphoton Advantage

In order to extend the dynamic range in an anisotropy measurement it is possible to use multi-photon excited (MPE) fluorescence [54]. Here the sample is placed within an intense radiation field from a focused laser beam causing the simultaneous absorption of  $i$  light quanta, which narrows the induced photo selection, and modifies  $R_0$  as

$$R_0 = \frac{2i}{2i + 3} \left[ \frac{3}{2} \cos^2 \beta_i - \frac{1}{2} \right], \quad (11)$$

where  $\beta_i$  is the intramolecular angle between the dominant absorption and emission transition dipoles. In the case of co-linear dipoles,  $\beta_i = 0$ , and  $i = 1$ ,

the time-zero anisotropy takes its usual value 0.4. However, if two or three photons are simultaneously absorbed  $R_0$  is increased by 43% and 67%, to 0.57 and 0.67, respectively. The situation is illustrated in Fig. 5 where synthetic data is presented for a spherical particle with a 5 ns rotational correlation time undergoing Brownian diffusion in a solvent of viscosity 1 cP. Data was re-analyzed for different values of the correlation time and the  $\chi^2$  parabola was constructed. It can be seen that the  $\chi^2$  parabola shows a significantly sharper minima when  $i > 1$ , which is carried through as a smaller statistical error in the fitted parameters.

By using two-photon excitation of R6G, silica clusters growing from 0.8 nm to 1.3 nm have been detected in acidic alkoxide sols [10, 11] and this probably represents the lowest limit of resolution yet obtained. A further advantage in MPE experiments is the anti-Stokes shifted fluorescence causing reduced light scatter that may otherwise be of concern in studying sols.

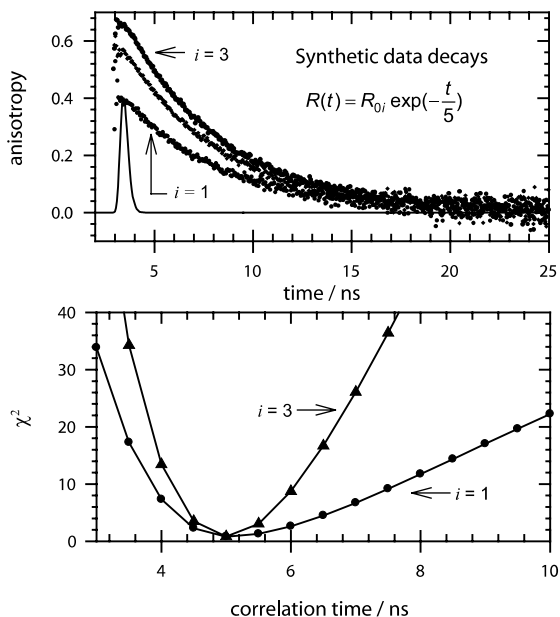


**Fig. 5** The *upper graph* shows synthetic anisotropy decay corresponding to a 5 ns correlation time under different modes of excitation, i.e.,  $i = 1, 2$  and  $3$ . The time per channel was set to 50 ps. Also shown is the Gaussian-shaped instrumental response function, FWHM  $\sim 450$  ps, used for the data generation. The *lower graph* shows the  $\chi^2$  parabola obtained when reanalyzing data and illustrates the better precision in fitted parameters achieved by using multiphoton-induced fluorescence. To construct the  $\chi^2$  parabola, one parameter was free to vary, the pre-exponential factor, and the  $\chi^2$  was calculated as function of  $\phi$ . The data was free from time-shift and distortions like pulse pile-up, radio-frequency interference, etc.

### 3.5

#### Sources of Error

It would be incorrect to associate all depolarization with Brownian rotation even for isolated and freely rotating dye molecules in solution. There are numerous examples in one and multiphoton studies of intra-molecular depolarization due to  $\beta_i$ , the intramolecular angle between the dominant absorption and emission transition dipoles, being non-zero. For example, the one-photon excitation of R6G at 400 nm leads to an  $R_0$  value as low as 0.09 as compared to the two-photon excitation at 800 nm giving a  $R_0$  value of 0.50 [31]. Here it is likely that different symmetry states are being populated, hence care needs to be taken in the choice of wavelength if the loss of dynamic range due to rapid intra-molecular processes is not to occur. Kowski [1] has considered the effect of excess vibrational energy of excitation by varying the excitation wavelength for R6G and found it to have no effect on  $\phi$ , although there was some evidence of an effect on  $R_0$ .

Potential sources of error in silica nanoparticle metrology concern the fluorescence lifetime being different for the free and silica particle bound dye and dye clustering leading to depolarization due to FRET or other energy migration mechanisms. A potential ambiguity also exists in the interpretation of data with respect to the possibility of viscosity and particle-size changes having comparable effects on  $\phi$  (Eq. 3). Indeed, early work incorrectly interpreted the anisotropy changes in sol-gels solely to viscosity without any consideration given to the presence of particles [16].

The dimensions of dyes obviously have a part to play in determining the smallest nanoparticle or cluster that can be measured, but the limitation is perhaps not so severe in ramified clusters where dye intercalation can occur.

Finally, it should be noted that Eq. 3 gives a radius dependent on the cube root of  $\phi$ ,  $\eta$  and  $T$ , thus minimizing the effect of errors in these parameters on the calculated value for  $r$ .

## 4

### Depolarization Due to Protein Structure and Dynamics

#### 4.1

##### Intrinsic Amino Acid Fluorescence

At first glance, it might seem that the intrinsic amino acid fluorescence of proteins may offer a viable nanometrology standard. After all, proteins have crystallographic structures that are well known in many cases, have dimension in the 10 nm region, which is comparable to many classes of nanoparticles and they fluoresce quite strongly. However, the experimental evidence usually reveals poor agreement between the crystallographic data and the hydrody-



dynamic radius obtained from the decay of fluorescence anisotropy [61]. This is probably linked to conformational differences between the frozen and native form and also the effect of the hydration shell.

Of course protein depolarization of fluorescence has received extensive attention in its own right and displays many of the characteristics already mentioned for silica nanoparticles. Hence the anisotropy decay in the presence of protein Brownian rotation and amino acid wobbling can be approximated by similar expressions to Eq. 7, bearing in mind the additional complication of the likelihood of there being several tryptophan or tyrosine residues contributing to the fluorescence and the rotations may be coupled and not separable.

It is a pity that more use cannot be made of proteins as nanometrology standards as there have been some recent developments in experimental capabilities which greatly facilitate the study of protein fluorescence. We are thinking in particular of the recent introduction of ultra-violet (UV) light-emitting diodes operating at 265 nm [62], 280 nm [63], and 295 nm [64] to provide intense UV optical pulses at low cost and negligible maintenance as compared with the hitherto alternative of Ti:Sapphire main-frame lasers. The greater convenience of light-emitting diodes is likely to lead to more widespread studies of proteins and new observations such as the recently reported evidence for rotamers in phenylalanine akin to the other two fluorescent amino acids [62].

Nevertheless it is instructive to dwell a while on some of the photophysics encountered in proteins as they provide a paradigm for several of the challenges to be successfully engaged in the search for fluorescence nanometrology standards. We are thinking mainly of the challenges associated with energy migration and its effect on polarization.

It can be seen from the orientational distribution function  $f_i(\theta)$  between the plane of polarization of excitation and that of the absorption dipole that every time energy is transferred there is a reduction in excited state anisotropy according to the angular dependence for  $i$  photons absorbed given by [54]:

$$f_i(\theta) = \cos^{2i} \theta. \quad (12)$$

Hence, no matter what the mechanism of energy transfer, be it radiative, FRET, or exciton, the net result is a reduction in anisotropy and, if it is beyond the time-resolution of the experiment, will appear as a reduction in  $R_0$ .

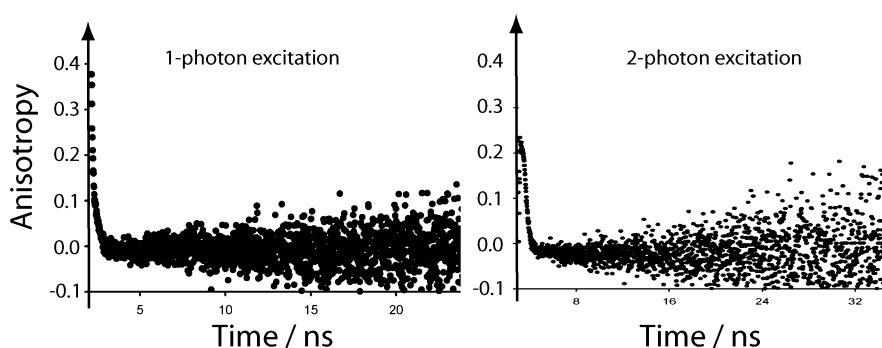
In proteins, efficient FRET occurs from tyrosine, which requires excitation at 280 nm, to tryptophan, such that most fluorescence observed in proteins originates from tryptophan and is usually detected at  $\sim 330$  nm [4]. The effect of this fundamental process manifests itself in depolarization data as illustrated in Table 3 for the single tryptophan protein human serum albumin (HSA). Here the anisotropy decay is analyzed using a faster component

**Table 3** Comparison of rotational decay parameters measured using a 295 nm and 280 nm LED. Errors are quoted to three standard deviations. Adopted from [64]

LED source	$\phi_1/\text{ns}$	Rel. int. %	$\phi_2/\text{ns}$	Rel. int. %	$R_0$	$\chi^2$
295 nm	$1.04 \pm 0.68$	0.4	$32.3 \pm 2.0$	99.6	0.198	0.98
280 nm	$0.72 \pm 0.32$	1.3	$20.6 \pm 1.3$	98.7	0.136	0.95

representing tryptophan wobbling and a longer component representing the Brownian rotation of the whole protein at 280 nm and 295 nm excitation. The shorter wavelength of excitation of tyrosine leads to FRET to tryptophan and apparent reduction in both rotational times and the initial anisotropy as compared to direct excitation of tryptophan at 295 nm. Note also how the longest rotational time of 32 ns is more than  $\sim 2$  times too short to represent rotation of the crystallographic dimensions of HSA of  $\sim 8 \times 8 \times 3$  nm.

The photophysics of tryptophan and tyrosine also bear testimony to the effect on depolarization of inter-conversion between complex excited states. In contrast to most common aromatic ring structures, the indole ring in fluorescent amino acids demonstrates a higher initial anisotropy for one photon than for two photon excitation (cf. Eq. 11) [54]. This is attributed to inter-conversion from an initially excited  $^1L_b$  state to the fluorescent  $^1L_a$  state. This behavior even propagates to nanoparticles containing indole rings as evidenced by those of the skin pigment melanin, which is a polymer particle of  $\pi$ -stacked di-hydroxyindole units [65]. Figure 6 shows the one- and two-photon fluorescence anisotropy decay of Sepia melanin using 400-nm and 800-nm Ti:Sapphire fs excitation, respectively [66]. The lower initial anisotropy in the two-photon case is clearly evident as is the rapid depolarization, believed to be due to energy migration.

**Fig. 6** One- and two-photon fluorescence anisotropy decay of Sepia melanin using 400-nm and 800-nm excitation [66]

Although departing from the natural form some of the complexity of the intrinsic fluorescence from amino acids in proteins can be removed by the use of bespoke labelling with extrinsic probes and aspects relevant to nanometrology in this approach are discussed in the next section.

## 4.2

### Extrinsic Probe FRET

Fluorescence resonance energy transfer (FRET) has been widely used as a nanometer ruler to measure distances between donor and acceptor molecules. The key expression was derived by Förster [67] who showed that the rate of energy transfer,  $\omega_{ij}$ , between two dipoles, here labelled  $i$  and  $j$ , separated by a distance  $d_{ij}(t)$  at a time  $t$  could be written

$$\omega_{ij}(t, \Omega) = \frac{3}{4} \frac{\kappa^2(t, \Omega)}{\tau} \left( \frac{R_{0f}}{d_{ij}(t)} \right)^6. \quad (13)$$

The characteristic Förster radius,  $R_{0f}$ , and the fluorescence lifetime in the absence of energy transfer,  $\tau$ , can be determined in an independent experiment. The angle dependence between the interacting dipoles,  $\Omega$ , enters through the orientational factor  $\kappa^2(t, \Omega)$  given by

$$\kappa_{ij}^2(t, \Omega) = \hat{\mu}_i(t) \cdot \hat{\mu}_j(t) - 3 (\hat{\mu}_i(t) \cdot \hat{d}_{ij}(t)) (\hat{\mu}_j(t) \cdot \hat{d}_{ij}(t)), \quad (14)$$

where  $\hat{\mu}_i$ ,  $\hat{\mu}_j$  and  $\hat{d}_{ij}$  indicates unit vectors of the transition dipole moments and distance, respectively, see Fig. 7. Thus, to evaluate Eq. 13 one needs to consider both reorientational motion, i.e., time dependence of  $\Omega$ , as well as

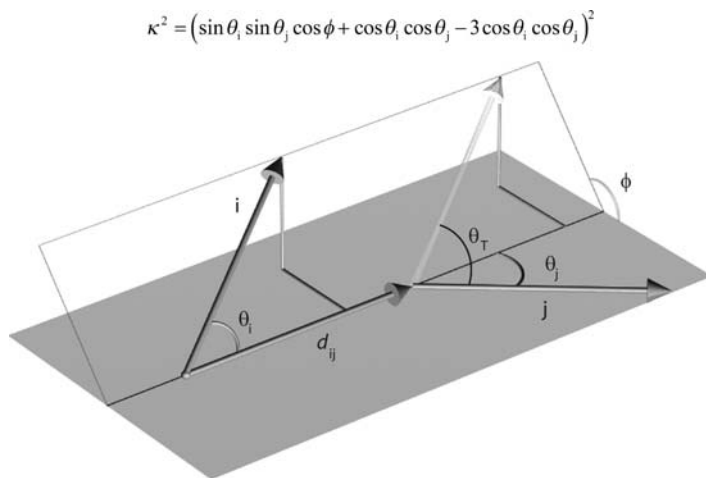


**Fig. 7** Visualization of the angle dependence of  $\kappa^2$

translational diffusion, i.e., time dependence of  $d_{ij}$ . This is a challenging task and to simplify the problem it is often assumed that translational diffusion can be neglected. Further, if the rate of energy transfer is time-independent, i.e., much faster or much slower than the rate of molecular reorientation,  $\kappa^2$  can be ensemble averaged, e.g., in the case of an isotropic distribution in the dynamic limit  $\kappa^2 = 2/3$ . If the orientational distribution is not known, which is most often the case, the range of  $\kappa^2$  can be calculated using the method described by Dale et al. [68].

In designing FRET experiments to obtain morphological information about nanostructured systems, e.g., proteins, sol-gels membranes, etc., one can choose between two different approaches, namely reversible or irreversible energy transfer. In the case of irreversible FRET, the rate of energy transfer from molecule 1 to 2 is much faster than the rate of energy transfer from molecule 2 to 1, i.e.  $\omega_{12} \gg \omega_{21}$ . This condition can be realized by finding a fluorescent donor and a non-fluorescent acceptor that have a spectral overlap, i.e., where the emission spectrum of the donor emission overlaps with the absorption spectrum of the acceptor. The rate of energy transfer can then be evaluated by measuring the quenching kinetics of the fluorescence signal. A situation of special interest is the use of metal ions as the acceptor since  $\kappa^2$  will then average to  $2/3$ , assuming that translational diffusion can be neglected, and one source of error is thus eliminated. This concept was used in sensors designed to specifically detect solvated cobalt [69] and copper(I) ions [70] and to probe phase transitions in the lipid bilayers of vesicles [71–73]. In these experiments, each donor is surrounded by an ensemble of acceptors that are distributed in a way that reflects the local morphology. Thus, buried in a recorded decay curve is additional information and to gather this extended morphological information, Rolinski and Birch developed an analyzing protocol with the potential to recover the underlying distance distribution making no prior assumption about its shape [74, 75].

Rather than labeling at random locations, which is effective in amorphous sol-gel nanoparticles, a higher degree of precision is often required for highly structured assemblies such as proteins. This can be achieved by site-directed mutagenesis where probes are inserted at specific positions in the amino acid sequence. However, the process requires the specific attachment of two different molecules, a donor and an acceptor, at two unique positions. Karolin et al. presented an alternative approach where the protein is labelled with the same kind of probe at two unique positions [76], an approach that offers a simplified preparation protocol. In this case, the energy-transfer process is reversible, i.e.,  $\omega_{12} = \omega_{21}$ , and can only be monitored by recording the depolarization of emitted light. To distinguish this process from the previous irreversible case it is often referred to as donor-donor energy migration DDEM.

A complication that is often encountered is that the rate of energy transfer is not independent of time, i.e., it occurs as the same time-scale as the local

reorientation of the probe, and there exists no closed analytical solution to the anisotropy decay function. A semi-analytical solution was presented by Johansson et al. [77–79] that is based on designing an experiment where three forms of the protein are synthesized, namely two single mutants where energy migration does not occur and one corresponding double mutant where energy migration does occur. From each single mutant form of the protein the local correlation function can be recorded, here labelled  $R_i(t)$  and  $R_j(t)$ , and if the correlation functions are considered as independent of the excitation probability,  $p(t)$ , one obtains [79]

$$R(t) = \frac{1}{2} \{R_i(t) + R_j(t)\} p(t) + \frac{1}{2} \{R_{ij}(t) + R_{ji}(t)\} (1 - p(t)), \quad (15)$$

where  $R_{ij}(t)$  and  $R_{ji}(t)$  represent the contribution to the recorded anisotropy from energy migrating from molecule 1 to 2 and 2 to 1, respectively.

Equation 15 was tested on rigid molecules as well as applied to the protein plasminogen activator inhibitor-1 (PAI-1) [76, 80–82]. Good agreement between the expected distance and the crystal structures was found.

## 5 Conclusions

So where does all this leave us in the search for standards for fluorescence depolarization in nanometrology, as clearly there is much progress still to be made towards the goal of making trusted and unambiguous measurements. The rotational dynamics of free dye molecules in solution can be easily determined or are already fairly well known in many cases. However, although having uses, such as helping to explain why dye molecules have dual rotational times during sol–gel nanoparticle formation [49, 53], the dimensions of free dye molecules are too small to be used as standards for most nanoparticles. However, the description we have given here for the Ludox colloids perhaps gives us some pointers as to the current status and where progress is needed. We have discussed a comprehensive list of depolarization mechanisms for dye molecules bound to nanoparticles in terms of particle Brownian rotation, wobbling, intramolecular processes, and surface contour diffusion. It is also clear from the Ludox data that even within a complex anisotropy decay, particle size information is present and under favorable circumstances can be obtained. This leads us to believe that further progress in the theoretical interpretation of anisotropy decay data combined with bespoke probes, which simplify and obey the theoretical models, will continue to contribute much towards establishing reliable standards.

**Acknowledgements** We would like to acknowledge the award of research grants contributing to this work from the EPSRC, the Wellcome Trust and Ineos Silicas Ltd.

## References

1. Kowski A (1993) *Crit Rev Anal Chem* 23:459
2. Soutar I (1991) *Polym Int* 26:35
3. Steiner RF (1992) In: Lakowicz JR (ed) *Principles (Topics in Fluorescence Spectroscopy)*, vol 2. Kluwer Academic/Plenum Publishers, New York, p 1
4. Eftink MR (1991) *Methods Biochem Anal* 35:127
5. Sorensen EM (1988) *Subcell Biochem* 13:159
6. Megens M, Sprik R, Wegdam GH, Lagendijk A (1997) *J Chem Phys* 107:493
7. Tleugabulova D, Duft AM, Zhang Z, Chen Y, Brook MA, Brennan JD (2004) *Langmuir* 20:5924
8. Tleugabulova D, Zhang Z, Chen Y, Brook MA, Brennan JD (2004) *Langmuir* 20:848
9. Tleugabulova D, Zhang Z, Brennan JD (2003) *J Phys Chem B* 107:10127
10. Geddes CD, Karolin J, Birch DJS (2002) *J Phys Chem B* 106:3835
11. Karolin J, Geddes CD, Wynne K, Birch DJS (2002) *Meas Sci Technol* 13:21
12. del Monte F, Ferrer ML, Levy D (2001) *J Mater Chem* 11:1745
13. Hungerford G, Suhling K, Ferreira JA (1999) *J Photochem Photobiol A - Chem* 129:71
14. Kikteva T, Star D, Zhao ZH, Baisley TL, Leach GW (1999) *J Phys Chem B* 103:1124
15. Sathy P, Penzkofer A (1997) *J Photochem Photobiol A - Chem* 109:53
16. Narang U, Wang R, Prasad PN, Bright FV (1994) *J Phys Chem* 98:17
17. Huston AL, Reimann CT (1991) *Chem Phys* 149:401
18. Cleary A, Karolin J, Birch DJS (2006) *Appl Phys Lett* 89:113125
19. Geddes CD, Apperson K, Birch DJS (2000) *Dyes Pigment* 44:69
20. Mateo CR, Tauc P, Tosti S, Duportail G, Lianos P (1996) *Spectroc Acta Pt A - Molec Biomolec Spectr* 52:565
21. Arcioni A, Tarroni R, Zannoni C, Dalcanale E, Duvosel A (1995) *J Phys Chem* 99:15981
22. Toptygin D, Brand L (1993) *Biophys Chem* 48:205
23. Mateo CR, Tauc P, Brochon JC (1993) *Biophys J* 65:2248
24. Borenstain V, Barenholz Y (1993) *Chem Phys Lipids* 64:117
25. Arcioni A, Tarroni R, Zannoni C (1993) *J Chem Soc - Faraday Trans* 89:2815
26. Eyl V, Muller S, Donner M, Maugras M, Stoltz JF (1992) *Cytotechnology* 8:5
27. Christiansson A, Kuypers FA, Roelofsen B, Wirtz KWA, Denkamp J (1984) *Chem Phys Lipids* 35:247
28. Aragonbirlouez I, Montenaygarestier T, Devynck MA (1984) *Clin Sci* 66:717
29. Billard C, Tuy FPD, Rosenfeld C, Tapiero H (1983) *FEBS Lett* 158:229
30. Hare F (1983) *Biophys J* 42:205
31. Volkmer A, Hatrick DA, Birch DJS (1997) *Meas Sci Technol* 8:1339
32. Birks JB, Birch DJS (1975) *Chem Phys Lett* 31:608
33. Parasassi T, Destasio G, Rusch RM, Gratton E (1991) *Biophys J* 59:466
34. Karolin J, Johansson LBA, Strandberg L, Ny T (1994) *J Am Chem Soc* 116:7801
35. Porter G, Sadtowski PJ, Tredwell CJ (1977) *Chem Phys Lett* 49:416
36. Fleming GR, Morris JM, Robinson GW (1976) *Chem Phys* 17:91
37. Best L, John E, Jahnig F (1987) *Eur Biophys J Biophys Lett* 15:87
38. Mateo CR, Lillo MP, Brochon JC, Martinezripoll M, Sanzaporicio J, Acuna AU (1993) *J Phys Chem* 97:3486
39. Iler RK (1979) *The chemistry of silica: solubility, polymerization, colloid and surface properties, and biochemistry*. Wiley, New York
40. Brinker CJ, Scherer GW (1990) *Sol-gel science*. Academic Press Limited, London

41. Ferrer ML, del Monte F, Levy D (2002) *Chem Mat* 14:3619
42. Veum L, Hanefeld U, Pierre A (2004) *Tetrahedron* 60:10419
43. Avnir D, Coradin T, Lev O, Livage J (2006) *J Mater Chem* 16:1013
44. Imhof A, Megens M, Engelberts JJ, de Lang DTN, Sprik R, Vos WL (1999) *J Phys Chem B* 103:1408
45. Tleugabulova D, Sui J, Ayers PW, Brennan JD (2005) *J Phys Chem B* 109:7850
46. Kinosita K, Kawato S, Ikegami A (1977) *Biophys J* 20:289
47. Szabo A (1984) *J Chem Phys* 81:150
48. Birch DJS, Geddes CD (2000) *Phys Rev E* 62:2977
49. Vandermeer BW, Cheng KH, Chen SY (1990) *Biophys J* 58:1517
50. Chen SY, Cheng KH, Vandermeer BW, Beechem JM (1990) *Biophys J* 58:1527
51. Krishna MMG, Das R, Periasamy N, Nityananda R (2000) *J Chem Phys* 112:8502
52. Geddes CD, Karolin J, Birch DJS (2002) *J Fluoresc* 12:113
53. Geddes CD, Karolin J, Birch DJS (2002) *J Fluoresc* 12:135
54. Birch DJS (2001) *Spectroc Acta Pt A – Molec Biomolec Spectr* 57:2313
55. Geddes CD, Chevers JM, Birch DJS (2000) *J Fluoresc* 10:421
56. Geddes CD, Birch DJS (2000) *J Non-Cryst Solids* 270:191
57. Birch DJS, Geddes CD (2000) *Chem Phys Lett* 320:229
58. Birch DJS, Geddes CD (2000) *Chem Phys Lett* 322:300
59. Birch DJS, Geddes CD (2000) *Proc Indian Acad Sci – Chem Sci* 112:311
60. Geddes CD, Chevers JM, Birch DJS (1999) *J Fluoresc* 9:73
61. Ferrer ML, Duchowicz R, Carrasco B, de la Torre JG, Acuna AU (2001) *Biophys J* 80:2422
62. McGuinness CD, Macmillan AM, Sagoo K, McLoskey D, Birch DJS (2006) *Appl Phys Lett* 89:63901
63. McGuinness CD, Sagoo K, McLoskey D, Birch DJS (2004) *Meas Sci Technol* 15:L19
64. McGuinness CD, Sagoo K, McLoskey D, Birch DJS (2005) *Appl Phys Lett* 86:261911
65. Birch DJS, Ganesan A, Karolin J (2005) *Synth Met* 155:410
66. Ganesan A (2003) PhD Thesis: Photophysics of epidermal chromophores melanin and urocanic acid. University of Strathclyde, Glasgow, UK
67. Forster T (1948) *Ann Physik* 2:55
68. Dale RE, Eisinger J, Blumberg WE (1979) *Biophys J* 26:161
69. Salthammer T, Dreeskamp H, Birch DJS, Imhof RE (1990) *J Photochem Photobiol A – Chem* 55:53
70. Birch DJS, Holmes AS, Darbyshire M (1995) *Meas Sci Technol* 6:243
71. Holmes AS, Birch DJS, Suhling K, Imhof RE, Salthammer T, Dreeskamp H (1991) *Chem Phys Lett* 186:189
72. Birch DJS, Suhling K, Holmes AS, Salthammer T, Imhof RE (1993) *Pure and Applied Chemistry* 65:1687
73. Holmes AS, Suhling K, Birch DJS (1993) *Biophys Chem* 48:193
74. Rolinski OJ, Birch DJS (2000) *J Chem Phys* 112:8923
75. Rolinski OJ, Birch DJS (2002) *J Chem Phys* 116:10411
76. Karolin J, Fa M, Wilczynska M, Ny T, Johansson LBA (1998) *Biophys J* 74:11
77. Edman P, Westlund PO, Johansson LBA (2000) *Phys Chem Chem Phys* 2:1789
78. Johansson LBA, Edman P, Westlund PO (1996) *J Chem Phys* 105:10896
79. Johansson LBA, Bergstrom F, Edman P, Grechishnikova IV, Molotkovsky JG (1996) *J Chem Soc – Faraday Trans* 92:1563
80. Fa M, Bergstrom F, Karolin J, Johansson LBA, Ny T (2000) *European J Biochem* 267:3729
81. Fa M, Bergstrom F, Hagglof P, Wilczynska M, Johansson LBA, Ny T (2000) *Struct Fold Des* 8:397

82. Bergstrom F, Hagglof P, Karolin J, Ny T, Johansson LBA (1999) Proc Natl Acad Sci USA 96:12477
83. Allinger NL, Yuh YH, Lii JH (1989) J Am Chem Soc 111:8551
84. Bowen JP, Allinger NL (1991) Rev Comput Chem 2:81
85. Burkert U, Allinger NL (1982) Molecular Mechanics. American Chemical Society, Washington, DC
86. Connolly ML (1985) J Am Chem Soc 107:1118
87. Connolly ML (1994) J Math Chem 15:339



# Fluorescence Polarization: Recent Bioanalytical Applications, Pitfalls, and Future Trends

Alevtina A. Goulko<sup>1</sup> · Qiang Zhao<sup>1</sup> · Jeffrey W. Guthrie<sup>1</sup> · Hanfa Zou<sup>2</sup> · X. Chris Le<sup>1</sup> (✉)

<sup>1</sup>Division of Analytical and Environmental Toxicology,  
Department of Laboratory Medicine and Pathology,  
Faculty of Medicine and Dentistry and School of Public Health,  
University of Alberta, Edmonton, Alberta, T6G 2G3, Canada  
*xc.le@ualberta.ca*

<sup>2</sup>Dalian Institute of Chemical Physics, Chinese Academy of Sciences, Dalian, China

<b>1</b>	<b>Principle of Fluorescence Polarization</b> . . . . .	304
<b>2</b>	<b>Applications of Fluorescence Polarization</b> . . . . .	306
2.1	Fluorescence Polarization Immunoassay (FPIA) . . . . .	307
2.2	Receptor – Ligand and Peptide – Ligand Based Fluorescence Polarization Assays . . . . .	308
2.3	Aptamer-Based Fluorescence Polarization Assays . . . . .	310
2.4	Immobilized Metal Assay for Phosphochemicals (IMAP™) . . . . .	311
2.5	Fluorescence Polarization Assays for Single Nucleotide Polymorphism . . . . .	313
2.6	Capillary Electrophoresis Based Fluorescence Polarization Assays . . . . .	317
<b>3</b>	<b>Advantages and Limitations of Fluorescence Polarization</b> . . . . .	318
<b>4</b>	<b>Future Trends</b> . . . . .	320
	<b>References</b> . . . . .	321

**Abstract** Fluorescence polarization (FP) is sensitive to changes in molecular size and, therefore, assays that make use of molecular interactions are particularly useful. FP immunoassays, which rely on antibody-antigen interactions are widely used for clinical analysis, food analysis, and environmental monitoring. Development of other FP techniques, such as receptor-ligand and peptide-ligand affinity assays, aptamer affinity assays, immobilized metal assays for phosphochemicals, assays for single nucleotide polymorphisms, and capillary electrophoresis laser-induced FP assays, have further extended the applications of FP techniques to drug discovery, protein–DNA interactions, disease diagnostics, and biochemical research. The use of microplate readers equipped with polarizing optics has led to the adoption of FP as a readout mode for high-throughput screening assays. This chapter briefly describes the basic principle of FP and summarizes some of the recent bioanalytical applications of FP. It also discusses the main advantages, limitations, and future prospects of FP assays.

**Keywords** Affinity binding capillary electrophoresis · Fluorescence polarization · Immobilized metal assay for phosphochemicals · Immunoassay · Molecular interactions · Single nucleotide polymorphism

**Abbreviations**

ATP	Adenosine triphosphate
CE	Capillary electrophoresis
CTL	Cytotoxic T lymphocyte
CsA	Cyclosporine A
DNA	Deoxyribonucleic acid
ddATP	Dideoxyadenoside triphosphate
ddGTP	Dideoxyguanoside triphosphate
ddNTP	Dideoxynucleoside triphosphate
dNTP	Deoxynucleoside triphosphate
FP	Fluorescence polarization
FPIA	Fluorescence polarization immunoassay
GPCR	G protein-coupled receptor
GTP	Guanoside triphosphate
HIV	Human immunodeficiency virus
HT	High throughput
HTS	High throughput screening
IgE	Immunoglobulin E
IMAP	Immobilized metal assay for phosphochemicals
LIF	Laser-induced fluorescence
LIFP	Laser-induced fluorescence polarization
MHC	Major histocompatibility complex
MPE	Multi-photon excitation
PCR	Polymerase chain reaction
PDE	Phosphodiesterase
PMT	Photomultiplier tube
PDGF	Platelet-derived growth factor
PKC	3'-phosphatidyl-inositol-dependent kinase I
RNA	Ribonucleic acid
RT	Reverse transcriptase
siRNA	Small interfering RNA
SBE	Single base extension
SPA	Scintillation proximity assay
SNP	Single nucleotide polymorphism
SSB	Single-stranded DNA binding protein
TDI	Template-directed dye-terminator incorporated assay

**1****Principle of Fluorescence Polarization**

Fluorescence polarization (FP) is an intrinsic property of molecules. FP was first described in 1926 by Perrin [1]. It is based on the observation that when fluorescent molecules are excited with plane-polarized light, the emitted light remains fixed in the same plane as the excitation plane (i.e., the light remains polarized), as long as the molecules remain stationary during excitation. However, molecules in solution are subject to rotation. As a result, if the molecule tumbles quickly with respect to the fluorescence lifetime (typic-

ally a few nanoseconds), light is emitted in both vertical and horizontal planes with respect to the excitation light, and the fluorescence is depolarized. However, if the molecule tumbles slowly with respect to the fluorescence lifetime, the observed fluorescence remains significantly polarized (Fig. 1).

The degree of polarization is measured by monitoring both the horizontally and vertically polarized light. This is done by employing polarized light as the excitation source, and using a polarizing beam splitter to split the emitted light into both horizontally and vertically polarized planes. The ratio of the horizontally and vertically polarized fluorescence intensity (Eqs. 1 and 2) can then be used to determine the degree of polarization ( $P$ ) or anisotropy ( $r$ ):

$$P = \frac{(I_v - I_h)}{(I_v + I_h)} \quad (1)$$

$$r = \frac{(I_v - I_h)}{(I_v + 2I_h)}, \quad (2)$$

where  $P$  is the polarization,  $r$  is anisotropy,  $I_v$  is the vertical component of the emitted light, and  $I_h$  is the horizontal component of the emitted light. Both  $P$  and  $r$  are ratio quantities independent of both the fluorophore concentration and the intensity of the emitted light, provided that the intensity is sufficient for accurate measurement.

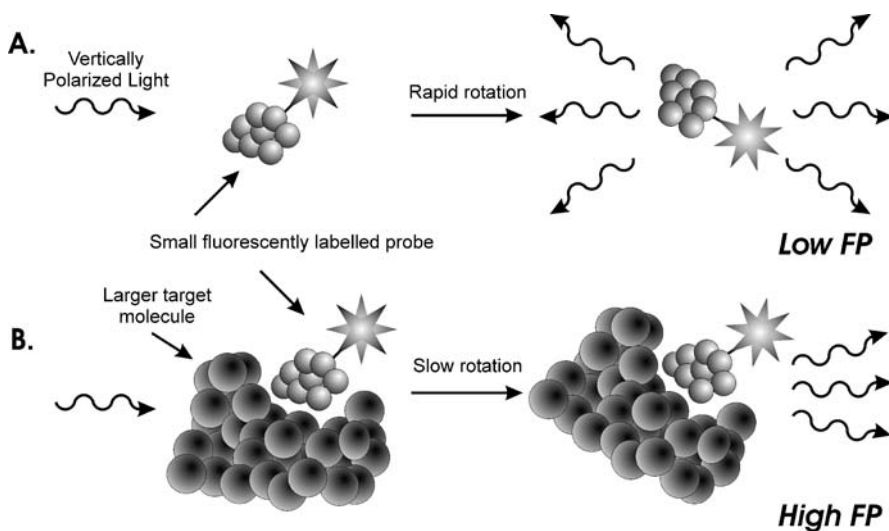


**Fig. 1** Schematic diagram of the FP difference between a small molecule (A) and a large, affinity-bound molecule (B). When plane-polarized light is used to excite the fluorescently labelled probe alone, the rapid rotation of the small molecule results in depolarization of the emitted fluorescence, resulting in low FP. When the same light is used to excite a larger molecule, such as when the probe is bound to a much larger protein target, the slow rotation of the large molecule maintains the polarization, resulting in high FP

The values for  $P$  can range from  $-0.33$  to  $0.5$ , and values for  $r$  from  $-0.25$  to  $0.4$ ; however, in practice, these limiting values are rarely attained. Typical values in bioanalytical applications for  $P$  range from  $0.01$  to  $0.3$  or  $10$  to  $300$  mP ( $1 \text{ mP} = 1/1000 \text{ P}$ ); smaller molecules, which rotate faster than larger molecules, have lower  $P$  and  $r$  values. This measurement range is not as narrow as it might appear to be, because very precise measurements ( $\pm 2$  mP) are readily obtainable with modern instrumentation.

The fundamental basis of FP is that it is related to the molecular volume via the rotational relaxation times. The rotational relaxation time ( $\rho$ ) is given by Stokes–Einstein equation (Eq. 3):

$$\rho = \frac{3\eta V}{k_B T}, \quad (3)$$

where  $\rho$  is the rotational relaxation time (the time required to rotate through an angle of approximately  $68.5^\circ$ ),  $\eta$  is the viscosity of the medium,  $V$  is the molecular volume of the molecule,  $k_B$  is the Boltzmann constant, and  $T$  is the temperature. For fluorescence emitted at right angles to the direction of excitation by linearly polarized light, the polarization,  $P$ , is given by

$$\left(\frac{1}{P} - \frac{1}{3}\right) = \left(\frac{1}{P_0} - \frac{1}{3}\right) \left(1 + \frac{\tau k_B T}{\eta V}\right), \quad (4)$$

where  $\tau$  is the fluorescence lifetime and  $P_0$  is the intrinsic polarization in the absence of rotational diffusion [1]. This indicates that FP is proportional to both the molecular size and the viscosity of the solution, and it is inversely proportional to the fluorescence lifetime and the temperature of the solution. In general, experiments are done at constant temperature and viscosity, and the change in fluorescence lifetime is negligible. Thus, a molecule's rotational relaxation time is directly proportional to its molecular volume.

Larger molecules are characterized by higher polarization values, since their rotational relaxation time is longer (slower rates of rotation), whereas smaller molecules have lower polarization values, due to their shorter rotational relaxation times (faster rates of rotation) (Fig. 1). By measuring the extent of fluorescence polarization, FP can be used to determine molecular interactions and to develop assays that make use of molecular interaction events.

## 2 Applications of Fluorescence Polarization

FP has been employed in several different applications, such as fluorescence polarization immunoassays [2], DNA hybridization and detection [3], DNA-protein binding [4], protein–ligand and peptide–ligand binding [5, 6], enzyme

assays [7–9], immobilized metal assay for phosphochemicals (IMAP) technology [10–13], high throughput screening FP (HTS-FP) for genotyping [14–21], capillary electrophoresis coupled laser-induced fluorescence polarization (CE/LIFP) assays [22, 23], and with the use of aptamers as affinity probes for FP detection of proteins [24–27]. The recent advent of microplate readers equipped with polarizing optics has led to the adoption of fluorescence polarization as a readout mode for high-throughput screening assays for drug discovery [5, 8, 9], detection of infectious diseases [6], and single nucleotide polymorphisms (SNPs) [14–21]. Microplate readers were traditionally in the 96-well plates format; however, 384-well plates ( $96 \times 4$ ) are now becoming more common, and soon 1536-well plates ( $96 \times 16$ ) (and even higher) will represent ultra-high throughput analysis, as the new technologies are adapted into the research labs. There are far too many other applications of FP to be covered in a single chapter. Therefore, we have decided to focus only on a few of the recent bioanalytical applications mentioned above.

## 2.1

### Fluorescence Polarization Immunoassay (FPIA)

Since the advent of FPIA in the 1970s by Dandliker [2], it has been used frequently in many fields. Several review papers have summarized these applications [28–30]. The largest group of bioanalytical applications utilizing FPIAs are those for clinical diagnostics; however, food analysis and environmental monitoring are also common. In clinical chemistry, FPIA is a powerful tool for monitoring therapeutic drugs [31, 32], determination of drugs of abuse in body fluids [33], and diagnosis of diseases [34, 35]. In food analysis, FPIA provides a simple and rapid means to detect toxins, such as ochratoxin and zearalenone [36, 37]. FPIAs have also been employed for the detection of contaminants in the environment, such as pesticides [30], herbicides [38, 39], nonylphenols [40], benzene [41], and metal ions [42].

The most common format for FPIA is the competitive immunoassay. In competitive assays, an unlabelled analyte competes with a labelled probe for the same binding partner, such as an antibody. Binding of the unlabelled analyte to the antibody displaces the antibody complex, resulting in depolarization. The degree of depolarization provides information on the amount of analyte bound to the antibody.

FPIA can be performed using a single reagent mixture, which involves pre-equilibration of the antibody with the fluorescent probe as a direct immuno-reagent [41, 43, 44]. When the sample is added to the pre-equilibrated reagent, the analyte in the sample displaces the probe from the complex. The quantification of analyte can be accomplished by monitoring the displaced probe. The change in the polarization value is determined by the concentration of analyte and the time of displacement. Single reagent FPIA is a one-step immunoassay, which reduces the detection time.

Both continuous flow and stopped-flow systems have been developed for FPIA. The flow format is particularly useful for HTS, because each measurement is usually completed within seconds. The stopped-flow FPIA uses the initial rate of the immunochemical reaction between the probe and the antibody as an analytical parameter instead of the signals obtained at the equilibrium state of the reaction [45]. FPIA reaction rate is measured by the variation of polarization with time ( $dP/dt$ ), which is also related to the concentration of analyte. Background signals do not contribute to the reaction rate; thus, stopped-flow FPIA yields a lower detection limit than conventional FPIA. The stopped-flow FPIA, also allows for kinetic measurements of a given reaction.

Although most FPIAs are conducted in aqueous solution, FPIA has also been employed in organic solvents by using micelles, enabling the measurement of analytes that are insoluble in water [46]. Reverse micellar systems of surfactants in non-polar organic solvents were used to dissolve the antibody in homogeneous media. The micelles are optically clear, and are able to retain the activity of the antibody. For example, a hydrophobic pesticide, dichlorophenoxyacetic acid, was determined in *n*-octane with a detection limit of  $0.1 \mu\text{gL}^{-1}$  by using the reverse micelles containing an antibody and a fluorescein labelled probe [46]. Such FPIA in micellar systems showed comparable sensitivity to that in aqueous system.

FPIA offers several advantages. FPIA is a homogeneous assay, which does not require separation and washing steps; FP is independent of sample concentration and volume, making it uniquely suited for assay miniaturization, which results in a reduction in reagents and cost; FPIA is suitable for high throughput screening due to its robustness and ease of automation.

Like other techniques, FPIA also has drawbacks. FPIA is sensitive to background fluorescence and light scattering. The sensitivity of FPIA is usually lower than the more commonly used enzyme linked immunosorbent assay. FPIA is also limited to low molecular weight analytes when fluorophores with short fluorescence lifetimes are used.

## 2.2

### Receptor – Ligand and Peptide – Ligand Based Fluorescence Polarization Assays

These assays are similar to FPIAs in that they involve competitive binding. The main difference is that the probe and ligand are not competing for the same antibody. Instead, they are competing for the same binding site on specific protein receptors or peptides. These assays are commonly used in HTS for drug discovery. For instance, Allen et al. demonstrated that FP is suitable for a high throughput (HT) receptor binding assays at G protein-coupled receptors (GPCR) and ligand-gated ion channels [5]. GPCRs are the largest family of cell surface proteins, and their inhibitors (peptide or non-peptide ligands) represent the major class of potential drugs. Radio-ligand binding

assays, such as the scintillation proximity assay (SPA), are the widely used HTS methods for GPCRs inhibitors. However, due to concerns with the use of radioactive materials, FP-based ligand-binding competition assays are great alternatives to the SPA. In the FP-based ligand assay, binding of GPCR to the fluorescently labelled ligand (reference or probe) results in high FP signal (Fig. 2). With the addition of a new non-fluorescent ligand (competitor or inhibitor) to the mixture, competition reactions result in the release of the fluorescently labelled ligand and a decrease in the FP signal. Thus, the screening of new binding ligands is possible using HTS-FP method.

Using a 384-well format, it was shown that miniaturization did not affect the sensitivity and precision required for the receptor FP binding assay, offer-

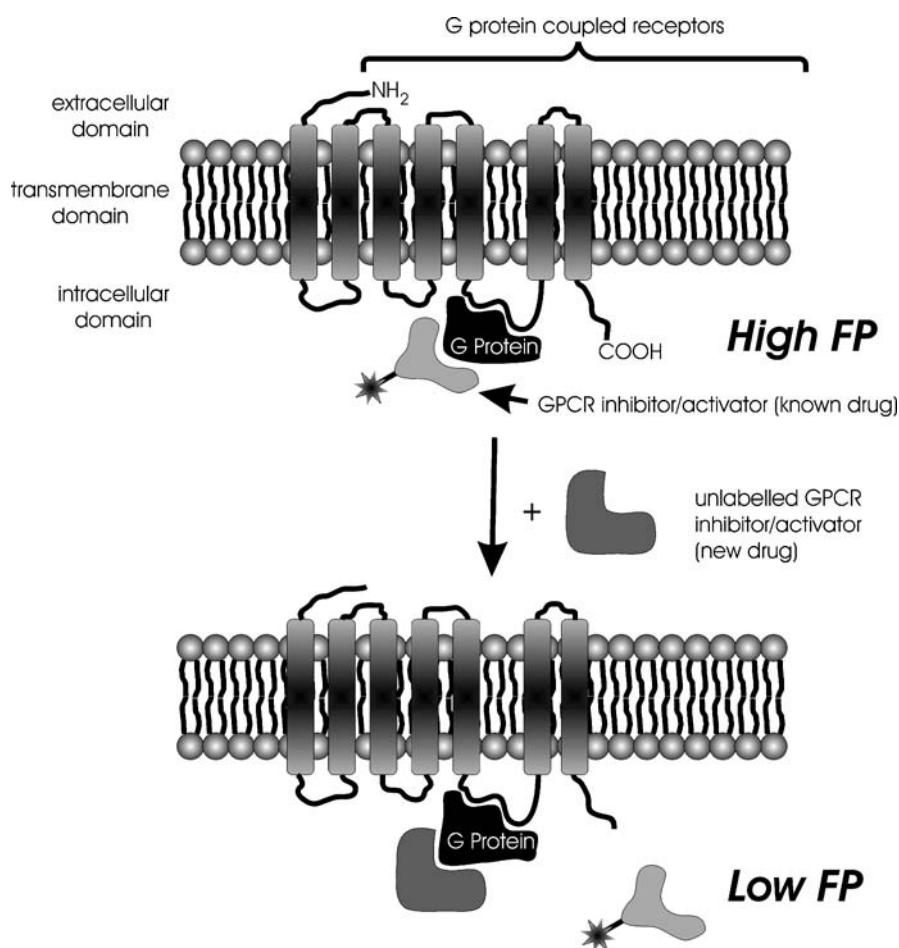


**Fig. 2** Competitive FP ligand-binding assay at G protein-coupled receptor (GPCR)

ing an advantage over low throughput cuvette-based FP methods and radio-ligand binding assays, which are rarely amenable to the 384-well assay [5].

An HTS-FP competitive peptide-binding assay was recently used as a new tool for epitope discovery [6]. A long-term goal is the development of vaccines which induce cytotoxic T lymphocyte (CTL) response as an approach to the treatment of cancer and/or infectious diseases. CTLs recognize peptide fragments of cellular or viral proteins in association with major histocompatibility complex (MHC) class-I molecules on the surface of infected or neoplastic cells. Thus, the identification of MHC-restricted CTL epitopes is important in the development of new treatments [6]. Standard procedures applied in CTL-epitope discovery are lengthy and labour-intensive. Therefore, the FP-based peptide competition assay offers a new tool for epitope discoveries [6].

This competition assay is similar to the one described for GPCRs: competitive binding to MHC class-I molecules between a labelled ligand and an unlabelled ligand is measured. Usually, an HT epitope discovery process starts with a rapid screening for large numbers of peptides, tested at a selected high threshold concentration, in order to eliminate peptides that are not incapable of binding to MHC. The HTS-FP based assays not only offer high speed, but also ease of automation, simplicity (one-step procedure, since no separation is needed), adaptation to existing instrumentation, and ease of standardization. The reproducibility is a key parameter in screening extensive sets of peptides for their affinity to MHC, and it provides important information from binding comparisons of various peptides [6]. Among features offered by FP-based assays, there are issues that have to be addressed specifically for the development of standardized assays. For instance, to achieve experimental accuracy and reproducibility, it is necessary to work with a standardized quantity of MHC class-I molecules. However, high concentrations of MHC receptors are needed to yield a significant change in FP. Consequently, a high concentration of ligand is required to compete with the probe for a 50% drop in the amount of the bound probe. Thus, the FP system is affected by the severe competitor depletion. Nevertheless, HTS-FP results remain useful in comparing relative affinities of ligands to the MHC receptor and in determining whether the ligand of interest belongs to a same group of compounds which can cause a similar response [6].

### 2.3

#### **Aptamer-Based Fluorescence Polarization Assays**

Aptamers have been recently used as affinity probes for the detection of a number of different proteins using FP [24–27]. Aptamers are short synthetic DNA and RNA oligonucleotides with high binding affinity and specificity to various targets, such as proteins and/or small molecules [47]. Aptamers offer the advantages of stability and ease of preparation and have been used in many analytical applications as alternatives to antibodies [48].



Potyralo et al. [24] developed aptamer-based biosensors to detect thrombin using FP. In this assay, fluorescently labelled aptamers were immobilized on a glass surface. Although immobilized, the aptamers were believed to rotate on the surface at the point of the attachment. The rotation rate decreased when the aptamers were bound to the target protein, resulting in an increase in FP. The biosensor could detect as little as 5 nM thrombin, and it had a dynamic range of three orders of magnitude [24]. McCauley et al. also used immobilized aptamers to develop an aptamer-based glass biosensor array for multiplex protein analysis with FP detection [26]. Specific detection and quantification of several cancer-associated proteins, including inosine monophosphate dehydrogenase II, vascular endothelial factor, and basic fibroblast growth factor, was accomplished [26].

Fang et al. demonstrated a fluorescence polarization assay in homogeneous solution for a platelet-derived growth factor (PDGF) based on its interaction with an aptamer [25]. A 35-base DNA aptamer for PDGF was labelled at the 5'-end with a fluorescein molecule. The binding of PDGF to the aptamer probe hindered the rotation of the aptamer probe, resulting in an increase in FP values. Fluorescence polarization of a solution containing the aptamer probe increased with the addition of PDGF. Titration of the 2 nM aptamer probe by PDGF showed that 0.22 nM PDGF could be detected.

Recently, Gokulrangan et al. reported an FP assay for IgE based on its fluorophore-labelled DNA aptamers as probes [27]. With this method, a detection limit of 350 pM for IgE was obtained. These examples show that the aptamer-based FP assay has a great potential for protein analysis.

## 2.4

### Immobilized Metal Assay for Phosphochemicals (IMAP™)

After GPCRs, protein kinases are the second major target in drug discoveries. Protein kinases phosphorylate proteins or peptides at hydroxy-bearing amino acid residues, which is a key regulatory mechanism in cells. Kinase activity plays an important role in many signalling processes, including the activation, growth, and differentiation of cells in response to any changes in intracellular or extracellular environments. While antibody-based FP assays [8, 9] are available for HTS of kinase inhibitors, a newly developed IMAP (Immobilized Metal Assay for Phosphochemicals) technology offers an additional advantage for HTS of kinases [10–12].

The principle of the IMAP kinase assay is shown in Fig. 3. A fluorescein-labelled peptide substrate is phosphorylated by a kinase enzyme. The reaction product, the fluorescein-labelled phosphopeptide, binds to the IMAP binding reagent through the interaction between the phosphate and the immobilized metal ( $M^{III}$ ) coordination complexes on the surface of the nanoparticles. The binding results in an increased FP value, due to a decreased molecular mobility of the fluorescein-labelled product.

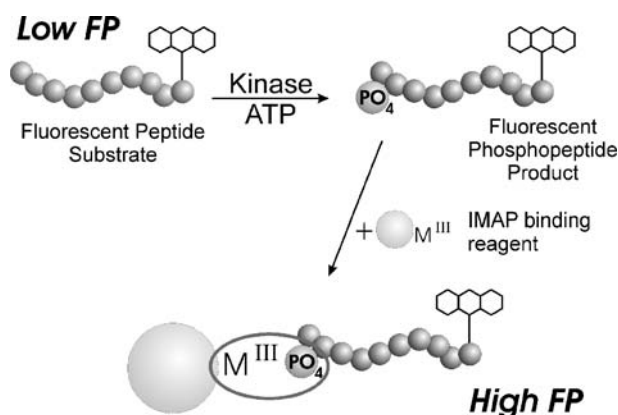


**Fig. 3** Principle of IMAP™ kinase assays [12]. Reprinted with permission from Sage Publications Inc.

The IMAP binding reagent binds to the products of a phosphodiesterase (PDE) reaction [10] and the products of a protein kinase reaction [12], but not to the fluorescein-labelled unphosphorylated substrate. The FP response achieved with the IMAP (maximum change >300 mP) is substantially greater than other FP assays (change ~50–150 mP). Although fluorophore concentrations in IMAP are relatively high ( $\geq 100$  nM), the large polarization change results in a high precision of polarization measurement and strong resistance to interfering compounds [12].

A modified IMAP technique has been developed to screen for inhibitors of kinase and upstream activation enzymes [13]. Libraries of inhibitors for upstream PDK1 (3'-phosphatidyl-inositol-dependent kinase 1) enzyme or activation sites of Akt enzymes are screened in the presence of fluorescently labelled substrate and the IMAP binding reagent (beads). If either the upstream PDK1 enzyme or the Akt enzyme is inhibited, then the substrate stays unphosphorylated and does not bind to the beads, resulting in low FP signal. If the Akt enzyme is activated, the fluorescently labelled substrate is phosphorylated, and it binds to the beads, resulting in high FP values. The coupled assay has the advantage of identifying not only compounds that inhibit kinase but also compounds that bind to the different activity states/conformations of a target kinase [13]. Therefore, this assay can be used to identify compounds that target other enzymes and block activation of the kinase [13].

The IMAP kinase assay requires no wash steps and can be scaled up for 96-, 384-, or 1536-well plate formats. It provides a powerful alternative to other widely used HTS kinase assays, which require costly reagents, such as radio-labelled substrates and antibodies. The IMAP assay offers a unique advantage over antibody-based assays because the IMAP assay measures the activity of kinase, and not the amount of protein as measured by the antibody-based assays. IMAP technology can also be applied to a broad range of targets, in-

cluding serine/threonine-specific protein kinases, protein tyrosine kinases, and protein phosphatases [12].

IMAP does have some limitations. High concentrations of ATP (>30  $\mu\text{M}$  in the 20  $\mu\text{L}$  enzyme reaction) will interfere with the assay response. Also, some peptides with numerous acidic residues can bind non-specifically to the binding reagent. Since FP requires a noticeable change in molecular volume to observe a significant change in FP signal, large protein substrates are expected to be a poorer choice than the peptide substrates [12]. Nevertheless, IMAP technology has a promising future for kinase-based drug discovery.

## 2.5

### Fluorescence Polarization Assays for Single Nucleotide Polymorphism

Single nucleotide polymorphism (SNP) is a DNA sequence variation, where a single nucleotide in genome is altered. SNP genotyping is the primary technique in genetic studies for mapping and identifying susceptible genes in complex diseases. Application of FP to SNPs differs from other FP applications, in that it is used for genomics rather than for classical pharmaceutical HTS applications. Since the size of the probe is altered during the SNP reactions, FP is an excellent detection technique for these assays. Kwok described three SNP assays that can be successfully used with FP [14]: (i) the template-directed dye-terminator incorporation assay with FP detection (TDI-FP) [16, 17]; (ii) the 5'-nuclease assay (the FP-TaqMan<sup>®</sup> assay) [18, 19]; and (iii) the FP-Invader<sup>®</sup> assay [20, 21].

The TDI-FP assay is reminiscent of a single base extension assay (SBE). Figure 4 shows the principle of the TDI-FP assay.

TDI-FP is accomplished in four steps in the same reaction vessel on a black 96- or 384-well plate. In the first step, genomic DNA is amplified by PCR to produce a template. Secondly, excess PCR primers and deoxynucleoside triphosphates (dNTPs) are enzymatically degraded in order to eliminate interferences with the subsequent primer extension step. In the third step, enzymes used in the second step are heat inactivated. Finally, a "master mix" containing DNA polymerase, SNP-primer, and allele-specific dye-terminators is added to the primer extension reaction with thermal cycling. The incorporation of a dye-labelled single nucleotide to the primer through the single base extension reaction results in an increased FP. This extension is SNP specific [14]. Using two dyes (ROX and BFL) attached to the allele-specific terminators (ddGTP and ddATP) (Fig. 4), the two SNPs can be detected with the FP assay [16, 17]. Likewise, using four dyes for each of the ddNTP terminators, all the four SNPs can be detected [14].

The second FP assay for SNPs is termed the FP-Taqman<sup>®</sup> assay, in which the amplification and allele discrimination steps are done at the same time; thus, no further manipulations are required after the reaction is set up.

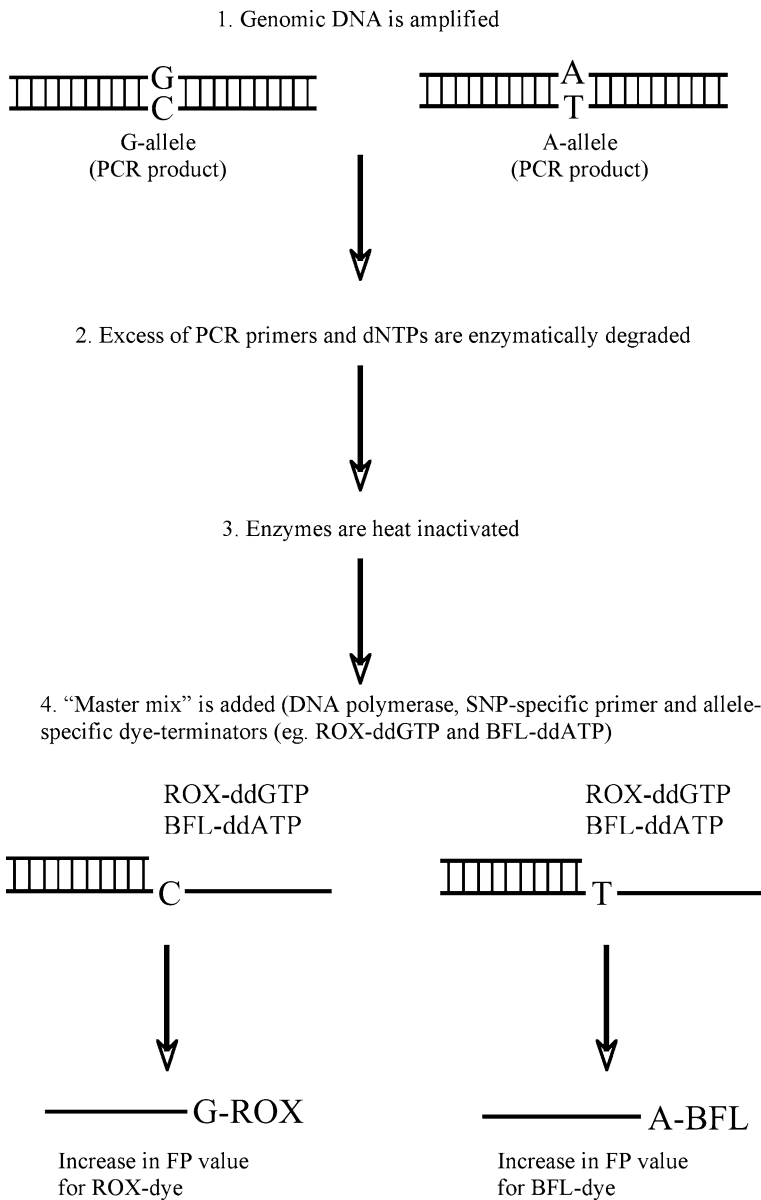


**Fig. 4** Schematic diagram of the TDI-FP assay [16]. Reprinted with permission from Cold Springs Harbor Laboratory Press

After 2-allele specific fluorescently labelled probes are annealed to the target, the perfectly hybridized product is cleaved by the DNA polymerase during the PCR. As a result, the fluorescent dye is released, resulting in a de-

crease in FP signal. In the mismatched product, DNA polymerase displaces, rather than cleaves, the probe. The FP signal remains unchanged, since the size of the fluorescently labelled molecule remains large (Fig. 5). In the FP-Taqman<sup>®</sup> assay, a less costly fluorescent probe is used, since there is no need for a fluorescent emitter and quencher pair as in the standard Taqman<sup>®</sup> assay.

The third FP assay for SNP is the FP-Invader<sup>®</sup> assay, which is based on the cleavage of a specific structure formed by overlapping probes annealed to the target.

In the FP-Invader<sup>®</sup> assay, the PCR product is incubated with the 1<sup>o</sup>-Invader<sup>®</sup> oligonucleotide (SNP specific) and the primary probe (allele specific). When there is a match between allele specific probe and PCR product at the base to be genotyped, an overlapping structure between the Invader<sup>®</sup> and allele specific probe is formed. A thermostable flap endonuclease, the Cleavase enzyme, recognizes this structure and cleaves the allele specific probe, releasing the 5'-flap. This 5'-flap acts as a 2<sup>o</sup>-invader in the second reaction, where the signal probe is cleaved and a fluorophore attached to a smaller flap is released, resulting in smaller FP signal (Fig. 6A). If the allele specific probe and PCR products do not match at the base to be genotyped, no overlapping structure is formed and no cleavage occurs; thus, a high FP signal is recorded for the dye (Fig. 6B).

FP assays are simple, cost-effective, and accurate for SNP genotyping. The use of FP as a detection method provides many possibilities for the utilization of unlabelled primers in the TDI assay, and less costly probes in the Taqman<sup>®</sup> and Invader<sup>®</sup> assays, since no quencher is needed. Improvements in the TDI-

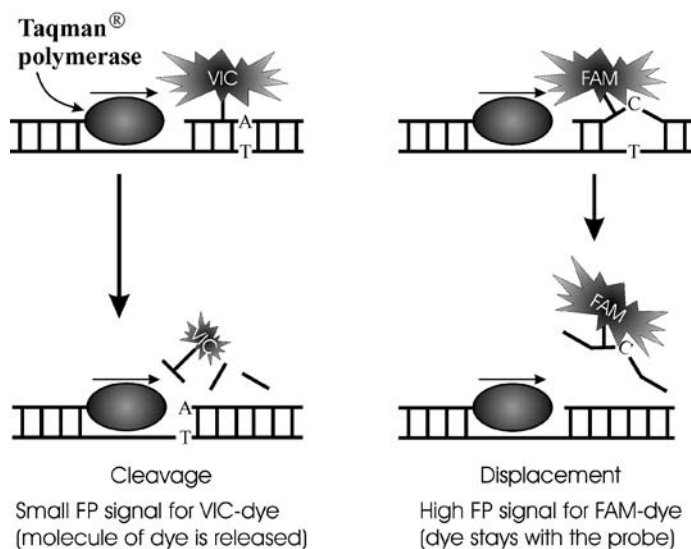


**Fig. 5** Schematic diagram of the FP-Taqman<sup>®</sup> assay

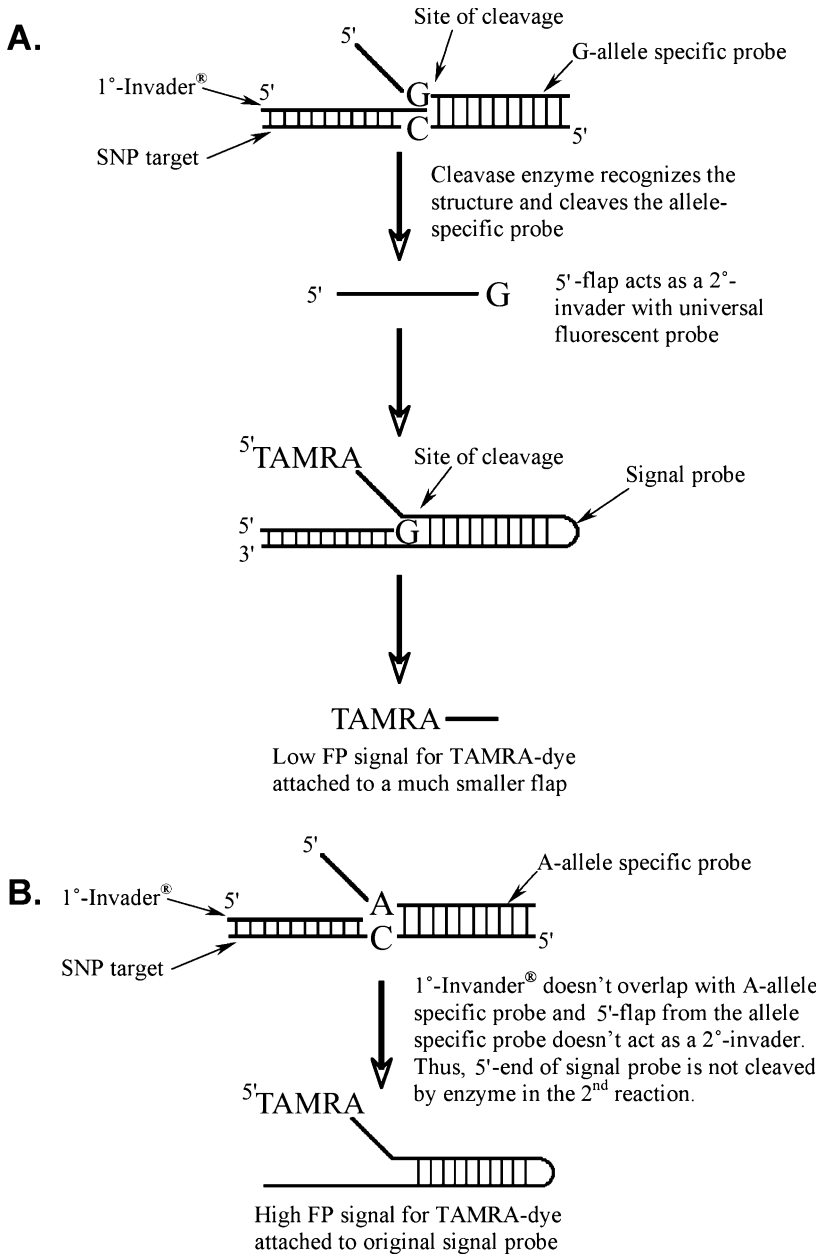


**Fig. 6** Schematic diagram of the FP-Invader<sup>®</sup> assay

FP assay include selecting appropriate fluorophores and/or single stranded DNA binding proteins [15].

## 2.6

### Capillary Electrophoresis Based Fluorescence Polarization Assays

Although fluorescence polarization is most commonly used in homogeneous assay formats which do not include separation, laser-induced fluorescence polarization (LIFP) has been shown to be particularly useful as a detector for capillary electrophoresis (CE) [22, 23]. Figure 7 shows the CE/LIFP configuration. The LIFP detector consists of a polarized laser for excitation, laser focusing, fluorescence collection optics, a polarizing beam-splitter and two photomultiplier tubes (PMTs). The LIFP detector can also be used as a single-channel laser induced fluorescence (LIF) detector when either one of PMTs is employed for detecting the fluorescence intensity, achieving similar sensitivity as conventional LIF measurement.

Conventional affinity CE distinguishes the complex from the free ligands by their electrophoretic mobility difference. Since FP is sensitive to changes in molecular size and rotation, FP facilitates the identification of complex peaks. Moreover, CE/LIFP maintains the advantages of high sensitivity from LIF detection. By combining the highly efficient separation and nanoliter sample delivering capability of CE with the sensitivity of LIFP, CE/LIFP provides additional information about complex formation, binding stoichiometry, and molecular interactions.

CE/LIFP has been utilized in competitive immunoassays to quantify therapeutic drugs, such as cyclosporine A (CsA) [49, 50], vancomycin [51], digoxin, and gentamicin [52]. The fluorescent probe, analyte and their complexes with the analyte's antibody were separated by CE, and the FP was measured for each of the fluorescent species. This is different from the con-

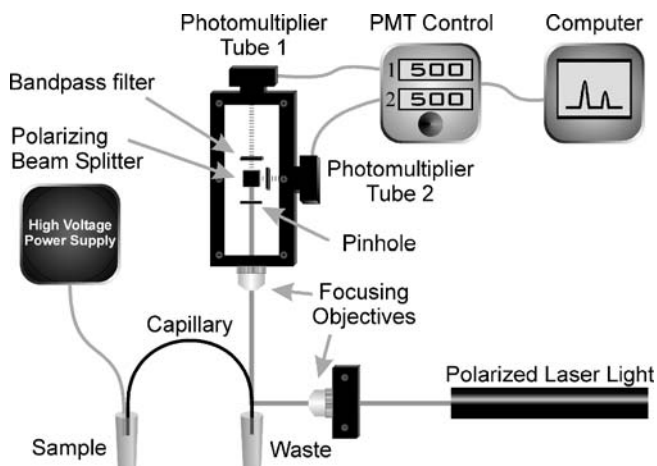


**Fig. 7** Schematic diagram of CE-LIFP configuration

ventional FPIA, where the measurement of polarization is obtained from a mixture of both unbound fluorescent probe (lower polarization value) and the antibody-bound probe (higher polarization value). The background fluorescence of the unbound probe in both vertical and horizontal planes leads to a lower value of fluorescence polarization of the mixture solution. However, in the case of CE/LIFP, the fluorescent probe and its antibody complex are separated. The fluorescence polarization measurement of the antibody-bound probe is not confounded by the unbound probe. As a consequence, CE/LIFP offers better sensitivity and detection limit compared to the conventional FPIAs. For example, the detection limit of CsA using CE/LIFP was 20 times lower than that obtained using the conventional FPIA [49].

CE/LIFP was also used for online monitoring of molecular interactions [53–57]. Different binding systems were investigated by CE/LIFP, such as vancomycin and its antibody, staphylococcal enterotoxin and its antibody, *trp* operator and *trp* repressor, and aptamer and protein, representing peptide–protein, protein–protein, and DNA–protein interactions [53–55]. CE/LIFP allows for the simultaneous measurement of changes in electrophoretic mobility and FP, which provides complementary information on binding interactions. The binding affinity and complex stoichiometry were readily determined by CE/LIFP in the investigation of the molecular interactions. With CE/LIFP, the binding constants of single-stranded DNA binding protein (SSB) with 11-mer and 37-mer oligonucleotides were determined to be  $5 \times 10^6 \text{ M}^{-1}$  and  $23 \times 10^6 \text{ M}^{-1}$ , respectively [54]. CE/LIFP revealed binding stoichiometry between different aptamers to HIV-1 reverse transcriptase (RT) [55]. For aptamers RT12, RT26, and ODN93, two binding stoichiometries were found, suggesting these aptamers can bind to two different subunits of HIV-1 RT.

Similarly, a CE-based FP technique was used to quantify proteins and to study peptide–protein interactions [56, 57]. A fluorescent probe is mixed with the electrophoresis buffer, and unlabelled protein partners are detected as they migrate through the detection window. The interaction of the protein with the fluorescent probe results in an increased polarization of the fluorescent probe. This technique does not require that the analyte be fluorescently labelled. Thus, simultaneous detection of multiple unlabelled analytes by their interactions with the fluorescent probe can be achieved.

### 3

#### **Advantages and Limitations of Fluorescence Polarization**

FP is mainly a homogeneous technology; however, some heterogeneous methods have also been developed. It is applicable to both equilibrium and non-equilibrium binding studies. For example, FP allows real-time measurements for kinetic assays. In addition, FP is insensitive to variations in fluo-



rophore concentrations and signal intensity, making it amenable to work with coloured solutions and cloudy suspensions. Since no separation or washing steps are required, both precision and speed are superior to other heterogeneous assays, and the amount of waste is also reduced.

Another advantage of FP over other fluorescent methods is that it gives a direct, nearly instantaneous (seconds to minutes) measure of the bound/free ratio of a fluorescent probe. This is especially useful in binding affinity studies (such as protein or DNA detection), since it provides direct evidence of complex formation.

FP also offers advantages in simple instrumentation requirements. Because FP is a measure of the ratio of fluorescence intensities of two polarization planes, it is relatively insensitive to instrument changes, such as drift, gain settings, lamp changes, etc., resulting in highly reproducible results and easy automation.

Despite the advantages, FP does have its limitations. The fluorescent molecule must be relatively small (<20 kD) compared to the target, otherwise the change in the rotational relaxation of the complexed molecule will not be sufficient to measure a difference in FP. Also, the fluorescence lifetime of the fluorophore must be suitable for a given application. Fluorophores with short fluorescence lifetimes, such as fluorescein and rhodamine (4 ns), can give sensitive polarization (or anisotropy) signals in response to changes in molecular size (e.g., due to binding to proteins) (Fig. 8) [58]. However, fluorescence polarization of these fluorophores rapidly approaches a limiting value at a molecular weight of ~50 kDa. Therefore, they are not suitable for most protein-protein interaction applications. On the other hand, polarization from very long lifetime fluorophores (ruthenium or lanthanide complexes, ~500 ns) is not sensitive to small changes in molecular size. It is difficult to

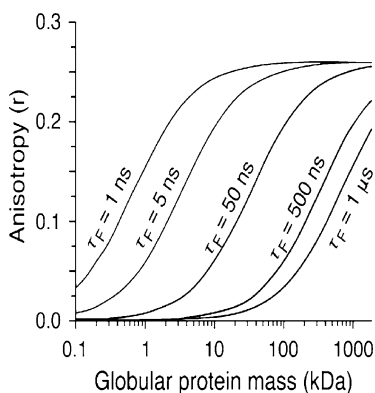


**Fig. 8** Simulated effect of fluorophore lifetime on fluorescence polarization/anisotropy as a function of globular protein mass [58]. Reprinted with permission from Elsevier

achieve changes in polarization values without complexation to very large systems (cells, membrane particle) or immobilization (Fig. 8).

Another consideration is that the FP method requires a fluorescent probe which can bind to the target. In some cases, appropriate probes are already commercially available. However, in other cases, appropriate probes must be developed. This can be challenging, particularly when the target is unknown or its amount is very limited.

## 4

### Future Trends

FP is particularly useful for studying molecular interactions, because FP is a sensitive measure of molecular size and, therefore, binding and dissociation. Although traditional FP assays commonly use antibodies for binding with antigens, future FP assays will likely make use of many more molecular interaction systems, such as aptamer and protein, small interference RNA (siRNA) and its complementary nucleic acid, oligosaccharide and lectin, enzyme and inhibitor, and guest/host chemistry.

The use of nanoparticles and beads to bind with fluorescence probes has shown enhancements in the magnitude of FP values [12]. With the rapid development of nanotechnology, we anticipate that more research will incorporate nanoparticles and quantum dots in FP assays to further improve sensitivity. The current fluorescent assays using nanoparticles and quantum dots have not taken advantage of FP.

Several FP techniques reported in recent years may be explored for further applications. Lakowicz et al. demonstrated preliminary results for an FP assay in HTS format using multi-photon excitation (MPE) [59]. MPE frequently results in larger polarization values than those obtained by traditional FP methods. Other interesting developments include time-resolved lifetime measurements [59], polarization sensing [60], and FP measurements done on single molecules [61].

Fluorescence polarization has been used as a detector for capillary electrophoresis [22, 23, 54, 56]. It can be extended to serve as a detector for other separation flow systems. The primary benefit of the separation of the affinity bound from the unbound fluorescent species includes the increased sensitivity of FP measurement and the ability to study binding stoichiometry [55].

Further research also needs to address standardization and quality assurance for routine, high throughput analysis in clinical, pharmaceutical, and biotechnology settings. Roehrl et al. suggested a procedural flowchart of a typical HT-FP assay project that may be very useful for the screening of new targets and/or development of a new assay [62]. Owicki showed very well how one could deal with issues and possible interferences in FP-based HTS methods [63]. Development and use of standard (certified) reference mate-

rials and inter-laboratory comparisons will be needed for validation of new analytical technology for routine applications.

**Acknowledgements** We acknowledge the support of the Natural Sciences and Engineering Research Council of Canada, the National Natural Science Foundation of China, the Terry Fox Foundation, the National Cancer Institute of Canada, the Canada Research Chairs Program, the Alberta Ingenuity Fund, and Alberta Health and Wellness.

## References

1. Perrin MF (1926) *J Phys Radium* 7:390
2. Dandliker WB, Kelly RJ, Dandliker J, Farquhar J, Levin J (1973) *Immunochem* 10:219
3. Kumke MU, Li G, McGown LB, Walker TG, Linn CP (1995) *Anal Chem* 67:3945
4. LeTilly V, Royer CA (1993) *Biochemistry* 32:7753
5. Allen M, Reeves J, Mellor G (2000) *J Biomol Screen* 5:63
6. Buchli R, VanGundy RS, Hickman-Miller HD, Giberson CE, Bardet W, Hildebrand WH (2005) *Biochemistry* 44:12491
7. Jameson DM, Seifried SE (1999) *Methods* 19:222
8. Seethala R, Menzel R (1997) *Anal Biochem* 253:210
9. Seethala R, Menzel R (1998) *Anal Biochem* 255:257
10. Huang W, Zhang Y, Sportsman JR (2002) *J Biomol Screen* 7:215
11. Sportsman JR, Daijo J, Gaudet EA (2003) *Comb Chem High Throughput Screen* 6:195
12. Gaudet EA, Huang KS, Zhang Y, Huang W, Mark D, Sportsman JR (2003) *J Biomol Screen* 8:164
13. Lu Z, Yin Z, James L, Syto R, Stafford JM, Koseoglu S, Mayhood T, Myers J, Windsor W, Kirschmeier P, Samatar AA, Malcolm B, Turek-Etienne TC, Kumar CC (2004) *J Biomol Screen* 9:309
14. Kwok PY (2002) *Human Mutat* 19:315
15. Chen X (2003) *Comb Chem High Throughput Screen* 6:213
16. Chen X, Levine L, Kwok PY (1999) *Genome Res* 9:492
17. Hsu TM, Chen X, Duan S, Miller RD, Kwok PY (2001) *Biotechniques* 31:560
18. Livak KJ (1999) *Genet Anal* 14:143
19. Latif S, Bauer-Sardina I, Ranade K, Livak KJ, Kwok PY (2001) *Genome Res* 11:436
20. Mein CA, Barratt BJ, Dunn MG, Siegmund T, Smith AN, Esposito L, Nutland S, Stevens HE, Wilson AJ, Phillips MS, Jarvis N, Law S, de Arruda M, Todd JA (2000) *Genome Res* 10:330
21. Hsu TM, Law SM, Duan S, Neri BP, Kwok PY (2001) *Clin Chem* 46:1373
22. Le XC, Pavski V, Wang H (2005) *Can J Chem* 83:185
23. Le XC, Wan QH, Lam TM (2002) *Electrophoresis* 23:903
24. Potyrailo RA, Conrad RC, Ellington AD, Hieftje GM (1998) *Anal Chem* 70:3419
25. Fang X, Cao Z, Beck T, Tan W (2001) *Anal Chem* 73:5752
26. McCauley TG, Hamaguchi N, Stanton M (2003) *Anal Biochem* 319:244
27. Gokulrangan G, Unruh JR, Holub DE, Ingram B, Johnson CK, Wilson GS (2005) *Anal Chem* 77:1963
28. Gutierrez MC, Gomez-Hens A, Perez-Bendito D (1989) *Talanta* 36:1187
29. Nasir MS, Jolley ME (1999) *Comb Chem High Throughput Screen* 2:177
30. Eremin SA, Smith DS (2003) *Comb Chem High Throughput Screen* 6:257
31. KuKanich B, B Lascelles DX, Papich MG (2005) *Ther Drug Monit* 27:389

32. Eremin SA, Murtazina NR, Ermolenko DN, Zherdev AV, Mart'ianov AA, Yazynina EV, Michura IV, Formanovsky AA, Dzantiev BB (2005) *Anal Lett* 38:951
33. Keller T, Schneider A, Dirnhofer R, Jungo R, Meyer W (2000) *Med Sci Law* 40:258
34. Lucero NE, Escobar GI, Ayala SM, Paulo PS, Nielsen K (2003) *J Med Microbiol* 52:883
35. Ragain JC, Cullum ME, Lininger LA, Schade SZ, Cope SE, Simonson LG (2003) *Mil Med* 168:915
36. Shim WB, Kolosova AY, Kim YJ, Yang ZY, Park SJ, Eremin SA, Lee IS, Chung DH (2004) *Int J Food Sci Technol* 39:829
37. Shim WB, Kolosova AY, Kim YJ, Yang ZY, Park SJ, Eremin SA, Lee IS, Chung DH (2004) *J Food Prot* 67:1039
38. Eremin SA, Ryabova IA, Yakovleva JN, Yazynina EV, Zherdev AV, Dzantiev BB (2002) *Anal Chim Acta* 468:229
39. Deryabina MA, Yakovleva YN, Popova VA, Eremin SA (2005) *J Anal Chem* 60:80
40. Yakovleva JN, Lobanova AY, Shutaleva EA, Kourkina MA, Mart'ianov AA, Zherdev AV, Dzantiev BB, Eremin SA (2004) *Anal Bioanal Chem* 378:634
41. Eremin SA, Knopp D, Niessner R, Hong JY, Park SJ, Choi MJ (2005) *Environ Chem* 2:227
42. Johnson DK (2003) *Comb Chem High Throughput Screen* 6:245
43. Hong JY, Choi MJ (2002) *Biol Pharm Bull* 25:1258
44. Choi MJ, Lee JR, Eremin SA (2002) *Food Agric Immunol* 14:107
45. Gomez-Hens A, Aguilar-Caballos MP (2003) *Comb Chem High Throughput Screen* 6:177
46. Matveeva EG, Popova VA, Eremin SA (1997) *J Fluoresc* 7:251
47. Ellington AD, Szostak J (1999) *Nature* 346:818
48. Tombelli S, Minunni A, Mascini A (2005) *Biosens Bioelectron* 20:2424
49. Wan QH, Le XC (1999) *J Chromatogr A* 853:555
50. Ye L, Le XC, Xing JZ, Ma M, Yatscoff R (1998) *J Chromatogr B* 714:59
51. Lam MT, Le XC (2002) *Analyst* 127:1633
52. Wan QH, Le XC (1999) *J Chromatogr B* 734:31
53. Wan QH, Le XC (1999) *Anal Chem* 71:4183
54. Wan QH, Le XC (2000) *Anal Chem* 72:5583
55. Fu H, Guthrie JW, Le XC (2006) *Electrophoresis* 27:433
56. Whelan RJ, Sunahara RK, Neubig RR, Kennedy RT (2004) *Anal Chem* 76:7380
57. Yang PL, Whelan RJ, Jameson EE, Kurzer JH, Argetsinger LS, Carter-Su C, Kabir A, Malik A, Kennedy RT (2005) *Anal Chem* 77:2482
58. Pope AJ, Haupts UM, Moore KJ (1999) *Drug Discovery Today* 4:350
59. Lakowics JR, Gryczynski I, Gryczynski Z (1999) *J Biomol Screen* 4:355
60. Lakowics JR, Gryczynski I, Gryczynski Z (2000) *J Biomol Screen* 5:123
61. Weiss S (1999) *Science* 283:1676
62. Roehrl MHA, Wang JY, Wagner G (2004) *Biochemistry* 43:16056
63. Owicki JC (2000) *J Biomol Screen* 5:297

**Part V**  
**Fluorescent Chemical Sensors:**  
**Principles, Problems, and Need for Quality Assurance**

# Classification of Chemical Sensors and Biosensors Based on Fluorescence and Phosphorescence

Stefan Nagl · Otto S. Wolfbeis (✉)

Institute of Analytical Chemistry, Chemo- and Biosensors, University of Regensburg,  
Universitätsstr. 31, D-93053 Regensburg, Germany  
*otto.wolfbeis@chemie.uni-regensburg.de*

1	Introduction . . . . .	326
2	Definition of Chemical Sensors and Biosensors . . . . .	327
3	Classification of Chemical Sensors and Biosensors . . . . .	330
3.1	Plain Fluorometric Sensors (Type A) . . . . .	332
3.2	Direct Indicator-Mediated Chemical Sensors (Type B) . . . . .	333
3.3	Indirect Indicator-Mediated Chemical Sensors (Type C) . . . . .	336
3.4	Direct Enzymatic Biosensors (Type D) . . . . .	338
3.5	Indicator-Mediated Enzymatic Biosensors (Type E) . . . . .	339
3.6	Affinity Biosensors (Type F) . . . . .	341
3.6.1	Antibody–Antigen Interactions . . . . .	341
3.6.2	Nucleic Acid Interactions . . . . .	342
3.6.3	Ligand–Receptor Interactions and Related Types . . . . .	343
4	Conclusions . . . . .	344
	References . . . . .	345

**Abstract** The field of chemical sensors and biosensors based on fluorescence and phosphorescence is becoming increasingly popular and advances are being reported at a rapid pace. It therefore appears worthwhile to classify these efforts to aid both newcomers and experts of the field in being able to view their work and those of others within a wider context. Among several classification schemes possible, here, one with respect to the mode of action is presented. After historical milestones and definitions of chemical sensors and biosensors are being reviewed briefly, the field is subdivided into six major types: Plain fluorometric sensors, direct- and indirect indicator-mediated chemical sensors, direct enzymatic biosensors, indicator-mediated enzymatic biosensors, and affinity biosensors. The discussion is accompanied by examples and further subdivisions for some sensor types.

**Keywords** Biosensors · Chemical sensors · Classification · Fluorescence · Luminescence · Phosphorescence

## Abbreviations

cAMP	Adenosine 3',5'-cyclic phosphate
CCD	Charge-coupled device
DNA	Deoxyribonucleic acid

ds	Double-stranded
FAD	Flavin adenine dinucleotide, oxidized or quinone form
FADH <sub>2</sub>	Flavin adenine dinucleotide, reduced or hydroquinone form
FRET	Förster resonance energy transfer
GOx	Glucose oxidase
HI	Indicator, protonated form
His <sub>6</sub>	Hexahistidine
HPTS	8-Hydroxypyrene-1,3,6 trisulfonic acid
I-	Indicator, deprotonated form
IgG	Immunoglobulin G
IR	Infrared spectral region
IUPAC	International Union of Pure and Applied Chemistry
MBP	Maltose binding protein
MIP	Molecularly imprinted polymer
NAD <sup>+</sup>	Nicotinamide adenine dinucleotide, oxidized form
NADH	Nicotinamide adenine dinucleotide, reduced form
NADPH	Nicotinamide adenine dinucleotide phosphate, reduced form
PNA	Peptide nucleic acid
PSD	Potential (or polarity) sensitive dye
PVC	Poly(vinylchloride)
Ribozyme	Ribonucleic acid enzyme
RNA	Ribonucleic acid
TIRF	Total internal reflection fluorescence
TNT	Trinitrotoluene
UV	Ultraviolet spectral region

## 1

### Introduction

Sensors have become part of our daily life to an extent we are not aware of: temperature sensors turn refrigerators on and off, pressure sensors display oil pressure in cars and elsewhere, and photosensors turn on and off city lights, to mention only a few.

Chemical sensors have been around for only about 30 years, with some notable exceptions such as the pH glass electrode reported in 1909 by Haber and Klemensiewicz [1] or Clark's oxygen electrode in 1956 [2]. The first biosensor can also be attributed to Clark when he described an experiment in 1962 using his oxygen electrode covered with a dialysis membrane filled with glucose oxidase [3]. Nowadays, the most often produced chemical sensor is the solid-state oxygen sensor (of the conductivity type, used by the millions in catalytic converters, and capable of continuously and reversibly recording oxygen levels in combustion gases). The literature on chemical sensors increased strongly after the 1970s. Following the success of electrochemical sensors and the invention of ion-selective electrodes, the first optical sensors were reported, in particular plain sensors, based on absorption or fluorescence, using the optical signal of the analyte itself, and indicator-mediated

sensors for oxygen and pH using indicator probes. Chemical sensors have experienced a further thrust following the availability of optical fibers, which enabled sensors to be used over large distances or invasively. The 1980s saw the widespread adaption of sensor technology to biochemical reactions. Biochemical interactions, however, often have some degree of irreversibility and are therefore limiting sensor utility. This is not often a problem in enzymatic and cell-based sensors, but more so with biosensors based on immunoreactions and in gene sensors. The main activities in this area involved electrochemical and optical approaches such as evanescent wave absorption and fluorescence. The surface plasmon resonance effect was applied to (mainly biochemical) sensing at about the same time as the first piezo-electric sensors in the 1980s. They are often referred to as quartz micro balances and used for continuous sensing of chemicals such as gases, but mainly for biochemical purposes. The most widely used (and produced) sensors are those for oxygen in the form of the lambda (oxygen) probe in catalytic converters and the glass pH electrode. Several books [4–7] describe the state of the art in chemical sensing and biosensing, and biannual reviews are available, focusing mainly on fiber-optic sensors [8].

The result of these (necessarily interdisciplinary) activities was an almost exponential increase in the number of scientific articles. Moreover, new journals on chemical sensors, materials aspects of sensors, and on biosensors have appeared that complement the work published in chemical and biological journals. Material aspects were found to be particularly critical since numerous sensing schemes have been proposed but many of them failed in practice due to limitations in the performance of the chemicals/materials used. It may be stated that we have more sensory schemes than sensors.

In order to classify optical (luminescence-based) sensors, it is mandatory first to define what chemical sensors are about, and what they are not.

## 2

### Definition of Chemical Sensors and Biosensors

There is no authoritative and universally accepted definition of any of the terms sensor, chemical sensor, or biosensor, yet, a fact to which much confusion and misperceptions of chemo- and biosensor terminology can be attributed. Part of the problem is the derivation of the word sensor. It is ultimately from the Latin words *sensus* and *sensorium*, having a meaning almost completely conserved in the English words sense and sensibility. Used to describe largely emotional rather than rational phenomena, they are ambiguous and individual in their meaning. Some of the proverbial senses of humans in particular and most of the animal kingdom are vision (sight), audition (hearing), gustation (taste), olfaction (smell) and tactition (touch). In all cases, a *receptor* responds to a particular stimulus, and this receptor in-



teracts with a *transducer* leading to a *signal cascade* ultimately arriving at the brain.

Simple logic reveals that this architecture can indeed also be used to identify and define any artificial sensor, and it was used by IUPAC in 1991 to identify the main constituents of a chemical sensor [9]. There are also a number of different definitions (e.g., [10], and ref. therein). The molecular receptor is often embedded into a *matrix* such as a *membrane*, which can also provide some selectivity. Alternative names for the receptor include primary element and recognition element. Much like in biology where the senses convert the input ultimately into an electrical signal in the brain, the sensor converts the input variable into an *electrical signal* suitable for measurement [9]. Importantly, a sensor works (in the ideal case) *reversibly*, and *continuously*. True sensors (independent of whether physical or chemical) enable a parameter (a chemical species) to be monitored over time. Ideally, a sensor is placed in contact with the sample, and the results are displayed over time. This has been accomplished almost perfectly with numerous physical sensors, but much less so with (bio)-chemical sensors.

The sensor may be self-contained or part of a larger signal-processing chain. If using *signal conditioning* such as amplification, filtering, or analog-digital conversion is contained within the sensor, the devices are often called *integrated sensors*. Such sensors, also possessing built-in *signal processing*, are called *intelligent* or *smart sensors* [11–13].

It is therefore easy to realize that simple test strips are not sensors, neither are complex analytical instruments, although they may in parts consist

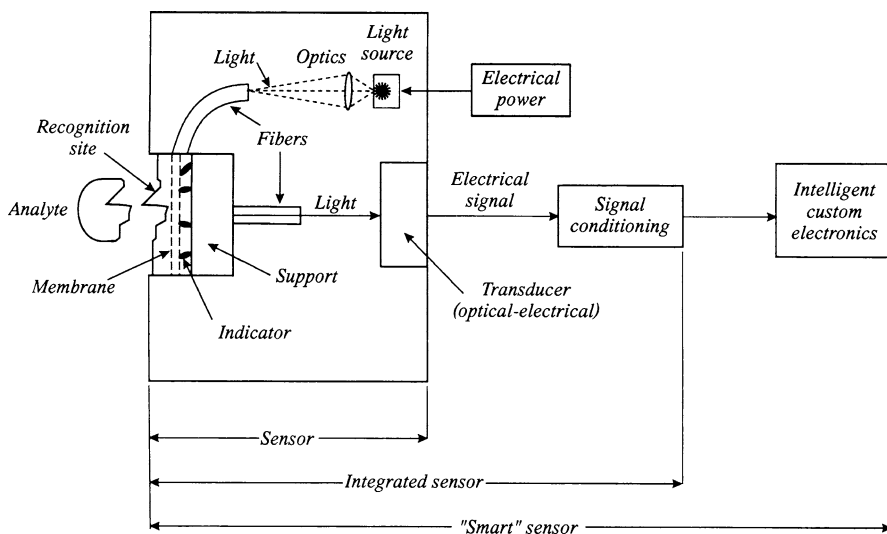


**Fig. 1** The integral components of a (fiber-optic) chemical sensor or biosensor. Revised from [13]

of even a multitude of different sensors, e.g., a fluorescence spectrometer may contain photosensors, thermal sensors, humidity sensors, etc.

In our opinion, the following definition of a chemical sensor (to which many colleagues refer to as the *Cambridge definition*) [14] is one of the most appropriate: *Chemical sensors are miniaturized devices which can deliver real-time and on-line information on the presence of specific compounds or ions in even complex samples.*

Definitions of biosensors are somewhat diverse [11, 15, 16], but most of them agree that their distinction from chemical sensors arises from the fact that they use a biological or bioengineered component such as an enzyme, an antibody, a polynucleic acid, or even whole cells or tissue slices as the receptor element for molecular recognition. A biosensor can therefore be regarded as a special type of a chemical sensor. More recently, the definition of biosensors has been extended to systems that can detect and determine biological species, for example by making use of molecularly imprinted polymers (MIPs). Thus, for example, a pH electrode capable of sensing the pH of blood is not a biosensor because it does not use a biological receptor, and neither detects a biological, but a chemical species, the proton. On the other hand, a gene sensor for lead ions in drinking water is a biosensor.

Optical sensors are, by definition, based on the measurement of photons. Therefore, the transducer in optical chemical sensors and biosensors always has to be a configuration involving one or more photodetectors such as a photodiode or a CCD chip. Optical sensors have also been named optodes and optrodes, both terms emphasizing the fact that the information collected by such sensors involves optical measurements of in analogy to electrons as in case of electrodes. It has been suggested [13] to use the term optrode for combinations of optical and electrochemical sensing methods such as those based on electroluminescence or electrochemically generated indicators, but mostly both terms are used interchangeably.

However, the term *sensor* is increasingly becoming a catchphrase much like *nano* or *bio* and this has led to sensor terminology becoming increasingly ambiguous. In the field of chemistry, researchers (mainly organic chemists) are increasingly using the term *sensor* for what is just the receptor part of a sensor and used to be referred to, for more than 100 years, as a (*molecular*) *probe* or an *indicator*. Conventional indicators (such as for pH or calcium) are being termed even *biosensors* if used *in vivo*, or *switches* even though they do not switch like mechanical or electrical switches but rather respond sigmoidally because their responses are governed by the mass action law. Similarly, classical chromoionophores are now sometimes being termed *ion sensors*, rather than probes or indicators. Some researchers argue that such indicators (in their terminology “sensors”) display all the properties of a (*molecular*) sensor, but this opinion is about as realistic as referring to a piece of silicon as a computer. Sensors are devices, not molecules. In order to function, sensors also need to possess a transducer or in other words a readout system, something organic

chemists and biologists tend to refer in a disparaging way as the “engineering step only”. In fact, it is a long way from an indicator dye to a functional sensor. In our opinion, more than 98% of the probes (“molecular sensors”) reported by organic chemists have had no impact at all in (bio)sensor science.

On the other hand, many physicists and engineers pay little attention to the receptor, and sometimes refer exclusively to transducers and transduction mechanisms when defining sensors (see e.g., [10] and references therein), taking the availability of a suitable receptor or primary element for granted.

### 3

#### **Classification of Chemical Sensors and Biosensors**

In principle, several classification schemes are possible. Chemical sensors and biosensors as defined above already contain a distinction with respect to the analyte. They sense a chemical or biochemical species, be it a gas, a fluid, or a dissolved or suspended molecule, complex or aggregate. Another broad distinction can be made with respect to the transduction mechanism such as optical in our case or electrochemical, piezoelectric, thermal, mechanical, etc. Although numerous kinds of optical sensors exist, this chapter is confined (in agreement with the scope of this book series) to fluorescence-based sensors, in contrast to other optical sensors based on absorption, reflectivity, light scattering, etc.

Another method to classify sensors is according to the analyte (sensors for  $H^+$ , glucose, albumins, etc.). This is most interesting to the end-user. Clinicians and producers sometimes classify sensors according to the field of application, such as critical care sensors, point-of-care sensors (home diagnostic sensors), in-vivo-, ex-vivo-, and in-vitro sensors, as well as “instant sensors”. Consequently, there are other fields of applications including sensors for use in the environment, in marine research, in industry, in meteorology, and in the car industry.

However, it is probably more significant to the researcher in the sensor field to classify sensors with respect to the mode of action, or, in other words, to the way the signal is generated. We suggest the classification of fluorescence sensors according to the scheme outlined in Table 1. The first group (type A) consists of the so-called plain sensors, which in fact are simply based on the measurement of the intrinsic fluorescence of an analyte.

A second class of sensors (type B) is based on the use of a luminescent indicator for a species that either has no useful (= measurable) intrinsic fluorescence, or that cannot be detected specifically in complex samples. Chemical sensors of type C utilize a fluorescent indicator that is involved in a reaction with the analyte such as a pH indicator, which is responsive to a reaction in which protons are generated or taken up. Examples include sensors for  $CO_2$ ,  $NH_3$  and gaseous HCl.

**Table 1** Classification of luminescence-based optical sensors

Sensor type	Description	Origin of the analytical signal
A	Plain sensor	Intrinsic fluorescence of an analyte
B	Directly indicator-mediated chemical sensor	Luminescence of an indicator for the species of interest
C	Indirectly indicator-mediated chemical sensor	Emission of an indicator for a species that is formed or consumed in the recognition process of the species of interest
D	Direct enzymatic biosensors	Luminescence of a cofactor which is formed or consumed during a biochemical reaction (analogous to type B)
E	Indicator-mediated biosensors	Fluorescence of an indicator which responds to a species formed or consumed during a biochemical reaction involving the analyte (analogous to type C)
F	Affinity sensors (mostly irreversible)	Fluorescent detection of noncovalent binding events such as antibody–antigen, complementary polynucleotide strands (DNA, RNA, PNA) receptor–ligand, enzyme–inhibitor, aptamers or MIPs and their substrates etc. (by analogy to types B or C)

The most direct form of biosensors is represented by class D, in which the emission change of a cofactor of particular enzymatic reaction is recorded. Mostly the  $\text{NAD}^+/\text{NADH}$  pair is employed, although there are also some examples with  $\text{FAD}/\text{FADH}_2$ . Most fluorescent biosensors, however, employ an indicator for a substrate or product that reacts with the analyte in an enzymatic reaction (class E). They can therefore be regarded as the biosensor analogs of type C. The most prominent representatives are glucose biosensors employing the generation of protons, oxygen, or hydrogen peroxide by glucose oxidase. The last class F is comprised of the wide area of affinity sensors, although strictly treated most of them do not qualify as sensors because they are based on irreversible, non-covalent high affinity interactions such as between particular proteins and monoclonal antibodies.

Note that all these sensors may also be coupled to fiber optics or other waveguides in order to achieve remote sensing capabilities, enhanced selectivity, or other special features.

Occasionally, sensors are classified according to the way they are engineered, for example into fiber-optic sensors, planar sensors, or distributed sensors. A generally applicable scheme for classifying fluorescent chemical sensors and biosensors obviously does not exist.

### 3.1

#### Plain Fluorometric Sensors (Type A)

These sensors rely on the continuous measurement of the intrinsic luminescent properties of a sample, a lot of which were among the first fluorometric sensors reported. Selectivity is achieved by proper choice of analytical wavelengths, time-resolved data acquisition, or by measurement of decay times. Often a fraction of the sample to be sensed is passed through an external loop where luminescence can be recorded.

Such sensors are often combined with fiber-optical technology. The fiber acts as a light guide and allows remote spectrometric analysis of any analyte displaying intrinsic luminescence that can be discerned from the background (Fig. 3). Such fiber sensors are referred to as bare-ended fiber sensors, plain fiber sensors, or passive opt(r)odes. Typical examples include the sensors listed in Table 2.

Plain sensors display both advantages and disadvantages with respect to quality assurance. In principle, it is usually preferable to use a signal which is generated directly by the analyte, thus avoiding any errors introduced by indirect detection. This is a convenient method, if the fluorescence of the analyte is in the red or near-IR, where the fluorescence background is normally very low, however, the luminescence of most analytes usually has to be excited in the deep UV (< 300 nm), where there is typ-

**Table 2** Examples for remote luminometric sensing of analytes by exploitation of the intrinsic fluorescence of the analyte

Analyte	Environment	Detection method used	Refs.
Algae	Natural waters	Remote measurement of the intrinsic fluorescence of chlorophylls	[19]
Diphenhydramine	Pharmaceuticals	Emission intensity at 285 nm, excited at 235 nm	[20]
NAD(P)H	Bioreactor	Fluorescence at 450–460 nm with excitation between 340 and 360 nm	[21]
Petroleum oil	–	Identification of oils using fluorescence spectra and lifetimes excited at 266, 355, 428, 532 nm	[22]
Proteins	Surfaces	Total internal reflection UV fluorescence	[23]
SO <sub>2</sub>	Air	Fluorescence intensity between 240 and 420 nm, excited at 213.8 nm (Zn flashlamp)	[24]
UO <sub>2</sub> <sup>2+</sup>	Groundwater	Luminescence intensity at 534 nm	[25]

ically a lot of interference, particularly in dense media, such as biological systems. Almost all organic matter and a lot of inorganic compounds absorb to some extent in the deep UV, and a lot of compounds also exhibit fluorescence. The use of plain sensors in this spectral region is thus not desirable. Some compounds such as polycyclic aromatic hydrocarbons exhibit remarkably long fluorescence lifetimes or phosphorescence, and temporal discrimination becomes feasible. The drawback of this method is the often poor quantum yield of long-lived emission, which along with the lower radiative rate can result in a poor *S/N* ratio. Phosphorescence is also typically dependent on the environmental conditions such as oxygenation, on the other hand deoxygenation is usually not feasible, as it leads to a much enhanced phosphorescence background of the support material. To recapitulate, plain fluorescence or phosphorescence-based sensors should only be used if the spectral or temporal features of the analyte are very distinct from the matrix, and should generally be avoided in the deep UV if background is present.

### 3.2

#### **Direct Indicator-Mediated Chemical Sensors (Type B)**

Numerous chemical species do not have analytically useful luminescence properties. Examples include hydrogen, oxygen, the proton (pH), most heavy metals and many organics. Thus, they cannot be probed or sensed directly. Moreover, various colored species may be contained in a matrix with optical properties similar to the species of interest so that they cannot be recognized by direct spectroscopy. This situation gave rise to the development of fluorosensors, in which the analytical information is mediated by some sort of indicator chemistry, usually deposited in the form of a thin sensor film. The film is composed of an analyte-permeable polymer that contains the chemically responsive probe. This film can be used in various ways but mostly in the form of a sensor spot as shown in Fig. 2 which is a schematic of the sensing unit of a widely used medical system.

Such films may, however, also be deposited inside a reaction bottle, a microwell plate, or at the core of a fiberoptic waveguide as shown in Fig. 3 where a fluorogenic enzyme substrate in a polymeric solid support is placed on either the core or the distal end of the fiber. The support also may contain indicator probes for analytes such as pH, oxygen, and the like. Other examples of such "opt(r)odes" are listed in Table 3.

A subgroup of such sensors is called "reservoir sensors": In this sensor type a reagent is continuously added to the sample at the tip of an optical fiber. A fluorogenic reaction occurs in the immediate vicinity of the fiber leading to the generated fluorescence being transmitted into it. Various species have been monitored in this way by simply adding the respective indicators

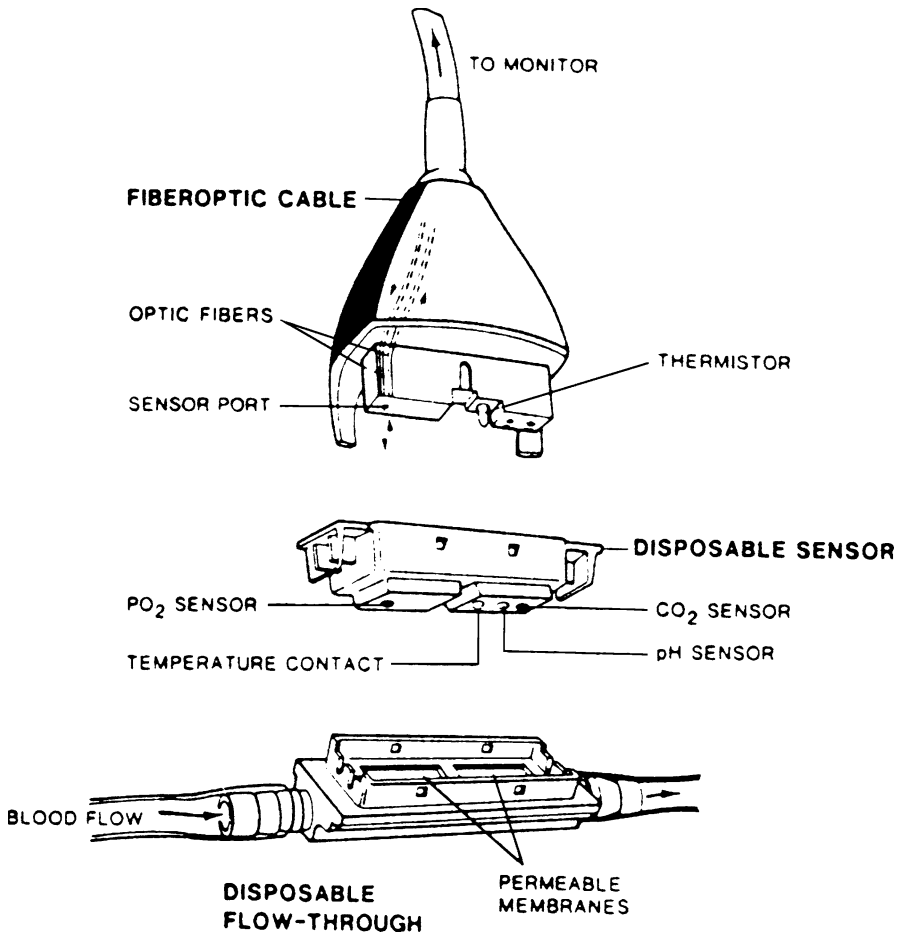


**Fig. 2** A disposable sensor for blood gas analysis containing an extracorporeal loop, from [17]. The three sensor spots (for pH, O<sub>2</sub>, and CO<sub>2</sub>) are interrogated via three 200- $\mu$ m fiber optic cables

to the sample. Effects of varying sample volume can be compensated for by making ratiometric techniques such as two-wavelength measurements.

The quality of this type of sensor is largely determined by the specificity of the probe, and the (typically polymer-based) matrix. Any compound that interferes with the indicator has to be retained inside the sample and not leak into the matrix. The matrix has not only got to provide specificity but must also be stable and not dissolve into the sample. Most commonly used polymers are stable against highly polar solvents like water only and big amounts of apolar compounds cause problems. The state-of-the-art in these schemes depends very strongly on the analyte. For many small-molecule compounds like oxygen, hydrogen, or heavy metals highly specific

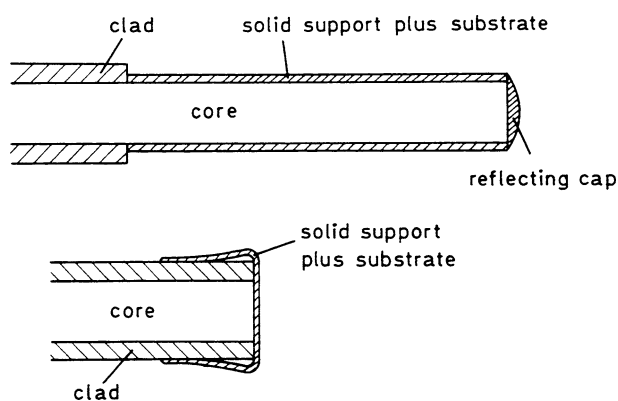


**Fig. 3** Two typical designs of fiber optic sensors. In the *upper one*, the solid support containing an indicator probe or a chromogenic enzyme substrate forms the cladding of the fiber and is interrogated by an evanescent wave. In the *lower one*, the material is fixed at the distal end of the fiber. Revised from [18]

**Table 3** Examples of direct indicator-mediated fluorosensors for chemical species

Analyte	Environment	Detection method used	Refs.
Cl <sup>-</sup>	Serum	Fluorescence quenching of lucigenin	[26]
Glucose	Eye	Saccharide-induced fluorescence quenching of boronic acid side groups-containing fluorophores	[27]
Halothane	Breath gas	Dynamic quenching of the fluorescence of decacyclene by halothane	[28]
H <sup>+</sup> , O <sub>2</sub>	Blood	Fluorescence intensity of appropriate indicators immobilized on a silica (O <sub>2</sub> ) or aminoethylcellulose (pH) layer	[29]
H <sup>+</sup>	Blood	H <sup>+</sup> without O <sub>2</sub> interference by fluorescence lifetime via Förster-type energy transfer	[30]
H <sup>+</sup>	Aqueous solutions	Emission intensities of HPTS at 530 and 610 nm (reservoir sensor)	[31]
K <sup>+</sup>	Serum	Fluorescence intensity of a fluoroionophore	[32]
Mg <sup>2+</sup>	Seawater	UV-excited fluorescence of a quinoline compound at 517 nm (reservoir sensor)	[33]

indicators exist, which ensure a very robust sensing capability, whereas the luminescence-based indicators for others are still very problematic (e.g., for the greenhouse gas CO<sub>2</sub>).



### 3.3

#### Indirect Indicator-Mediated Chemical Sensors (Type C)

Ideally, chemical sensing is performed with direct sensors, type B. Direct sensors usually provide a more robust assay procedure and less complexity than indirect ones. Unfortunately, for a variety of analytes there are no or only poorly suitable indicators known, which suffer from problems like poor reversibility or sensitivity, the need for high temperature, the addition of aggressive reagents or adjustment of a certain pH, which may be incompatible with the analyte or the medium. In order to circumvent such difficulties, an indirect indicator, which responds to a species which is formed or consumed in a reaction involving the analyte, can be employed. For example, a lot of these sensors are based on a pH indicator contained in a polymer membrane, which is permeable to the analyte, but not to acids or bases in the medium. As the most prominent application, many indirect carbon dioxide sensors work according to the general principle:



The indicator ( $\text{I}^-$ ) is protonated by  $\text{CO}_2$ , causing its fluorescence properties to change. Other schemes involve a phase transfer can occur from the (usually) aqueous sample into a polymer, for example by ion exchange from a lipophilic cation carrier (such as valinomycin). The carrier extracts the ion from an aqueous sample phase into a polymer phase containing a deprotonable indicator dye. In order to maintain electroneutrality, a proton of the dye has to be released from the polymer phase to enter the aqueous phase. Deprotonation causes the fluorescence of the dye to change. In the case of anions, a coextraction process occurs: A carrier extracts an anion such as chloride from an aqueous phase into a polymer phase. The process would soon come to an end unless a proton is coextracted. Any protonable dye contained in the polymer phase, which will become protonated and thus change its fluorescence. A schematic of the ion-exchange schemes is shown in Figs. 4 and 5.

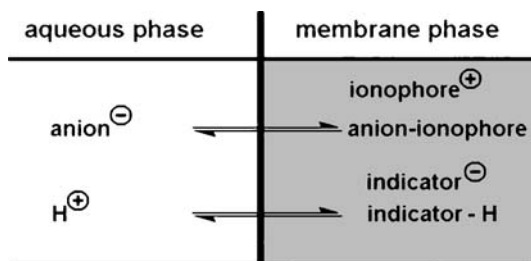


**Fig. 4** Schematic of the coextraction scheme of an anion along with a proton. The latter causes the indicator dye to change its fluorescence

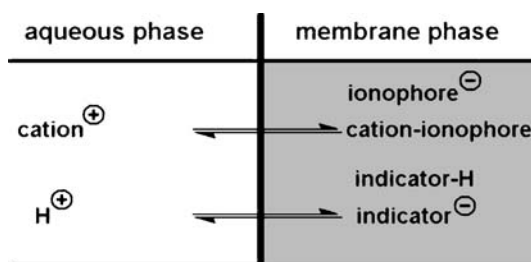


**Fig. 5** Schematic of the ion-exchange scheme for a cation and a proton. Deprotonation of the dye causes its fluorescence to change

Another type B scheme makes use of so-called potential-sensitive (or polarity-sensitive) fluorescent dyes (“PSDs”). Similar to the above extraction mechanisms, analyte ions are extracted from the sample to a polymer phase. However, PSDs are not protonated or deprotonated, but rather move inside the membrane in response to the analyte. The solid phase, in this case displays two distinct environments or some kind of gradient in between them, one being more hydrophilic the other being more lipophilic. Movement of the PSDs causes the fluorescence to change as a result of solvatochromism or aggregation. An example is outlined in Fig. 6.

It just takes simple logic to reveal that with indirect indicator-based schemes at least one further component is being introduced that is possibly susceptible to interference by non-analytes, so experimental conditions have to be monitored and validated even more rigorously than with type B sensors. The inherent complexity of these schemes usually limits their usefulness to a smaller set of conditions compared to B-type sensor schemes. Taking the outlined CO<sub>2</sub> sensing scheme as an example, it is easy to realize that any acidic or basic component has the potential to interfere into the measurement.

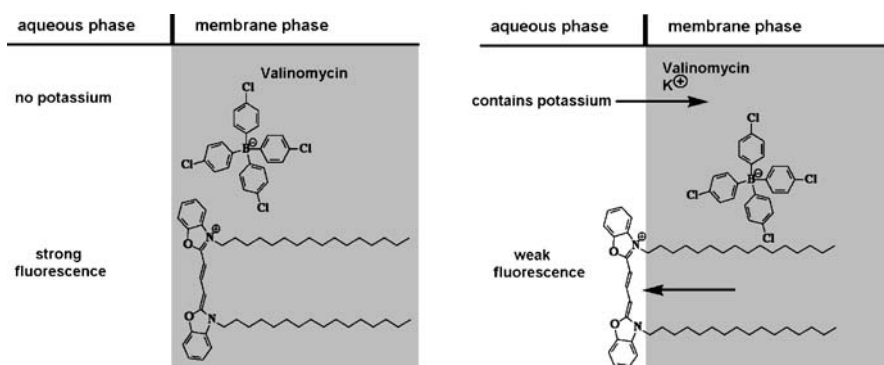


**Fig. 6** Mechanism of action of a potential sensitive cyanine dye for K<sup>+</sup>. Revised from [35]

**Table 4** Examples of indirect indicator-mediated fluorosensors

Analyte	Environment	Detection method used	Refs.
CO <sub>2</sub>	Food packaging	Luminescence decay time of a pH indicator contained in a sol-gel layer incorporated into the packaging	[34]
K <sup>+</sup>	Serum	Coupling of transport to a proton exchange process. The luminescence intensity of a pH indicator contained into a thin layer of plasticized PVC is measured	[35]
K <sup>+</sup>	Serum	Recognition of the cation by an ion carrier and transports onto lipid beads. A potential-sensitive dye changes its fluorescence	[36]
NH <sub>3</sub>	Aqueous solutions	Penetration of a proton-impermeable silicone polymer that contains a pH indicator, the luminescence intensity of it is monitored	[37]
NO <sub>3</sub> <sup>-</sup>	Drinking water	Luminescence intensity of a potential-sensitive dye	[38]

### 3.4

#### Direct Enzymatic Biosensors (Type D)

Certain coenzymes and co-factors of enzymes undergo a change in their optical properties when undergoing metabolic transformations. Two examples are representative. The first is the well-known cofactor NAD<sup>+</sup> that is reductively converted into the strongly fluorescent NADH during the action of enzymes out of the group of dehydrogenases. Thus, by monitoring the increase in the fluorescence of NADH over time, a direct kinetic parameter is obtained that reflects the concentration of the substrate of the enzyme. This has been shown to work for immobilized enzymes, but NAD<sup>+</sup> has to be added. In a certain sense, such a system also may be referred to as a kind of reservoir sensor.

The second type of direct optical enzyme biosensor is based on the finding that the intrinsic fluorescence of the coenzyme FAD undergoes a change in intensity and decay time upon addition of suitable substrates. This has been exploited to sense glucose, lactate, and other substrates.

Direct enzymatic biosensors can be regarded as being analogous to chemical sensors of type B, as they are based on changes in the fluorescence of species that are involved in a reaction with the analyte, although this analogy

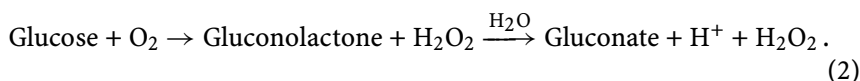
is not perfect, as the coenzyme does not directly react with the molecule of interest.

Apart from what has already been said for sensors of type B, enzyme-based sensors are typically advantageous because of the large specificity and selectivity being engineered by nature, however, the main drawback in using enzymes as well as many other biomolecules as recognition elements is their lack of thermal stability, which results in great problems with respect to storage and data reproducibility.

### 3.5

#### Indicator-Mediated Enzymatic Biosensors (Type E)

The lack of specific indicators for some compounds, which would give changes in luminescence at room temperature without addition of aggressive reagents, and at near neutral pH, in reasonably short time and in a fully reversible way, has led researchers to look for other alternatives than to use indirect chemical sensors. One solution is to employ a biocatalytic system and to screen for chemicals formed or consumed in the course of the reaction. Since many enzymatic reactions require co-reactands such as O<sub>2</sub> (for which good indicators are abundant), they are well suited for sensing. Such biosensors can be regarded as analogous to chemical sensors type C. Typical examples are listed in Table 5. The glucose sensors are some of the most successful, both in terms of performance and on the marketplace. Almost all functions on the basis of the enzymatic action of glucose oxidase (GOx) according to



The production of protons or H<sub>2</sub>O<sub>2</sub>, or the consumption of oxygen may be monitored optically. The cross section of a typical layer for enzymatic sensing of glucose (or other enzyme substrates) is shown in Fig. 7. It is clear from this figure that response times become longer with increasing layer thickness.

**Table 5** Examples of direct enzymatic biosensors

Substrate	Enzyme	Coenzyme/Indicator	Refs.
Ethanol	Alcohol dehydrogenase	NADH	[39]
Glucose	Glucose dehydrogenase	NADH	[40]
Glucose	Glucose oxidase	FAD	[41]
Lactate, Pyruvate	Lactate dehydrogenase	NADH	[42]
Lactate	Lactate monooxy-genase	FAD	[43]

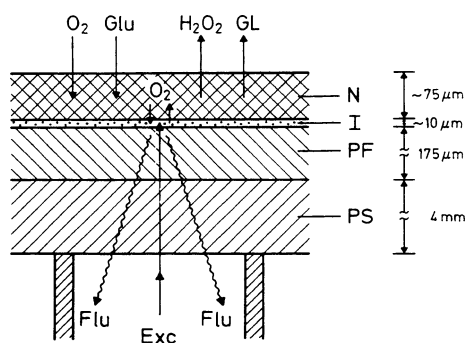


**Fig. 7** Cross section of a glucose-sensing layer using fluorescence quenching of oxygen as detection method. *PS* PMMA support, *PF* polyester film, *I* indicator layer, *N* nylon membrane, *Glu* glucose, *GL* gluconolactone

As with type C sensors, problematic with such sensors is potential of interference of compounds into various steps of the sensing process. A further problem with these sensors is that enzymes are also only working in the native conformation and may undergo denaturation in response to the sample,

**Table 6** Examples of chemical species determined via optical enzymatic biosensors using chemical transducers

Substrate	Enzyme	Indicator	Refs.
Ascorbate	Ascorbate oxidase	O <sub>2</sub>	[44]
Bilirubin	Bilirubin oxidase	O <sub>2</sub>	[45]
Cholesterol	Cholesterol oxidase	O <sub>2</sub>	[46]
Creatinine	Creatinine Iminohydrolase	NH <sub>4</sub> <sup>+</sup>	[47]
Ethanol	Alcohol oxidase	O <sub>2</sub>	[48]
Glucose	Glucose oxidase	H <sub>2</sub> O <sub>2</sub>	[49]
Glucose	Glucose oxidase	O <sub>2</sub>	[50]
Glucose	Glucose oxidase	pH	[51]
Glutamate	Glutamate decarboxylase	CO <sub>2</sub>	[53]
Glutamate	Glutamate oxidase	O <sub>2</sub>	[54]
Lactate	Lactate monooxygenase	O <sub>2</sub>	[53]
Lactate	Lactate oxygenase	O <sub>2</sub>	[54]
Oxalate	Oxalate decarboxylase	CO <sub>2</sub>	[55]
Penicillin	Penicillinase	pH	[56]
Phenols	Phenolase	O <sub>2</sub>	[55]
Sulfite	Sulfite oxidase	O <sub>2</sub>	[55]
Urea	Urease	NH <sub>3</sub> /NH <sub>4</sub> <sup>+</sup>	[57]
Urea	Urease	pH	[58]
Uric Acid	Uricase	O <sub>2</sub>	[55]

which is typically not a problem with type C sensors, as the conformation of small molecules, particularly chromophores, is much more restricted. Nevertheless, the gain in selectivity by the use of enzymatic reaction often outweighs these disadvantages.

### 3.6

#### **Affinity Biosensors (Type F)**

Given the above definition of (bio)sensors (as being continuously recording devices), one cannot refer to affinity sensors as true sensors since they display a rather high degree of irreversibility. This is true for both metal ion indicators (where indicators have a very high affinity to certain ligands), and for immunosensors and gene sensors. It is the binding constant and the (un)binding kinetics that determines—to a wide extent—the irreversibility of a sensor. Of course, the rates of the forward and back reactions, respectively, determine whether a sensor is reversible or not, but in case of immunosensors the back reaction is mostly so slow that a sensor is unlikely to be reversed at room temperature in reasonable time. However, regenerating agents such as acid or detergent are added. Hence, such “sensors” are in fact single shot probes.

#### 3.6.1

##### **Antibody–Antigen Interactions**

Antibodies are some of nature’s most effective molecular recognition tools. Substantial advances have been made in the analysis of biological compounds by the use of specific, mainly monoclonal, antibodies against a molecule of interest. They typically show nano- to picomolar dissociation constants, enabling the detection of minute quantities of compounds. Also, antibodies are not restricted to proteins, but are available against almost all kinds of compounds, e.g., small toxins or even fluorescent probes. However, due to the high affinities they act mostly in an irreversible way. Another problem is the poor stability at room temperature or above, even more so than with other biosensors, which suffer similar problems. Fluorescent detection can be performed in a classical sandwich manner or by using direct designs such as incorporation of a fluorescent dye into the antibody, which changes its properties upon antigen binding. Table 7 shows some representative antibody-based biosensor applications.

Although the binding constants of antibodies are very disadvantageous with respect to continuous sensing, they also enable a sensitivity and specificity that is pretty much unmatched by other compounds. However, the main disadvantages of antibodies are the elaborate production process, which results in high costs and the thermal instability, which is often even more pronounced than in enzymes.

**Table 7** Examples of antibody–antigen–interaction–based biosensors

Analyte	Detection method used	Refs.
Benzo[ <i>a</i> ]pyrene	Time-resolved, low-temperature, laser-induced fluorescence	[59]
Rabbit anti-horse IgG	Supercritical angle-based fluorescence immunoassay	[60]
Testosterone	Total internal reflection fluorescence (TIRF)-based Immunoassay	[61]
TNT	Direct, competitive, displacement or sandwich immunoassay on planar waveguides	[62]
Zn(II)	Fluorescence quenching of catalytic antibodies upon Zn(II) binding	[63]

### 3.6.2

#### Nucleic Acid Interactions

The ability of nucleic acids to form stable duplexes (and in some cases multiplexes) with their matching counterparts forms one of the integral bases of life and has been exploited widely for analytical purposes in many areas of research. DNA displays many advantageous properties for sensor design with respect to other biomolecules such as chemical and thermal stability, and the ability to control duplex formation via temperature adjustment. This has found widespread use in sensor development. Synthetic analogues of naturally occurring bases include peptide nucleic acids (PNA) which exhibit an uncharged backbone. They have further widened the scope of applications for sensors based on nucleic acid interactions. One popular detection design is based on

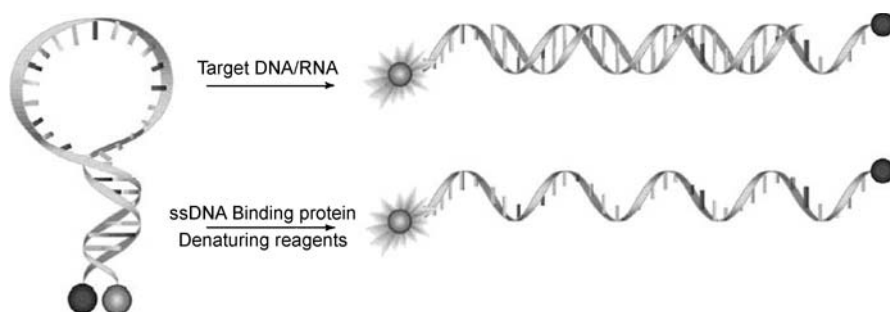


**Fig. 8** Schematic representation of the molecular beacon mechanism. The target binds to the probe DNA, causes the loop to vanish and therefore release of the donor fluorescence in a FRET pair. From [64]

the so-called “molecular beacon”, where the ends of the probe oligonucleotides are labeled with a donor and acceptor dye, respectively. They form a hairpin loop, which unfolds upon acceptor binding and causes the donor fluorescence to emerge (Fig. 8). For a comprehensive discussion see [64].

### 3.6.3

#### Ligand–Receptor Interactions and Related Types

Interactions of large biomolecules (“receptors”) with small natural or synthetic compounds (“ligands”) may also be utilized for sensory purposes. The most prominent example is certainly the avidin–biotin interaction. It is often used for detection via direct labeling, but biotin–avidin binding can also serve as building block for the construction of biosensor surfaces. It features a femtomolar dissociation constant, and occurs between readily available compounds. The glycoprotein avidin, however, is seldomly employed, because of its basic isoelectric point and its sugar moiety which causes some unspecific binding at neutral pH. The nonglycosylated analogue streptavidin and the bioengineered neutravidin are free of these drawbacks. Problems associated with the use of biotin (such as poor water solubility) have also been largely overcome by use of synthetic analogues.

A large number of ligand–receptor interactions are known. A special case involves the use of metal–ligand interactions such as the specific formation of complexes between Ni(II) ions and six histidine residues. The metal-binding capacity of DNA has also been used in biosensors. As another example, a group of proteins called lectins bind specific sugar residues. Enzymes, for example cannot only be used along with their specific substrates, but also with inhibitors. Synthetic short DNA chains called aptamers, which bind to molecules of different types such as proteins, have been developed and used for sensing. The ability of certain molecules to intercalate into DNA can

**Table 8** Examples of nucleic-acid-interaction-based biosensors

Analyte	Detection method used	Refs.
Double-stranded DNA	Binding of dye-labelled PNA to ds DNA, FRET upon addition of conjugated cationic polymers	[65]
Endocrine disruptors	TIRF-based detection using immobilized PNA's	[66]
Rat $\gamma$ -actin	Molecular beacons on optical fibers	[67]
Salmonella	Evanescent wave, analyte binding to both an immobilized probe and a dye-labeled oligonucleotide	[68]
Staphylococcus aureus	Fluorescence unquenching of molecular beacons on gold films	[69]



**Table 9** Examples of ligand–receptor–interaction-based biosensors

Analyte	Detection method used	Refs.
Acetylcholine	Fluorescence of probe molecule upon binding of the analyte to a MIP	[70]
B. anthracis	RNA detection using biotin–streptavidin and fluorescein–antibody recognition	[71]
cAMP	Fluorescence quenching upon binding of cAMP to a MIP	[72]
Maltose	Quenching of quantum dot luminescence upon binding of His <sub>6</sub> -tagged maltose binding protein (MBP)	[73]
Organophosphate pesticides	Binding of labeled, biotinylated organophosphate hydrolases to avidinylated fibers	[74]
Polyaromatic hydrocarbons	Displacement of fluorescent DNA intercalators	[75]
Theophyllin	FRET-based detection using an aptamer-ribozyme assembly	[76]
Zn(II)	Indirect displacement of an enzyme-fluorescent inhibitor complex yielding fluorescence increase	[77]

also be used in sensing schemes. Recently, molecularly imprinted polymers (MIPs) have been employed for quantification of biological content, particularly of proteins. Strictly speaking, one cannot not refer to these schemes as biosensors though, because MIPs are not biomolecules. Rather, they act as mimics of these, and are thus also often referred to under this label.

## 4 Conclusions

Although having been around for a long time, definitions and classifications of chemical sensors and biosensors are rather diverse, sometimes misleading or even contradictory. Important features of the most common definitions are highlighted here, and an integral scheme for the classification of sensors based on fluorescence or phosphorescence is presented, highlighting the different requirements needed for validation and to ensure robust quality. The scheme is based on the molecular mode of action of these sensors. It is therefore expected of particular use for researchers in the chemical sensor and biosensor field. Possibly, it can make a contribution towards avoiding misunderstandings and misinterpretations in sensor terminology, and increase sensor quality, and therefore may help to further advance this important and highly interdisciplinary field.

## References

1. Haber F, Klemensiewicz Z (1909) *Z Phys Chem* 67:385
2. Clark LC Jr (1956) *Trans Am Soc Artif Intern Organs* 2:41
3. Clark LC Jr (1962) *Ann NY Acad Sci* 102:29
4. Wolfbeis OS (ed) (2004–2006) *Springer Series on Chemical Sensors and Biosensors, Vol 1–4*. Springer, Berlin Heidelberg New York
5. Eggins BR (2002) *Chemical Sensors and Biosensors*. Springer, Berlin Heidelberg New York
6. Ligler FS, Rowe-Taitt CA (eds) (2002) *Optical Biosensors: Present and Future*. Elsevier, Amsterdam
7. Thompson RP (2006) *Fluorescence Sensors and Biosensors*. CRC Press, Boca Raton
8. Wolfbeis OS (2006) *Anal Chem* 78:3859 (and references A1–A3 therein)
9. Hulanicki A, Glab S, Ingman F (1991) *Pure Appl Chem* 63:1247
10. Grandke T, Hesse J (1991) Introduction, in *Sensors. A Comprehensive Survey, Vol 1*. Wiley, Weinheim, p 1
11. Goepel W, Schierbaum KD (1991) Definitions and Typical Examples. In: Goepel W, Hesse J, Zemel JN (eds) *Sensors: A Comprehensive Survey, Vol 2*. Wiley, Weinheim, p 1
12. Hauptmann P (1990) *Sensoren – Prinzipien und Anwendungen*. Hanser, München (in German)
13. Boisdé G, Harmer A (1996) *Chemical and biochemical sensing with optical fibers and waveguides*. Artech House, Norwood
14. Cammann K, Guibault EA, Hall H, Kellner R, Wolfbeis OS (1996) The Cambridge Definition of Chemical Sensors. In: *Proceedings of the Cambridge Workshop on Chemical Sensors and Biosensors*. Cambridge University Press, New York
15. Brecht A, Gauglitz G (1995) *Biosens Bioelectron* 10:923
16. Thévenot DR, Toth K, Durst RA, Wilson GS (2001) *Biosens Bioelectron* 16:121
17. Wolfbeis OS (1991) Biomedical Application of Fiber Optic Chemical Sensors. In: Wolfbeis OS (ed) *Fiber Optic Chemical Sensors and Biosensors, Vol 2*. CRC Press, Boca Raton, p 267
18. Wolfbeis OS (1991) Sensing Schemes. In: Wolfbeis OS (ed) *Fiber Optic Chemical Sensors and Biosensors, Vol 1*. CRC Press, Boca Raton, p 61
19. Samuelsson G, Oquist G (1977) *Physiol Plant* 40:315
20. Reguera IP, Rubio MG, Diaz AM (2004) *Anal Sci* 20:799
21. Mukherjee J, Lindemann C, Scheper T (1999) *Appl Microbiol Biotechnol* 52:489
22. Alaruri S, Rasas M, Alamedine O, Jubian S, Al-Bahrani F, Quinn M (1995) *Opt Eng* 34:214
23. Van Wagenen RA, Rockhold S, Andrade JD (1982) *Adv Chem* 199:351
24. Schwarz FP, Okabe H, Whittaker JK (1974) *Anal Chem* 46:1024
25. Hirschfeld T, Deaton T, Milanovich F, Klainer S (1983) *Opt Eng* 22:27
26. Huber C, Werner T, Krause C, Wolfbeis OS (2003) *Microchim Acta* 142:245
27. Badugu R, Lakowicz JR, Geddes CD (2005) *Talanta* 65:762
28. Wolfbeis OS, Posch HE, Kroneis H (1985) *Anal Chem* 57:2556
29. Leiner MJP (1995) *Sens Actuators B* 29:169
30. Kosch U, Klimant I, Wolfbeis OS (1999) *Fres J Anal Chem* 364:48
31. Luo S, Walt DR (1989) *Anal Chem* 61:174
32. He H, Mortellaro MA, Leiner MJP, Fraatz RJ, Tusa JK (2003) *J Am Chem Soc* 125:1468
33. Inman SM, Stromvall EJ, Lieberman SH (1989) *Anal Chim Acta* 217:249
34. Wang K, Seiler K, Morf WE, Spichiger UE, Simon W, Lindner E, Pungor E (1990) *Anal Sci* 6:715

35. von Bueltingsloewen C, McEvoy AK, McDonagh C, MacCraith BD, Klimant I, Krause C, Wolfbeis OS (2002) *Analyst* 127:1478
36. Huber C, Klimant I, Krause C, Werner T, Wolfbeis OS (2001) *Anal Chim Acta* 449:81
37. Mohr GJ, Murkovic I, Lehmann F, Haider C, Wolfbeis OS (1997) *Sens Actuators B* 39:239
38. Werner T, Klimant I, Wolfbeis OS (1995) *Analyst* 120:1627
39. Walters BS, Nielsen TJ, Arnold MA (1988) *Talanta* 35:151
40. Narayanaswamy R, Sevilla F III (1988) *Anal Lett* 21:1165
41. Trettnak W, Wolfbeis OS (1989) *Anal Chim Acta* 221:195
42. Wangsa J, Arnold MA (1988) *Anal Chem* 60:1080
43. Trettnak W, Wolfbeis OS (1989) *Fres Z Anal Chem* 334:427
44. Schaffar B, Dremel BAA, Schmid RD (1989) *GBF Monographs* 13:229
45. Li X, Fortuney A, Guilbault GG, Suleiman AA (1996) *Anal Lett* 29:171
46. Trettnak W, Wolfbeis OS (1990) *Anal Biochem* 184:124
47. Wolfbeis OS, Li H (1992) *Proc SPIE* 1587:48
48. Wolfbeis OS, Posch HE (1988) *Fres Z Anal Chem* 332:255
49. Wolfbeis OS, Schaeferling M, Duerkop A (2003) *Microchim Acta* 143:221
50. Trettnak W, Leiner MJP, Wolfbeis OS (1988) *Analyst* 113:1519
51. Kulp TJ, Camins I, Angel SM (1988) *Proc SPIE* 906:134
52. Dremel BAA, Schmid RD, Wolfbeis OS (1991) *Anal Chim Acta* 248:351
53. Trettnak W, Wolfbeis OS (1989) *Anal Lett* 22:2191
54. Dremel BAA, Trott-Kriegeskort G, Schaffar BP, Schmid RD (1989) *GBF Monographs* 13:225
55. Schaffar BPH, Wolfbeis OS (1991) *Bioprocess Technol* 15:163
56. Kulp TJ, Camins I, Angel SM, Munkholm C, Walt DR (1987) *Anal Chem* 59:2849
57. Rhines TD, Arnold MA (1989) *Anal Chim Acta* 227:387
58. Luo S, Walt DR (1989) *Anal Chem* 61:1069
59. Grubor NM, Shinar R, Jankowicz R, Porter MD, Small GJ (2004) *Biosens Bioelectron* 19:547
60. Ruckstuhl T, Rankl M, Seeger S (2003) *Biosens Bioelectron* 18:1193
61. Tschmelak J, Kumpf M, Kaepfel N, Proll G, Gauglitz G (2006) *Talanta* 69:343
62. Sapsford KE, Charles PT, Patterson CHJ, Ligler FS (2002) *Anal Chem* 74:1061
63. Stewart JD, Roberts VA, Crowder MW, Getzoff ED, Benkovic SJ (1994) *J Am Chem Soc* 116:415
64. Tan W, Wang K, Drake TJ (2004) *Curr Opin Chem Biol* 8:547
65. Baker ES, Hong JW, Gaylord BS, Bazan GC, Bowers MT (2006) *J Am Chem Soc* 128:8484
66. Kroger K, Jung A, Reder S, Gauglitz G (2002) *Anal Chim Acta* 469:37
67. Liu X, Farmerie W, Schuster S, Tan W (2000) *Anal Biochem* 283:56
68. Furch M, Ueberfeld J, Hartmann A, Bock D, Seeger S (1996) *Proc SPIE* 2928:220
69. Du H, Disney MD, Miller BJ, Kraus TD (2003) *J Am Chem Soc* 125:4012
70. Inouye M, Hashimoto KI, Isagawa K (1994) *J Am Chem Soc* 116:5517
71. Baeumner AJ, Jones C, Wong CY, Price A (2004) *Anal Bioanal Chem* 378:1587
72. Turkewitsch P, Wandelt B, Darling GD, Powell WS (1998) *Anal Chem* 70:2025
73. Medintz IL, Clapp AR, Mattoussi H, Goldman ER, Fisher B, Mauro JM (2003) *Nature Mater* 2:630
74. Viveros L, Paliwal S, McCrae D, Wild J, Simonian A (2006) *Sens Actuators B* 115:150
75. Pandey PC, Weetall HH (1995) *Appl Biochem Biotechnol* 55:87
76. Rueda D, Walter NG (2006) *Methods Mol Biol* 335:289
77. Thompson RB, Whetsell WO, Maliwal BP, Fierke CA, Frederickson CJ (2000) *J Neurosci Methods* 96:35

# Fibre-Optic and Nanoparticle-Based Fluorescence Sensing Using Indicator Dyes: Pitfalls, Self-Referencing, Application, and Future Trends

Gerhard J. Mohr

Institute of Physical Chemistry, Friedrich-Schiller University Jena, Lessingstrasse 10,  
07743 Jena, Germany  
*gerhard.mohr@uni-jena.de*

1	Fluorescence-Based Fibre-Optical Chemical Sensors . . . . .	347
1.1	Principle of Referencing Using Ratiometric Dyes or Reference Dyes . . . . .	348
1.2	Principle of Referencing Using Luminescence Lifetime Measurements . . . . .	350
1.3	Principle of Referencing Using Dual Luminophore Ratioing . . . . .	352
1.4	Principle of Referencing Using Luminescence Anisotropy . . . . .	354
1.5	Referenced Fibre-Optic Chemical Sensors for pH . . . . .	354
1.6	Referenced Fibre-Optic Chemical Sensors for Cations and Anions . . . . .	357
1.6.1	Ion-Exchange and Co-Extraction Based Sensors . . . . .	357
1.6.2	Sensors Using Fluoroionophores . . . . .	359
1.7	Referenced Fibre-Optic Sensors for Neutral Analytes . . . . .	361
1.8	Referenced Fibre-Optic Biosensors for Neutral and Ionic Analytes . . . . .	364
2	Fluorescent Sensor Nanoparticles . . . . .	365
2.1	Referenced Sensor Nanoparticles for Ions . . . . .	366
2.2	Referenced Sensor Nanoparticles for Neutral Analytes . . . . .	368
2.3	Future Trends for Optical Fibres and Sensor Nanoparticles . . . . .	369
	References . . . . .	371

**Abstract** Herein is described how reliable measurements of ionic analytes and biomolecules can be performed using fibre-optic sensors or sensor nanoparticles. Referenced signal readings are achieved by using ratiometric dyes or by combination of indicator dyes with inert luminophores. Thus, it becomes possible to minimize effects from light source instability, leaching, photobleaching or sample colouration. Similarly, a combination of reference and indicator dyes in nanoparticles enables quantitative measurements, for example, in cells and tissues.

**Keywords** Fibre-optic chemical sensors · Fluorescent sensor nanoparticles

## 1 Fluorescence-Based Fibre-Optical Chemical Sensors

Fibre-optic chemical sensors (FOCS) are used in medical research, for diagnostic applications, for environmental monitoring, for food quality analysis and for detection of chemical warfare agents. Fibre optics enable optical

spectroscopy to be performed on sites inaccessible to conventional spectroscopy, over large distances, and even on several spots along the fibre. They offer a high degree of miniaturization, have no electric contacts, and are unaffected by electromagnetic fields. However, the reliability of signal readings of FOCS can be compromised by various parameters such as dye photobleaching, dye leaching, autoluminescent molecules in the analyte sample, ambient light, light source fluctuations, detector and electronics fluctuations, optical fibre bending, changes in the sensor geometry by detachment of the sensor layer or changes in the optical properties of the dye and polymer matrix. Four general approaches have been introduced to overcome these limitations and guarantee stable signal readings, namely (a) measurements using ratiometric dyes, (b) the measurement of luminescence lifetime, (c) a combination of both methods (e.g. dual lifetime referencing), and (d) measurement of luminescence anisotropy. This overview does not give a complete coverage on all self-referencing FOCS but rather an introduction into the different reference methods using exemplary analytes. For a comprehensive overview on FOCS, the biannual reviews "Fiber-Optic Chemical Sensors and Biosensors" by Otto S. Wolfbeis in Analytical Chemistry are recommended. Furthermore, only "true" sensors are discussed, i.e. sensors that enable the concentration of certain species to be sensed *continuously*.

## 1.1

### Principle of Referencing Using Ratiometric Dyes or Reference Dyes

Fibre-optic chemical sensors for neutral and ionic analytes are often based on the selective interaction of an indicator dye with the analyte. The indicator dye is typically immobilized in (or on) a polymer support attached to the tip of the optical fibre. Two major optical transduction principles are used: (A) a specific functional group of the indicator dye that is an integral part of the fluorophore performs a selective interaction with the analyte molecule (Fig. 1). This interaction affects the electron acceptor or donor strength of the functional group and thus changes the electron delocalization within the dye molecule. As a consequence, the dye shows significant changes in fluorescence which are usually accompanied by a shift in fluorescence maxima. (B) The receptor function is connected to the fluorophore via a spacer. Thus, the interaction of the receptor moiety with the analyte does not affect the electron delocalization of the fluorophore directly but modulates photo-induced electron transfer from the receptor to the fluorophore. As a consequence, changes in luminescence intensity (but no spectral shifts) are observed.

Most reported optical chemical sensors use changes in intensity at one defined wavelength as the analytical information because intensity-based optical fibre sensors are commercially available. Since light emitting diodes, laser diodes, photodiodes and filters can be used for their fabrication, they are

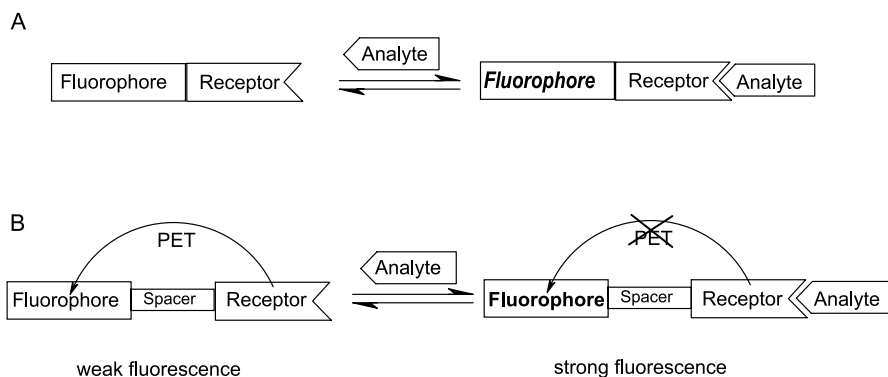


**Fig. 1** Analyte recognition **A** via selective interaction with the fluorophore causing electron delocalization and fluorescence to change and **B** via complexation with a receptor not directly linked to the fluorophore but modulating PET

usually not expensive. However, they are limited in accuracy due to drifts in opto-electronical set up, indicator leaching and photo-bleaching or transmission changes in the optics. Consequently, ratiometric methods based on the use of an internal reference were later established because they are less prone to errors related to non-analyte-induced intensity changes.

When developing fibre-optic sensors, indicator dyes of type (A) are preferred that exhibit intramolecular charge transfer upon interaction with the analyte. These dyes usually show different fluorescence maxima for the free dye and the analyte-bound dye, and it is possible to quantify analyte recognition via a decrease in fluorescence of one form and an increase in intensity of the other form of the dye (on each side of the isosbestic point, Fig. 2). Consequently, measuring intensities of two different forms (e.g. complexed/uncomplexed or protonated/deprotonated) and calculating the ratio of these two intensities allows one to obtain signal changes that are not compromised by dye leaching or fluctuations of the light source. Fibre bending can also be partially compensated although the out-coupling of light through bending is wavelength-dependent.

Indicator dyes of type (B) and fluorescent indicators that exhibit luminescence quenching upon interaction with the analyte (e.g. oxygen sensor dyes, and halide indicators such as lucigenin) require another approach to achieve referenced sensor signals. Here, the use of an analyte-insensitive reference dye together with the indicator dye is a feasible way to obtain a ratio of signals (Fig. 3). The reference dye has to be completely insensitive to changes in the analyte concentration and should have comparable absorbance to the indicator dye in order to allow a common excitation light source to be used. Furthermore, the reference dye must emit at a significantly different wavelength than the indicator dye to separate indicator signal from reference

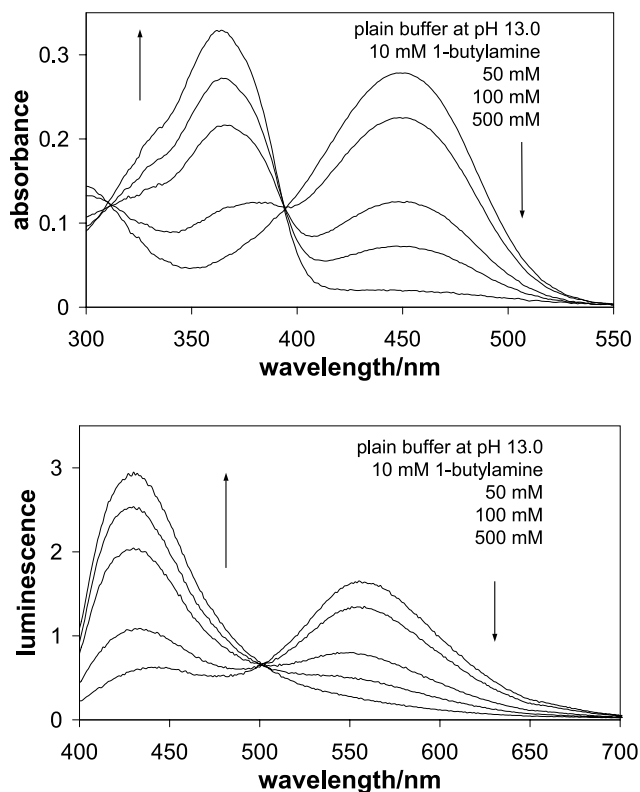


**Fig. 2** Optical sensor based on an indicator (type A) whose electron delocalization changes upon interaction with the analyte, causing changes in both absorbance and fluorescence (excitation set to 400 nm) [1]. Here, ratiometric measurements are possible

signal. However, often a minor change in intensity of the inert reference upon exposure to the analyte can be observed (Fig. 3).

This is due to a small but significant spectral overlap of analyte-dependent indicator emission and analyte-independent reference emission. Care has to be taken in the choice of the reference dye not to encounter inner filter effects or energy transfer between the two fluorophores. And both dyes must have comparable rates of photo-bleaching and leaching, otherwise considerable changes in intensity ratio are observed.

## 1.2

### Principle of Referencing Using Luminescence Lifetime Measurements

A very convenient method to obtain stable signal readings is the measurement of luminescence lifetime because this parameter is not compromised by leaching or instability of light source/detector. Luminescence lifetime is

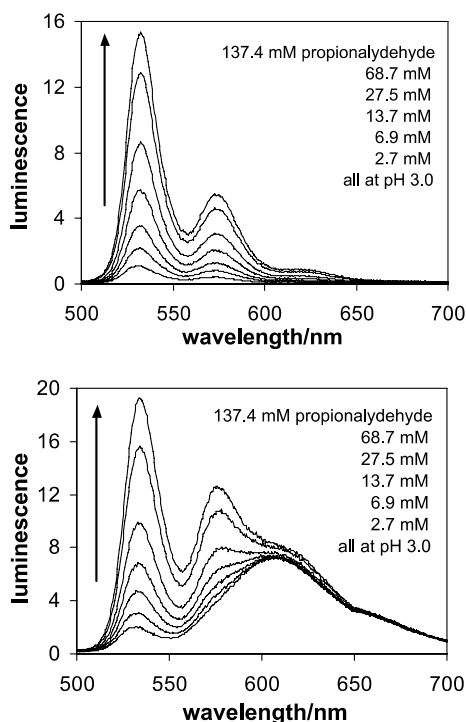


**Fig. 3** Optical sensor based on an indicator (type B) that responds to changes in analyte concentration via photoinduced electron transfer [2]. Referencing is only possible when an inert reference fluorophore (peak emission at 620 nm) is added to the sensor layer (*lower graph*)

intrinsically independent of the overall signal intensity but almost all indicator dyes have lifetimes in the ns range which would require expensive instrumental set-up. One very prominent exception are the phosphorescent indicators for oxygen, i.e. the ruthenium bipyridyl or phenanthroline complexes and the palladium/platinum porphyrins that have lifetimes in the  $\mu\text{s}$ –ms range. These dyes can be used in phase-fluorimetric sensors, where the sensor layer is illuminated with modulated light (sine or square wave excitation), while monitoring the luminescence signal with respect to the excitation. The delay in emission (phase shift  $\phi$ , measured in degrees angle) relates to the lifetime ( $\tau$ ) of the dye according to:  $\tan \phi = 2\pi\nu\tau$ , with  $\nu$  = frequency of excitation. For dyes with long decay times, modulation frequencies of excitation in the kHz range are sufficient, which can be achieved using low-cost LEDs and photodiodes. In contrast, dyes with nanosecond decay times require modulation frequencies in the megahertz range, making the experimental set-up more expensive. The resulting sensors can operate under ambient light and the signals are independent of dye concentration



(e.g. leaching and bleaching are not problematic as long as the products of photodecomposition themselves are not luminescent and enough dye is in the layer to provide adequate signal to noise ratio). Unfortunately, there is limited availability of selective indicator dyes with long luminescence lifetime. This, however, has partially been overcome by making use of fluorescence energy transfer between a donor fluorophore and an absorber dye to modulate the luminescence lifetime. An analyte-insensitive but long-lived fluorophore (e.g. a ruthenium complex) is combined with an analyte-sensitive indicator dye (e.g. a pH sensitive indicator) in one polymer layer. To obtain sufficiently high signal changes in both intensity and decay time, a strong overlap between the absorbance of the deprotonated or protonated form of the pH indicator with the inert emission of the donor is mandatory. Depending on sample pH, the acceptor deactivates the excited state of the donor, modulating both the luminescence intensity and the decay time.

### 1.3

#### Principle of Referencing Using Dual Luminophore Ratioing

Another approach to referenced fluorescence signals combines an inert reference dye with long luminescence lifetime and an analyte-sensitive indicator dye with short lifetime. When using modulated excitation light, the inert reference dye provides a constant phase angle that is modified by analyte-dependent changes in fluorescence signal of the indicator dye. Consequently, a phase shift of modulated light caused by the analyte rather than the overall change in luminescence signal is measured. Since measurements are performed at low modulation frequencies adjusted to the long-lived reference dye, a cheap and small experimental sensor set-up can be developed. This approach is referred to as dual luminophore referencing (DLR).

Two different luminescent dyes are present in one sensor layer. The first is the indicator dye which changes its fluorescence intensity upon interaction with the analyte. The second is a phosphorescent dye which, for the sake of chemical and physical inertness, is embedded in gas-impermeable poly(acrylonitrile) beads. Both dyes exhibit overlapping excitation and emission spectra (Fig. 4).

The indicator dye exhibits a short fluorescence lifetime. Consequently, there is virtually no phase shift between the modulated light of the LED and the emitted light of the indicator (Fig. 5). The ruthenium reference, in contrast, has a lifetime in the range of microseconds causing a strong phase shift compared to the light source. If the indicator is present in its uncomplexed form (here: showing strong luminescence), then the amplitude composed of the luminescence signal of indicator and reference luminophore is measured (A). This causes a shift of the phase angle of the overall luminescence,  $\phi_m$ , compared to the phase angle of the reference dye  $\phi_{ref}$ . As soon as the indicator reacts with the analyte (here: causing weak luminescence), then the

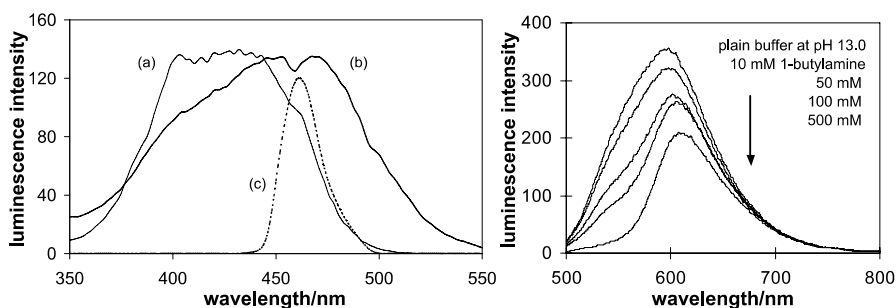


**Fig. 4** *Left*: Luminescence excitation spectra of (a) reference beads, (b) the indicator ETH<sup>T</sup> 4003 in plasticized PVC, and (c) emission spectrum of the blue LED (all showing strong spectral overlap). *Right*: Luminescence emission of the sensor layer composed of plasticized PVC, ETH<sup>T</sup> 4003 and reference beads in contact with water and aqueous 1-butylamine. The referenced signal is encoded in the ratio of amplitudes of indicator and reference (see text)

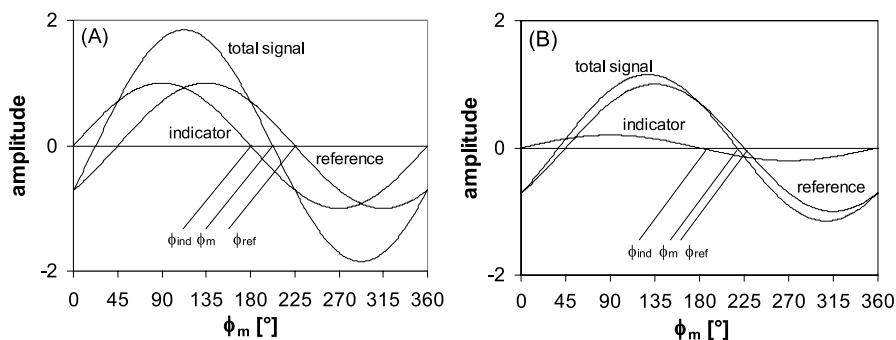


**Fig. 5** Phase shift of the overall luminescence ( $\phi_m$ ), the reference ( $\phi_{ref}$ ) and the indicator dye ( $\phi_{ind}$ ). **A** Luminescence of the indicator before interaction with the analyte, **B** luminescence of the indicator after interaction with the analyte

overall amplitude consists only of the reference dye, and a phase angle,  $\phi_m$ , being equal to the phase angle of the reference,  $\phi_{ref}$ , is observed (B). Therefore, the phase angle  $\phi_m$  directly reflects the intensity of the indicator and consequently the concentration of the analyte. The modulation frequency is adjusted to the decay time of the reference dye. The calculation of the phase shift and of  $\cot \phi$  is performed according to:

$$\cot \phi_m = \cot \phi_{ref} + 1 / \sin \phi_{ref} A_{ind} / A_{ref}$$

provided that the phase angle of the indicator,  $\phi_{ind}$ , is equal to zero and  $\phi_{ref}$  is constant. Consequently, the measured phase angle  $\phi_m$  depends on the ratio of amplitudes of indicator,  $A_{ind}$ , and reference beads  $A_{ref}$ , since  $\phi_{ref}$  is constant.

A significant advantage of dual luminophore referencing is the fact that both the indicator and reference are excited by one common light source and

the signals are detected by a single filter-detector combination. This makes the instrumental set-up less complex and enhances stability in the signal readings.

## 1.4

### Principle of Referencing Using Luminescence Anisotropy

Anisotropy is a fundamental property of the fluorescent emission and is often used in biosensing, mainly to evaluate and quantify antigen–antibody interactions. A small antigen labelled with a small fluorescent dye rotates very easily in solution. Therefore, anisotropy is low. When binding to a large antibody takes place, rotation of the fluorescent dye is slower and anisotropy increases. Similarly to luminescence lifetime, anisotropy is intrinsically referenced. When developing optical sensors for analytes such as oxygen, a different approach is used. Here, a highly polarized reference fluorophore is combined with a non-polarized fluorescence indicator. A stretched polymer layer containing a dye with linear structure and short luminescence lifetime is used as the reference, while the indicator embedded in a second polymer layer has a long luminescence lifetime and consequently yields low polarization. Because the total anisotropy is the weighed sum of the anisotropy contributions of the separate emissions of both dyes, an increase in the intensity of the sensor fluorophore results in decreased anisotropy, and vice versa. Since excitation and emission polarizers are necessary to evaluate changes in anisotropy, polarization-based sensors using fibre optics have not yet been applied in practice [3].

## 1.5

### Referenced Fibre-Optic Chemical Sensors for pH

In optical sensors for pH measurement, a pH indicator dye is immobilized in a polymer matrix at the distal end of an optical fibre. The indicator exists, in the acidity range of interest, in both acid and base forms which can be differentiated by their luminescence properties. The luminescence of the indicator is then related to the concentration of protons present in the samples solution. Often pH optodes are inadequate for real applications because they measure the signal change at one defined emission wavelength. The single excitation and single emission optodes are vulnerable to light source fluctuations (*vide supra*) and leaching/bleaching of the dye. Sample turbidity, changes in temperature, or presence of luminescence quenchers (e.g. heavy metal ions, halides, etc.) can cause the signal intensity to change even when the pH is kept constant.

Zhujun and Seitz presented the first self-referenced fibre-optic sensor for physiological pH values by immobilizing 1-hydroxypyrene-3,6,8-trisulfonate onto an anion exchange membrane [4]. The electronically excited pH indi-

cator dye undergoes rapid deprotonation, therefore only the emission of the base form at 520 nm is observed around near neutral pH. However, the acid and base forms of the dye can be selectively detected by appropriate choice of wavelengths. The ratio of intensities resulting from excitation at 470 and 405 nm can be used to quantify pH values between 6 and 9. Response times were reported to be in the range of 70–120 s, and no interferences by heavy metal ions (all at  $10^{-3}$  M), sulfate, phosphate, carbonate, acetate, oxalate (all at 500 mg/L) and 10% proteins was observed. The low interferences were attributed to the anion exchange membrane, excluding ions by electrostatic effects and proteins because of size.

Parker and co-workers presented a pH sensor with enhanced chemical stability using a seminaphthorhodafluor indicator [5]. This dye was covalently linked to poly(2-hydroxyethylmethacrylate) and sensors were prepared by dissolving the pH polymer in acetone and applying the solution to the distal end of the 125  $\mu\text{m}$  optical fibre via dip-coating. The dye had a pK around 7.9 in the polymer matrix and exhibited a 95% response in less than 90 s. Using a green LED as the light source, the basic form exhibited a maximum at around 650 nm, the acid form at 590 nm and the isosbestic point was at 605 nm.

Song and co-workers developed a pH-microsensor with a diameter of 2  $\mu\text{m}$  using carboxynaphthofluorescein entrapped in a polyacrylamide gel matrix via photopolymerization [6]. The response to pH was almost linear in a pH 7–8 range and response was in the ms time regime. Excitation of the dye was performed at convenient wavelengths such as 488, 514.5 or 632.8 nm and the two emission maxima corresponding to the acid and base form were found at around 590 nm and 680 nm, respectively, with the isosbestic point at 640 nm. The preparation of the polymer layer at the tip of the fibre was originally proposed by Walt et al. [7]. It is of special interest because it can be used for other pH and ion sensors as well. First, the tip of the optical fibre is surface-silanized with [3-(methacryloyloxy)propyl]trimethoxysilane. Then, a mixture composed of acrylamide, *N,N'*-methylene-bis(acrylamide) and the fluorescent indicator dye is prepared and the activated optical fibre is placed into this polymerization solution. Polymerization is initiated by passing light through the optical fibre. This causes the formation of the sensor polymer only in the region of the fibre tip. Furthermore, the polymer is covalently linked to the fibre via the methacrylate groups obtained in the pre-activation step. Walt et al. used a polymerizable acryl derivative of fluorescein to obtain stable cross-linked pH sensors, but it is also possible to physically embed the dye without the need for covalent attachment. This has been shown by Song et al. (*vide supra*) who simply added the plain dye into the monomer mixture and embedded carboxynaphthofluorescein only physically during the polymerization, yet obtaining an operational lifetime of around 14 days.

Another approach to achieve stable pH sensors is to use the sol-gel process for the fabrication of layers on the distal end of optical fibres. These glass-

like layers are made by hydrolysis and polycondensation of tetraalkoxysilanes at room temperature, usually in the presence of water and alcohols. The response time of the sensor layers depends strongly on whether acidic or alkaline catalysis is applied during their preparation, basic catalysts usually giving larger pores in the polysiloxane network. Grant et al. prepared a ratiometric pH sensor by simply mixing seminaphthorhodamine-1-carboxylate with sol-gel precursors and dip-coating the end of an optical fibre in this mixture. A linear response within pH 6.8–8.0 in human blood was obtained and the sensor had low coating leachability [8]. A non-invasive excitation-ratiometric pH sensor for continuous on-line fermentation monitoring was presented by Kermis et al. who immobilized 8-hydroxypyrene-1,3,6-trisulfonate onto Dowex anion exchange resin. The resin was embedded in a hydrogel layer and then polymerized onto a white microfiltration membrane that provided an optical barrier to the fluorescence and scatter of the fermentation medium. The ratio of emission intensity at 515 nm excited at 468 nm to that excited at 408 nm enabled detection of pH within a pH 6.0–9.0 range. Response of the indwelling sensor patch was <9 min and the sensor was sterilizable [9].

Fluorescence lifetime-based pH sensors are limited in number, because the amount of long-lived pH indicators is limited as well. However, it is possible to use chemically modified oxygen-sensitive ruthenium complexes to monitor changes in pH. Ruthenium(II) polypyridyl complexes have been synthesized where at least one heterocyclic ligand responded to pH via, for example, photoinduced electron transfer [10, 11]. These pH sensors remained cross-sensitive to molecular oxygen so that oxygen had to be determined in parallel, or calibrations had to be performed with different oxygen background.

Another more facile way to achieve pH optodes with luminescence decay in the microsecond time regime is to use fluorescence energy transfer from a pH-insensitive luminescent donor to a pH-sensitive coloured acceptor. Kosch et al. used bromothymol blue as the acceptor whose deprotonated form strongly overlapped the emission of the pH-insensitive ruthenium(II) bipyridine fluorophore (donor). Consequently, the excited state of the donor was deactivated, thereby causing a decrease in both the quantum yield and the decay time of the donor [12]. The resulting phase shift of the luminescence signal was dependent on sample pH (excitation 470 nm, emission above 570 nm), and was highest in the pH 7–9 range.

Sanchez-Barragan and co-workers recently presented a new ratiometric approach to fibre-optic pH sensing using a single fluorescent pH indicator entrapped in sol-gel glass [13]. They measured the pH-dependent emission of 2',7'-dibromo-5'-(hydroxymercurio)fluorescein at 550 nm and used the reflected light from the sensing phase at 470 nm (i.e. the excitation light) as the reference signal. The reference intensity was composed of a large fraction of specular reflectance (pH independent, since no interaction with the sensing phase occurred) and a smaller fraction of diffuse reflectance (pH-dependent through the absorbance of the indicator dye). The resulting sensor signal was

obtained by dividing the indicator intensity by the sum of intensities of indicator and reference signals. The pH optode exhibited a linear range from pH 4–6, operational lifetime of one day and shelf life of >8 months.

## 1.6

### Referenced Fibre-Optic Chemical Sensors for Cations and Anions

#### 1.6.1

##### Ion-Exchange and Co-Extraction Based Sensors

The detection of ions via FOCS is mainly based on two different methods, namely (a) using the Charlton/Simon approach of co-extraction or ion-exchange and (b) using fluoroionophores selective for a specific ion.

In the first case, the optical sensors are composed of ion-selective carriers (ionophores), pH indicator dyes (chromoionophores), and lipophilic ionic additives dissolved in thin layers of plasticized PVC. Ionophores extract the analyte from the sample solution into the polymer membrane. The extraction process is combined with co-extraction or exchange of a proton in order to maintain electroneutrality within the unpolar polymer membrane (Fig. 6). This is optically transduced by the pH indicator dye [14–16].

The preparation of sensor layers on the optical fibre is relatively simple. It only requires dissolving the components (pH indicator dye, ionophore, ionic additive) together with poly(vinyl chloride) and a plasticizer in tetrahydrofuran (similar to ion-selective electrode membranes). The solutions are then coated onto the distal end of optical fibres. Since the recognition element (ionophore) and the optical transducer (pH indicator) are different molecules, almost any ionophore pH indicator combination is possible, giving sensors for a wide range of analytes. The sensor performance is math-

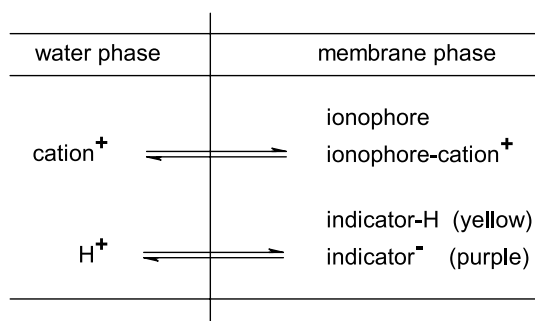


**Fig. 6** Mechanism of ion-exchange of cations and protons between the aqueous sample and the sensor membrane. The cation is extracted into the membrane phase by the selective ionophore. In turn, a proton is released from the membrane by the deprotonable pH indicator dye and this causes a change in fluorescence

ematically well-defined which allows one to predict both dynamic range and selectivity.

Several FOCs have been presented where this type of chemical sensor is used in a ratiometric procedure or where reference dyes were used to provide stable signals. Shortreed and co-workers investigated Nile Blue derivatives as pH chromoionophores and combined them with a 1,3-bridged calix[4]crown sodium ionophore and potassium tetrakis[3,5-bis(trifluoromethyl)phenyl]borate. A mixture with poly(vinyl chloride) and bis(2-ethylhexyl)sebacate in tetrahydrofuran was attached to the silanized fibre tip by a dip-coating procedure. This approach has the advantage that the sensitivity of the optode can be modified by substituting the chromoionophore by another whose  $pK_a$  differs. Consequently, Nile Blue derivatives with different  $pK_a$  gave sodium-sensitive optodes with different sensitivity but similar selectivity because the ionophore remained the same [17]. Thus, the optodes could be adjusted to both measurements in whole blood or intracellular medium. Koronczi et al. used a lipophilic fluorescein derivative in combination with valinomycin to develop an aluminium-coated fibre sensor for potassium, taking advantage of scanning near-field optical microscope technology [18]. In order to provide stable signal readings, they used Nile Red as a reference dye. An increase in potassium caused an intensity increase of fluorescein at around 550 nm while the emission of Nile Red at 600 nm remained unaffected. The authors reported that the error of the referenced signal due to photobleaching was reduced by a factor of  $\sim 100$ . However, it has to be taken into consideration that errors with internal calibration may occur if the two dyes are bleached, leached or quenched to a different extent.

Huarui He and co-workers were the first to combine inert fluorescent particles with absorbance-based sensor dyes to develop fluorosensors for ions [19]. They presented a potassium sensor based on the inner filter effect of fluorescence, using valinomycin as the selective ionophore. Exposure to potassium ion increased the absorbance of the pH indicator at around 640 nm, causing the fluorescence of the inert particles at 605 nm to decrease (with excitation set to 560 nm). Sensitivity was in the range of  $1 \mu\text{M}$ – $10 \text{ mM}$  potassium ion and response times were in the range of 2–6 min for full signal changes.

Making use of co-extraction of anions and protons into plasticized PVC, Barker et al. have presented nano- and micro-optodes for nitrite and chloride for in vitro applications [20]. Nile Blue chromoionophores were combined with a Vitamin B12-based ionophore for nitrite and an indium octaethylporphyrine derivative for chloride. Sensitivity was in the range of  $5 \mu\text{M}$ – $5 \text{ M}$  for nitrite and  $63 \text{ mM}$ – $5 \text{ M}$  for chloride (at pH 7.4).

Kosch et al. had already shown that pH-insensitive ruthenium(II) bipyridyl donor dyes in combination with pH-sensitive acceptor dyes were useful to develop luminescence lifetime-based sensors for pH (vide supra). By further adding selective ionophores for chloride and potassium and making use of

ion exchange or co-extraction into plasticized PVC, they also developed selective optodes for cations and anions [21, 22].

A severe disadvantage of all co-extraction or ion-exchange sensors is the intrinsic cross-sensitivity to pH because sensors based on ion-exchange measure the ratio of activities between analyte ion and the proton, and sensors based on co-extraction measure the product of activities of analyte and protons. In other words, it is not possible to distinguish whether colour changes are due to changes in analyte concentration or due to changes in pH. Consequently, the pH of the sample solution has to be determined or to be adjusted by addition of buffer. Huber et al. have addressed this problem by using a polarity-sensitive dye (PSD) to detect nitrate in drinking water, rather than a pH indicator dye as an optical transducer for the recognition process [23]. In sensor membranes based on PSDs, signal changes are induced by selective ionophores, which, similar to the mechanisms of co-extraction or ion exchange, extract analyte ions from the sample solution into the polymer membrane [24]. However, the response to the increase of analyte ions in the polymer phase is different. In the case of ion exchange or co-extraction, electroneutrality in the membrane is maintained via protonation/deprotonation of pH indicator dyes. PSDs usually do not possess functional groups that can be protonated or deprotonated. Therefore, electroneutrality can only be established if the PSD itself moves between the aqueous and the polymer phase. As a consequence of the motion of the PSD between phases of different polarity, fluorescence changes are induced which are not cross-sensitive to pH.

Another problem for the ion-exchange/co-extraction approach is leaching of the components from the polymer matrix, both relevant for the reference and indicator dye, as well as for the selective ionophore and for additional ionic additives. All of them have to be highly lipophilic and even if only one of the components is leaching, then the whole sensor exhibits a significant drift. Bakker et al. tackled this issue by covalently immobilizing a  $\text{Ca}^{2+}$ -selective ionophore to a plasticizer-free methacrylate copolymer, but still the indicator dye and the anionic additive were not covalently linked to the sensing layer [25].

## 1.6.2

### Sensors Using Fluoroionophores

A more reliable and practically relevant approach to FOCS is the use of one selective fluorogenic indicator dye for ions (fluoroionophore) and to immobilize this fluoroionophore (and the reference dye) to the tip of the optical fibre. The response of optical sensors based on fluoroionophores is completely different to the sensing schemes discussed previously. The above schemes (ion-exchange, co-extraction) make use of non-selective pH indicator dyes and selective ionophores. However, fluoroionophores are a combination of selective recognition and optical transduction in one molecule.



They consist of a fluorogenic part directly connected with the recognition moiety. Whereas ion-exchange and co-extraction work best in a lipophilic polymer matrix (usually plasticized PVC), fluoroionophores should be dissolved in a hydrophilic matrix in order to allow rapid diffusion of analyte ions to and from the fluoroionophore. Furthermore, due to the facilitated ion diffusion in hydrophilic matrices, no strong pH-cross-sensitivity comparable to the pH-cross-sensitivity of ion-exchange/co-extraction-based sensors is observed. Typical hydrophilic polymers are polyacrylamides, polyurethanes, cellulose, poly(hydroxyalkyl methacrylates) or poly(vinyl alcohols). Often, rather hydrophilic fluoroionophores are embedded in these hydrophilic polymers. Therefore, leaching is an issue and covalent immobilization of the fluoroionophores turns out to be almost mandatory.

The amount of fibre-optic ion sensors based on fluoroionophores is limited because the synthesis of selective indicator dyes with functions to covalently attach them to a polymer support is quite tedious. Nevertheless, Shortreed and co-workers presented a fluorescent calcium sensor for physiological measurements where they covalently linked Calcium Green acrylamide to the optical fibre via the polymerization procedure introduced by Walt and co-workers. However, the selective calcium sensor was limited by photobleaching of the indicator because Calcium Green is not a ratiometric fluorophore and because no reference dye was used [26]. Ji and co-workers have immobilized two dyes, namely the calcium-sensitive 1,2-bis(2-aminophenoxy)ethane-*N,N,N',N'*-tetraacetic acid derivative of 4-carboxy-2',7'-difluorofluorescein and the pH-sensitive seminaphthorhodafluor dye, both as dextran conjugates within poly(2-hydroxyethyl methacrylate) adsorbed to the distal end of the optical fibre [27]. It was not necessary to covalently immobilize the dyes to the polymer matrix because the dextran derivatives were large enough to be retained in the polymer network. Both dyes were excited at 488 nm and the emission of fluorescein at 520 nm and of the seminaphthorhodafluor at 584 and 630 nm were correlated to pH and calcium ion concentration by spectral processing of the sensor signals.

Mayr et al. applied the scheme of dual luminophore referencing to detect copper(II) using the indicator Lucifer Yellow and inert luminescent reference beads composed of ruthenium(II) tris(4,7-diphenyl-1,10-phenanthroline) in polyacrylonitrile (denoted  $\text{Ru}(\text{dpp})_3^{2+}$ -PAN). Both the fluoroionophore and the reference beads were immobilized in a hydrogel matrix. The copper(II)-dependent fluorescence intensity change of Lucifer Yellow was converted in either a phase shift or time-dependent parameter. The sensing membrane was capable of selectively determining copper(II) over a dynamic range between 1 and 1000  $\mu\text{M}$  under neutral or weakly acidic conditions [28]. This approach also addressed one problem when using ruthenium(II) complexes for the preparation of optical ion sensors, namely their cross-sensitivity to oxygen. The ruthenium(II) complexes were encaged in gas-impermeable nanoparticles. Therefore, quenching by molecular oxygen was no longer observed and

stable reference materials with long luminescence lifetimes were obtained. Using the same referencing approach, Huber and co-workers developed a selective optical sensor for chloride [29]. They prepared optodes by covalently linking the indicator lucigenin to polymer beads and by using  $\text{Ru}(\text{dpp})_3^{2+}$ -PAN reference nanoparticles. Both types of beads were then embedded in hydrophilic polyurethane hydrogel to give materials with a sensitive range of 1–1000 mM chloride.

## 1.7

### Referenced Fibre-Optic Sensors for Neutral Analytes

The majority of self-referencing fibre-optical sensors for neutral analytes are based on indicators whose luminescence lifetime is modulated during interaction with the analyte. All types of polymer matrices can be used because the diffusion of the analyte is not as strongly affected by the polymer matrix as it is in the case of ions.

Fibre-optic sensors for oxygen based on luminescence lifetime measurements are commercially available from several companies (Ocean Optics Foxy, Interlab Optosen, Presens Microx, Luxcel Oxygen Sensor System), and have found practical application in process-monitoring, clinical diagnostics, environmental monitoring and medical research. They are almost exclusively based on ruthenium(II) tris(4,7-diphenyl-1,10-phenanthroline) [30, 31] and platinum or palladium porphyrins [32, 33], all of which show a decrease in luminescence intensity and lifetime upon exposure to molecular oxygen (Table 1). The polymer-dissolved ruthenium complexes have luminescence lifetimes in the range of 0.8–5  $\mu\text{s}$  while the porphyrins can have lifetimes in the range from 40–>1000  $\mu\text{s}$ . Both systems are compatible with LEDs as excitation light sources and their long-lived luminescence makes them compatible with inexpensive (phase-fluorimetric) instrumentation. The advantage of the porphyrins is that oxygen-sensitivity can be tailored more strongly via their different chemical structures, and they absorb and emit at longer wavelengths. Thus, background light from, for example, cellular autofluorescence is minimized.

Oxygen sensors have a linear calibration function, because the luminescence intensity and decay time is reduced (quenched) by molecular oxygen via a photophysical quenching process. This process is described by the linear Stern–Volmer equation, rather than by mass action law used to describe the complexation of indicators with analytes. Unfortunately, often the calibration is not completely linear because the dye is embedded in polymers that have different microdomains. As a consequence, the same dye is quenched differently in different sites with a resultant downward curved Stern–Volmer plot.

Park and co-workers reported a fibre-optic sensor for oxygen with linear calibration [34]. Furthermore, rather than measuring luminescence lifetime,

**Table 1** Spectral properties and sensitivities of optical oxygen sensors

Oxygen sensor	Excitation [nm]	Emission [nm]	Lifetime (under N <sub>2</sub> ) [ $\mu$ s]	Sensitive range [hPa]
Ruthenium(II) tris(bipyridine) chloride in silicone	460	605	0.8	0–1013
Ruthenium(II) tris(4,7-diphenyl-1,10-phenanthroline) chloride in silicone	460	610	5	0–1013
Platinum(II)-tetrakis(pentafluorophenyl)porphine in polystyrene	539	653	27	0–210
Platinum(II)-octaethylporphine-ketone in polystyrene	592	759	61	0–210
Palladium(II)-octaethylporphine-ketone in polystyrene	602	790	480	0–20

they measured the ratio of intensities between oxygen-sensitive platinum(II) octaethylporphine ketone (at 760 nm) and oxygen-insensitive octaethylporphine (at 620 nm). However, the authors used plasticized PVC as the polymer matrix which is problematic in terms of leaching, especially in the case of nano-sized optodes.

In order to compensate for the significant temperature dependence of oxygen sensors, Liebsch et al. have embedded a ruthenium(II) complex in poly(acrylonitrile) nanoparticles. Thus, the complex was no longer oxygen-sensitive and could be used to monitor temperature via luminescence lifetime measurements. A linear calibration from 10 to 40 °C was reported [35]. Another issue for fibre-optic sensors is biofouling of polymer surfaces. The rapid accumulation of adsorbed biomaterials (proteins, cells, microorganism) leads to drift and sensor failure. Navarro et al. addressed this problem by coating their oxygen sensors with a 50 nm protective layer of phosphorylcholine-substituted methacrylate. Adsorption of thrombocytes was reduced by 90%, of fibrinogen by 92%, of albumin by 64%, and of adhered bacteria by 70% [36].

Barker et al. developed a fibre-optical nitric oxide sensor for cellular applications based on fluorescein attached to colloidal gold. The gold colloid was attached to the fibre, then the fibre immersed in a solution of the indicator 4-carboxy-2',7'-difluorofluorescein, succinimidyl ester and finally treated with a solution of fluorescent reference spheres. A change in orientation of the fluorophore was reported when the gold colloid reacted with nitric oxide, causing fluorescence quenching within less than 0.25 s [37]. Grant et al. presented a sol-gel-based optode for nitrogen dioxide that measured changes in luminescence lifetime via a miniature optoelectronics package. Ruthenium(II) tris-(2,2'-bipyridyl) dichloride was quenched by the paramagnetic

analyte gas with sensitivity in the 0.5%–2% range and response times of less than 15 s [38]. There was no response to nitric oxide but cross-sensitivity to oxygen was not investigated. Generally, when evaluating optodes based on the mechanism of luminescence quenching, it is recommended to investigate cross-sensitivity to notorious luminescence quenchers such as heavy metal ions, halides and nitroaromatic compounds.

Sensors for gaseous carbon dioxide frequently make use of modified pH sensors which have a carbon dioxide permeable membrane and a hydrogen carbonate reservoir. When in contact with the sample, carbon dioxide diffuses into the bicarbonate reservoir until equilibrium of balanced partial pressure occurs. This causes a change in pH of the bicarbonate reservoir and protonation/deprotonation of the pH-sensitive indicator dye. A comparable approach can also be used to detect ammonia [39].

Orellana and co-workers used a pH indicator dye with long luminescence lifetime to detect carbon dioxide. The ruthenium(II) tris-[2-(2-pyrazinyl)thiazole] complex was electrostatically immobilized in carboxymethyl Sephadex and the gel equilibrated with pH 7.25 buffer. The sensor material was physically attached to the optical fibre and was protected from the analyte sample via a gas-permeable silicone layer. Diffusion of carbon dioxide through the silicone layer to the sensor material caused a shift in buffer pH, protonation of the dye, and a change in luminescence lifetime [40]. Response times of ca. 2–10 min were found and highest sensitivity to carbon dioxide in the 1%–25% range. Tabacco et al. reported an autonomous fibre sensor and telemetry for low level  $p\text{CO}_2$  measurements in seawater. They immobilized pH-sensitive carboxysemaphthofluorescein in a poly(*N*-vinylpyrrolidone) copolymer that was equilibrated with bicarbonate buffer and coated with an ion-impermeable layer. In order to provide stable readings over periods of up to 8 months, signal changes of the dye were measured in ratiometric mode, giving a working dynamic range between 200 and 1000 ppm  $p\text{CO}_2$  [41].

Using the dual-luminophore approach, von Bültzingslöwen et al. combined the pH-sensitive indicator 1-hydroxypyrene-3,6,8-trisulfonate with inert  $\text{Ru}(\text{dpp})_3^{2+}$ -PAN nanoparticles [42]. The pH indicator responded to carbon dioxide via changes in fluorescence intensity while the (both pH- and oxygen-insensitive) nanoparticles provided the reference intensity to be evaluated in the phase domain. In this specific case, the pH indicator was not in contact with aqueous buffer but with a lipophilic quaternary ammonium hydroxide that acted as the ligand for carbon dioxide. Consequently, the sensors had response times in the range of 20–30 s. Furthermore, the use of sol-gel glass as the polymer matrix gave an operational and shelf lifetime of 20 weeks. The sensors were used to monitor the integrity of modified atmosphere packaging (MAP) of foodstuff. In MAP it is necessary to monitor the carbon dioxide content on the inner side of the packaging without sample destruction. This is possible with optical fibres that are placed close to the

transparent packaging foil in order to evaluate the response of the sensor on the inner side of the foil.

In a similar referencing approach, Mohr et al. developed a fibre-compatible optical sensor for amines that made use of the amine and alcohol-sensitive reactand 4-*N,N*-dioctylamino-4'-trifluoroacetylstilbene dissolved in plasticized PVC into which  $\text{Ru}(\text{dpp})_3^{2+}$ -PAN reference beads were suspended [43]. The optode exhibited the highest sensitivity to 1-butylamine in the 1–100 mM range and response times between 5–10 min. These materials can also be used for the detection of alcohols, biogenic amines and thiols.

## 1.8

### Referenced Fibre-Optic Biosensors for Neutral and Ionic Analytes

A wide range of analytes cannot be detected directly via optical sensors because adequate fluoroionophores or fluoroligands for e.g. glucose, lactate or urea do not exist. Therefore, biosensors have been developed where optical sensors for oxygen, carbon dioxide or ammonia are combined with selective enzymes. Rather than measuring the analyte directly, the optical sensor detects substances produced or consumed during the enzymatic conversion of the analyte. The enzyme glucose oxidase for example converts glucose with stoichiometric amounts of oxygen into gluconolactone and hydrogen peroxide. The consumption of oxygen (measured by the optical sensor) is then related to the quantity of glucose present in the sample solution. Sensitivity depends on the enzyme activity and the rate of diffusion of both oxygen and glucose to the immobilized enzyme and optical sensor layer.

On the basis of oxygen sensors, several fibre-optic biosensors for different analytes have been developed. Papkovsky et al. prepared stable glucose-sensitive optodes by dissolving both the oxygen sensitive polymer and glucose oxidase in the same microporous light-scattering support material. Thus, they obtained materials with enhanced mechanical stability, optical isolation against ambient light and sample colouration, close contact between sensor layer and enzyme, and good stability against elevated temperatures. A sensitive range of 0.1–15 mM glucose at pH 7.0 was found with response times of less than 7 min and storage stability >4 months [44]. Wolfbeis and co-workers introduced a two-sensor system consisting of a plain oxygen optode and a glucose optode to compensate varying oxygen partial pressure in analyte samples [45]. An optical fibre-sensor to estimate the biological oxygen demand (BOD) within minutes rather than days even made use of microbial cells immobilized on top of an oxygen sensor. Response times of 5–10 min, sensitivity within 0–110 mg/L BOD, operational stability up to 1 month and storage stability of one year were reported [46]. Sensors for alcohols can be developed by using alcohol oxidase in combination with the oxygen sensor material [47] and for lactate based on lactate oxidase [48]. While enzyme-based biosensors are very useful for analytical applications, it has to be taken

into consideration that, dependent on the type of enzyme used for sensor preparation, significant pH sensitivity, ionic strength and temperature dependence, limited stability and sensitivity to inhibitors can occur.

Similarly to using oxygen sensors in combination with enzymes to detect different analytes, optical sensors for ammonia and carbon dioxide are combined with enzymes to detect substrates where carbon dioxide and/or ammonia is produced, e.g. urea via its conversion by urease to form ammonia [49].

## 2

### Fluorescent Sensor Nanoparticles

There is a significant interest to detect ions in cells and tissues in order to obtain information on intra- and intercellular communication, transport mechanism, energy metabolism, pathogenic effects, and to evaluate the development/use of new drugs. A wide range of fluoroionophores is available and thoroughly characterized in aqueous buffer solution, but when it comes to the cellular environment, the situation can change completely. Two major challenges are (a) the high background of interfering ions in cells and (b) the fact that intracellular proteins often show strong interaction with dye molecules. Especially the interaction of indicator dyes with proteins can lead to very strong changes in fluorescence intensity and lifetime, but also to spectral shifts. Often, signal changes with proteins are much larger than the signal changes upon interaction with the analyte ion.

One approach to circumvent the limitation of indicator dyes is to protect them from proteins by entrapping them in nanoparticles. Thus, the indicator dyes are embedded in a stable polymer matrix which allows the entrance of ions and small biomolecules, but not of proteins. The resulting nanoparticles show significant changes in fluorescence with ions/biomolecules, but do no longer respond to proteins. Another advantage of the nanoparticles is that both indicator and reference dyes can be embedded together in the nanoparticles. This is mandatory when monitoring ion concentrations with a fluorescence microscope where focus and light source intensity may change during measurements. Finally, the nanoparticles can be inserted at specific locations in cells and, in contrast to dissolved indicator dyes, they do not enrich in certain cell compartments. It has to be mentioned that the presence of nanoparticles provides stress to the cells, but dissolved indicator dyes can even be toxic to the cell.

Different matrices have been reported for the development of luminescent sensor nanoparticles, e.g. hydrophilic poly(acrylamide), hydrophobic poly(decyl methacrylate) and sol-gel silica. Often the photostability of the dyes in nanoparticles was reported to be higher than in aqueous solution indicating, for example, partial shielding from oxygen once the dye was in the matrix.

## 2.1 Referenced Sensor Nanoparticles for Ions

Fluoroionophores in aqueous solution are highly sensitive to proteins but turn insensitive to proteins when embedded in polymer particles. For example, both the fluorescence intensity and emission maximum of the chloride indicator dye lucigenin in phosphate buffer is affected by the addition of bovine serum albumine. This undesirable behaviour is no longer observed after embedding (and protecting) lucigenin in polyacrylamide nanoparticles. While chloride is able to diffuse into the particle and to quench the luminescence of lucigenin, proteins are too large to enter the particle. In order to provide ratiometric nanoparticles, both the indicator lucigenin and the reference dye Sulforhodamine 101 are used in nanoparticle preparation [50]. Increasing the concentration of chloride ion causes the fluorescence of lucigenin in the nanoparticles to decrease while the fluorescence of Sulforhodamine 101 remains unaffected (Fig. 7). Since both dyes are protected in the particles, this response is not compromised by the presence of proteins.

The particles can be inserted into living cells by using a commercially available transfection solution. Other possible insertion methods are the use of a gene gun, micropipette, phagocytosis or attaching cell penetrating peptides to the nanoparticle surface [51]. When measuring separately the fluorescence intensities of indicator and reference dye a significant drift is observed. However, when measuring the intensity of the indicator signal divided by the intensity of the reference signal, then stable signals without drift are obtained.

To date, various sensor nanoparticles for ions have been presented, most of them based on hydrophilic polyacrylamide as the polymer matrix (Table 2). Kopelman and co-workers, who pioneered this type of sensor chemistry presented referenced nanoparticles for pH and  $\text{Ca}^{2+}$  [52],  $\text{Mg}^{2+}$  [53],  $\text{Zn}^{2+}$  [54],  $\text{Cu}^{2+}$  [55] and  $\text{Fe}^{3+}$  [56]. All of them were similar to the approach explained

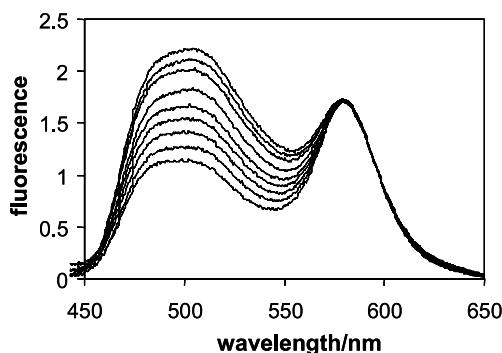


**Fig. 7** Decrease in luminescence of lucigenin at around 500 nm in polyacrylamide nanoparticles upon exposure to  $\text{Cl}^-$ , normalized against the inert luminescence of Sulforhodamine 101 at around 580 nm.  $K_{SV} = 53 \text{ M}^{-1}$  at pH 7.4

**Table 2** Performance and spectral properties of selected sensor nanoparticles

Analyte	Sensitive range	Excitation [nm]	Emission of indicator and reference [nm]	Response time
pH	6.2–7.4	488/568	500/590	1 ms
Ca <sup>2+</sup>	0–0.15 $\mu$ M	488/568	500/590	1 ms
Mg <sup>2+</sup>	1–30 mM	445	483/600	< 4 s
Zn <sup>2+</sup>	4–50 $\mu$ M	488	530/600	< 4 s
Cu <sup>+</sup> /Cu <sup>2+</sup>	200–5000 nM	488	583/517	3 min
Fe <sup>2+</sup>	1–15 $\mu$ M	493	517/600	3 min

above in that (commercially available) indicator dyes were combined with reference dyes. For example, the particles for pH monitoring were composed of 5-(and 6-) carboxy-4',5' dimethylfluorescein (pH indicator) and Sulforhodamine 101 (reference) with a pH working range from 6.2–7.4. Magnesium ion was detected by using Coumarin 343 where Texas Red Dextran was used as the reference, giving a sensitive range from 1–30 mM. Leaching of Coumarin 343 was in the range of 30–50% per 48 h, clearly because it was not covalently linked to the polymer matrix and because the particles had small size ( $\sim 20$  nm). Since measurements in cells are usually performed within a period of several hours, leaching does not pose a major problem. However, cross-contamination of neighbouring beads may become an issue as soon as different sensing chemistries are used simultaneously in one cell.

When developing referenced nanosensors, the reference dye often shows a small change in intensity upon exposure to the analyte (although there is no response of the reference dye alone to the analyte). This is mostly due to a spectral overlap of analyte-dependent indicator emission and analyte-independent reference emission (see also Fig. 3). However, fluorescence resonance energy transfer between indicator and reference must also be evaluated which can complicate calibration. Another aspect that deserves attention is the fact that embedding of indicator dyes into acrylamide nanoparticles can cause a loss in analyte-sensitivity and signal magnitude. The origin of both has not yet been investigated in detail. Finally, for guaranteeing accurate measurements over longer periods of time, photo-bleaching of both the indicator and reference dye must be comparable.

McNamara et al. developed phospholipid-based beads for the preparation of pH-sensitive nanoparticles with a sensitive range from pH 5.5–7.0 [57]. Fluorescein and tetramethylrhodamine were covalently labeled to phospholipids. The fluorescent phospholipids were coated onto carboxylated polystyrene beads to give 1.6  $\mu$ m-sized hybrid lipobeads with high stability against leaching. Fast response (<1 s) was observed because the dyes were immobilized close to the particle surface.



Kopelman and co-workers also prepared sensor nanoparticles for  $K^+$  [58],  $Na^+$  [59] and  $Cl^-$  [60], albeit with a different type of polymer matrix and a diameter of 500–1000 nm. Rather than using hydrophilic polyacrylamide, they chose poly(decyl methacrylate-*co*-hexanedioldimethacrylate) as the matrix in order to make use of the Charlton/Simon approach to combine selective ionophores with pH indicator dyes. Consequently, the composition of the sensors became more complex in that a nanoparticle for e.g.  $Na^+$  contained sodium-selective ionophore IV, Nile Blue derivative ETH 2439 as the pH indicator dye, the ionic additive potassium tetrakis-[3,5-bis(trifluoromethyl)]-phenyl borate, an indocarbocyanine reference dye, and the plasticizer bis(2-ethylhexyl)sebacate. As mentioned previously, sensor signals obtained by this approach are highly cross-sensitive to changes in pH, and thus can only be performed if the pH in the cells is continuously monitored and used to correct the data. Furthermore, leaching of one single component changes the calibration significantly. Finally, the response of the particles often deviates significantly from theory. Consequently, this type of sensor has limited practical relevance. Using the same recognition mechanism, Tsagkatakis et al. presented a mass production approach for microspheres with a diameter adjustable within 2–30  $\mu m$  [61]. All sensing components (indicator dye, ionophore, ionic additive, PVC, plasticizer) were dissolved in an organic solvent and then precipitated into aqueous solution at a rate of 20 000 drops/s. The major advantage of the microsensors over optode layers was an improvement in response time from hours to minutes due to small size and additionally, the need for only small amounts of analyte to reach sensor equilibrium. Furthermore, such miniaturized sensors also allow a high spatial resolution and their use in sensor arrays, similar to biochips.

## 2.2

### Referenced Sensor Nanoparticles for Neutral Analytes

Similar to FOCS, selective fluorogenic ligands embedded in nanoparticles can be used to detect neutral analytes or to detect the enzymatic conversion of the analyte. In order to monitor dissolved oxygen in cells, Xu et al. synthesized sol-gel-based nanoparticles in a modified Stöber method with poly(ethylene glycol) as a steric stabilizer. Ru(II)-tris(4,7-diphenyl-1,10-phenanthroline) chloride was the oxygen-sensitive indicator and 4-carboxy-2',7'-difluorofluorescein-dextran the reference fluorophore [62]. The sol-gel was prepared from these dyes, tetraethoxysilane, water, ammonia and poly(ethylene glycol) to give particles with a diameter in the 100–600 nm range (albeit after extensive filtration procedures to remove larger and smaller particles). The surfactant poly(ethylene glycol) helped in reducing both the size of the particles and aggregation effects, and was beneficial for a high sensitivity towards oxygen, probably by enhancing the hydrophobicity of the particle. Particle excitation was set to 488 nm and emission ratio was

detected at around 520 and 605 nm. A linear sensitive range from 0–30 ppm oxygen was achieved and response times less than 1 s.

Cao and co-workers prepared poly(decyl methacrylate)-based nanoparticles containing the oxygen indicator dye platinum octaethylporphine ketone (PtOEPK) and the reference dye octaethylporphyrin (OEP) [63]. The nanoparticles were synthesized via modified emulsion polymerization using sonication to reduce the size of the particles to a range of 150–250 nm. Both dyes were excited at 570 nm and the emission maxima of OEP and of PtOEPK were at 622 and 754 nm, respectively. The authors reported sensor nanoparticles with a linear calibration range (for the ratio of sensing dye over reference dye emission) for dissolved oxygen in the 0–45 ppm range and response times in the range of 0.4 s. Because of the high lipophilicity of the dyes and their compatibility with the lipophilic polymer matrix, no significant leaching was observed within a period of three days. While the poly(decylmethacrylate) particles are highly lipophilic, the surface of the particles is less so because the polyethylene glycol surfactant (used during synthesis) is still present at the surface of the particles. Consequently, good biocompatibility and suppression of protein binding was found.

By combining an oxygen-sensitive indicator, a reference dye and glucose oxidase in polyacrylamide nanoparticles, sensors for intracellular glucose were developed. The dynamic range was 0.3–8 mM glucose and response times of 150–200 s were observed. The materials were modified to be either ratiometric in excitation or emission mode, dependent on the reference dyes used [64]. Brown and co-workers designed glucose-sensitive multi-layer particles for intradermal implantation and for diabetes mellitus management. They prepared calcium alginate microspheres in the presence of glucose oxidase and impregnated them with an oxygen-sensitive ruthenium complex. Then, the 20–30  $\mu\text{m}$  diameter microspheres were coated with poly(styrene sulfonate), poly(allylamine hydrochloride) and the reference dye Alexa Fluor 488 conjugated to poly(allylamine hydrochloride) giving two bilayer polyelectrolyte films. Leaching of the fluorescent dyes was negligible and significant response to glucose in the range 0–20 mM was observed. The polyelectrolyte nanofilms were discussed to perform several functions, namely (a) to provide a diffusion barrier to inhibit leaching of encapsulated material out of the spheres, (b) to provide a transport barrier to slow inward diffusion of substrates, allowing control over the sensitivity, and (c) to introduce a reference dye for allowing ratiometric measurements [65].

### 2.3

#### **Future Trends for Optical Fibres and Sensor Nanoparticles**

David Walt and co-workers have presented an innovative approach to combine sensor nanoparticles with optical fibres. They created randomly ordered addressable high-density optical sensor arrays by combining optical imaging

fibres, selective etching, chemical assays, and optical encoding schemes [66]. First, a high-density array of micrometer wells was produced by etching the distal end of imaging fibres that are composed of thousands of individually cladded optical fibres. Second, nanoparticles were individually encoded and identified using different ratios of dyes that fluoresce at different wavelengths, for example indocarbocyanine DiIC and Texas Red cadaverine. Third, the nanoparticles from e.g. amino-functionalized poly(methylstyrene-co-divinylbenzene) or silicate were chemically functionalized to contain indicator dyes [67] or DNA probes [68]. Finally, the multifunctional nanoparticles were immobilized into the wells of the etched imaging fibre by electrostatic interaction. The presence of hundreds of identical nanosensors in each array afforded the opportunity for sensitivity enhancement through signal summing. Through encoding and using different sensor chemistries, a multitude of analytes could be detected simultaneously. The small dimensions of the optical fibre bundle and the resulting reduced sample volumes made this approach amenable to be integrated into portable instruments. A related approach was based on polymeric sensor microspheres immobilized in micromachined cavities on silicone wafers. A commercial-grade 24-bit video camera was used to detect colour changes of the microsphere array [69].

New relevant materials for the preparation of fluorescent sensor nanoparticles are continuously developed. Accordingly, Yang and co-workers reported hybrid silica particles using sol-gel precursors prepared by the chemical reaction of 3-aminopropyltrimethoxysilane with organic fluorophores (e.g. fluorescein isothiocyanate). The fluorescent particles of a diameter of around 40 nm were further surface functionalized with 3-aminopropyltrimethoxysilane for covalent immobilization to antibodies. However, immobilization of indicator dyes is also conceivable. Furthermore, the authors reported significantly enhanced photostability of the fluorophore inside the particles when they were coated with additional thin silica layers [70]. Ow et al. prepared similar fluorescent particles with a diameter of 20–30 nm and photostability comparable to quantum dots [71]. Mayes et al. reported core-shell nanoparticles which may consist of an inert fluorescent core and an indicator-containing shell that may additionally be made selective by the process of molecular imprinting [72].

It is to be expected that the operationally stable self-referencing optodes and nanosensors reported here will facilitate real-time, in situ, continuous optical detection of analytes relevant for medical research, and will find more applications in process monitoring, food quality control, high-throughput screening, and environmental monitoring. The future success of optodes and nanosensors also relies upon new sensing chemistries and indicator dyes [73, 74]. To design new selective probes and indicators has become a major challenge because the new application-oriented dyes have to absorb and emit in the visible spectral range, must show strong and selective colour

changes upon interaction with the analyte, and need functional groups to covalently link them to polymer materials.

## References

1. Mohr GJ, Demuth C, Spichiger-Keller UE (1998) *Anal Chem* 70:3868
2. Mohr GJ, Spichiger UE, Jona W, Langhals H (2000) *Anal Chem* 72:1084
3. Gryczynski I, Gryczynski Z, Rao G, Lakowicz JR (1999) *Analyst* 124:1041
4. Zhujun Z, Seitz WR (1984) *Anal Chim Acta* 160:47
5. Parker JW, Laksin O, Yu C, Lau ML, Klima S, Fisher R, Scott I, Atwater BW (1993) *Anal Chem* 65:2329
6. Song A, Parus S, Kopelman R (1997) *Anal Chem* 69:863
7. Munkholm C, Walt DR, Milanovich FP, Klainer SM (1986) *Anal Chem* 58:1427
8. Grant SA, Glass RS (1997) *Sens Actuators B* 45:35
9. Kermis HR, Kostov Y, Harms P, Rao G (2002) *Biotech Progr* 18:1047
10. Malins C, Glever HG, Keyes TE, Vos JG, Dressick WJ, MacCraith BD (2000) *Sens Actuators B* 67:89
11. Clarke Y, Xu WY, Demas JN, DeGraff BA (2000) *Anal Chem* 72:3468
12. Kosch U, Klimant I, Werner T, Wolfbeis OS (1998) *Anal Chem* 70:3892
13. Sanchez-Barragan I, Costa-Fernandez JM, Sanz-Medel A, Valledor M, Ferrero FJ, Campo JC (2006) *Anal Chim Acta* 562:197
14. Charlton SC, Fleming RL, Zipp A (1982) *Clin Chem* 28:1857
15. Bakker E, Simon W (1992) *Anal Chem* 64:1805
16. Seiler K, Simon W (1992) *Anal Chim Acta* 266:73
17. Shortreed M, Bakker E, Kopelman R (1996) *Anal Chem* 68:2656
18. Koronczi I, Reichert J, Heinzmann G, Ache HJ (1998) *Sens Actuators B* 51:188
19. He H, Li H, Mohr GJ, Kovacs B, Werner T, Wolfbeis OS (1993) *Anal Chem* 65:123
20. Barker SLR, Thorsrud BA, Kopelman R (1998) *Anal Chem* 70:100
21. Werner T, Klimant I, Huber C, Krause C, Wolfbeis OS (1999) *Mikrochim Acta* 131:25
22. Wolfbeis OS, Klimant I, Werner T, Huber C, Kosch U, Krause C, Neurauter G, Dürkop A (1998) *Sens Actuators B* 51:17
23. Huber C, Klimant I, Krause C, Werner T, Wolfbeis OS (2001) *Anal Chim Acta* 449:81
24. Mohr GJ, Wolfbeis OS (1995) *Anal Chim Acta* 316:239
25. Qin Y, Peper S, Radu A, Ceresa A, Bakker E (2003) *Anal Chem* 75:3038
26. Shortreed M, Kopelman R, Kuhn M, Hoyland B (1996) *Anal Chem* 68:1414
27. Ji J, Rosenzweig Z (1999) *Anal Chim Acta* 397:93
28. Mayr T, Klimant I, Wolfbeis OS, Werner T (2002) *Anal Chim Acta* 462:1
29. Huber C, Klimant I, Krause C, Wolfbeis OS (2001) *Anal Chem* 73:2097
30. O'Keeffe G, MacCraith BD, McEvoy AK, McDonagh CM, McGilp JF (1995) *Sens Actuators B* 29:226
31. Xu W, McDonough RC, Langsdorf B, Demas JN, DeGraff BA (1994) *Anal Chem* 66:4133
32. Papkovsky DB, Olah J, Troyanovsky IV, Sadovalsky NA, Romyantseva VD, Mironov AF, Yaropolov AI, Savitsky AP (1991) *Biosens Bioelectron* 7:199
33. Papkovsky DB, Ponomarev GV, Trettnak W, O'Leary P (1995) *Anal Chem* 67:4112
34. Park EJ, Reid KR, Tang W, Kennedy RT, Kopelman R (2005) *J Mater Chem* 15:2913
35. Liebsch G, Klimant I, Wolfbeis OS (1999) *Adv Mater* 11:1296
36. Navarro-Villoslada F, Orellana G, Moreno-Bondi MC, Vick T, Driver M, Hildebrand G, Lieveith K (2001) *Anal Chem* 73:5150

37. Barker SLR, Kopelman R (1998) *Anal Chem* 70:4902
38. Grant SA, Satcher JH, Bettencourt K (2000) *Sens Actuators B* 69:132
39. Mohr GJ, Draxler S, Trznadel K, Lehmann F, Lippitsch ME (1998) *Anal Chim Acta* 360:119
40. Orellana G, Moreno-Bondi MC, Segovia E, Marazuela MD (1992) *Anal Chem* 64:2210
41. Tabacco MB, Uttamlal M, McAllister M, Walt DR (1999) *Anal Chem* 71:154
42. Von Bültzingslöwen C, McEvoy AK, McDonagh C, MacCraith BD, Klimant I, Krause C, Wolfbeis OS (2002) *Analyst* 127:1478
43. Mohr GJ, Klimant I, Spichiger-Keller UE, Wolfbeis OS (2001) *Anal Chem* 73:1053
44. Papkovsky DB, Ovchinnikov AN, Ogurtsov VI, Ponomarev GV, Kopela T (1998) *Sens Actuators B* 51:137
45. Wolfbeis OS, Oehme I, Papkovskaya N, Klimant I (2000) *Biosens Bioelectron* 15:69
46. Preininger C, Klimant I, Wolfbeis OS (1994) *Anal Chem* 66:1841
47. Mitsubayashi K, Kon T, Hashimoto Y (2003) *Biosens Bioelectron* 19:193
48. Ignatov SG, Ferguson JA, Walt DR (2001) *Biosens Bioelectron* 16:109
49. Xie XF, Suleiman AA, Guilbault GG (1991) *Talanta* 38:1197
50. Gräfe A, Mohr GJ, personal communication
51. Webster A, Compton SJ, Aylott JW (2005) *Analyst* 130:163
52. Clark HA, Kopelman R, Tjalkens R, Philbert MA (1999) *Anal Chem* 71:4837
53. Park EJ, Brasuel M, Behrend C, Philbert MA, Kopelman R (2003) *Anal Chem* 75:3784
54. Sumner JP, Aylott JW, Monson E, Kopelman R (2002) *Analyst* 127:11
55. Sumner JP, Westerberg NM, Stoddard AK, Fierke CA, Kopelman R (2006) *Sens Actuators B* 113:760
56. Sumner JP, Kopelman R (2005) *Analyst* 130:528
57. McNamara KP, Nguyen T, Dumitrascu G, Ji J, Rosenzweig N, Rosenzweig Z (2001) *Anal Chem* 73:3240
58. Brasuel M, Kopelman R, Miller TJ, Tjalkens R, Philbert MA (2001) *Anal Chem* 73:2221
59. Brasuel M, Kopelman R, Kasman I, Miller TJ, Philbert MA (2002) *Proc IEEE Sensors IEEE Int Conf on Sensors* 1:288
60. Brasuel MG, Miller TJ, Kopelman R, Philbert MA (2001) *Analyst* 128:1262
61. Tsagkatakis I, Peper S, Retter R, Bell M, Bakker E (2001) *Anal Chem* 73:6083
62. Xu H, Aylott JW, Kopelman R, Miller TJ, Philbert MA (2001) *Anal Chem* 73:4124
63. Cao Y, Koo YEL, Kopelman R (2004) *Analyst* 129:745
64. Xu H, Aylott JW, Kopelman R (2002) *Analyst* 127:1471
65. Brown JQ, Srivastava R, McShane MJ (2005) *Biosens Bioelectron* 21:212
66. Michael KL, Taylor LC, Schultz SL, Walt DR (1998) *Anal Chem* 70:1242
67. Dickinson TA, Michael KL, Kauer JS, Walt DR (1999) *Anal Chem* 71:2192
68. Song L, Ahn S, Walt DR (2006) *Anal Chem* 78:1023
69. Goodey A, Lavigne JJ, Savoy SM, Rodruigez MD, Curey T, Tsao A, Simmons G, Wright J, Yoo SJ, Sohn Y, Anslyn EV, Shear JB, Neikirk DP, McDevitt JT (2001) *J Am Chem Soc* 123:2559
70. Yang HH, Qu HY, Lin P, Li SH, Ding MT, Xu JG (2003) *Analyst* 128:462
71. Ow H, Larson DR, Srivastava M, Baird BA, Webb WW, Wiesner U (2005) *Nano Lett* 5:113
72. Mayes AG, Whitcombe MJ (2005) *Adv Drug Deliv Rev* 57:1742
73. Wolfbeis OS (2005) *J Mater Chem* 15:2657
74. Mohr GJ (2005) *Sens Actuators B* 107:2

# Intrinsically Referenced Fluorimetric Sensing and Detection Schemes: Methods, Advantages and Applications

Michael Schäferling (✉) · Axel Duerkop

Institute of Analytical Chemistry, Chemo- and Biosensors, University of Regensburg,  
93040 Regensburg, Germany  
*Michael.schaeferling@chemie.uni-regensburg.de*

<b>1</b>	<b>Introduction</b> . . . . .	375
<b>2</b>	<b>Dual Wavelength Probes</b> . . . . .	376
2.1	Sensors Based on pH-Sensitive Probes . . . . .	376
2.2	Metal Ion and Anion Probes . . . . .	380
2.3	Fluorescent Boronic Acid Compounds for Carbohydrate Determination . . . . .	382
<b>3</b>	<b>Dual Luminophore Assays</b> . . . . .	383
3.1	Sensors and Assays Including Inert Reference Dyes . . . . .	383
3.2	Resonance Energy Transfer-Based Sensors . . . . .	387
<b>4</b>	<b>Ratiometric Luminescence Lifetime Determination</b> . . . . .	389
4.1	Time-Domain Determination Methods . . . . .	389
4.2	Frequency-Domain Determination Methods . . . . .	397
<b>5</b>	<b>Fluorescence Polarization and Emission Anisotropy</b> . . . . .	402
5.1	Emission Anisotropy or Polarization: Definitions and Theoretical Background . . . . .	402
5.2	Measurement Principles . . . . .	403
5.3	Effect of Rotational Diffusion on Fluorescence Anisotropy . . . . .	406
<b>6</b>	<b>Conclusion</b> . . . . .	407
	<b>References</b> . . . . .	409

**Abstract** The precision of analytical methods using fluorescent probes or biomolecular labels often is compromised of a variety of conceivable interferences that may originate from the instrumental system, the sample, or the underlying sensor chemistry. Instrumental drifts of the optoelectronic system, photobleaching of luminophores, or high intrinsic color and background fluorescence of the sample cannot be eliminated even by extensive calibration procedures. As a result, intrinsically referenced methods are preferred to improve optical chemo- or biosensor technology, and fluorescent bioimaging. Intrinsic referencing is often accomplished by ratiometric techniques. These include (1) dual wavelength probes, (2) dual luminophore sensors, (3) lifetime-based assays, (4) dual lifetime referencing (in the time and frequency-domain), and (5) fluorescence anisotropy. Applications and advantages of the various approaches are outlined in this review, with a focus on widely used sensing methods for oxygen, pH, carbon dioxide, calcium, glucose, or temperature, and on biomolecular screening. In addition to ratiometric methods,

fluorescence correlation spectroscopy represents another attractive tool to determine analyte concentrations via fluorescent probes. Many of these ratiometric approaches have the potential to pave the way for the development of calibration-free sensor and imaging schemes.

**Keywords** Fluorescence lifetime imaging · Fluorescence polarization · Intrinsic referencing · Phase fluorometry · Resonance energy transfer

### Abbreviations

A	Amplitude
ATP	Adenosine-triphosphate
BCEFC	2',7'-Bis(2-carboxyethyl)-5-carboxyfluorescein
CCD	Charge coupled device
5-CMANBA	5-( <i>tert</i> -Butoxycarbonylmethyl-methylamino)-naphthalene-1-boronic acid
DLR	Dual lifetime referencing
dpp	4,7-Diphenyl-1,10-phenanthroline
5-DMANBA	5-Dimethylaminonaphthalene-boronic acid
EDTA	Ethylene-diamine-tetraacetic acid
ESIPT	Excited states intramolecular proton transfer
<i>f</i>	Frequency
FCS	Fluorescence correlation spectroscopy
FLIM	Fluorescence lifetime imaging microscopy
HPTS	8-Hydroxypyrene-1,3,6-trisulfonic acid
<i>I</i>	Intensity
LOD	Limit of detection
<i>m</i>	Demodulation ratio
OEP	Octaethylporphyrin
<i>P</i>	Polarization
PEBBLE	Probes encapsulated by biological localized embedding
PCR	Polymerase chain reaction
phen	1,10-Phenanthroline
PDR	Phase delay ratioing
PMT	Photomultiplier tube
PSP	Pressure-sensitive paint
<i>r</i>	Emission anisotropy
ref	Reference
resp	Response
RLD	Rapid lifetime determination
SBFI	Sodium-binding benzofuran isophthalate
SPT	Single photon timing
<i>t</i>	Time
TCSPC	Time-correlated single photon counting
TFPL	Tetra(pentafluorophenyl)porpholactone
TFPP	5,10,15,20-Tetrakis(2,3,4,5,6-pentafluorophenyl)porphyrin
TOA	Tetraoctylammonium
TSP	Temperature-sensitive paint
$\lambda_{\text{exc}}, \lambda_{\text{em}}$	Wavelength of excitation/emission maximum
$\Phi$	Phase angle
$\tau$	Luminescence lifetime

## 1

### Introduction

Fluorescent sensing methods have become essential tools in highly diverse applications like medical research and diagnostics, environmental analysis, biomolecular screening, and fluid mechanics. Detection of analytes can be carried out with outstanding sensitivity and a sufficient selectivity thanks to specially designed molecular probes, sensor materials, or biomolecular affinity assays. Instrumental methods and devices for fluorescence analysis include spectroscopy, fluorescence microscopy and imaging, fluorescence lifetime determination, high-throughput screening of microwell plates and microarrays, or fiber-optical sensors.

Generally, fluorophores can be applied in two different forms: on the one hand as labels, indicating biomolecular interactions, on the other hand as probes (sometimes termed as “molecular sensors”). In the second case, the influence of external chemical stimuli, mainly quenching agents, and the microenvironment on the excited fluorophores is detected. Together with a transducer unit, fluorescent probes form the core element of an optical sensor. The fluorescent probes can be dispensed directly into the sample, casted in sensor films and layers, or encapsulated in spherical nano- and microparticles [1–6]. Fluorophores used as labels are either covalently conjugated to biomolecules like DNA or antibodies, or can be coupled to single molecules or supramolecular aggregates by electrostatic or lipophilic interactions, e.g., as stains for electrophoresis gels and blots, cell membranes and other cellular compartments, or applied as DNA intercalators [7–9]. Besides labeling with single dyes, nanometer-scale architectures like luminescent quantum dots or fluorophores incorporated in polymer or silica nanoparticles have become an interesting alternative as biomarkers in the last few years [10–12].

The determination of fluorescence emission for analytical purposes has some significant drawbacks and limitations, particularly in combination with imaging methods where signal distributions have to be recorded in a two-dimensional resolution. First of all, the sensitivity to unsteadiness of the light source intensity and to fluctuations in the light field is an important factor. Inhomogeneities of the dye concentration are a severe problem if it is used as a probe. Furthermore, bleaching of dyes can affect the detected fluorescence intensity, as well as light scatter, irregularities in the optical path (particularly in fiber-optic sensors or instruments containing waveguides), unspecific background signals or autofluorescence of biological samples. If the sensor is casted as a thin film, varieties of the film thickness can lead to differing intensities.

To overcome these difficulties, intrinsically referenced methods are of great interest in fluorescence sensor and imaging technology. Their usefulness does not only occur from the elimination of the above itemized interferences leading to an improved assay “robustness,” but also the avoidance of exten-



sive calibration procedures accompanying each experiment is a worthwhile challenge for the development of internally referenced systems. In case of steady-state intensity sensing, kinetic measurements like enzymatic oxygen consumption or pH changes can be referenced by dividing the actual intensity by the initial value recorded before starting the reaction. However, it is not possible to convert these normalized intensities into actual analyte concentrations without accurate calibration of each single sensor. Thus, calibration-free sensor systems like ready for use microwell plate assays or fiber-optic devices save expenses and labor time, which is beneficial for the end user. Not all of these objectives can be achieved for every type of assay. But several approaches have been established, initially developed in fluorescence microscopy and meanwhile adapted to the different fields of applications. Summarized, they can be characterized best as ratiometric measurements [13]. Ratiometric methods in the simplest form use the addition of reference dyes which behave inertly towards the respective analyte. Instead of applying a second dye, luminescent probes can also be analyzed ratiometrically by dual wavelength measurements. More advanced techniques include luminescence decay determination, phase-modulated fluorometry, fluorescence polarization, fluorescence correlation spectroscopy, and their combinations with dual luminophore measurements. These concepts will be highlighted in the following chapter, focusing on sensing methods based on fluorescent probes.

## 2

### Dual Wavelength Probes

A very straightforward approach to obtain internal referencing is the use of dual wavelength probes. Two basic principles are feasible: detection of fluorescence emission at two different excitation wavelengths or the detection at two different emission wavelengths at a fixed excitation wavelength. Prominent examples are ratiometric pH or ion-sensitive probes. Most instruments for fluorescence analysis, like microscopes, and scanning or imaging devices, are equipped for dual wavelength excitation and contain a set of narrow bandpass filters for separation of emission wavelengths. Furthermore, miniaturized low-cost devices specially designed for ratiometric fluorescence measurements have been developed [14].

### 2.1

#### Sensors Based on pH-Sensitive Probes

Fiber-optic pH sensors have found widespread applications in environmental analysis, biomedical research, medical monitoring and industrial process control [6]. Fluorescent pH-sensitive dyes like pyrene, coumarin, or fluorescein derivatives can be immobilized on the tip of a waveguide by sol-gel tech-

niques [15–17] or by embedding in polymeric hydrogels [18–20]. Disposable microplates (e.g., a 96-well format) with integrated fluorescent pH sensors can be used for screening of enzyme reactions or monitoring the proliferation of cells [21]. Ratiometric measurements take advantage of the different absorption and emission maxima in the protonated and basic form of the pH-sensitive dye. The dual wavelength 2- $\lambda$  method can be illustrated by means of 8-hydroxypyrene-1,3,6-trisulfonic acid (HPTS), a bright fluorophore with a fluorescence quantum yield close to unity and a  $pK_a$  of  $\sim 7.3$  in aqueous buffers. Embedded in a polymer matrix, the dye was used for example in diagenetic studies of marine sediments [22]. The conjugate acid and basic forms of HPTS are shown in Fig. 1 along with the resulting excitation and emission spectra [20]. HPTS exhibits a pH-dependent shift of its absorption band, which enables the calculation of the excitation ratio of 405 and 450 nm by the detection of the corresponding emission at 520 nm. These excitation wavelengths perfectly match the lines of the violet and blue diode laser, respectively.

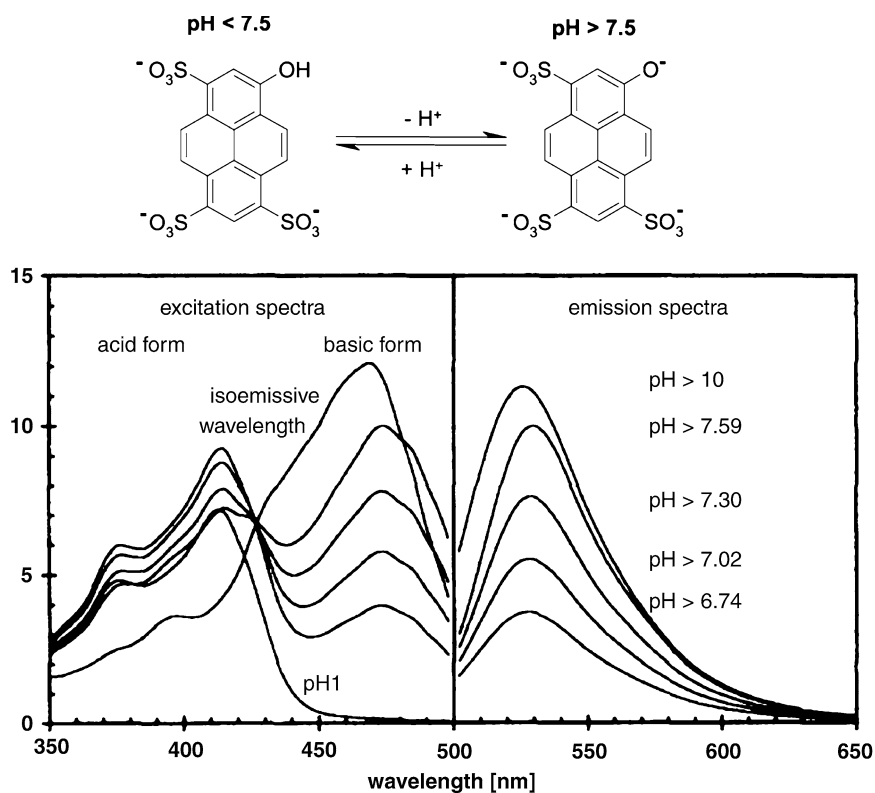


**Fig. 1** Excitation and emission spectra of a HPTS-based sensor membrane. The excitation spectra for pH 6–10 were acquired at an emission wavelength of 520 nm [20]

Other commercially available fluorophores with different absorption of the protonated and deprotonated form are fluorescein derivatives. They have been optimized regarding water solubility, polarity, cell membrane permeability, and exhibit a  $pK_a$  that enables the detection of small pH changes around pH 7. The polar fluorescein derivative BCEFC (2',7'-bis(2-carboxyethyl)-5-carboxyfluorescein) (Fig. 2) is a typical dual excitation ratiometric pH indicator, which is used for intracellular pH measurements [7, 23]. The absorption of the phenolate anion (basic form) undergoes a bathochromic shift with increased absorption coefficient relative to the protonated (acidic) form. The excitation ratio of 450 to 490 nm (or 505 nm, alternatively) is calculated at an emission wavelength typically of 535 nm. Signal errors caused by variations of the probe concentration, path length of light, and photobleaching are significantly reduced applying  $2-\lambda$  ratiometric measurements. The excitation wavelengths are ideally suited for blue and blue-green LEDs. A class of seminaphthorhodamine and seminaphthofluorescein derivatives (SNARF and SNAFL) [7] have both dual emission and dual excitation properties, making them particularly useful for confocal laser-scanning microscopy and imaging, flow cytometry, microwell plate-based assays, and fiber-optic sensors [24–29]. In these cases, also the fluorescence emission shows a significant pH-dependent shift. Thus, the ratio in fluorescence emission at the two differ-

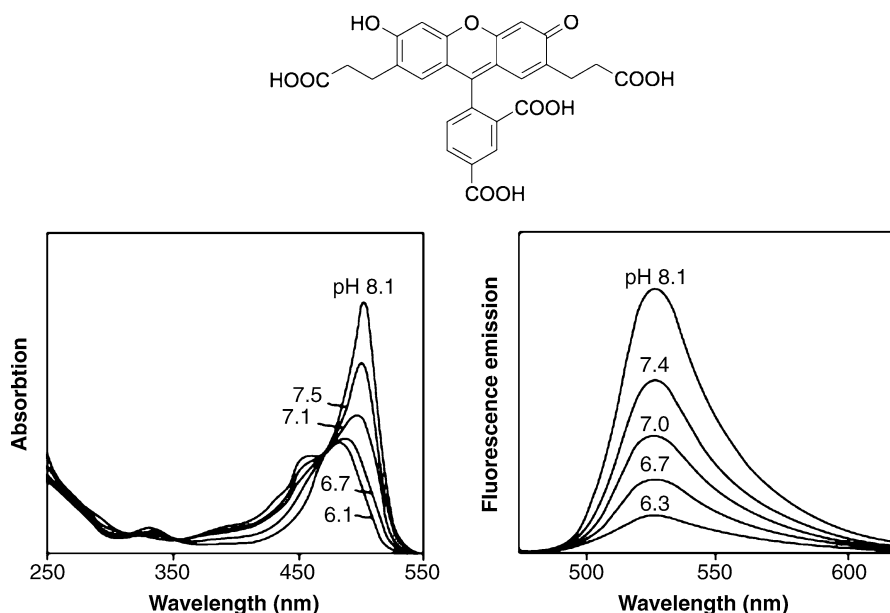


**Fig. 2** Absorption and emission spectra of BCEFC at different pH between 6.1 and 8.1 [7]. The signal ratio for the excitation wavelengths 450 and 490 nm is calculated at a fixed emission wavelength between 510 and 535 nm

ent maxima associated with the protonated and deprotonated structure can be used as internally referenced signal (Fig. 3). The fluorophores can be excited at one wavelength, e.g., by the 488 or 514 nm lines of an argon-ion laser. Systems based on pH-sensitive probes can also be applied for the determination of  $\text{CO}_2$ . Fluorescent pH sensors in a natural environment like marine systems or body fluids show a strong dependence on the ionic strength of the aqueous medium. Cross-sensitivity towards ionic strength can be delimited using carboxy-fluorescein ester derivatives as ratiometric indicators [30]. The dynamic range of a pH sensor is adjusted by the  $\text{pK}_a$  value of the corresponding indicator. The accuracy and the resolution of a pH determination are affected by the sensor design and the complexity of the sample. Fiber-optic dual wavelength pH sensors achieve precisions of 0.01 pH units [29, 30]. Particularly in the case of pH sensors, the response time is a critical issue. Typical  $t_{90}$  values are in the magnitude of 90–120 s.

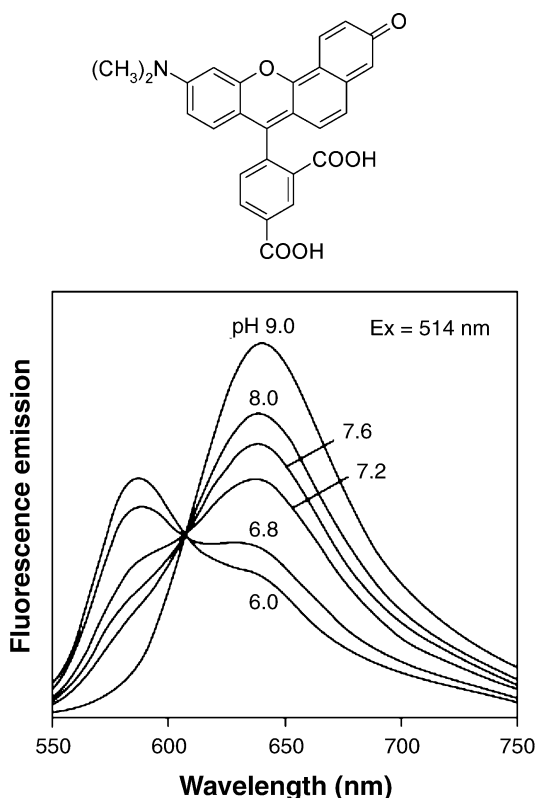


**Fig. 3** The pH-dependent emission spectra of 5-carboxy SNARF-1 at an excitation wavelength of 514 nm [7]. The signal ratio for the two emission maxima at 580 nm (protonated form) and 640 nm (anionic form) can be calculated at excitation wavelengths between 480 and 550 nm

## 2.2

### Metal Ion and Anion Probes

Fluorescent indicators for metal ions like  $\text{Ca}^{2+}$ ,  $\text{Mg}^{2+}$ ,  $\text{Zn}^{2+}$ ,  $\text{Na}^+$  or  $\text{K}^+$  have found widespread application in clinical chemistry and biomedical imaging. Imaging of the intracellular  $\text{Ca}^{2+}$  concentration and its distribution is an important tool in medical and pharmaceutical research. For example, the increase in cytosolic  $\text{Ca}^{2+}$  is a marker for the activation of pharmaceutically relevant cell membrane-bound receptors and enzymes. Fluorescent probes conjugated to dextrans for improved cellular retention, and lipophilic dyes for studying near-membrane  $\text{Ca}^{2+}$  concentrations are commercially available. The choice of proper cell loading and intracellular calibration methods are major tasks. The dissociation constant of the indicator must be compatible with the  $\text{Ca}^{2+}$  concentration range of interest. Ion indicators exhibiting spectral shifts upon ion binding are suitable for ratiometric dual wavelength methods. These tend to be independent of non-uniform dye loading, dye leakage, different cell thickness or photobleaching effects. Among the numerous fluorescent calcium indicators, the class of fura dyes (e.g., fura-2 [31]) with varying dissociation constants to  $\text{Ca}^{2+}$  are prominent examples. These show a significant hypsochromic shift of their absorbance after binding to  $\text{Ca}^{2+}$  ions (Fig. 4, fura-2). The emission is monitored typically at 510 nm at dual excitation wavelengths of 340 and 380 nm, respectively [32, 33]. As an alternative derivatives of indo-1 [34] can be used, a  $\text{Ca}^{2+}$ -sensitive dye with dual emission properties ( $\lambda_{\text{em}} = 400/470$  nm with/without  $\text{Ca}^{2+}$ , respectively). Covalently attached to polystyrene microspheres it can be used for intracellular pH imaging [35].

As this class of dyes can only be excited with UV light, several calcium-sensitive probes have been developed that are excitable with visible light, e.g., calcium green-1 and 2 [7, 36], the Oregon green BAPTA dyes [7, 37], or fluorescein and rhodamine derivatives [38]. However, these probes show only a change in fluorescence quantum yield on ion binding and therefore have no capability for dual wavelength measurements. If determinations using indicators like calcium green have to be referenced, other ratiometric methods like addition of inert reference dyes [39] (see Sect. 3.1) or fluorescence lifetime imaging [40] have to be applied (see Sect. 4.1). The same applies for virtually all other fluorescent metal ion indicators, particularly for  $\text{Mg}^{2+}$  (magnesium green) [41],  $\text{Zn}^{2+}$  (FluoZin-3),  $\text{Cu}^{2+}$  (Phen Green FL), or  $\text{K}^+$  (PBF1) [42], which, in addition, have the problem of high cross-sensitivity. Most common heavy metal or anion-sensitive probes and assays are not applicable for dual wavelength referencing, as they are usually based on dynamic (collisional) quenching. Only the sodium-sensitive dye SBFI [43], a benzofuranyl fluorophore linked to crown ether for selective sodium complexation, provides dual excitation properties (340/380 nm, at an emission wavelength of 505 nm). Ratiometric probes for  $\text{Zn}^{2+}$  have been designed that are based on cation-induced inhibition of excited states intramolecular proton transfer

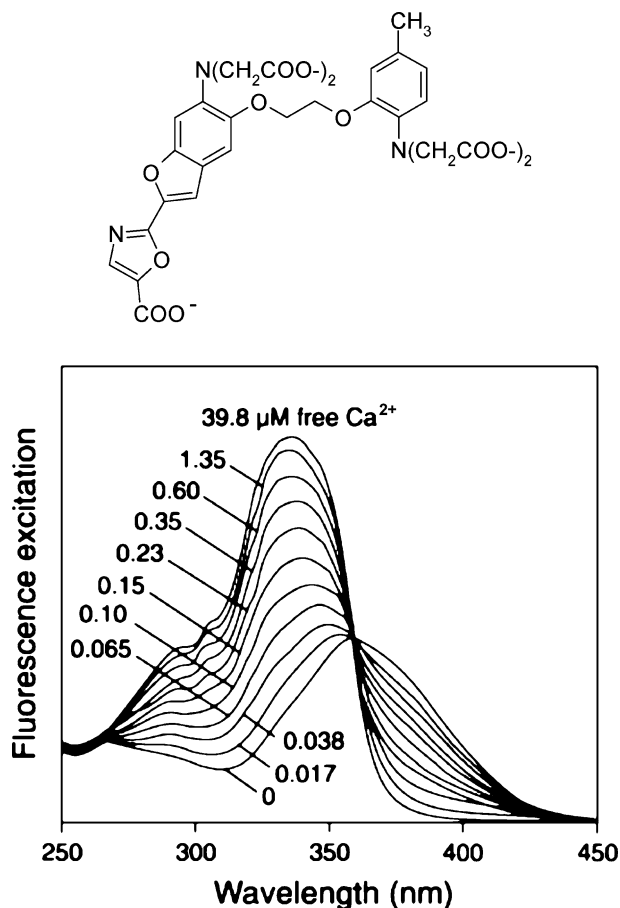


**Fig. 4** Fluorescence excitation spectra of fura-2 at varying Ca<sup>2+</sup> concentrations from 0–39.8 μmol L<sup>-1</sup> (emission wavelength = 510 nm) [7]

(ESIPT) using imidazole derivatives. Coordination of zinc inhibits the highly Stokes-shifted ESIPT process and yields a hypsochromic shift of the emission maximum [44]. Proton transfer processes in fluorescent imidazole derivatives can be inhibited by deprotonation induced by fluoride anions, a property that can be used for the development of ratiometric dual wavelength fluoride chemosensors [45]. A fluorescent sensor for ammonium ions is based on the dye merocyanine 540, which operates as a dual excitation/dual emission ratiometric probe with high selectivity towards NH<sub>4</sub><sup>+</sup> [46]. A ratiometric probe for pyrophosphate anions is composed of a 2',7'-dichlorofluorescein derivative that forms a complex with two Zn<sup>2+</sup> ions. The complex acts as receptor for pyrophosphate anions, accompanied by a bathochromic shift of its excitation maximum from 504 to 517 nm and its emission maximum from 523

to 534 nm upon ligation of the anion [47]. Selectivity towards  $\text{H}_2\text{PO}_4^-$  was reported, but interferences by other biologically relevant phosphoric esters (e.g., ATP or ADP) are not addressed in this study.

### 2.3

#### Fluorescent Boronic Acid Compounds for Carbohydrate Determination

Boronic acids are capable of recognizing saccharides with sufficient selectivity [48] and can be conjugated to fluorophores like quinolinium [49] or anthracene units [50–52]. The activity of the boronic acid moiety is based on the formation of stable complexes between boronic acids and compounds that bear two adjacent nucleophiles such as diols and carbohydrates. Consequently, artificial fluorescent receptors have been developed that are water-soluble, photochemically stable and change their fluorescence properties upon binding to mono- and oligosaccharides. Naphthalene derivatives were found to be useful for carbohydrate sensing. Among these, dyes like 5-(*tert*-butoxycarbonylmethyl-methylamino)-naphthalene-1-boronic acid (5-CMANBA) or 5-dimethylaminonaphthaleneboronic acid (5-DMANBA) (Fig. 5) can be applied as ratiometric probes at physiological pH with a high association constant to fructose, which is typical for monoboronic acids. Fluorescence emission is detected at 433 and 513 nm, respectively [53, 54]. Generally, diboronic acids are known to be more specific and more responsive to glucose than their monoboronic analogues. The drawback of these compounds is their short-wavelength excitation maximum around 320 nm. Spectral shifts upon saccharide binding can alternatively be obtained with 6-aminoquinolinium derived boronic acids [55]. Ratiometric response can either be calculated from their 340/388 nm excitation bands or 540/546 nm emission bands. These probes are also sensitive towards cyanide anions [56]. Other UV-excitable ratiometric indicators are based on diphenylpolyenes [57]. Artificial boronic acid receptors based on ruthenium metal-ligand complexes can be excited with visible light and provide a long luminescence lifetime. Thus, they can be easily referenced by lifetime determination methods (see Sect. 4) [58]. Boronic acid-based molecular sensors for glucose monitoring have been reviewed by Wang et al. [59], including ratiometric probes and internal charge transfer compounds (ICT).

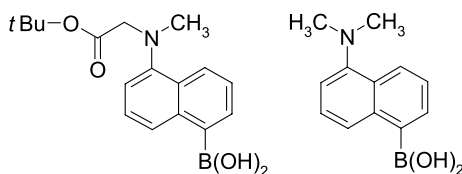


**Fig. 5** Water-soluble fluorescent naphthalene boronic acid derivatives for saccharide sensing

### 3 Dual Luminophore Assays

While the last section highlighted radiometric dual wavelength fluorescent probes which respond towards analytes like metal ions, pH or carbohydrate, this part will point out referenced sensor systems. These make use of an internal fluorescence standard that is not interfered by the analyte. Many different approaches have been presented so far, and some of them found their way into commercial utilization. One type of dual luminophore sensors can be read out at different excitation and emission wavelengths. If the absorption of one luminophore coincides with the emission band of the second, resonance energy transfer (RET) assays can be configured. They found widespread application in bioanalysis because of their unsurpassed high sensitivity. These methods require costly instruments with diverse light sources or an assortment of appropriate excitation filters. In more simplified systems, both indicator and inert reference fluorophores can be excited at the same wavelength, but show sufficiently separated emission spectra. In this case, the signals can easily be separated by a change of the emission filters. Examples for all different kinds of these analytical approaches will be elucidated in the following section. Related methods based on the determination of different luminescence lifetimes of probe and reference dye will be outlined in Sect. 4. Dual labeling techniques for the screening of biomolecular interactions, e.g., differential gene expression profiling with help of DNA microarrays, are beyond the scope of this review.

#### 3.1 Sensors and Assays Including Inert Reference Dyes

The application of inert, non-responding fluorophores is a general referencing method in fluorescence detection and mainly utilized associated with solid-phase sensor materials. These include thin polymer films, layers for the coating of microwell plates, fiber-optic devices, and sensitive paints like PSPs (pressure-sensitive paints). Variable probe/reference combinations enable the determination of such diverse analytes like  $pO_2$ , pH,  $pCO_2$ , metal ions, anions, glucose or physical parameters like atmospheric pressure and temperature. Severe interferences like instrumental drifts, light scatter within the sensor film, and inhomogeneous dye loading can be compensated by means of a reference dye and ratiometric detection. Other effects like dye leaching and photobleaching, background fluorescence and intrinsic color of the sample cannot be corrected. Nevertheless, signal referencing with a second inert dye is one of the frequently applied methods in the field of fluorescent sensors.

The determination of oxygen partial pressure ( $pO_2$ ) is an important tool in pharmaceutical screening, medical chemistry, and environmental analysis.



Typical oxygen-sensitive probes like pyrene derivatives, transition metal complexes of  $\text{Ru}^{2+}$ ,  $\text{Os}^{2+}$ ,  $\text{Ir}^3$ , or platinum and palladium porphyrins, and their specific properties and application formats have been reviewed in several articles [2, 60, 61]. Changes in oxygen partial pressure in extracellular fluids can monitor status and dysfunctions of the cell metabolism, e.g., after exposure to toxins and drugs. The control of oxygen supply in hypoxic tumorous tissue plays an important role in the development of radio and chemotherapeutic treatments of tumors [62]. The significance of blood gas analysis including  $p\text{O}_2$ ,  $p\text{CO}_2$  and pH in clinical diagnostics is generally accepted.

Furthermore, oxygen sensors arouse an increasing interest in applications aligned with microwell plate-based screening techniques. Sensor layers containing the oxygen-sensitive probe and a reference dye can be immobilized on the bottom of each well in a microplate and used for the screening of enzyme inhibitors or activators, monitoring of cell growth, screening of proliferation of cells and respiratory assays [63]. Oxygen sensor plates have been commercialized [64, 65], the performance of OxoPlates is shown in Fig. 6. Both fluorophores can be excited at a wavelength of 540 nm and the emission can be analyzed at wavelengths of 650 nm (indicator) and 590 nm (reference). The precision of such oxygen assays is at least 1% (referred to air saturation).

Plates can be coated similarly with pH-sensitive layers (HydroPlate [64]), containing a fluorescent pH indicator and a reference dye. These are used for screening of enzymes inducing pH changes and monitoring of cell prolifera-

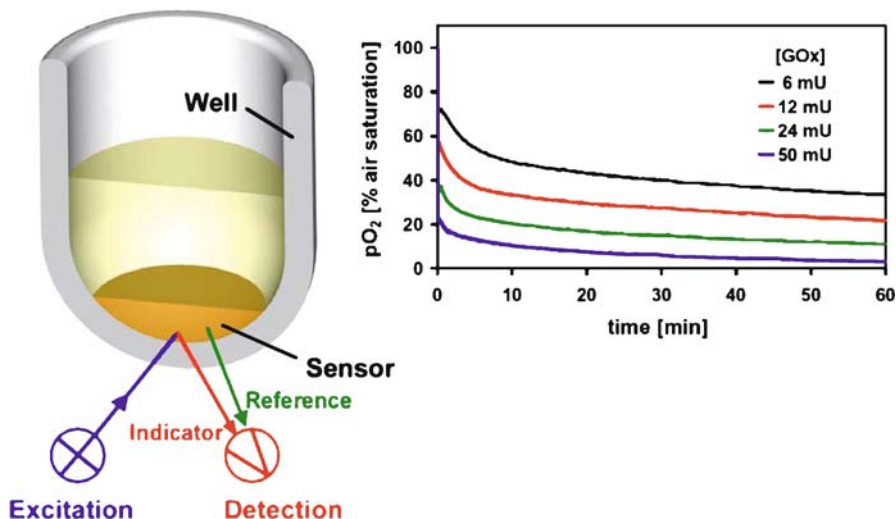


**Fig. 6** (Left) Well of a microplate which is coated by a fluorescent layer at the bottom, including an oxygen-sensitive probe (red) and a reference dye (green). (Right) The microwell plates can be applied for screening of enzyme activities by kinetic monitoring of the oxygen consumption, e.g., of glucose oxidase [64]

tion, as respiratory activity releases CO<sub>2</sub> which is accompanied by a decrease in pH. Such plates are advertised as “calibration-free” sensor arrays. Because of internal referencing absolute pH or pO<sub>2</sub> quantifications require a two-point calibration only on several spots for a whole batch of microplates. However, a two-point calibration is necessary because differing light source intensities, instrumental settings, and drifts of the optoelectronic system of the plate reader affect the overall intensity of the signal. Moreover, the accuracy and reliability of the measurement is significantly improved by applying a reference fluorophore. Accuracies of 0.05 pH units can be obtained, pH values can be determined typically with a resolution of 0.01. Cell respiration assays and cytotoxic screening with oxygen (or pH) sensor plates is not only a beneficial tool in pharmaceutical research and drug development [66, 67], but has also attracted attention in the field of environmental analysis. For this purpose the inhibition of cell respiration by toxins in waste water (e.g., with the standardized *Pseudomonas putida* assay) or the proliferation of bacteria like *Escherichia coli* can be monitored [68, 69].

Nanosensors for determination and imaging of oxygen or pH inside cells are known as PEBBLE (probes encapsulated by biological localized embedding) [70]. These ratiometric fluorescent oxygen sensors consist of poly(decyl methacrylate) nanobeads of 150–250 nm diameter encapsulating platinum octaethylporphyrin ketone as oxygen-sensitive probe and octaethylporphyrin as reference dye [71]. Organically modified silicate (ormosil) is another well-suited material for the preparation of oxygen nanosensors by means of a sol-gel process [72]. Ormosil PEBBLE nanopores were also developed for monitoring singlet oxygen using 9,10-dimethyl-anthracene as indicator dye and octaethylporphyrin as reference [73]. The red fluorescent protein (DsRed) was encapsulated in polyacrylamide in combination with Alexa Fluor 488 as reference dye to form nanobiosensors for copper ions [74].

Ormosil [75, 76] or polymer matrices like PVC [77] are preferred materials for the functionalization of fiber-optic microsensors (optodes). Usually the tips of optical waveguides are coated with such analyte-permeable sensitive layers containing the fluorescent probe. Oxygen and pH-sensitive needle-type microsensors that are integrated in syringes, and also implantable optical sensors, are commercially available [21]. Referenced fiber-optical oxygen trace sensors are available with a limit of detection (LOD) of 1 ppb of oxygen and a dynamic range from 0 to 40 hPa. Fiber-optic sensors can be referenced either by means of two-wavelength measurements using an inert non-sensitive dye [77], dual emission pH-sensitive dyes [78] or phase-modulated detection (see Sect. 4.2). Fiber-optic chemical sensors and biosensors have been reviewed recently [79].

Other sensor materials which were improved by incorporation of reference dyes are pressure-sensitive paints (PSPs) used in fluid mechanics and aerodynamic tests. The functionality of pressure-sensitive dyes is based on the principle of fluorescence quenching by oxygen. The probe and reference

molecules are incorporated into polymer solutions. These kinds of paints can be sprayed on different surfaces with high homogeneity by using air guns.

The real-time imaging of dynamic flow processes on models in wind tunnel tests are of high significance for aerospace and car industry. The addition of a reference dye improves the accuracy by compensating interferences caused by light scatter, irregular illumination and deformations of the model. Commonly used PSP dyes are pyrene, and platinum or palladium porphyrine derivatives [80–83]. The added reference dyes should be insensitive towards oxygen and temperature quenching. A typical binary PSP formulation consists of pyrene as indicator and a europium complex as reference. Both can be excited at a wavelength of 337 nm, the emission wavelengths ( $\lambda_{\max} = 470$  and 650 nm, respectively) can be easily separated by changing the emission filters or using a set-up with two different cameras equipped with appropriate filters [84]. Another approach uses platinum tetra(pentafluorophenyl)porpholactone as pressure-sensitive fluorophore and magnesium tetra(pentafluorophenyl)porphyrine as reference. Both can be simultaneously excited at 400 nm (e.g., by violet LEDs) [85]. Dual pressure and temperature-sensitive paints (PSP/TSP) make use of a temperature-sensitive dye instead of the reference dye. In this case, the measurement is performed better by means of fluorescence lifetime imaging (see Sect. 4.1).

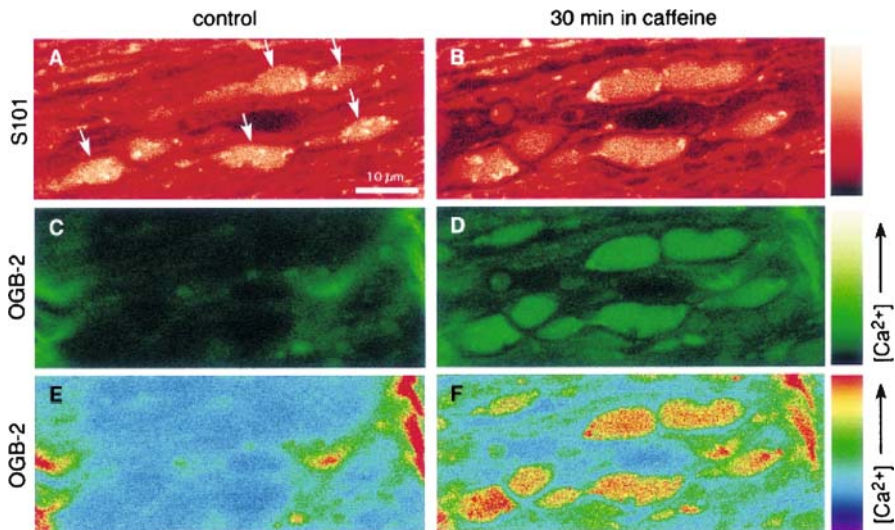


**Fig. 7** Caffeine-induced axonal  $\text{Ca}^{2+}$  imaging in live optic nerves. Single optical sections showing baseline red (A) and green fluorescence (C). The green channel is weak because the fibers are healthy with a low resting  $[\text{Ca}^{2+}]$ . After addition of caffeine to release internal  $\text{Ca}^{2+}$  stores, the red channel appears unchanged (B) but green fluorescence becomes more than doubled (D). The  $\text{Ca}^{2+}$ -sensitive channel is shown in pseudocolor to emphasize the  $\text{Ca}^{2+}$  rise in (E) and (F) [87]

The two-dye approach is also useful for the imaging of intracellular calcium concentrations. Cell cultures were coloaded with calcium green as indicator and brilliant-sulflavine as reference. Referenced fluorescence images displaying the intracellular calcium distribution can be obtained by ratiometric detection of the signals derived at excitation wavelengths of 420 and 488 nm [86]. In a different approach, the  $\text{Ca}^{2+}$ -sensitive indicator Oregon green 488 BAPTA-2 was administered to neuronal cells in combination with sulforhodamine 101 as reference to visualize axonal profiles of calcium activity (Fig. 7) [87].

## 3.2

### Resonance Energy Transfer-Based Sensors

The non-radiative transfer of excitation energy requires a spectral overlap between a donor and an acceptor molecule and has found widespread application for the detection of biomolecular interactions like DNA hybridization, protein–protein interactions or antigen–antibody binding. Energy transfer occurs if the emission spectrum of the donor partially coincides with the absorption spectrum of the acceptor. Such transitions are in resonance, so the term fluorescence resonance energy transfer (FRET) is often used in literature, but actually not the fluorescence is transferred but the electronic energy of the donor. Many luminescent donor/acceptor pairs are well-established [88]. Biomolecular recognition brings the donor/acceptor couple in close spatial proximity, and the resulting energy transfer can be detected via the quenching of the fluorescence of the donor or the specific emission of the acceptor dye if the donor is excited. This Förster type of resonance energy transfer takes place over a distance of around 1–10 nm between donor and acceptor and results from long-range dipole–dipole interactions. FRET technologies (Fig. 8) have found numerous applications and are essential in cellular imaging and diagnosis [89], monitoring of enzymatic activities [90, 91], DNA analysis [92, 93] and quantification by real-time PCR [94], pharmaceutical screening [2, 95–97], immunoassays [98] and analysis of conformational changes in biopolymers [99, 100]. Changes in the spectral overlap will alter the FRET efficiency and therefore the fluorescence emission and fluorescence lifetime of both the donor and the acceptor. Ratiometric detection is best performed by measuring the fluorescence emission of donor and acceptor while only the donor is excited.

Because of its very high sensitivity, FRET-based fluorophore systems can be used not only as labels in biomolecular screening but can also be integrated into chemical sensors. The sensitive dye is usually applied as FRET acceptor. Applying dual wavelength probes, only the absorption of one species (e.g., the free and metal-complexed form of a chelating ligand) should coincide with the donor emission. However, approaches using FRET as basis for chemosensors have received only limited attention. Energy transfer sys-

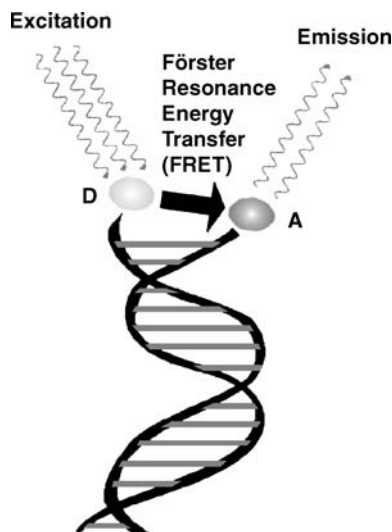


**Fig. 8** Illustration of resonance energy transfer. Specific interactions of biomolecules (e.g., hybridization of DNA) implicate a close proximity (<10 nm is required for an effective Förster transfer) of a fluorescent donor (*D*) and an acceptor (*A*), which acts as the second emitter in ratiometric measurements

tems can feature an unusually high efficiency of fluorescence quenching by oxygen. This effect was first observed by means of pyrene and perylene as donor/acceptor system casted in silicon rubber as oxygen-sensitive layer. Stern–Volmer quenching constants increased fourfold compared to a sensor with pyrene alone [101]. A fluorescent probe for transition metal cations has been reported that is composed of a naphthalene-EDTA conjugate as donor and metal ion chelator ( $\lambda_{\text{exc}} = 440 \text{ nm}$ ,  $\lambda_{\text{em}} = 555 \text{ nm}$ ) and a benzofurazan fluorophore as acceptor [102]. The emission spectrum of the chelator changes after addition of different metal ions. A disposable sensor for copper ions was developed by coating a polyester support with a PVC membrane containing a porphyrazine as donor and the copper reagent Zincon as non-fluorescent acceptor [103]. It can be assumed, that interferences which are not compensated by a single-dye dual wavelength measurement can also not be reduced by additional resonance energy transfer mechanisms. It has to be considered that dye bleaching and leaking can affect both donor and acceptor if FRET-based sensors are used. Furthermore, new challenges arise, like the preparation of uniform films where the donor and acceptor dyes are evenly dispersed in nanometer-size proximity. A higher capability for implementation in ratiometric sensors emanates from the combination of long-lived fluorescent donors like ruthenium complexes with an ion or pH-sensitive acceptor. With these systems, responses of the donor fluorescence lifetime can be determined, taking advantage of signal referencing by time-resolved meas-

urements or phase-modulation fluorometry. Both methods will be illustrated in the next section.

## 4

### Ratiometric Luminescence Lifetime Determination

The self-referenced methods outlined so far are all based on the determination of fluorescence intensity and require a dual wavelength measurement. The decay time of the excited state of a fluorophore is probably the most attractive parameter in being self-referenced. The decay of fluorescence intensity after a short pulse of light is, in the first approximation, monoexponential, given by:

$$I = I_0 \exp^{-t/\tau}, \quad (1)$$

with  $I_0$  as the intensity at  $t = 0$ , and  $\tau$  the fluorescence lifetime. This is the time that is required until the fraction of molecules in the excited state has decreased to  $1/e$ . Unlike intensity, fluorescence lifetime is, to a certain extent, not affected by the concentration of the fluorophores, static quenching effects and the brightness of the light source. In contrast, dynamic (“collisional”) quenching, FRET and temperature have a strong impact on the fluorescence decay. That makes the fluorescence lifetime  $\tau$  a preferred parameter in fluorescence sensing and imaging. Methods for lifetime determination can be classified into time-domain and frequency-domain approaches.

#### 4.1

##### Time-Domain Determination Methods

The most precise instrumental set-up for the determination of luminescence lifetimes is based on the time-correlated single photon counting (TCSPC) method, alternatively called single-photon timing (SPT) [104]. By timing and recording the single photons hitting the detector, a large number of short excitation pulses can be integrated. On the basis of this set of data the fluorescence decay curve is assembled. A typical example has been described by Draxler and Lippitsch by means of a pH sensor [18]. This method requires complex instrumentation and synchronization of the modules like mode-locked lasers, avalanche photodiodes as detectors and a time-to-amplitude converter, and generates extensive data. More straight-forward ratiometric lifetime determinations using gated detection have been widely accepted in sensing or imaging applications. In particular fluorescence lifetime imaging microscopy (FLIM) is an important method in life sciences [105, 106]. The first optical set-ups for FLIM were introduced by Wang et al., both in the time [107] and frequency-domain [108]. The output of ratiometric lifetime

detection in the time-domain is the calculated ratio of the intensities recorded in two successive time gates after a short pulse of light.

In principle, there are two different ways of performing ratiometric detection. If the first gated intensity is measured during the excitation period (light source on), and the second gate is acquired in the emission period (light source off), the acquisition process can be referred to as phase delay ratioing (PDR) [109]. The second approach is known as the rapid lifetime determination (RLD) method [110, 111]. Here, the two gates are placed in the decay period (Fig. 9). Both techniques can also be applied for imaging purposes by means of gated CCD cameras [112]. In case of monoexponential decay and an identical length of the time gates  $\Delta t$ , the lifetime  $\tau$  can be calculated from four experimental parameters according to the RLD method:

$$\tau = \frac{t_2 - t_1}{\ln(I_1/I_2)}, \quad (2)$$

where  $t_1$  and  $t_2$  are the times when the respective gates  $I_1$  and  $I_2$  are opened.

In practice, the images of the two different gates are taken separately in subsequent acquisition cycles. The integration of the two sets of pictures is followed by a subtraction of the corresponding background dark pictures (de-

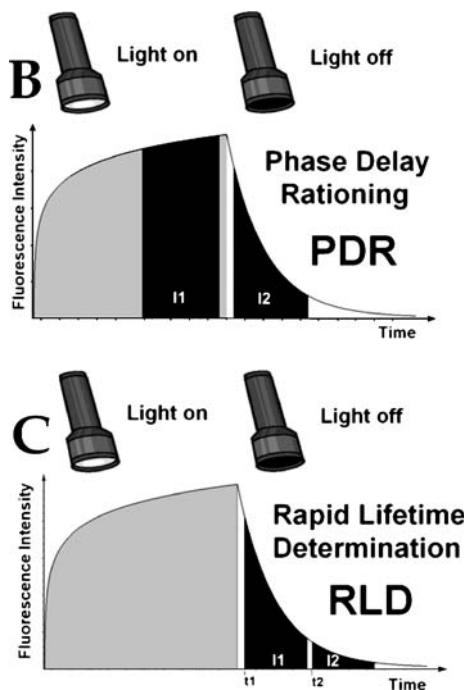


**Fig. 9** Phase delay ratioing (PDR) and rapid lifetime determination (RLD) method. The latter can be used for ratiometric calculations of luminescence lifetimes  $\tau$

tected with the same time gates and frequency but without illumination). Figure 10 illustrates the whole acquisition process for the RLD method where four sets of images are obtained: images 1 ( $I_1$ ), images 2 ( $I_2$ ), dark images 1 ( $D_1$ ) and dark images 2 ( $D_2$ ). The resulting ratio  $R$  is calculated according to

$$R = \frac{\sum I_1 - \sum D_1}{\sum I_2 - \sum D_2} \tag{3}$$

By executing these processes, thousands of single screens can be integrated and averaged within a split second. This affords a high sensitivity and reduces interferences by imprecisions in the exact lengths of single pulses. In combination with long-lived fluorescent probes, RLD offers a multitude of advantages compared to intensity measurements: (1) elimination of fast-decaying background fluorescence, (2) fluorescence lifetime serves as very sensitive analytical parameter and provides additional contrast enhancement in imaging, (3) independency of intensity fluctuations of the light source

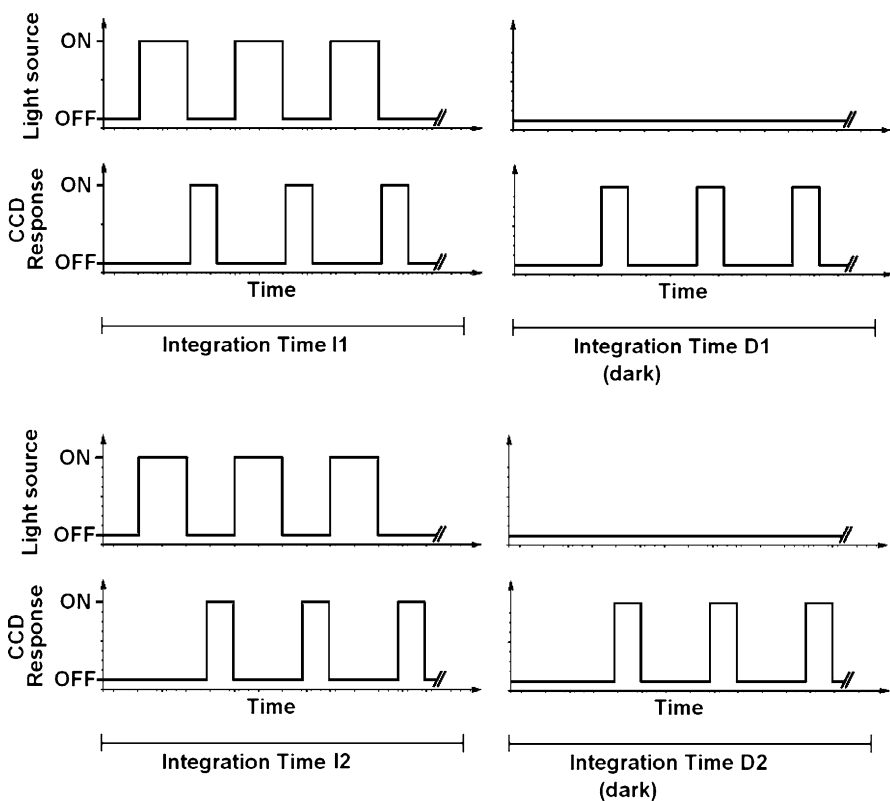


**Fig. 10** Total data acquisition process for ratiometric fluorescence lifetime imaging according to the RLD method



or inhomogeneities in the light field, (4) lower sensitivity towards the local fluorophore concentration and photobleaching, and (5) elimination of light scatter effects. In contrast to self-referenced dual wavelength methods, lifetime determination can be accomplished by applying only one excitation and one emission wavelength.

Sensing and imaging of oxygen partial pressure, barometric pressure and temperature (in aerodynamic PSP/TSPs) are just a few examples for the versatile applications of FLIM using fluorescent probes. Novel probes have been developed for the sensing of glucose, hydrogen peroxide, citrate or phosphates. Most of them can be dispersed in sensor films, layers or nanoparticles. Some typical examples are summarized in Table 1. It is difficult to compare the specifications of different referenced sensor systems for the same analyte, as a great variety of analytical problems in diverse samples is approached. Oxygen sensors with a preferably broad dynamic range ( $pO_2 = 0\text{--}400$  hPa) exhibit accuracies of typically 2 to 5.3 hPa at 210 hPa [112, 113]. As Stern-Volmer plots are not strictly linear, analytical figures of merit like accuracy and precision are also a function of  $pO_2$ . Deviating dynamic ranges and accuracies apply to trace oxygen sensors (see Sect. 3.1). In the case of  $pO_2$  or pH measurements in tissue (or intracellular) internal referencing is essential, as intensity measurements reflect only the accumulation of dyes in different environments. In terms of accuracy ( $pO_2$ ) and resolution (pH), no significant differences between the respective referenced methods can be gathered from the literature.

It should be noted that sensor films for oxygen, pH or hydrogen peroxide detection can be applied for glucose sensing. This can be achieved by monitoring the enzymatic production of hydrogen peroxide, consumption of oxygen or the associated change of pH by glucose oxidase in presence of glucose [124, 125]. The hydrogen peroxide-sensitive probe Eu-tetracycline paves the way for enzyme activity assays by fluorescence lifetime determination. This includes enzymatic assays for glucose oxidase [126], catalase [127] or peroxidase [128]. The latter can be used as fluorescent indicator for enzyme-linked immunosorbent assays (ELISA). Heavy metal ions can be detected by the dynamic quenching of lanthanide complexes [129–131].

For many analytes like pH or ions only fluorescent probes with nanosecond lifetimes exist. These depend on CCD cameras with image intensifier and pumped (mode-locked) lasers, which makes the equipment very expensive. A combination of lifetime detection and dual luminophore referencing overcomes this problem. The method called time-domain dual lifetime referencing ( $tDLR$ ) was first described for a pH-sensitive layer for 2D imaging. The sensor layer was composed of pH-sensitive microbeads consisting of a poly(acrylonitrile) core that contains the inert luminophore  $Ru(dpp)_3$  and a hydrogel shell with the covalently bound indicator carboxy-fluorescein dispersed in a polyurethane matrix. The hydrogel cocktail was spread on a polyester support and dried. In this case the long-lived ruthenium complex

**Table 1** Applications of fluorescent ratiometric lifetime determination and imaging

Analyte/parameter	Fluorescent probe	Sensor specification	Refs.
$pO_2$ in air	Ru-phenanthroline complex	Probe adsorbed to silica gel particles in silicone matrix	[113]
Transcutaneous $pO_2$	Pt-OEP	Polystyrene matrix on polyester	[114]
$pO_2$ in engineered tissue	Pt-OEP	Silicone hydrogel with $TiO_2$	[115]
Intracellular $pO_2$	Ru-bipyridyl complex	Dye applied in cultured human epithelial cells	[116]
Extracellular pH in epidermis	BCEFC	Indicator applied on skin	[117]
Intracellular pH	Carboxy SNAFL-1	Indicator applied in cells	[118]
pH gradients in microbial biofilms	Carboxyfluorescein	Film stained with soluble indicator	[119]
Glucose	Ru-bipyridyl conjugate with boronic acid	Water-soluble molecular sensor	[58]
$H_2O_2$ in aqueous solution	Eu-tetracycline complex (3 : 1)	Dye in poly (acrylamide-co-acrylonitrile) matrix	[120]
Citrate in aqueous solution	Eu-tetracycline complex (1 : 1)	Microwell plate-based assay	[121]
Phosphate in aqueous solution	Eu-tetracycline complex (1 : 1)	Microwell plate-based assay	[122]
Temperature	Ru-phenanthroline complex	Poly(acrylonitrile) matrix	[112]
Pressure/temperature	Pt-TFPL/EuD2	Dual PSP/TSP	[123]

serves as reference dye and the short-lived fluorescein as pH indicator. The data acquisition process of  $t$ DLR is illustrated in Fig. 11 [132]. With a standard deviation between 1 and 2% in a pH range from 5 to 8.5 the sensor shows a comparable performance to the referenced methods described above (dual wavelength, lifetime). The  $t$ DLR concept has its merits in terms of the reduction of experimental expenses for ratiometric lifetime determination at a constant level of accuracy.

Similar to the PDR method,  $t$ DLR imaging is based on the acquisition of two images, one taken in the excitation period when the light source is on,

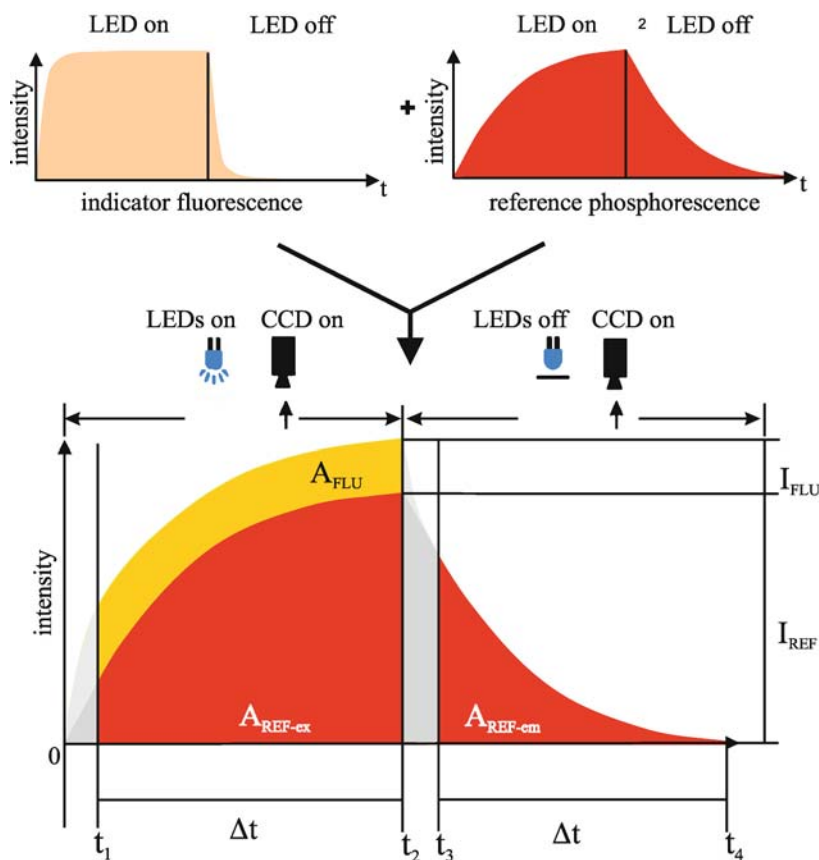


**Fig. 11** Schematic representation of the time-domain DLR ( $t$ DLR) scheme. The short-lived indicator fluorescence and the long-lived phosphorescence of the inert reference beads are simultaneously excited and measured in two time gates. The first ( $A_{ex}$ ) is set in the excitation period where the light source is on and the signal obtained is composed of short-lived fluorescence and long-lived luminescence. The second gate ( $A_{em}$ ) is opened in the emission period where the intensity is exclusively composed of the reference luminescence [132]

and one in the decay period when the light source is off. The luminescence in the decay period is measured after a certain time delay in order to eliminate short-lived interferences. The resulting image  $A_{ex}$  represents the sum of short-lived indicator and long-lived reference luminescence, while image  $A_{em}$  originates exclusively from the long-lived reference dye (Fig. 11). By dividing both images  $A_{ex}$  and  $A_{em}$ , virtually all significant interferences can be referenced.

With the dual lifetime referencing method also metal ion sensors and sensor arrays are accessible for ratiometric lifetime imaging [133]. Generally, for the application of the  $tDLR$  scheme in optical sensors, the following conditions have to be fulfilled:

1. The inert reference luminophore and indicator fluorophore need highly differing decay times (separated by a factor of  $> 100$ ).
2. The decay time and the quantum yield of the reference dye is not affected by the sample.
3. The indicator changes its fluorescence intensity as a function of the analyte concentration.
4. The excitation spectra of reference and indicator overlap; thus, simultaneous excitation at a single wavelength is possible.
5. The luminescence of reference and indicator are detectable at a common wavelength range by appropriate filters.

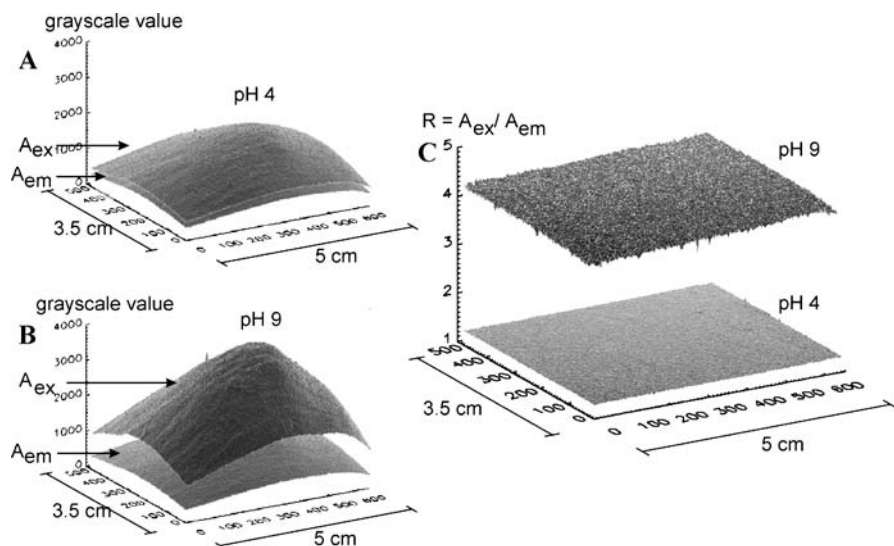


**Fig. 12** Illustration of the effect of internal referencing by  $tDLR$  on the homogeneity of images. **A** Sensor surface plots  $C_{ex}$  and  $C_{em}$  at pH 4. **B** Plots  $C_{ex}$  and  $C_{em}$  at pH 9. **C** Intrinsically referenced parameter  $R$  at pH 4 and pH 9, combined into one surface plot [132]

6. Both luminophores are in close spatial proximity.
7. The ratio of the concentration of two dyes remains constant.

The effect of  $t$ -DLR on the quality and homogeneity of images is shown Fig. 12. For imaging applications, time-domain lifetime referencing is the preferred method, whereas in case of fiber-optical sensors or sensor arrays the frequency-domain is favored (see Sect. 4.2).

Not only is the dual lifetime method suited for intrinsic referencing, but also FRET can be combined with lifetime determination. In time-resolved FRET, usually a long-lived fluorophore like a metal-ligand complex is utilized as resonance energy donor and the indicator dye as acceptor. The principle can be illustrated by means of a pH sensor. A ruthenium bipyridyl complex acts as the luminescent donor, bromothymol blue as pH-sensitive acceptor. Only the absorption band of the deprotonated form of the indicator coincides with the emission maximum of the ruthenium donor. Protonation of the indicator interrupts the non-radiative energy transfer. Thus, with decreasing pH the luminescence lifetime of the ruthenium complex increases. Corresponding sensor films were prepared in a polyurethane matrix [112]. The resolution of this sensor amounts to 0.1 pH units, which is not enhancement related to other referenced methods. But using the ruthenium complex as donor, the sensor can easily be combined with other sensor elements (e.g., for oxygen, carbon dioxide or temperature) to form sensor arrays. Similar systems were composed of Texas red hydrazide as donor and bromothymol blue as acceptor in a sol-gel film [134]. These pH sensor materials can also be used as  $p\text{CO}_2$  sensors, because dissolved carbon dioxide induces a change of pH in a humid environment (e.g., polymer matrices with entrapped water). Several sensor systems have been developed, containing the following donor/acceptor pairs: Ru-diphenylbipyridyl/*m*-cresolpurple (in ethyl cellulose) [112], or Ru-diphenylphenanthroline/Sudan III (in silica/ethyl cellulose hybrid material) [135], correspondingly. The latter sensor has a dynamic range from 0 to 100%  $\text{CO}_2$  with a LOD of 0.06%  $\text{CO}_2$ . On the basis of the pH-sensitive ruthenium complex/bromothymol blue FRET system in PVC, a sensor for chloride ions was developed [136]. A sensor for ammonia was presented consisting of sulforhodamin 101 as donor and bromocresol green as the acceptor in ethyl cellulose. In these cases, lifetime changes were detected by phase-modulated fluorometry (see Sect. 4.2) [137].

Making use of fluorophores as labels for biopolymers, time-resolved fluorescence detection and, particularly, time-resolved FRET have found numerous applications in biomolecular screening [138, 139].

## 4.2 Frequency-Domain Determination Methods

The phase-modulation (frequency-domain) method is a well-established technique for the measurement of luminescence decay times. Here, the sample is excited with light that is sinusoidally modulated at a frequency approximately reciprocal to the decay time. Hence, the emission of the probe follows the modulation, but with a certain delay. This is measured as a change of the phase angle. The luminescence decay time  $\tau$  can be calculated from the phase angle  $\Phi$  measured at a modulation frequency ( $f_{\text{mod}}$ ) if the luminescence decay is a single exponential:

$$\tau = \frac{\tan \Phi}{2\pi f_{\text{mod}}}. \quad (4)$$

The peak ratio of the modulated emission decreases relative to that of the excitation light and thus delivers another independent lifetime parameter, the demodulation  $m$ . The decay time can be calculated from the demodulation using:

$$\tau = \frac{1}{\omega} \sqrt{\frac{1}{m^2} - 1}. \quad (5)$$

The data is analyzed by non-linear least square analysis to obtain a lifetime from the best fit. Hence, frequency-domain measurements give lifetimes from two observables  $\Phi$  and  $m$ . Oxygen sensors have been developed composed of Ru-phenanthroline complexes in different polymer matrices [140]. Frequency lifetime measurements are prone to interferences by optoelectronic drifts, temperature effects and scatter. Consequently, methods for suppression of short-lived background fluorescence in phase fluorometry have been presented [141, 142] and used to design a glucose sensor [143]. Also in the phase-domain ratiometric methods can be based on FRET [144] and applied to imaging [106, 108].

Detection of nanosecond decay times requires complex and expensive optoelectronic instrumentation (electrooptical modulator, frequency synthesizers, radio-frequency amplifiers). This motivated the search to find a way of employing inexpensive instrumentation based on lock-in amplifiers (which are capable of measuring microsecond ( $\mu\text{s}$ ) decay times) for the detection of nanosecond decay times by phase fluorometry. For this purpose the dual lifetime referencing method for frequency-domain measurements ( $f\text{DLR}$ ) was developed [145].

$f\text{DLR}$  is a universal scheme to convert a fluorescence intensity into a phase shift which is not prone to the many factors that can interfere with fluorescence intensity measurements [146–148]. In the DLR scheme, two luminophores are used. One is referred to as the indicator and has a nanosec-

ond decay time ( $\tau_{\text{ind}}$ ). This is the analyte-sensitive fluorophore. The second luminophore is the reference with a decay time in the microsecond ( $\mu\text{s}$ ) range ( $\tau_{\text{ref}}$ ), unbiased by the analyte. Their excitation and emission spectra should display a distinct overlap so that they can be excited at the same wavelength and their fluorescence can be detected using the same emission window. Upon excitation with sinusoidally modulated light adjusted to the decay time of the reference dye from an LED or another light source that can be modulated in the kHz range, a phase shift  $\Phi_m$  of the overall luminescence occurs. This shift is detected by a PMT or PIN photodiode synchronized with a dual phase lock-in amplifier with a phase resolution of at least  $0.01^\circ$  or better. The frequency of  $\Phi_m$  depends on the ratio of intensities of the reference luminophore and the indicator dye. This signal is a superposition of the sine-shaped emissions of the indicator and the reference luminophores. The reference luminophore gives a constant background signal (ref) whereas the fluorescence signal of the indicator (ind) depends on the concentration of the analyte. If the intensity of the indicator is high (large amplitude, Fig. 13a), the observed overall phase shift  $\Phi_m$  is small. On the other hand  $\Phi_m$  becomes larger, if the indicator is quenched (low amplitude, Fig. 13b). Therefore, the phase shift  $\Phi_m$  directly renders the intensity of the indicator dye and, consequently, the analyte concentration. The phase signals of the reference dye and the indicator superimpose as shown in Eq. 6 and Eq. 7:

$$A_m \cos \Phi_m = A_{\text{ref}} \cos \Phi_{\text{ref}} + A_{\text{ind}} \cos \Phi_{\text{ind}}, \quad (6)$$

$$A_m \sin \Phi_m = A_{\text{ref}} \sin \Phi_{\text{ref}} + A_{\text{ind}} \sin \Phi_{\text{ind}}, \quad (7)$$

where  $A$  is the amplitude (or intensity) of either total signal ( $m$ ), reference luminophore (ref), or indicator (ind), and  $\Phi$  is the phase angle of either the overall signal ( $m$ ), the reference luminophore (ref), or the indicator (ind), respectively. In case of optimized modulation frequency ( $f_{\text{mod}}$ ),  $\tan \Phi_{\text{ref}}$  is described by:

$$\tan \Phi_{\text{ref}} = 2\pi f_{\text{mod}} \tau_{\text{ref}} = 1, \quad (8)$$

and  $\tan \Phi_{\text{ind}}$  is

$$\tan \Phi_{\text{ind}} = 2\pi f_{\text{mod}} \tau_{\text{ind}} = \frac{2\pi \tau_{\text{ind}}}{2\pi \tau_{\text{ref}}} = \frac{\tau_{\text{ind}}}{\tau_{\text{ref}}}. \quad (9)$$

The decay time of the reference luminophore should be three orders of magnitude higher than that of the indicator. Consequently, at low modulation frequencies in the kilohertz range (for measurement of microsecond ( $\mu\text{s}$ ) decay times)  $\Phi_{\text{ind}}$  equals zero. The decay time of the reference luminophore remains constant. The correlation of the phase angle ( $\Phi_m$ ) and the inten-

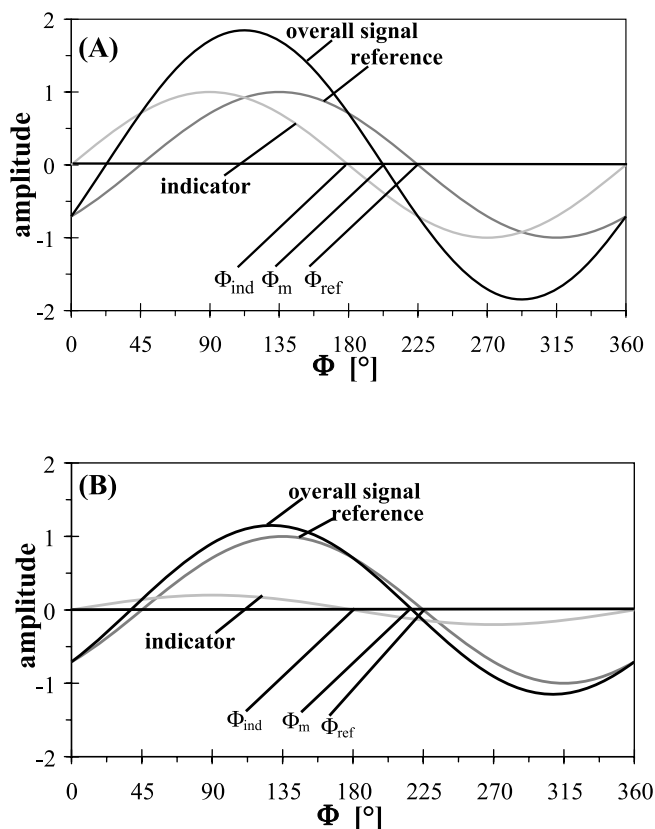


**Fig. 13** Dependency of the overall signal and phase shift  $\Phi_m$  on the amplitudes of indicator dye and reference standard. (Top) A high intensity of the indicator (A) results in a large phase angle  $\Phi_m$ , whereas  $\Phi_m$  is small if the indicator is quenched (bottom, B)

sity ratio of the indicator dye ( $A_{ind}$ ) and reference luminophore ( $A_{ref}$ ) is given by:

$$\frac{A_m \cos \Phi_m}{A_m \sin \Phi_m} = \cot \Phi_m = \frac{A_{ref} \cos \Phi_{ref} + A_{ind}}{A_{ref} \sin \Phi_{ref}} = \cot \Phi_{ref} + \frac{1}{\sin \Phi_{ref}} \frac{A_{ind}}{A_{ref}}. \quad (10)$$

As a result, a linear relation is obtained between  $\cot \Phi_m$  and the ratio of  $A_{ind}/A_{ref}$ , because the phase angle of  $\Phi_{ref}$  of the reference luminophore is assumed to be constant.

The *f*DLR method is advantageous in various respects because it eliminates fluctuations of the excitation source, temperature effects (if the reference fluorophore is suitably protected), and scattering. Drifts caused by the optoelectronic system, optical parameters of the sample, bending effects of filter optics, and light losses in the optical path are referenced. On the other



hand, losses of the luminescence intensity of the indicator, e.g., by leaching or photobleaching, will not be compensated. At lower frequencies in the kilohertz range, electronic cross-talk between components is almost excluded.

The application of DLR requires appropriate reference luminophores. Particularly, metal-ligand complexes of ruthenium, osmium, rhenium and iridium with polypyridine ligands in various substitution patterns combine high quantum yields and large Stokes shifts with high photophysical stability [149–151]. Other promising transition metal complexes include porphyrines of Pd<sup>2+</sup> and Pt<sup>2+</sup> and lanthanide chelates of Eu<sup>3+</sup> and Tb<sup>3+</sup>. These show decay times of up to a few milliseconds, which makes them ideal for the excitation with kilohertz-modulated electroluminescent light sources. It should be noted that any assay or sensor scheme based on the measurement of fluorescence intensity can be converted into a referenced *f*DLR scheme by addition of an appropriate reference fluorophore. A selection of sensors together with the luminophores employed for phase-modulation DLR can be found in Table 2. The accuracy and robustness of phase-modulated sensors for pH, *p*CO<sub>2</sub> or *p*O<sub>2</sub> are comparable to other intrinsic referenced methods. Their advantage is that they require only a comparatively simple instrumental set-up.

It is essential to protect the long-decaying reference dyes from quenching by oxidants, reductants and singlet oxygen. Therefore, the reference luminophore should be embedded in a separate, oxygen-impermeable layer or inside oxygen-impermeable nano- or microbeads. It is important that the reference fluorophore is distributed uniformly and does not tend towards sedimentation or aggregation. If the ratio between the fluorescent indicator and the reference standard is known and constant, a calibration-free quantification of the fluorescence signal can be obtained.

The latest developments are two-analyte sensors [158] for simultaneous detection of, e.g., oxygen and carbon dioxide. This system works with two optically independent sensing systems. The sensor for CO<sub>2</sub> is based on phase-domain DLR. It uses HPTS indicator beads and a long-lifetime iridium complex in polyacrylonitrile-co-acrylic acid beads as reference standard which are integrated into a highly gas-permeable polymer layer. Below this layer, another layer containing a Pt-porphyrin in polystyrene as oxygen probe was spread onto a polyester support. The spectral properties of the three dyes are carefully selected. The emission of the oxygen sensor does not interfere with the emission of the CO<sub>2</sub>-sensing system. The two-analyte sensor allows non-invasive and precise detection of O<sub>2</sub> and CO<sub>2</sub> in growing microbial cultures.

Another two-analyte sensor [159] for simultaneous detection of oxygen (0–20 kPa) and pH (pH 5–8) is based on an indicator and reference dye like the usual *f*DLR scheme, but in this case the reference dye is replaced by an oxygen-sensitive probe. The indicator is covalently attached to poly-HEMA particles and dispersed together with the reference dye in ormosil microparticles in a polyurethane hydrogel. Data are evaluated by

**Table 2** Applications of dual lifetime referencing in the frequency-domain

Analyte/ parameter	Indicator/ reference	Sensor specification	Figures of merit	Refs.
Water salinity via chloride	Lucigenin/ Ru(phen) <sub>3</sub> complex	Indicator in Nafion, reference embedded in poly-acrylonitrile particles	Range: 0.1–2 M, $t_{\text{resp}} = 100$ s LOD = 19 mM, pH-indept: 4–9	[152]
Cl <sup>-</sup>	Lucigenin/ Ru(dpp) <sub>3</sub> complex	Lucigenin in hydrogel beads, Ru in poly- acrylonitrile beads dispersed in polyurethane	Range: 0.01–1 $\mu\text{M}$ , $t_{\text{resp}} = 300$ s LOD = 0.01 $\mu\text{M}$ , pH-independent	[153]
NO <sub>3</sub> <sup>-</sup> in water	Styryl dye/ Ru(phen) <sub>3</sub> complex	Indicator in hydrogel with reference in sol-gel particles	Range: 0.1–50 mM, $t_{\text{resp}} = 180$ s pH-indept: 4.5–9	[154]
pH in seawater	Fluorescein derivatives/ Ru(dpp) <sub>3</sub>	Indicator in hydrogel, Ru in polyacrylo- nitrile beads	pH-range: 7.2–9.2, $t_{\text{resp}} = 120$ s Indept. of ionic strength	[30]
pCO <sub>2</sub> in food packaging	HPTS/ Ru(dpp) <sub>3</sub>	Indicator in ormosil matrix and reference in polyacrylonitrile	Range: 0–100% $t_{\text{resp}} = 20$ –30 s LOD = 0.08%, pH-independent	[155]
1-Butylamine	Fluoro-reactant/ Ru(dpp) <sub>3</sub> complex	Indicator in PVC-DOS co-polymer, Ru reference in polyacrylonitrile beads	Range: 1–100 mM, $t_{\text{resp}} \sim 300$ s LOD = 0.01 mM, (pH 13)	[156]
Cu <sup>2+</sup>	Lucifer yellow/ Ru(dpp) <sub>3</sub>	Indicator in cellulose beads, Ru in poly- acrylonitrile beads dispersed in a poly- urethane hydrogel	Range: 1–1000 $\mu\text{M}$ , $t_{\text{resp}} \sim 240$ s LOD = 0.4 $\mu\text{M}$ Best sensitivity at pH 5	[157]
pO <sub>2</sub> and pCO <sub>2</sub> simultaneously	Pt-TFPP and HPTS-TOA/ Ir-coumarin	See text	CO <sub>2</sub> : 0–20% $t_{\text{resp}} \sim 180$ s	[158]
pH and pO <sub>2</sub> simultaneously	5(6) Carboxy-fluorescein/ Ru(dpp) <sub>3</sub>	See text	O <sub>2</sub> : 0–18%, $t_{\text{resp}} = 30$ s pH: 5–8, $t_{\text{resp}} \sim 60$ s pO <sub>2</sub> : 0–21.3 kPa, $t_{\text{resp}} \sim 6$ s	[159]

a modified dual luminophore referencing (m-DLR) method, which relates the phase shift measured at two different frequencies to pH and to oxygen partial pressure, correspondingly. Dual sensor systems with integrated temperature-sensitive dyes are considered to be another promising tool for high-precision measurements, as the temperature sensitivity of the probe can be compensated.

## 5

### Fluorescence Polarization and Emission Anisotropy

Interactions of linearly polarized light with molecules in homogeneous solution can be regarded as excitation of a fraction of those molecules that have a transition moment predominantly parallel to the electric field of the excitation light (photoselection). This creates an anisotropic spatial distribution of excited molecules. This anisotropy can persist until the moment of luminescence emission. Consequently, luminescence emission of these molecules is also partially polarized. The common source of depolarization of luminescence emission is rotational diffusion which depends on the size and shape of the molecule under investigation and the (micro)-viscosity of the surrounding medium. These factors are the basis for numerous applications of fluorescence anisotropy in sensing methods, e.g., for the measurement of antigen–antibody interactions (polarization immunoassay) [160], kinase assays based on immunological detection of phosphorylation products [161], DNA genotyping by hybridization [162, 163], monitoring of real-time PCR [164], or for cytometric studies and cellular bioassays [165]. Polarization measurements are also suited for the study of segmental flexibility of macromolecules and membrane fluidity via hindered rotation [166].

Polarization bioassays are particularly interesting, because in this case a fluorescent label can be utilized as a probe to monitor biomolecular interaction and recognition processes.

#### 5.1

##### Emission Anisotropy or Polarization: Definitions and Theoretical Background

Two different definitions for emission anisotropy and polarization are commonly used. The polarization ratio  $P$  is defined as the fraction of light that is linearly polarized:

$$P = \frac{I_{\parallel} - I_{\perp}}{I_{\parallel} + I_{\perp}}, \quad (11)$$

which is the standard definition for polarization.

The emission anisotropy  $r$  is defined as the ratio of the intensity of the polarized component to the total intensity  $I_T$  (see Fig. 14). If the excitation

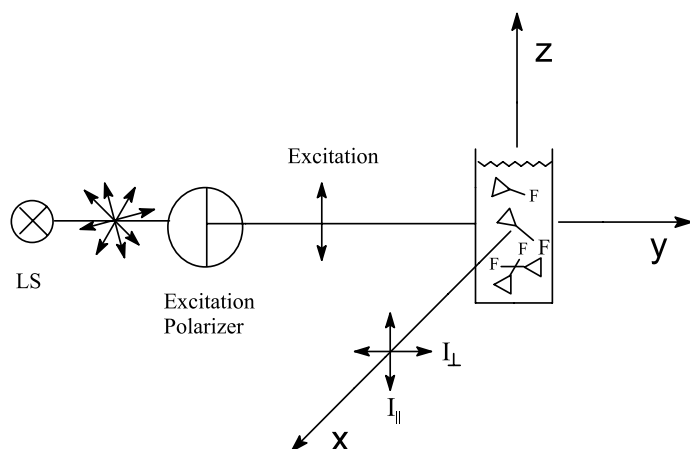


**Fig. 14** Scheme indicating the spatial components of emission anisotropy  $r$  with vertically polarized excitation light. The term  $r$  describes the ratio of the excess intensity parallel to the  $z$ -axis to the total intensity which is  $I_{\parallel} + 2I_{\perp}$

light is polarized along the  $z$ -axis and dipolar radiation from a fluorophore is symmetric around the  $z$ -axis ( $I_x = I_y$ ), the standard definition for emission anisotropy is obtained:

$$r = \frac{I_{\parallel} - I_{\perp}}{I_{\parallel} + 2I_{\perp}}, \quad (12)$$

with  $I_z = I_{\parallel}$  and  $I_y = I_{\perp}$ .

Thus, the anisotropy describes the ratio of the excess intensity parallel to the  $z$ -axis to the total intensity which is  $I_{\parallel} + 2I_{\perp}$ . Both polarization and anisotropy are dimensionless quantities. The values can be converted into each other using:

$$P = \frac{3r}{2+r} \quad \text{and} \quad r = \frac{2P}{3-P}. \quad (13)$$

Typically, the largest  $r$  values are observed for the longest wavelength absorption band of the fluorophore. Therefore, a polarization spectrum is a plot of the polarization versus the excitation wavelength of a fluorophore in diluted vitrified solution [167]. This spectrum is required for selecting the best excitation wavelength leading to an optimized dynamic range of an anisotropic assay.

## 5.2

### Measurement Principles

Two methods are commonly used for steady-state measurements of fluorescence anisotropies. These are the  $T$ -format and the  $L$ -format method. The

*L*-format is the most commonly used method since most fluorometers only have one emission channel. The transmission efficiencies of the components in the emission channel are different for light of parallel or perpendicular orientation. Therefore, a method was introduced that corrects these different transition efficiencies ( $S_V$  and  $S_H$ ).  $S_V$  and  $S_H$  have to be taken into account for an objective measurement of  $I_{\perp}$  and  $I_{\parallel}$  unbiased by the detection system. If a sample is excited with vertically polarized light and the emission is detected via a monochromator or an emission filter (Fig. 15, top) the observed polarized intensities are:

$$\frac{I_{VV}}{I_{VH}} = \frac{kS_V I_{\parallel}}{kS_H I_{\perp}} = G \frac{I_{\parallel}}{I_{\perp}}, \quad (14)$$

where  $k$  is a proportionality factor to account for the quantum yield of the fluorophore and other instrumental factors, and  $G$  is the ratio of the sensitivities of the detection system for vertically and horizontally polarized light.  $G$  is dependent on the emission wavelength and the bandpass of the emission monochromator.

$G$  is determined with horizontally polarized excitation where both the vertical and the horizontal component of the emission light are equal and proportional to  $I_{\perp}$  (see Fig. 15, bottom) because both orientations are perpendicular to the polarization of the excitation light. Therefore, any measured difference in  $I_{HV}$  and  $I_{HH}$  reflects the different transition efficiencies of the detection system:

$$\frac{I_{HV}}{I_{HH}} = \frac{S_V I_{\perp}}{S_H I_{\perp}} = \frac{S_V}{S_H} = G. \quad (15)$$

Changes of the excitation intensity due to rotation of the excitation polarizer do not affect the  $G$ -factor. Using Eq. 12, divided by  $I_{\perp}$  and Eq. 14 the anisotropy is given by:

$$r = \frac{I_{VV} - GI_{VH}}{I_{VV} + 2GI_{VH}}. \quad (16)$$

In the *T*-format method the intensities are measured simultaneously in two separate emission channels, one for the detection of the parallel and one for the detection of the perpendicular intensity. The different sensitivities of the two detection systems have to be determined using horizontally polarized excitation:

$$R_H = \frac{G_{\parallel}}{G_{\perp}}, \quad (17)$$

where  $G_{\parallel}$  and  $G_{\perp}$  are the gains of the respective emission channels, and with vertical excitation:

$$R_V = \frac{G_{\parallel} I_{\parallel}}{G_{\perp} I_{\perp}}. \quad (18)$$

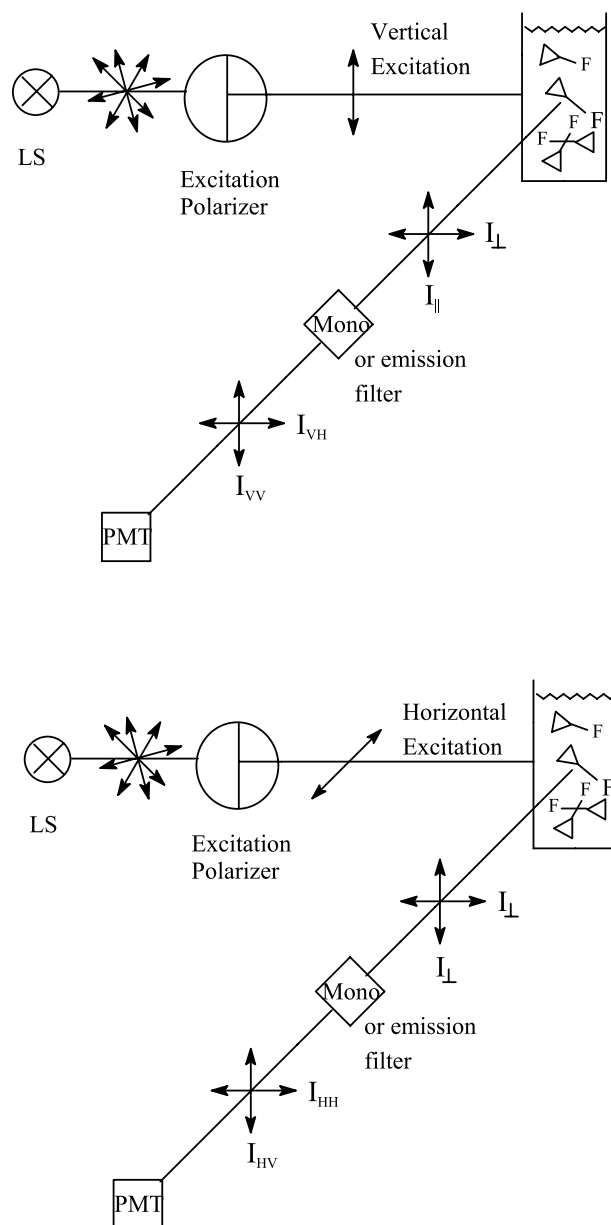


**Fig. 15** Lightpath of L-format devices for anisotropy measurements with vertically (*top*) and horizontally (*bottom*) polarized excitation light, and respective orientations of the emission intensities

Division of Eq. 18 by Eq. 17 yields:

$$\frac{R_V}{R_H} = \frac{I_{\parallel}}{I_{\perp}}. \quad (19)$$

This can be used to calculate the anisotropy according to Eq. 16.

In addition to the shorter acquisition time, the *T*-format method has more advantages over the *L*-format method. A *T*-format measurement is not prone to interferences from fluctuations from the excitation source. Simultaneous measurement in two separate channels is a more accurate referencing method. Light losses in the optical path are compensated in both *L*- and *T*-format methods, as well as losses in the intensity of the light source.

### 5.3

#### Effect of Rotational Diffusion on Fluorescence Anisotropy

Rotational diffusion is an important cause of depolarization of the emission light coming from a fluorescent labeled macromolecule. This depolarization is dependent on the molecular mass. Therefore, labeled macromolecules can act as indicators for biomolecular recognition like antigen–antibody interactions in immunoassays. This is expressed by:

$$r = \frac{r_0}{1 + \frac{\tau}{\theta}}, \quad (20)$$

which is one of different forms of the Perrin equation [167]. For globular proteins, the rotational correlation time is approximately related to the molecular mass *M* of the protein by:

$$\theta = \frac{\eta V}{RT} = \frac{\eta M}{RT}(\bar{v} + h), \quad (21)$$

where  $\bar{v}$  is the specific volume and *h* the hydration volume of the protein, *T* is the temperature in Kelvin, *R* the universal gas constant and  $\eta$  is the viscosity in poise [167].

As the ratio ( $\tau/\theta$ ) determines the anisotropy (Eq. 20), there is a demand for fluorophores with fluorescence lifetimes of  $\tau$  and  $\theta$  in a comparable order of magnitude. Ruthenium metal-ligand labels offer lifetimes of several hundred nanoseconds [160, 168]. This makes them suitable for fluorescence polarization immunoassays with medium weight antigens. Re(I) complexes display very long lifetimes of up to 2.7  $\mu$ s [169] and are well-suited labels for heavy weight antigens of >500 000 g/mol. In contrast to FRET, polarization immunoassays require only one luminescent label. Therefore, they can be performed as homogeneous assays without washing and separation steps.

For non-spherical and ellipsoidal molecules corresponding relations between anisotropy and rotational diffusion coefficients can be found in the literature [170–173]. Another common case where anisotropy displays complex decay behavior is the hindered rotor (e.g., a luminescent probe in

a membrane). Theoretical models dealing with these problems have been published [174, 175]. Measurement of depolarization via rotational diffusion can also be used to determine the fluidity of membranes, vesicles or micelles, membrane transitions [176], local viscosity of polymers [172], internal viscosity of micelles [177] and molecular orientation in solid polymer [178].

The commercial availability of instruments for anisotropy measurements in microwell plate-based assays reflects the growing number of applications of this method, even in high-throughput screening approaches, e.g., binding assays to study aptamer/protein interactions [179], or to identify selective steroid hormone receptor ligands [180]. As immobilized molecules are trapped at a certain orientation, their emission is strongly anisotropic. Thus, polarization assays can be adapted to protein microarray formats. As an example, fluorescently labeled aptamers were spotted on a glass slide to screen their interactions with different proteins which act as biomarkers for cancer [181]. Equipment for time-resolved anisotropy is only available on a research-instrument basis.

## 6

### Conclusion

Intrinsically referenced fluorescence sensing and imaging represent promising tools to obtain analytical information free of interferences and background signals. This survey gives an introduction into the most perspective ratiometric methods and demonstrates their significance in terms of biosensor and chemosensor technology by means of selected application examples. We focus on fluorescent probes that are integrated in different sensor formats. Methods for internal referencing by ratiometric methods include the use of (1) dual wavelength fluorophores, (2) dual fluorophore assays (incl. FRET), (3) luminescence lifetime assays in the time-domain or frequency-domain, and (4) fluorescence polarization. If lifetime measurements are combined with dual fluorophore referencing, the dual lifetime referencing (DLR) method is obtained. The resistance of the various techniques to assay interferences are summarized in Table 3. In case of sensor layers, interferences can also be suppressed by a proper choice of materials. For example, interferences by quenchers such as oxygen or heavy metal ions can be reduced by incorporating the fluorescent probe into appropriate materials like polymer layers or nanoparticles with a low permeability for the interfering species. In order to compensate photobleaching in frequency-domain FLIM, reversed phase [182] or permuted order [183] acquisition protocols may be applied. In case of imaging, straylight, background fluorescence and noise may be reduced by a confocal configuration, where the excitation light is focused on a certain small-sized plane within the sample. Emission light out of this focus is rejected by the confocal lens and pinhole system.



**Table 3** Referencing methods for fluorescence signals and their ability to minimize interferences from different sources<sup>a</sup>

Interference source	2- $\lambda$ <sup>b</sup>	Dual dye	FRET	$\tau$ (RLD)	$\tau$ (Phase-domain)	$t$ DLR	$f$ DLR	Anisotropy
Optical components	0	0	0	++	+	+	+	0
Instrumental drift (light source, detector)	+	+ <sup>c</sup>	+	++	++	++	++	+
Misalignment of optical fibers	++	++	- <sup>d</sup>	++	++	++	++	++
Background fluorescence sample	0	0	0	+ <sup>e</sup>	0	0	0	0
Light scatter by sensor material/sample	+	+	+	++	++	++	++	+
Intrinsic color of sample (inner filter effect)	0	0	0	++	++	+	+	+
Dye leaching/bleaching	+	0	0	+	+	-	-	+
Inhomogeneous dye loading	++	0	0	++	++	+	+	+

<sup>a</sup> ++ Good compensation, + partial compensation, 0 no compensation<sup>b</sup> Dual wavelength probe<sup>c</sup> Only compensated if detected with the same set of optical components<sup>d</sup> Not used in fiber optical sensors<sup>e</sup> Good compensation only for probes with lifetimes in the  $\mu$ s or ms range

The robustness of an assay or a sensor format is the main motive for internal referencing. It defines how the signal readout tolerates interferences in real-world samples. The implementation of calibration-free sensor systems is still a challenge. Ratiometric fluorescence detection, either by dual wavelength or lifetime measurements, is a basic requirement to achieve this objective, provided such experiments are carried out with calibrated instruments under well-defined conditions.

Calibration-free chemical sensing also is likely to be possible using fluorescence correlation spectroscopy (FCS), where temporal fluctuations of fluorescence are recorded. This method is usually applied to study the translational or rotational diffusion of biomolecules by means of their autocorrelation function [184] and not related to chemosensor technology. However, such fluctuations also can occur as a result of chemical reactions that cause a change in the fluorescence intensity (or lifetime) of a probe. Therefore, rate constants of chemical reactions can be determined [185]. Tailored fluorescent probes may then be used to measure the concentrations of reactants in a calibration-free mode. Recently, an example for local pH determination was presented [186], in which two-photon excitation of a pH-sensitive dyes enabled sensing of pH between 4 and 6. In this case, the pH can be deduced from the correlation curve. The increasing importance of *in vivo* imaging methods, particularly in medical diagnosis and therapy, will secure a continuing interest in robust intrinsically referenced fluorescence detection.

**Acknowledgements** We thank Prof. Peter K. Stys (Loeb Health Research Institute, Division of Neuroscience, University of Ottawa), Prof. Otto S. Wolfbeis (Institute of Analytical Chemistry, Chemo- and Biosensors, University of Regensburg), Dr. Sarina Arain (Pre-sens GmbH, Regensburg) and Dr. Gregor Liebsch (BIOCAM GmbH, Regensburg) for the provision of images and figures.

## References

1. Wolfbeis OS, Böhmer M, Dürkop A, Enderlein J, Gruber M, Klimant I, Krause C, Kürner J, Liebsch G, Lin Z, Oswald B, Wu M (2002) Advanced Luminescent Labels, Probes and Beads, and Their Application to Luminescence Bioassay and Imaging. In: Kraayenhof R, Visser AJWG, Gerritsen HC (eds) Springer Series on Fluorescence 2 (Fluorescence Spectroscopy, Imaging and Probes). Springer, Berlin Heidelberg New York, pp 3–42
2. Schäferling M (2005) Luminescence Lifetime-Based Imaging of Sensor Arrays for High-Throughput Screening Applications. In: Orellana G, Moreno-Bondi MC (eds) Springer Series on Chemical Sensors and Biosensors 3 (Frontiers in Chemical Sensors). Springer, Berlin Heidelberg New York, pp 45–92
3. Orellana G, Moreno-Bondi MC, Garcia-Fresnadillo D, Marazuela MD (2005) The Interplay of Indicator, Support and Analyte in Optical Sensor Layers. In: Orellana G, Moreno-Bondi MC (eds) Springer Series on Chemical Sensors and Biosensors 3 (Frontiers in Chemical Sensors). Springer, Berlin Heidelberg New York, pp 189–225

4. Mingoarranz FJ, Moreno-Bondi MC, Garcia-Fresnadillo D, de Dios C, Orellana G (1995) *Mikrochim Acta* 121:107
5. Amao Y (2003) *Microchim Acta* 143:1
6. Lin J (2000) *Trends Anal Chem* 19:541
7. Haugland RP (2002) *Handbook of Fluorescent Probes and Research Products. Molecular Probes*. <http://probes.invitrogen.com/handbook>. Accessed Oktober 2007
8. Amersham Biosciences (2007) *Reactive cyanine dyes*. <http://www.amershambiosciences.com>. Accessed Oktober 2007
9. Horobin RW (1980) *J Microsc* 119:345
10. Nagl S, Schäferling M, Wolfbeis OS (2005) *Microchim Acta* 151:1
11. Chan WCW, Maxwell DJ, Gao X, Bailey RE, Han M, Nie S (2002) *Curr Opin Biotechnol* 13:40
12. Costa-Fernandez JM (2006) *Anal Bioanal Chem* 384:37
13. Swanson JA (2002) Ratiometric fluorescence microscopy. In: Sansonetti P, Zychlinsky A (eds) *Methods in Microbiology*, 31 (*Molecular Cellular Microbiology*). Elsevier, Amsterdam, pp 1–18
14. Kostov Y, Rao G (1999) *Rev Sci Instrum* 70:4466
15. Wang E, Chow KF, Kwan V, Chin T, Wong C, Bocarsly A (2003) *Anal Chim Acta* 495:45
16. Shahriari MR, Ding JY (1994) In: Klein LC (ed) *sol-gel Optics: Processing and Applications*, chap 13. Kluwer, Boston, p 279
17. Lobnik A, Oehme I, Murkovic I, Wolfbeis OS (1998) *Anal Chim Acta* 367:159
18. Draxler S, Lippitsch ME (1995) *Sens Actuators B* 29:199
19. Wroblewski W, Roznicka E, Dybko A, Brzozka Z (1998) *Sens Actuators B* 48:471
20. Schulman SG, Chen S, Bai F, Leiner MJP, Weis L, Wolfbeis OS (1995) *Anal Chim Acta* 304:165
21. *Precision Sensing* (2007) <http://www.presens.de>. Accessed Oktober 2007
22. Hulth S, Aller RC, Engstrom P, Selander E (2002) *Limnol Oceanogr* 47:212
23. Paradiso AM, Tsien RY, Machen TE (1984) *Proc Natl Acad Sci USA* 81:7436
24. Muller-Borer BJ, Yang H, Marzouk SAM, Lemasters JJ, Cascio WE (1998) *Am J Physiol* 275:H1937
25. Ishaque A, Al-Rubeai M (1998) *J Immunol Methods* 221:43
26. Boyer MJ, Hedley DW (1994) *Methods Cell Biol* 41:135
27. Qian T, Nieminen AL, Herman B, Lemasters JJ (1997) *Am J Physiol* 273:C1783
28. Xu Z, Rollins A, Alcalá R, Marchant RE (1998) *J Biomed Mater Res* 39:9
29. Parker JW, Laksin O, Yu C, Lau ML, Klima S, Fisher R, Scott I, Atwater BW (1993) *Anal Chem* 65:2329
30. Schroeder C, Weidgans BM, Klimant I (2005) *Analyst* 130:907
31. Poenie M, Alderton J, Tsien RY, Steinhardt RA (1985) *Nature* 315:147
32. Silver RB (1998) *Methods Cell Biol* 56:237
33. Xu T, Yang W, Huo XL, Song T (2004) *J Biochem Biophys Methods* 58:219
34. Valet G, Raffael A, Rüssmann L (1985) *Naturwissenschaften* 72:600
35. Sanchez-Martin RM, Cuttle M, Mittoo S, Bradley M (2006) *Angew Chem* 118:5598
36. Lee SK, Lee JY, Lee MY, Chung SM, Chung JH (1999) *Anal Biochem* 273:186
37. Sun XP, Callamaras N, Marchant JS, Parker I (1998) *J Physiol* 509:67
38. Minta A, Kao JP, Tsien RY (1989) *J Biol Chem* 264:8171
39. Oheim M, Naraghi M, Muller TH, Neher E (1998) *Cell Calcium* 24:71
40. Lakowicz JR, Szmacinski H, Johnson ML (1992) *J Fluoresc* 2:47
41. Budinger GR, Duranteau J, Chandel NS, Schumacker PT (1998) *J Biol Chem* 273:3320
42. Meuwis K, Boens N, De Schryver FC, Gally J, Vincent M (1995) *Biophys J* 68:2469

43. Minta A, Tsien RY (1989) *J Biol Chem* 264:19449
44. Henary MM, Wu Y, Fahrni CJ (2004) *Chem Eur J* 10:3015
45. Peng X, Wu Y, Fan J, Tian M, Han K (2005) *J Org Chem* 70:10524
46. Stromberg N, Hulth S (2003) *Sens Actuators B* 90:308
47. Jang YJ, Jun EJ, Lee YJ, Kim YS, Kim JS, Yoon J (2005) *J Org Chem* 70:9603
48. Deng G, James TD, Shinkai S (1994) *J Am Chem Soc* 116:4567
49. Badugu R, Lakowicz JR, Geddes CD (2005) *Bioorg Med Chem* 13:113
50. Kaur G, Fang H, Gao X, Li H, Wang B (2006) *Tetrahedron* 62:2583
51. Zhao J, James TD (2005) *J Mater Chem* 15:2896
52. Yoon J, Czarnik AW (1992) *J Am Chem Soc* 114:5874
53. Zhang Y, Gao X, Hardcastle K, Wang B (2006) *Chem Eur J* 12:1377
54. Gao X, Zhang Y, Wang B (2005) *New J Chem* 29:1
55. Badugu R, Lakowicz JR, Geddes CD (2005) *Talanta* 66:569
56. Badugu R, Lakowicz JR, Geddes CD (2004) *Anal Biochem* 327:82
57. DiCesare N, Lakowicz JR (2001) *J Photochem Photobiol* 143:39
58. Wolfbeis OS, Klimant I, Werner T, Huber C, Kosch U, Krause C, Neurauder G, Duerkop A (1998) *Sens Actuators B* 51:17
59. Kaur G, Lin N, Fang H, Wang B (2006) Boronic Acid-Based Fluorescence Sensors for Glucose Monitoring. In: Geddes CD, Lakowicz JR (eds) *Topics in Fluorescence Spectroscopy*, vol 11 Glucose Sensing. Springer, Berlin Heidelberg New York, pp 377–397
60. Mingoarranz FJ, Moreno-Bondi MC, Garcia-Fresnadillo D, de Dios C, Orellana G (1995) *Microchim Acta* 121:107
61. Amao Y (2003) *Microchim Acta* 143:1
62. Molls M, Vaupel P (1998) The Impact of the Tumor Environment on Experimental and Clinical Radiation Oncology and other Therapeutic Modalities. In: Molls M, Vaupel P (eds) *Blood Perfusion and Microenvironment of Human Tumors – Implications for Clinical Radiooncology*. Springer, Berlin Heidelberg New York
63. John GT, Klimant I, Wittman C, Heinzle E (2003) *Biotechnol Bioeng* 81:829
64. Precision Sensing (2007) Presens OxoPlate. <http://www.presens.de>. Accessed Oktober 2007
65. BD Biosciences (2007) BD Oxygen Biosensor System. <http://www.bd.com>. Accessed Oktober 2007
66. Deshpande RR, Koch-Kirsch Y, Maas R, John GT, Krause C, Heinzle E (2005) *Assay Drug Develop Technol* 3:299
67. Wodnicka M, Guarino RD, Hemperly JJ, Timmins RM, Stitt D, Pitner JB (2000) *J Biomol Screen* 5:141
68. Arain S, John GT, Krause C, Gerlach J, Wolfbeis OS, Klimant I (2006) *Sens Actuators B* 113:639
69. O'Mahony FC, Papkovsky DB (2006) *Appl Environ Microbiol* 72:1279
70. Brasuel M, Kopelman R, Aylott JW, Clark H, Xu H, Hoyer M, Miller TJ, Tjalkens R, Philbert MA (2002) *Sens Mater* 14:309
71. Cao Y, Koo Y-EL, Kopelman R (2004) *Analyst* 129:745
72. Koo Y-EL, Cao Y, Kopelman R, Koo SM, Sang M, Brasuel M, Philbert MA (2004) *Anal Chem* 76:2498
73. Cao Y, Koo Y-EL, Koo SM, Kopelman R (2005) *Photochem Photobiol* 81:1489
74. Sumner JP, Westerberg NM, Stoddard AK, Fierke CA, Kopelman R (2006) *Sens Actuators B* 113:760
75. McEvoy AK, McDonagh CM, MacCraith BD (1996) *Analyst* 121:785
76. Klimant I, Ruckruh F, Liebsch G, Stangelmayer A, Wolfbeis OS (1999) *Microchim Acta* 131:35

77. Park EJ, Reid KR, Tang W, Kennedy RT, Kopelman R (2005) *J Mater Chem* 15:2913
78. Song A, Parus S, Kopelman R (1997) *Anal Chem* 69:863
79. Wolfbeis OS, Weidgans BM (2006) *Fiber Optic Chemical Sensors and Biosensors: A View Back*. In: Baldini F, Chester AN, Homola J, Martellucci S (eds) *Optical Chemical Sensors*. Springer, Berlin Heidelberg New York, pp 17–44
80. Bell JB, Schairer ET, Hand LA, Mehta RD (2001) *Annu Rev Fluid Mech* 33:155
81. Engler RH, Merienne MC, Klein C, LeSant Y (2002) *Aerospace Sci Technol* 6:313
82. Kingsley-Rowe JR, Lock GD, Davies AG (2003) *Royal Aeronaut J* 107:1
83. Asai K, Amao Y, Iijima Y (2002) *J Thermophys Heat Transf* 16:109
84. Klein C, Engler RH, Henne U, Sachs WE (2005) *Exp Fluids* 39:475
85. Khalil GE, Costin C, Crafton J, Jones G, Grenoble S, Gouterman M, Callis JB, Dalton LR (2004) *Sens Actuators B* 97:13
86. Oheim M, Naraghi M, Muller TH, Neher E (1998) *Cell Calcium* 24:71
87. Ren Y, Ridsdale A, Coderre E, Stys PK (2000) *J Neurosci Methods* 102:165
88. Selvin PR (2000) *Nat Struct Biol* 7:730
89. Jares-Erijman EA, Jovin TM (2003) *Nat Biotech* 21:1387
90. Kircher MF, Weissleder R, Josephson L (2004) *Bioconj Chem* 15:242
91. Takakusa H, Kikuchi K, Urano Y, Kojima H, Nagano T (2003) *Chem Eur J* 9:1479
92. Gonzalez-Gomez F, Vergara F, Fernandez A, Pedrosa C, Ramirez JP, Castilla JA, Ruiz R, Galan JJ, Ruiz A, Real LM (2003) *Clin Chem Lab Med* 41:392
93. Selvin PR (2002) *Ann Rev Biophys Biomol Struct* 31:275
94. Bustin SA (2002) *J Mol Endocrinol* 29:23
95. Mere L, Bennett T, Coassin P, England P, Hamman B, Rink T, Zimmerman S, Negulescu P (1999) *Drug Discovery Today* 4:363
96. Boute N, Jockers R, Issad T (2002) *Trends Pharmacol Sci* 23:351
97. Augustin CM, Oswald B, Wolfbeis OS (2002) *Anal Biochem* 305:166
98. Deniz AA, Laurence TA, Dahan M, Chamla DS, Schultz PG, Weiss S (2001) *Ann Rev Phys Chem* 53:233
99. Suzuki Y, Yasunaga T, Ohkura R, Wakabayashi T, Sutoh K (1998) *Nature* 396:380
100. Hudgins RR, Huang F, Gramlich G, Nau WM (2002) *J Am Chem Soc* 124:556
101. Sharma A, Wolfbeis OS (1988) *Anal Chim Acta* 212:261
102. Miura M, Miyahara T, Kato M, Toyooka T (2004) *Anal Chim Acta* 501:45
103. Cano-Raya C, Fernandez-Ramos MD, Capitan-Vallvey LF (2006) *Anal Chim Acta* 555:299
104. Valeur B (2002) *Molecular Fluorescence*. Wiley-VCH, Weinheim
105. Schneider PC, Clegg RM (1997) *Rev Sci Instrum* 68:4107
106. Herman P, Lin HJ, Lakowicz JR (2003) *Lifetime-Based Imaging*. In: Vo-Dinh T (ed) *Biomedical Photonics*. CRC, Boca Raton, pp 9.1–9.30
107. Wang XF, Uchida T, Coleman DM, Minami S (1991) *Appl Spectrosc* 45:360
108. Wang XF, Uchida T, Minami S (1989) *Appl Spectrosc* 43:840
109. Hartmann P, Ziegler W, Holst G, Lübbers DW (1997) *Sens Actuators B* 38:110
110. Woods RJ, Scypinski S, Cline Love LJ, Ashworth HA (1984) *Anal Chem* 56:1395
111. Ballew RM, Demas JN (1989) *Anal Chem* 61:30
112. Liebsch G, Klimant I, Frank B, Holst G, Wolfbeis OS (2000) *Appl Spectrosc* 54:548
113. Hartmann P, Ziegler W (1996) *Anal Chem* 68:4512
114. Babilas P, Schacht V, Liebsch G, Wolfbeis OS, Landthaler M, Szeimies R-M, Abels C (2003) *Br J Cancer* 88:1462
115. Kellner K, Liebsch G, Klimant I, Wolfbeis OS, Blunk T, Schulz MB, Göpferich A (2002) *Biotech Bioeng* 80:73
116. Zhong W, Urayama P, Mycek M-A (2003) *J Phys D Appl Phys* 36:1689

117. Hanson KM, Behne MJ, Barry NP, Mauro TM, Gratton E, Clegg RM (2002) *Biophys J* 83:1682
118. Sanders R, Draaijer A, Gerritsen HC, Houpt PM, Levine YK (1995) *Anal Biochem* 227:302
119. Vroom JM, De Grauw KJ, Gerritsen HC, Bradshaw DJ, Marsh PD, Watson GK (1999) *Appl Environ Microbiol* 65:3502
120. Schäferling M, Wu M, Enderlein J, Bauer H, Wolfbeis OS (2003) *Appl Spectrosc* 57:1386
121. Lin Z, Wu M, Schäferling M, Wolfbeis OS (2004) *Angew Chem Int Ed* 43:1735
122. Duerkop A, Turel M, Lobnik A, Wolfbeis OS (2006) *Anal Chim Acta* 555:292
123. Zelelew B, Khalil GE, Phelan G, Carlson B, Gouterman M, Callis JB, Dalton LR (2003) *Sens Actuators B* 96:304
124. Schäferling M, Wu M, Wolfbeis OS (2004) *J Fluoresc* 14:561
125. Duerkop A, Schäferling M, Wolfbeis OS (2006) In: Geddes CD, Lakowicz JR (eds) *Topics in Fluorescence Spectroscopy*, vol 11 *Glucose Sensing*. Springer, Berlin Heidelberg New York, pp 351–375
126. Wu M, Lin Z, Schäferling M, Dürkop A, Wolfbeis OS (2005) *Anal Biochem* 340:66
127. Wu M, Lin Z, Wolfbeis OS (2003) *Anal Biochem* 320:129–135
128. Lin Z, Wu M, Wolfbeis OS, Schäferling M (2006) *Chem Eur J* 12:2730
129. Arakawa T, Akamine M (2003) *Sens Actuators B* 91:252
130. Kessler MA (1998) *Anal Chim Acta* 364:125
131. Cano-Raya C, Fernandez Ramos MD, Capitan Vallvey LF, Wolfbeis OS, Schäferling M (2005) *Appl Spectrosc* 59:1209
132. Liebsch G, Klimant I, Krause C, Wolfbeis OS (2001) *Anal Chem* 73:4354
133. Mayr T, Igel C, Liebsch G, Klimant I, Wolfbeis OS (2003) *Anal Chem* 75:4389
134. Bambot SB, Sipior J, Lakowicz JR, Rao G (1994) *Sens Actuators B* 22:181
135. Von Bültzingslöwen C, McEvoy AK, McDonagh C, MacCraith BD (2003) *Anal Chim Acta* 480:275
136. Huber C, Werner T, Krause C, Klimant I, Wolfbeis OS (1998) *Anal Chim Acta* 364:143
137. Chan Q, Sipior J, Lakowicz JR, Rao G (1995) *Anal Biochem* 232:92
138. Pfeifer L, Stein K, Fink U, Welker A, Wetzl B, Bastian P, Wolfbeis OS (2005) *J Fluoresc* 15:423
139. Hoefelschweiger BK, Pfeifer L, Wolfbeis OS (2005) *J Biomol Screen* 10:687
140. Hartmann P, Ziegler W, Holst G, Lübbers DW (1997) *Sens Actuators B* 38/39:110
141. Szmazinski H, Lakowicz JR (1999) *Appl Spectrosc* 53:490
142. Herman P, Maliwal BP, Lakowicz JR (2002) *Anal Biochem* 309:19
143. Tolosa L, Gryczynski I, Eichhorn LR, Dattelbaum JD, Castellano FN, Rao G, Lakowicz JR (1999) *Anal Biochem* 267:114
144. Chang Q, Randers-Eichhorn L, Lakowicz JR, Rao G (1998) *Biotechnol Prog* 14:326
145. Klimant I, Huber C, Liebsch G, Neurauter G, Stangelmayer A, Wolfbeis OS (2002) In: Valeur B and Brochon JC (eds) *New Trends in Fluorescence Spectroscopy, Applications to Chemical and Life Sciences* (Springer Series on Fluorescence). Springer, Berlin Heidelberg New York, pp 257–274
146. Klimant I (1997) German Patent Application DE 198 29 657
147. Klimant I, Wolfbeis OS (1998) In: *Book of Abstracts of the 6th European Conference on Optical and Chemical Sensors & Biosensors (EUROPT(R)ODE)*, Manchester, UK, 7–10 April 2002, p 125
148. Lakowicz JR, Castellano JD, Dattelbaum L, Tolosa L, Rao G, Gryczynski I (1998) *Anal Chem* 70:5115
149. Kosch U, Klimant I, Werner T, Wolfbeis OS (1998) *Anal Chem* 70:3892

150. Dürkop A, Lehmann F, Wolfbeis OS (2002) *Anal Bioanal Chem* 372:688
151. Wolfbeis OS, Klimant I, Werner T, Huber C, Kosch U, Krause C, Neurauter G, Dürkop A (1998) *Sens Actuators B* 51:17
152. Huber C, Klimant I, Krause C, Werner T, Mayr T, Wolfbeis OS (2000) *Fres J Anal Chem* 369:196
153. Huber C, Klimant I, Krause C, Wolfbeis OS (2001) *Anal Chem* 73:2097
154. Huber C, Klimant I, Krause C, Werner T, Wolfbeis OS (2001) *Anal Chim Acta* 449:81
155. Von Bültzingslöwen C, McEvoy AK, McDonagh C, MacCraith BD, Klimant I, Krause C, Wolfbeis OS (2002) *Analyst* 127:1478
156. Mohr GJ, Klimant I, Spichiger-Keller U, Wolfbeis OS (2001) *Anal Chem* 73:1053
157. Mayr T, Klimant I, Wolfbeis OS, Werner T (2002) *Anal Chim Acta* 462:1
158. Borisow SM, Krause C, Arain S, Wolfbeis OS (2006) *Adv Mater* 18:1511
159. Vasylevska GS, Borisov SM, Krause C, Wolfbeis OS (2006) *Chem Mater* 18:4609
160. Vedvik KL, Eliason HC, Hoffmann RL, Gibson JR, Kupcho KR, Somberg RL, Vogel KW (2004) *Assay Drug Dev Technol* 2:193
161. Latif S, Bauer-Sardina I, Ranade K, Livak KJ, Kwok PY (2001) *Genome Res* 11:436
162. Murakami A, Nakaura M, Naktatsuji Y, Nagahara S, Tran-Cong Q, Makino K (1991) *Nucleic Acids Res* 19:4097
163. Crane BL, Hogan NC, Sudo H, Thilly WG, Hunter IW (2005) *Anal Chem* 77:5129
164. Yishai Y, Fixler D, Cohen-Kashi M, Zurgil N, Deutsch M (2003) *Phys Med Biol* 48:2255
165. Augustin CM, Wolfbeis OS (2003) *J Mol Liq* 107:141
166. Lakowicz JR (1999) *Principles of Fluorescence Spectroscopy*, 2nd edn. Kluwer Academic/Plenum, New York, pp 291–304
167. Terpetschnig E, Szmacinski H, Malak H, Lakowicz JR (1995) *Biophys J* 68:342
168. Guo X-Q, Castellano FN, Li L, Lakowicz JR (1998) *Anal Chem* 70:632
169. Perrin F (1926) *J Phys Radium* 7:390
170. Jabłonsky A (1960) *Bull Acad Pol Sci* 8:529
171. Kowski A (1993) *Crit Rev Anal Chem* 23:459
172. Steiner RF (1991) In: Lakowicz JR (ed) *Topics in Fluorescence Spectroscopy*, vol 2, Principles. Plenum, New York, pp 1–52
173. Lapari G, Szabo A (1980) *Biophys J* 30:489
174. Lentz BR (1989) *Chem Phys Lipid* 50:171
175. Neilson RDM, Soutar I, Steedman W (1977) *Macromolecules* 10:1193
176. Cogan U, Shinitzky M, Weber G, Nishida T (1973) *Biochemistry* 12:521
177. Nobbs JH, Bower DI, Ward IM, Patterson D (1974) *Polymer* 15:287
178. Scust J, Berg T (2004) *Anal Biochem* 330:114
179. McCauley TG, Hamaguchi N, Stanton M (2003) *Anal Biochem* 319:244
180. Blommel P, Hanson GT, Vogel KW (2004) *J Biomol Screen* 9:294
181. Webb WW (1976) *Quart Rev Biophys* 9:49
182. Gadella TWJ, Clegg RM, Jovin TM (1994) *Bioimaging* 2:139
183. Van Munster EB, Gadella TWJ (2004) *Cytometry A* 58:185
184. Thompson RL (1991) *Correlation Spectroscopy*. In: Lakowicz JR (ed) *Topics in Fluorescence Spectroscopy*, vol 1, Techniques. Plenum, New York, pp 337–378
185. Madge D (1976) *Quart Rev Biophys* 9:35
186. Charier S, Meglio A, Alcor D, Cogne-Laage E, Allemand J-F, Julien L, Lemarchand A (2005) *J Am Chem Soc* 127:15491



# Total Internal Reflection Fluorescence Sensing – Quality Assurance and Application to Water Analysis

Guenter Gauglitz (✉) · Guenther Proll (✉)

Eberhard-Karls Universität, Institut für Physikalische und Theoretische Chemie,  
Auf der Morgenstelle 8, 72076 Tübingen, Germany  
*guenter.gauglitz@ipc.uni-tuebingen.de, guenther.proll@ipc.uni-tuebingen.de*

<b>1</b>	<b>Introduction</b> . . . . .	415
<b>2</b>	<b>Fluorescence Based Trace Analysis in Water</b> . . . . .	417
2.1	Analytical Requirements . . . . .	417
2.2	Realization of Automated Immunological Low Concentration Direct Detection . . . . .	418
2.2.1	Principle of Total Internal Reflection Reference . . . . .	418
2.2.2	Why Use Total Internal Reflection Fluorescence – How Does a Binding Inhibition Assay Work? . . . . .	420
<b>3</b>	<b>Quality Assurance</b> . . . . .	422
3.1	Calibration and Validation Parameters . . . . .	422
3.2	How to Validate a Total Internal Reflection Fluorescence Immunoassay for Water Analysis . . . . .	424
<b>4</b>	<b>Conclusion</b> . . . . .	426
	<b>References</b> . . . . .	427

**Abstract** Based on the water directives of the European Union, the results of a biosensor system using total internal reflection fluorescence (TIRF) are demonstrated. The optical principal, the assay type, as well as the calibration and validation parameters are discussed. Results for endocrine disrupting compounds are given, and the validation parameters are outlined. These are applied to a measurement in comparison to a collaborative test in cooperation with accredited water laboratories using high performance liquid chromatography (HPLC) and gas chromatography (GC) techniques.

**Keywords** Quality assurance · Total Internal Reflection fluorescence · Water analysis

## 1 Introduction

A fundamental aspect of environmental policy in all European countries is the protection of water quality as an important factor of human health. Industry, agriculture, and other human activities have polluted waterways throughout Europe and beyond. Rivers, lakes, groundwater, and oceans can be contaminated by a variety of pollutants that can have a dramatic impact on aquatic life



and pose risks to human health [1, 2]. Examples are especially small organic molecules like herbicides, insecticides, fungicides, endocrine disrupting compounds (EDCs), carcinogens, and antibiotics.

At present, the most commonly used technologies in water analyses are liquid chromatography, such as high performance liquid chromatography (HPLC) and gas chromatography (GC), in combination with detection principles, such as mass spectrometry. These methods are well established and have proven to be successful applications for decades. Both principles require enrichment of water samples by several orders of magnitude prior to analysis. Typically, time consuming solid phase extraction is used as an enrichment procedure. However, the step of sample pretreatment makes these methods rather expensive, unsuitable for automation, and trained personnel is required to perform them.

At present, there are quite a few European directives, such as the Urban Waste Water Directive of 1991 [3]. A new water framework directive has been adopted to match the European needs providing an operational tool by setting the objectives for water protection well suited for the next century [4]. Since endocrine disruptors are of special interest in Europe, in Framework VI the strategy of the community for endocrine disruptors has been developed and is considered necessary as an implementation of methods to control a range of substances suspected to interfere with the hormone system of humans and wildlife [5]. These European directives have been transferred to many countries, and it is expected that within a short time a permanent control of drinking water will be enforced within Europe.

Accordingly, to protect water resources and control water quality, it is necessary to develop fast, sensitive, cost-effective, and user-friendly analytical systems capable of measuring a variety of small organic pollutants in aqueous samples. Classical methods requiring sample enrichment have to be replaced by methods supplying very low limits of detection (the European Commission requires a detection limit of less than  $0.1 \mu\text{L}^{-1}$ , e.g., in the case of pesticides) and allowing online monitoring.

The first requirement can be met by promising analytical techniques such as enzyme linked immunosorbant assays (ELISA) based on immunochemistry. It requires neither clean-up steps nor pre-concentration. However, automation is out of scope. The use of fluorescence is still one of the most sensitive detection principles. If combined with a suitable test format, these immunoassays can easily be carried out by flow injection analysis.

New approaches in array technology, miniaturization, and transduction in sensor signals have led to a new generation of such immunosensor systems [6]. Recently, one of the first portable and fully automated total internal reflexion fluorescence (TIRF) based biosensor systems suitable for multianalyte detection [7, 8] has been developed.

Within Framework V and VI, TIRF based sensor systems have been developed in the course of projects called RIANA and AWACSS [9, 10]. In lab-

oratories, both systems provided the intended low limits of detection and allowed automated measurements as required for future water control. With regard to the system development, both devices were successful. However, new analytical methods need to be accredited and validated. Accordingly, these new analytical tools, their automated instrumentation, and the potential application in daily water analysis has to be based on the fundamentals of quality control being part of a total quality management system.

Therefore, in this chapter, application of TIRF in water analysis is discussed with regard to instrumentation and results, giving the analytical principle, demonstrating the approach of calibration, and demonstration instruments of quality assurance. Especially the necessity of internal quality control and validation of this new analytical procedure will be discussed, but also the necessity of reference analytics and round robin tests. Accordingly, the results of both comparing the analyses using this new AWACSS systems in competition to other accredited laboratories and the proof of quality in a field test will be surveyed.

## 2 Fluorescence Based Trace Analysis in Water

### 2.1 Analytical Requirements

As mentioned above, the European directives regulate the quality of permanent water analysis in drinking, ground, and waste water. Within few years these directives will govern any analytics in most European countries. According to these regulations, an analytical method for pesticides in water must be able to detect and quantify concentrations at the given EU limit for drinking water of  $0.1 \mu\text{g L}^{-1}$ . Up to now, there are no limits for hormones or other EDCs. However, because of the no-effect-levels of hormone active compounds at and below  $0.001 \mu\text{g L}^{-1}$ , it is necessary to have limits of detection (LOD) towards sub-nanogram per liter range.

Classical analytical methods like HPLC or GC can achieve these very low LODs only after enrichment of the water sample by a factor of 1000 to 10 000. This time consuming and expensive pretreatment step makes these well established methods unsuitable for continuous monitoring of water sources as claimed in the EU [11] by the end of 2007. Accordingly, research on development of instrumentation using immunological based analytical techniques has been well funded in recent years. ELISA methods have shown to be able to overcome this drawback of an enrichment step. To achieve the very low LODs, great efforts have been made to develop fully automated biosensors capable for detecting compounds in a multi-analyte mode. In terms of detection sensitivity, immunochemistry combined with fluorescence detection is superior

to other transduction methods. Especially Total Internal Reflection Fluorescence (TIRF) has proved to meet the requirements in environmental trace analytics.

## 2.2

### **Realization of Automated Immunological Low Concentration Direct Detection**

#### 2.2.1

##### **Principle of Total Internal Reflection Reference**

Detection principles based on the measurement of fluorophores provide very low limits of detection as required in trace analysis in water. A combination with wave guide structures in planar transducers have the additional advantages of directed excitation of fluorophores, spatially resolved monitoring in a multi-analyte system, and the approach of low detection volumes. TIRF provides selective excitation of fluorophores close to the interface planar transducer and biomolecular sensitive layer. No fluorophores in the sample volume are excited. Therefore, total internal reflection fluorescence techniques have been considered advantageous.

The evanescent field arises at the interface between two dielectric media if the condition for total internal reflection is complied with. It decays exponentially into the media of lower refractive index. The penetration depth is of the order of half the operating wavelength. In evanescent field sensor applications an optical waveguide is used as the transducer element. A fraction of the total guided power in the waveguide is carried by the evanescent field [12]. The sample covers part of the waveguide surface and interacts with the guided light via the evanescent field. Among the demonstrated planar devices in the literature [13] are grating and directional couplers [14, 15], surface plasmon resonance [16, 17], resonant mirror [18], interferometric [19, 20], and fluorescence based sensors [21]. All of the transducers have (bio-)chemically modified surfaces to allow for specific recognition.

Radiation can be guided inside a waveguide, either bulk or a channel waveguide, microstructured by photolithography. At the interface between waveguide and fluidics, a bulk polymer layer which has to avoid non-specific binding is immobilized. This layer is also the basis for immobilized derivatives of analytes which are considered to be detected in the sample solution. Modern spotting techniques allow the preparation of areas at different spots with different analyte derivatives immobilized. Therefore, multiple analytes can be measured in parallel in one sample (see Fig. 1).

The flow injection setup allows mixing of antibodies and sample solution containing different analytes in various concentrations. High concentration of a specific analyte blocks the related antibody. This means, the labeled non-inhibited antibodies can diffuse to the surface of the transducer, interact with

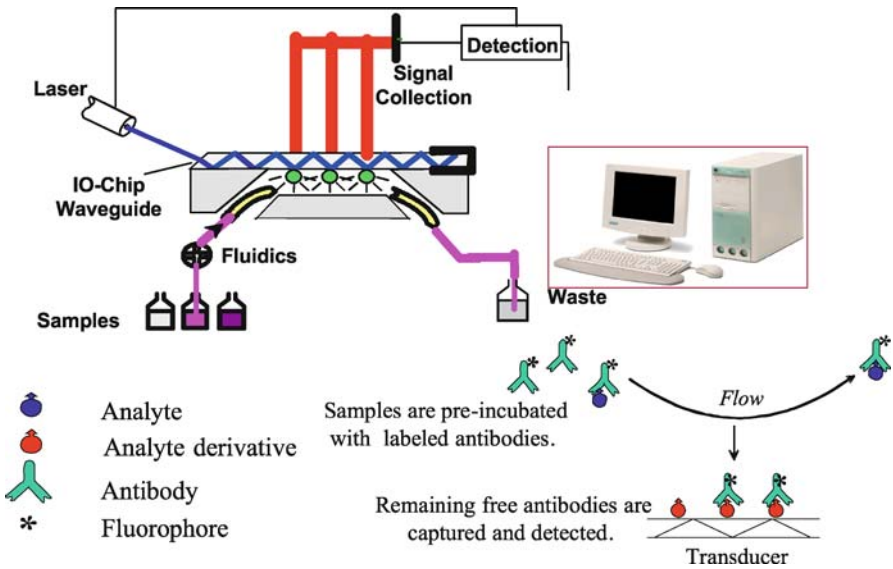


**Fig. 1** Setup: in-coupling of laser radiation in integrated optics chip; evanescent field excites fluorophores interacting with immobilized analyte derivatives; fluorescence is monitored by fiber optics, collected to detection unit

the immobilized analyte derivatives, and provide a readout signal which can be guided to the detector by the detection fibers. This binding inhibition test allows a kind of inverse concentration monitoring (see Fig. 2). A high concentration of analytes blocks the antibodies, and, therefore, the detected signal is very low. Low concentration of analyte allows non-blocked to get to the surface in large numbers and form a high signal. Since the different analyte derivatives have been immobilized and laterally resolved, the antibodies can all be labeled by the same fluorophore.

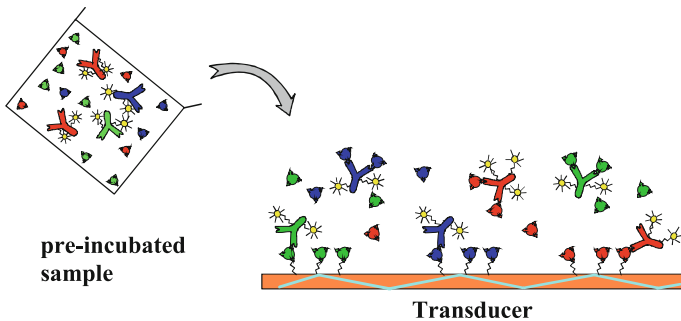


**Fig. 2** Binding inhibition: analyte derivatives are immobilized and laterally resolved; in a pre-incubation phase, sample can interact with different added antibodies; non-blocked antibodies interact at selected spots

Details of the instrumentation are published elsewhere in detail [24, 26, 27]. Just in brief; laser radiation is incoupled into the embelled wave guide, which can be either a bulk one or a planar transducer containing monomode integrated optical wave guide arms. A flow injection system passes by the sample after incubation. The guided wave excites at laterally resolved spots areas where the immobilized analyte derivatives (for test format, see next chapter) can interact with labeled antibodies. A spatially resolved detection using fiber optics allows the determination of concentration even in a multi-analyte system.

In the RIANA system, six spots are used and placed on a bulk waveguide transducer [23]. In AWACSS, four monomode waveguide arms [25] are spotted with 32 different derivatives to allow even multi-analyte analysis for simultaneous measurements of up to 32 analytes. In both cases, the overload time for one measurement cycle is up to 12 min, including the preincubation time, the baseline measurement, the regeneration, and the determination of the fluorescence signal itself. The overall system is shown in Fig. 1. For further details, see [26–28].

### 2.2.2

#### **Why Use Total Internal Reflection Fluorescence – How Does a Binding Inhibition Assay Work?**

To understand the technical requirements for setting up a biosensor capable for trace analytics, some theoretical considerations should be taken into account.

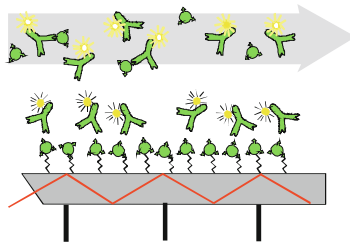
#### **Test Format**

Direct test formats with antibodies immobilized on a solid-phase, like it is for ELISA, can be further rationed as competitive and non-competitive. Although this principle is widely used, it struggles with the instability of the immobilized antibodies during regeneration procedures as they are necessary for a long-term continuous monitoring.

The other possibility is to immobilize the antigen to the heterogeneous phase and to use a binding inhibition test format, which is non-competitive if performed under mass transport limited conditions. Making use of this advantageous test format capable of detecting a LOD of  $1 \mu\text{g L}^{-1}$  requires a concentration of active antibody which has to be used in the same order of magnitude. This type of assay is demonstrated in Fig. 3.

Biosensors usually perform the mentioned test formats in combination with Flow Injection Analysis (FIA). If one mL water sample is used for carrying out a binding inhibition assay with fluorescently labeled antibodies with a FIA and the incubation step under mass transport limited conditions of the sample over the sensor takes approx. 5 min, only a few million dye molecules

Low concentration



High concentration

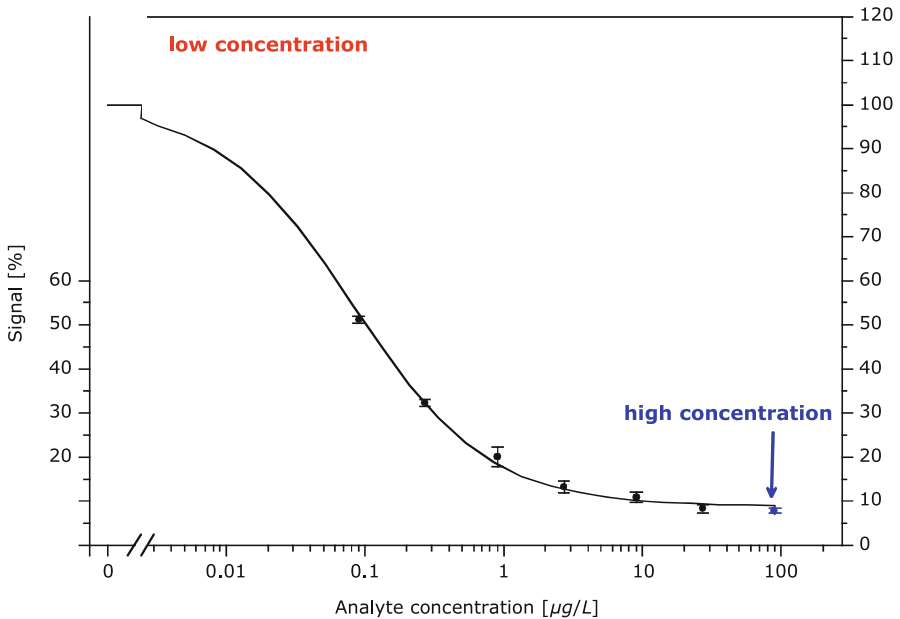
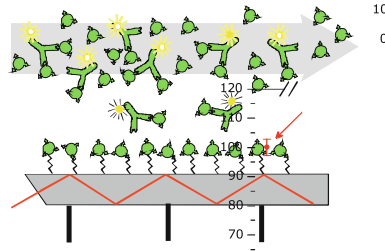


**Fig. 3** Testformat: detected high and low fluorescence intensity in correlation with low and high concentration of pollutant in the sample which is passing the transducer after pre-incubation phase, using a flow injection device

(atto moles) will bind to an area of one  $\text{mm}^2$ . This amount of dye molecules and following fluorescent intensity will even decrease with increasing antigen concentration. As demonstrated in Fig. 3, the binding inhibition assay kind of gives inverse information. Low analyte concentration causes a high fluorescence signal, since just a few antibodies are blocked during incubation phase. The non-blocked ones can interact with the immobilized analyte derivatives at the transducer sensitive layer and can be excited by the evanescent field. Their fluorescence is monitored by the optical fibers. Accordingly at high analyte concentrations most antibodies are blocked. Low fluorescence intensity results are as shown in the calibration curve.

TIRF is a very good technique for the selective illumination of the surface bound fluorescent labeled antibody molecules. Combined with detectors for low light intensities it is possible to setup fully automated biosensors for water analysis (RIANA, AWACSS). The very few photons to be detected require expensive cooled charge-coupled devices (CCD) or photodiode-arrays to be able to read out a two dimensional array for multi-analyte detection.

### 3 Quality Assurance

#### 3.1 Calibration and Validation Parameters

The standard experimental design for a calibration routine consists of nine independent blank (e.g., Milli-Q water) measurements and eight concentration steps (each measured as three replica) of the analyte (e.g., spiked Milli-Q water). For all concentration steps and the blank measurements (nine replica), the mean value and the Standard Deviation (SDV) for the replica was calculated. The measured signal for the mean value of the blanks was set to 100% and all spiked samples could be obtained as a relative signal below this blank value.

In immunoassays, the calibration curves follow a sigmoidal behavior if the signal is plotted over the concentration in the logarithmic scale (see Figs. 3, 4). To fit the data set, a Logistic Fit function (parameters of a logistic function:  $A_1$ ,  $A_2$ ,  $x_0$ , and  $p$ ) [29] was used:

$$y = \frac{A_1 - A_2}{1 + (x/x_0)^p} + A_2,$$

where  $A_1$  is the upper asymptote and  $A_2$  the lower one. The range between  $A_1$  and  $A_2$  is the dynamic signal range. The inflection point is given by the variable  $x_0$  and represents the analyte concentration, which corresponds to a decrease of 50% of the dynamic signal range – the Inhibitory Concentration

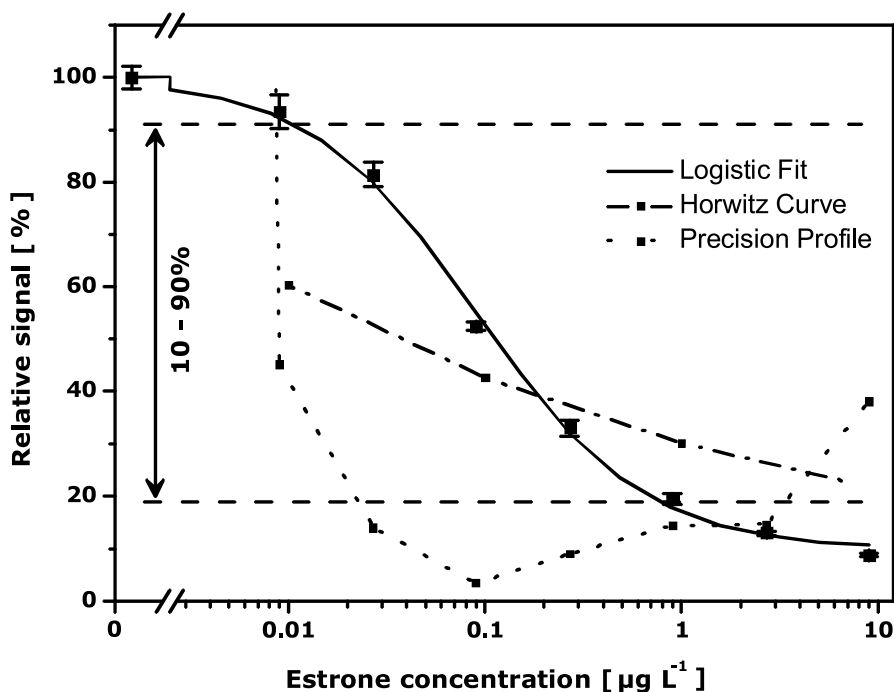


**Fig. 4** Calibration: Test calibration curve for estrone approximated with the logistic function (parameter  $A_1$  fixed to 100%). The 10–90% block of the dynamic signal range is compared to the working range depending on the Horwitz Curve and the Precision Profile

50% ( $IC_{50}$ ). The slope of the tangent in this point is given by the parameter  $p$ . Out of the Logistic Fit data, the 10% to 90% range of the dynamic signal can be calculated, which gives the first impression of the possible utilization range of the received calibration curve.

According to the calibration parameters received by this non-linear fit, there are no common rules for evaluating the corresponding analytical performance. In compliance with the International Union of Pure and Applied Chemistry (IUPAC) rules, “The Orange Book” [30] for linear calibration plots, the LOD is calculated as three times the Standard Deviation of the blanks ( $SDV_b$ ) and the LOQ is calculated as ten times the  $SDV_b$ .

If applied to immunoassays approximated with this logistic model, it can happen that the parameter  $A_1$  is above 100% and outside the standard deviation of the blanks. Following this, it is possible to receive a calculated LOD which is in the signal range also above 100%. In extreme cases, this value can even be outside the error margin of the blanks. Having this in mind, it would make sense to fix the parameter  $A_1$  to 100% during the approximation of the logistic model. Studying these two strategies, we obtained better results for most cases when approximation was carried out for all four parameters.



The use of LOQ for logistic calibration curves is also a contentious issue, because with its non-linear behavior the results for immunoassays are often worse than they need to be. A real alternative is the use of the 95% Confidence Belt and the associated Minimum Detectable Concentration (MDC) and Reliable Detection Limit (RDL), which can easily be calculated for the sigmoidal calibration curves [31]. These authors reported on calibration and assay development using the four-parameter logistic model and assay quality control procedures.

To determine the working range, the Precision Profile ( $x_{cv,i}$ ) and its intersections with the Horwitz Curve [32, 33] has to be calculated. Based on scores of Association of Analytical Communities (AOAC) intercomparison programs, Horwitz developed an empiric correlation between the comparative SD and the concentration. For laboratory intercomparison programs, Horwitz proposed an equation for the reproducibility  $\sigma_R = f \cdot c^{0.8495}$  with a factor  $f = 0.02$ . The corresponding error is the relative standard deviation  $RSD = 100(\sigma_R/c)$  that can be calculated with the reproducibility  $\sigma_R$  and the analyte concentration  $c$ . For intralaboratory reproducibility, Horwitz found a higher precision and, consequently, lower RSD values. In this case, the factor  $f$  can be reduced to two-thirds up to half of its former value. RSD values can be calculated for each concentration and they represent the Horwitz Curve.

An applicable concentration determination is possible only if the Precision Profile is below the Horwitz Curve. The SD values of the inverse function ( $SDVx_i$ ) can be calculated using the SD values of the measured data ( $SDVy_i$ ) and the associated values of the first derivative ( $y'$ ) of the Logistic Fit ( $y$ ) for each concentration.

Then, the variation coefficients ( $x_{cv,i}$ ) can be calculated and plotted together with the values of the Horwitz Curve and the calibration data, including the Logistic Fit in the semilogarithmic graph. Finally, the range between the intersection points of the Horwitz Curve and the Precision Profile represents the working range.

### 3.2

#### **How to Validate a Total Internal Reflection Fluorescence Immunoassay for Water Analysis**

The development of a new TIRF immunoassay for water monitoring carried out with a fully automated biosensor should undergo the same four step validation procedure as usually performed for other techniques:

1. Lab based calibration and replica measurement spiked buffer samples;
2. measurement of spiked real water samples and comparison to classical analytical methods;
3. collaborative trial together with accredited laboratories;
4. field test in comparison with accredited laboratories.

During the development of the AWACSS, this four step strategy has been taken into account.

The first exemplary calibration of the AWACSS has been performed for estrone. As introduced above, the validation parameters can be calculated according to two different strategies, as shown in Figs. 4, 5. The corresponding validation parameters are summarized in Table 1. The resulting working ranges calculated for the two calibration functions do not differ much. However, the valid concentration range for the Horwitz based evaluation method is wider compared to the 10–90% dynamic signal range. This example also demonstrates the problematic situation arising with the IUPAC based determination of the LOQ. In this case, the LOQ value is far above the lower boarder of the valid working range, which makes the results worse then they need to be.

In a next step, the system has been calibrated for six analytes (estrone, atrazine, isoproturon, bisphenol A, propanil, and sulphamethizole) in parallel. During our studies, we compared the two different evaluation strategies and in most cases we obtained better results and recovery rates for the IUPAC recommended method for the determination of LOD and LOQ based on

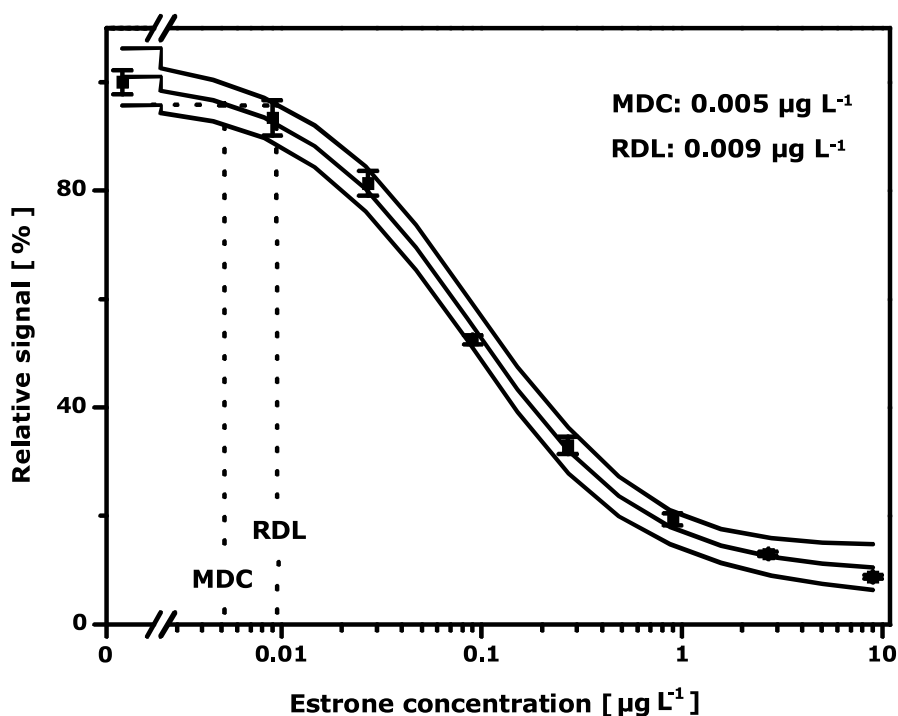


**Fig. 5** Confidence belt: Calibration curve and 95% Confidence Belt for estrone approximated with the four parameter logistic function. The Minimum Detectable Concentration (MDC) and the Reliable Detection Limit (RDL) are indicated

**Table 1** Validation parameters

Approximation with fixed A1				Approximation for 4 parameters			
A <sub>1</sub> fixed	100		[%]	A <sub>1</sub>	100.95 ± 1.91		[%]
A <sub>2</sub>	9.91 ± 1.56		[%]	A <sub>2</sub>	9.72 ± 1.75		[%]
x <sub>0</sub>	0.09 ± 0.01		[µg L <sup>-1</sup> ]	x <sub>0</sub>	0.09 ± 0.01		[µg L <sup>-1</sup> ]
p	1.03 ± 0.07		[-]	p	1.01 ± 0.08		[-]

WR-%	WR-H	LOD <sup>1</sup>	LOQ <sup>1</sup>	WR-%	WR-H	MDC <sup>2</sup>	RDL
[µg L <sup>-1</sup> ]	[µg L <sup>-1</sup> ]	[µg L <sup>-1</sup> ]	[µg L <sup>-1</sup> ]	[µg L <sup>-1</sup> ]	[µg L <sup>-1</sup> ]	[µg L <sup>-1</sup> ]	[µg L <sup>-1</sup> ]
0.011–0.764	0.009–4.3	0.008	0.030	0.010–0.781	0.009–4.3	0.002	0.012

<sup>1</sup> According to IUPAC recommendations

<sup>2</sup> Associated to the Confidence Belt

the approximation of the logistic model with the A1 parameter fixed to 100%. This multi-analyte calibration was successfully applied for analyzing drinking water as a real water sample spiked with different concentrations of the corresponding analytes. All recovery rates – except for bisphenol A because of contamination from plastic labware – could match the recommended range of the AOAC international between 70 and 120% [34].

The third validation step has been the collaborative trial together with three accredited water laboratories employing different HPLC and GC techniques. As published in [35] [36], the overall performance of the AWACSS was fully comparable to common analytical techniques.

As the most important test regarding robustness and precision during this validation procedure, a field test has been performed. It could be demonstrated under realistic measurement conditions that online monitoring of river water representing a complex matrix can be carried out by the AWACSS. The results obtained with this fully automated biosensor system could be confirmed by an accredited water laboratory [34]. All data during this field test have been treated according to IUPAC rules for pure and applied chemistry to obtain validation parameters for each analyte of the multi-analyte assays. The evaluation procedures for evaluating the analytical performance are in compliance with the recommendations given by the AOAC international. The results support the data of the collaborative trial mentioned before.

## 4 Conclusion

Upcoming directives in permanent control of drinking water and protection of ground water require new approaches in instrumental analysis. Immunological techniques provide the necessary low limits of detection and quantification as well as the opportunity to introduce automatic low-cost water

analysis systems operating in unattended mode. These also offer the opportunity of early warnings and fresh water control. On the other hand, high quality assurance requirements are necessary in order to secure high quality water surveillance. This requires best validation of these new methods, including reference analytics and field tests as well as effective quality assurance systems, including internal and external evaluation.

The presented instrumentation meets the requirements of method validation, of modern calibration procedures, and offers the opportunity to meet the mentioned requirements of quality assurance, as demonstrated above. Because of the very low LODs in the lower ng per liter range – and even below – for many small organic compounds this system is not only useful as a monitoring device but also as a novel analytical instrument for trace analysis without the need of any sample preconcentration. In addition, as a device for prescreening of thousands of water samples per day analyzed by specialized laboratories, this system can help to significantly reduce costs per sample. In principle, the employed immunochemistry based technique can be used to analyze other aqueous samples coming from food safety, diagnostics, or from the detection of other hazardous agents in the environment.

The AWACSS biosensor is a fully automated analytical system capable of multi-analyte detection, ready to be used for the monitoring of different water bodies. Therefore, this system can be a very helpful tool for the implementation of the surface-water-monitoring programs which have to be defined by the end of 2007 by each EU member state.

## References

1. Barceló D, Hennion MC (1997) Trace Determination of Pesticides. Elsevier, Amsterdam
2. Barceló D, Hennion MC (1997) *Anal Chim Acta* 338:3
3. European Urban Waste Water Directive 91/271/EEC (1991)
4. European Water Framework Directive 2000/60/EC (2000)
5. European Directives: COM (1999) 706, COM (2001) 262
6. Krämer PM, Franke A, Standfuss-Gabisch C (1999) *Anal Chim Acta* 399:89
7. Ligler FS, Golden JP, Rowe-Taitt CA, Dodson JP (2001) Array biosensor for simultaneous detection of multiple analytes. In: *Proceedings of SPIE* 4252:32
8. Sapsford KE, Shubin YS, Delhanty JB, Golden JP, Taitt CR, Shriver-Lake LC, Ligler FS (2004) *J Appl Microbiol* 96:47
9. RIANA ENV4-CT95-0066 (4th Framework: Environment and Climate Programme 1994–1998; Research Area 2: Environmental Technologies (Instruments, Techniques and Methods for Monitoring the Environment))
10. AWACSS EVK1-CT-2000-00045 (5th Framework Programme: Energy, Environment, and Sustainable Development)
11. Griffiths M (2002) European water management online, official publication of the European Water Association (EWA). [http://www.ewaonline.de/journal/2002\\_05.pdf](http://www.ewaonline.de/journal/2002_05.pdf)
12. Bergmann L, Schaefer C (2004) *Optik* 10. Auflage. Walter de Gruyter, Berlin New York

13. Gauglitz G (2005) *Anal Bioanal Chem* 381(1):141
14. Kunz RE, Duebendorfer J, Morf RH (1996) *Biosens Bioelectron* 11:653
15. Luff BJ, Harris RD, Wilkinson JS, Wilson R, Schiffrin DJ (1996) *Opt Lett* 21:618
16. Homola J, Ctyroky J, Skalsky M, Hradilova J, Kolarova P (1997) *Sens Actuators B* 286:38–39
17. Mouvet C, Harris RD, Maciag C, Luff BJ, Wilkinson JS, Piehler J, Brecht A, Gauglitz G, Abuknesha RA (1997) *Anal Chim Acta* 338:109
18. George AJT, French RR, Glennie MJ (1995) *J Immunol Methods* 183:51
19. Brandenburg A, Henninger R (1994) *Appl Opt* 33:5941
20. Lukosz W, Stamm C, Moser HR, Ryf R, Dubendorfer J (1997) *Sens Actuators B* 38–39:316
21. Plowman TE, Reichert WM, Peters CR, Wang HK, Christensen DA, Heron JN (1996) *Biosens Bioelectron* 11:149
22. Klotz A, Brecht A, Gauglitz G (1997) *Sens Actuators B* 39:310–315
23. Brecht A, Barzen C, Klotz A, Gauglitz G, Harris R, Quigley G, Wilkinson J, Fraval S, Sztajn bok P, Barcelo D, Gascon J, Steinwand M, Abuknesha R (1998) *River Analyser-Multiresidue Immunoanalytical Monitoring Tools*. In: Hock, Barcelo, Cammann, Hansen, Turner (eds) *Biosensors for Environmental Diagnostic*. Teubner-Reihe Umwelt, Teubner Verlag, Stuttgart, pp 147–160
24. Mallat E, Barzen C, Klotz A, Brecht A, Gauglitz G, Barcelo D (1999) *Environ Sci Technol* 33:965–971
25. Hua P, Hole JP, Wilkinson JS, Proll G, Tschmelak J, Gauglitz G, Jackson MA, Nudd R, Griffith HMT, Abuknesha RA, Kaiser J, Kraemmer P (2005) *Opt Express* 13:1124
26. Klotz A (1998) *Fluoreszenzbasiertes optisches Biosensorsystem: Entwurf, Modellierung und Optimierung* (PhD thesis) University of Tuebingen <http://www.ub.uni-tuebingen.de/pro/elib/tobias.php>
27. Reder S (2003) *Multi-Analyt-Bestimmung von endokrinen Disruptoren im Wasser mit Hilfe eines Fluoreszenz-Immunoassays unter Verwendung von neuronalen Netzen* (PhD thesis) University of Tuebingen <http://www.ub.uni-tuebingen.de/pro/elib/tobias.php>
28. Tschmelak JM (2005) *New ultra-sensitive immunoassays for (Total Internal Reflectance Fluorescence) TIRF-based biosensors* (PhD thesis) Shaker Verlag Aachen
29. Dudley RA, Edwards P, Ekins RP, Finney DJ, McKenney IGM, Raab GM, Rodbard D, Rodgers RPC (1985) *Clin Chem* 31:1264
30. Inczedy J, Lengyel T, Ure AM (1998) *Compendium of analytical nomenclature. Definitive rules*. In: *The Orange Book*, 3rd edn. Blackwell Science, Oxford
31. O'Connell MA, Belanger BA, Haaland PD (1993) *Chemometr Intell Lab Sys* 20:97
32. Horwitz W, Kamps LR, Boyer KW (1998) *J Assoc Off Anal Chem* 63:1344
33. Meyer VR (2003) *Schweizerische Laboratoriums-Zeitschrift* 60:63
34. Proll G, Tschmelak J, Kaiser J, Krämer P, Stien J, Gauglitz G (2006) *Advanced Environmental Sensor for Water Monitoring*. In: *Nato Science Series IV: Earth and Environmental Sciences*, vol 69, 131–145
35. Tschmelak J, Proll G, Riedt J, Kaiser J, Kraemmer P, Bárzaga L, Wilkinson JS, Hua P, Hole JP, Nudd R, Jackson M, Abuknesha R, Barceló D, Rodriguez-Mozaz S, López de A, Sacher F, Stien J, Slobodník J, Oswald P, Kozmenko H, Korenková E, Tóthová L, Krascšenits Z, Gauglitz G (2005) *Biosens Bioelectron* 20:1499
36. Tschmelak J, Proll G, Riedt J, Kaiser J, Kraemmer P, Bárzaga L, Wilkinson JS, Hua P, Hole JP, Nudd R, Jackson M, Abuknesha R, Barceló D, Rodriguez-Mozaz S, López de A, Sacher F, Stien J, Slobodník J, Oswald P, Kozmenko H, Korenková E, Tóthová L, Krascšenits Z, Gauglitz G (2005) *Biosens Bioelectron* 20:1509

# Fluorescence Sensing and Imaging Using Pressure-Sensitive Paints and Temperature-Sensitive Paints

Matthias I. J. Stich · Otto S. Wolfbeis (✉)

Institute of Analytical Chemistry, Chemo- and Biosensors, University of Regensburg,  
93040 Regensburg, Germany  
*otto.wolfbeis@chemie.uni-r.de*

<b>1</b>	<b>Introduction</b> . . . . .	432
<b>2</b>	<b>Background</b> . . . . .	432
2.1	Quenching of Luminescence . . . . .	433
2.2	Pressure-Sensitive Paints (PSPs) and Temperature-Sensitive Paints (TSPs) . . . . .	434
<b>3</b>	<b>Materials for Use in Pressure-Sensitive Paints and Temperature-Sensitive Paints</b> . . . . .	435
3.1	Indicators for Use in Pressure-Sensitive Paints . . . . .	435
3.2	Polymers for Use in Pressure-Sensitive Paints . . . . .	438
3.3	Electrochemical Coating . . . . .	441
3.4	Indicators for Use in Temperature-Sensitive Paints . . . . .	442
3.5	Polymers for Use in Temperature-Sensitive Paints . . . . .	443
<b>4</b>	<b>Spectroscopic Methods of Interrogation</b> . . . . .	445
4.1	Rapid Lifetime Determination (RLD) . . . . .	448
4.2	Multiple Gate Methods . . . . .	450
<b>5</b>	<b>Requirements and Characteristics of the Imaging Setup</b> . . . . .	451
5.1	Camera Systems . . . . .	451
5.1.1	Interline Charge Coupled Device Cameras . . . . .	452
5.1.2	Frame Transfer Charge Coupled Device Cameras . . . . .	453
5.1.3	Full Frame Charge Coupled Device Cameras . . . . .	453
5.1.4	Intensified Charge Coupled Device Cameras . . . . .	454
5.1.5	Areas of Application of the Various Cameras . . . . .	454
5.2	Light Sources . . . . .	455
5.3	Software . . . . .	456
<b>6</b>	<b>State of the Art</b> . . . . .	456
<b>7</b>	<b>Current Challenges and Limitations</b> . . . . .	457
	<b>References</b> . . . . .	457

**Abstract** Pressure-sensitive paints (PSPs) and temperature-sensitive paints (TSPs) are widely used in aerodynamic research and wind tunnel testing. Both systems are based on the incorporation of the respective indicators into a matrix polymer (often referred

to as the “binder”) to be cast on the area of interest. Spatially resolved distributions of oxygen partial pressure ( $pO_2$ ) and temperature can be instantly visualized by making use of respective paints and appropriate techniques of fluorescence imaging.

This chapter summarizes state of the art in probes and polymers for use in PSPs and TSPs. Fluorescence spectroscopic methods for the interrogation of the paints are described along with the components and respective experimental setups. Finally, we discuss the advantages and drawbacks of various systems and methods, along with their utility in various fields of applications.

**Keywords** Fluorescence · Optical imaging · Temperature-sensitive paint · Pressure-sensitive paint (PSP) · Sensor

### Abbreviations

A	Absorption
$A_X$	Number of gate/window
Abs.	Absorption
Bs	Brightness
CCD	Charge coupled device
DLD	Dual lifetime determination
DLR	German Aerospace Center (Deutsches Zentrum für Luft- und Raumfahrt) Dual Lifetime referencing
E	Emission
$\varepsilon$	Extinction coefficient
EC	Ethyl cellulose
Em.	Emission
EMCCD	Electron multiplying CCD
Eq.	Equation
Eu(tta) <sub>3</sub> (pat)	Europium-tris(thenoyltrifluoroacetyl-acetonato)-(2,6-di(dimethyl-pyrazole)-4- <i>N,N</i> -diethylaniline)-triazine
F	Fluorescence intensity
fd	Frequency domain
FII	Fluorescence intensity imaging
$\phi_f$	Quantum yield
$\Delta\Phi$	Phase shift
FIB	Random co-polymer of heptafluoro- <i>n</i> -butyl methacrylate and hexafluoroisopropyl methacrylate
FLIM	Fluorescence lifetime imaging
$\Gamma$	Emissive rate
Gate width	The time over which luminescence intensity is gathered
$h\nu$	Energy of a photon
IC	Internal conversion
ICCD	Intensified charge coupled device
Int.	Intensity
ISC	Intersystem crossing
JAXA	Japan Aerospace Exploration Agency
$k_{nr}$	Rate of nonradiative decay
$K_{SV}$	Stern–Volmer constant
$\lambda$	Wavelength
LED	Light emitting diode

LT	Lifetime
MgTFPP	Magnesium-5,10,15,20-tetrakis-(2,3,4,5,6-pentafluorophenyl)-porphyrin
MLC	Metal-ligand complex
MLCT	Metal-to-ligand charge transfer
NASA	National Aeronautic and Space Administration (USA)
norm.	Normalized
$p$	Pressure
$P$	Diffusion coefficient
PAN	Poly(acrylonitrile)
PBA	Pyrene butylic acid
$p\text{CO}_2$	Partial pressure of carbon dioxide
PDMS	Poly(dimethylsiloxane)
PDR	Phase delay rationing
PdTFPP	Palladium-5,10,15,20-tetrakis-(2,3,4,5,6-pentafluorophenyl)-porphyrin
PdOEP	Palladium-2,3,7,8,12,13,17,18-octaethyl-porphyrin
PMMA	Poly(methyl methacrylate)
$p\text{O}_2$	Partial pressure of oxygen
poly(IBM- <i>co</i> -TFEM)	Poly(isobutyl methacrylate- <i>co</i> -trifluorethyl methacrylate)
PolyTMSP	Poly(1-trimethylsilyl-1-propyne)
PS	Polystyrene
PSA	Pyrene sulfonic acid
PSAN	Poly(styrene- <i>co</i> -acrylonitrile)
PSP	Pressure-sensitive paint
PtOEP	Platinum-2,3,7,8,12,13,17,18-octaethyl-porphyrin
PtTFPP	Platinum-5,10,15,20-tetrakis-(2,3,4,5,6-pentafluorophenyl)-porphyrin
PtTFPPL	Platinum-5,10,15,20-tetrakis-(2,3,4,5,6-pentafluorophenyl)-porpholactone
PVC	Poly(vinyl chloride)
PVMK	Poly(vinyl methyl ketone)
PVP	Poly(vinyl pyrrolidone)
QY	Quantum yield
R	Relaxation
RLD	Rapid lifetime determination
$\text{Ru}(\text{dpp})_3^{2-}$	Ruthenium-tris(4,7-diphenyl-1,10-phenanthroline)
$\text{Ru}(\text{phen})_3^{2-}$	Ruthenium-tris(1,10-phenanthroline)
$S_0$	Electronic ground state (singlet)
$S_1$	First excited singlet state
$S_2$	Second excited singlet state
SNR	Signal-to-noise ratio
$T_1$	First excited triplet state
$t$	Time
$\tau$	Lifetime
td	Time domain
Trans.	Transmission
TSP	Temperature-sensitive paint



## 1

### Introduction

The determination of oxygen is most important in almost every field of science, research, and technology. Pressure (or oxygen partial pressure) as well as temperature are omnipresent factors, influencing almost every measurement of other parameters. The problem of determining the pressure of the ambient atmosphere was solved in the seventeenth century. However, it took quite a long time until man was able to continuously measure the concentration of oxygen in liquids. This was achieved by Leland Clark in 1954 with his so-called Clark oxygen electrode [1]. This was the first commercially available device for  $pO_2$  determination, but it was not applicable to measurement of oxygen distribution or surface flow.

In the early 1930's, Kautsky and Hirsch described the decrease of the luminescence intensity of organic dyes adsorbed onto silica when exposed to oxygen [2]. Fifty years later, Peterson and Fitzgerald utilized this effect for studies of flow over airfoil shapes [3]. The idea of pressure-sensitive paints was born therewith. First research on the application of pressure-sensitive paints (PSPs) was performed in the former Soviet Union at the Central Aerohydrodynamic Institute, Moscow (TsAGI). Since then, numerous other aerodynamic research facilities all over the world have applied and advanced the technique. These include National Aeronautic and Space Administration (NASA) (USA) [4], Japan Aerospace Exploration Agency (JAXA) [5], ONERA (France) [6], and the German Aerospace Center (DLR) [7].

Since every pressure-sensitive dye displays a more or less strong cross-sensitivity towards temperature, there is also a large interest in temperature-sensitive paints (TSPs) to gather information on the overall temperature distribution, so to compensate for the effect of temperature on the PSP.

Aside from its use in aerodynamic research, pressure/oxygen imaging has become important in the medical and pharmaceutical sciences, due to the possibility of performing noninvasive measurements [8–20].

## 2

### Background

The phenomenon of the quenching of luminescence by quenchers, such as oxygen not only forms the basis for various methods and applications in (bio)analytical chemistry and in physics [21–26], but is also the fundamental process of pressure-sensitive paints.

## 2.1

### Quenching of Luminescence

The intensity of fluorescence can be decreased by various processes and mechanisms. One of these processes, beside energy transfer and electron transfer, is called quenching. Common quenchers include oxygen, halides, heavy metal ions, amines, and electron deficient molecules like nitroaromatics and acrylamide. Generally, two different mechanisms of quenching are observed, namely, collisional dynamic and static quenching. The phenomenon of static quenching, where the quencher is forming a complex with the fluorophore, will not be discussed here, since it plays no role in pressure-sensitive and temperature-sensitive paint technology. Collisional quenching occurs when the excited state of a fluorophore is deactivated via molecular collisions. The fluorophores are not chemically altered in this process. The excited state is depopulated in a nonradiative way. The quantum yield decreases with the rate of nonradiative decay. The luminescence lifetime also decreases with decreasing quantum yield [24, 27–29]. Most organic luminophores emit from a singlet excited state with decay times up to 20 ns (with a few exceptions). In contrast, metal-ligand complexes (MLCs), emit from a state of higher multiplicity and have much longer decay times. Therefore, they are easily quenched by oxygen (which itself has a triplet ground state) via triplet-triplet annihilation. MLCs are not quenched by oxygen to the same extent. For example, ruthenium complexes are more strongly affected than europium complexes. This is due to the possibility of the transition of the triplet state to the *f*-orbital of the europium metal center, resulting in a long lived luminescence from that state. Thus, the triplet state is depopulated by this mechanism before being annihilated by triplet oxygen.

For collisional quenching, a relationship between the luminescence intensity, and thus in lifetime, and air pressure was described by Stern and Volmer in 1919:

$$\frac{I_{\text{ref}}}{I} = 1 + K_{\text{SV}} \cdot [Q] = \frac{\tau_{\text{ref}}}{\tau}, \quad (1)$$

where  $K_{\text{SV}}$  is the Stern–Volmer quenching constant,  $[Q]$  the concentration of the quencher,  $I$  the intensity, and  $\tau$  the lifetime, whilst  $I_{\text{ref}}$  and  $\tau_{\text{ref}}$ , respectively, are the intensities and lifetimes under reference condition, in the majority of cases in absence of the quencher. Equation 1 is the simplest form of the Stern–Volmer equation, and is well applicable to molecules in solution. The term  $K_{\text{SV}}$  contains the unquenched luminescence lifetime and a diffusion-controlled bimolecular rate constant. In solution, the diffusion of the dye molecule and the quenching species remains the same throughout the entire volume. Plotting the intensity or lifetime ratio versus the quencher concentration gives a linear dependency with the Stern–Volmer constant as the slope.

The PSP and TSP technique makes use of solid phases. Thus, free diffusion of the dye and the quencher is compromised, and deviations can occur from the strictly linear dependence of the intensity or lifetime on the quencher concentration. Hence, a modified Stern–Volmer equation, which reflects the fact that fluorophores are located at different chemical environment and, thus, have different quencher accessibility, has to be applied:

$$\frac{I_{\text{ref}}}{I} = \frac{\tau_{\text{ref}}}{\tau} = \left( \frac{f_1}{1 + K_{\text{SV}}^{(1)} \cdot [Q]} + \frac{f_2}{1 + K_{\text{SV}}^{(2)} \cdot [Q]} + \frac{f_3}{1 + K_{\text{SV}}^{(3)} \cdot [Q]} + \dots \right)^{-1}. \quad (2)$$

It turns out that terminating Eq. 2 after the second term is an acceptable simplification to describe quenching in heterogeneous polymers. The simplified equation is referred to as the two-site-model [27–34].

Quenching by temperature (in contrast to oxygen quenching) is not based on the interaction of two species. Rather, it is directly affected by the energy levels of the orbitals involved, e.g., the  $d-d$  orbital and the metal-ligand charge transfer (MLCT) in metal-ligand complexes, and the energy gaps between these. For luminescence to occur, the  $d-d$  state has to lie above the MLCT state. The energy of the states can be altered by the addition of thermal energy. Furthermore, additional thermal energy increases the probability of electron transitions between the two states involved. This happens with a defined rate constant and depends on the characteristics of the molecule. The rate constant changes with temperature and can be described by

$$\frac{d \ln k}{dT} = \frac{E_a}{RT^2} \quad (3)$$

or the integrated form

$$\ln k = \ln A - \frac{E_a}{RT}, \quad (4)$$

where  $k$  is the rate constant,  $R$  the real gas constant,  $T$  the temperature, and  $E_a$  the Arrhenius activation energy. The temperature sensitivity of a pressure-sensitive paint can be described by

$$\ln \left( \frac{I_{\text{ref}}(T_{\text{ref}})}{I(T)} \right) = - \frac{E_a}{R} \left( \frac{1}{T} - \frac{1}{T_{\text{ref}}} \right). \quad (5)$$

If the energy gap between the electronic states involved is small, the luminescence is quenched by temperature. An increase in temperature will then cause a large decrease of both luminescence intensity and lifetime [35, 36].

## 2.2

### Pressure-Sensitive Paints (PSPs) and Temperature-Sensitive Paints (TSPs)

The function of PSPs relies on the principle of collisional quenching by oxygen of the luminescence intensity and, accordingly, of lifetime. The indicator

dyes are incorporated into a polymeric matrix or encapsulated inside polymer particles. The PSP is then cast on the surface or structure of interest. The photoluminescence intensity depends on the oxygen partial pressure of the ambient air. The process is fully reversible. By imaging the surface, pressure distributions can be visualized with high spatial resolution.

Unfortunately, all dyes employed in PSPs are more or less sensitive to temperature. Metal-ligand complexes (MLCs) are often used as pressure indicators, due to their large Stokes' shifts. The temperature dependence of MLCs is particularly expressed. Since altering the pressure flow often entails a change in temperature, the calculation of the pressure at a certain point is only possible with the knowledge of the temperature at this very point.

Intensity is the most frequently acquired parameter. This is convenient but it implies several problems and sources of error. These include (a) small deviations in the PSP distribution, (b) inhomogeneities of the paint, (c) defects on the sample surface, and (d) imperfectly installed light sources. Time-gated fluorescence lifetime imaging can help to avoid some of these disadvantages [37, 38].

### 3

#### **Materials for Use in Pressure-Sensitive Paints and Temperature-Sensitive Paints**

These have to meet a variety of stipulations. Indicators are expected to possess high quantum yields, large absorption coefficients (and, thus, brightness), to be photostable, and to be excitable with low-cost light sources. Polymers for use in PSPs are expected to be good solvents for the luminophores, to have good and fast permeability for oxygen, to be sprayable, and to have good adhesion to the support.

#### 3.1

##### **Indicators for Use in Pressure-Sensitive Paints**

Amongst the variety of luminescent molecules, only few are suitable for use in pressure-sensitive paints. With respect to luminescence intensity, the dyes have to be as bright as possible. The brightness ( $B_s$ ) of a luminophore is defined as the product of molar absorbance ( $\epsilon$ ) and the quantum yield ( $\phi$ ). For example, the  $\text{Ru}(\text{dpp})_3^{2+}$  complex has a molar absorbance ( $\epsilon$ ) of  $\sim 30\,000\text{ L}/(\text{mol cm})$ , and a quantum yield of 0.36 and, thus, a brightness of 10 800 for deoxygenated conditions. Under ambient air pressure, the quantum yield drops to about 0.2, and, therefore, the brightness drops to  $\sim 6000$ .

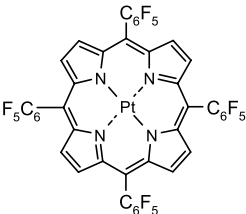
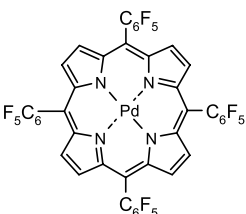
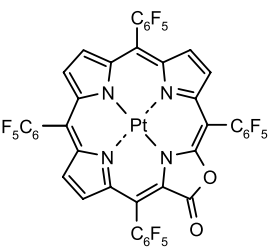
One of the widely used classes of molecules is the family of the polycyclic aromatic hydrocarbons (PAHs), such as pyrene. The luminescence decay of pyrene occurs in the nanosecond timescale, which makes it more difficult to determine lifetime changes due to quenching. Metal-ligand complexes typic-

ally display lifetimes between hundreds of nanoseconds up to several milliseconds, but only few have quantum yields comparable to the PAHs. In fact, there is no ideal luminescent molecule suitable for all kinds of PSP measurements. Important probes for use in PSPs are listed in Tables 1 and 2.

**Table 1** Names, acronyms, and chemical structures of typical indicators for use in PSPs

Compound [acronym]	Chemical structure
Pyrene	
Decacyclene	
Ruthenium(II)-tris(4,7-diphenyl-1,10-phenanthroline) [Ru(dpp) <sub>3</sub> <sup>2+</sup> ] (various counter ions)	
Platinum(II)-2,3,7,8,12,13,17,18-octaethyl-porphyrin [PtOEP]	
Palladium(II)-2,3,7,8,12,13,17,18-octaethyl-porphyrin [PdOEP]	

**Table 1** (continued)

Compound [acronym]	Chemical structure
Platinum(II)-5,10,15,20-tetrakis-(2,3,4,5,6-pentafluorophenyl)-porphyrin [PtTFPP]	
Palladium(II)-5,10,15,20-tetrakis-(2,3,4,5,6-pentafluorophenyl)-porphyrin [PdTFPP]	
Platinum(II)-5,10,15,20-tetrakis-(2,3,4,5,6-pentafluorophenyl)-porpholactone [PtTFPL]	

The polycyclic aromatic hydrocarbons (PAHs) are efficiently quenched by oxygen and were first applied in optical (fiber) sensors [40, 56]. They exhibit bright emission, but many of them lack photostability and some need short-wave excitation.

Ruthenium-tris(4,7-diphenyl-1,10-phenanthroline) is not a very bright luminophore compared to the PAHs, but it possesses an unusually long luminescence lifetime. The complexes are more stable against photodecomposition and are excitable with blue light. In the past, this was a great advantage due to the high costs of light sources for the UV region [50].

The porphyrin platinum complexes show intense luminescence at room temperature, possess a high quantum yield of over 50%, and are, therefore, very bright: PtTFPP, for example, has a  $\phi$  of 0.6 at an  $\varepsilon$  of 323 000 (Soret band) and 23 200 (non-Soret band), respectively [57]. Obviously, the brightness is

**Table 2** Properties of typical indicators for use in PSPs

Compound	$\lambda_{\text{abs}}(\text{max})$	$\lambda_{\text{em}}(\text{max})$	Refs.
Pyrene	335 nm	395 nm (monomer) 475 nm (excimer)	[6, 7, 39]
Decacylcene	385 nm	510 nm	[40–42]
Ru(dpp) <sub>3</sub> <sup>2+</sup>	337 nm 457 nm	610 nm	[43–48]
PtOEP	381 nm (Soret) 535 nm (non-Soret)	646 nm	[37, 49, 50]
PdOEP	393 nm (Soret) 512 nm (non-Soret) 546 nm (non-Soret)	663 nm	[50, 51]
PtTFPP	395 nm (Soret) 541 nm (non-Soret)	648 nm	[52, 53]
PdTFPP	407 nm (Soret) 518 nm (non-Soret) 552 nm (non-Soret)	653 nm	[34]
PtTFPL	392 nm (Soret) 572 nm (non-Soret)	745 nm	[38, 54, 55]

much higher if excitation is performed at the wavelength of the Soret band. The palladium or platinum octaethyl porphyrins immobilized in polymer matrices undergo photobleaching [50, 58]. Fluorinated porphyrin derivatives, like PtTFPL, are more photostable [52, 59].

### 3.2

#### Polymers for Use in Pressure-Sensitive Paints

The polymer (often referred to as the “binder”) is the second important component of a PSP [60, 61]. It attaches the indicator on the solid support. However, not all kinds of polymers are suitable for the use in PSP formulations. The pressure-sensitive indicator dye has to be soluble in the binder (unless it is suspended). Furthermore, the binder has to be soluble in an appropriate solvent, so that it can be sprayed or spread on the surface of interest. It is of particular importance that the polymer is inert. It should not contain any functional groups that may affect the luminescence of the PSP. Even carboxy groups, for instance, can act as quencher.

Moreover, the polymer has to comply with two important conditions; It should be mechanically stable and it should display a high and constant permeability for oxygen. This permeability depends on various factors and is not directly a function of the polymer’s chemical structure. Rather, it depends on the orientation and density of the macromolecules, and on the thickness of the coating. The most common parameter for quantifying the diffusion of

oxygen through a polymer is the so-called permeability coefficient,  $P$ .

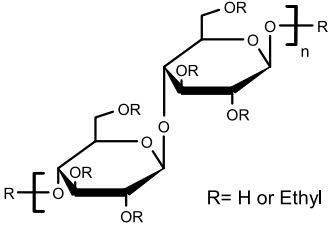
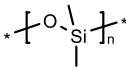
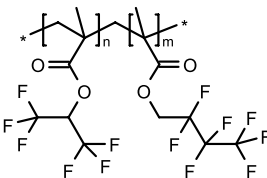
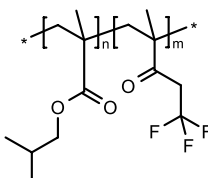
$$P = \frac{(\text{thickness of the polymer film}) \cdot (\text{quantity of oxygen})}{(\text{area}) \cdot (\text{time}) \cdot (\text{pressure drop across the film})} \quad (6)$$

The temperature dependence of the permeability coefficient is given by:

$$P = P_0 \cdot \exp\left(-\frac{E_p}{RT}\right), \quad (7)$$

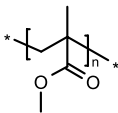
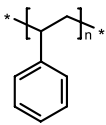
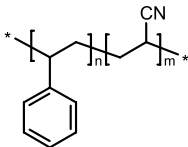
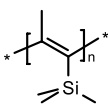
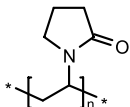
where  $P_0$  is a pre-exponential factor,  $E_p$  the activation energy of permeation,  $R$  the gas constant, and  $T$  the temperature in Kelvin. For the application in PSP, the permeability coefficient should be constant over a wide temperature range or, ideally, be completely independent of temperature. An overview on polymers for the application in PSPs is given in Table 3.

**Table 3** Names, acronyms, and chemical structures of selected polymers for use in PSPs

Polymer [acronym]	Structure
Ethyl cellulose [EC]	 <p>R = H or Ethyl</p>
Poly(dimethylsiloxane) [PDMS]	
Poly(hexafluoroisopropyl methacrylate- <i>co</i> -heptafluoro- <i>n</i> - butyl methacrylate) [FIB]	
Poly(isobutyl methacrylate- <i>co</i> -trifluoroethyl methacrylate) [Poly(IBM- <i>co</i> -TFEM)]	



**Table 3** (continued)

Polymer [acronym]	Structure
Poly(methyl methacrylate) [PMMA]	
Polystyrene [PS]	
Poly(styrene-co-acrylonitrile) [PSAN]	
Poly(trimethylsilyl-propyne) [PolyTMSP]	
Poly(vinyl pyrrolidone) [PVP]	

**Table 4** Figures of merit for selected polymers for use in PSPs

Polymer	$T$ [°C]	$P$ $\left[ 10^{-13} \frac{\text{cm}^3 \text{ cm}}{\text{cm}^2 \text{ s Pa}} \right]$	Refs.
EC	25	11.0	[62]
PDMS	35	695	[63]
FIB		n.d.	[64, 65]
Poly(IBM-co-TFEM)		n.d.	[65, 66]
PMMA	34	0.116	[65, 67]
PS	25	1.9	[65, 67]
PSAN	25	0.0032	[65, 68]
PolyTMSP		n.d.	[69]

Polymers for use in PSPs can be divided in three classes: silicones, organic glassy polymers, and fluoropolymers. Silicones like poly(trimethylsilyl-1-propyne) excel in oxygen permeability, but often are not stable over a longer

period of time. In case of the double bond is not stable towards irradiation. This makes the polymer lose its outstanding permeability over time.

Organic glassy polymers like polystyrene or poly(styrene-*co*-acrylonitrile) are much easier to handle. They do not possess the high permeability compared to the silicones, but are mechanically stable, and their properties are not altered when cast on solid supports in PSP applications. The field of practicability of some components is limited, due to the rather low glass transition temperature and the rather low melting point of certain polymers. Polystyrene, for example, has a glass transition temperature of  $\sim 90^\circ\text{C}$  [70] and a melting point of  $\sim 240^\circ\text{C}$  [71]. Thus, polystyrene is not suitable for application in high-temperature oxygen sensing. Due to the simple chemistry behind the synthesis of the organic glassy polymers, it is possible to tailor binders with properties close to those desired.

The fluoropolymers feature high oxygen permeability and often are more stable than the silicones. Like highly fluorinated indicators, they are more resistant to photo-oxidation. The carbon-fluorine bond is stable towards singlet oxygen which is being formed after photoexcitation of the probe [72]. Because of their outstanding properties, the fluorinated polymers have become important in aeronautic applications. Poly(hexafluoroisopropylmethacrylate-*co*-heptafluoro-*n*-butyl methacrylate) ("FIB", from fluoro/isopropyl/butyl) is the American standard binder in PSPs [64]. However, FIB polymers require the use of hazardous solvents, such as  $\alpha,\alpha,\alpha$ -trifluorotoluene, in order to make it sprayable.

Polymers like poly(vinyl pyrrolidone) or some polyurethane-based polymers are soluble in water and ethanol, and easier to handle. The corresponding solvents are less toxic or less environmentally harmful. Unfortunately, the permeability of these polymers for oxygen strongly depends on the fraction of water in the polymer. Thus, the binders are cross-sensitive to humidity. Accordingly, these kinds of polymers are not suitable for high-temperature PSPs [73–76].

### 3.3

#### Electrochemical Coating

Any binder will decrease the accessibility of oxygen to the luminescent indicator. This compromises the response time of paints. The groups of Sakaue et al. and of Asai et al. have developed an approach in which no polymer binder is needed, reducing the response time to a minimum. Aluminum surfaces were treated with different acids and bases, and were then electrochemically anodized. This results in a porous metal surface. The size and depth of the pores are very uniform, with a pore diameter of  $\sim 20$  nm and a layer thickness of  $\sim 10$  mm. If treated with its concentrated solution, the pressure indicator will diffuse into the pores and will be adsorbed at the surface of the anodized aluminum. In this kind of PSPs, the response time to pressure shocks

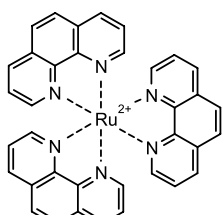
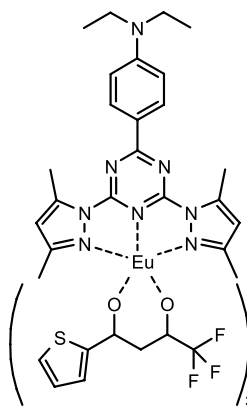
is only limited by the luminescence lifetime of the indicator applied and can be compared to those of electric pressure transducers [6, 43, 65, 77–79]. Unfortunately, this approach is limited to aluminum surfaces. Furthermore, the adsorption of indicators onto the porous aluminum surface turns out to be difficult in some cases.

### 3.4 Indicators for Use in Temperature-Sensitive Paints

All known indicators used in pressure-sensitive paints have a temperature-dependent luminescence. This affects both intensity and lifetime. Nevertheless, in most cases mathematical algorithms can be used to correct the effects of temperature. Alternatively, a temperature-sensitive (but oxygen-insensitive) probe may be added to the pressure-sensitive paint [80].

There is also a need to determine temperature only, for example in cryogenic wind tunnel tests or for combustion studies in turbochargers and turbines. Consequently, certain indicators have to withstand tempera-

**Table 5** Structure of important indicators for use in TSPs

Compound	Structure
La <sub>2</sub> O <sub>2</sub> S:Eu <sup>3+</sup>	
Ruthenium-tris(1,10-phenanthroline) [Ru(phen) <sub>3</sub> <sup>2+</sup> ] (various counter ions)	
Europium-tris(thenoyltrifluoroacetyl- acetonato)-(2,6-di(dimethylpyrazole)- 4- <i>N,N</i> -diethylaniline)-triazine [Eu(tta) <sub>3</sub> (pat)]	

**Table 6** Properties of important indicator materials for use in TSPs

Compound	$\lambda_{\text{abs}}(\text{max})$	$\lambda_{\text{em}}(\text{max})$	Refs.
$\text{La}_2\text{O}_2\text{S}:\text{Eu}^{3+}$	385 nm	514 nm	[81, 83]
$\text{Ru}(\text{phen})_3^{2+}$	448 nm	579 nm	[85–87]
$\text{Eu}(\text{tta})_3(\text{pat})$	417 nm	614 nm	[68, 87, 88]

tures up to 2000 °C. The first substances applied for that purpose were inorganic compounds, the so-called thermographic phosphors. Temperature distribution imaging was formerly termed thermographic phosphor thermography (TPT). They are now referred to as temperature-sensitive paints (TSP) [76, 81–84]. More recently, metal-ligand complexes are being used as temperature probes but are hardly applicable at temperatures above 200 °C. Important indicators for application in TSPs are listed in Tables 5 and 6, respectively.

Temperature sensing may also be performed using infrared cameras. This method (IR-thermography) is a powerful tool for direct visualization of temperature gradients, but is applicable only to a limited extent, since the spatial resolution of infrared cameras is poor and the sensitivity at low temperatures is inadequate. This can be improved, however, by cooling the charge coupled device (CCD) chip with liquid nitrogen or helium [89].

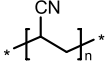
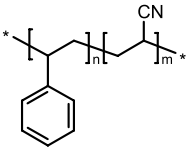
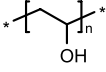
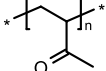
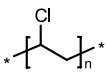
There is a large variety of indicators for thermographic phosphor thermography, for example,  $\text{La}_2\text{O}_2\text{S}:\text{Eu}^{3+}$ ,  $\text{Y}_2\text{O}_3:\text{Eu}$ , or  $\text{YAG}:\text{Dy}$  [82]. These inorganic compounds are very robust in terms of thermal stability. Nevertheless, a lot of research is required in order to develop temperature-sensitive metal-ligand complexes for certain temperature ranges. This is because of (a) the lack of sensitivity in the temperature range between 0 and 100 °C, and (b) the limited brightness ( $B_s$ ; see Sect. 3.1) of thermographic phosphors, due to their low molar absorbances.

### 3.5

#### Polymers for Use in Temperature-Sensitive Paints

As in the case of PSPs, the polymers for use in TSPs have to be mechanically stable, of course. On the other hand, they do not need not be permeable to oxygen or other gases [61]. The chemical stability and photostability of the paints is a critical issue, as they tend to crack because of the uneven thermal contraction and expansion of the binder and the thermographic phosphor, respectively [81–83]. To eliminate any cross-sensitivities of temperature probes to oxygen, gas-blocking polymers have been used. The chemical structures and properties of common binders for TSP applications are listed in Tables 7 and 8, respectively. The polymers listed in Table 7 have very low  $P$

**Table 7** Chemical structures and permeability coefficients ( $P$ ; at 25 °C) of polymers for use in TSPs

Polymer	Chemical structure
Poly(acrylonitrile) [PAN]	
Poly(styrene- <i>co</i> -acrylonitrile) [PSAN]	
Poly(vinyl alcohol) [PVA]	
Poly(vinyl methyl ketone) [PVMK]	
Poly(vinyl chloride) [PVC]	

**Table 8** Permeability coefficients ( $P$ ; at 25 °C) of typical polymers for use in TSPs

Polymer	$P \left[ 10^{-13} \frac{\text{cm}^3 \text{cm}}{\text{cm}^2 \text{s Pa}} \right]$	Refs.
PAN	0.00015	[87, 90]
PSAN	0.0032	[87, 90]
PVA	0.00665 <sup>a</sup>	[90]
PVMK	n.d.	[87]
PVC	0.034 <sup>b</sup>	[90]

<sup>a</sup> at 0% relative humidity<sup>b</sup> unplasticized

values and, thus, prevent diffusion of singlet oxygen, which can be harmful to both the probe and the polymer.

## 4 Spectroscopic Methods of Interrogation

There is a large variety of methods for calibrating and evaluating PSPs and TSPs. The most common optical parameters determined are the intensity or decay time of luminescence. They can be measured using different calibration schemes, each of them having its own advantages and limits. The parameters intensity and lifetime are compared in Table 9, with respect to their pros and cons.

In the simplest case, luminescence is excited continuously and luminescence intensity is imaged. The light source and the CCD camera are controlled and triggered by a computer. The data are conveyed to the CPU and processed. This method is common not only in case of PSPs and TSPs, but also in fluorescence microscopy, where the analyte (oxygen in the case of PSPs) causes a change in the luminescence intensity of the sensor, which is related to its concentration [90–92]. However, the luminescence intensity detected by the CCD camera is not only dependent on the probe concentration ( $c$ ). This makes intensity-based methods prone to errors. The intensity response is directly dependent on the intensity of the excitation light. On one hand, this is advantageous because very high intensities can be achieved by making use of lasers. On the other hand, small deviations in the excitation light field will cause variations in the local intensity (see Fig. 1). Furthermore, the light in-

**Table 9** Advantages and disadvantages of pressure sensing and temperature sensing based on measurement of  $I$  and  $\tau$ , respectively

Pros	Cons
<i>Intensity</i>	
high intensity in case of strong light sources	prone to errors (caused by e.g. uneven coatings or deviations in dye concentration)
simple	dependent on several factors
inexpensive	light field has to be very homogeneous
numerous indicators available	not self-referenced
–	sensitive to changes in the experimental geometry
<i>Lifetime</i>	
independent of the intensity of the excitation light	more expensive experimental setup
self-referenced	more complex data handling
independent of the setup	limited number of indicators available
defined lifetime for given indicator	–

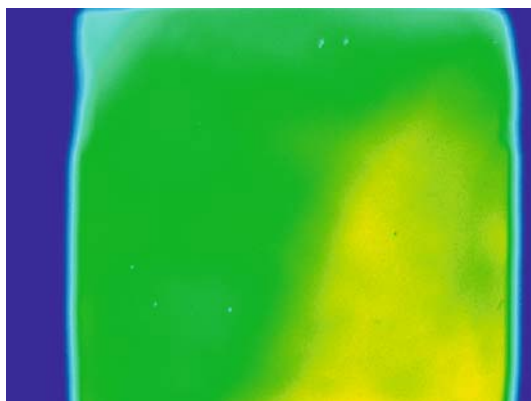


**Fig. 1** Pseudo-color intensity image of Platinum-5,10,15,20-tetrakis-(2,3,4,5,6-pentafluorophenyl)-porphyrin (PtTFPP) in poly(styrene-*co*-acrylonitrile) (PSAN) with a non-ideal excitation light alignment. The resulting deviations in the intensity response result from strong excitation light coming from the lower right corner

tensity is a function of distance. The geometry of the system also plays an important role, causing deviations in the response when slightly changed.

At present, there is no perfect PSP. Deviations in the layer thickness and dye concentration,  $c$ , result in a non-homogeneous intensity response of the sensor. To avoid this problem, reference dyes, which are widely inert to temperature, are incorporated into the PSP composition. Thus, the intensity response of the indicator can be related to the intensity of the reference dye, resulting in a ratio of intensities being only dependent on oxygen concentration.

Additionally, white pigments are often added in order to increase luminescence intensity. The emission of light from PSPs and TSPs has no preferred direction. White additives like titanium dioxide can increase the luminescence seen by the camera.

When studying non-flat surfaces and models with a 3D-structure, additional problems may arise. The excitation light can be reflected at a surface and can excite the PSP or TSP of another area, leading to falsified images. This effect can be prevented to some extent by using base coats. These are pigments either applied as additional layer with an extra polymer, or incorporated in the paint. Base coats can be designed to absorb in the UV-region, thus, eliminating the reflection of UV excitation light.

One example for such an intensity based PSP formulation is the system applied at the German Aerospace Centre (DLR). It is composed of a pyrene derivative acting as the pressure-sensitive probe, and a europium complex as a reference dye whose emission is not affected by pressure. Both components are excited at 337 nm. The excimer emission of the pyrene is monitored to acquire the pressure information, while the emission of the reference dye is

only dependent on the amount of the complex excited [7]. The ratio,  $R$ , between  $S_{\text{PSP}}$  and  $S_{\text{ref}}$  is independent of light source fluctuations and effects of reflection. As a result, such effects and self-illumination can be referenced out. In addition, the adverse effect of uneven surfaces and reflections of the excitation beam can be eliminated for the most part. In wind tunnel applications, these measurements are called wind-off images, taken at a well known pressure and defined temperature. The pressure dependence and temperature dependence of the paint can be described by a modified Stern–Volmer relationship [33]:

$$f_T(p, p_0) = \frac{I(p_0, T)}{I(p, T)} \quad (8)$$

for the pressure dependence of the intensity at a constant temperature, and

$$g_p(T, T_0) = \frac{I(p, T)}{I(p, T_0)} \quad (9)$$

for the temperature dependence of the intensity at constant pressure, with  $p_0$  and  $T_0$  as reference pressure and temperature, respectively. The pressure-sensitive paint is referred to as ideal if the function  $f_T(p, p_0)$  is independent of temperature and if  $g_p(T, T_0)$  is independent of pressure. In wind tunnel applications, the intensity of the wind-off measurements is divided by the results of the intensity obtained at airflow. For the ideal paints, the ratio can be written as

$$\frac{I(p_0, T_0)}{I(p, T)} \approx \frac{f(p, p_0)}{g(T, T_0)}. \quad (10)$$

If the temperature dependency of the luminescence of the paint has been determined experimentally, Eq. 10 can be rewritten as

$$g(T, T_0) \frac{I(p_0, T_0)}{I(p, T)} \approx f(p, p_0). \quad (11)$$

If temperature is known, e.g. from IR thermography, the ratio of signals obtained at wind-off and at wind-on can be multiplied by a single function,  $g(T, T_0)$ , in order to obtain the temperature-corrected pressure dependent function  $f(p, p_0)$ . In the non-ideal case, the ratio of wind-off and wind-on measurements has to be multiplied by a function  $g_p(T, T_0)$ , which is unfortunately dependent on pressure. Thus, the temperature correction becomes more difficult, if not completely impossible [63, 64].

The measurement of fluorescence lifetime is superior to the intensity-based approach, because it is affected neither by scattering or reflection, the overall intensity of the light field, or by inhomogeneous thicknesses of



the paint. Lifetime can be measured in the time domain or the frequency domain [93–98]. The time-domain approach has rarely been applied for detecting lifetimes of PSPs in the nanosecond time scale. On the other hand, the required setup is less complex compared to the frequency-domain approach. Since the decay times of metal-ligand complexes (MLCs) are in the microsecond time scale, the time-domain approach along with the use of MLCs is the method of choice for aerodynamic and wind tunnel applications. The use of MLCs also enables the elimination of background fluorescence that usually decays with max. 100 ns and can thus be suppressed by starting the data acquisition after a delay time of typically >500 ns [93].

There are various methods and schemes for measuring luminescence lifetimes, for example, the “phase delay ratioing” (PDR) and the “dual lifetime referencing” (DLR) methods [99, 100]. They are described in another Section of this book. Important approaches (as they apply to PSPs and TSPs) will be discussed in the following sections.

#### 4.1

##### Rapid Lifetime Determination (RLD)

In the rapid lifetime determination (RLD) method, a square-shaped excitation pulse is applied, and luminescence is detected in two different gates, both located in the emission phase of the probe ( $A_1$  and  $A_2$ , see Fig. 2). The lifetime-dependent ratio of the two intensity images represents the intrinsically referenced response of the paint. It is often determined empirically [93–95, 101, 102]. The decay time  $\tau$  can be calculated according to

$$\tau = \frac{t_2 - t_1}{\ln \frac{A_1}{A_2}}, \quad (12)$$

where  $A_1$  and  $A_2$ , respectively, are the intensities of the two gates in the emission phase, and  $t_1$  and  $t_2$  are the times when the different gates are opened (relative to the end of the excitation pulse).

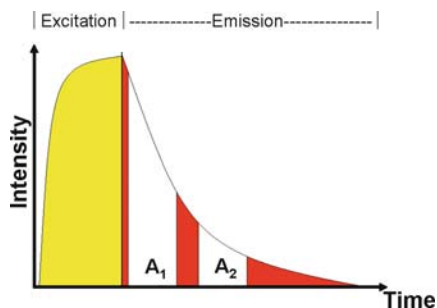


**Fig. 2** Schematic presentation of the Rapid Lifetime Determination (RLD) method

For calculating the lifetimes according to Eq. 12, the two time windows ( $A_1$  and  $A_2$ ) have to have the same length. As in the PDR method (see the chapter on “Intrinsically Referenced Fluorimetric Sensing and Detection Schemes” in this book.), it is difficult to obtain true values for the decay time, because the equation is only valid for monoexponentially decaying luminophores [103–105]. However, for imaging application, it is often sufficient to detect relative changes in lifetime.

Furthermore, RLD is less prone to interferences. It is not necessary to correct the alignment of the lightfield, because the luminescence decay time is independent of the overall intensity (see Fig. 3). On account of this, the effects of inhomogeneous indicator distribution within the sensor layer, coloration, turbidity, reflections, variations in the opto-electronic system, background luminescence, and varying distances between surface and camera also do not adversely affect accuracy. The method even tolerates low levels of ambient light and displacements in the optical setup between calibration and measurement [93, 101].

The RLD approach is a very powerful tool for the evaluation of luminescence lifetimes. However, the calculation (see Eq. 12) assumes monoexponential decay times. The RLD method is often performed with metal-

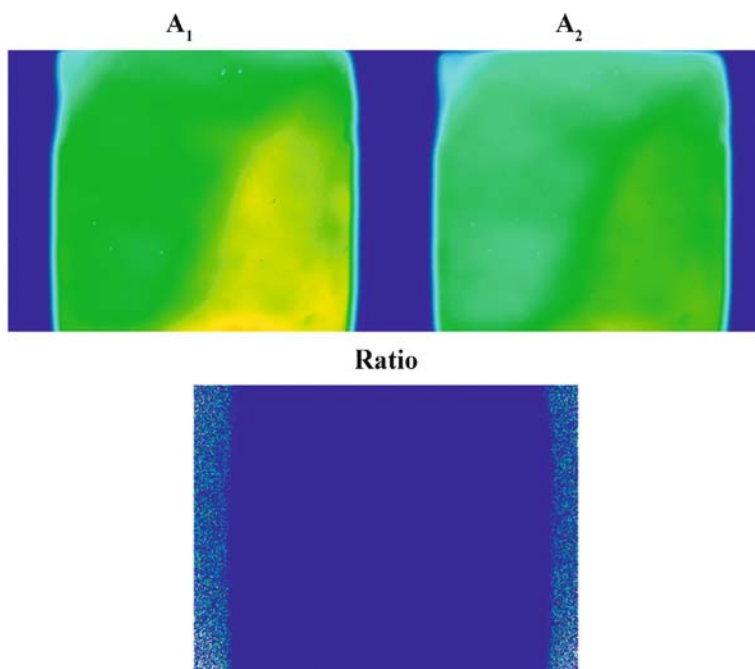


**Fig. 3** Pseudo-color images of PtTFPP in PSAN (same system as in Fig. 1) measured applying the RLD method. Variations in intensity are referenced out in the ratio image

ligand complexes, many of which exhibit a decay that is at least biexponential. Hence, much effort was made to modify the existing scheme in order to obtain more accurate data. This can be achieved by appropriate positioning of the gates. In case of a biexponential decay, a 50% overlap of the two gates ( $A_1$  and  $A_2$ ) enormously improves accuracy and precision of the resulting data [106]. Furthermore, the length of the gates and the relative position to each other play an important role for evaluating lifetimes [107]. Two or more different  $\tau$ -values are dominant for the slope of a multi-exponential decay curve at different times, respectively. Thus, the position of the gates may decisively influence the lifetime result data obtained. A look at a bi-exponential decay curve reveals that positioning windows  $A_1$  and  $A_2$  in the initial part of the decay curve will result in a smaller  $\tau$  than if placed at the end.

## 4.2

### Multiple Gate Methods

Modified time-resolved imaging approaches that make use of multiple gating (and are more precise) have been developed for both the td-DLR and the RLD method. This also is the results of advancements made in CCD, LED, and laser technologies. It is possible, at least in principle, to obtain the complete decay function of the luminescence of a paint by subsequently opening a large number of gates. The more gates are used, the better the resolution and the more precise are the results, this leading (theoretically) to an infinite number of gates, all of an infinitesimally small width [107].

In case of indicators of well known decay time, refining the parameter settings will make the data more precise [104]. With proper settings along with appropriate positions and widths of the gates, it is even possible to monitor two parameters with one measurement. In Japanese aerodynamic and wind tunnel research, a tailor made calibration scheme was developed for the

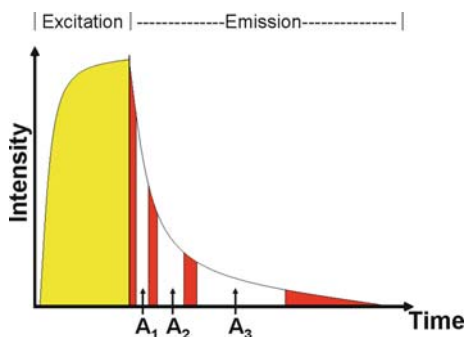


**Fig. 4** Calibration scheme for PtTFPP in poly(IBM-co-TFEM) applied at Japan Aerospace Exploration Agency (JAXA)

PSP probe platinum tetra-(pentafluorophenyl)-porphyrin in poly(isobutyl methacrylate-*co*-trifluoroethyl methacrylate), as shown in Fig. 4. It accounts for the non-mono-exponential luminescence decay of the porphyrin. The parameters are adjusted, such that all three gates have the same intensity at reference conditions.

The ratios of the intensities of the gates are evaluated like applying the standard RLD method (see Eqs. 13 and 14).

$$R_{12} = \frac{I_1}{I_2} = f(p, T) \quad (13)$$

$$R_{13} = \frac{I_1}{I_3} = f'(p, T) \quad (14)$$

Thus, it is possible to obtain two equations for two unknown parameters (pressure and temperature) by only one measurement. Accordingly, pressure and temperature can be measured simultaneously with just one single probe [108].

In the majority of cases, the signals obtained with dually sensing paints are separated via the spectral differences of the indicators, either by absorbance or emission, and are measured separately. A more elegant way consists in the acquisition of both signals within one measurement if they can be separated on the basis of differences in spectra and/or lifetimes [109, 110].

## 5

### Requirements and Characteristics of the Imaging Setup

From observations made in Sect. 4, it is obvious that in order to determine luminescence lifetimes by the time-domain method, the components of the setup have to be well coordinated. Unlike in measurements of frequency phase shifts, a CCD (charge coupled device) camera can be used to acquire the luminescence information in time-domain methods.

#### 5.1

##### Camera Systems

Time-resolved measurements require the camera and the light source to be triggered synchronously in the nanosecond time regime. This can be achieved using an expensive image intensifier. When making use of metal-ligand complexes (decaying in microsecond time scale), a CCD camera with a fast shutter is sufficient and it eliminates the need for an image intensifier. It even tolerates interfering ambient light, which is highly practical in many applications. Cooled CCD chips are adequate, due to their very low

signal-to-noise ratio. Usually, computers control the trigger steps and the data acquisition.

Other systems are available for intensity signal detection, but all have their merits and drawbacks. For example, photomultiplier tubes are capable of detecting weak signals, but they do not offer the possibility of imaging intensity distributions, due to the nonselective multiplication of all incoming intensity information, resulting in a single overall intensity signal. Common techniques and configurations of the black/white CCD-based cameras are specified and explained in the following sections. It has to be pointed out that the class of electron multiplying CCDs (EMCCDs) is not discussed in the following, because they are not applicable to time-resolved imaging.

### 5.1.1

#### Interline Charge Coupled Device Cameras

Every second serial pixel column of an interline CCD camera is covered with a thin layer of a light-impermeable metal such as aluminum. The “dark” pixels do not register incoming photons (see Fig. 5). During the readout of the chip, the light intensity information is transferred from the active columns to the inactive columns, thus, being protected from re-exposure. After the transfer, the columns are shifted to the output amplifier and are read out [111]. The transfer of the pixels to the vicinal “dark” pixel is very fast. Once accomplished, the next image can be taken without the readout being completed. In other words, a second photo can be shot while the first one is still on the chip.

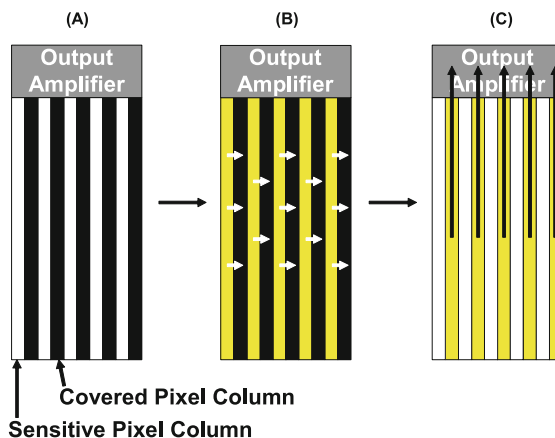


**Fig. 5** Operating mode of an interline CCD chip. **A** The initial state; **B** Chip after exposure; the intensity information is located exclusively on the sensitive pixels and is transferred to the covered pixel column. **C** The covered pixels are read out. The chip is ready again for re-exposure

### 5.1.2 Frame Transfer Charge Coupled Device Cameras

This kind of chip is also composed of active areas and a storage areas. The active pixels register light intensity when exposed to light. The storage area – as in interline CCD chips – is blinded. After image recording, the image information on the active area is transferred to the coated (inactive) region. The pixels are read row by row from this storage array (see Fig. 6). The active pixel array can be re-exposed already during readout [111]. The process of transferring the information to the inactive area is not as fast as the analog process in interline chips. Furthermore, the frame transfer technique is susceptible to cross-talk.

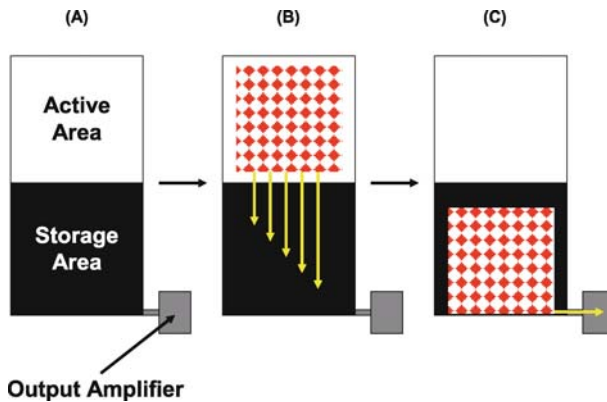


**Fig. 6** Operating mode of a frame transfer CCD chip. **A** The initial state; **B** Chip after exposure. The image information is located on the active area, it is transferred en bloc to the storage area, and it is then **C** read out row by row

### 5.1.3 Full Frame Charge Coupled Device Cameras

Unlike in interline and frame transfer CCDs, full frame arrays do not possess a storage area. All pixels are sensitive to light. The intensity information is read row by row after exposure. A new image can be taken as soon as the “old” image is completely read by the output amplifier. This limits the speed and performance of the system. In addition, the full frame technique is prone to image smearing. This disadvantage can be widely eliminated by the application of shutters, but this necessitates fast and precise triggering steps.

### 5.1.4 Intensified Charge Coupled Device Cameras

The intensified CCD (ICCD) chip is suitable for detecting even weak signals. Before reaching the chip, the incoming photons are converted into electrons by a photocathode. Each single electron is then converted into a cloud of electrons (more than 1000 electrons per incident electron) by a multiplier, the so-called microchannel plate. The cloud hits an electroluminescent screen and causes the emission of many more photons than initially entered the photocathode. Light is then guided to a CCD chip by a tapered fiber-bundle [112, 113].

### 5.1.5 Areas of Application of the Various Cameras

There are mainly four characteristics to be considered when selecting the most appropriate camera, including viz. speed, resolution, sensitivity, and noise. A first differentiation has to be made between ordinary CCD and ICCDs, because different CCD techniques feature virtually the same main characteristics, however, with differences in terms of speed.

CCD-based systems can acquire and process image data much faster than intensified cameras. However, for luminescence imaging applications, this advantage in speed has to be put into perspective. Usually, luminescence is not of strong intensity. Thus, the exposure time has to be increased when using conventional CCD cameras, and this compromises the advantage of faster electronic processing. In case of low intensity, the CCDs are slower than the ICCDs. Intensified CCDs detect thousands of signals per incoming photon, and this results in better-quality images at a given exposure time. The ICCDs are also faster, because they have fewer pixels, so less information has to be read out. Accordingly, the spatial resolution is not very high. On the other hand, CCD cameras enable binning. In this process, a certain number of pixels is combined to form a single (combined) pixel. For example, when applying  $4 \times 4$  binning, the intensity will be higher by a factor of 16 but, of course, at only 1/16 of the spatial resolution. This is a very efficient way to speed up CCD cameras.

The choice of the camera system also depends on the field of application. If the signal is low and the observed process is fast, an ICCD camera is preferable. However, for the bigger part of aerodynamic applications, a cooled CCD camera is more than adequate. The typical time needed for cooled CCD cameras to acquire a single image is  $\sim 100$  ms (including parameter transfer from the PC to the camera and image readout). The intensity of the luminescence emitted by the (usually bright) indicator dyes also depends on the brightness of the light source. However, in case of indicators with low absorbance or poor quantum yield, in case of weak light sources (see Sect. 5.2), and imaging over large distances, intensified CCD cameras are clearly preferable.

The performance of any CCD system is limited by several noise sources. They can be divided into three main types: shot noise, dark current noise, and readout noise. The shot noise is an inescapable effect based on the quantum nature of photons. It emerges from statistical variations in the overall number of photons emitted from the object (indicator). This noise source is the limit for any CCD in terms of signal-to-noise ratio.

CCD chips are made of silicone. In this kind of substrate, temperature can generate electrons. Hence, there is a temperature-dependent current in CCD-chips causing the so-called dark current noise. Cooling of the camera can significantly reduce the dark current. For example, a noncooled chip might generate a dark current of approximately 300 e/s/pixel at 20 °C. This effect can be reduced to a value of 1 e/s/pixel when cooling the CCD chip down to -40 °C. However, the dark current effect is reproducible for a given temperature and can, thus, be corrected by dark image subtraction.

After exposing the CCD chip to light, the generated charge on each pixel has to be digitalized and processed. Therefore, the charges have to be shifted. It may then happen that electrons are left behind or change their relative position. This effect causes the readout noise, which is, thus, dependent on the frame rate.

The signal-to-noise ratio of a CCD is limited by the readout noise, especially at low light intensity. Under these conditions, the SNR of ICCDs is shot-noise limited, which is the ideal case for any camera system. As it was said before, the ICCD outperforms the cooled CCD at low light conditions, until the limit of approximately 400 photons per pixel is reached. At values greater than that, the cooled CCD is preferable [114].

## 5.2

### Light Sources

Light sources are expected to have a high output and – in case of time-resolved measurements – to allow for high pulse frequencies. Suitable lasers represent the ideal form of such light sources. However, certain types of lasers are expensive, and the available wavelengths are limited. More seriously, the laser beam is rather focused. Thus, only a confined area of the paint is excited. For imaging a whole aircraft model, a scanning system needs to be installed. This increases the complexity of the setup. Alternatively, the laser light may be guided to the site of interest by applying lenses, mirrors, and/or fiber optics. This has been shown to work for pressure or temperature imaging using microplates or confocal microscopes [115–117]. Laser diodes are particularly attractive in being compact, easy to drive, and (mostly) suitable for high frequency operation. They cover the wavelength range from 280 to above 1000 nm, but those of <370 nm are expensive.

With a wavelength range from approximately 250 nm up to 600 nm, mercury lamps and xenon flash lamps are most useful. Almost any desired exci-



tation wavelength can be chosen by using appropriate optical filters. These systems are rather compact.

Light emitting diodes (LEDs) are the light sources of choice, due to their low costs, compactness, output, efficiency, pulse rates, and flexibility. LEDs can be triggered in the nanosecond timescale and driven via computer, and they are bright and easy to handle, thereby reducing the demands on the experimental setup. They are mostly employed in the form of LED arrays (“batteries”).

Given the number of possible combinations of materials for use in PSPs and TSPs, of possible spectroscopic schemes (from intensity to decay time to time resolution), of geometries, cameras, and light sources, it does not come as a surprise that there is no generally applicable approach.

### 5.3

#### Software

The core of an efficient imaging system is its software. It controls the optoelectronic components and processes the received information. On transferring the PSP and TSP techniques from the lab experiment to industrial applications, the requirements on the software further increase. If two parameters are to be sensed simultaneously, there is twice the quantity of information to be processed (independent of whether two indicators are used, or only one indicator and one reference dye), and two cameras need to be triggered. The two-camera method is attractive, because it is not necessary to change emission filters. The object is viewed by the two cameras from slightly different angles, and the software is used to correct for this effect. Small positional markers are usually placed on the surface, which enables the calculation of the true shape of the image and the positions of the pixels acquired. This step is particularly important in case of lifetime imaging, where the ratio of two images serves as information and where even small deviations in the alignment of the images may cause errors in the calculations of the images. Examples for commonly used software are “ToPas” (3-dimensional pressure analysis software, applied for example at DLR [7]), MatLab, and IDL.

## 6

### State of the Art

PSPs and TSPs have been, and are, widely applied to aerodynamic wind tunnel testing. A cooperation between NASA and the University of Washington (WA), resulted in a dual PSP system, which makes use of a platinum fluorophenyl-porphyrin (or a platinum porpholactone) as the oxygen-sensitive probe, and a magnesium fluorophenylporphyrin as a temperature reference probe, all contained in a fluorinated co-polymer called FIB [38, 54, 64, 118, 119].

Intense research is also being performed in Japan within the MOSAIC project. The PSPs are based on the use of ruthenium polypyridyl complexes and on platinum porphyrins. New binders and polymers with superior permeability for oxygen were also developed. New approaches, such as the anodized aluminum PSPs and polymers acting as pressure-sensitive indicators, were also elaborated, and the accuracy and performance of existing paints was improved [120–134] (see Sect. 3.3).

Polycyclic aromatic hydrocarbons (PAHs), such as pyrene, pyrene butyric acid, and pyrene sulfonic acid, have had a large impact on wind tunnel research. The PSPs used in Europe are mainly based on pyrene, and are applied in aerodynamic research facilities, such as those of DLR [135, 136], ONERA [137, 138], and BAE Systems [139].

## 7

### Current Challenges and Limitations

Nowadays, the intensity-based PSPs are applied mainly in aeronautic research and in wind tunnel tests. However, time-resolved lifetime imaging is gaining in importance, due to the lower susceptibility for erroneous data. Thus, there is a need for novel pressure-sensitive paints, with decay times in the microsecond time regime. Present-day paints have been optimized for high pressures. This renders them less useful for testing automobiles (and racing cars) in low-speed wind tunnels.

The use of polymers as a type of solvent also limits the response time of PSPs by forming a diffusional barrier. Some paints (such as hydrogels) are soluble in water or swell at high humidity, and this changes their permeability for oxygen. With respect to TSPs, a polymer that is completely impermeable to oxygen is desirable but has not been described so far (keeping in mind that other conditions also need to be fulfilled) [61].

Two probes are needed in case of dual PSP/TSP systems. This further limits the number of indicators available, because the signals of the two probes have to be differentiated. For spectral separation, the emission of the dyes must not overlap, which is, in fact, not easy to accomplish, because many of the metal-ligand complexes (except for those of the lanthanides) show rather broad emission bands. Thus, research in the areas of probe design, polymer chemistry, spectroscopy, and system design remains quite challenging.

### References

1. Clark LC Jnr (1956) *Trans Am Soc Artif Intern Organs* 2:41
2. Kautsky H, Hirsch A (1935) *Z Anorg Allg Chem* 222:126
3. Peterson JL, Fitzgerald RV (1980) *Rev Sci Instrum* 51:670

4. Baron AE, Danielson JDS, Gouterman M, Wan JR, McLachlan B (1993) *Rev Sci Instrum* 64:3394
5. Nakakita K, Kurita M, Mitsuo K, Watanabe S (2006) *Meas Sci Technol* 17:359
6. Merienne M-C, Le Sant Y, Ancelle J, Soulevant D (2004) *Meas Sci Technol* 15:2349
7. Klein C, Engler RH, Henne U, Sachs WE (2005) *Exp Fluids* 39:475
8. Papkovsky DB, O'Riordan TC, Guilbault GG (1999) *Anal Chem* 71:1568
9. Preininger C, Klimant I, Wolfbeis OS (1994) *Anal Chem* 66:1841
10. Kellner K, Liebsch G, Klimant I, Wolfbeis OS, Blunk T, Schulz MB, Göpferich A (2002) *Biotechnol Bioeng* 80:73
11. Arain S, John GT, Krause C, Gerlach J, Wolfbeis OS, Klimant I (2006) *Sens Actuators, B* 113:639
12. Arain S, Weiss S, Heinze E, John GT, Krause C, Klimant I (2005) *Biotechnol Bioeng* 90:271
13. Gerlach J, Pohn B, Karl W, Scheideler M, Uray M, Bischof H, Schwab H, Klimant I (2006) *Sens Actuators, B* 114:984
14. Ogurtsov VI, Papkovsky DB (2006) *Sens Actuators, B* 113:608
15. Ogurtsov VI, Papkovsky DB (2006) *Sens Actuators, B* 113:917
16. Hynes J, O'Riordan TC, Curtin J, Cotter TG, Papkovsky DB (2005) *J Immunol Methods* 306:193
17. O'Mahony FC, O'Donovan C, Hynes J, Moore T, Davenport J, Papkovsky DB (2005) *Environ Sci Technol* 39:5010
18. Alderman J, Hynes J, Floyd SM, Krüger J, O'Connor R, Papkovsky DB (2004) *Biosens Bioelectron* 19:1529
19. Apostolidis A, Klimant I, Andrzejewski, Wolfbeis OS (2004) *J Comb Chem* 6:325
20. John GT, Klimant I, Wittmann C, Heinze E (2003) *Biotechnol Bioeng* 81:829
21. Lakowicz JR (1999) *Principles of Fluorescence Spectroscopy*, 2nd edn. Kluwer Academic/Plenum Publishers, New York, Boston, Dordrecht, London, Moscow
22. Becker HGO (1991) *Einführung in die Photochemie*, 3rd revised edn. Verlag der Wissenschaften, Berlin
23. Valeur B (2002) *Molecular Fluorescence – Principles and Applications*. Wiley-VCH, Weinheim
24. Schulman SG (1977) *Fluorescence and phosphorescence spectroscopy: physicochemical principles and practice*. Pergamon Press, Oxford
25. Demas JN, DeGraff BA (1991) *Anal Chem* 63:829A. In: Lakowicz JR (1999) *Principles of Fluorescence Spectroscopy*, 2nd edn. Kluwer Academic/Plenum Publishers, New York, Boston, Dordrecht, London, Moscow
26. Wolfbeis OS (2006) *Anal Chem* 78:3859
27. Atkins P, DePaula (2002) *Physical Chemistry*, 7th edn. Oxford University Press, pp 920–934
28. Alberty AA, Silbey RJ (1997) *Physical Chemistry*, 2nd edn. Wiley & Sons, New York, Chichester, Brisbane, Toronto, Singapore, pp 690–697
29. Maron SH, Lando JB (1974) *Fundamentals of Physical Chemistry*. Collier MacMillan Publishers, London, pp 720–728
30. Valeur B, Bronchon JC (2001) *New Trends in Fluorescence Spectroscopy – Application to Chemical and Life Science* Springer Series on Fluorescence, Methods and Applications. Springer, Berlin Heidelberg
31. Lakowicz JR, Weber G (1973) *Biochem* 12:4161
32. Bowen EJ (1954) *Trans Farad Soc* 50:97
33. Stern V, Volmer M (1919) *Physik Z* 20:183
34. Lu X, Winnik MA (2001) *Chem Mater* 13:3449

35. Liu T, Campbell BT, Sullivan JP (1995) *Exp Therm Fluid Sci* 10:101
36. Woodmansee MA, Dutton JC (1998) *Exp Fluid* 24:163
37. Amao Y, Asai K, Okura I (2000) *J Porphyrin Phthalocyanine* 4:292
38. Zelelew B, Khalil GE, Phelan G, Carlson B, Gouterman M, Callis JB, Dalton LR (2003) *Sens Actuators, B* 96:304
39. Basu JB, Rajam KS (2004) *Sens Actuators, B* 99:459
40. Wolfbeis OS, Posch HE, Kroneis HW (1985) *Anal Chem* 57:2556
41. Brugman CJM, van Scerpenzeel PJ, Rettschnik RPH (1973) *J Chem Phys* 58:3468
42. Cox ME, Dunn B (1985) *Appl Optics* 24:2114
43. Kameda M, Tabei T, Nakakita K, Sakae H, Asai K (2005) *Meas Sci Technol* 16:2517
44. Sakamura Y, Matsumoto M, Suzuko T (2005) *Meas Sci Technol* 16:759
45. Bowyer WJ, Xu W, Demas J (2004) *Anal Chem* 76:4374
46. Carraway ER, Demas JN, DeGraff BA, Bacon JR (1991) *Anal Chem* 63:332
47. Bacon JR, Demas JN (1987) *Anal Chem* 59:2780
48. Li XM, Wong HY (1992) *Anal Chim Acta* 262:27
49. Lee S-K, Okura I (1998) *Spectrochim Acta A* 54:91
50. Amao Y (2003) *Microchim Acta* 143:1
51. Amao Y, Miyashita T, Okura I (2000) *J Porphyrin Phthalocyanine* 5:433
52. Lee S-K, Okura I (1997) *Anal Comm* 34:185
53. McGraw CM, Bell JH, Khalil G, Callis JB (2006) *Exp Fluids* 40:203
54. Gouterman M, Callis J, Dalton L, Khalil G, Mebarki Y, Cooper KR, Grenier M (2004) *Meas Sci Technol* 15:1986
55. Gouterman M, Hall RJ, Khalil G-E, Martin PC, Shankland EG, Cerny RL (1989) *J Am Chem Soc* 111:3702
56. Peterson JL, Fitzgerald RV, Buckhold DK (1984) *Anal Chem* 56:63
57. Lai S-W, Hou Y-J, Che C-M, Pang H-L, Wong K-Y, Chang CK, Zhu N (2004) *Inorg Chem* 43:3724
58. Papkovsky DB, Ponomarev GV, Trettnak W, O'Leary P (1995) *Anal Chem* 67:4112
59. Asai K, Nakakita, Kameda M, Teduka K (2001) 19th International Congress in Instrumentation in Aerospace Simulation Facilities (ICIASF), pp 25–36
60. Wolfbeis OS (1991) *Fiber Optic Chemical Sensors and Biosensors*, vols. 1–2. CRC Press, Boca Raton, Florida.
61. Potyrailo RA (2006) *Angew Chem* 118:718
62. Liebsch G, Klimant I, Frank B, Holst G, Wolfbeis OS (2000) *Appl Spec* 54:548
63. Gouin S, Gouterman M (2000) *J Appl Polym Sci* 77:2805
64. Puklin E, Carlson B, Gouin S, Costin C, Green E, Ponomarev S, Tanji H, Gouterman M (1999) *J Appl Polym Sci* 77:2795
65. Asai K, Amao Y, Iijima Y, Okura I, Nishide H (2002) *J Thermophys Heat Transfer* 16:109
66. Amao Y, Asai K, Miyashita T, Okura I (2000) *Polym Adv Tech* 11:705
67. Gouin S, Gouterman M (2000) *J Appl Polym Sci* 77:2815
68. Borisov SM, Wolfbeis OS (2006) *Anal Chem* 78:5094
69. Amao Y, Komori T, Nishide H (2005) *Reactive & Functional Polymers* 63:35
70. Reding FP, Faucher JA, Whitman RD (1962) *J Polym Sci* 57:483
71. Dedeurwaerder R, Oth JFM (1959) *J Chim Phys* 56:940
72. Yi-Yan N, Felder RM, Koros WJ (1980) *J Appl Polym Sci* 25:1755
73. Compan V, Lopez L, Andrio A, Lopez-Aleman A, Refojo MF (1998) *J Appl Polym Sci* 72:321
74. Lim C-W, Kim C-G, Kim W-Y, Jeong Y-S, Lee Y-S (1999) *Bull Korean Chem Soc* 20:672

75. Weinmüller C, Langel C, Fornasiero F, Radke CJ, Prausnitz JM (2005) *J Biomed Mat Research* 77A:230
76. Eldridge JI, Benic TJ, Allison SW, Beshears DL (2004) *J Therm Spray Tech* 13:44
77. Nakakita K, Yamazaki T, Asai K, Teduka N, Fuji A, Kameda M (2000) 21st AIAA Aerodynamic Measurement Technology and Ground Testing Conference, June 19–22 2000, Denver, USA
78. Sakaue H, Sullivan JP, Egami Y, Iijima Y, Asai K, Engler RH, Beifuss U, Doering F (2001) *Instrumentation in Aerospace Facilities*, 19th International Congress on ICI-ASF, 186–195
79. Kameda M, Tezuka N, Hangai T, Asai K, Nakakita K, Amao Y (2004) *Meas Sci Technol* 15:489
80. Köse ME, Omar A, Virgin CA, Carrol BF, Schanze KS (2005) *Langmuir* 21:9110
81. Omrane A, Särner G, Alden M (2004) *Appl Phys B* 79:431
82. Feist JP, Heyes AL, Seefeldt S (2003) *Meas Sci Technol* 14:N17
83. Coyle LM, Gouterman M (1999) *Sens Actuators, B* 61:92
84. Allison SW, Gillies GT (1997) *Rew Sci Instrum* 68:2615
85. Liebsch G, Klimant I, Wolfbeis OS (1999) *Adv Mater* 11:1296
86. Wang Z, McWilliams A, Evans C, Lu X, Chung S, Winnik M, Manners I (2002) *Adv Funct Mater* 12:415
87. Borisov SM, Mayr T, Karasyov AA, Klimant I, Chojnacki P, Moser C, Nagl S, Schaeferling M, Stich MI, Vasilevskaya GS, Wolfbeis OS (2006) *Springer Series on Fluorescence* 4:431–463
88. Yang C, Fu L-M, Wang Y, Zhang J-P, Wong W-T, Ai X-C, Qiao Y-F, Zou B-S, Gui L-L (2004) *Angew Chem Int Ed* 43:5009
89. Le Sant Y, Marchand M, Millan P, Fontaine J (2002) *Aerospace Sci Technol* 6:355
90. Brandrup J, Immergut EH, Grulke EA (1999) *Polymer Handbook*, 4th edn. John Wiley & Sons, New York, Chichester, Weinheim, Brisbane, Singapore, Toronto
91. Miller DS, Letcher S, Barnes DM, David M (1996) *Am J Physiol* 271:508
92. Paglarlo L (1995) *Adv Mol Cell Biol* 11:93
93. Liebsch G, Klimant I, Frank B, Holst G, Wolfbeis OS (2000) *Appl Spectrosc* 54:548
94. Mariott G, Clegg RM, Arndt-Jovin DJ, Jovin TM (1991) *Biophys J* 60:1374
95. Wang XF, Uchida T, Coleman DM, Minami S (1991) *Appl Spec* 45:360
96. Morgan CG, Mitchel AC (1996) *Chromosome Res* 4:261
97. König K, Böhme S, Leclerc N, Ahuja R (1998) *Cell Mol Biol* 44:763
98. Gadella TWJ, van Hoek A, Visser AJWG (1997) *J Fluoresc* 7:35
99. Hartmann P, Ziegler W (1996) *Anal Chem* 68:4512
100. Hartmann P, Ziegler W, Holst G, Lübbers DW (1997) *Sens Actuators, B* 38:110
101. Demas JN, Jones WM, Keller RA (1986) *Anal Chem* 58:1717
102. Woods RJ, Scypinski S, Cline Love LJ, Ashworth HA (1984) *Appl Spec* 45:360
103. Ballew R, Demas JN (1989) *Anal Chem* 61:30
104. Chan SP, Fuller ZJ, Demas JN, DeGraff BA (2001) *Anal Chem* 73:4486
105. Chan SP, Fuller ZJ, Demas JN, Ding F, DeGraff BA (2001) *Appl Spec* 55:1245
106. Sharman KK, Periasamy A, Ashworth H, Demas JN, Snow NH (1999) *Anal Chem* 71:947
107. Moore C, Chan SP, Demas JN, DeGraff BA (2004) *Appl Spec* 58:603
108. Mitsuo K, Asai K, Suzuki H, Mizushima H (2006) *AIAA Journal* 44:600
109. Liebsch G, Klimant I, Krause C, Wolfbeis OS (2001) *Anal Chem* 73:4354
110. Schroeder CR, Polerecky L, Klimant I (2006) *Anal Chem*, submitted
111. Feltz JC, Karim MA (1990) *Appl Opt* 29:717
112. Frenkel A, Sartor MA, Wlodawski MS (1997) *Appl Opt* 36:5288

113. Fordham JLA, Moorhead CF, Galbraith RF (2000) *Mon Not R Astron Soc* 312:83
114. Dussault D, Hoess P (2004) *Proceedings of SPIE* 5563:195
115. Schaeferling M, Wu M, Enderlein J, Bauer H, Wolfbeis OS (2003) *Appl Spec* 57:1386
116. Cubeddu R, Comelli D, D'Andrea C, Taroni P, Valentini G (2002) *J Phys D: Appl Phys* 35:R61
117. Mayr T, Igel C, Liebsch G, Klimant I, Wolfbeis OS (2003) *Anal Chem* 75:4389
118. Khalil GE, Costin C, Crafton J, Jones G, Grenoble S, Gouterman, Callis JB, Dalton LR (2004) *Sens Actuators, B* 97:13
119. Morris RJ, Donovan JK, Kegelmann JT, Schwab SD, Levy RL, Crites RC (1993) *AIAA Journal* 31:419
120. Amao Y, Asai K, Okura I (2000) *J Porphyrin Phthalocyanine* 4:179
121. Amao Y, Asai K, Miyashita T, Okura I (2000) *J Porphyrin Phthalocyanine* 4:19
122. Amao Y, Asai K, Miyashita T, Okura I (1999) *Chem Lett* 10:1031
123. Obata M, Tanaka Y, Araki N, Hirohara S, Yano S, Mitsuo K, Asai K, Harada M, Kakuchi T, Ohtsuki C (2005) *J Polym Sci A: Polym Chem* 43:2997
124. Fujiwara Y, Amao Y (2004) *Sens Actuators, B* 99:130
125. Fujiwara Y, Amao Y (2003) *Sens Actuators, B* 89:187
126. Fujiwara Y, Amao Y (2003) *Sens Actuators, B* 89:58
127. Amao Y, Okura I (2003) *Sens Actuators, B* 88:162
128. Fujiwara Y, Amao Y (2002) *Sens Actuators, B* 85:175
129. Amao Y, Tabuchi Y, Yamashita Y, Kimura K (2002) *Eur Polym J* 38:675
130. Amao Y, Ishikawa Y, Okura I (2001) *Anal Chimica Acta* 445:177
131. Amao Y, Miyashita T, Okura I (2001) *React Funct Polym* 47:49
132. Amao Y, Okura I, Miyashita T (2000) *Chem Lett* 11:1286
133. Amao Y, Okura I, Miyashita T (2000) *Chem Lett* 8:1286
134. Amao Y, Asai K, Miyashita T (1999) *Anal Commun* 36:367
135. Engler RH, Klein C, Trinks O (2000) *Meas Sci Technol* 11:1077
136. Fey U, Engler RH, Egami Y, Iijima Y, Asai K, Jansen U, Quest J (2003) 20th International Congress on Instrumentation in Aerospace Simulation Facilities ICIASF 2003 Record, Göttingen, Germany, August 25–29 2003, pp 77–88
137. Engler RH, Merienne M-C, Klein C, Le Sant Y (2002) *Aerospace Sci Technol* 6:313
138. Le Sant Y, Merienne M-C (2005) *Aerospace Sci Technol* 9:285
139. Kingsley-Rowe JR, Lock GD, Davies AG (2003) *Royal Aeronautical J* 107:1

**Part VI**  
**Fluorescence Analysis of Actinides**

# Luminescence Analysis of Actinides: Instrumentation, Applications, Quantification, Future Trends, and Quality Assurance

I. Billard<sup>1</sup> · G. Geipel<sup>2</sup> (✉)

<sup>1</sup>IPHC/DRS, Chimie Nucléaire, Bat. 35, BP 28, 67037 Strasbourg Cedex 2, France

<sup>2</sup>Forschungszentrum Rossendorf, Institute of Radiochemistry, P.O. Box 510 119,  
01314 Dresden, Germany

*G.Geipel@fzd.de*

<b>1</b>	<b>Introduction</b> . . . . .	467
<b>2</b>	<b>Instrumentation and Applications</b> . . . . .	468
2.1	Photon Counting Techniques for the Determination of Actinides . . . . .	469
2.2	Boxcar Technique . . . . .	470
<b>3</b>	<b>Luminescence of Actinides</b> . . . . .	470
3.1	Protactinium . . . . .	471
3.2	Uranium . . . . .	471
3.2.1	Uranium(IV) . . . . .	472
3.2.2	Uranium(V) . . . . .	473
3.2.3	Uranium(VI) . . . . .	473
3.3	Neptunium(VI) and Plutonium(VI) . . . . .	476
3.4	Americium(III) . . . . .	477
3.5	Curium . . . . .	478
3.6	Other Actinides . . . . .	480
3.6.1	Berkelium(III) . . . . .	481
3.6.2	Californium(III) . . . . .	481
3.6.3	Einsteinium(III) . . . . .	481
3.7	Radioluminescence . . . . .	482
<b>4</b>	<b>Concentration Determination and Quality Assurance</b> . . . . .	482
<b>5</b>	<b>Trends</b> . . . . .	487
	<b>References</b> . . . . .	489

**Abstract** Since the discovery of uranium, the impact of actinides has dramatically increased in our everyday life, firstly through the naturally occurring elements Th, Pa, and U (that were first used mainly as color pigments or for cancer treatment) and secondly through the artificial ones, produced in all steps of the nuclear power process (mostly Pu, Np, Am, and Cm). Considering the huge problem of providing safe and sustainable energy in order to supply the fast increasing world demand, nuclear power will be one of the major concerns of this century. It is therefore of tremendous importance to tackle associated problems, which are related to the remediation of old mining and milling sites, to the control of fissile products throughout the nuclear power production cycle,



and finally to the long term disposal of generated wastes. In this field, and according to public concern, quantification and quality assurance are of utmost importance. However, owing to the radioactive properties of actinides, these objectives are liable to even more difficulties than for other more stable elements. Other problems that need to be overcome are mainly related to the complexity of the chemical behavior of actinides, which display numerous oxidation states, a large tendency to hydrolysis, and, for the short-lived ones (mostly elements above Cm), handling problems. Furthermore, the range of concentration of these elements found in the environment (mainly as a consequence of mining, milling, nuclear bomb testing, and accidents) limits the use of speciation techniques, which need to be safe, fast, reliable, and very sensitive. Fortunately, some major actinides display luminescence, which can be used for the determination of complex stabilities as well as for the direct detection of the formed species in different environments over a wide concentration range, from ultra-traces to chemically usable concentrations up to reprocessing conditions.

In this chapter, we will present an overview of the field of actinide luminescence analysis (time-resolved laser-induced fluorescence spectroscopy, TRLIFS), focusing on applications related to the nuclear fuel cycle, from reprocessing to validation of nuclear waste repositories. However, it is not possible to include all publications in this contribution and a personally influenced selection has been made, that highlights applications in solution.

**Keywords** Actinides · Complexes · Excitation wavelength · Laser-induced · Oxidation states · Speciation · Time-resolved

### Abbreviations

3D	Three dimensional
CCD	Charge coupled device
CEA	Commissariat à l'énergie atomique
EDTA	Ethylene-diamine-tetraacetic acid
EXAFS	Extended X-ray absorption fine structure
FWHM	Full width at half maximum
Gly	Glycine
LIPAS	Laser-induced photoacoustic spectroscopy
LN <sub>2</sub>	Liquid nitrogen
MEDUSA	Make equilibrium diagrams using sophisticated algorithms
NEA	Nuclear energy agency
Nd:YAG	Neodymium-doped yttrium aluminium garnet
OPO	Optical parametric oscillator
PTr	O-Phospho-L-threonine
SSA	5-Sulfosalicylic acid
Tr	L-threonine
Triton	X100 octylphenol ethoxylate
TOPO	Trioctylphosphine oxide
TRLIFS	Time-resolved laser-induced fluorescence spectroscopy
TTA	Thenoyltrifluoroacetone

## 1 Introduction

Since the discovery of uranium, the impact of actinides has dramatically increased in our everyday life, firstly through the naturally occurring elements Th, Pa, and U, (that were first used mainly as color pigments or for cancer treatment) and secondly through the artificial ones, produced in all steps of the nuclear fuel cycle (mostly Pu, Np, Am, and Cm). Considering the huge problem of providing safe and sustainable energy in order to supply the fast increasing world demand, nuclear power will be one of the major issues of this century. It is therefore of tremendous importance to tackle associated problems, which are related to the remediation of old mining and milling sites, to the control of fissile products throughout the nuclear power production cycle, and finally to the long term disposal of generated wastes. In this field, and according to the public concern, quantification and quality assurance are of utmost importance. However, owing to the radioactive properties of actinides, these objectives are liable to even more difficulties than for other more stable elements. Other problems that need to be overcome are mainly related to the complexity of the chemical behavior of actinides, which display numerous oxidation states, a large tendency to hydrolysis, and, for the short-lived ones (mostly, elements above Cm), handling problems. Furthermore, the range of concentration of these elements in the environment (as a consequence of mining, milling, nuclear bomb testing and accidents, mainly) limits the use of speciation techniques, which need to be safe, fast, reliable, and very sensitive. Fortunately, some major actinides display luminescence, which can be used for the determination of complex stabilities as well as for the direct detection of the formed species in different environments over a wide concentration range, from ultra-traces to chemically usable concentrations up to reprocessing conditions, even in different oxidation states.

In this chapter, we will present an overview of the field of actinide luminescence analysis (time-resolved laser-induced fluorescence spectroscopy, TRLIFS), focusing on applications related to the nuclear fuel cycle, from reprocessing to validation of nuclear waste repositories. However, it is not possible to include all publications in this contribution and a personally influenced selection has been made that highlights applications in solution. Also it should be mentioned that the contribution of laser-induced spectroscopy to actinide speciation has been reviewed recently in several publications [1–6]. Owing to the limited space allocated, the reader is also referred to books on basic actinide chemistry [7] and to reviews [8].

## 2 Instrumentation and Applications

Determination of actinides should be performed exploiting their spectroscopic properties and the changes in the decay constants and emission peaks depending on the speciation prevailing in solution. This means that several coexisting species of one luminescent actinide ion can be determined with one time-resolved spectroscopic measurement.

TRLIFS measurements were usually carried out in two ways:

- Photon counting mode
- Boxcar technique

In both techniques, the excitation source is a pulsed laser system, allowing for time-resolved data. However, the excitation wavelengths for the different actinides vary over a wide range. Therefore, dedicated laser systems are mostly used. Table 1 summarizes the useable excitation wavelengths for dedicated actinides, together with the common range of emission and average lifetimes (which are very sensitive to the speciation), in order to illustrate the diversity of luminescence properties of actinides. Besides tunable laser systems (dye laser, optical parametrical amplifier), laser systems with fixed output wavelength have been used.

**Table 1** Excitation wavelength applicable to luminescent oxidation states of the actinide series protactinium to einsteinium, emission range and usual lifetimes

Ion	Excitation [nm]	Lifetime	Emission [nm]	Refs.
Pa(IV)	278 (308)	15 ns	350–550	[9]
U(IV)	248	150 ns (N <sub>2</sub> ) <sup>a</sup>	275–450	[10]
U(V)	255	1.1 μs	440	[11]
U(VI)	266	2–180 μs	470–580	[12, 13]
	337			[14]
	355			[15]
	380–440			[16]
Np(VI)	633	20 μs	1400–1600	[17]
Am(III)	504 (aq. solution)	20 ns	550–1100	[18]
	337/355 (solid)			[19]
				[20]
Cm(III)	395	65 μs–1.2 ms	593–615	[21]
Bk(III)	391	0.1 μs	647	[22, 23]
Cf(III)	Ar-ion	n.d.	685	[22]
Es(III)	495, 355	1 μs	1080	[24, 25]

<sup>a</sup> Measured at liquid nitrogen temperature

With further development of laser sources as well as detection devices it also seems to be possible to observe the hitherto unknown luminescence properties of some of the other actinide elements in aquatic environments.

According to the excitation wavelengths listed in Table 1, a selection of several laser systems may be suggested. In many cases tunable dye laser systems are applicable. These systems use excimer laser systems or a Nd:YAG laser as pump source. Besides this, during the last 15 years the application of tunable solid state lasers (Nd:YAG pumped optical parametric oscillators, OPO) has also been established. These laser systems provide laser pulses for the excitation of the samples to be studied over a wide wavelength range and avoid the problems with the handling of the dyes (toxicity, cancer stimulating, and short wavelength ranges of about 30 nm). In addition, the OPO pumped systems operate over long time periods, providing very stable output energies.

For uranium(VI) mostly laser systems with a fixed wavelength are used, especially the third (355 nm) and fourth (266 nm) harmonic generation of a Nd:YAG laser but in the past nitrogen laser (337 nm) have been used [26].

Curium(III) may be excited with several laser sources. Besides excimer pumped dye lasers, a frequency doubled Ti:sapphire laser or a Nd:YAG pumped OPO system can also be used.

The excitation energies are usually in the range of about 5 mJ per pulse. Higher pulse energies may be attenuated by polarizing prism arrangements. However, in many cases much less laser energy should be applied to the samples due to decomposition and/or photochemical reactions of the chemical components under investigation. This is especially necessary if the interaction of organic ligands like humic substances with actinides has to be studied [27, 28].

## 2.1

### Photon Counting Techniques for the Determination of Actinides

In this type of setup, the photons emitted after the laser pulse are detected by a fast photomultiplier, after being selected through a monochromator. One excitation pulse is usually not enough to get decay spectra liable to reasonable data fitting so that data arising from a few laser pulses are averaged in order to get a decay spectrum at a given wavelength. A scan of the monochromator allows reconstruction of the 3D data (counts versus emission wavelength and time). In this kind of setup, which is very cheap as compared to the boxcar system described below, the decay spectra are very rapidly acquired, while the emission spectra are time-consuming. Data deconvolution allows a precise emission spectrum to be ascribed to each lifetime, thus leading to the complete characterization of all the luminescent species present in the sample. On a practical aspect, however, it is often hard to distinguish species displaying close lifetimes and/or rather similar emission spectra (see Sect. 4).

## 2.2

### Boxcar Technique

The determination of emission spectra and lifetimes within one measurement is the most important advantage of this technique. The use of this technique requires, besides the laser system and a spectrograph (in contrast to a monochromator, here the output has no slit), a so-called intensified CCD-camera system combined with a delay generator for the time-resolved mode. In comparison to the photon counting setup the camera system is more expensive. However, the summation over a reasonable number of laser pulses (often not more than 100) leads to an acceptable luminescence spectrum. The selection of the delay steps for one time-resolved spectrum is more problematic. The commercially available software to control the delay generator allows only one type of step. As already stressed, several uranium(VI) species may exist simultaneously in solution, all of them participating in the luminescence spectroscopy of uranium(VI), and presenting very different luminescence decay times that would require dedicated conditions of the boxcar system to be ideally detected. Therefore, the Institute of Radiochemistry, FZR, has developed its own computer code [13], allowing up to three delay step sizes. This allows the collection, *within one measurement*, of enough spectra for short decaying species as well as for the longer decaying ones.

As mentioned above, owing to the differences in the spectral and decaying properties of the various species of the luminescent actinides, the determination of up to four species with one measurement has been achieved (uranyl case) [15].

## 3

### Luminescence of Actinides

Through the actinides series, the elements protactinium (Pa), uranium (U), americium (Am), neptunium (Np), curium (Cm), berkelium (Bk), as well as californium (Cf) and einsteinium (Es) show luminescence properties in one or more of their oxidation states. However, owing to the difficulties arising from either supplying or handling of the heavier actinides, most of the studies have been restricted to U, Cm, and Am, while studies dealing with Bk, Cf, and Es are limited to pioneer studies. The case of Pa is somehow indicative of a renewal of the interest of the radiochemical community in the luminescence properties of rather “unusual” actinides. Actually, Pa might be one of the element of concern in the case of generation IV nuclear power plants, so that Pa studies are now appearing in the literature (either by TRLIFS or other techniques) [29], though this element was practically not studied at all, by any means, for decades.

### 3.1

#### Protactinium

The only publication on Pa luminescence in solution has been reported by Marquardt et al. [9]. It was found that Pa in oxidation state +4 shows a luminescence emission around 460 nm. Depending on the solution conditions, the absorption and emission maxima vary slightly. Table 2 summarizes the data from [9]. Note that Pa(IV) is not the only stable oxidation state of this element in solution; it also exists as Pa(V), which is not known to be luminescent.

The shifts of the absorption and emission maxima compared to the 5 M HClO<sub>4</sub> solution are explained by the complex formation between the various anions of mineral acids. One should note that the given decay times are influenced by the laser excitation, due to the fact that an excimer laser was used for this study. This has at least two disadvantages: Firstly, the pulse width of such a laser system is about 24 ns. As a boxcar setup is used in this study a deconvolution between the excitation and the luminescence decay should be performed in order to obtain correct luminescence lifetimes. Secondly, the maxima of the absorption band are located between 278 and 290 nm. The output wavelength of the excimer laser is 308 nm. This leads to a less intense excitation of the samples.

**Table 2** Spectroscopic properties of Pa(IV) in various acidic solutions

Solution	Maximum absorption band [nm]	Maximum of luminescence emission [nm]	Decay time [ns]
1 M HClO <sub>4</sub>	278	–	–
5 M HClO <sub>4</sub>	279	464	18.3
2 M HCl	279	465	14.7
5 M HCl	284	456	12.6
2 M H <sub>2</sub> SO <sub>4</sub>	288	460	16.5
5 M H <sub>2</sub> SO <sub>4</sub>	290	455	17.3

### 3.2

#### Uranium

Most studies on luminescent actinides have been performed with uranium. This is for two reasons: Firstly, uranium is the last element in the periodic table occurring naturally and it is available for chemical purposes in higher amounts. Secondly, the amount of uranium used for luminescence experiments can be handled in the laboratory much more easily than the other relevant actinides, which need special equipment for safety and radiation protection (e.g., glove boxes) due to their high specific radioactivity.

Several oxidation states of uranium are known. Under normal chemical conditions the most stable oxidation state is +6. However, uranium does not form such highly charged ions in solution; it occurs as dioxouranium(VI) ion, more commonly named the uranyl ion. Under reducing conditions uranium is stable in the oxidation state +4. In this oxidation state uranium hydrolyzes very easily and the solvated uranium(IV) exists only in strong acid solutions of non-complexing mineral acids like perchloric acid or in some ionic liquids [29].

Uranium(V) occurs also as dioxo-cation [30]. In this oxidation state uranium disproportionates easily into its +6 and +4 states. The oxidation state +3 is also known in non-aquatic, strong reducing media.

### 3.2.1

#### Uranium(IV)

The luminescence of uranium in solution in its oxidation state +4 has been observed by Kirishima et al. [10, 32]. The excitation occurs at 245 nm.

As excitation source, the frequency doubled output of a dye laser at 490 nm was used, resulting in a 245 nm laser pulse. The dye laser was pumped by an excimer laser at 308 nm. Due to the pulse duration of the excimer laser it was not possible to determine the decay time of the luminescence at room temperature. It was only mentioned that the lifetime is shorter than 20 ns. It should be noted that the same problem exists with the determination of the lifetime of the excited state of Pa(IV). From measurements of the excitation the FWHM (full width at half maximum) of the excitation band was calculated to be 2.7 nm [33].

Freezing the sample to the temperature of liquid nitrogen, the lifetime increases to 149 ns in H<sub>2</sub>O and to 198 ns in D<sub>2</sub>O [32].

The application of a Nd:YAG pumped OPO system to the excitation of the uranium(IV) luminescence resulted in much shorter lifetimes [33] of  $2.69 \pm 0.08$  ns. The determination was possible due to the shorter pulse length of the laser system.

Uranium(IV) shows at least 12 emission bands. The most intense are located at 319, 335, 410, and 525 nm. Additionally, emission peaks were located at 289, 292, 313, 321, 339, 346, 394, and 447 nm. The emission maxima are in agreement with the possible transitions derived from the absorption spectrum.

Some studies are performed on the luminescence of uranium(IV) in solid matrices. The luminescence of uranium(IV) in LiYF<sub>4</sub> [34] is a good example as data for other actinides are also available for this system. The excitation energy for uranium(IV) in this matrix is somewhat higher, resulting in a maximum of the excitation at a wavelength of 242 nm. The resulting luminescence emissions are located at 262, 282, 304, 328, and 334 nm as well as two weak emission peaks at 430 and 490 nm. The lifetime of the luminescence

was observed to be about 17 ns. This value was observed at 300 K as well as at 77 K.

### 3.2.2 Uranium(V)

The luminescence properties of uranium(V) have been described recently [11]. The uranium(V) was prepared in a solution of 0.5 M 2-propanol by use of an Hg-lamp. The spectrum was excited at 255 nm and the luminescence is emitted at around 440 nm with a decay time of 1.1  $\mu$ s.

### 3.2.3 Uranium(VI)

Uranium(VI) emits light from two emission levels. These levels are located at 21 270  $\text{cm}^{-1}$  (470.1 nm) and 20 502  $\text{cm}^{-1}$  (487.8 nm) [35]. The intensity of the emission of the higher level is relatively low and mostly reaches not more than about 5% of the total emission. Therefore this emission is often not detected. The emission from the other energy level shows six vibration levels in the ground state. The energy distance between these levels is about 855  $\text{cm}^{-1}$  [35] and differs slightly for the several solution species.

The FWHM (full width at half maximum) of the several emission bands ranges from about 12 to 30 nm. The FWHM depends on the speciation of the uranium(VI). Especially the several hydroxo species show an increasing FWHM for the higher hydrolyzed species. Within the series of emission bands from the 20 502  $\text{cm}^{-1}$  level a broadening of the FWHM with increasing emission wavelength is also observed.

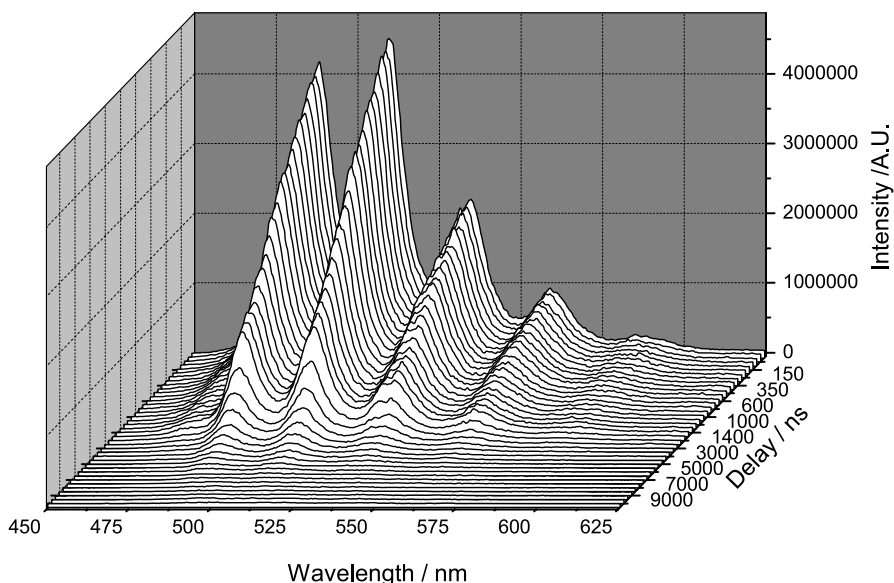
Information about the intensity ratios of the bands from the emitting level 20 507  $\text{cm}^{-1}$  are not available in the literature. As a first rough estimation, the intensity should decrease with increasing ground state vibrational levels, i.e., with increasing emission wavelength. However, it has often been observed that it is not the emission to the ground state, but to the first vibrational level, that shows the highest luminescence intensity.

Figure 1 shows a typical time-resolved luminescence spectrum of the uranyl ion using the acquisition program with three different, increasing delay steps (50, 100 and 500 ns). A small influence of the exciting laser pulse at 532 nm, corresponding to a second order image, can be observed.

The uranium(VI) luminescence decay depends first on the speciation of the uranium(VI) ion. Note that the decay time is also strongly influenced by the ionic strength of the medium [36]. In general, an increase of the decay time with increasing ionic strength is observed. The decay times summarized in Table 3 therefore are compiled for an ionic strength of 0.1 M.

Usually uranium(VI) species formed with organic carboxylic ligands show no luminescence properties. Some exceptions are summarized in Table 3.





**Fig. 1** Typical time-resolved luminescence spectrum of the  $\text{UO}_2^{2+}$  ion (see text)

This behavior is sometimes connected to uranium bond via other than carboxylic groups (i.e., phosphate, sulfate) to the organic ligand.

In addition to the species in Table 3, the uranium(VI) nitrate complexes should be mentioned, owing to the importance of this ion in environmental and reprocessing conditions. The nitrate complexation is very weak and can be only determined in highly concentrated nitric acid solutions ( $>0.5$  M  $\text{HNO}_3$ ). Unfortunately, nitrate ions are well known to suffer photochemical reactions [54] and it has been shown that they also quench uranyl luminescence [55], so that no complete data set (emission and lifetime values) on the luminescence of the species  $\text{UO}_2\text{NO}_3^+$  and  $\text{UO}_2(\text{NO}_3)_2$  has been reported [56].

Additionally it has to be noted that many effects may influence the luminescence of uranium(VI). A number of quenching substances have been studied in the past: Firstly, the solvent water as well as carbonate ions, which play an important role in environmental samples, should be mentioned. Besides these, iron and chloride are also often present in solution and influence the luminescence of uranium(VI) through their dynamic quench properties. A list of quenchers and the quenching constants are summarized in [57]. Such a phenomenon can be used in order to assay the concentration of the quenching substances.

As Table 3 shows, uranium(VI) shows a wide variety in luminescence emission bands as well as in decay times, depending on the solution species. Nevertheless it can be also seen that determination of the luminescence de-

**Table 3** Emission wavelength and decay times of U(VI) solution species (lifetimes are usually compiled for room temperature, 25 °C)

Species	Emission wavelength [nm]						Decay time [ns]	Refs.
UO <sub>2</sub> <sup>2+</sup>	472	488	510	535	560	587	1600	[37, 38]
	470	488	509	533	559	585	2000	[39, 40]
	470	489	510	535	560	588	1700	[41]
		488	509	534	560		900	[42]
		488	510	534	560		7900	[12] <sup>a</sup>
UO <sub>2</sub> F <sub>3</sub> <sup>-</sup> /UO <sub>2</sub> F <sub>4</sub> <sup>2-</sup>	500	522	546	571			300 000	[43]
UO <sub>2</sub> F <sup>+</sup>	495	517	541				76 500	[44]
UO <sub>2</sub> F <sub>2</sub>	498	520	544				214 000	[44]
UO <sub>2</sub> IO <sub>3</sub> <sup>+</sup>	494	515	538	565			< 2000	[43]
UO <sub>2</sub> (IO <sub>3</sub> ) <sub>2</sub>	501	522	545	572			< 2000	[43]
UO <sub>2</sub> IO <sub>4</sub> <sup>+</sup>	503	524	547	574			< 2000	[43]
UO <sub>2</sub> OH <sup>+</sup>	482	498	519	543	570	599	35 000	[37]
		497	519	544	570		80 000	[39]
		496	518	542	566		32 800	[41]
UO <sub>2</sub> (OH) <sub>2</sub>		488	508	534	558		< 20 000	[39]
(UO <sub>2</sub> ) <sub>2</sub> (OH) <sub>2</sub> <sup>2+</sup>	481	498	519	543	566	603	9500	[41]
	480	497	519	542	570	598	9000	[39]
		499	519	542	566		2900	[42]
UO <sub>2</sub> (OH) <sub>3</sub> <sup>-</sup>	482	499	519	543	567	594	800	[39]
		506	524	555	568		400	[41]
K <sub>2</sub> UO <sub>2</sub> (OH) <sub>4</sub>	491	510	531	551	586		154 000	<sup>b</sup>
(UO <sub>2</sub> ) <sub>3</sub> (OH) <sub>5</sub> <sup>+</sup>	484	496	514	535	556	583	23 000	[39]
		500	515	536	554		6600	[41]
		498	516	533	557		7000	[42]
			514	534			19 800	[45]
(UO <sub>2</sub> ) <sub>3</sub> (OH) <sub>7</sub> <sup>-</sup>		503	523	547	574		230 000	[39]
UO <sub>2</sub> SO <sub>4</sub>	477	493	515	538	563	590	4300	[13]
UO <sub>2</sub> (SO <sub>4</sub> ) <sub>2</sub> <sup>2-</sup>		493	515	538			11 000	[13]
UO <sub>2</sub> (SO <sub>4</sub> ) <sub>3</sub> <sup>4-</sup>		493	515	538			18 800	[13]
UO <sub>2</sub> H <sub>2</sub> PO <sub>4</sub> <sup>+</sup>		494	515	539	559		11 000	[46]
		493	514	538			11 100	[44]
UO <sub>2</sub> HPO <sub>4</sub>		497	519	543	570		6000	[46]
UO <sub>2</sub> PO <sub>4</sub> <sup>-</sup>		499	520	544	571		24 000	[46]
UO <sub>2</sub> (H <sub>2</sub> PO <sub>4</sub> )(H <sub>3</sub> PO <sub>4</sub> ) <sup>+</sup>		500	522	546	571		180 000	[43]
UO <sub>2</sub> (H <sub>2</sub> PO <sub>4</sub> ) <sub>2</sub>		494	516	540			67 900	[44]
(UO <sub>2</sub> ) <sub>x</sub> (PO <sub>4</sub> ) <sub>y</sub>	488	503	524	547	573	601	4700	[47]
(UO <sub>2</sub> ) <sub>x</sub> (K <sub>y</sub> P <sub>2</sub> O <sub>7</sub> ) <sub>z</sub>	484	499	520	544	568	598	75 000	[47]
UO <sub>2</sub> HAsO <sub>4</sub>		504	525	547			< 1000	[38]
UO <sub>2</sub> H <sub>2</sub> AsO <sub>4</sub> <sup>+</sup>	478	494	514	539	563		12 200	[38]
UO <sub>2</sub> (H <sub>2</sub> AsO <sub>4</sub> ) <sub>2</sub>	481	497	518	541	571		38 300	[38]
UO <sub>2</sub> CO <sub>3</sub>			520				35 000	[42]
Ca <sub>2</sub> UO <sub>2</sub> (CO <sub>3</sub> ) <sub>3</sub>	465	484	504	524			43	[48]

**Table 3** (continued)

Species	Emission wavelength [nm]						Decay time [ns]	Refs.
UO <sub>2</sub> OSi(OH) <sub>3</sub> <sup>+</sup>		500	521	544	570		19 000	[49]
UO <sub>2</sub> C <sub>3</sub> H <sub>2</sub> O <sub>4</sub>	477	494	515	540	564	594	1240	[37]
UO <sub>2</sub> (C <sub>3</sub> H <sub>2</sub> O <sub>4</sub> ) <sub>2</sub> <sup>2-</sup>	479	496	517	542	566	597	6480	[37]
UO <sub>2</sub> ATP <sup>2-</sup>	480	495	517	540	565	594	> 20 000	[47]
UO <sub>2</sub> (C <sub>6</sub> H <sub>11</sub> O <sub>6</sub> PO <sub>3</sub> )	479	497	519	543	569	598	130	[50]
UO <sub>2</sub> (HGly) <sup>2+</sup>	476	492	513	537	562	587	3350	[51]
UO <sub>2</sub> (HGly) <sub>2</sub> <sup>2+</sup>	479	495	517	541	565	594	690	[51]
UO <sub>2</sub> (Gly) <sub>4</sub> <sup>2+</sup>		495	516	538	561			[52] <sup>c</sup>
UO <sub>2</sub> HTr <sup>2+</sup>	475	492	514	539	565	591	810	[53]
UO <sub>2</sub> H <sub>2</sub> Tr <sub>2</sub> <sup>2+</sup>	476	494	516	541	566	595	330	[53]
UO <sub>2</sub> H <sub>3</sub> PTr <sup>2+</sup>	478	494	515	540	564	594	17 400	[53]
UO <sub>2</sub> H <sub>2</sub> PTr <sup>+</sup>	479	496	517	541	566	595	4900	[53]
UO <sub>2</sub> HPTr	484	502	523	547	573	601	540	[53]

*Gly* glycine, *Tr* L-threonine, *PTr* O-phospho-L-threonine

<sup>a</sup> 1 M HClO<sub>4</sub>; values are rounded, the errors in emission wavelength are 2, 0.8, 0.6, 0.6, 0.6 and 2 nm, the error of the decay time is 0.7 μs

<sup>b</sup> Tits J, private communication; measured at LN<sub>2</sub>

<sup>c</sup> 0.019 M solution, excitation at 416.5 nm

cay times may be influenced by a number of factors, leading to differences in the published data. The round-robin test (see Sect. 4) has shown that there is a need for more comparative measurements to get consistent data sets in the luminescence determination of uranium(VI) species.

### 3.3

#### Neptunium(VI) and Plutonium(VI)

Beitz and coworkers have reported on the luminescence of NpF<sub>6</sub> and PuF<sub>6</sub> [58]. However, these studies were performed in the gaseous state. The NpF<sub>6</sub> as well as the PuF<sub>6</sub> were excited at 1064 nm. The luminescence was observed for the Np compound at 1360, and 2300 nm for the plutonium compound. The decay times are dependent on the vapor pressure. The <sup>237</sup>NpF<sub>6</sub> shows a lifetime of 3.49 ms at 21 Torr, and the <sup>242</sup>PuF<sub>6</sub> a lifetime of the excited state of 0.218 ms at 18 Torr.

Additionally, Wilkerson et al. [17] studied the luminescence of Np(VI). They found a near-infrared emission in Cs<sub>2</sub>U(Np)O<sub>2</sub>Cl<sub>4</sub> from the 6890 cm<sup>-1</sup> level (1451 nm). Also, the main emission occurs at 1473.8 nm and 1509.4 nm. The luminescence decay time at 295 K is reported to be 20 μs, whereas this decay time increases at 75 K to 71 μs.

### 3.4 Americium(III)

Luminescence studies of americium in solution have not been performed with the same intensity as the studies of uranium(VI) and curium(III). This may be caused by the high molar absorption coefficient of  $\text{Am}^{3+}$  in solution (allowing studies in absorption mode by laser-induced photoacoustic spectroscopy, LIPAS) [59, 60], as well as the radioactivity of the mostly used isotope ( $^{243}\text{Am}$ , half-life 7400 years), and the short luminescence decay time (nanosecond range).

The excitation of Americium(III) occurs depending on the solution species in the wavelength range 503–510 nm. The luminescence is emitted in the range 660–740 nm. The excitation is very sensitive to the speciation of the americium. Figure 2 shows the emission spectrum of  $\text{Am}(\text{EDTA})^-$ -complex excited at 503.2 nm, the excitation wavelength of the aqueous species, and at 507.6 nm, which is the wavelength to excite the  $\text{Am}(\text{EDTA})^-$  species to its maximum extent.

Following the pioneer work of Horrocks and coworkers on europium luminescence lifetimes [61] (the “Horrocks’ method”), an empirical correlation between the luminescence decay constant and the number of water molecules

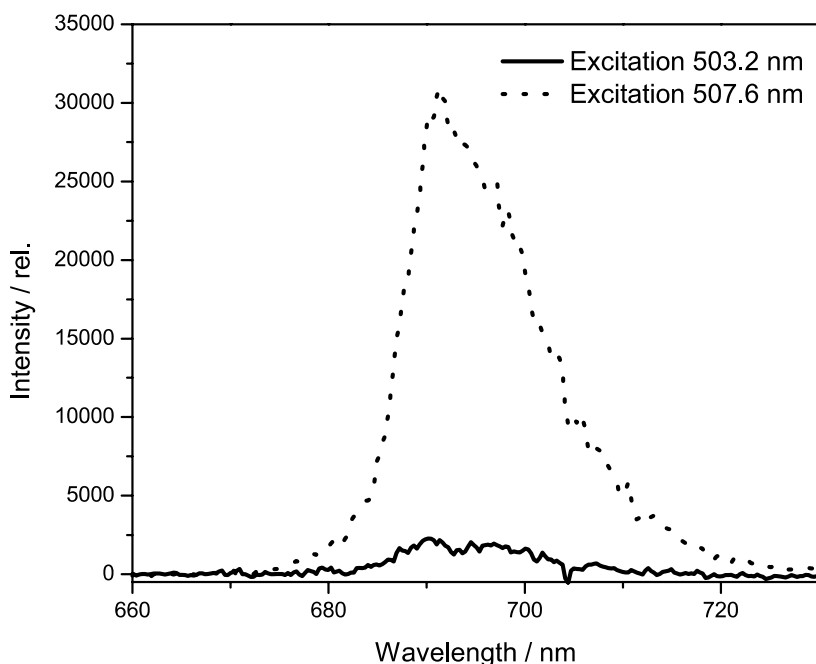


**Fig. 2** Intensity of the emission spectra of  $\text{Am}(\text{EDTA})^-$  excited at different wavelengths

in the inner sphere hydration shell has been derived by Kimura [18]. Such relationships have also been established for several lanthanides such as  $\text{Sm}^{3+}$ ,  $\text{Eu}^{3+}$ ,  $\text{Tb}^{3+}$ , and  $\text{Dy}^{3+}$ , and for  $\text{Cm}^{3+}$ .

In this particular case,  $\text{Am}^{3+}$  was excited at 504 nm and the emission at 691 nm was used for the determination of the decay constant. According to the Horrocks' procedure, americium(III) was dissolved in solutions with increasing concentrations of  $\text{D}_2\text{O}$ . The lifetime value was determined to be 24.6 ns in pure  $\text{H}_2\text{O}$  and increases to 162 ns in pure  $\text{D}_2\text{O}$ . A linear relationship between the decay constant and the concentration of  $\text{D}_2\text{O}$  in the solution was found. Assuming nine water molecules to be in the inner sphere hydration shell and neglecting any isotopic exchange leading to HDO for example, the relationship was derived to be:

$$N_{\text{H}_2\text{O}} = 2.56 \times 10^{-7} k_{\text{obs}}(\text{Am}) - 1.43, \quad (1)$$

where  $N_{\text{H}_2\text{O}}$  is the number of water molecules coordinating to the  $\text{Am}(\text{III})$  ion and  $k_{\text{obs}}$  is the decay constant (in  $\text{s}^{-1}$ ).

A recently performed study [62] has lead to an equation that is very close to the data given in [18]. It should be mentioned that this study has been performed with a Nd:YAG pumped OPO system, which has a pulse duration of about 1.6 ns. The result is given in Eq. 2:

$$N_{\text{H}_2\text{O}} = 2.27 \times 10^{-7} k_{\text{obs}}(\text{Am}) - 1.32. \quad (2)$$

Such empirical formulae, although interesting, suffer from the rough approximations on which they are based. These hypotheses have been discussed at length in various papers [63] and reviews [4].

Cavallec and coworkers reported on the  $^5\text{F}_6$  transition of  $\text{Am}^{3+}$  in a  $\text{LiYF}_3$  matrix [64]. The data were obtained at 10 K. The most intense excitation line at 501.5 nm was used. The emission was observed in two main groups of narrow lines. The highest intensities were observed at 669.7 and 719.4 nm. The luminescence decay time of 1.5 ms at 583.5 and 669.7 nm is assigned to  $^5\text{D}_1$  levels of the crystal field, whereas the shorter 7  $\mu\text{s}$  decay originates from the  $^5\text{L}_6$  level.

### 3.5

#### Curium

The short luminescence decay time of americium in combination with the high specific radioactivity (shorter half-life and formation of gamma rays emitting daughter nuclides) of the commercially available Am isotopes have led to fewer studies than those performed with Cm, for which  $^{248}\text{Cm}$  (half-life 340 000 years) is mostly used. However, the availability of this isotope is very limited. Fortunately enough, curium(III) shows the highest luminescence yield among the actinide series. Therefore, luminescence studies at very

low concentrations of this element in solution are possible. While uranium speciation studies at room temperature are usually performed in a concentration range of about  $1 \times 10^{-5}$  to  $1 \times 10^{-6}$  M, for curium studies concentrations of  $1 \times 10^{-7}$  M and less are applied.

As in the case of U(VI), Cm(III) displays a wide variety of luminescence decay times and emission spectra (mainly spectral shifts), depending on the speciation. This characteristic has been used to determine the equilibrium constant by use of very low concentrations of Cm in order to mimic environmental conditions and to avoid radioactive concerns. As curium is a spherical ion, comparable to the lanthanides and to americium, a simple equation has been derived by Choppin and Kimura [65] to correlate the decay time with the number of water molecules in the first hydration shell:

$$N_{\text{H}_2\text{O}} = 0.65 \times 10^{-3} k_{\text{obs}}(\text{Cm}) - 0.88 . \quad (3)$$

A typical luminescence spectrum of  $\text{Cm}^{3+}$  in an aquatic environment is shown in Fig. 3. The luminescence decay is mono-exponential with a decay time of 65  $\mu\text{s}$  and the maximum of the emission is located at 593.8 nm.

Besides curium(III) it is also reported that curium in its uncommon oxidation state +4 shows luminescence properties [66]. About 0.1 at. % Cm was doped into a  $\text{CeF}_4$  matrix . Luminescence excitation was observed at around 501.3 nm. The emission occurs at about 602 nm and the decay time was determined to be in the 50  $\mu\text{s}$  region.

The most important data on the luminescence of curium are summarized in Table 4.

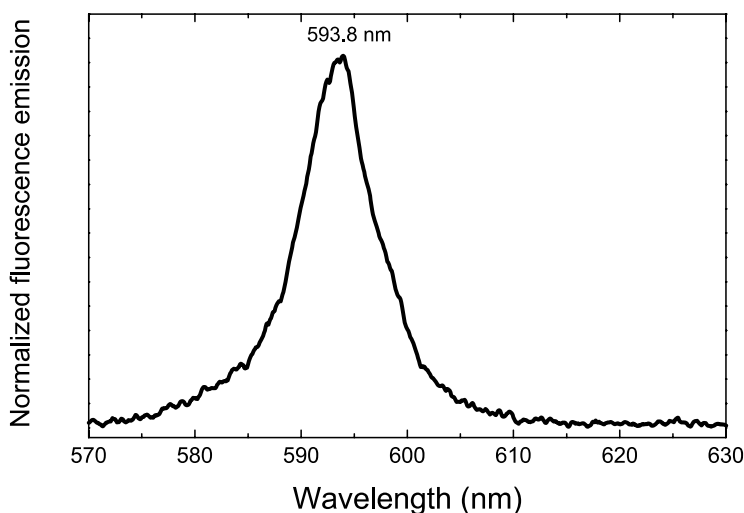


**Fig. 3** Luminescence spectrum of  $3.0 \times 10^{-7}$  M  $\text{Cm}^{3+}$  in 0.1 M  $\text{NaClO}_4$ , pH 2.93

**Table 4** Emission wavelength and decay times of Cm(III) solution species

Species	Emission wavelength [nm]	Lifetime [μs]	Refs.
Cm <sup>3+</sup>	593.8	67 ± 3	[67]
	593.8	65 ± 2	[68]
CmCl <sup>2+</sup>	592.9		[69]
CmCl <sub>2</sub> <sup>+</sup>	598.3		[69]
CmCl <sub>3</sub>	605		[69]
CmCl <sub>4</sub> <sup>-</sup>	615		[69]
Cm(OH) <sup>2+</sup>	598.7	72 ± 2	[70]
	598.8		[68, 71]
Cm(OH) <sub>2</sub> <sup>+</sup>	603.5	80 ± 10	[70]
	603.5		[68]
CmSO <sub>4</sub> <sup>+</sup>	596.2	88 ± 2	[72]
Cm(SO <sub>4</sub> ) <sub>2</sub> <sup>-</sup>	599.5	95 ± 8	[72]
Cm(SO <sub>4</sub> ) <sub>3</sub> <sup>3-</sup>	602.2	195 ± 3	[72]
CmHCO <sub>3</sub> <sup>2+</sup>	594.9		[73]
CmCO <sub>3</sub> <sup>+</sup>	598.0	85 ± 4	[68]
	598.5		[74]
Cm(CO <sub>3</sub> ) <sub>2</sub> <sup>-</sup>	605.9	105 ± 5	[68]
	603.0		[74]
Cm(CO <sub>3</sub> ) <sub>3</sub> <sup>3-</sup>	607.6	215 ± 6	[68]
	605.7		[74]
	607.4		[75]
Cm(CO <sub>3</sub> ) <sub>4</sub> <sup>5-</sup>	607.5		[74]
Cm(H <sub>3</sub> SiO <sub>4</sub> ) <sup>2+</sup>	598.5	85.1 ± 2.5	[67]
Cm(H <sub>3</sub> SiO <sub>4</sub> ) <sub>2</sub> <sup>+</sup>	603.2	198.2 ± 7.2	[67]
CmH <sub>2</sub> ATP <sup>+</sup>	598.6	88	[76]
CmHATP	600.3	96	[76]
CmATP <sup>-</sup>	601.0	187 ± 7	[76]
CmEDTA <sup>-</sup>	599.4	234	[77]
Cm(EDTA) <sub>2</sub> <sup>5-</sup>	609.1	347	[77]
	601.2?	72 ± 5	[78]
CmHA	601		[79]
	601.2	70 ± 5	[78]
CmFA	600.3		[79]
	597.8		[80]
CM(SSA) <sub>2</sub> <sup>3-</sup>	603.5		[80]

SSA 5-sulfosalicylic acid

### 3.6

#### Other Actinides

Bk, Cf, and Es can be considered rather “exotic” actinides. They are not formed in measurable amounts in the core of nuclear power plants so that

the supply is actually very limited. On another hand, the radioactive problems linked to these elements render their (luminescence) studies very difficult to perform, which explains why papers are scarce.

### 3.6.1

#### Berkelium(III)

The spectroscopic properties of berkelium have been studied by Carnall et al. [81]. The luminescence was excited with a nitrogen laser pumped dye system tuned to 391 nm. Measurements were carried out at 295 K in 0.5 M DCl in D<sub>2</sub>O. The luminescence peaks at 647 nm. The observed lifetime was  $0.1 \pm 0.02 \mu\text{s}$ . As the computed pure radiative decay time was calculated to be about 0.5 ms the authors conclude a quantum yield for Bk<sup>3+</sup> of about 0.0002 in D<sub>2</sub>O.

Bk(III) shows emission lines at 651.5 nm ( $15\,340 \text{ cm}^{-1}$ ) and 742 nm ( $13\,475 \text{ cm}^{-1}$ ) [22] in a silicate matrix. The emission was stimulated by use of an argon-ion laser. The intensity ratio between these two bands depends on the intensity of the exciting light source and the temperature of the sample.

### 3.6.2

#### Californium(III)

Evidence for an emission spectrum has been reported by Conway 1962 [82]. Three regions of emission were given with at least 14 lines (370.6–378.9 nm, 384.4–389.3 nm, and 426.7–433.5 nm). However, these emissions may result from radioluminescence of this element. No other data about the luminescence of Cf<sup>3+</sup> have been reported up to now [2, 83]. From the calculated free ion *f*-state energies of Cf<sup>3+</sup> [75], no emission is expected. In contrast to this, Nugent expected a very low intense emission in the far infrared region [84].

In the same silicate matrix as used for Bk(III) studies, an emission of Cf(III) at  $14\,600 \text{ cm}^{-1}$  (684.9 nm) has also been observed. However, the spectrum is dominated by the emission of the daughter nuclide curium, which exhibits an emission at  $16\,100 \text{ cm}^{-1}$  (621.1 nm) [22].

### 3.6.3

#### Einsteinium(III)

The behavior of Es<sup>3+</sup> in a LaF<sub>3</sub> matrix has been studied by Beitz [85]. The spectra were recorded using the 526 nm excitation. A short initial decay was assigned to the influence of radiation damage-induced color centers. For the <sup>5</sup>F<sub>5</sub> deactivation, a decay time of  $2060 \pm 100 \mu\text{s}$  was observed.

The luminescence of einsteinium(III) in aqueous solution has been reported by Beitz and coworkers [86]. Two different laser systems were used to excite the einsteinium, a nitrogen laser pumped dye laser (495 nm) and a fre-



quency tripled Nd:YAG laser (355 nm). One of the most important problems during the measurements was due to the high radioactivity of  $^{253}\text{Es}$ , which leads to a warming of the solution up to its boiling point, a situation that is rather common with such highly radioactive elements. The emission occurs in a broad band in the near infrared at 1080 nm. In the solvent water the lifetime has been determined to be 1.05  $\mu\text{s}$ . This lifetime increases to 2.78  $\mu\text{s}$  if the solvent is exchanged by  $\text{D}_2\text{O}$ . From the comparison with the decay of the hydrated lanthanides it was concluded that the 5f actinides show a more strong interaction with their inner sphere coordination shell.

### 3.7

#### Radioluminescence

All isotopes of the elements in the actinide series are radioactive. This is connected to a release of energy during the radioactive decay process. On the other hand, the released energy sometimes excites luminescence of the actinide elements. This phenomenon, called radioluminescence, is mostly observed in solid samples.

Evidence for luminescence of uranium(III) has been reported by Conway [87]. The data were derived in a  $\text{LaCl}_3$  crystalline matrix. Seven emission bands were observed in the region 545–692 nm. Data on the decay constant were not given.

As for uranium(III), data for the luminescence of neptunium(III) were also reported [87]. In the  $\text{LaCl}_3$  crystalline matrix four emission lines around 503 nm were observed. Besides these lines, one line at 512 nm and six lines around 623 nm were determined.

The relevant data of Pu(III) in  $\text{LaCl}_3$  were reported by Cunningham [88]. Some 25 lines were observed, the most intense being located in the range 516.3–518.3 nm as well as at 614.7 nm.

Also, Am(III) in the  $\text{LaCl}_3$  matrix was studied by Gruen [89]. Some 34 lines were observed between 424 and 671 nm. The most intense bands are located at 462.6 and 611.9 nm.

The radioluminescence of  $\text{Cm}^{3+}$  in the  $\text{LaCl}_3$  matrix is also reported [87]. The emission occurs around 450 nm (three lines) and 399 nm (four lines).

The radioluminescence of californium has been reported by Conway [82]. The emission occurs in the visible region.

## 4

### Concentration Determination and Quality Assurance

The determination of actinide concentrations by luminescence spectroscopic methods is usually performed by use of calibration methods, with the help of samples of known concentration, from which a relationship between intensity

and concentration is derived. Clearly, measurements should be performed using exactly the same setup (geometry, energy etc.). However, even if such precautions are taken, such calibration curves require the same speciation to be present in the known and unknown samples but it has already been stressed that actinide chemistry is very diverse. The problem can only be solved easily if one or two species are present at maximum. In particular, for uranium(VI) solutions in the mid-pH range, a large number of species co-exist in the solution that all have different luminescence yields and lifetimes and, last but not least, present relative ratios that are extremely dependent on the chemical conditions prevailing in solution (total uranium concentration, ionic strength,  $T$  etc.). As an example, the speciation of uranium at pH 6 in a carbonate-free medium as function of the total uranium concentration is shown in Fig. 4. For the calculations, the data of the NEA database [90, 91] as well as the program code MEDUSA [92] were used.

The ionic strength of the solution under investigation has also to be taken into consideration. For uranium(VI) a series of studies [36, 93] has been performed showing that the luminescence lifetime is strongly dependent on the ionic strength of the solution. It could be shown that the decay time as well as the luminescence intensity increases, whereas the emission maxima are

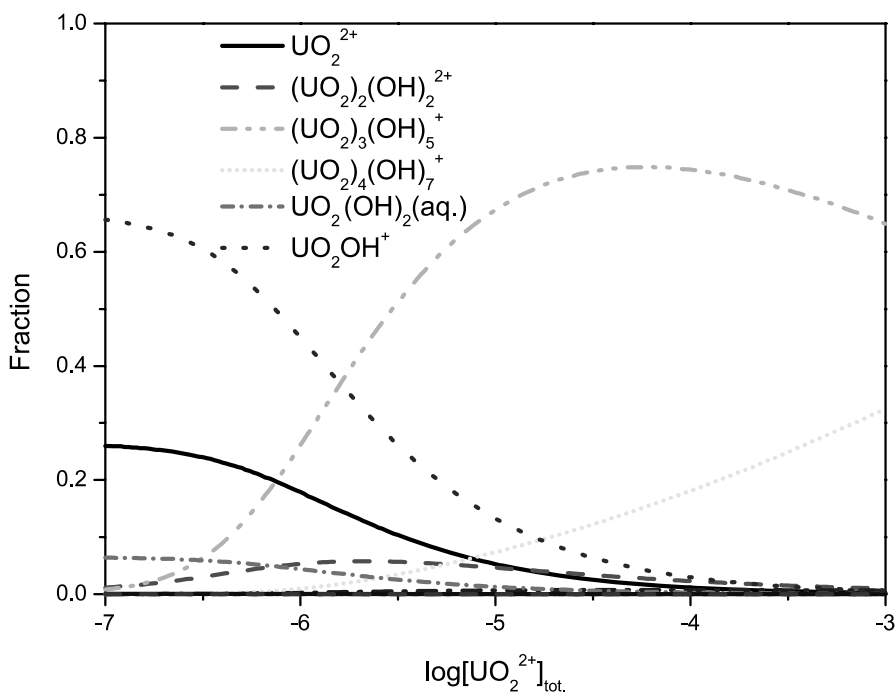


**Fig. 4** Relative species distribution of uranium(VI) as a function of the concentration at pH 6,  $I = 0.1$  M,  $t = 25$  °C

not affected. This is caused by the negligible complexing interaction of the perchlorate ion. The change in the decay time is discussed as a result of a photochemical excited state reaction of the uranyl ion. However, the decreasing activity of the solvent water, acting as a quencher on the luminescence, may also be taken into consideration.

Table 5 summarizes the detection limits described in the literature for several actinides. The given values can differ from our personally derived data due to the following reasons:

1. The setup for the fluorescence spectroscopic systems differs from one laboratory to another. The use of a wide variety of spectrographs, gratings, photosensitive devices, multichannel plates (intensifiers) with the possibility to vary the amplification factor leads to different sensitivities of the used setup and therefore the detection limits may differ.
2. The use of different light sources induces variation in the excitation wavelength and thus in its efficiency, especially in the case of U(VI) spectroscopy. According to the excitation spectrum, the light absorption changes and subsequently the emission intensity also varies. Turning the argument around, adapting the excitation wavelength may allow the highlighting of the spectroscopic properties of a specific species in order to focus on its study.

Detection limits for the other luminescent actinides are not available. However, it can be stated, due to the low available amounts of these elements, that the limit of detection is in the same order of magnitude. The only statement found was by Yusov [2], that the relative luminescence intensity decreases in the order  $\text{Cm}^{3+} > \text{Es}^{3+} > \text{Bk}^{3+} > \text{Am}^{3+} > \text{Cf}^{3+}$ .

In the nuclear field, TRLIFS data are mainly used in order to derive equilibrium constants [13, 96–99]. In order to do so, either lifetime values and/or emission spectra and their variation with a given parameter (such as ligand concentration, ionic strength etc.) are examined. In turn, such equilibrium constants are used to predict actinide migration in the environment, for example. Therefore, the confidence that can be ascribed to the primary data (lifetimes, emission spectra) is essential for the quality of the predictions derived from them [100]. However, it has been rapidly acknowledged through the radiochemical community that TRLIFS data of very basic systems (such as the uranyl ion in water as a function of pH) present a large variation from one research group to another. Although clear differences between samples (pH, total ionic strength, concentration of *U* etc.; see Fig. 4 for an illustration of these variations) could be possible reasons for such deviations, it was necessary to ascertain more firmly the TRLIFS technique in order to validate predictions derived from such studies. With this aim, a round-robin test was organized in 2001 in order to compare data obtained on identical uranyl ion samples of perfectly known composition. The samples were prepared in CEA (CETAMA group, Marcoule, France) and identical aliquots were shipped

**Table 5** Detection limits for actinide species in solution

	Detection limit [M]	Refs.
Pa(IV)	$1.0 \times 10^{-7}$	[9]
U(IV)	$1.0 \times 10^{-6}$	[32] <sup>1</sup>
U(VI)	$8.0 \times 10^{-8}$	[51] <sup>2</sup>
	$4.0 \times 10^{-12}$	[51] <sup>3</sup>
	$2.0 \times 10^{-9}$	[42] <sup>4</sup>
	$2.0 \times 10^{-10}$	[42] <sup>5</sup>
Am(III)	$1.0 \times 10^{-8}$	[19] <sup>6</sup>
	$1.0 \times 10^{-11}$	[19] <sup>7</sup>
Cm(III)	$5.0 \times 10^{-13}$	[94, 95]

<sup>1</sup> At liquid nitrogen temperature

<sup>2</sup> 4.1 M HNO<sub>3</sub> at 40 °C

<sup>3</sup> H<sub>3</sub>PO<sub>4</sub>

<sup>4</sup> 5 M H<sub>2</sub>SO<sub>4</sub>

<sup>5</sup> Solution TTA/TOPO/Triton X100

<sup>6</sup> Solid, ThO<sub>2</sub> matrix

<sup>7</sup> In 10<sup>-3</sup> M TTA/5 × 10<sup>-5</sup> TOPO

to the 14 participating laboratories worldwide (France, Great Britain, Japan, Germany, Portugal, Poland, USA).<sup>1</sup> The exact composition of the samples was kept secret to the participants. They were asked to provide, by use of their own TRLIFS setup, the number of decaying species, associated lifetime values, and peak positions of the corresponding emission spectra. In the case of multiple decaying spectra, they were requested to ascribe a given lifetime to a given group of emission peaks, if possible. The detailed analysis of this round-robin test has been published [12], so we will just summarize the main results.

First, it appears that the exact components of the TRLIFS setup have no influence on the values collected. This means that excitation by use of either a Nd:YAG or a dye laser, or detection by use of a photomultiplier (photon counting setup) or boxcar apparatus have no real impact onto the data values, as expected. However, the sensitivity of the whole setup is a very important parameter in deriving data that can be easily separated from background, especially in the case of the rather diluted samples of the round-robin test.

More important, it has been demonstrated that for simple samples, such as uranium in an acidic solution (1 M HClO<sub>4</sub>) for which it is well known that a single uranyl species (UO<sub>2</sub><sup>2+</sup><sub>aq</sub>) is present, data are consistent within a very narrow range from one laboratory to another. This allowed researchers to ob-

<sup>1</sup>The financial support of the French "Groupement de Recherches PRACTIS" is greatly acknowledged.

tain reliable emission peak and lifetime values for this system (see Table 3), thus leading to an easy-to-prepare solution for routine tests of any TRLIFS setup. However, such a solution cannot be considered as a *standard*.

Careful examination of the other results led to the following conclusions:

1. The  $\text{UO}_2^{2+}$  <sub>aq</sub> lifetime depends strongly on the ionic strength, while its emission spectrum remains unchanged
2. As long as no more than two luminescent species are present in solution, data obtained are consistent and reliable
3. In the case of three species, discrepancies are observed, which could be ascribed to two different reasons: (a) either the luminescence properties of the various species are too similar to be able to distinguish between them, whatever the intrinsic quality of the TRLIFS setup used, or (b) the analysis methods used are not efficient enough

As a consequence, it appears that the uranyl/ $\text{H}_2\text{O}$  system, as a function of pH, might well be too intricate, as far as its chemistry is concerned [90, 91], to be safely examined in the neutral pH range through TRLIFS alone.

Further studies in the laboratories of the two authors of this chapter, in collaboration with the editor of this book, have shown that the usual luminescent standards (such as quinine sulfate in methanol) are not user-friendly means of improving the quality of TRLIFS data collected in the radiochemical community. Actually, these standard solutions display lifetimes that are very short, thus making their time-resolved detection with ns-laser photon counting setups impossible. Furthermore, luminescence yields (more than 50%) are far from those of the usual uranium solutions (in the range of 0.05%). This situation is even more difficult because of the usual available setups in the laboratories. While actinide chemists are more interested in the determination of species, mostly it is spectrometers that are available for time-resolved measurements. However, determination of luminescence yields need steady state intensity measurements over much more than five orders of magnitude. The luminescence yield value of U(VI) obtained from a comparison of a dye and an uranium(VI) solution performed in our laboratory is therefore only a first rough estimation. To this end, it was necessary to open the camera gate to a value of about five times that of the luminescence decay time of the uranyl ion (i.e. 10  $\mu\text{s}$ ) to collect the whole emitted luminescence. Comparison with the luminescence yield of quinine sulfate (51%) leads to a luminescence yield of the uranyl ion in 0.1 M  $\text{HClO}_4$  of about 0.04%.<sup>2</sup> In conclusion, owing to the limited community to which dedicated luminescent standards would be of some help, there is little chance that this situation will improve in the near future.

On another hand, the fundamental question of the physical meaning of the data has to be tackled. It is well known that many chemical systems, once

---

<sup>2</sup> For supporting of these measurements the assistance of U. Resch-Genger is gratefully acknowledged.

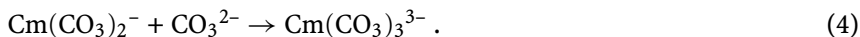
excited through a laser pulse, may (but not always) undergo excited-state reactions such as proton transfer, ligand exchange etc. [101, 102]. Chemical systems containing luminescent radionuclides do not escape this rule and there is clear evidence in the literature of such a phenomenon [103], which is also known for lanthanide-containing systems [104, 105]. The mathematical description of such systems, in order to derive the *ground-state* equilibrium constant from the TRLIFS data, is not straightforward and thus deserves attention [106]. Depending on the relative values of the excited and ground state reaction rate constants at work, such a data analysis is feasible or not. Indeed, numerous publications have demonstrated that in favorable cases, the ground state equilibrium value derived from TRLIFS data is perfectly accurate and valuable [13, 15, 56]. However, some other systems, especially those containing Cm, may display fast excited state kinetics, rendering the determination of the ground state equilibrium constant impossible without a better knowledge of the photophysical properties of  $\text{Cm}^{3+}$  in its excited state [105]. As a consequence, TRLIFS experiments will be required in order to deepen our understanding of the fundamental aspects of actinide luminescence before applied studies can be performed.

## 5

### Trends

New trends in the luminescence analysis of actinides can be divided into several aspects: new experimental parameters, new solvents and media, new luminescence concerns and, last but not least, multiple experimental devices. These aspects will be briefly introduced.

First, experiments are now performed under rather difficult conditions, i.e., under high pressure or at rather elevated temperatures. Temperature-dependent measurements of the luminescence of actinides have the potential to be used for determination of thermodynamic data ( $\Delta H$ ,  $\Delta G$ ,  $\Delta S$ ). Vercoouter et al. [75] have used measurements of the luminescence of  $\text{Cm}^{3+}$  in the temperature range 10–70 °C to determine the reaction enthalpy for:



The study of uranium(VI) speciation at variable temperatures was also performed. As one example, we refer to some data given by Zanonato [107]. Besides the calculated thermodynamic data, information about the change of the luminescence decay time is available, showing a decrease over one order of magnitude in the temperature range 20–80 °C. This leads to an activation parameter of about 35 kJ mol<sup>-1</sup>.

Measurements at low temperatures have a high potential for time-resolved luminescence spectroscopic studies. Due to the luminescence quenching effect of the water molecules in the hydration shell of the actinides, freezing of

the samples can improve sensitivity, resulting in more intense and more detailed spectra. This leads, last but not least, to a lower detection limit and to the possibility of studying the speciation of actinides in environmental samples, provided that the freezing process does not disturb the speciation under investigation. The same effect occurs in the case of the pure uranium carbonate species. It is known that these solution species do not emit any luminescence, also caused by the dynamic quench effect of the carbonate bonding to the uranium(VI). This leads to a total output of luminescence in the species  $\text{UO}_2(\text{CO}_3)_2^{2-}$  and  $\text{UO}_2(\text{CO}_3)_3^{4-}$ . However, Wang and coworkers [108] showed that freezing of such samples allows detection of the carbonate species in the soil of the Hanford site. Very interesting experiments have also been performed under hydrothermal conditions. Although the work already published is focused on lanthanide ions [109], it represents a first step towards the luminescence studies of actinides under delicate environmental conditions.

On another hand, although not as difficult as those previously described, experiments in new media are another interesting trend of actinide luminescence studies. As a brief review, we will first mention data acquired in supercritical  $\text{CO}_2$ , a medium of potential interest for extraction studies for the reprocessing of nuclear fuels or for the remediation of contaminated soils [110]. Luminescence studies in ionic liquids are also an emerging field. Ionic liquids are solvents composed of ions, which present interesting features often gathered under the “green solvent” definition. However, at the moment, no publication has appeared evidencing actinide luminescence in this class of solvents, most probably because of the very efficient quenching of the luminescence by the ionic liquid itself. In contrast, papers on the very intense luminescence of lanthanides in such solvents have already appeared [111], and it is expected that, by tuning the exact chemical structure of the ionic liquid, efficient actinide luminescence will be observed soon [112].

Thirdly, the application of tunable short pulse lasers may allow in the future the exact determination of the luminescence decay times of protactinium(IV), uranium(IV), and americium(III). It can also be expected that the detection limits for these ions will be improved, allowing the determination of the stability constants of the various complexes formed by these actinides. Finally, the interaction of organic ligands is of great interest in the coordination chemistry of the actinides. The application of fs-laser systems to excite the non-complexed organic ligand has been shown to be very useful for the determination of stability constants [103, 113]. In addition, an increase in studies of energy transfer reactions [114, 115] as well as investigations with excited state reactions may be expected in the future.

As a last trend, it should also be mentioned that the combination of various techniques such as EXAFS (extended X-ray absorption fine structure), electrochemistry, chromatographic techniques etc. with TRLIFS may have a great future potential in the determination of intricate chemical behavior in actinide chemistry. This is, however, a general trend observed in various fields,

where the conjunction of various techniques is of clear benefit for the understanding of complex systems.

The extremely low detection limits for luminescent actinides, resulting in studies of the behavior of these elements under environmental conditions, are the greatest advantage of luminescence detection methods.

## References

1. Kim JI (1986) Chemical behaviour of transuranium elements in natural aquatic systems. In: Freeman AJ, Keller C (eds) Handbook on the physics and chemistry of the actinides, vol. 4. Elsevier Science, Amsterdam, p 413
2. Yusof AB (1993) *Radiokhimiya* 35:3–25
3. Baird CP, Kemp TJ (1997) *Prog React Kinet* 22:87–139
4. Billard I (2003) Lanthanide and actinide solution chemistry studied by time-resolved laser-induced spectroscopy (TRLS). In: Bünzli J-C, Gschneidner KA (eds) Handbook on the physics and chemistry of rare earths, vol 33. Elsevier, Amsterdam, p 465
5. Choppin GR (2003) *Radiochim Acta* 91:645–649
6. Geipel G (2005) Speciation of actinides. In: Cornelis R, Caruso J, Crews H, Heumann K (eds) Handbook of elemental speciation II. Wiley, Chichester, pp 509–563
7. Reed DT, Clark SB, Rao L (eds) (1999) Actinide speciation in high ionic strength media. Kluwer Academic/Plenum, New York
8. Lever B (ed) (2006) Actinide chemistry. Special issue, *Coord Chem Rev* 250:729–974
9. Marquardt CM, Panak PJ, Apostolidis C, Morgenstern A, Walther C, Klenze R, Fanghänel T (2004) *Radiochim Acta* 92:445–446
10. Kirishima A, Rimura T, Tochiyama O, Yoshida Z (2003) *Chem Commun*, pp 910–911
11. Steudtner R, Arnold T, Großmann K, Geipel G, Brendler V (2006) *Inorg Chem Commun* 9:939–941
12. Billard I, Ansoborlo E, Apperson K, Arpigny S, Azenha ME, Birch D, Bros P, Burrows HD, Choppin G, Coustin L, Dubois V, Fanghänel T, Geipel G, Hubert S, Kim JI, Kimura T, Klenze R, Kronenberg A, Kumke M, Lagarde G, Lamarque G, Lis S, Madic C, Meinrath G, Moulin C, Nagaishi R, Parker D, Planque G, Scherbaum F, Simoni E, Sinkov S, Viallesoubranne C (2003) *Appl Spectrosc* 57:1027–1031
13. Geipel G, Brachmann A, Brendler V, Bernhard G, Nitsche H (1996) *Radiochim Acta* 75:199–204
14. Deniau H, Decambox P, Mauchien P, Moulin C (1993) *Radiochim Acta* 61:23–28
15. Brendler V, Geipel G, Bernhard G, Nitsche H (1996) *Radiochim Acta* 74:75–79
16. Wang Z, Zachara JM, McKinley JP (2005) *Environ Sci Technol* 39:2651–2659
17. Wilkerson MP, Berg JM, Hopkins TA, Dewey HJ (2005) *J Solid State Chem* 178:584–588
18. Kimura T, Kato Y (1998) *J Alloys Compd* 271–273:867–871
19. Thouvenot P, Hubert S, Moulin C, Decambox P, Mauchien P (1993) *Radiochim Acta* 61:15–21
20. Beitz JV (1994) *J Alloys Compd* 207/208:41–50
21. Wimmer H, Kim JI, Klenze R (1992) *Radiochim Acta* 58/59:165–171
22. Assefa Z, Haire RG, Stump NA (1998) *J Alloys Compd* 271–273:854
23. Carnall WT, Beitz JV, Crosswhite H (1984) *J Chem Phys* 80:2301–2308
24. Beitz JV, Hessler JP (1980) *Nucl Technol* 51:169–177
25. Beitz JV, Wester WD, Williams CW (1983) *J Less Common Met* 93:331–338



26. Moulin C, Decambox P, Couston L, Pouyat D (1994) *J Nucl Sci Technol* 31:691–699
27. Pompe S, Brachmann A, Bubner M, Geipel G, Heise KH, Bernhard G, Nitsche H (1998) *Radiochim Acta* 82:89–92
28. Günther A, Bernhard G, Geipel G, Reich T, Rossberg A, Nitsche H (2003) *Radiochim Acta* 91:319–328
29. Trubert D, Le Naour C, Jaussaud C (2002) *J Sol Chem* 31:261–265
30. Nikitenko SI, Cannes C, Le Naour C, Moisy P, Trubert D (2005) *Inorg Chem* 44:9497–9505
31. Bell JT, Friedman HA, Billings MR (1974) *J Inorg Nucl Chem* 36:2563–2567
32. Kirishima A, Kimura T, Nagaishi R, Tochiyama O (2004) *Radiochim Acta* 92:706–71
33. Geipel G (2004) Annual report 2003; FZR-400. Institute of Radiochemistry, Forschungszentrum Rossendorf, Dresden, p 1
34. Godbole SV, Page AG, Sangeeta A, Sabharwal SC, Gesland JY, Sastry MD (2001) *J Luminesc* 93:213–221
35. Bell JT, Biggers RE (1968) *J Mol Spectrosc* 25:312–329
36. Billard I, Rustenholtz A, Semonand L, Lützenkirchen K (2001) *Chem Phys* 270:345–354
37. Brachmann A, Geipel G, Bernhard G, Nitsche H (2002) *Radiochim Acta* 90:147–149
38. Rutsch M, Geipel G, Brendler V, Bernhard G, Nitsche H (1999) *Radiochim Acta* 86:135–141
39. Laszak I, Moulin V, Moulin C, Mauchien P (1997) First Technical Report on EC Project: Effects of humic substances on the migration of radionuclides. CEA contribution to Task 2, EU report
40. Moulin C, Laszak I, Moulin V, Tondre C (1998) *Appl Spectrosc* 52:528–535
41. Eliet V, Bidoglio G, Omenetto N, Parma L, Grenthe IJ (1995) *Chem Soc Faraday Trans* 91:2275–2285
42. Kato Y, Meinrath G, Kimura T, Yoshida Z (1994) *Radiochim Acta* 64:107–111
43. Karbowski M, Hubert S, Fourest B, Moulin C (2004) *Radiochim Acta* 92:489–494
44. Kirishima A, Kimura T, Tochiyama O, Yoshida Z (2004) *Radiochim Acta* 92:889–896
45. Sachs S, Brendler V, Geipel G (2007) *Radiochim Acta* 95:103
46. Scapolan S, Ansoborlo E, Moulin C, Madic C (1998) *J Alloys Compd* 271–273:106–111
47. Geipel G, Bernhard G, Brendler V, Reich T (2000) Extended abstracts 5th international conference on nuclear and radiochemistry (NRC5), Pontresina, Switzerland, 3–8 Sept 2000, vol 2. pp 473–476
48. Bernhard G, Geipel G, Reich T, Brendler V, Amayri S, Nitsche H (2001) *Radiochim Acta* 89:511–518
49. Moll H, Geipel G, Brendler V, Bernhard G, Nitsche H (1998) *J Alloys Compd* 271–273:765–769
50. Koban A, Geipel G, Roßberg A, Bernhard G (2004) *Radiochim Acta* 92:903–908
51. Günther A, Geipel G, Bernhard G (2007) *Polyhedron* 26:59–65
52. Alcock ND, Flanders DJ, Kemp TJ, Shand MA (1985) *J Chem Soc Dalton Trans* 517–521
53. Günther A, Geipel G, Bernhard G (2006) *Radiochim Acta* 94:845–851
54. Mack J, Bolton JR (1999) *J Photochem Photobiol A* 128:1–3
55. Deniau P, Decambox P (1993) *Radiochem Acta* 61:23–28
56. Couston L, Pouyat D, Moulin C, Decambox P (1995) *Appl Spectrosc* 49:349–353
57. Hoffman MZ, Bolletta F, Moggi L, Hug GL (1989) *J Phys Chem Ref Data* 18:219–543
58. Beitz JV, Williams CW, Carnall WT (1982) *J Chem Phys* 75:2756–2757
59. Kim JI, Buckau G, Bryant E, Klenze R (1989) *Radiochim Acta* 48:135–141
60. Wruck DA, Palmer CEA, Silva R (1996) Report UCRL-JC-125198
61. Horrocks WD, Suddnick DR (1979) *J Am Chem Soc* 101:334–340

62. Geipel G, Stumpf T (2005) Annual Report 2004; FZR-419. Institute of Radiochemistry, Forschungszentrum Rossendorf, Dresden, p 18
63. Beeby A, Clarkson IM, Dickins RS, Faulkner S, Parker D, Royle L, de Sousa AS, Williams JAG, Woods M (1999) *J Chem Soc Perkin Trans* 2:493–503
64. Cavallec R, Hubert S, Simoni E (1997) *J Solid State Chem* 129:189–195
65. Kimura T, Choppin GR (1994) *J Alloys Compd* 213/214:313
66. Liu GK, Beitz JV (1990) *J Luminesc* 45:254–257
67. Panak PJ, Kim MA, Klenze R, Kim JI, Fanghänel T (2005) *Radiochim Acta* 93:133–139
68. Wimmer H, Kim JI, Klenze R (1992) *Radiochim Acta* 58/59:165–171
69. Arisaka M, Kimura T, Nagaishi R, Yoshida Z (2006) *J Alloys Compd* 408:1307–1311
70. Fanghänel T, Kim JI, Paviet P, Klenze R, Hauser W (1994) *Radiochim Acta* 66/67:81–87
71. Wimmer H, Klenze R, Kim JI (1992) *Radiochim Acta* 56:79–83
72. Paviet P, Fanghänel T, Klenze R, Kim JI (1994) *Radiochim Acta* 74:99–103
73. Fanghänel T, Weger WT, Schubert T, Kim JI (1998) *Radiochim Acta* 82:55–57
74. Fanghänel T, Weger WT, Könnecke T, Neck V, Paviet-Hartmann P, Steinle E, Kim JI (1998) *Radiochim Acta* 82:47–53
75. Vercoouter T, Vitorge P, Amekraz B, Giffaut E, Hubert S, Moulin C (2005) *Inorg Chem* 44:5833–5843
76. Moll H, Geipel G, Bernhard G (2005) *Inorg Chim Acta* 358:2275–2282
77. Wang Z, Felmy AR, Xia XY, Mason MJ (2003) *Radiochim Acta* 91:329–337
78. Choi JG, Oum KW, Choi CY, Moon H, Sin HS, Park SM, Chong PJ (1993) *Bull Korean Chem Soc* 14:72–78
79. Kim JI, Wimmer H, Klenze R (1991) *Radiochim Acta* 54:35–41
80. Klenze R, Panak P, Kim JI (1998) *J Alloys Compd* 271–273:746–750
81. Carnall WT, Beitz JV, Crosswhite H (1984) *J Chem Phys* 80:2301–2308
82. Conway JG, Hulet EK, Modrow RJ (1962) *J Opt Soc Am* 52:222–223
83. Beitz JV (1994) *J Alloys Compd* 207:41–50
84. Nugent LJ, Burret JL, Werner GK, Tanner S, Tarrant JR, Keller OL (1969) *J Phys Chem* 73:1540–1549
85. Beitz JV, Williams VW, Liu GK (1998) *J Alloys Compd* 271–273:850–853
86. Beitz JV, Wester DW, Williams CW (1983) *J Less Common Metals*, 93:331–338
87. Conway JG, Wallmann JC, Cunningham BB, Shalimoff GV (1957) *J Chem Phys* 17:1416–1417
88. Cunningham BB, Gruen DM, Conway JG, McLaughlin RD (1956) *J Chem Phys* 24:1275
89. Gruen DM, Conway JG, McLaughlin RD, Cunningham BB (1956) *J Chem Phys* 24:1115–1116
90. Grenthe I, Fuger J, Konings RJ M, Lemire RJ, Muller AB, Nguyen-Tung Cregu C, Wanner H (1992) *Chemical thermodynamics, vol 1: chemical thermodynamics of uranium*. NEA-OECD, North-Holland, Amsterdam
91. Guillaumont G, Fanghänel T, Fuger J, Grenthe I, Neck V, Palmer DA, Rand MH (2003) *Chemical thermodynamics, vol 5: update of the chemical thermodynamics of uranium, neptunium, plutonium, americium and technetium*. Elsevier, Amsterdam
92. Puigdomenech I (2001) *MEDUSA: make equilibrium diagrams using sophisticated algorithms*. Inorganic Chemistry Royal Institute of Technology (KTH), Stockholm, Sweden, <http://w1.156.telia.com/%7Eu15651596/>: Last visited 14 Mar 2008
93. Rustenholz A, Billard I, Duplatre G, Lützenkirchen K, Semon L (2001) *Radiochim Acta* 89:83–89
94. Moulin C, Decambox P, Mauchien P (1991) *Anal Chim Acta* 254:145–151
95. Moulin C, Decambox P, Mauchien P (1997) *J Radioanal Nucl Chem* 226:135–138

96. Moulin C, Decambox P, Moulin V, Decaillon JG (1995) *Anal Chem* 67:348–353
97. Beitz JV (1991) *Radiochim Acta* 52:35–39
98. Kim JI, Wimmer H, Klenze R (1991) *Radiochim Acta* 54:35–41
99. Arisaka M, Kimura T, Suganuma H, Yoshida Z (2001) *Radiochim Acta* 89:593–698
100. Nitzsche O, Meinrath G, Merkel B (2000) *J Contam Hydrol* 44:223–237
101. Valeur B (2002) *Molecular fluorescence*. Wiley-VCH, Weinheim
102. Plaza P, Leray I, Changenet-Barret P, Martin MM, Valeur B (2002) *Chem Phys Chem* 3:668–674
103. Geipel G, Acker M, Vulpius D, Bernhard G, Nitsche H, Fanghänel T (2004) *Spectrochim Acta A* 60:417–424
104. Horrocks WD, Arkle VK, Liottaand FJ, Sudnick DR (1983) *J Am Chem Soc* 105:3455–3459
105. Billard I, Montavon G, Markai S, Galindo C (2006) *Radiochim Acta* 94: 275–282
106. Billard I, Lützenkirchen K (2003) *Radiochim Acta* 91:285–294
107. Zanonato PL, Di Barnardo P, Bismondo A, Liu G, Chen X, Rao L (2004) *J Am Chem Soc* 126:5515–5522
108. Wang Z, Zachara JM, Yantasee W, Gassman PL, Liu C, Joly AG (2004) *Environ Sci Technol* 38:5591–5597
109. Kimura T, Nagaishi R, Arisaka M, Ozaki T, Yoshida Z (2002) *Radiochim Acta* 90:715–719
110. Addleman RS, Wai CM (1999) *Phys Chem Chem Phys* 1:783–790
111. Billard I, Mekki S, Gaillard C, Hesemann P, Moutiers G, Mariet C, Labet A, Bunzli JCG (2004) *Eur J Inorg Chem* 6:1190–1197
112. Stumpf S, Billard I, Panak P, Mekki S (2007) *Dalton Trans*, pp 240–248
113. Vulpius D, Geipel G, Baraniak L, Bernhard G (2006) *Spectrochim Acta A* 63:603–608
114. Kumke MU, Eidner S, Kruger T (2005) *Environ Sci Technol* 39:9528–9533
115. Panak P, Klenze R, Kim JI, Wimmer H (1995) *J Alloys Compd* 22:261–166

---

# Subject Index

- ABC values 21
- Absolute fluorescence measurements 91
- Actinides, luminescence 470
  - , luminescence analysis 465
  - , photon counting techniques 469
- Actinometry 101, 122
- Affinity binding capillary electrophoresis 303
- Affinity biosensors (Type F) 341
- Americium(III) 477
- Amino acid fluorescence, intrinsic 293
- Antibody–antigen interactions 341
- Aptamer-based fluorescence polarization assays 310
- Autofluorescence 219
  
- Berkelium(III) 481
- Binder 429
- Binding inhibition assay 420
- Biosensors 327
  - , neutral/ionic analytes, referenced fibre-optic 364
- Bispectral luminescent radiance factor 187
- Boronic acid compounds, carbohydrate determination 382
- Boxcar technique 470
  
- Calibration 65
- Calibration curve 22
- Californium(III) 481
- Calorimetry 101
- Camera systems 451
- Cameras, frame transfer charge coupled device 453
  - , full frame charge coupled device 453
  - , intensified charge coupled device 454
  - , interline charge coupled device 452
  - , streak 208
  
- Capillary electrophoresis, fluorescence polarization assays 317
- Chemical sensors 325
  - , direct indicator-mediated (Type B) 333
  - , indirect indicator-mediated (Type C) 336
- Chromophore-based wavelength standards 45
- Color effect 221
- Color measurement concepts 164
- Colorimetry 163
- Concentration determination 482
- Curium 478
  
- Data inversion 238
- Deoxygenation 223
- Depolarization, protein structure/dynamics 293
- Detectors 264
- Diode lasers, picosecond 260
- Distribution parameters 24
- DNA sequencing 147
- Dual lifetime referencing 373
- Dual luminophore sensors 373
- Dual wavelength probes 376
- Dyes, inert reference 383
  
- Einsteinium(III) 481
- Electrochemical coating 441
- Electrophoresis, affinity binding capillary 303
- Emission anisotropy 402
- Emission standards 65, 82
- Enzymatic biosensors, direct (Type D) 338
  - , indicator-mediated (Type E) 339
- Enzyme linked immunosorbant assays (ELISA) 416
- Excitation channel, spectral irradiance 87

- Excitation sources 260  
Extrinsic probe FRET 296
- FI calibration curve 13  
Fibre laser 262  
Fibre-optic chemical sensors (FOCS) 347  
Filter effects 219  
Filter-based instruments 53  
FLCS (fluorescence lifetime correlation spectroscopy) 259, 270  
FLIM, accuracy of fitting parameters 255  
–, data analysis 233, 249  
Flow cytometry 3  
Fluorescence 3  
Fluorescence anisotropy 373  
Fluorescence calibration, quantitative 16  
–, standards 39  
Fluorescence instruments 71  
Fluorescence intensity standards 3, 33, 65  
–, application-specific 46  
Fluorescence kinetics 195  
Fluorescence lifetime correlation spectroscopy (FLCS) 259, 270  
Fluorescence lifetime imaging 373  
Fluorescence lifetime standards 225  
Fluorescence measurements 71  
–, equation 13  
Fluorescence polarization 303, 373  
–, advantages/limitations 318  
–, applications 306  
–, emission anisotropy 402  
Fluorescence polarization assays, capillary electrophoresis 317  
–, single nucleotide polymorphism 313  
Fluorescence polarization immunoassay (FPIA) 307  
Fluorescence properties 17  
Fluorescence quantum yields 101  
–, absolute 106  
–, calorimetric methods 115  
–, optical methods 107  
–, relative 123  
–, standards 47, 136  
Fluorescence sensing 429  
Fluorescence standards 33, 36, 65, 147  
–, absolute/relative 16  
Fluorescence-based fibre-optical chemical sensors 347  
Fluorescent color, standardization 172  
Fluorescent sensor nanoparticles 347, 365
- Fluorochrome standards, characterization 16  
Fluorometric sensors 332  
Fluorometry, radiometry 65  
Fluorophores, tandem long-wavelength 153  
FOCS 347  
Frequency-domain determination/method 207, 397  
Frequency-domain fluorometries 215, 217, 228  
–, artifacts 224  
FRET 279  
–, extrinsic probe 296
- Gain switching 259  
Green fluorescent protein (GFP) 150
- Imaging setup 451  
Immobilized metal assay for phosphochemicals (IMAP) 303, 311  
Immunoassays 147, 303  
Immunophenotyping, receptor quantification 26  
Instrument performance validation (IPV) 89  
Intrinsic referencing 373
- Lasers, pulsed diode 259  
LEDs, spectroscopy 263  
Lifetime assays 147  
Lifetime data, accuracy 228  
Lifetime measurements, standardization 226  
Lifetime standards 215, 225, 230  
Lifetime-based assays 373  
Lifetimes 248  
Ligand–receptor interactions 343  
Light sources 455  
Light-emitting diodes (LEDs) 263  
Long-wavelength fluorescence instrumentation 154  
Long-wavelength fluorophores 150  
Long-wavelength standards 158  
Ludox 279  
Luminescence 325  
–, quenching 433  
Luminescence lifetime determination, radiometric 389  
Luminophore assays, dual 383

- Matrix 17  
MESF calibrators 21  
MESF concept 48  
Metal anion probes 380  
Metal ion probes 380  
Microarrays 27  
Microbead suspension arrays 26  
Modulation domain method 207  
MPF, time-resolved fluorescence 217  
Multifrequency phase-modulation  
  fluorometry (MPF) 217  
Multiphoton advantage 291  
Multiple gate methods 450  
Multiplexed analysis 26
- Nanometrology 279  
Neptunium(VI) 476  
Nucleic acids 342
- One-nonochromator method 176  
Optical imaging 429
- Paints, pressure-sensitive paints, materials 435  
-, temperature-sensitive paints, materials 435  
PCR 28  
Peptide–ligand based fluorescence  
  polarization assays 308  
pH sensing 147  
Phase fluorometry 373  
Phase of frequency domain method 195  
Phosphochemicals, immobilized metal  
  assay 311  
Phosphorescence 325  
-, quantum yields 136  
Photoacoustic spectroscopy 101, 116  
Photobleaching effects 223  
Photoluminescence 163  
Photon counting techniques, actinides 469  
Phycobiliprotein allophycocyanin (APC) 150  
Picosecond diode lasers 260  
Plain fluorometric sensors (Type A) 332  
Plutonium(VI) 476  
Polarization effects, magic angle  
  configurations 220  
Polymorphism, single nucleotide 303  
Pressure-sensitive paints (PSPs) 429, 434  
-, indicators 435, 442  
-, polymers 438, 443  
Probe Brownian depolarization 280  
Protactinium 471  
Pulse fluorometry, artifacts 224  
Pulse pile-up effect 224  
Pulsed diode lasers 259
- QFC 6  
-, calibration curve 15  
-, formalization 13  
-, procedures 20  
Quality assurance 3, 33, 65, 415, 422, 482  
Quantification 3  
Quantitative fluorescence calibration (QFC) 6  
Quantum yield 101
- Radiance factor, reflected 187  
Radioluminescence 482  
Radiometric reference quantity 86  
Rapid lifetime determination (RLD) 448  
Real-time polymerase chain reaction 28  
Receptor–ligand based fluorescence  
  polarization assays 308  
Red fluorescent proteins (RFPs) 150  
Reference dyes 348  
Referencing, dual luminophore ratioing 352  
-, luminescence anisotropy 354  
-, luminescence lifetime measurements 350  
-, ratiometric dyes 348  
Reflection spectrophotometry 163  
Resonance energy transfer 373  
RFI calibrators 21  
Rotational diffusion, fluorescence  
  anisotropy 406
- Sensors, co-extraction based 357  
-, fluoroionophores 359  
-, fluorometric 332  
-, for cations/anions, referenced fibre-optic  
  chemical 357  
-, for neutral analytes, referenced  
  Fibre-Optic Sensors 361  
-, for pH, referenced fibre-optic chemical 354  
-, ion-exchange based 357

- , nanoparticles, referenced, ions/ neutral analytes 366, 368
- , pH-sensitive probes 376
- , resonance energy transfer-based 387
- Silica 279
- Silica hydrogel nanoparticle growth kinetics 290
- Silica nanoparticles, probe depolarization 284
- , stable (Ludox) 285
- Single nucleotide polymorphism 303
- Single photon counting, time-correlated 201
- Single-photon timing (SPT) 215, 217
- Sol–gel 279
- Solid-phase particulate ligand binding assays 25
- SPAD 259
- Spectral correction 65
- Spectral irradiance, excitation unit 184
- Spectral responsivity, emission channel 80
- Spectrofluorimetry metrology 163
- SPT, time-resolved fluorescence 217
- Streak camera 195, 208
- Surface fluorescence 163
  - , measurements 163, 181
- Surface fluorescent colors 171
- Surface-contour diffusion (SCOD) 289
  
- TAC, linearity of time response 224
- Tandem long-wavelength fluorophores 153
- TCSPC, data analysis 233
- TCSPC electronics 266
- Temperature-sensitive paints (TSPs) 429, 434
  
- , materials 435
- Temporal behaviour, modelling 236
- Thermal lensing 101, 119
- Ti:sapphire lasers 262
- Time fluorometries 217
- Time tagging 259
- Time-correlated single photon counting 195
- Time-domain determination 389
- Time-resolved fluorescence 259
  - , data evaluation 233
- Time-resolved fluorometry 215
- Time-resolved laser-induced fluorescence spectroscopy (TRLIFS) 465
- Time-resolved measurements 201
- Total internal reflection fluorescence (TIRF) 415, 420
- Transfer standards 65
- TRLIFS 465
- TTTR 259
- Two-monochromator method 163, 177
  
- Up-conversion 209
- Uranium 471
- Uranium(IV) 472
- Uranium(V)/(VI) 473
  
- Water, fluorescence-based trace analysis 417
- Water analysis 415
- , total internal reflection fluorescence immunoassay 424
- Wavelength accuracy 78
- Wavelength probes 373
- Wavelength standards, chromophore-based 45
- Western blotting 147